UNCLASSIFIED

AD 274 825

Reproduced
by the

ARMED SERVICES TECHNICAL INFORMATION AGENCY
ARLINGTON HALL STATION
ARLINGTON 12, VIRGINIA



UNCLASSIFIED

NOTICE: When government or other drawings, specifications or other data are used for any purpose other than in connection with a definitely related government procurement operation, the U. S. Government thereby incurs no responsibility, nor any obligation whatsoever; and the fact that the Government may have formulated, furnished, or in any way supplied the said drawings, specifications, or other data is not to be regarded by implication or otherwise as in any manner licensing the holder or any other person or corporation, or conveying any rights or permission to manufacture, use or sell any patented invention that may in any way be related thereto.

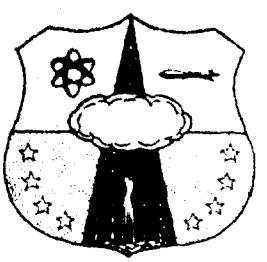
1-2-3-2

274 825

GEOLOGIC STRUCTURE STABILITY AND DEEP PROTECTION CONSTRUCTION

Technical Documentary Report No. AFSWC-TDR-61-93
November 1961

AD NO. 274 825



Research Directorate
Air Force Special Weapons Center
Air Force Systems Command
Kirtland Air Force Base
New Mexico

Project No. 1080, Task No. 108001

(Prepared under Contract No. AF 29(601)-2821 by G. B. Clark and R. D. Caudle, University of Missouri, School of Mines and Metallurgy.)

ASTIA

REPRODUCTION QUALITY NOTICE

This document is the best quality available. The copy furnished to DTIC contained pages that may have the following quality problems:

- Pages smaller or larger than normal.
- Pages with background color or light colored printing.
- Pages with small type or poor printing; and or
- Pages with continuous tone material or color photographs.

Due to various output media available these conditions may or may not cause poor legibility in the microfiche or hardcopy output you receive.

☐ If this block is checked, the copy furnished to DTIC contained pages with color printing, that when reproduced in Black and White, may change detail of the original copy.

ABSTRACT

A study is made of the problems associated with protective construction in rock, particularly deep protective structures. Information from the experience of mining engineers and from past weapons tests is given on rock structure and properties and on theories relating these to the stability of underground openings under both static and dynamic loads. Recommendations are made for meeting design problems for underground protective structures and for research to improve the reliability of the designs.

PUBLICATION REVIEW

This report has been reviewed and is approved.

DONALD L. PRICKETT
Colonel USAF
Director, Research Directorate

JOHN J. DISHUCK
Colonel USAF
Deputy Chief of Staff for Operations

DISTRIBUTION (con't)

No. Cys	
1	Commandant, The Industrial College of the Armed Forces, Ft McNair, Wash 25, DC
1	Commandant, Armed Forces Staff College, Norfolk 12, Va
10	ASTIA (TIPDR), Arlington Hall Sta, Arlington 12, Va
	AEC ACTIVITIES
1	US Atomic Energy Commission (Technical Reports Library, Mrs. J. O'Leary for DMA), Wash 25, DC
1	President, Sandia Corporation (Document Control Division), Sandia Base, N Mex
	OTHER
1	University of Illinois, Talbot Laboratory, Room 207, Urbana, Ill
1	Massachusetts Institute of Technology, ATTN: Dr. R. V. Whitman, Civ Engr Dept, 77 Massachusetts Avenue, Cambridge, Mass
1	Armour Research Foundation, ATTN: Dr. Eugene Sevin, 3422 South Dearborn Street, Chicago 16, Ill
1	American Machine & Foundry Company, ATTN: T. G. Morrison, 7501 North Natchez Avenue, Niles, Ill
1	Stanford Research Institute, ATTN: F. M. Sauer, Menlo Park, Calif
1	Purdue University, School of Civil Engineering, ATTN: Dr. Leonards, Lafayette, Ind
1	University of Massachusetts, Dept of Civil Engineering, ATTN: Dr. M. P. White, Amherst, Mass
1	Broadview Research Corp, 1811 Trousdale Drive, Burlingame, Calif
3	Dept of Mining Engineering, University of Missouri School of Mines and Metallurgy, Rolla, Mo
1	Colorado School of Mines, ATTN: Dr. J. S. Rinehart, Golden, Colo
1	Ralph M. Parsons, ATTN: M Agbabian, 617 Olive Street, Los Angeles 14, Calif
1	Iowa State University, Dept of Civil Engineering, ATTN: Dr. D. A. Van Horn, Ames, Iowa
1	School of Mines & Technology, ATTN: Prof. Oshier, Rapid City, South Dakota
1	Official Record Copy (SWRS, Mr. Walsh)
1	OTS, Department of Commerce, Wash 25, DC

DISTRIBUTION (con't)

No. Cys

ESD, Hanscom Fld, Bedford, Mass

1 (Tech Library

1 (Dir of Civil Engineering, Murphey Inst, 424 Trapelo Road, Waltham, Mass. ATTN: Mr. Minichiello)

1 (ESF)

RADC, Griffiss AFB, NY

1 (RCSST)

1 (RCS/Div of Engr/ATTN: Mr. Dana Benson)

KIRTLAND AFB ORGANIZATIONS

AFSWC, Kirtland AFB, N Mex

1 (SWEH)

5 (SWOI)

4 (SWR)

OTHER AIR FORCE AGENCIES

Director, USAF Project RAND, via: Air Force Liaison Office, The RAND Corporation, 1700 Main Street, Santa Monica, Calif

1 (RAND Library)

1 (ATTN: Dr. Judd)

ARMY ACTIVITIES

1 Chief of Engineers, Department of the Army (ENGEB), Wash 25, DC

1 Office of the Chief, Corps of Engineers, US Army (Protective Construction Branch), Wash 25, DC

NAVY ACTIVITIES

1 Chief, Bureau of Yards and Docks, Department of the Navy, Wash 25, DC

OTHER DOD ACTIVITIES

Chief, Defense Atomic Support Agency, Wash 25, DC

1 (Document Library Branch)

1 (Blast and Shock Division)

1 Director, Defense Research & Engineering, The Pentagon, Wash 25, DC

HEADQUARTERS
AIR FORCE SPECIAL WEAPONS CENTER
Air Force Systems Command
Kirtland Air Force Base
New Mexico

When Government drawings, specifications, or other data are used for any purpose other than in connection with a definitely related Government procurement operation, the United States Government thereby incurs no responsibility nor any obligation whatsoever; and the fact that the Government may have formulated, furnished, or in any way supplied the said drawings, specifications, or other data, is not to be regarded by implication or otherwise as in any manner licensing the holder or any other person or corporation, or conveying any rights or permission to manufacture, use, or sell any patented invention that may in any way be related thereto.

This report is made available for study upon the understanding that the Government's proprietary interests in and relating thereto shall not be impaired. In case of apparent conflict between the Government's proprietary interests and those of others, notify the Staff Judge Advocate, Air Force Systems Command, Andrews AF Base, Washington 25, DC.

This report is published for the exchange and stimulation of ideas; it does not necessarily express the intent or policy of any higher headquarters.

Qualified requesters may obtain copies of this report from ASTIA. Orders will be expedited if placed through the librarian or other staff member designated to request and receive documents from ASTIA.

TABLE OF CONTENTS

Chapter		Page
I.	PHYSICAL AND MECHANICAL PROPERTIES OF ROCKS.	1.1
	A. Introduction	1.1
	B. Rock Properties.	1.3
	1. Classification of Rock Properties.	1.3
	2. Petrofabric.	1.4
	3. Elastic Properties	1.4
	a. Young's Modulus of Elasticity.	1.8
	b. Modulus of Rigidity.	1.8
	c. In Situ Moduli Tests	1.9
	d. Comparison of Static and Dynamic Measurements.	1.11
	e. Specific Damping Capacity.	1.12
	4. Rock Strength.	1.12
	a. Tensile Strength	1.12
	b. Modulus of Rupture	1.12
	c. Compressive Strength	1.15
	d. Shear Strength	1.15
	5. Hardness of Rocks.	1.15
	a. Scleroscope Hardness	1.15
	b. Abrasive Hardness.	1.16
	c. Impact Toughness	1.16
	d. Ball Mill Grindability	1.16
	6. Volumetric Properties.	1.16
	a. Apparent Porosity.	1.16
	b. Apparent Specific Gravity.	1.17
	7. Other Properties	1.17
	a. Fatigue.	1.17
	b. Creep.	1.17
	c. Thermal Expansion of Rock.	1.18
	d. Compressibility.	1.18
	8. Granular Structure and Strength.	1.20
	9. Behavior of Rocks under High Confining Pressures.	1.22
	a. Quartz and Limestone	1.22
	10. Effect of Time on Strength	1.25
	11. Effect of Pressure on Fracture and Flow. . .	1.25
	12. Fundamental Strength	1.25
	13. Velocity of Longitudinal Waves in Rocks. . .	1.27
	a. Method of Measurement.	1.29
	b. State of Stress.	1.29
	c. Effect of Wave Amplitude	1.31
	d. Water Content and Velocity	1.31
	e. Velocity vs. Porosity.	1.36
	f. Effects of Stratification.	1.36
	g. Rock Texture and Velocity.	1.42
	h. Field and Laboratory Measurements. . . .	1.44
	14. Correlation of Physical Properties	1.44
	E. References	

TABLE OF CONTENTS (Continued)

Chapter		Page
II.	STRUCTURAL ENGINEERING GEOLOGY	2.1
	A. Introduction	2.1
	B. Geological Engineering Structures	2.1
	1. Folds	2.1
	2. Joints	2.8
	3. Bedding Planes	2.14
	4. Faults	2.14
	a. Post-Mineral Movement	2.18
	5. Secondary Foliation and Lineation	2.21
	6. Unconformities	2.21
	7. Lava Flows	2.23
	C. Rock Types	2.23
	a. Sedimentary Rocks	2.23
	b. Igneous Rocks	2.25
	c. Metamorphic Rocks	2.30
	D. Primary Metamorphism	2.35
	E. Secondary Metamorphism	2.36
	a. Strength of Ore	2.38
	b. Geology and Underground Water	2.38
	F. References	
III.	GEOLOGY AND UNDERGROUND STRUCTURE STABILITY	3.1
	A. Introduction	3.1
	B. Mining Methods - Classification	3.1
	C. Physical Factors and Selection of Stoping Methods	3.2
	1. Strength of Ore and Wall Rocks	3.3
	2. Shape, Size, and Dip of Deposit	3.4
	3. Depth below Surface and Character of Overburden	3.4
	D. Influence of Geology on Rock Structure and Geometry	3.5
	a. Bedded and Sedimentary Deposits	3.6
	b. Veins in Fractures, Shear, and Fault Zones	3.6
	c. Massive Deposits	3.8
	E. Mining Methods, Geology and Rock Stability	3.9
	1. Open Stopes with Pillars	3.9
	2. Sublevel Stoping	3.14
	3. Shrinkage Stoping	3.17
	4. Cut-and-Fill Stoping	3.21
	5. Square-Set Stoping	3.24
	6. Top Slicing and Sublevel Caving	3.26
	7. Block Caving	3.30
	8. Summary and Conclusions	3.33
	F. Rock Stability Intensity Factors for Non-Caving Methods	3.35
	1. Geology and Protective Construction	3.36
	a. Favorable Overlying Geological Configurations	3.37
	b. Favorable Local Geology	3.37
	G. References	

TABLE OF CONTENTS (Continued)

Chapter		Page
IV.	WAVE MECHANICS AND INSTRUMENTATION	4.1
	A. Introduction	4.1
	B. Propagation in an Extended Medium	4.1
	1. Propagation in an Extended Elastic Medium	4.2
	a. Rayleigh Waves	4.4
	b. Love Waves	4.4
	c. Reflection and Refraction	4.4
	d. Propagation in an Extended Anelastic Medium	4.10
	e. Wave Attenuation in Rock	4.12
	f. Plastic Waves	4.14
	g. Shock Waves	4.14
	C. Wave Mechanics and Crater Formation	4.17
	a. Instrumentation for Dynamic Response	4.18
	b. Strain Instrumentation	4.20
	c. Acceleration Measurements	4.21
	d. Pressure Measurements	4.21
	e. Displacement Instrumentation	4.21
	D. References	
V.	ROCK FAILURE	5.1
	1. Introduction	5.1
	2. Criteria of Failure	5.1
	3. Theories of Strength	5.2
	a. Maximum Stress Theory	5.4
	b. Maximum Elastic Strain Theory	5.4
	c. Theory of Constant Elastic Energy of Deformation	5.4
	d. Theory of Constant Distortion Elastic Strain Energy	5.4
	e. Theory of Maximum Shearing Stress	5.5
	f. Mohr's Theory of Failure	5.6
	g. Griffith's Theory of Fracture	5.9
	A. Rock Bursts	5.17
	a. Rock Burst Energy	5.18
	B. Mechanisms of Dynamic Failure	5.21
	1. General	5.21
	2. Failure Due to Plane Tension Waves	5.21
	a. Breakage Processes	5.24
	b. Strain Reflection	5.24
	3. Crater Tests	5.26
	a. General	5.26
	b. Nomenclature of Crater Tests	5.26
	c. Critical Factors in Effective Breakage	5.28
	d. Rocks Tested	5.30

TABLE OF CONTENTS (Continued)

Chapter		Page
V.	e. Granite.	5.30
	f. Discussion	5.56
	g. Failure in Flexure	5.58
	4. Rock Failure and Nuclear Bursts.	5.58
	C. References	
VI.	STATIC STRESSES AND DESIGN OF OPENINGS	6.1
	A. Introduction	6.1
	1. Initial Stresses and Stress Concentrations in the Earth's Crust	6.3
	a. Stresses around Openings in Solid Homogeneous Materials.	6.5
	2. Early Underground Stress Analysis.	6.5
	3. Theory of Elasticity Applied to Underground Mine Structure	6.7
	4. Photoelasticity Applied to Underground Mine Structures.	6.7
	5. Stress Distribution around a Single Opening.	6.8
	a. Circular Openings.	6.8
	b. Elliptical Openings.	6.13
	c. Ovaloidal Openings	6.15
	d. Rectangular Openings	6.18
	6. Summary.	6.20
	a. No Lateral Restraint	6.20
	b. Laterally Restrained	6.23
	c. Hydrostatic Pressure	6.23
	7. Stress Distribution around Multiple Openings	6.23
	a. Circular Openings	6.25
	b. Ovaloidal Openings	6.31
	c. Rectangular Openings	6.37
	8. Summary.	6.37
	B. Stresses in Simple Stratified Roofs.	6.39
	C. Centrifugal Testing to Simulate Stresses Occurring in Rock Beams Underground.	6.40
	D. Rock Beams with Three Types of Loads	6.42
	1. Mathematical Analysis of Stresses in Simple Roof Strata.	6.43
	2. Simple Beams	6.43
	a. Uniform Load	6.43
	b. Loaded by Own Weight	6.43
	c. Centrifugal Loading.	6.46
	3. Restrained Beams	6.46
	4. Summary.	6.48
	E. Design of Openings in Bedded Rock.	6.53
	1. General.	6.53
	2. Single Layer - Beams	6.53

TABLE OF CONTENTS (Continued)

Chapter		Page
VI.	3. Multiple Layer - Beams	6.54
	4. Rectangular Roof - Plate	6.54
	5. Field Tests of Design	6.56
	F. Failure Probability and Fracture Patterns	6.58
	1. Multiple Rock Cantilever Beams	6.60
	2. Voussoir Structures	6.61
	G. References	
VII.	DYNAMIC STRESSES AND DESIGN OF OPENINGS	7.1
	A. Introduction	7.1
	a. Elastic Plane Stress and Cylindrical Openings	7.1
	b. Geologic Structure	7.2
	c. Transfer of Stresses - Rock Bursts	7.14
	d. Artificial Support	7.14
	B. References	
VIII.	SIMILITUDE AND DEEP PROTECTIVE CONSTRUCTION	8.1
	A. Introduction	8.1
	B. Similitude and Confined Explosives	8.1
	a. Damage Scaling - Tuff	8.2
	b. Cratering and Scaling	8.4
	c. ERDL Tunnel Demolition	8.4
	d. Scaled Cratering and Underground Damage Prediction	8.4
	C. References	
IX.	SUPPORT OF UNDERGROUND OPENINGS	9.1
	A. Introduction	9.1
	B. Static Support	9.1
	a. Mine Timbering	9.1
	1. Steel Support	9.4
	a. Static Load Assumptions	9.13
	2. Forces and Stresses in Blocked Ribs	9.14
	a. Blocking Points	9.19
	b. Transfer of Forces	9.23
	c. Force and Stress Computation	9.23
	3. Evaluation of Proctor Method	9.26
	a. Yielding Arches	9.26
	4. Rock Bolts	9.28
	a. Suspension	9.31
	b. Beam Building	9.31
	c. Reinforcement of Openings	9.38
	C. References	

TABLE OF CONTENTS (Continued)

Chapter		Page
X.	GEOLOGIC EXPLORATION METHODS	10.1
	A. Exploration Geophysics	10.1
	1. Seismic Prospecting	10.1
	2. Seismic Refraction	10.3
	3. Theory of Refraction Method	10.3
	4. Seismic Reflection Method	10.5
	a. Summary-Seismic Methods	10.14
	5. Gravity Method	10.14
	6. Magnetic Method	10.15
	7. Electrical Prospecting Methods	10.23
	B. Exploration Drilling	10.23
	1. Geologic Mapping	10.23
	C. Aerial Photography	10.25
	1. Rock Types	10.25
	2. Structural Geology	10.26
	a. Faults	10.26
	b. Joints	10.26
	c. Bedding	10.26
	d. Schistosity and Gneissosity	10.26
	3. Summary	10.26
	D. References	
XI.	CONCLUSIONS AND RECOMMENDATIONS	11.1
	1. Rock Properties	11.1
	2. Structural Engineering Geology	11.2
	3. Geology and Mine Stability	11.2
	4. Geology and Stability of Underground Protective Construction	11.2
	5. Wave Mechanics and Instrumentation	11.3
	6. Rock Failure	11.4
	7. Static Stresses and Design of Openings	11.4
	8. Dynamic Stresses and Design of Openings	11.5
	9. Similitude and Scaling	11.5
	10. Support of Underground Openings	11.6
	11. Geophysics, Drilling and Aerial Photography	11.6

TABLE OF CONTENTS (Continued)

Appendix		Page
I-A	PHYSICAL AND MECHANICAL PROPERTIES ROCKS	
	YOUNG'S MODULUS	I-A.1
	1. Young's Modulus	I-A.1
	a. Static Method	I-A.1
	b. Dynamic Method	I-A.1
	2. Modulus of Rigidity	I-A.3
	3. Tensile Strength	I-A.3
	4. Modulus of Rupture	I-A.5
	5. Compressive Strength	I-A.5
	6. Scleroscope Hardness	I-A.5
	7. Abrasive Hardness	I-A.5
	8. Impact Toughness	I-A.7
	9. Apparent Porosity	I-A.7
	10. Apparent Specific Gravity	I-A.7
	A. Strength of Rock Samples of Irregular Shape	I-A.7
	1. Tensile Strength	I-A.8
	a. Direct Tensile Test	I-A.8
	b. Indirect Tensile Test	I-A.8
	c. Failure of a Ring	I-A.8
	2. Combined Compression and Shear	I-A.10
	B. In Situ Determinations	I-A.10
	a. Seismic	I-A.10
	b. Load Bearing Tests	I-A.12
	c. Additional Mechanical Property Tests Performed in the U.S.S.R.	I-A.13
	d. Laboratory Tests	I-A.13
	e. Static In Situ Tests	I-A.18
	C. References	
I-B	ANNOTATED TABLES OF PHYSICAL PROPERTIES OF ROCK	I-B.1
	1. General	I-B.1
	2. Table I-B.1 - Triaxial Compression Test Data	I-B.1
	3. Equation of Mohr's Envelope	I-B.1
	a. Principle Stress Relationship	I-B.2
	b. References	I-B.2
	4. Table I-B.2 - Physical and Mechanical Properties of Rock	I-B.2
	a. Source	I-B.3
	b. Type of Rock	I-B.3
	c. Static Elastic Constants	I-B.3
	d. Poisson's Ratio	I-B.3
	e. Dynamic Elastic Constants	I-B.3
	f. Selected Mechanical and Physical Properties	I-B.4
	5. Table I-B.3 - Heat Capacities of Minerals and Rocks	I-B.5
	6. Table I-B.4 - Heats of Transformation and Fusion of Minerals	I-B.6
	7. Table I-B.5 - Thermal Conductivity of Rocks	I-B.6
	A. References	

TABLE OF CONTENTS (Continued)

Appendix		Page
III-A	CASE HISTORIES OF UNDERGROUND STRUCTURE STABILITY	III-A.1
	1. Open Stopes with Pillars	III-A.1
	a. Southeast Missouri District	III-A.1
	b. Jonathan Limestone Mine	III-A.1
	A. Oil Shale, Rifle, Colorado	III-A.7
	1. Introduction	III-A.7
	2. Geology	III-A.8
	3. Physical Properties of Oil Shale	III-A.8
	4. Limestone Mine	III-A.13
	B. Sublevel Stoping	III-A.13
	1. Horne Mine	III-A.13
	2. Burra Burra Mine	III-A.21
	C. Shrinkage Stoping	III-A.22
	1. Creighton Mine	III-A.22
	2. Hollinger Mine	III-A.24
	D. Cut-and-Fill Stoping	III-A.29
	1. McIntyre Porcupine Mines	III-A.29
	2. Anaconda Copper Mining Company	III-A.33
	a. Rock Alteration	III-A.34
	b. Ore-Anaconda Vein	III-A.38
	c. Faults in Anaconda Veins	III-A.38
	d. Blue Vein Systems	III-A.38
	e. Geological Factors and Operations	III-A.39
	3. Conclusions	III-A.40
	4. Bunker Hill & Sullivan Mine	III-A.41
	5. McIntyre Mine	III-A.42
	6. Frood Mine	III-A.43
	7. Lake Shore Mine	III-A.45
	a. North Vein Zone	III-A.46
	b. South Vein Zone	III-A.46
	c. Nature of Ore and Wall Rocks	III-A.47
	d. Effects of Pressure	III-A.47
	e. Rock Bursts	III-A.47
	E. Top Slicing and Sublevel Caving	III-A.49
	1. Gogebic Range	III-A.49
	F. Block Caving	III-A.52
	1. Climax Molybdenum Mine	III-A.52
	a. Shape	III-A.54
	b. Dimensions	III-A.54
	c. Dip	III-A.54
	d. Capping	III-A.54
	e. Estimated Tonnage	III-A.54
	f. Ore Mineralization	III-A.54
	g. Ore Characteristics	III-A.54
	h. Mineral Content of Ore	III-A.54
	i. Physical Characteristics of Ore Body	III-A.54
	j. Physical Characteristics of Capping	III-A.54

TABLE OF CONTENTS (Continued)

Appendix		Page
III-A	2. Conclusions	III-A.60
	3. Inspiration Mine	III-A.61
	G. Case History of Underground Power Station	III-A.62
	1. Power Station, Snowy Mountains, Australia	III-A.62
	a. Geology	III-A.62
	b. Geological Structure of the Site	III-A.62
	H. References	
IX-A	DETAILED PROCEDURE FOR COMPUTATION OF STRESSES	IX-A.1
	1. Introduction	IX-A.1
	2. Construction of Load Diagram	IX-A.1
	3. Construction of Force Polygon	IX-A.3
	4. Determination of Thrusts	IX-A.4
	5. Bending Moment	IX-A.4
	6. Maximum Total Stress	IX-A.4
	7. Computations for Stresses in Arch Rib	IX-A.4
	8. Leg Checked as a Column	IX-A.5
	9. Stresses in Leg	IX-A.6
	a. Example No. 2 - Tunnel Support Subject to Side Pressure	IX-A.7
	10. Case 1 - Vertical Load Only on Straight Legged Rib	IX-A.9
	11. Case 2 - Side Unit Pressure Equal to 1/3 the Unit Vertical Pressure Acting on the Straight Legged Rib	IX-A.9
	12. Case 3 - Full Circle Rib	IX-A.13
IX-B	CONTINUOUS RIBS (TABLES)	IX-B.1

LIST OF ILLUSTRATIONS

Figure No.		Page
1.1	INFLUENCE OF FREQUENCY ON DYNAMIC VALUES OF YOUNG'S MODULUS.	1.14
1.2	COMPRESSIBILITY OF GRANITES, GABBROS AND DIABASES AS A FUNCTION OF PRESSURE (GUTENBERG).	1.21
1.3	INCREASE OF STRENGTH WITH CONFINING PRESSURE FOR SINGLE QUARTZ CRYSTALS CUT PARALLEL TO THE e AXIS	1.23
1.4	ULTIMATE STRENGTH AS A FUNCTION OF CONFINING PRESSURE. EACH POINT REPRESENTS THE MAXIMUM DIFFERENTIAL PRESSURE SUPPORTED BY A SPECIMEN TESTED AT THE APPROPRIATE CONFINING PRESSURE	1.24
1.5	STRESS-STRAIN DIAGRAMS FOR SOLENHOFEN LIMESTONE TESTED IN COMPRESSION WITH VARYING CONFINING PRESSURE FROM 1 TO 10000 ATMOSPHERES. EACH CURVE REPRESENTS ONE COMPLETE EXPERIMENT ON AN INDIVIDUAL SPECIMEN. (GRIGGS)	1.26
1.6	VARIATION OF LONGITUDINAL VELOCITY (km/s) WITH UNIAXIAL AND HYDROSTATIC PRESSURE (kg/cm^2)	1.30
1.7	RESULTS OF THREE DIFFERENT METHODS OF COMPRESSION ON THE SAME MATERIAL.	1.30
1.8	LONGITUDINAL WAVE VELOCITY (km/s) VERSUS PRESSURE (BARS) FOR ROCKS SHOWING A LARGE INCREASE AT LOW PRESSURES.	1.32
1.9	LONGITUDINAL WAVE VELOCITY (km/s) VERSUS PRESSURE FOR ROCKS SHOWING A SMALL INCREASE AT LOW PRESSURES.	1.32
1.10	DILATATIONAL VELOCITY (km/s) VERSUS PRESSURE (BARS). VELOCITY MEASURED WHEN DECREASING PRESSURE IS HIGHER THAN VELOCITY MEASURED WHEN INCREASING PRESSURE.	1.33
1.11	STRESS-STRAIN CURVES AND POISSON'S RATIO VERSUS STRESS FOR A SANDSTONE	1.33
1.12	COMPARISON BETWEEN MEASURED PROPAGATION VELOCITY AND VELOCITY COMPUTED FROM THE STRESS-STRAIN CURVES OF FIGURE 1.11	1.34

LIST OF ILLUSTRATIONS (Continued)

Figure No.		Page
1.13	LONGITUDINAL WAVE VELOCITY (km/s) VERSUS PRESSURE (BARS) FOR DIFFERENT WATER CONTENT. THE GREAT DIFFERENCE IN VELOCITY FOR 95 PERCENT AND 100 PERCENT SATURATED SPECIMENS IS DUE TO THE DIFFERENCE IN THE CONDITIONS OF PRESSURE.	1.34
1.14	LONGITUDINAL WAVE VELOCITY VERSUS PRESSURE. PRESSURE DIFFERENCE APPEARS TO BE IMPORTANT PARAMETER.	1.35
1.15	VELOCITY VERSUS SATURATION FOR THREE SANDSTONES	1.35
1.16	LONGITUDINAL WAVE VELOCITY AS A FUNCTION OF WATER SATURATION AT 350 BARS	1.37
1.17	LONGITUDINAL VELOCITY VS. POROSITY FOR DOLOMITE. . .	1.37
1.18	DEDUCED CURVE FOR LONGITUDINAL WAVE VELOCITY VS. POROSITY FOR SANDSTONE CORES	1.38
1.19	LONGITUDINAL WAVE VELOCITY VS. POROSITY. EXPERIMENTAL AVERAGE CURVE COMPARED WITH TIME AVERAGE FORMULA.	1.38
1.20	COMPARISON BETWEEN MEASURED POROSITY AND POROSITY DEDUCED FROM THE VALUE OF MEASURED VELOCITY AND THE EXPERIMENTAL AVERAGE CURVE OF FIGURE 1.19.	1.39
1.21	LONGITUDINAL VELOCITY AS FUNCTION OF POROSITY IN SANDSTONE FOR DIFFERENT VALUE OF σ-p.	1.40
1.22	LONGITUDINAL VELOCITY VS. POROSITY. COMPARISON BETWEEN RESULTS GIVEN BY BIOT'S THEORY AND EXPERIMENTAL RESULTS FOR SANDSTONE	1.41
1.23	SLOW AND FAST ARRIVAL PULSES FOR PITTSFORD MARBLE	1.43
1.24	COMPARISON OF FIELD CONTINUOUS VELOCITY LOG WITH SYNTHETIC LABORATORY LOG.	1.43
1.25	COMPARISON BETWEEN LABORATORY AND FIELD VALUES OF YOUNG'S MODULUS	1.45
1.26	INSTANTANEOUS AND SUSTAINED MODULUS OF ELASTICITY OF CONCRETE	1.46

LIST OF ILLUSTRATIONS (Continued)

Figure No.		Page
1.27	RELATIONSHIP BETWEEN ROCK TYPE AND YOUNG'S MODULUS .	1.48
1.28	RELATIONSHIP BETWEEN CERTAIN ROCK TYPES AND STATICALLY DETERMINED VALUES OF YOUNG'S MODULUS. . .	1.49
1.29	RELATIONSHIP OF ACTUAL TO PREDICTED COMPRESSIVE STRENGTH	1.50
1.30	SKETCHES OF COMPARATIVE SCATTERGRAMS	1.52
1.31	CORRELATION BETWEEN DYNAMIC AND STATIC E. (LABORATORY DETERMINATION.	1.53
2.1	TYPES OF ANTICLINES.	2.3
2.2	TYPES OF SYNCLINES	2.4
2.3	FLEXURE FOLDING. A-FOLDS RESULTING FROM SIMPLE COMPARISON. B-FOLDS DEVELOPED BY (1) A COUPLE OR (2) COMPRESSION AND A COUPLE COMBINED	2.5
2.4	SHEAR FOLDING BEFORE AND DURING DISPLACEMENT ALONG FRACTURES.	2.6
2.5	REGIONS OF TENSION AND SHEAR IN FLEXURE FOLDING. . .	2.7
2.6	SIMPLE FOLD SHOWING TENSION JOINTS	2.9
2.7	GEOMETRIC CLASSIFICATION OF JOINTS	2.10
2.8	JOINT MAP OF A HYPOTHETICAL AREA. ATTITUDE OF INDIVIDUAL JOINTS SHOWN BY DIP-STRIKE SYMBOLS. . . .	2.11
2.9	JOINT DIAGRAMS OF AREA SHOWN IN FIGURE 2.8	2.11
2.10	POINT AND CONTOUR DIAGRAMS OF 311 JOINT IN ADIRONDACK MOUNTAINS	2.12
2.11	TYPICAL JOINT PATTERNS. A - ROUGH AND IRREGULAR MINIMUM CAVING. B - SMOOTH SURFACE, MAXIMUM CAVING. C - SMOOTH AND ROUGH, CONSIDERABLE CAVING	2.13
2.12	DIAGRAM OF BLOCK FAULTING WITH TOPOGRAPHIC RESULTS .	2.16
2.13	FAULT SCARP BEFORE AND AFTER EROSION	2.17

LIST OF ILLUSTRATIONS (Continued)

Figure No.		Page
2.14	A- FAULT-LINE WITHOUT SCARP, FORMATIONS RESISTANT TO EROSION. B- FAULT SCARP DOWN THROW FORMATIONS EASILY ERODED. C- SCARP DUE TO GREATER RESISTANCE OF DOWN THROW BLOCK.	2.17
2.15	TYPES OF FAULTS. A-CLEAR SHARP BREAK, NO ALTERATION OF WALL ROCKS. B-SHARPLY DEFINED, NO SUBSIDIARY FRACTURES, PERVASIVE ALTERATION. C-SHARPLY DEFINED, WITH SUBSIDIARY FRACTURES, LOCALIZED ALTERATION. D-BRAIDED, WITH SUBSIDIARY FRACTURES, GENERAL ALTERATION. E-OPEN, POROUS, FILLED WITH BRECCIA.	2.19
2.16	FAULT MOVEMENT WITH FRACTURES INDUCED BY IRREGULARITIES ALONG THE FAULT PLANE	2.20
2.17	CLEAVAGE BANDING AND SEGREGATION BANDING	2.22
2.18	LINEATION. A-ELONGATED PEBBLES. B-ELONGATED CRYSTALS OF HORNBLENDE. C-LINEATION CAUSED BY CIRCULAR PLATES OF MICA. D-CLEAVAGE REPRESENTED BY TOP OF BLOCK AND PLANES SHOWN BY DOTTED LINES. . . .	2.22
2.19	VARIOUS TYPES OF UNCONFORMITIES	2.24
2.20	ANGULAR UNCONFORMITIES	2.24
2.21	PLAN VIEW OF AN IGNEOUS ROCK WITH FLOW LINES AND DIAGONAL FAULTS AND JOINTS	2.26
2.22	DIAGONAL JOINTS IN DIKES. FRACTURES IN DIKES REPRESENT EITHER DIAGONAL JOINTS IN DIKES OR CROSS JOINTS IN ENCLOSING SYENITE.	2.26
2.23	A. HORIZONTAL FLOW LAYERS; B. VERTICAL FLOW LAYERS AND VERTICAL FLOW LINES; C. VERTICAL FLOW LAYERS WITH HORIZONTAL FLOW LINES; D. VERTICAL FLOW LAYERS WITH PITCHING FLOW LINES	2.27
2.24	RELATIVE FREQUENCY OF OCCURRENCE OF SiO_2 IN IGNEOUS ROCKS IN THE EARTH'S CRUST	2.29
2.25	IDEALIZED RELATIONS BETWEEN FLOW LINES IN IGNEOUS ROCK AND ARTIFICIAL PARTING. (ABCF, CFED, AFGE.). .	2.31
2.26	IDEALIZED RELATIONS BETWEEN FLOW LINES IN IGNEOUS ROCK AND ARTIFICIAL PARTING.	2.31

LIST OF ILLUSTRATIONS (Continued)

Figure No.		Page
2.27	PRIMARY STRUCTURAL ELEMENTS AND DIRECTIONS OF PARTING IN GRANITE MASS, STREHLEN, GERMANY.	2.32
2.28	IDEALIZED SUPERPOSITION OF FLOW STRUCTURES AND FRACTURE SYSTEMS IN A MASSIVE INTRUSIVE AND SURROUNDING ROCKS	2.33
2.29	PLAN VIEW OF LEDGE OF GRANITE GNEISS, FOLIATED NORTH-SOUTH, TAVERNED BY A 6-FOOT DIKE OF FOLIATED GRANITE. THIS IS ILLUSTRATIVE OF COMPLICATED STRUCTURES WHICH MIGHT OCCUR IN IGNEOUS AND METAMORPHIC ROCKS	2.34
3.1	DIAGRAMMATIC SKETCH OF CROSS SECTION OF VEIN IN GRANITE SHOWING TYPES OF FRACTURES AND OTHER STRUCTURE	3.7
3.2	ROOM AND PILLAR METHOD WITH REGULAR PILLARS	3.10
3.3	ROOM AND PILLAR METHOD WITH RANDOM PILLARS	3.11
3.4	SCHEMATIC OF SUBLEVEL STOPING WHICH IS ADAPTED TO STRONG ORE AND STRONG WALL CONFIGURATIONS. . . .	3.15
3.5	DIAGRAMMATIC SKETCH ILLUSTRATING PRINCIPLES OF SHRINKAGE STOPING METHOD.	3.18
3.6	METHOD OF CUT-AND-FILL STOPING IS ADAPTED TO MODERATELY WEAK ORE AND WALL STRUCTURES	3.22
3.7	SQUARE SET METHOD IS USED UNDER CONDITIONS REQUIRING MAXIMUM SUPPORT FOR ORE AND WALLS	3.25
3.8	BLOCK DIAGRAM ILLUSTRATING PRINCIPLES INVOLVED IN APPLICATION OF TOP SLICING METHOD.	3.28
3.9	BLOCK DIAGRAM ILLUSTRATING PRINCIPLES INVOLVED IN APPLICATION OF BLOCK CAVING METHOD	3.31
4.1	REFLECTION OF P WAVES AT AN INTERFACE BETWEEN TWO ELASTIC SOLIDS.	4.5
4.2	REFLECTION OF SV WAVES AT AN INTERFACE BETWEEN TWO ELASTIC SOLIDS.	4.5

LIST OF ILLUSTRATIONS (Continued)

Figure No.		Page
4.3	SQUARE ROOTS OF RATIO OF REFLECTED OR TRANSMITTED TO INCIDENT ENERGY IF NO CHANGE IN WAVE TYPE OCCURS.	4.6
4.4	SQUARE ROOTS OF RATIO OF REFLECTED OR TRANSMITTED TO INCIDENT ENERGY IF INCIDENT AND REFLECTED OR TRANSMITTED WAVES ARE OF DIFFERENT TYPE	4.7
4.5	NORMAL INCIDENCE ON AN INTERFACE SEPARATING AN INCIDENT BED WITH VELOCITY 8000 FT./SEC. FROM A REFRACTING BED OF VELOCITY 16,000 FT./SEC. . . .	4.8
4.6	A TWO INTERFACE SYSTEM IN WHICH THE INCIDENT STRATUM OF VELOCITY 8000 FT./SEC. IS SEPARATED FROM THE FINAL REFLECTING STRATUM OF VELOCITY 16,000 FT./SEC. BY A BED OF INTERMEDIATE VELOCITY, 12,000 FT./SEC.	4.8
4.7	A 4-INTERFACE SYSTEM IN WHICH THE HIGHEST AND LOWEST VELOCITY BEDS ARE SEPARATED BY THREE INTERMEDIATE LAYERS WITH EQUAL VELOCITY INCREMENTS	4.9
4.8	THE REFLECTIONS AT NORMAL INCIDENCE FROM A TYPICAL SEDIMENTARY SECTION WITH A LOW VELOCITY INTERMEDIATE STRATUM	4.9
4.9	MODELS OF VISCO-ELASTIC SOLIDS (AFTER KOLSKY) . . .	4.11
4.10	TWO EQUIVALENT MECHANICAL MODELS (AFTER KOLSKY) . .	4.11
4.11	SCHEMATIC REPRESENTATION OF DISTRIBUTION OF STRAIN IN A PLASTIC WAVE (AFTER KOLSKY)	4.15
4.12	A CYLINDRICAL MASS OF MATERIAL OF UNIT CROSS-SECTION PASSING FROM RIGHT TO LEFT THROUGH A SHOCK FRONT. REFERENCE SYSTEM FIXED IN THE TRANSITION ZONE (AFTER KOLSKY).	4.15
4.13	CALCULATED PRESSURE DISTRIBUTION UNDER 2 MEGATON SURFACE SHOT AT 105 MILLISECONDS.	4.19
5.1	LIMITING STATES OF STRESS FOR FRACTURE OF BRITTLE METALS ACCORDING TO D. J. McADAM.	5.3
5.2	MOHR'S DIAGRAM.	5.7

LIST OF ILLUSTRATIONS (Continued)

Figure No.		Page
5.3	DIAGRAMMATIC REPRESENTATION OF CRACK AND STRESS SYSTEM FOR NORMAL ORIENTATION - GRIFFITH THEORY . .	5.12
5.4	DIAGRAMMATIC REPRESENTATION OF CRACK AND STRESS SYSTEM FOR ANGULAR ORIENTATION - GRIFFITH THEORY. .	5.14
5.5	GEOMETRICAL REPRESENTATION OF THE BIAXIAL FRACTURE CRITERION OF GRIFFITH.	5.16
5.6	PRINCIPAL STRESS AT FAILURE - MOHR'S THEORY	5.16
5.7	THE CONDITIONS PREVAILING IN THE GROUND AROUND AN EXCAVATION AT DEPTH.	5.19
5.8a	PROBABLE EFFECT OF ARTIFICIAL DE-STRESSING ON THE STRESS DISTRIBUTION AHEAD OF THE FACE	5.20
5.8b	PROBABLE EFFECT OF NATURAL DE-STRESSING ON THE STRESS DISTRIBUTION AHEAD OF THE FACE	5.20
5.9	THE DISTRIBUTION OF STRESS IN THE SOLID CORE OF A REMNANT AS IT BECOMES WORKED OUT	5.22
5.10	TENSILE FRACTURE BY REFLECTION OF A COMPRESSIVE STRAIN PULSE.	5.23
5.11	REFLECTION OF A TRIANGULAR COMPRESSIVE STRAIN PULSE	5.25
5.12	PLAN AND SECTION DRAWINGS ILLUSTRATING CRATER TESTS VARIABLES	5.27
5.13	STRAIN RECORD MEASUREMENTS.	5.29
5.14	STRAIN DATA - GRANITE	5.31
5.15	STRAIN DATA - MARLSTONE	5.32
5.16	STRAIN DATA - SANDSTONE	5.33
5.17	STRAIN DATA - CHALK	5.34
5.18	SCALED CRATER RADIUS VS. SCALED CHARGE DEPTH - GRANITE AND MARLSTONE	5.35
5.19	SCALED CRATER RADIUS VS. SCALED CHARGE DEPTH - SANDSTONE AND CHALK	5.36

LIST OF ILLUSTRATIONS (Continued)

Figure No.		Page
5.20	SCALED CRATER DEPTH VS. SCALED CHARGE DEPTH - GRANITE AND MARLSTONE	5.37
5.21	SCALED CRATER DEPTH VS. SCALED CHARGE DEPTH - SANDSTONE AND CHALK	5.38
5.22	SCALED CRATER VOLUME VS. SCALED CHARGE DEPTH - GRANITE AND MARLSTONE	5.39
5.23	SCALED CRATER VOLUME VS. SCALED CHARGE DEPTH - SANDSTONE AND CHALK	5.40
5.24	SCALED RADIUS OF RUPTURE VS. SCALED CHARGE DEPTH - GRANITE AND MARLSTONE	5.41
5.25	SCALED RADIUS OF RUPTURE VS. SCALED CHARGE DEPTH - SANDSTONE AND CHALK	5.42
5.26	SCALED CRATER RADIUS VS. SCALED CRATER DEPTH - UNAWEEP GRANITE	5.43
5.27	SCALED CRATER DEPTH VS. SCALED CHARGE DEPTH - UNAWEEP GRANITE	5.44
5.28	SCALED CRATER VOLUME VS. SCALED CHARGE DEPTH - UNAWEEP GRANITE	5.45
5.29	SCALED RADIUS OF RUPTURE VS. SCALED CHARGE DEPTH - UNAWEEP GRANITE	5.46
5.30	SCALED CRATER RADIUS VS. SCALED CHARGE DEPTH - NAVAJO SANDSTONE.	5.47
5.31	SCALED CRATER DEPTH VS. SCALED CHARGE DEPTH - NAVAJO SANDSTONE.	5.48
5.32	SCALED CRATER VOLUME VS. SCALED CHARGE DEPTH - NAVAJO SANDSTONE.	5.49
5.33	SCALED RADIUS OF RUPTURE VS. SCALED CHARGE DEPTH - NAVAJO SANDSTONE.	5.50
5.34	COMPARISON OF RESPONSE OF ROCK BEAMS TO IMPACT LOADING BY DROP WEIGHT AND NO. 6 BLASTING CAPS. . .	5.59
5.35	U12B RAINIER PLAN VIEW.	5.63

LIST OF ILLUSTRATIONS (Continued)

Figure No.		Page
5.36	U12B RAINIER CROSS SECTION A-A'	5.64
5.37	U12B RAINIER CROSS SECTION B-B'	5.65
5.38	SHOCK TIME-OF-ARRIVAL - RAINIER EVENT	5.67
5.39	PEAK SHOCK PRESSURE - RAINIER EVENT	5.68
5.40	U12C-03-NEPTUNE PLAN VIEW - PLATE 1	5.70
5.41	U12C-03-NEPTUNE CROSS SECTION A-A'	5.71
5.42	U12C-03-NEPTUNE CROSS SECTION B-B'	5.72
6.1	ASSUMED STATES OF STRESS IN THE EARTH AT A GREAT DISTANCE FROM ANY DISTURBING INFLUENCE	6.4
6.2	PRESSURE DOME AND STRESS TRAJECTORIES AROUND A DRIFT	6.4
6.3	TANGENTIAL STRESSES FOR A CIRCULAR CYLINDRICAL OPENING IN A SEMI-INFINITE MASS AS AFFECTED BY INCREASING DEPTH	6.10
6.4	UNIFORM COMPRESSIVE STRESSES IN AN INFINITE PLATE AT A GREAT DISTANCE FROM ANY DISTURBING INFLUENCE	6.11
6.5	AREAL DISTRIBUTION OF RADIAL STRESS ALONG THE HORIZONTAL AND VERTICAL AXES OF SYMMETRY FOR A CIRCULAR HOLE IN AN INFINITE PLATE	6.11
6.6	AREAL DISTRIBUTION OF TANGENTIAL STRESS ALONG THE HORIZONTAL AND VERTICAL AXES OF SYMMETRY FOR A CIRCULAR OPENING IN AN INFINITE PLATE	6.11
6.7	TANGENTIAL STRESS CONCENTRATION ON THE BOUNDARY OF A CIRCULAR OPENING IN AN INFINITE PLATE	6.12
6.8	STRESS CONCENTRATION ON THE BOUNDARY OF AN ELLIPSE AT THE MAJOR AND MINOR AXES AS THE HEIGHT-TO-WIDTH RATIO VARIES	6.12
6.9	TANGENTIAL STRESS CONCENTRATION ON THE BOUNDARY OF AN OVALOIDAL OPENING (SQUARE WITH SEMI-CIRCLES ATTACHED TO OPPOSITE ENDS)	6.16

LIST OF ILLUSTRATIONS (Continued)

Figure No.		Page
6.10	MAXIMUM STRESS CONCENTRATION AS A FUNCTION OF HEIGHT-TO-WIDTH RATIO FOR OVALOIDAL OPENING - UNIDIRECTIONAL STRESS FIELD.	6.19
6.11	STRESS CONCENTRATION AT END OF AXIS PERPENDICULAR TO THE DIRECTION OF APPLIED STRESS AS A FUNCTION OF HEIGHT-TO-WIDTH RATIO - UNIDIRECTIONAL STRESS FIELD.	6.19
6.12	MAXIMUM STRESS CONCENTRATION AS A FUNCTION OF HEIGHT-TO-WIDTH RATIO FOR RECTANGULAR OPENINGS HAVING SLIGHTLY ROUNDED CORNERS - UNIDIRECTIONAL STRESS FIELD	6.21
6.13	TANGENTIAL STRESS CONCENTRATION ON THE BOUNDARY OF A SQUARE OPENING IN AN INFINITE PLATE FOR THE THREE INITIAL STATES OF STRESS	6.21
6.14	EFFECT OF SHAPE OF OPENING ON MAXIMUM STRESS CONCENTRATION - UNIDIRECTIONAL STRESS FIELD	6.22
6.15	COMPARISON OF CRITICAL COMPRESSIVE TANGENTIAL STRESS FOR RECTANGLES AND ELLIPSE.	6.22
6.16	COMPARISON OF CRITICAL COMPRESSIVE TANGENTIAL STRESS FOR RECTANGLES AND ELLIPSE UNDER CONDITIONS OF HYDROSTATIC PRESSURE.	6.24
6.17	STRESS CONCENTRATION AS A FUNCTION OF THE RATIO OF OPENING WIDTH TO PILLAR WIDTH IN AN APPLIED STRESS FIELD PERPENDICULAR TO LINE OF CENTERS. . . .	6.26
6.18	DISTRIBUTION OF SHEAR STRESS IN PILLAR FORMED BY TWO CIRCULAR HOLES - APPLIED STRESS FIELD PERPENDICULAR TO LINE OF CENTERS	6.29
6.19	SHEAR STRESS DISTRIBUTION IN CENTRAL PILLARS - PLATE CONTAINING FIVE CIRCULAR OPENINGS IN AN APPLIED STRESS FIELD PERPENDICULAR TO LINE OF CENTERS.	6.29
6.20	RELATION BETWEEN MAXIMUM STRESS CONCENTRATION AND NUMBER OF PILLARS FOR RATIO OF OPENING WIDTH TO PILLAR WIDTH OF 4.0	6.32

LIST OF ILLUSTRATIONS (Continued)

Figure No.		Page
6.21	MAXIMUM STRESS CONCENTRATION IN PILLARS FORMED BY CIRCULAR OPENINGS AS A FUNCTION OF THE RATIO OPENING WIDTH TO PILLAR WIDTH IN AN APPLIED STRESS FIELD PERPENDICULAR TO LINE OF CENTERS	6.32
6.22	STRESS CONCENTRATION AS A FUNCTION OF OPENING WIDTH TO PILLAR WIDTH RATIO IN AN APPLIED STRESS FIELD PERPENDICULAR TO LINE OF CENTERS	6.33
6.23	SHEAR STRESS DISTRIBUTION IN CENTRAL PILLARS - PLATE CONTAINING FIVE OVALOIDAL OPENINGS (HEIGHT-TO-WIDTH RATIO = 0.5) IN AN APPLIED STRESS FIELD PERPENDICULAR TO LINE OF CENTERS	6.36
6.24	MAXIMUM STRESS CONCENTRATION AS A FUNCTION OF PERCENT OF RECOVERY FOR PILLARS FORMED BY FIVE OPENINGS	6.36
6.25	COMPARISON OF THE EMPIRICAL EQUATION AND THE EXPERIMENTAL DATA	6.36
6.26	SIMPLE BEAMS SHOWING METHOD OF SUPPORT, LOADS AND COORDINATE SYSTEMS	6.44
6.27	RESTRAINED BEAMS SHOWING LOADS, RESTRAINTS AND COORDINATE SYSTEMS	6.47
6.28	ROOF SPAN VS. ROOF THICKNESS AND WORKING STRESS. . .	6.55
6.29	RELATIONSHIP BETWEEN SAG AND SPAN FROM THEORY AND MEASUREMENTS IN PLACE.	6.57
6.30	STRESS DISTRIBUTION IN TWO FIXED CANTILEVERS WITH A POINT LOAD AT THE END OF THE LARGE MEMBER . .	6.62
6.31	A, B, C. A. A NORMAL VOUSSOIR ARCH WITH LOOSE COVER FILL. B. THE SAME AS A, WITH JOINTS VERTICAL. C. SIMILAR TO B, WITH ALL VOUSSOIRS EQUAL BUT TOTAL LOAD NOT INCREASED	6.63
6.32	EVANS' ASSUMED STRESSES FOR SIMPLE VOUSSOIR ANALYSIS	6.65
7.1	HOOP STRESS VS. CENTRAL ANGLE.	7.3

LIST OF ILLUSTRATIONS (Continued)

Figure No.		Page
7.2	SKETCH OF MODEL ILLUSTRATING LOCATION OF HOLE AND SYMMETRIC FREE FIELD POINT	7.4
7.3	APPLIED STRESS AS A FUNCTION OF TIME AT THE SYMMETRIC FREE FIELD POINT	7.4
7.4	STATIC AND DYNAMIC STRESS DISTRIBUTIONS ON THE HOLE BOUNDARY - 1,320 MICROSECONDS AFTER IMPACT. . .	7.5
7.5	STATIC AND DYNAMIC STRESS DISTRIBUTIONS ON THE HOLE BOUNDARY - 3,075 MICROSECONDS AFTER IMPACT. . .	7.6
7.6	HOOP STRESS VS. TIME	7.7
7.7	ROCK STRATA WOULD CAUSE ADDITIONAL STRESSES DUE TO VIBRATION (INERTIA) EFFECTS IN ROOF MEMBERS . . .	7.8
7.8	DIAGRAMMATIC SKETCH OF INCLINED STRATA WITH IMPEDANCE CONDITION WHICH WOULD TEND TO CHANNEL-IZE WAVE ENERGY, ACCENTUATED BY DETONATION IN DEEP RAVINE OR CANYON.	7.8
7.9	PLACING OF OPENINGS WITH LONG AXIS NEARLY PARALLEL AND TOO CLOSE TO FAULT CREATES AREA OF HIGH STRESS CONCENTRATION WHICH MAY BE CRITICAL IN HIGH MAG-NITUDE STRESS FIELD.	7.10
7.10	FAULTS SHOULD BE CROSSED AT 90° TO MINIMIZE POSSIBILITY OF HIGH STRESS CONCENTRATION ZONES . . .	7.10
7.11	OPENINGS IN VARIED GEOLOGIC STRUCTURES	7.11
7.12	OPENINGS IN VARIED GEOLOGIC STRUCTURES	7.12
7.13	RESIDUAL PRINCIPAL STRESSES PLOTTED UPON DEVELOPED INSIDE SURFACE OF TUNNEL	7.13
7.14	RESIDUAL TANGENTIAL STRESS: STATION 4 + 96.	7.13
7.15	FORMATION OF FRACTURED OR DESTRESSED ZONE BY EXPLOSIVES AROUND CIRCULAR OPENING, LEAVING A RING OF SOLID SUPPORTING ROCK, SURROUNDED BY A DESTRESSED ZONE OF BROKEN ROCK WITH THE MAJOR STATIC STRESSES TRANSFERRED BEYOND THE FRACTURE ZONE	7.15
7.16	HYPOTHETICAL LONG TIME RESPONSE CURVES FOR RIGID STEEL, YIELDABLE ARCHES AND TIMBER, MAY BE ADAPT-ED TO IMPACT LOADING	7.16

LIST OF ILLUSTRATIONS (Continued)

Figure No.		Page
8.1a	SCALING OF HE AND Ne SHOTS WHICH WERE EFFECTIVE IN CRATERING. ALL UNDERGROUND NUCLEAR SHOTS ALSO INCLUDED	8.7
8.1b	SCHEMATIC DIAGRAM SHOWING DAMAGE-DISTANCE NOTATION AND ZONES OF DAMAGE	8.8
8.2	SCHEMATIC CURVE OF SCALED CRATER VOLUME VS. SCALED CHARGE DEPTH UTILIZED TO PREDICT ZONAL DAMAGE TO TARGET UNDERGROUND OPENINGS	8.10
9.1	POST	9.2
9.2	REINFORCED STULL	9.2
9.3	TWO-PIECE STULL SET	9.3
9.4	THREE-PIECE SET, INCLINED POSTS	9.3
9.5	FOUR-PIECE SET, SAWED TIMBER	9.3
9.6	HEAVY TIMBERING AT BROKEN HILL, N.S.W.	9.3
9.7a	SUPPORT AT UNITED VERDE MINE	9.5
9.7b	SUPPORT AT UNITED VERDE MINE	9.6
9.8	TUNNEL CROSS-SECTIONS	9.7
9.9	COMPARISON OF STEEL AND WOOD SUPPORTS	9.7
9.10	CONTINUOUS RIB TYPE	9.8
9.11	RIB AND POST TYPE	9.8
9.12	RIB AND WALL PLATE TYPE	9.8
9.13	RIB, WALL PLATE AND POST TYPE	9.8
9.14	FULL CIRCLE RIB TYPE	9.9
9.15	INVERT STRUT	9.9
9.16	FULL CIRCLE RIBS CLOSELY SPACED	9.11
9.17	YIELDING LINING FOR SWELLING ROCK	9.12

LIST OF ILLUSTRATIONS (Continued)

Figure No.		Page
9.17a	OVER-MINING IN STIFF SWELLING GROUND TO INDUCE SOFTENING.	9.15
9.18	THE TOTAL COMBINED ACTIVE AND PASSIVE FORCES AT CORRESPONDING BLOCKING POINTS ARE THE SAME IN EACH LOADING ASSUMPTION	9.15
9.19	CONCENTRATED LOAD ASSUMPTION , ...	9.16
9.20	OBLIQUE LOAD ASSUMPTION.	9.17
9.21	WHERE IT IS POSSIBLE TO APPLY THE EXACT AMOUNT OF ACTIVE LOAD TO EACH BLOCKING POINT TO BALANCE ALL FORCES, THE LOADING DIAGRAM COULD BE ASSUMED AS IN THIS FIGURE	9.18
9.22	EFFECT ON RIB STRESS OF CHANGES IN BLOCKING POINT SPACING.	9.20
9.23	TRANSFER OF FORCE FROM ROCK TO RIB	9.20
9.24	FORCES ACTING AT OVERBREAK BLOCKING POINT.	9.21
9.24	FORCES ACTING AT OVERBREAK BLOCKING POINT (CONT.). .	9.22
9.25	RESOLUTION OF FORCES AT OVERBREAK BLOCKING POINTS. .	9.24
9.26	ACTION OF FORCES AT BLOCKING POINT 3	9.25
9.27	DEFLECTION OF LEG.	9.25
9.28	PRINCIPLE OF YIELDABLE ARCH.	9.27
9.29	YIELDABLE CONNECTIONS	9.29
9.30	TYPICAL YIELDABLE ARCH SHAPES.	9.30
9.31	ROOF BOLTING DESIGN CHART.	9.32
9.32	A. GRAVITY-LOADED BEAM. B. BENDING AND SHEARING STRESSES ON SECTION Z-Z'. C. DISTRIBUTION OF OUTER-FIBER BENDING STRESS AND MIDDLE-SURFACE SHEARING STRESS ACROSS THE SPAN. D. STRESSES ACTING ON ELEMENT AT A	9.36
9.33	FLEXURE OF GRAVITY-LOADED BEAMS.	9.37
9.34	LOAD-STRAIN GRAPHS	9.39
9.35	LOAD-STRAIN GRAPHS	9.40

LIST OF ILLUSTRATIONS (Continued)

Figure No.		Page
9.36	LOAD-STRAIN GRAPHS	9.41
9.37	ROOF BOLTING REQUIRED FOR FRACTURING AND OVERBREAK CAUSED BY CONVENTIONAL BLASTING.	9.42
9.38	ROOF BOLTS EMPLOYED FOR BOLTING BACKS AND WALLS OF OPENINGS.	9.43
9.39	BOLTING OF A LOOSE HANGING WALL IN AN OPERATING STOPE IN MINING ORE.	9.43
9.40	BOLTING IN A FAULT ZONE.	9.45
9.41	USE OF BOLTS IN STRATA CUT BY FAULTS OR JOINTS . . .	9.45
9.42	DIAGRAM OF ZONE OF TENSION IN ARCHED OPENING	9.46
9.43	TORQUE-BOLT LOAD RELATIONSHIPS FOR 1-INCH BOLTS IN SANDSTONE AND SHALE	9.46
10.1	MECHANISM FOR TRANSMISSION OF REFRACTED WAVES IN TWO-LAYERED EARTH.	10.4
10.2	RAY PATHS OF LEAST TIME AND TIME-DISTANCE CURVE FOR TWO LAYERS SEPARATED BY HORIZONTAL INTERFACE . .	10.4
10.3	RAY PATHS OF LEAST TIME FOR THREE LAYERS SEPARATED BY HORIZONTAL INTERFACES	10.6
10.4	RAY PATHS, TIME-DISTANCE CURVE, AND CRITICAL DISTANCES FOR MULTILAYER CASE.	10.6
10.5	TIME-DISTANCE CURVE AND RAY PATHS FOR HIGH-SPEED MARKER BELOW OVERBURDEN WITH LINEAR SPEED-DEPTH RELATION	10.7
10.6	WAVE PATHS AND TIME-DISTANCE CURVE FOR REFRACTION ACROSS FAULT (SHOT IS ON UPTHROWN SIDE).	10.7
10.7	REFRACTION ALONG AN INTERFACE DIPPING AT AN ANGLE α	10.8
10.8	WAVE REFLECTED FROM A NUMBER OF INTERFACES IN AREA WHERE SPEED INCREASES CONTINUALLY WITH DEPTH, EXCEPT FOR DISCONTINUITIES AT INTERFACES THEMSELVES	10.8
10.9	WAVE REFLECTED FROM SINGLE INTERFACE	10.8

LIST OF ILLUSTRATIONS (Continued)

Figure No.		Page
10.10	TIME-DISTANCE CURVES FOR REFLECTED AND REFRACTED WAVES OBSERVED WITH SINGLE VELOCITY DISCONTINUITY	10.10
10.11	REFLECTIONS FROM A DIPPING INTERFACE	10.10
10.12	REFLECTION OF SEISMIC WAVES AT AN EROSIONAL SURFACE.	10.11
10.13	REFLECTION OF SEISMIC WAVES FROM ZONE OF PINCHOUT AGAINST UNCONFORMITY	10.11
10.14	CONSTRUCTION OF GEOLOGIC SECTION IN FOOTHILLS AREA OF ALBERTA BY COMBINING SURFACE GEOLOGY, WELL INFORMATION, AND SEISMIC REFLECTION DATA. . . .	10.12
10.15	AN ALTERNATIVE INTERPRETATION OF THE GEOLOGICAL AND SEISMIC DATA USED TO OBTAIN CROSS SECTION OF FIGURE 10.14.	10.12
10.16	REFLECTION DIP SECTION FROM HIGHLY FAULTED AND FOLDED AREA BEFORE ADDITION OF GEOLOGICAL INFORMATION	10.13
10.17	SECTION OF 10.16 AFTER INFORMATION FROM TWO WELLS AT OPPOSITE ENDS IS USED FOR GEOLOGICAL INTERPRETATION.	10.13
10.18	NORTHEAST-SOUTHWEST PROFILE OF ANOMALOUS RELATIVE GRAVITY ACROSS DAMON MOUND SALT DOME, TEXAS.	10.16
10.19	AVERAGE MAGNETIC SUSCEPTIBILITIES OF SURFACE SAMPLES AND CORES AS MEASURED IN LABORATORY.	10.16
10.20	VERTICAL MAGNETIC FIELD OF BURIED ISOLATED NEGATIVE POLE.	10.18
10.21	VERTICAL INTENSITY OVER BURIED VERTICAL DIPOLE . . .	10.18
10.22	APPROXIMATE VERTICAL FIELD ON SURFACE FROM BURIED VERTICAL CYLINDER	10.18
10.23	CURVES SHOWING FALL OFF WITH HORIZONTAL DISTANCE OF VERTICAL MAGNETIC INTENSITY FOR VARIOUS GEOMETRIC FORMS.	10.18
10.24	HORIZONTAL FIELD INTENSITY X ABOVE VERTICAL DIPOLE .	10.19
10.25	VERTICAL MAGNETIC FIELD OF INCLINED DIPOLE	10.19
10.26	FORMULAS AND TYPICAL PROFILES FOR VERTICAL AND INCLINED DIKES	10.20

LIST OF ILLUSTRATIONS (Continued)

Figure No.		Page
10.27	MAGNETIC ANOMALIES ACROSS KURSK IRON DEPOSIT	10.21
10.28	MAGNETIC FIELD OVER DRIFT-COVERED SULFIDE-ORE BODY AT SUDBURY, ONTARIO	10.21
10.29	MAGNETIC INTENSITIES OBSERVED OVER CUMBERLAND FIELD, OKLA. GEOLOGIC SECTION ALSO SHOWN.	10.22
10.30	NEGATIVE MAGNETIC ANOMALY OVER HOCKLEY SALT DOME, TEXAS.	10.22
I-A.1	BLOCK DIAGRAM OF ELECTRONIC EQUIPMENT UTILIZED IN DYNAMIC MODULUS DETERMINATION BY THE RESONANT FREQUENCY METHOD	I-A.2
I-A.2	TENSILE TEST CONFIGURATIONS.	I-A.4
I-A.3	MODULUS OF RUPTURE TEST CONFIGURATION.	I-A.6
I-A.4	COMPRESSIVE TEST CONFIGURATION	I-A.6
I-A.5	CONFIGURATION OF TENSILE TESTS PERFORMED BY RUSSIAN INVESTIGATORS ON IRREGULARLY SHAPED SPECIMENS.	I-A.9
I-A.6	COMBINED COMPRESSION AND SHEAR TEST CONFIGURATION AS APPLIED TO IRREGULARLY SHAPED SPECIMENS BY SOVIET ENGINEERS	I-A.11
I-A.7	CONFIGURATIONS OF RUSSIAN STANDARD TENSILE TESTS . .	I-A.14
I-A.8	TWO METHODS UTILIZED BY RUSSIAN INVESTIGATORS TO PRODUCE SIMULTANEOUS SHEAR AND COMPRESSION STRESSES	I-A.16
I-A.9	FLAT DISC LOADED BY COAXIAL DIES	I-A.17
I-A.10	TEST CONFIGURATIONS OF HYDROSTATICALLY LOADED TEST SPECIMENS	I-A.17
I-A.11	MEASUREMENT OF ROCK SPECIMEN DEFORMATION DUE TO HYDROSTATIC PRESSURES.	I-A.19
I-A.12	MEASUREMENT OF ROCK BEAM DEFLECTION UNDER SIMULTANEOUS CENTRAL LOADING AND HYDROSTATIC PRESSURE . .	I-A.19

LIST OF ILLUSTRATIONS (Continued)

Figure No.		Page
I-A.13	CONFIGURATION FOR DYNAMIC MODULUS OF ELASTICITY TEST AS PERFORMED BY SOVIET SCIENTISTS USING A PULSE VELOCITY TECHNIQUE ON SPECIMENS SUBJECTED TO HYDROSTATIC PRESSURES	I-A.20
I-A.14	IN SITU TEST CONFIGURATION AS USED BY SOVIET INVESTIGATORS TO DETERMINE TENSILE STRENGTH.	I-A.21
I-A.15	CONFIGURATION OF IN SITU TESTS FOR THE DETERMINATION OF PILLAR COMPRESSIVE STRANGTHS AND COMBINED COMPRESSION AND SHEAR STRENGTHS	I-A.22
III-A.1	GENERALIZED SECTION OF GEOLOGIC STRUCTURE IN LEAD MINES IN SOUTHEAST MISSOURI.	III-A.2
III-A.2	PLAN AND SECTION OF EXPERIMENTAL ROOM.	III-A.5
III-A.3	LOGS OF DRILL HOLES INTO ROOF.	III-A.6
III-A.4	LOG OF CORES AND MINE OPENING.	III-A.9
III-A.5	GENERALIZED GEOLOGIC COLUMN OF WESTERN MISSOURI. . .	III-A.14
III-A.6	TYPICAL DETERIORATION OF SHALEY PORTION OF PILLARS IN LIMESTONE MINE IN WESTERN MISSOURI. . . .	III-A.15
III-A.7	AN ISOMETRIC DRAWING OF THE GEOLOGY OF THE HORNE ORE BODIES	III-A.17
III-A.8	VERTICAL SECTION THROUGH THE HORNE MINE SHOWING THE ORE BODIES AND THE ENCLOSING ROCKS	III-A.18
III-A.9	PLAN VIEW OF THE GEOLOGY ON THE 200 LEVEL OF THE HORNE MINE	III-A.19
III-A.10	BLOCK DIAGRAM OF THE MASSIVE LOWER H ORE BODY SHOWING THE METHOD OF SUBLEVEL STOPING APPLIED TO MINE THE ORE.	III-A.20
III-A.11	GEOLOGIC STRUCTURE PATTERN OF THE SUDBURY BASIN AND THE LOCATION OF THE IMPORTANT MINING CENTERS . .	III-A.23
III-A.12	TYPICAL CROSS SECTION OF THE HOLLINGER MINE SHOWING THE DISTRIBUTION OF ROCKS AND ORE.	III-A.25

LIST OF ILLUSTRATIONS (Continued)

Figure No.		Page
III-A.13	VERTICAL GEOLOGICAL SECTION OF THE McINTYRE MINE DEPICTING THE RELATIONSHIP BETWEEN THE IGNEOUS COUNTRY ROCKS, THE ORE AND MINE OPENINGS	III-A.26
III-A.14	OFFSET BLOCK DIAGRAM OF THE GEOLOGY OF THE McINTYRE-PORCUPINE MINE. ORE OCCURS IN THE McINTYRE FLOW.	III-A.30
III-A.15	PLAN VIEW OF GEOLOGY OF McINTYRE MINE.	III-A.31
III-A.16	STOPE SECTION SHOWING THE TYPE OF STOPE GEOLOGY ENCOUNTERED IN THE McINTYRE MINE	III-A.32
III-A.17	HORIZONTAL SECTION OF THE BUTTE DISTRICT, 4,600 FT. ABOVE SEA LEVEL (1,500 FT, BELOW SURFACE), SHOWING STRUCTURAL RELATIONS OF THE FISSURE SYSTEMS	III-A.35
III-A.18	NORTH-SOUTH VERTICAL SECTION THROUGH THE COPPER DISTRICT NEAR THE ANACONDA SHAFT, SHOWING THE STRUCTURAL RELATIONS OF THE VEINS AND FISSURES.	III-A.36
III-A.19	BLOCK DIAGRAMS OF THE ORE FORMATIONS IN THE GOGEBIC RANGE.	III-A.50
III-A.20	GENERALIZED GEOLOGICAL SECTION OF THE GOGEBIC RANGE.	III-A.51
III-A.21	LONGITUDINAL SECTION OF THE IRON DEPOSITS SHOWING THE SUCCESSION OF FORMATIONS OVERLYING THE ORE . . .	III-A.53
III-A.22	PLAN VIEW OF THE PHILLIPSON LEVEL AND THE ROCK DISTRIBUTION ACCORDING TO TYPE AND CLASS	III-A.55
III-A.23	VERTICAL SECTION AT RIGHT ANGLES TO THAT IN FIGURE III-A.24.	III-A.56
III-A.24	VERTICAL SECTION THROUGH THE CLIMAX ORE BODY	III-A.57
III-A.25	REGIONAL GEOLOGY	III-A.63
III-A.26	PLAN SHOWING ROCK TYPES T.1. POWER STATIONS - GENERAL LAYOUT	III-A.64
III-A.27	GEOLOGY OF SITE.	III-A.65

LIST OF ILLUSTRATIONS (Continued)

Figure No.		Page
IX-A.1	A TUNNEL 24 FT. WIDE, SEMI-CIRCULAR ARCH, 13 FT. VERTICAL SIDE WALLS.	IX-A.2
IX-A.2	SETS FORTH THE COMPUTATIONS MADE TO ILLUSTRATE THE ADVANTAGES OF A FULL CIRCLE RIB OVER A STRAIGHT LEGGED RIB WHEN SIDE PRESSURES ARE ENCOUNTERED.	IX-A.8

LIST OF TABLES

Table No.		Page
1.1	A MINERALOGIC AND TEXTURAL CLASSIFICATION OF IGNEOUS ROCKS.	1.5
1.2	A MINERALOGIC AND TEXTURAL CLASSIFICATION OF SEDIMENTARY ROCKS.	1.6
1.3	A MINERALOGIC AND TEXTURAL CLASSIFICATION OF METAMORPHIC ROCKS.	1.7
1.4	COMPARISON OF RESULTS, IN PLACE AND LABORATORY STUDIES.	1.10
1.5	YOUNG'S MODULUS.	1.13
1.6	COMPRESSIBILITY OF ROCKS (HYDROSTATIC PRESSURE. DIRECT MEASUREMENT OF VOLUME CHANGE. PRESSURE RANGE, 2,000 TO 12,000).	1.19
1.7	COMPRESSIBILITY OF ROCKS (HYDROSTATIC PRESSURE. VOLUME CHANGE, DETERMINED FROM CHANGE TO LENGTH) . .	1.19
1.8	VARIATION IN VELOCITY WITH ROCK TYPE	1.28
2.1	CLASSIFICATION OF TYPES OF FOLIATION	2.21
3.1	OPEN STOPES WITH PILLARS	3.13
3.2	SUBLEVEL STOPING	3.16
3.3	SHRINKAGE STOPING.	3.19
3.3	SHRINKAGE STOPING (CONT.).	3.20
3.4	CUT-AND-FILL STOPING	3.23
3.5	SQUARE SET STOPING	3.27
3.6	TOP SLICING AND SUBLEVEL CAVING.	3.29
3.7	BLOCK CAVING	3.32
5.1	PHYSICAL PROPERTIES OF ROCKS (UET & USBM).	5.51
5.2	CRATER TEST DATA - UNAWEEP GRANITE	5.52

LIST OF TABLES (Continued)

Table No.		Page
5.2	CRATER TEST DATA - UNAWEEP GRANITE (CONT.)	5.53
5.2	CRATER TEST DATA - NAVAJO SANDSTONE (CONT.).	5.54
5.3	TUNNEL DEMOLITION SHOTS IN BASALT.	5.55
5.4	SUMMARY OF EFFECTIVE BREAKAGE CRITERIA - SURFACE CRATERS.	5.57
5.5	MAJOR FEATURES OF UNDERGROUND NUCLEAR EXPLOSIVES . .	5.61
5.6	SEISMIC VELOCITY, VERTICAL DISTRIBUTION OVER RAINIER.	5.62
5.7	RADII OF RADIOACTIVE SHELLS.	5.62
5.8	RAINIER ENERGY DISTRIBUTION.	5.66
6.1	CRITICAL VALUES OF TANGENTIAL STRESS ON AN ELLIPTICAL BOUNDARY.	6.14
6.2	OVALOIDAL OPENINGS - UNIDIRECTIONAL STRESS FIELD . .	6.17
6.3	STRESS CONCENTRATION FOR OVALOIDS - HYDROSTATIC STRESS FIELD	6.17
6.4	CRITICAL COMPRESSIVE TANGENTIAL STRESS FOR A PAIR OF CIRCULAR HOLES.	6.27
6.5	STRESS CONCENTRATION FOR A PLATE CONTAINING TWO CIRCULAR OPENINGS.	6.28
6.6	STRESS CONCENTRATION FOR A PLATE CONTAINING THREE CIRCULAR OPENINGS.	6.28
6.7	STRESS CONCENTRATION FOR A PLATE CONTAINING FIVE CIRCULAR OPENINGS.	6.30
6.8	STRESS CONCENTRATION FOR A PLATE CONTAINING TWO OVALOIDS	6.34
6.9	STRESS CONCENTRATION FOR A PLATE CONTAINING FIVE OVALOIDS	6.34
6.10	STRESS CONCENTRATION FOR A PLATE CONTAINING FIVE OVALOIDAL OPENINGS	6.35

LIST OF TABLES (Continued)

Table No.		Page
6.11	COMPILATION OF STRESS EQUATIONS FOR SIMPLE BEAM LOADED BY THREE TYPE LOADS	6.45
6.12	COMPILATION OF ANALOGOUS STRESS EQUATIONS FOR SIMPLE BEAM LOADED BY THREE TYPE LOADS	6.49
6.13	COMPILATION OF STRESS EQUATIONS FOR RESTRAINED BEAM LOADED BY THREE TYPE LOAD	6.50
6.14	COMPILATION OF ANALOGOUS STRESS EQUATIONS FOR RESTRAINED BEAM LOADED BY THREE TYPE LOADS	6.52
6.15	CONSTANTS FOR USE IN EQUATIONS 11, 12, AND 13.	6.56
6.16	RELATIVE STRENGTH OF BEAMS WITH EQUAL SPACING.	6.61
8.1	TABULATION OF SCALING FACTORS.	8.3
8.2	TUNNEL CLOSURE DISTANCES FOR UNDERGROUND NUCLEAR BLASTS	8.2
8.3	CRUSH AND FRACTURE ZONES - RAINIER & NEPTUNE	8.3
8.4	MAJOR FEATURES OF UNDERGROUND NUCLEAR EXPLOSIVES	8.5
8.5	ERDL TUNNEL DEMOLITION	8.6
8.6	CAMOUFLET SCALED DEPTHS AND FRACTURE ZONES FOR ROCKS.	8.6
9.1	LIMITS WITHIN WHICH RESULTS OF FACTORIAL EXPERIMENT ARE APPLICABLE.	9.33
10.1	COMPARISON OF MAJOR GEOPHYSICAL PROSPECTING METHODS.	10.2
I-B.1	TRIAXIAL COMPRESSION TEST DATA	I-B.7
I-B.2	PHYSICAL AND MECHANICAL PROPERTIES OF ROCK	I-B.12
I-B.3a	HEAT CAPACITY OF MINERALS.	I-B.22
I-B.3b	HEAT CAPACITY OF ROCKS	I-B.36

LIST OF TABLES (Continued)

Table No.		Page
I-B.4	HEATS OF TRANSFORMATION AND OF FUSION.	I-B.41
I-B.5	THERMAL CONDUCTIVITY OF ROCKS.	I-B.48
I-B.6	EFFECT OF WETTING AND OF SIMPLE COMPRESSION ON THE THERMAL CONDUCTIVITY OF CERTAIN ROCKS.	I-B.60
III-A.1	PHYSICAL PROPERTIES OF LIMESTONE AND SHALE (HOLES 1, 2, AND 3).	III-A.3
III-A.2	PHYSICAL PROPERTIES OF LIMESTONE AND SHALE PARALLEL TO BEDDING (HOLES 15, 16, 17, AND 18).	III-A.7
III-A.3	PHYSICAL PROPERTIES OF OIL-SHALE SAMPLES FROM ROOF CORED PARALLEL TO BEDDING, COLLEGE PARK, MD . .	III-A.10
III-A.4	PHYSICAL PROPERTIES OF OIL-SHALE SAMPLES FROM ROOF CORED PERPENDICULAR TO BEDDING, COLLEGE PARK, MD.	III-A.10
III-A.5	COMPRESSIVE STRENGTH OF OIL-SHALE SAMPLES FROM ROOF AND PILLAR SPECIMENS CUT PERPENDICULAR TO BEDDING, COLUMBIA UNIVERSITY	III-A.11
III-A.6	SHEAR STRENGTHS OF OIL-SHALE SAMPLES FROM ROOF, COLUMBIA UNIVERSITY.	III-A.12
III-A.7	MODULUS OF RUPTURE OF OIL-SHALE SAMPLES FROM ROOF BEAMS CUT PERPENDICULAR TO BEDDING, COLUMBIA UNIVERSITY	III-A.12
III-A.8	MODULUS OF ELASTICITY OF OIL-SHALE SAMPLES FROM ROOF AND PILLAR, COLUMBIA UNIVERSITY	III-A.12
IX-B.1	CONTINUOUS RIBS	IX-B.1
IX-B.2	WALL PLATE RIBS.	IX-B.2

NOTATIONS

a	=	interatomic distance, or dimension
A	=	area, or a constant
A_k	=	area of crater at surface
α	=	specific surface energy
α_o	=	parameter of ellipse
b	=	dimension
B	=	compressibility, or a constant
β	=	velocity
c	=	unit cohesive strength, or a distance
C_p	=	heat capacity, or chord length
d	=	bolt-hole diameter, inches
d'	=	bolt diameter, inches
D	=	depth in feet
$D_k/\bar{r}$	=	scaled crater depth
$D/\bar{r}$	=	scaled charge depth
δ	=	angle of inclination
E	=	Young's Modulus
E'	=	modulus of elasticity of bolt material
ϵ	=	unit strain
f	=	frequency
F	=	scale factor, or coefficient of friction on bedding planes
g	=	acceleration of gravity
G	=	modulus of rigidity
h	=	specimen thickness, or dimension
H	=	thrust, or effective compressive force
H_d	=	abrasive hardness
H_m	=	Moh's hardness
I	=	moment of inertia, or amplitude
i_c	=	critical angle
K	=	maximum stress concentrations in pillars, bulk modulus, or centrifugal loading ratio
L	=	length

NOTATIONS (Continued)

L_p = load supported by one pillar

λ = viscous constant, or Lame's constant

m = material entering transition zone per unit time, or inverse of Poisson's ratio

M = bending moment

n = revolutions per second

N = number of bolts per set across opening

ν = Poisson's Ratio

P = pressure

$\bar{\omega}$ = rotation component

$p(\tau)$ probability function

q = dissipative factor, or a constant depending upon material

r = radius, or uniform normal stress

r/h = radius of fillets to minor axis

R = radius, or percent recovery

ρ = density

S = modulus of deformation, or scale factor

SH = shore scleroscope hardness

τ = normal and shearing stress

σ = unit stress

θ = coordinate angle

t = thickness of plate, or time

T = thickness, thrust, or temperature

V = volume, or velocity

w = deflection, or unit weight of immediate roof rock

w' = unit weight of bolt material

W = weight of explosive in lbs, energy release in kilotons of TNT, or width

x = shot-detector distance

X = dynamic Young's modulus

z = couple arm

Z = radius of load applying die

x,y,z = rectangular coordinates

CHAPTER I

PHYSICAL AND MECHANICAL PROPERTIES OF ROCKS

Introduction

Physical (intrinsic) and mechanical (response) properties of rock may be measured in several different ways and experimentally determined values of mechanical properties often depend upon the method of measurement. Engineering design requires a relatively accurate evaluation of characteristics which affect the behavior of rock in a particular environment. In its response to nuclear blasts rock reaction is of interest from the zero point out to distances where stresses, accelerations, etc., become subcritical as far as damage to underground openings is concerned. Thus, the melting point under intense shock, strength, elastic parameters, visco-elastic characteristics, wave propagation capabilities and related properties are of vital interest. Some properties can be measured both in the field and in the laboratory. Dynamic moduli may approximate statically measured ones, or may differ by more than 100 percent. Methods of measurement and available data from all types of tests are included in Chapter I and Appendices. Correlation studies of measured properties are proving fruitful in static design applications. Although only few quantitative engineering criteria have been established, rapid initial advances have been made for static design purposes. Applications for resistance to dynamic loads are much less completely developed. The greatest need for research is in the evaluation of effective properties which will define the response of the rock to imposed loads.

The properties of rock and soil have been the subject of intense research and considerable controversy within recent years, and like soil mechanics, the field of rock mechanics is unique in that it deals with materials which must be used for construction purposes in the state in which they occur in nature. A detailed knowledge of the physical and mechanical characteristics of the rock at the site of underground openings is a necessity if the construction and utilization of the installation are to be made with efficiency and security. The design of an underground structure requires knowledge of load distributions and reactions of the inter-dosal rock to these loads. The properties of the rock are prime factors in engineering design in both surface and underground structures. Those which are of greatest interest in the problem of static support of super-incumbent rock are ultimate strength, density, permeability, and elastic and visco-elastic moduli. The physical properties of rock which determine response of underground structures to dynamic loadings have not been clearly defined but could reasonably be assumed to include all of the properties mentioned above.

Of the characteristics which are important, density and permeability are recognized as being relatively independent of the size of sample chosen and results obtained may be applied to *in situ* as well as labora tory investigations. This is not the case of ultimate strength, elastic

or visco-elastic moduli. In addition, these physical properties are strongly dependent upon the type of test employed as well as the time scale of the test. Since underground excavation operations are concerned with the reaction of rock masses to forces which range in time duration from a few micro-seconds in the case of blasting operations to a period of years in the case of underground opening utilization, it is apparent that time dependency of mechanical properties must also be considered.

Nadai[1] has classified solid materials as being either (1) elastic (2) viscous or (3) plastic when subject to deforming loads. More recently, a rheologic explanation of behavior has been applied to materials originally considered elastic. The principle of materials exhibiting time dependent behavior is characterized by Eirich's[2] statement, "Real materials exhibit a whole spectrum of behavior from dependence of the forces on the speed of deformation only shown by liquids, to the practical independence on speed of deformation and dependence on the extent of deformation only, of the ideally elastic bodies. Any materials may be caused to flow, i.e., become fluid, by varying temperature and force field." There seems little doubt that a particular rock may fall into several of the categories described by Nadai and Eirich depending upon the load configuration, magnitude, rate of loading and the duration of the load.

Rock is, in general, a non-homogeneous, anisotropic, discontinuous medium. The degree of departure from an ideal medium depends upon the rock type, composition, depth, conditions of deposition, etc. The rock may range from a practically ideal salt to an extremely anisotropic conglomerate. Spaulding[3] suggests that rock properties are a function of depth, at depth the rock becoming more compact, denser, and generally harder and heavier, while the number of open pores and cavities decreases.

The fact that rock is generally not homogeneous has resulted in considerable discussion of the validity of application of test results from laboratory samples to field conditions. Spaulding[3] states "the determination of the elastic constants and other physical properties of rock by tests on small specimens will necessarily give very inaccurate results. The selection of a specimen which will be truly representative of the rock is an almost impossible task; the piece chosen will usually be more homogeneous than the average rock which is sure to have a number of weaknesses in it."

Isaacson[4] has stated quite aptly that conclusions of a static pressure behavior based on conditions of pure elasticity should be accepted with great caution if falling into gross error is to be avoided. Although many rocks exhibit a pronounced elastic phase over a limited pressure range, some local volumes of the rock mass may be stressed beyond the elastic limit and a plastic phase may occur before the ultimate point of failure is reached. A further modification of the elastic theory, Isaacson states, is required as a consequence of the anisotropic nature of some rocks. For example, schists and shales are anisotropic in that the elastic constants may differ according to the coordinate direction considered.

Rock Properties

Classification of Rock Properties.

For most purposes rock characteristics may be considered as follows:

I. Petrographic Properties

II. Elastic Properties - (static and dynamic)

- A. Young's Modulus
- B. Modulus of Rigidity
- C. Poisson's Ratio

III. Strength of Rock

- A. Tensile Strength and Modulus of Rupture
- B. Compressive Strength
- C. Shear Strength

IV. Hardness and Similar Properties

- A. Scleroscope Hardness
- B. Abrasive Hardness
- C. Moh's Hardness
- D. Impact Toughness

V. Volumetric Properties

- A. Apparent Porosity
- B. Apparent Specific Gravity

VI. Other Properties

- A. Fatigue
- B. Creep - Viscosity of Plasticity
- C Thermal Expansion
- D. Compressibility
- E. Granular Structure and Strength

VII. Behavior of Rocks Under High Confining Pressures

VIII. Fundamental Strength of Rock

IX. Miscellaneous

- A. Drilling Characteristics of Rock
- B. Blasting Characteristics of Rock
- C. Other - Artificial Weathering

Emphasis is placed on those properties which are directly pertinent to the subject of this report

Petrofabric.

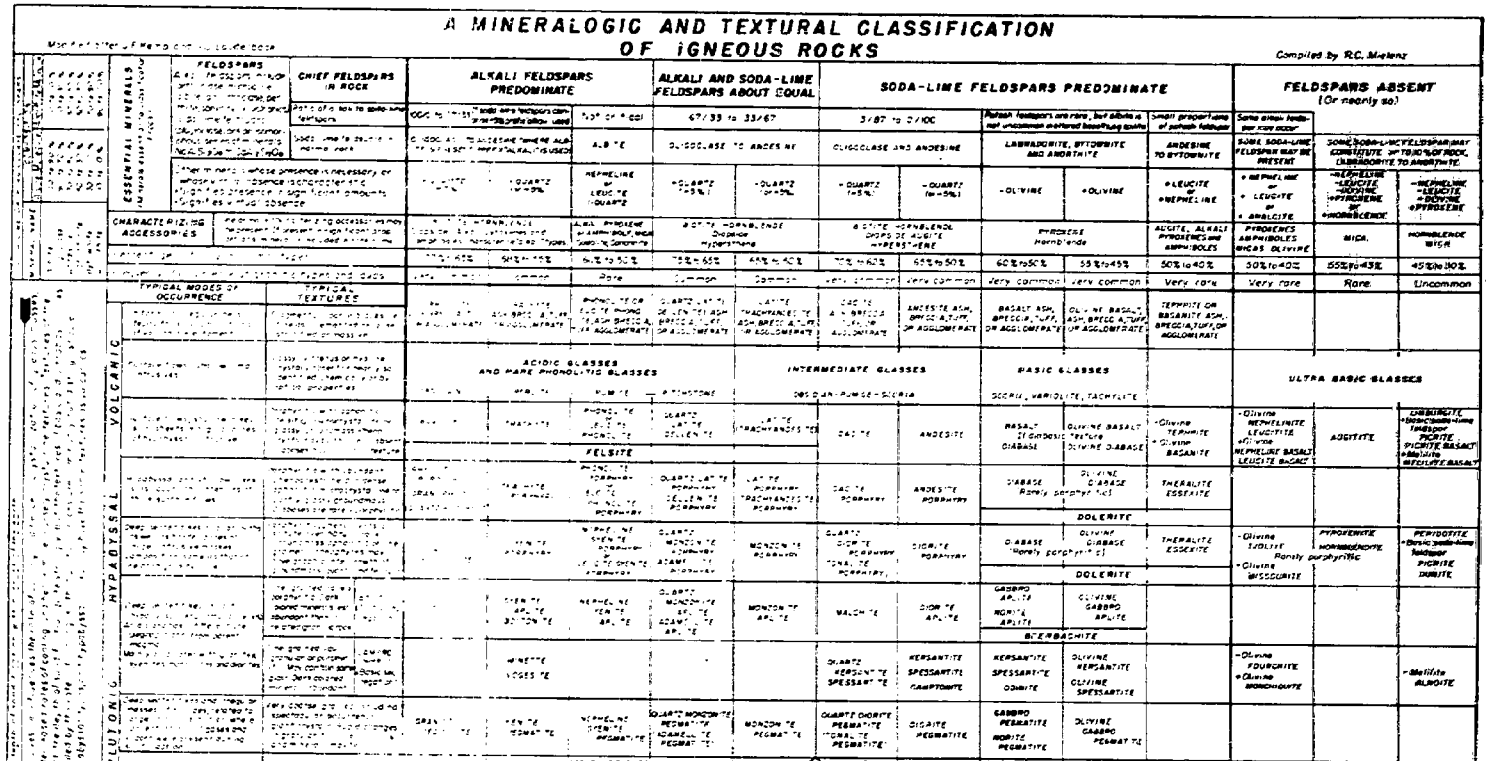
One primary difference in rocks and soils is the degree of cementation. An illustrative study of rock fabric in its relation to physical properties was published by the Bureau of Reclamation[5]. Other detailed descriptions of special rock types found on the Nevada Test Site are given in Reference 6. Just as is the case with metals, the grain size and structure of rocks are determining factors in their properties. Rock specimens tested by the Bureau of Reclamation are first classed according to their genetic origin, i.e., whether they are igneous, sedimentary or metamorphic (Tables 1.1, 1.2, 1.3), and are examined under the petrographic microscope. Further subdivisions are according to compressive strength in descending order. Careful evaluation is made of spacing, continuity and orientation of structural planes such as stratification, jointing, fracture or schistosity. The grouping of rock types according to strength is based on the detailed microscopic examination of sections which are usually taken from the ends of the test specimens. Observed features include size, shape, packing and orientation of the constituent grains; mineralogic composition; degree of cementation; articulation of grain boundaries; degree of alteration; identity and description of alteration products; development and description of seams, fractures and other discontinuities; and the kind and amount of seam and fracture fillings.

The petrographic analysis represents a qualitative method of evaluating some of the important characteristics of rock materials, as well as providing a comprehensive classification and description of the rock. It further serves as a guide for correlation of strength and elastic properties, although the latter cannot be predicted from a petrofabric description. Results of numerous laboratory tests (Appendix I-B) show that rocks with almost identical geological classification vary widely in their physical properties. Therefore, to be accurate and realistic, engineering designs should be based on measured physical properties of rocks, or estimated by comparison with a petrographically similar rock whose optical characteristics correlate.

Elastic Properties.

Birch[7] states that the elastic properties of rocks differ somewhat from those of metals. It has been found that the elastic constants of structural metals are nearly independent of the magnitude of stress within the stress range which is employed in engineering structures. However, a number of investigations have shown that the elastic "constants" of rocks are dependent upon the magnitude of stress in the stress range involved. This is particularly true at low stresses where the relation between unit strain and unit stress is often not linear. For example, the effective Young's Modulus, if defined for small displacements about the equilibrium displacement corresponding to zero or equilibrium stress, often increases or decreases with increase in stress, sometimes by large factors. The other elastic constants vary in a similar manner. This type of behavior has been attributed to the initial porosity of most rocks. If a rock is tested in compression by the static method, the pore spaces are at least partially closed by the initial compression and the initial strain. In the dynamic method of testing the pore spaces and heterogeneity of rocks also cause deviations from the assumed behavior of an ideal specimen.

TABLE 1.1



RE-DRAWN FROM BUREAU OF RECLAMATION, U.S. DEPARTMENT OF THE INTERIOR, ENGINEERING MONOGRAPH NO. 1

TABLE 1.2

A MINERALOGIC AND TEXTURAL CLASSIFICATION OF SEDIMENTARY ROCKS

Prepared by R. C. Mielens

Texture	Essential constituent	Definitive characteristic		Petrographic type
Clastic (composed predominantly of rock and mineral grains derived by weathering and erosion, and deposited by water, wind, ice, or gravity; showing varying degrees of cementation or consolidation)	Volcanic ejecta	Fragments > 32 mm		Agglomerate or breccia
		Particles > 4 mm < 32 mm		Lapilli tuff
		Particles < 4 mm		Tuff
	Gravel	Abraded particles > 4 mm over 50 percent, clay < 25 percent		Conglomerate
	Rock and mineral fragments	Angular particles > 4 mm over 50 percent, clay < 25 percent		Breccia
	Rock fragments and clay	Fragments are greatly varied, occasionally exhibit faceting, high range of sizes usually unsorted; matrix usually clay, sometimes sand, usually greatly in excess of fragments	Loose	Till
			Compact	Tillite
	Sand	Particles < 4 mm > 1/16 mm over 50 percent, clay < 25 percent		Sandstone, quartzite, arkose, graywacke, subgraywacke
	Detrital grains of calcite	Calcite more than 50 percent, clay < 25 percent		Limestone
	Silt	Particles < 1/16 mm over 50 percent, clay < 25 percent; massive to stratified		Siltstone
		Predominant particles < 1/16 mm, fissile		Shale
		Predominant particles < 1/16 mm, open structure		Loess
	Clay minerals	Clay more than 25 percent, massive to stratified		Claystone
		Predominantly clay or silt, fissile		Shale
		Predominantly clays and sericite, incipient recrystallization		Argillite
		Montmorillonite clays more than 75 percent		Bentonite
		Kaolinite clays more than 75 percent		Kaolin
	Clay and calcite	Very fine grained; carbonates 25 to 75 percent		Marl, marlstone
Crystalline (composed predominantly of coarse to fine or microcrystalline to cryptocrystalline aggregates of crystals precipitated chemically or biochemically from surface or subsurface waters)	Calcite	Carbonate > 50 percent of which calcite is more than 50 percent	Coarse to microcrystalline, compact	Limestone
			Fine to microcrystalline, porous, firm to friable	Chalk
			Spongy, porous, firm to friable, fine to microcrystalline	Tufa
			Compact to porous, banded, fine to microcrystalline	Travertine
	Calcite and clay	Very fine-grained; calcite 25 to 75 percent		Marl, marlstone
	Carbonates	Carbonates more than 25 percent, compact to earthy; deposited by ground water		Caliche
	Dolomite	Carbonate > 50 percent of which dolomite > 50 percent; coarse to fine, compact		Dolomite
	Chalcedony	Chalcedony > 25 percent, microcrystalline to cryptocrystalline, conchoidal fracture, compact		Chalcedonic chert
	Cryptocrystalline quartz	Cryptocrystalline quartz, > 50 percent		Novaculite
	Chalcedony	Chalcedony > 25 percent; friable to firm; earthy to porous		Tripoli
	Crystalline phosphates	Crystalline phosphates > 50 percent		Phosphorite
	Anhydrite	Anhydrite > 50 percent		Rock anhydrite
	Gypsum	Gypsum > 50 percent		Rock gypsum
	Halite	Halite > 50 percent		Rock salt
	Hematite	Hematite > 50 percent		Hematite rock
	Crystalline hydrous aluminum oxides	Hydrous aluminum oxides > 50 percent of which > 50 percent are crystalline		Bauxite
Amorphous (composed predominantly of noncrystalline substances precipitated or produced by chemical or biochemical action in surface or ground water or within sediments by geologic processes)	Opal	Opal > 50 percent, massive to banded, compact		Opal, opaline chert
		Opal > 50 percent, porous, massive to laminated		Siliceous sinter
		Deposited by geysers		Geyserite
	Collophane	Accumulated bird excrement		Guano
		Amorphous phosphates > 50 percent		Phosphorite
	Limonite	Limonite > 50 percent		Limonite, bog iron ore
	Amorphous hydrous aluminum oxides	Hydrous aluminum oxides > 50 percent, of which > 50 percent are amorphous		Bauxite
	Hydrocarbons	Solid		Asphalt, mineral tar, gilsonite, grahamite
	Amorphous carbon	Fibrous to spongy to compact, carbonized plant remains < 50 percent; black to brown		Coal (see below)
	Oxygenated hydrocarbons	Resinous, various light colors		Amber
Biofragmental (composed of whole or fragmental remains of plants or animals)	Calcareous shells and fragments	Whole or fragmental shells > 50 percent		Coquina
	Diatom tests	Diatom tests > 50 percent		Diatomite, diatomaceous earth
	Radiolarian tests	Radiolarian tests > 50 percent		Radiolarite, radiolarian earth
	Foraminifera tests	Foraminifera tests > 50 percent		Foraminiferal limestone
	Algal structures	Algal structures > 50 percent		Algal limestone
	Coral structures	Coral structures > 50 percent		Coral limestone
	Phosphatic shells teeth, bones	Phosphatic fossils > 50 percent		Phosphorite
	Partially or completely carbonized plant remains	Brown to black, spongy to compact, plant remains readily visible		Peat
		Brown to black, fibrous to compact, slakes readily		Lignite
		Black, massive to banded, compact, slakes slowly		Bituminous coal
		Black, massive to banded, submetallic, conchoidal fracture		Anthracite coal

TABLE 1.3

A MINERALOGIC AND TEXTURAL CLASSIFICATION OF METAMORPHIC ROCKS

Prepared by R. C. Mielenz

Structure	Essential constituent	Definitive characteristic	Petrographic type
Cataclastic (composed of crushed, sheared, broken, and strained, angular fragments of rocks and minerals, usually with some recrystallization)	Crushed, sheared, and granulated fragments of rocks and minerals	Angular particles > 4 mm over 50 percent; in granulated or recrystallized matrix	Breccia
		Fractured and sheared, with partial recrystallization and development of new minerals, but original texture, structure and mineralogy largely preserved	Original rock name with prefix "meta" as metasandstone, metarhyolite, metatuff, etc.
		Fragments of original rock sheared into lenses and streaks surrounded by finely granulated and recrystallized material	
		Planar structure poorly developed	Original rock name with prefix "flaser" as flaser-granite, flaser-conglomerate, etc.
		Planar structure well developed	Flaser-gneiss
			Augen-gneiss
		Fragments of original rock pulverized to microscopical or submicroscopical dimensions, or locally fused; partially recrystallized; massive to laminated	Mylonite
		Fissile; cryptocrystalline to microcrystalline; partially recrystallized; closely spaced, well developed fractures cut across bedding	Slate
Foliated (marked lamellar, plicated, or planar structure developed by tabular or prismatic minerals in parallel orientation; completely or largely recrystallized)	Tabular and/or prismatic minerals	Microcrystalline to fine grained	Phyllite
		Fine to coarse grained	Schist
	Antigorite	Fine to coarse grained; antigorite > 50 percent	Serpentine, serpentinite
Banded (composed of alternating foliated and granular lenses, the latter being conspicuous or dominant, completely recrystallized)	Tabular or prismatic and granular minerals abundant	Fine to coarse grained	Gneiss
Granular (composed predominantly of equidimensional grains, largely or completely recrystallized)	Calcite	Coarse to fine grained: Total carbonates, > 90 percent, of which calcite > 50 percent	Marble
	Dolomite	Coarse to fine grained: Total carbonates > 90 percent, of which dolomite > 50 percent	Dolomite marble
	Calcic and magnesian silicates	Coarse to fine grained: Calcite and/or dolomite usually abundant, calcic and magnesian silicates conspicuous or predominant	Calc-silicate rock Calc-silicate hornfels Calc-flinta
	Quartz	Coarse to fine grained: Quartz > 90 percent	Quartzite
	Tabular and prismatic minerals predominant	Coarse to fine grained: Decussate texture, normally tabular and prismatic minerals abundant and almost equidimensional	Hornfels
	Granular minerals	Coarse to fine grained: Equidimensional minerals predominant, normally tabular and prismatic minerals inconspicuous	Granulite
	Amphibole	Coarse to fine grained: Amphibole conspicuous or predominant	Amphibolite
	Tabular and prismatic minerals predominant	Micro- to cryptocrystalline: Decussate texture, normally tabular and prismatic minerals abundant and almost equidimensional	Hornfels
	Granular minerals	Micro- to cryptocrystalline: Equidimensional minerals predominant, normally tabular and prismatic minerals inconspicuous	Granulite
	Quartz and/or chalcedony and iron oxides	Micro- to cryptocrystalline: Banded, with alternating layers of quartz and chalcedony and of iron oxides	Jaspilite
	Quartz	Micro- to cryptocrystalline: Banded to massive, micro- to cryptocrystalline quartz predominant	Novaculite
	Micaceous minerals	Micro- to cryptocrystalline: Banded, laminated, or massive, mixed granular and micaceous minerals without conspicuous foliation; incomplete recrystallization	Argillite
Felted (composed predominantly of tabular or prismatic minerals, in random, decussate, or subradiate arrangement, without foliation, completely or largely recrystalized)	Tabular and/or prismatic minerals	Decussate texture, tabular minerals thick and prismatic minerals stumpy	Hornfels
		Random or subradiate arrangement; amphibole conspicuous or predominant	Amphibolite
		Random or subradiate arrangement; antigorite predominant	Serpentine, serpentinite
		Random or subradiate arrangement; one, two, or three minerals predominant	Use mineral names as prefix, as cummingtonite-garnet rock

Thus, some calculated values of Poisson's ratio may turn out to be negative when calculated from dynamically determined elastic moduli. Certain sedimentary rocks may show discrepancies due to processes involved in their deposition. Thus, all elastic constants should be employed only with the knowledge of how they were determined and what they really represent.

Young's Modulus of Elasticity. Young's modulus of elasticity is defined as stress divided by the strain for any given elastic substance under stress. For many metals and other materials this relationship is considered to be constant up to the yield point as in mild steel, for example. Similarly, Poisson's ratio and the modulus of rigidity are assumed to be constant over a given range of stress. For many rocks, however, these values are not constant over the "elastic range".

If dynamic specimens are vibrated unstressed, the resulting value of Young's modulus is the tangent value at zero load. Secant values and average values are sometimes employed.

Various types of stress-strain curves, concave downward, concave upward and straight line have been obtained from static tests for different rocks. The flat initial portion of the curve for some sandstones is most likely due to an initial stage of compression which involves little elastic strain but consists largely of forcing grains closer together and partially filling the voids in the rock. The flattening of some curves in their upper portion might be due to a failure of some of the weaker constituents of the rock.

Modulus of Rigidity. If a small block of elastic material is acted upon by two non-colinear forces (couple) a shearing stress is produced and the body is deformed. The modulus of rigidity is defined as the shearing stress divided by the deformation. It can also be shown that the three elastic constants E, G and ν (Poisson's ratio) are related by the following equation

$$G = \frac{E}{2(1 + \nu)} \qquad (1.1)$$

The third constant can always be calculated if the other two are known. Poisson's ratio is a pure number and E and G are in lb/in^2 in the English system of units.

The rigidity of rocks is a function of the confining pressure (the pressure around the rock other than the deforming force). Very large changes in rigidity are observed in many rocks upon the application of the first few hundred atmospheres of confining pressure. Where such pressures are very high the change of rigidity with pressure becomes nearly linear and smaller.

Rigidity might be defined as the ability of solid matter to offer instantaneous resistance to deformation. If the modulus of rigidity can be taken as a measure of this property, then sandstone has a low rigidity, while that of limestone, granite, marble, slate, and greenstone vary increasingly in the order named. If a rock were perfectly rigid, its shape would remain unchanged no matter what the magnitude or

length of duration of the applied stress. In a single crystal, rigidity is largely determined by the arrangement of the atoms (and related factors), with interatomic forces holding them in equilibrium. Most rocks, however, are masses of various size crystals and grains, so stresses and deformation are concerned with intercrystalline bonds as well.

The dynamic modulus of rigidity may be determined with ease by a laboratory method. The fundamental frequency of torsional vibration of a cylindrical specimen is measured. The torsional velocity of sound and dynamic rigidity modulus of the specimen is then calculated from appropriate equations.

In Situ Moduli Tests. Nicholls[8] has reported a new technique in the determination of elastic constants of rock in situ. Longitudinal and shear waves were generated in rock by small explosive charges in shallow drill holes. Accelerometers and strain gages were employed to measure arrival time for both waves. From wave velocities and measured density, Poisson's ratio, modulus of elasticity, modulus of rigidity, Lame's constant and the bulk modulus were calculated. The same types of waves and values of elastic constants were determined by laboratory methods and the results compared (Table 1.4).

The equations employed to calculate the elastic constants from field studies are as follows:

$$\nu = \frac{\frac{1}{2}\left(\frac{V_p}{V_s}\right)^2 - 1}{\left(\frac{V_p}{V_s}\right) - 1} = \text{Poisson's Ratio} \qquad (1.2)$$

$$E = \rho V_s^2 \frac{\left[\left(\frac{V_p}{V_s}\right)^2 - 4\right]}{\left(\frac{V_p}{V_s}\right)^2 - 1} = \text{Young's Modulus} \qquad (1.3)$$

$$G = \rho V_s^2 = \text{Modulus of rigidity} \qquad (1.4)$$

$$\lambda = \rho V_s^2 \left[\left(\frac{V_p}{V_s}\right)^2 - 2\right] = \text{Lame's constant} \qquad (1.5)$$

$$k = \rho V_s \left[\left(\frac{V_p}{V_s}\right)^2 - \frac{4}{3}\right] = \text{bulk modulus} \qquad (1.6)$$

TABLE 1.4 - Comparison of results, in place and laboratory studies[8]

Property	Units	Salt			Granite-gneiss		
		Value	No. of readings	% deviation	Value	No. of readings	% deviation
Weight density (ρ)	lb./ ft.^{3}	135	11	± 1.0	164	6	± 0.5
Longitudinal velocity (V_p):							
Velocity study	ft./ sec.	14,350	32	± 0.7	18,230	58	± 0.3
Laboratory (bar)	ft./ sec.	12,810	11	± 4.0	8,860	6	± 3.8
Shear velocity (V_s):							
Velocity study	ft./ sec.	8,380	27	± 1.2	10,340	28	± 0.4
Laboratory (bar)	ft./ sec.	8,800	11	± 2.6	6,950	6	± 2.6
Poisson's ratio (σ):							
Velocity study		.241	--	± 6.1	.263	-	± 1.9
Laboratory		.059	11	±76.2	-.190	6	±31.
Modulus of elasticity (E):							
Velocity study	lb./ in.^{2} x 10^6	5.09	--	± 4.5	9.55	-	± 1.6
Laboratory	lb./ in.^{2} x 10^6	4.79	11	± 7.9	2.78	6	± 5.0
Modulus of rigidity (μ):							
Velocity study	lb./ in.^{2} x 10^6	2.05	--	± 3.3	3.78	-	± 1.2
Laboratory	lb./ in.^{2} x 10^6	2.26	11	± 5.3	1.71	6	± 9.4
Lame's constant (λ):							
Velocity study	lb./ in.^{2} x 10^6	1.91			4.20		
Laboratory	lb./ in.^{2} x 10^6	1/			1/		
Bulk modulus (k):							
Velocity study	lb./ in.^{2} x 10^6	3.28			6.72		
Laboratory	lb./ in.^{2} x 10^6	1/			1/		

1/ These values not calculated for laboratory tests because of large error in Poisson's ratio.

where

ρ = density

V_p = longitudinal velocity

V_s = shear velocity

The calculations from field data are primarily from the ratio of longitudinal and shear velocities. The field studies gave higher values for E than laboratory tests and more reasonable values for Poisson's ratio.

Comparison of Static and Dynamic Measurements. Since laboratory dynamic determination of Young's modulus usually involves low stresses, a comparison of static and dynamic values of Young's modulus is meaningful only if the values of the static Young's modulus are taken at comparable stress levels, i.e., using initial or zero stress tangent modulus.

It has been found that values obtained by static techniques are lower than those obtained by dynamic methods, the difference in the constants so determined varying from 0 to 300 percent. The difference has been explained[9,10] as being due to the presence of fractures, cracks or cavities, with the static yielding being increased by deformation of cracks and cavities and the dynamic measurements being less influenced. A stress wave is transmitted by the matrix of rock, and high frequency components are reflected and refracted from the crevices and cavities. The greater the degree of compactness of the rock, the more nearly static and dynamic constants may agree, as illustrated by the following:

	Young's modulus		Poisson's ratio	
	Static	Dynamic	Static	Dynamic
	(dynes/cm^2)			
Quincy granite	3.5×10^{11}	4.3×10^{11}	0.10	0.33
Sudbury norite	8.36×10^{11}	8.82×10^{11}	0.22	0.27

The higher value of Young's modulus and the closer agreement of the static and dynamic values indicate that Sudbury norite is more compact than the Quincy granite.

The Bureau of Reclamation[11] investigated the difference between dynamic and static moduli of the Davis Dam foundation rock and their results agree with the conclusions of Zisman and Ide.[9,10] The mean value of Young's modulus in dynamic measurements was found to be 1,000,000 psi and that in static measurements was 50,000 psi. A longitudinal pulse transmitted across water-filled gaps in concrete or across a crushed concrete specimen showed little attenuation of velocity. Dynamic measurements could therefore indicate a fictitiously high value of modulus for rock or concrete that was completely fractured. Similar results were obtained by Dvorak[12] for a medium under pressure, but differences did not exceed 50 percent because fractures were partially closed by pressure.

The ratio of the dynamic to static moduli varies between 0.85 and 2.9,[13] based on data determined by the Bureau of Reclamation[14] (Table 1.5). (The description of the rocks investigated and the value of Young's modulus and Poisson's ratio for static and dynamic tests (Tables 1.1 - 1.3) does not detail such factors as open fractures, porosity, alteration, or boundaries between crystals). The discrepancy between static and dynamic values is less for rocks which have a larger elastic modulus. It should be emphasized that equations relating velocity to Young's modulus are based upon the ideal assumptions that rocks are homogeneous and isotropic.

The variation of values of dynamic constants is dependent on frequency in a range from 40 to 140 cps[15] for different rocks (Figure 1.1). Test results indicate that the higher the frequency, the higher Young's modulus, with values being from 2.1 - 2.6 percent higher for the various rocks tested. For higher frequencies Birch and Bancroft[16] found that in the frequency range 140 - 4500 cps the variation is less than 1 percent, and the increase of Young's modulus does not exceed 4 percent.

Specific Damping Capacity. This factor is a measure of the vibrational energy absorbed by the rock and may be considered to be a measure of the internal friction. It is determined by the "sharpness" of resonance that is evident when a specimen is vibrated through a range of frequencies centered on the fundamental longitudinal resonant frequency. (See U.S. Bureau of Mines R.I. 3891 for mathematical expressions). For damping of the dry type (coulomb damping), the damping is commonly assumed to be independent of the velocity and thus independent of the frequency. The specific damping capacity is somewhat sensitive to moisture content.

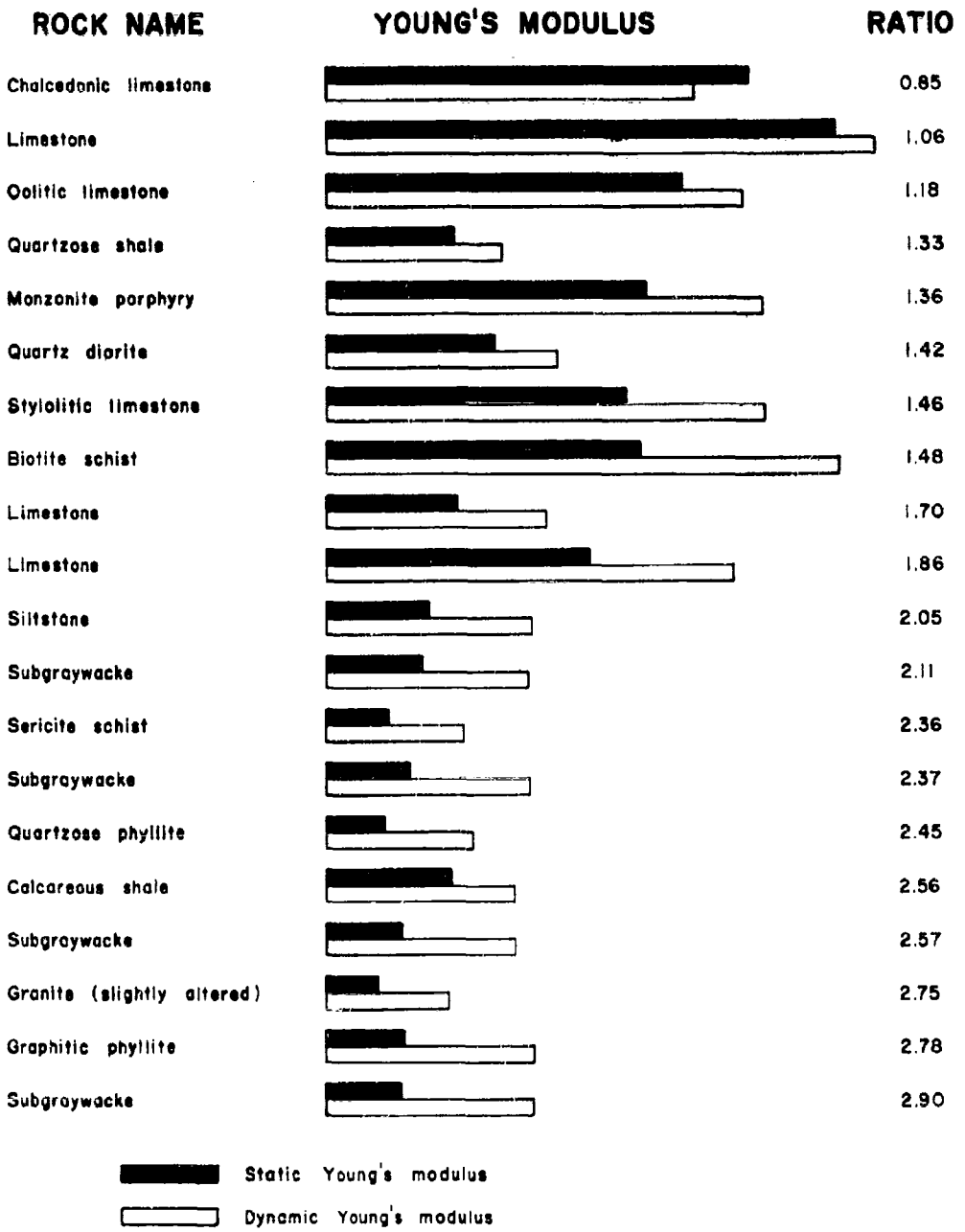
Rock Strength.

Tensile Strength. The strength of rock in tension is one of its most important engineering properties, because a large portion of rock structure failures are due to failure in tension. The blasting action of conventional explosives on rock depends largely upon the rock's tensile strength as well as other physical properties. Rocks are much weaker in tension than in shear or compression.

Modulus of Rupture. The modulus of rupture has the units of stress, and is computed from the flexure formula $\sigma = \frac{Mc}{I}$. Where σ is the stress, M the bending moment at failure, c the distance from the neutral axis and I the moment of inertia of the cross-section. Tests are performed on laboratory-size rock specimens.

Test values obtained by this method are higher than those obtained by a tensile strength test, possibly due to the small area of the specimen under tension in the rupture test. From the formula it can be seen that the modulus is proportional to the load the specimen will support. Flexure strengths of rocks so tested vary from 500 to 8000 lb./in^2 which values are roughly one-tenth to one-twentieth their compressive strengths.

TABLE 1.5[13]


ROCK NAME
YOUNG'S MODULUS
RATIO
Chalcedonic limestone
0.85
Limestone
1.06
Oolitic limestone
1.18
Quartzose shale
1.33
Monzonite porphyry
1.36
Quartz diorite
1.42
Stylolitic limestone
1.46
Biotite schist
1.48
Limestone
1.70
Limestone
1.86
Siltstone
2.05
Subgraywacke
2.11
Sericite schist
2.36
Subgraywacke
2.37
Quartzose phyllite
2.45
Calcareous shale
2.56
Subgraywacke
2.57
Granite (slightly altered)
2.75
Graphitic phyllite
2.78
Subgraywacke
2.90
Static Young's modulus
Dynamic Young's modulus

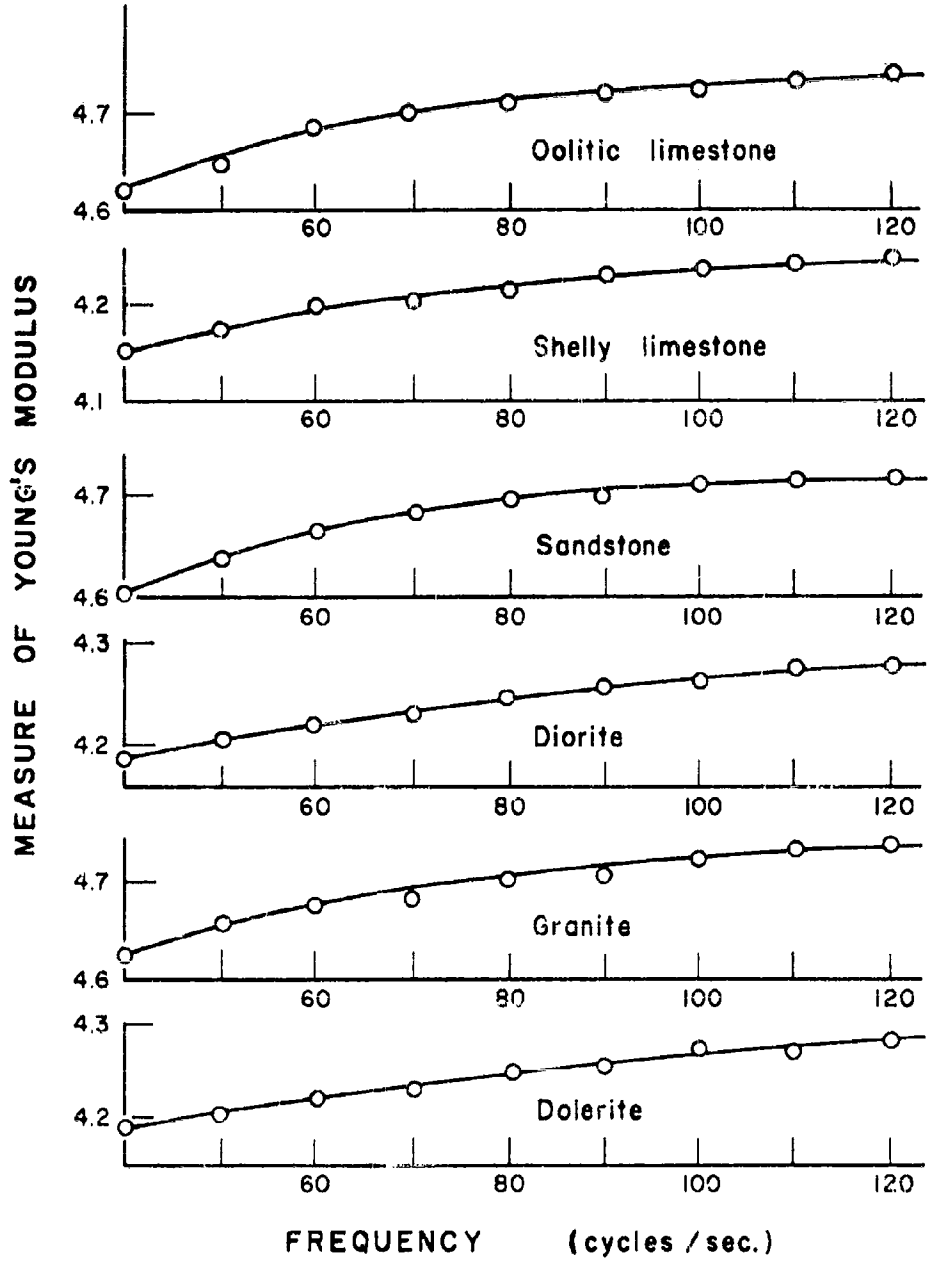


Figure 15. Influence of frequency on dynamic values of Young's modulus [5].

Compressive strength. Limestones and sandstones are weak in compression, and granite, marble, slate, and greenstone exhibit greater strength. Some are stronger parallel to the bedding and others perpendicular to the bedding.

Where a test specimen is subject to a compressive unidirectional load, a study of Mohr's circle for stress distribution shows that a shear stress exists at an angle to the direction of loading. Thus it is possible for the specimen to fail in shear. The only case where pure compression exists is where the specimen is subject to equal pressure (hydraulic) in all directions. Failure in this case could only occur due to compression of pore space with resultant fracture of grains and movement along grain or crystal boundaries.

Shear strength. There appear to be few data available relative to the shear strength of rocks and no accepted tests to determine this property. However, rocks subject to load are seldom free from shear stresses, and if weak in shear, stress caused by a compressive load may cause them to fail due to induced stresses along shear planes, the angle of failure depending upon confinement.

Hardness of Rocks.

Various concepts of hardness do not lend themselves to exact definitions in usual physical units. The hardness scale (Moh's) employed in mineralogy is based upon the ability of one substance to scratch another. This familiar scale of hardness gives talc a hardness of 1 and diamond a hardness of 10, the difference in hardness between 9 and 10 being much greater than that between 1 and 9. Relatively homogeneous substances such as metals are much easier to classify as to their hardness than rocks. The majority of rocks is heterogeneous in character and, hence, a type of integrated or average hardness over a representative surface is usually determined.

Scleroscope Hardness. A Shore Scleroscope indicates the Scleroscope hardness of a substance by the height (or an arbitrary scale of 0 to 120 divisions) of rebound of a diamond pointed (pin-point - 0.03 $in.^2$) hammer which is dropped vertically on the test surface. The impact of the point may produce some crushing of a microscopic nature, but this may be neglected for practical purposes.

Basically, the scleroscope reading is a measure of an elastic property of the material being tested. That is, the distance of rebound of the hammer depends upon the coefficients of restitution of the diamond point and the rock. If the rock crushes, this decreases the rebound energy and the consequent height of rebound by an amount equal to the crushing energy and the energy otherwise absorbed by the rock and the instrument.

The direct application of scleroscope readings to the engineering design of underground openings is not clearly defined, as is the case with many of the other physical properties of rock. However, it is at least superficially a measure of the response of rock to an impact load

of a given type and as such might be employed as a guide to the manner in which rocks will behave when subjected to the repeated impact of shock waves from explosions in drill round.

Abrasive Hardness. This test employs a rotating abrasive wheel or plate against which specimens are held. The specimens are abraded for a given number of revolutions and the weight of material lost is a measure of the abrasive hardness.

Impact Toughness. This method involves determining the impact toughness of a rock by dropping a weight from successively greater heights until such a height is reached that the specimen is fractured. Impact toughness may be related to compressive strength, but seems to be affected to a greater extent by foliation weakness. Inasmuch as axial compressive stresses are accompanied by shear stresses, the impact toughness would be affected by shear strength as well. The ability of the rock to absorb or dissipate impact energy must also be considered.

Ball Mill Grindability. Although the procedure for this test is prescribed in certain standardized tests, it is not considered an essential part of the program of study of underground structures. A crushed specimen of a given size range of particles is placed in a ball mill and the reduction in size of particles for a given number of revolutions of the mill is interpreted in terms of a grindability index.

Volumetric Properties.

Apparent Porosity. This characteristic is defined as the ratio of the volume of open pore space in the specimen to the exterior volume. It is obtained by measuring the difference in weight of a rock which is dessicator dried and then water saturated. The porosity of a rock so determined is also an indication of its granular structure.

All rocks which are composed of crystals have measurable amounts of porosity, and these pore spaces, both open and closed, are the cause of many difficulties involved in the measurement of the elastic properties of rock. The pore spaces are made up largely of irregular thin cracks separating the crystal grains. Granites, gabbros, and other igneous rocks exhibit rather low porosities, granites, having porosities which average about 1 percent. Gabbros ordinarily have a porosity whose order of magnitude is about 0.1 percent of the volume. Sandstones and limestones possess much higher porosities, depending upon their particular physical characteristics such as grain size, cementing material, etc. It is the porosity of some limestones plus their chemical nature that makes them amenable to mineralization or replacement.

Porosity at relatively low confining pressures has at least two effects which contribute to the anomalous elastic behavior of rock: (1) Complicated stress conditions are created due to the existence of discontinuities caused by crystal boundaries and spaces between crystals, and (2) a looseness of structure which may be caused by crystalline composition or granular structure.

Apparent Specific Gravity. This property is determined by the standard method of dividing the weight of a rock by the weight of an equal volume of water. The term "apparent specific gravity" is used because water cannot penetrate the closed pore spaces inside of the rock, and, hence, the specific gravity measured by water displacement methods includes the effect of internal pore spaces as well as that of the constituent minerals.

Other Properties.

Fatigue. Repeated stresses in a rock structure may cause it to fail through fatigue failure, even though the stresses are well below the ultimate strength. It is a well known fact that metals may resist a steady load of considerable magnitude without rupture, but fail when this stress is repeated many times. During the thousands of years which have elapsed since the original formation of rock structures they have been subjected to repeated stresses of different types and magnitudes but their time distribution is of such a character that the rocks had time to relieve themselves of one stress before another was applied. In this case plastic or viscous flow usually would take place. However, Philips[17] conducted a test on marble which illustrates the response of rock to repeated loadings and a final sustained load to failure, i.e., a type of fatigue failure.

Creep. Griggs[18] performed a series of experiments on rocks to determine their creep (visco-elastic) characteristics. Many substances including metals, plastics, etc., will yield continuously or creep when they are subjected to stresses below their elastic limit for a long period of time. Allowance for this characteristic must be made in some heavy machinery. While experimentation on rocks has been primarily concerned with the geological behavior of rocks under stress, i.e., the flow of rocks subject to tectonic forces, the results obtained from these studies indicate some important facts that are of interest in the study of rock mine structures.

When rocks are subject to stresses for long periods of time, the terms "elastic limit," "set point" and "strength" lose their ordinary meaning because they usually define properties in terms of short period tests. Creep may be analyzed, according to Griggs, as an aggregate of two types of flow: (1) "pseudo-viscous flow," which is deformation at a constant rate, and (2) "elastic flow," which decreases logarithmically with time.

The data plotted on logarithmic coordinates for the creep of Solenhofen limestone under a load of 1400 kg.km^2 at 23°C. (normal strength 2560 kg.km^2), resulted in a curve whose equation is:

$$s = (6.10 - 5.20 \log_{10} t)\ 10^{-5} \qquad (1.7)$$

where s is the shortening per unit length and t is the time in days.

The same curve plotted on cartesian coordinates shows that the rock shortens rapidly during the first part of the test period and then the curve levels off rapidly as time goes on. The time for limestone to shorten is well within the range of time periods over which mine pillars

are required to support stresses which may be even closer to their ultimate strength than the load on the limestone discussed above.

Flow or creep of rocks is largely a result of rearrangement of atoms within crystals (intracrystalline slip). For example, evidence points to the hypothesis that creep in lead is largely due to intergranular motion whereas rapid deformation occurs largely by intracrystalline slip.

Thermal Expansion of Rock. The thermal expansion of various rocks, particularly those of a heterogeneous character like granite, which is composed of a mixture of non-oriented crystals, involves a complex group behavior. Investigators,[19] however, believe that the tendency of silica to expand may persist and exhibit itself throughout the variations of structure and chemical complexity. The coefficients of expansion in those rocks which contain silicates are considered as being conditioned by the presence of alumina and silica independent of other variables. This generalization does not apply to those rocks such as limestone, travertine, and marble, which do not contain appreciable amounts of silica.

Some rocks show a low rate of expansion for lower temperatures, and the rate increases as the temperature increases. When specimens are cooled after heating, their contraction is less than their expansion, i.e., they show a permanent set. Coefficients of expansion (in Fahrenheit scale) vary from 0.0000067 for cherts and quartzites to a minimum of 0.0000022 for diabases, gabbros, and basalts, with an average of 0.0000045 for granites, limestones, sandstones, slates and marbles.

Compressibility. The compressibility of a substance is usually defined as the relative change in volume per unit change in pressure referred to an arbitrary initial pressure. This may be represented in terms of partial differentials or in terms of finite changes in volume and pressure,

$$B = \frac{1}{V_o} \cdot \frac{\partial V}{\partial P} \quad \text{or} \quad B = \frac{1}{V_o} \frac{(V - V_o)}{(P - P_o)} = \frac{1}{K} \tag{1.8}$$

the latter being for small changes and both defined for changes at constant temperature. In these equations B is the compressibility, V the volume of the sample at pressure P, V_o the volume at an initial pressure, P_o, and K is the bulk modulus in the elastic range. It is assumed that the temperature, chemical composition and physical state of the sample remain constant and that the pressure is hydrostatic. The unit pressure commonly employed is the **bar**. (1 bar = 10^6 dynes/cm.^{2} or 0.987 atmospheres). The units of measurement of compressibility are the reciprocal of the pressure units employed.

Compressibility[20] of common minerals is given in Tables 1.6 and 1.7. These values were obtained by means of testing specimens in a heavy walled cylinder under high pressure. Volume changes were measured by appropriate electrical devices which were selected for their accuracy.

TABLE 1.6

COMPRESSIBILITY OF ROCKS

(Hydrostatic pressure. Direct measurement of volume change. Pressure range, 2,000 to 12,000)

Description	Pressure, bars	$10^6\beta$	$-10^4\frac{1}{\beta_o}\frac{\partial\beta}{\partial P}$
Westerly granite	2,000	2.12	0.19
Washington granite	2,000	2.23	0.24
Stone Mountain granite	2,000	2.06	0.17
Sudbury diabase	2,000	1.37	0.11
Palisade diabase	2,000	1.54	0.2
Maryland diabase	2,000	1.23	0.16
New Glasgow gabbro	2,000	1.34	0.2
Whin Sill diabase	2,000	1.70	0.3
New Jersey basalt	2,000	2.4	0.4
Balsam Gap dunite	7,000	0.79	...
Serpentine	2,000	1.79	0.31
Colorado marble	7,000	1.37	...
Obsidian	2,000	2.82	0.07
Tachylite (basalt glass)	7,000	1.45	...
(Plate glass)	2,000	2.22	0.10

TABLE 1.7

COMPRESSIBILITY OF ROCKS

(Hydrostatic pressure. Volume change, determined from change of length)

Description	Pressure, bars	$10^6\beta$	Pressure, bars	$10^6\beta$
Quartzite sandstone	300	3.55	600	3.15
Quincy granite (from 235 ft.)	300	3.18	600	2.55
Rockport granite	300	3.39	600	2.71
French Creed norite	300	2.64	600	1.69
Sudbury norite	300	1.75	600	1.68
Olivine diabase	300	1.46	600	1.33
Vermont marble	300	2.09	600	1.53
Limestone	300	2.60	600	2.40
Solenhofen limestone (not covered)	6,000	1.39	...	...
Dolomite	300	1.89	600	1.51
Lipari obsidian	300	3.01	600	3.01
Lipari obsidian	5,000	2.7	...	...
Ascension Island obsidian	5,000	2.61	...	...
Diabase glass	5,000	1.62	...	...

It is noteworthy that whereas the concept of compressibility can be applied to anisotropic materials which are made up of grains or crystals, other purely elastic properties such as rigidity, Young's modulus and Poisson's ratio can be applied with accuracy only to those materials which are isotropic, or which approach a condition of isotropy such that elastic conditions may be assumed without any degree of error.

A comparison of the compressibilities of various rocks with those of the minerals of which the rocks are composed show that the acidic rocks have much lower compressibilities and in general consist of less compressible minerals. For pressure above 2000 bars the compressibility of a rock can be calculated with satisfactory accuracy from the individual compressibilities of the various minerals. Below this pressure the agreement between calculated and measured results vary as much as 5 percent. To calculate the compressibility on this basis the volume percentage of each mineral is multiplied by its compressibility and the sum of these products is then the calculated compressibility.

Figure 1.2 shows that at pressures of about 2000 bars the compressibility of various rocks of given types is nearly the same. The width of the shaded areas between the curves indicates the degree of variation that might be expected for ordinary rocks within a given class, in this case granites, gabbros and diabases. Open and closed pore spaces probably account for the abnormally high compressibility at low pressures. Gabbroic rocks may have a porosity of about 0.1 percent of the total volume while that of granitic rocks is notably higher, but seldom exceeds 1.0 percent.

A general criterion seems to be derivable from the initial effect of pressure on rigidity: A larger initial change in rigidity with the application of pressure is an indication of high porosity.

Granitic rocks may sometimes exhibit anomalous elastic behavior because (1) they are composed of highly compressible and less compressible mineral grains, which result in a complicated set of stress conditions with respect to individual mineral grains, or (2) they possess an original looseness of structure which allows the elastic behavior to become simplified only after the application of sufficient pressure to make the mineral grains tightly locked together.

Granular structure and strength.

It has been found that grain size in metals is very closely related to the strength of the metal, the decrease in grain size being accompanied by an increase in strength. Also, the addition of small amounts of carbon to iron forms steel. In this case the greater strength of the steel over the iron is believed to be partly due to the formation of hard shells around the soft iron crystals. The constituents of igneous rocks, however, do not form alloys in the same manner that metals do. Consequently, there seems to be only a very limited parallelism between the properties of rocks and metals.

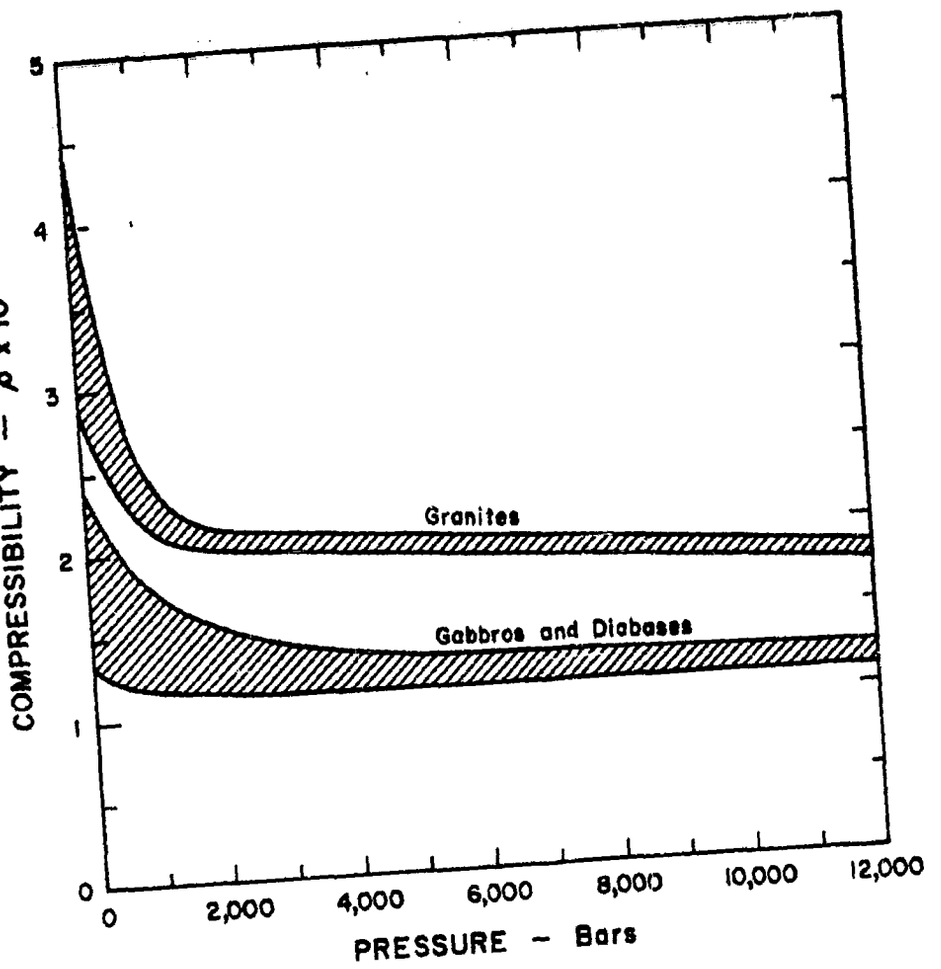


Figure 1.2. Compressibility of granites, gabbros and diabases as a function of pressure. (Gutenberg).

Fine grained rocks have been shown to break under compression with so-called "extensional rupture." According to Rove[21] these rocks are brittle, competent, strong and have a high crushing strength. Because of the high resistance to compressive stresses, and frequently low ratio of tensile to crushing strength, these rocks are believed to commonly develop tension joints or faults which are characterized by the development of open spaces. Breakage of coarse grained rock of low crushing strength and a higher ratio of tensile to shear strength may result in development of faulting characterized by shear zones and the development of possible gouge. In a medium grained rock a shattered condition is postulated by Rove.

The depth of the rocks in the earth's crust plus their physical character thus have an important effect upon their perviousness to solutions, particularly along fault zones. Their physical character is also a determining factor in their deformation or failure under the stresses of post-mineral faulting, which is a dominant factor in the processes which effect the strength of mine structures.

The results of test data accumulated by the U.S. Bureau of Mines (Appendix I-B) are not conclusive concerning the relation of petrographic fabric of rocks to their physical properties. For example, only one quartzite was tested in the groups whose properties have been published. In this type of rock, not only the grain size but the cementing material would affect the physical character of the rock. The grain size of the mineral constituents of various igneous rocks is also a prominent factor in determining their properties, but the presence of soft minerals or the effects of alteration are often more important than grain size and obscure the effects of the latter. Also, the physical properties of various rocks are particularly sensitive to the percentage composition of the minerals in the rock. These relations have only been observed in a qualitative manner, however.

Behavior of Rocks under High Confining Pressures

Quartz and limestone. Experiments which were conducted by Griggs[22] and others in which crystals of quartz were subjected to compressive stresses up to 138,000 atmospheres while the crystal was under a confining pressure of 20,000 atmospheres did not show that quartz had any degree of plasticity. (The compressive force which was applied is equivalent to pressures that might be encountered at a depth of 280 miles under the earth's surface). At a high temperature of 400° C. and a pressure of 4000 atmospheres, quartz showed a tendency to fracture into needles with definite crystallographic features. Under the highest confining pressures employed, single crystals of quartz ruptured only under stresses approaching the extremely high value of 2,000,000 lb. in.^{2}

Figure 1.3 shows how rapidly the strength of quartz increases with increasing confining pressures. Figure 1.4[23] shows similar curves for limestone and marble, whose ultimate strength increased 600 percent when the rocks were subjected to confining pressures up to 10,000 atmospheres. It is remarkable that these rocks showed less plastic flow for slowly applied stresses than for those applied more rapidly, which is an opposite effect from that postulated by geologists to explain rock flow in the earth's crust.

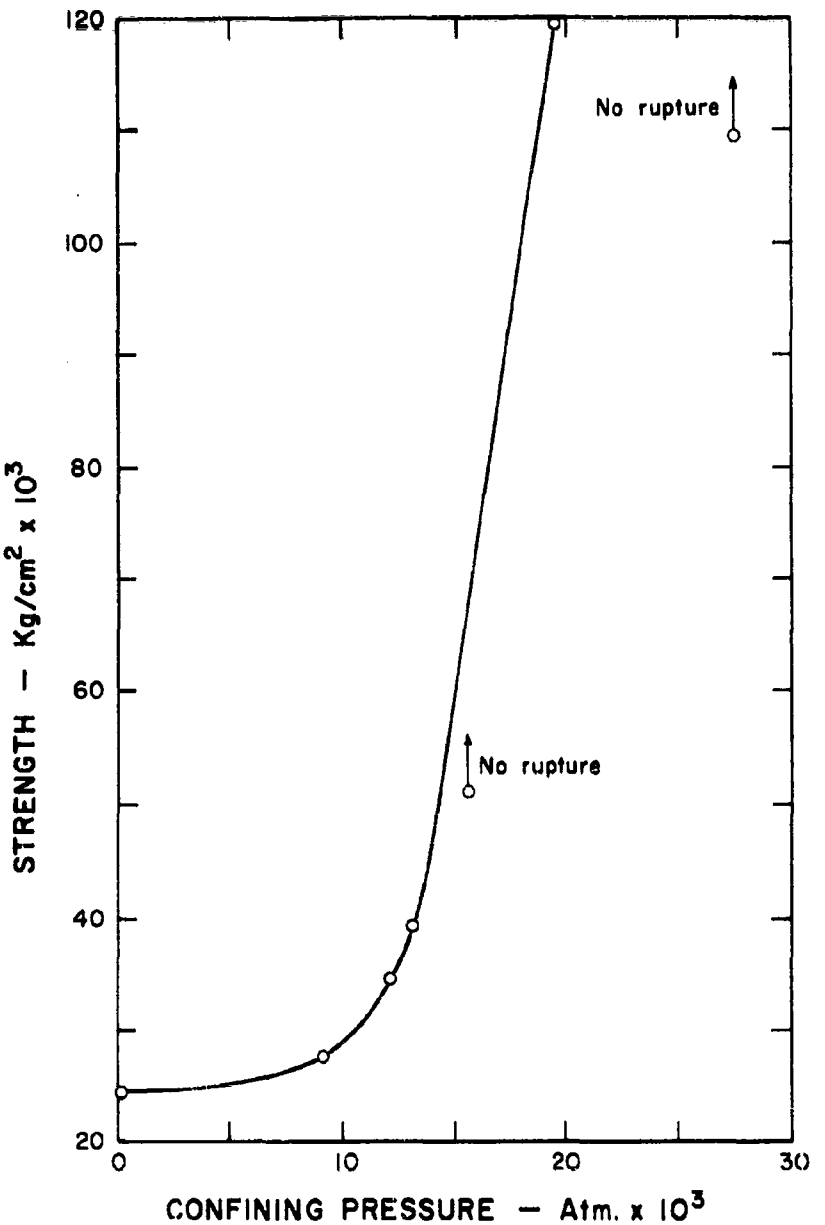


Figure 1.3. Increase of strength with confining pressure for single quartz crystals cut parallel to the e axis. (Griggs)

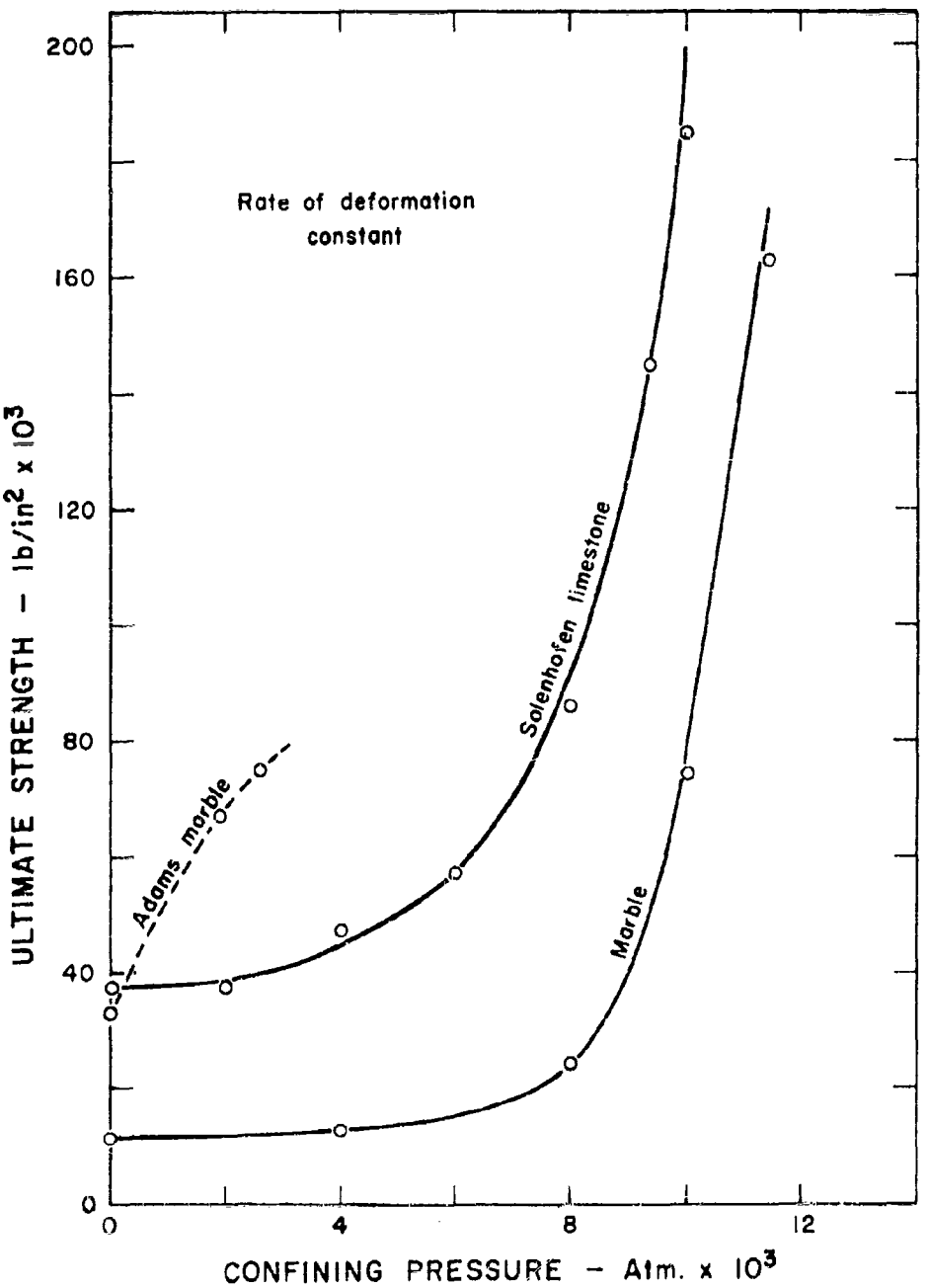


Figure 1.4. Ultimate strength as a function of confining pressure. Each point represents the maximum differential pressure supported by a specimen tested at the appropriate confining pressure. (Griggs)

A microscopic study of the effects of deformation upon the rock fabric of marble showed that the deformation seemed to be purely plastic. Two important observations were that (1) there was no marked change in grain size or shape in the marble, and (2) the crystals of the deformed marble were highly twined with traces of orientation of the twining.

Effect of Time on Strength.

Research data indicate that solid relatively homogeneous specimens of rock under confining pressure which are subjected to stresses below their "elastic limit" will not fail, no matter how long the force is applied. Under these conditions the "elastic limit" is a constant independent of the length of time of application of the force, but the ultimate strength is found to vary considerably with the duration of the deforming force, and if any force below a limiting value is applied to the rock for any definite time the rock will not fail.

Effect of Pressure on Fracture and Flow.

Geologists have long believed that when a rock is deformed under high confining pressures such as those postulated to exist at depth in the earth's surface that it will flow. That is, they have made a distinction between a "zone of fracture" and a deeper "zone of flow", but laboratory experiments have failed to produce continuous flow under high confining pressures. Completely reversing predictions, however, limestone at a confining pressure of 10,000 atmospheres behaved as a brittle substance. No plastic deformation before rupture was measured and the character of fracture was the same as at atmospheric pressure. This pressure corresponds roughly to that at 22 miles depth in the earth. The change in physical character of rock (i.e., stress-strain properties) with confining pressure is shown in Figure 1.5. The curves for the tests at low confining pressures (1200 and 4000 atmospheres) are characteristic of brittle materials. That is, the rocks rupture without deviating from approximately elastic behavior. The curves at high pressures are characteristic of materials such as some metals, which have a yield point at ordinary pressures, show a region of plastic deformation, and some work hardening before they rupture.

Fundamental Strength.

From the previous discussion concerning the properties of rock, it is evident that no simple equation of state or no single usable stress equation can be derived which will be applicable to complex geologic structures which may occur around mine openings. Equations based upon elastic theory have been applied with success to the relatively ideal geologic structures in the oil shale mines at Rifle, Colorado.[24, 25] However simple undisturbed mine structures such as these are unusual. The effects of bedding planes, joints, faults, cracks, alteration, mineralization, etc., and the resultant heterogeneity of composition and structure, make practical mathematical analysis of complex structures impossible. The strength of the component parts of a mine structure, their position

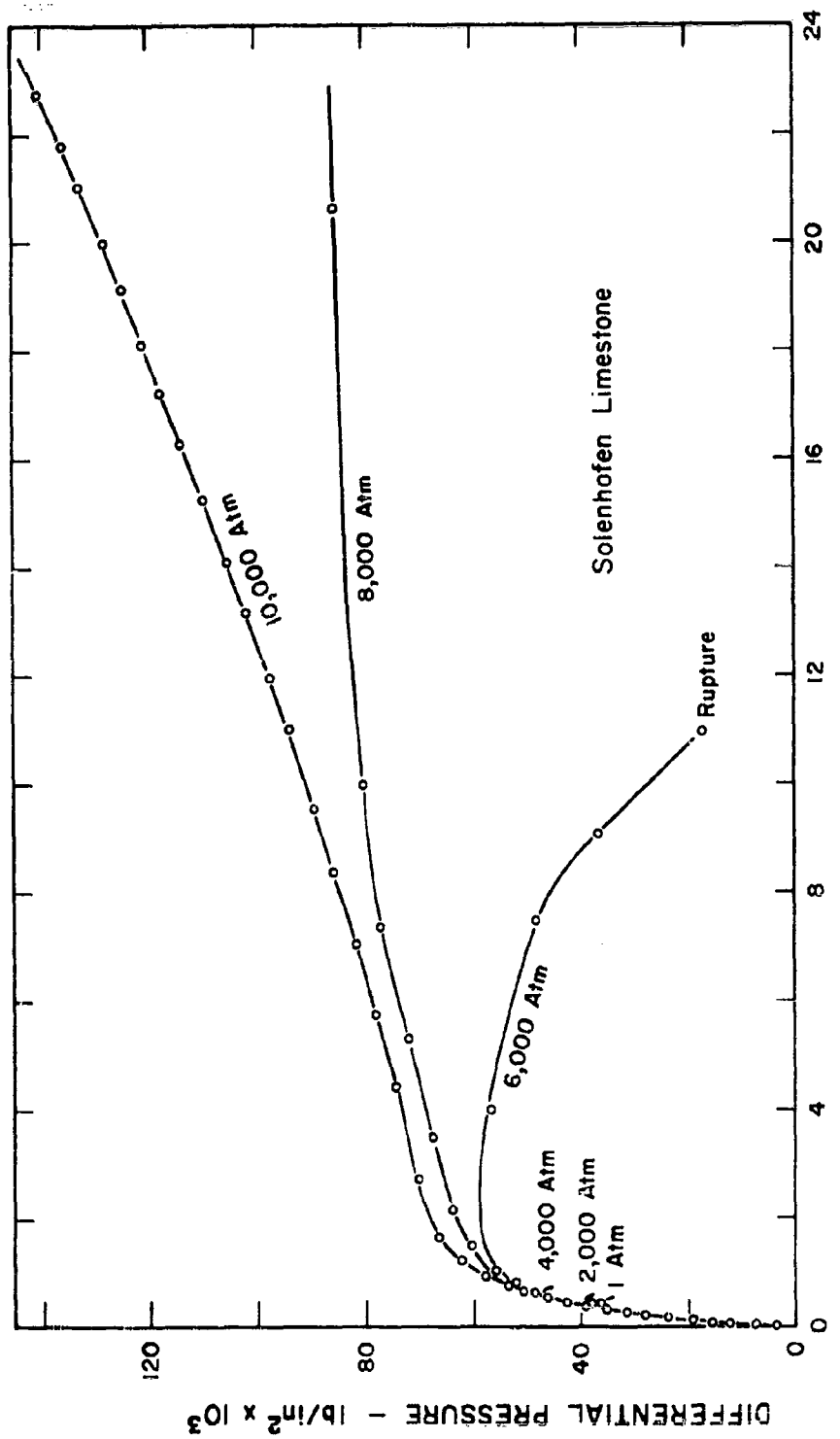


Figure 1.5. Stress-strain diagrams for Solenhofen limestone tested in compression with varying confining pressure from 1 to 10000 atmospheres. Each curve represents one complete experiment on an individual specimen. (Griggs)

relative to each other, their size, etc., are all determining factors in the strength of the over-all structure.

It has also been emphasized above that the element of time has a very important effect upon the reaction of solid materials to stresses. Crystal structure, porosity, grain size and other small scale physical characteristics further increase the complexity of evaluating the strength of rock.

While a mathematical evaluation is not in all cases attainable, Billings[26] has suggested a general criterion which is most useful to both mining engineers and geologists. The fundamental strength of solid materials has been defined by him as the stress which a material is able to withstand, regardless of time, under any given conditions--temperature, pressure, being subject to solutions--without rupturing or deforming continuously.

This concept can be easily extended to apply to a mine structure of any size or complexity, and does not depend upon approximations of elastic constants or the evaluation of strengths of large-scale mine structures from specimens of laboratory size. It is obvious from the outset that the quantitative determination of an exact number which would represent the fundamental strength of a given mine structure is an impossibility. On the other hand, from the mass of geological data usually available in any mining district it should be possible to arrive at an index of fundamental strength of structures which can be employed as a reliable guide in fixing the safe size of openings, choosing the proper excavation method, locating permanent mine openings, etc.

It has been found, for example, that the percentage recovery of rock core from diamond drill operations is a very good indication of the strength of the rock structure being drilled. The ability of rock to remain as a solid core is dependent largely upon the same characteristics which make for competent mine structures. These include tensile and shear strength, and lack of cracks, fissures and other weaknesses. Other valuable data which may be obtained from core drilling are discussed by Loofbourow.[27]

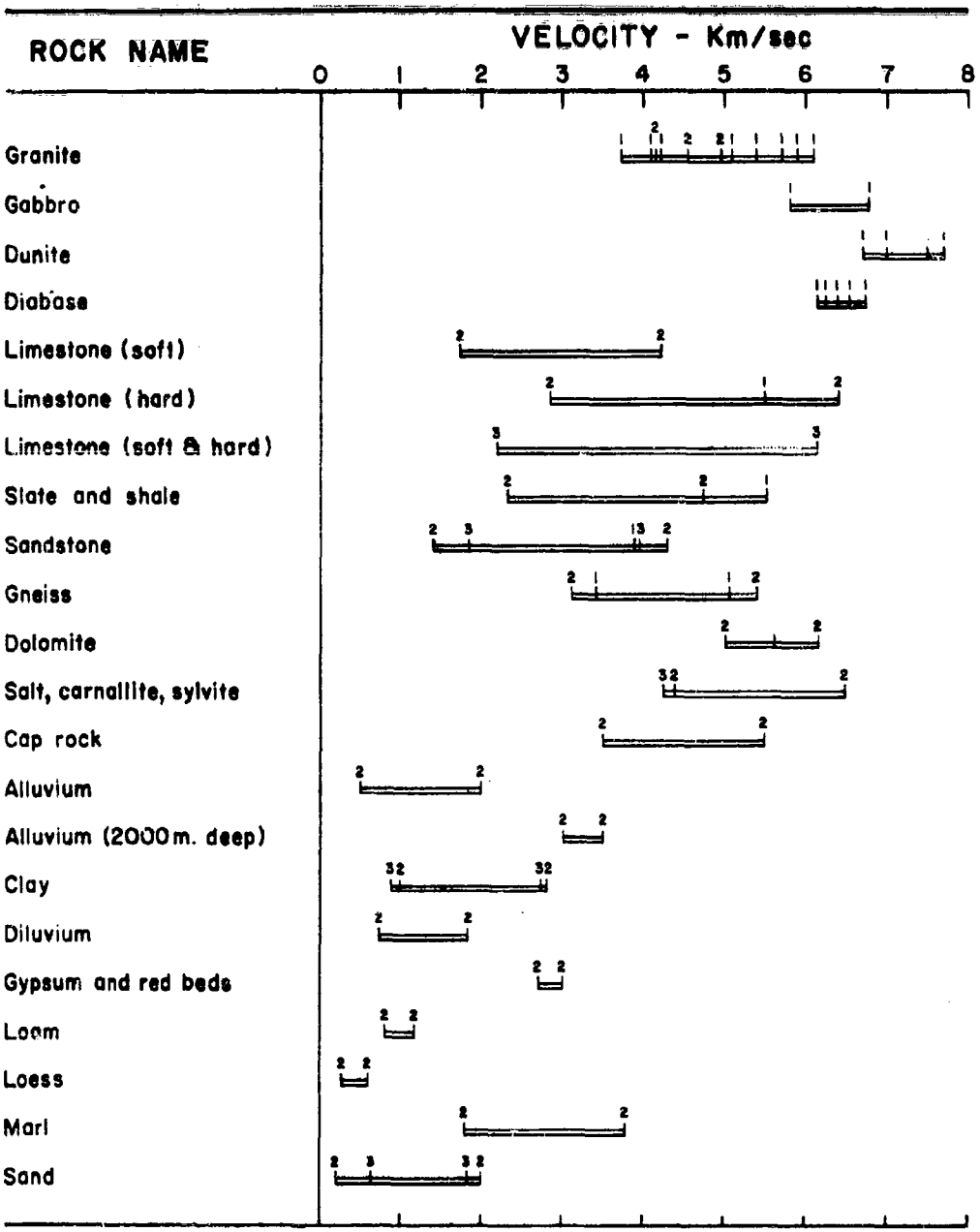
Velocity of Longitudinal Waves in Rocks.

The velocity of longitudinal stress waves in rocks is a function of several factors: the state of stress, stress level of the wave, water content, rock porosity, texture, temperature, and direction of propagation with respect to stratification. Generally, velocities are higher for rocks which are more dense and compact and are much lower for unconsolidated materials. Average values of velocity for some common rocks and earth materials are given below and in Table 1.8:[13]

Compact		Less Compact	
Rock	Av. Value	Rock	Av. Value
Dunite	7 km/s	Limestone	4 km/s
Diabase	6.5 km/s	Slate and shale	4 km/s
Gabbro	6.5 km/s	Sandstone	3 km/s
Dolomite	5.5 km/s		
Granite	5 km/s		

TABLE 1.8

Variation in Velocity with Rock Type[13]



1 - Ref. 28
2 - Ref. 29
3 - Ref. 30

Unconsolidated

Rock	Av. Value
Alluvium	1 km/s
Loam	1 km/s
Sand	1 km/s
Loess	0.5 km/s

The longitudinal bar velocity is related to the propagation velocity in an infinite medium by the equation:

$$V = V_o \sqrt{\frac{1 - \nu}{(1 + \nu)(1 - 2\nu)}} \qquad (1.9)$$

where V is the velocity in an infinite medium; V_o, the longitudinal bar velocity; and ν, Poisson's ratio.

Method of Measurement. Two methods are commonly employed for laboratory and field determination of velocities; (1) a frequency resonance method and (2) a pulse technique. In the first, a cylindrical specimen is vibrated longitudinally and the velocity calculated from the measured fundamental frequency of vibration. In the second, a pulse is sent through a rock specimen or a rock in situ, and the travel time of the pulse is measured between two points. (See Appendix I-A.) Various methods include seismic velocity logging methods using a transmitter capable of producing discrete sound pulses, laboratory experiments in which the pulse is provoked by a piezo-electric crystal of quartz or polarized barium titanate ceramic, and creation of a pulse by impact from a pendulum-type hammer on an end of the specimen. The different pulse methods may yield different values for the propagation velocity in a given rock, and no comparison of results or specific advantages appears to have been made for them.

State of Stress. Laboratory tests by Toucher[31], Wyllie and others[32,33] indicate that velocity values under various types of compressive loading are not significantly different except when the specimen is under uniaxial pressure and the velocity is measured in a direction perpendicular to the stress. A sample may be subjected to either a hydrostatic pressure, a triaxial pressure or a uniaxial pressure with the velocity measured parallel or perpendicular to the higher stress. Velocity values measured parallel to a uniaxial stress are 3 percent lower than those determined under a triaxial pressure. Toucher found values measured perpendicular to a uniaxial stress were 10 percent lower than those above and suggests that the anisotropic behavior of the rocks under simple axial pressure can give a possible method for determining the state of stress in rock in situ. Figure 1.6 demonstrates data obtained by Toucher for granite and Figure 1.7 similar results by Wyllie for sandstone.

For the majority of rocks velocities increase with state of stress. As pressure is increased from 0 to 500 bars, velocities increase 10 to 30 percent of their zero stress value. For an increase from 500 to 2,000 bars, the rise in velocity is 3 to 8 percent and above 2,000 bars it increases very slowly from 0.3 to 2 percent per 1,000 bars, as indicated

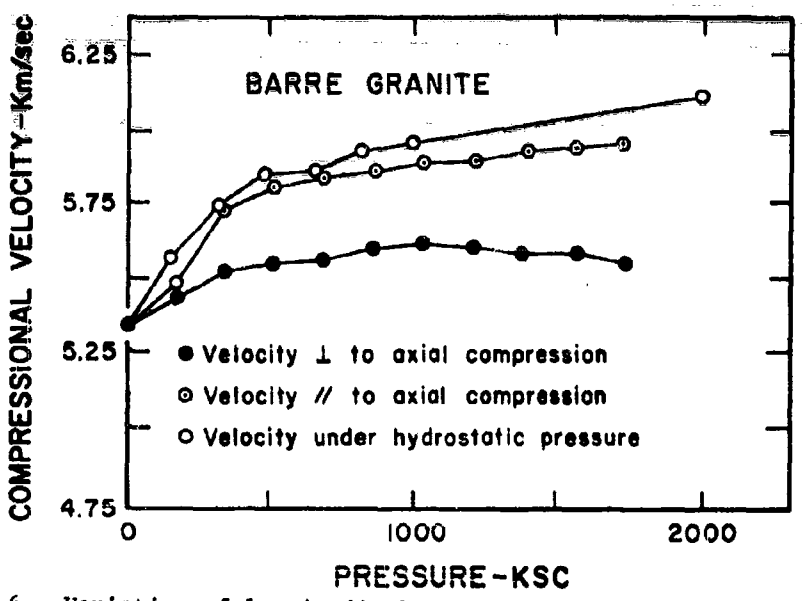


Figure 1.6. Variation of longitudinal velocity (km/s) with uniaxial and hydrostatic pressure (kg/cm^2). (31)

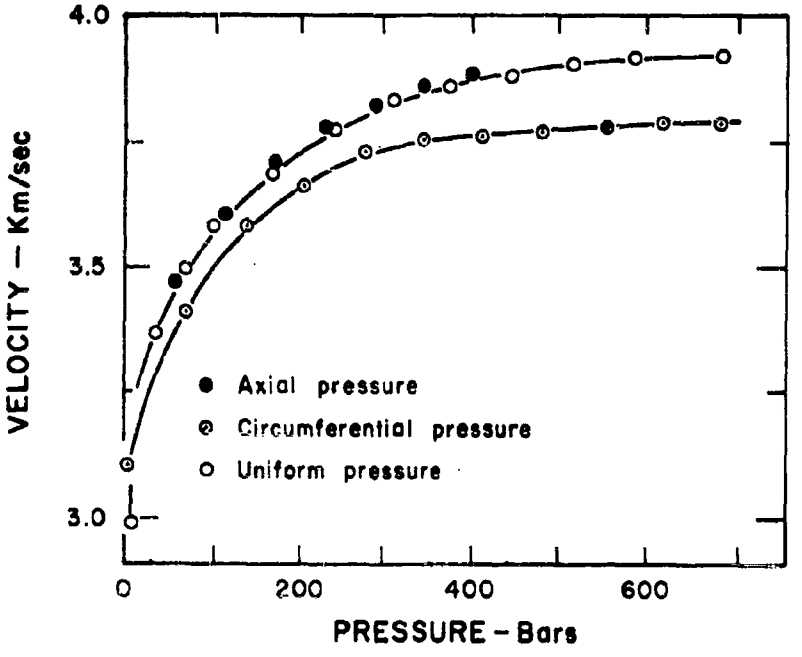


Figure 1.7. Results of three different methods of compression on the same material. (32).

in Figure 1.8. Some rocks show very little increase; Modoc obsidian (Figure 1.9) is anomalous in that it shows a decrease.

At low pressure (0 - 1,000 bars), the initial increase in velocity caused by stresses can be attributed to the presence of cracks. Transient stress pulses cannot be transmitted across narrow air gaps without very large loss in amplitude[11]. Thus, when there is no pressure on the rock, the open cracks impede the progress of the wave which must be refracted and reflected around the cracks. The transit time is greater than that of a wave in unfractured rock, or rock in which pressure has closed the cracks (Figure 1.10).

By means of the dilatational wave equation values of E and ν in Berea sandstone have been computed and compared to the measured values at the same stress level. The measured quantities are very different from those which were computed (Figures 1.11 and 1.12). This indicates that the velocity at different stress levels cannot always be deduced from slope of a stress-strain curve.

Effect of Wave Amplitude. The velocity of a stress wave may also depend on the amplitude or stress level of the wave itself. Stress waves generated by a near explosion have higher amplitudes than those of pulses encountered in laboratory tests. If the difference in amplitude results in a difference in velocities, dispersion phenomena will occur. Rinehart[13] has pointed out that the relationship between propagation velocity and stress levels of the wave may be deduced from theory of elasticity.

Water Content and Velocity. The influence of the water content on the velocity of a stress wave can be studied at atmospheric or higher pressure. It has been observed[32,33,34] that it is important to evaluate the pressure applied both to the rock grains and to the water in the pores. When the external pressure applied to the sample is equal to zero and when the water content increases from zero to saturation, the velocity increases, for example in Berea sandstone (Figure 1.11), and for the curves a and b in Figure 1.11, the water pressure is low and the rock framework under high pressure. For curve c, the water pressure is high and the rock pressure low. If there is an external pressure, the important factor is the rock pressure. If the solid phase or the differential pressure ΔP remains constant, the velocity is almost independent of external pressure for sandstone (Figure 1.14).

The velocity vs. water content at atmospheric pressure for three sandstones (Figure 1.15) showed marked decrease as saturation was reduced from 100 percent to about 70 percent, nearly constant velocities between 70 percent and 10 percent and variable trends below 10 percent. The variation at 350 bars is much less than at atmospheric pressure. At atmospheric pressure the stresses are transmitted through water filled spaces and not through air, significantly increasing the velocity. At high pressure the water or air content becomes less important because the closing of cracks increases the transmission of wave energy, and the velocity in the compacted rock is much greater than that in air or water.

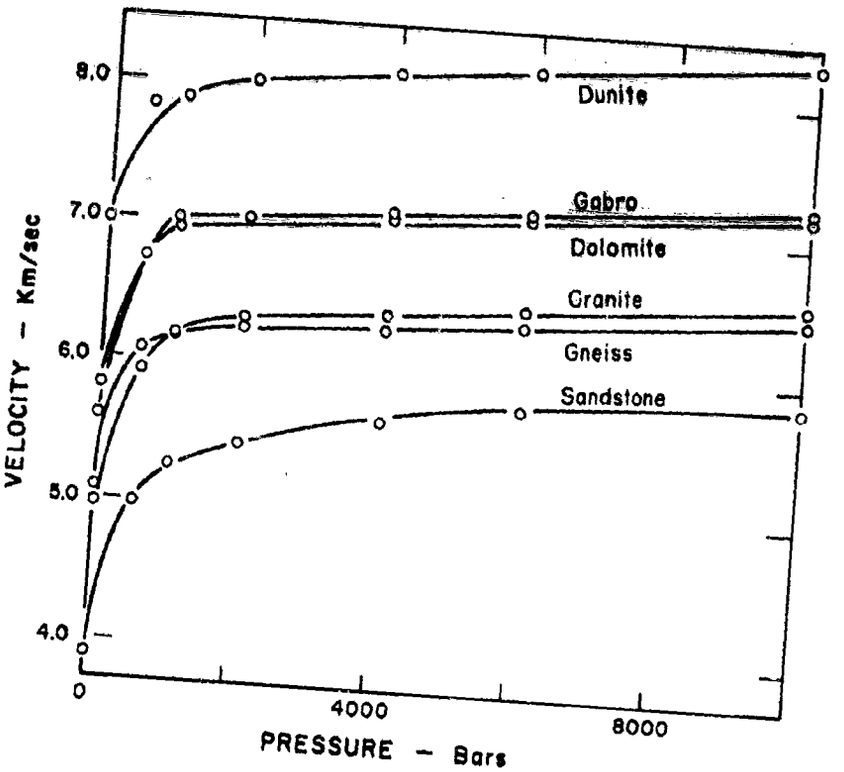


Figure 1.8. Longitudinal wave velocity (km/s) versus pressure (bars) for rocks showing a large increase at low pressures. (28)

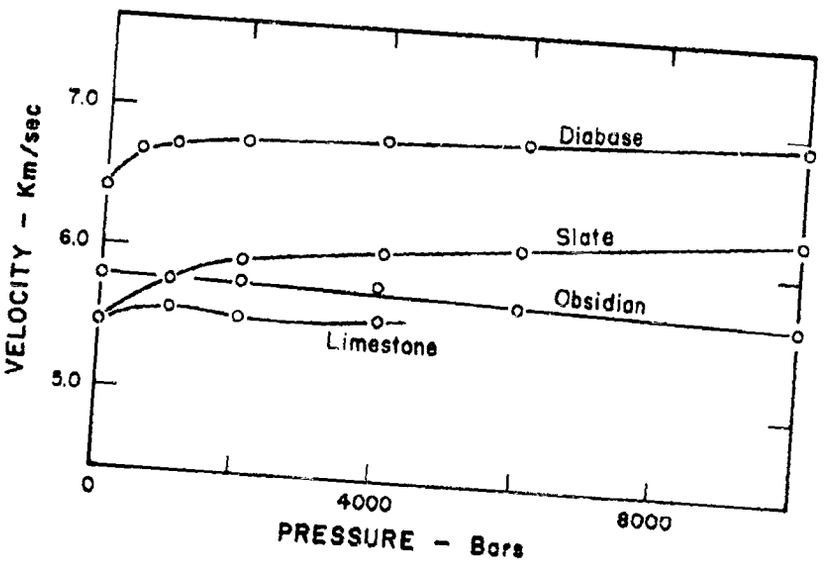


Figure 1.9. Longitudinal wave velocity (km/s) versus pressure for rocks showing a small increase at low pressures. (28)

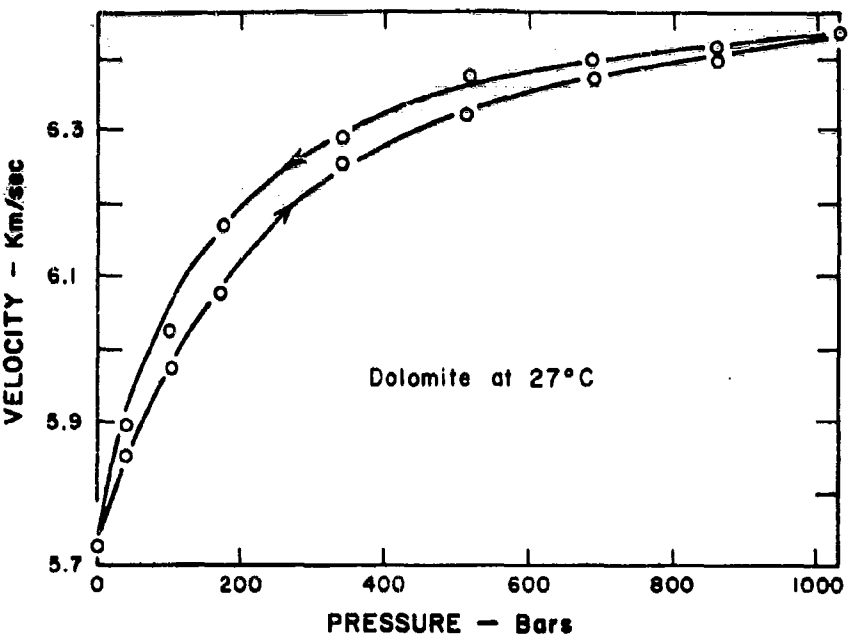


Figure 1.10. Dilatational velocity (km/s) versus pressure (bars). Velocity measured when decreasing pressure is higher than velocity measured when increasing pressure.[35]

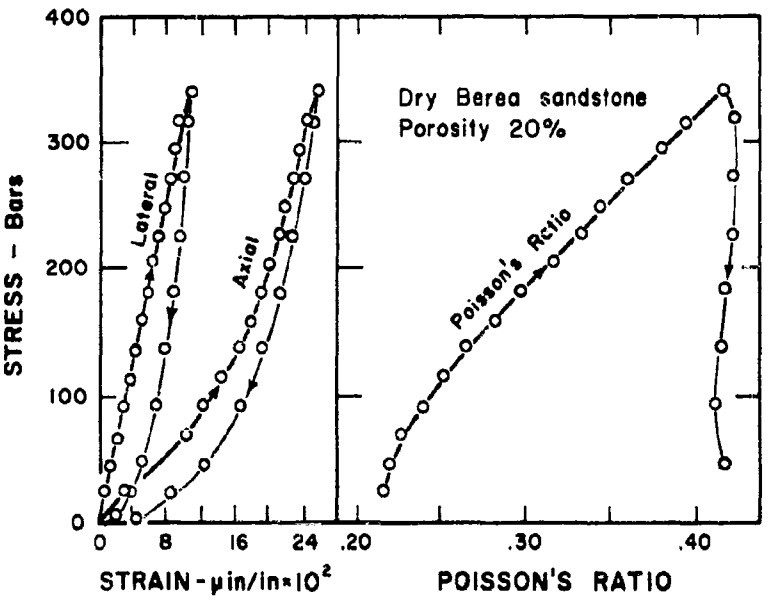


Figure 1.11. Stress-strain curves and Poisson's ratio versus stress for a sandstone.[36]

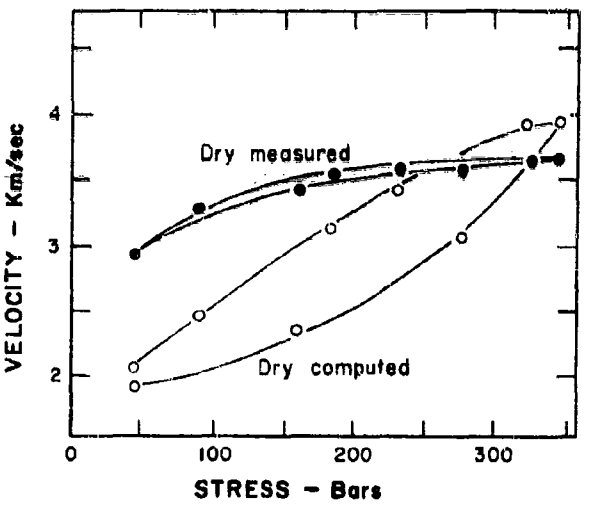


Figure 1.12. Comparison between measured propagation velocity and velocity computed from the stress-strain curves of Figure 1.11. (32)

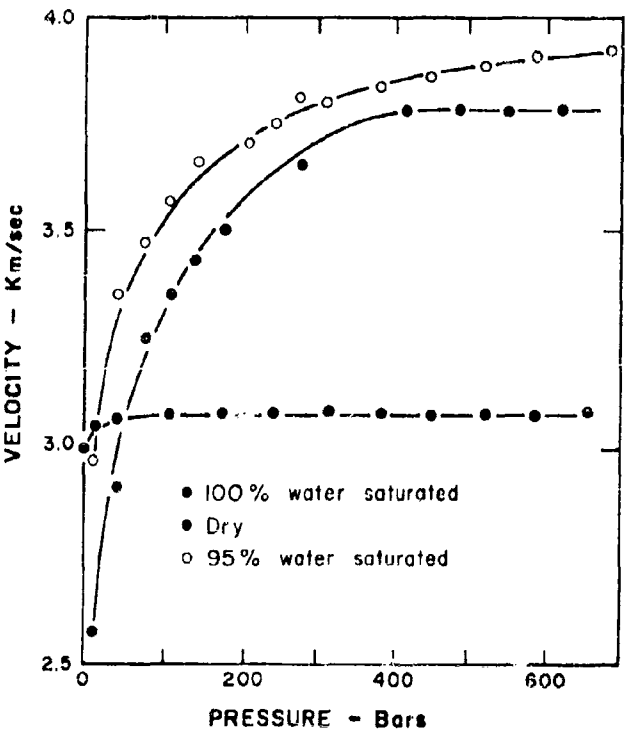


Figure 1.13. Longitudinal wave velocity (km/s) versus pressure (bars) for different water content. The great difference in velocity for 95 percent and 100 percent saturated specimens is due to the difference in the conditions of pressure. (32).

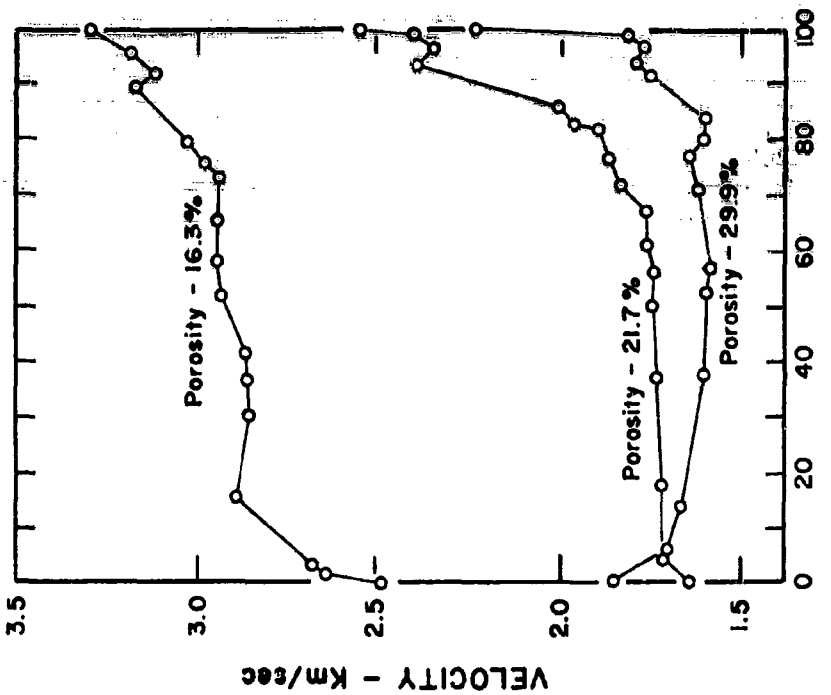


Figure 1.15. Velocity versus saturation for three sandstones.

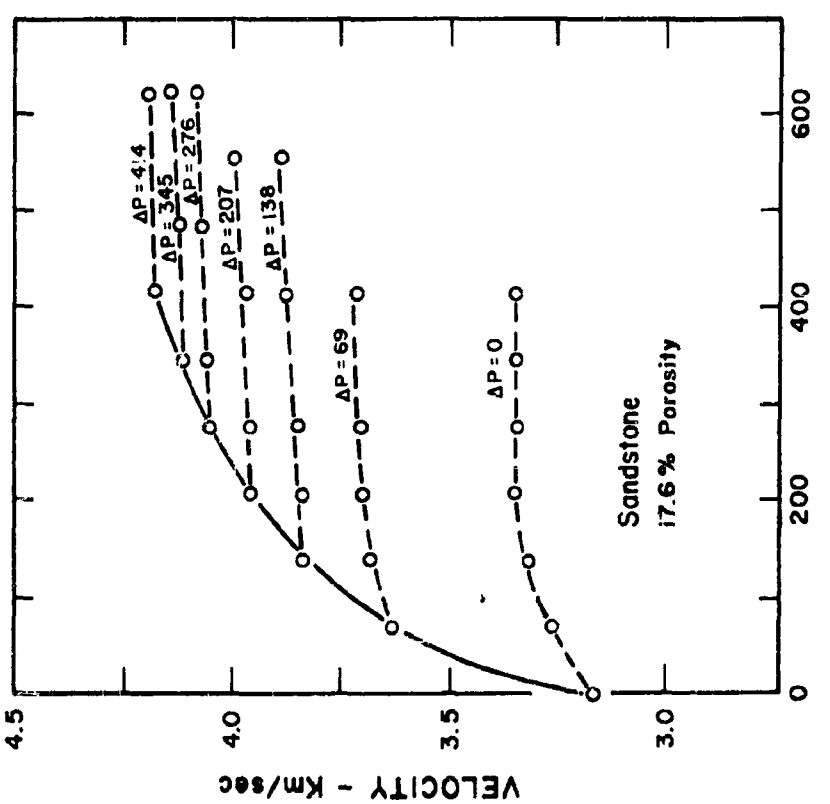


Figure 1.14. Longitudinal wave velocity versus pressure. Pressure difference appears to be important parameter.

The Bureau of Mines[37] found a 20 percent decrease in velocity for two sandstones at saturation. This abnormal behavior has not been explained and may be due to absorption phenomena.

Velocity vs. Porosity. In general, the wave velocity decreases as porosity increases due to two kinds of porosity[32]: (1) intergranular porosity, and (2) secondary porosity caused by natural fracturing or solution of the primary rock structure. Porosity due to solution differs from intergranular porosity in that the spaces formed are larger and less uniformly distributed. Secondary porosity does not have much influence upon the propagation velocity of stress waves in dolomite (Figure 1.17).

Experimental values for velocities in various types of dry and saturated sandstone with different types of cementing material (calcite, silica or clay), show that the relationship between velocity and porosity considerably outweighs the importance of cementing materials.

Similar data obtained from oil wells[32] show a trend relating decreased velocity with increased porosity (Figure 1.19). The average curve deduced from these data and the values of the velocities and porosities obtained from measurements in a specific oil well (Figure 1.20) shows a good degree of correlation. The experimental data of Figure 1.19 were obtained from different types of rock: sandstone, and limestone, from various depths (2,000 to 10,000 ft.) and from different geographical locations.

Among several theories proposed to relate propagation velocity to porosity, a time average relation by Wyllie[32] has given good results. Opposing this, Geertsma[38] believes that such a relation is fortuitous. Paterson[39] classifies theories according to the degree of coupling between the pore filler and the framework of the porous medium. Geertsma utilizes Biot's theory for a relation between velocity and porosity which is applicable when the deformation properties of the material are known. From measured deformation properties of sandstone, Geertsma computed the velocity as function of porosity and compared it with experimental values (Figures 1.21 and 1.22). The application of theory to limestone is more complicated because a distinction must be made between the effects of shell-shaped pores and spherical pores. It has been found that the effect of porosity on velocity is smaller for limestones with shell-shaped pores.

Effects of Stratification. Most rocks are anisotropic[40,36] described by an anisotropy factor which is defined as the ratio of the velocity along layers or cleavages to the velocity perpendicular to layers or cleavages. The velocity parallel to the layers has been found to be greater than the velocity perpendicular to the layers with some values as follows:

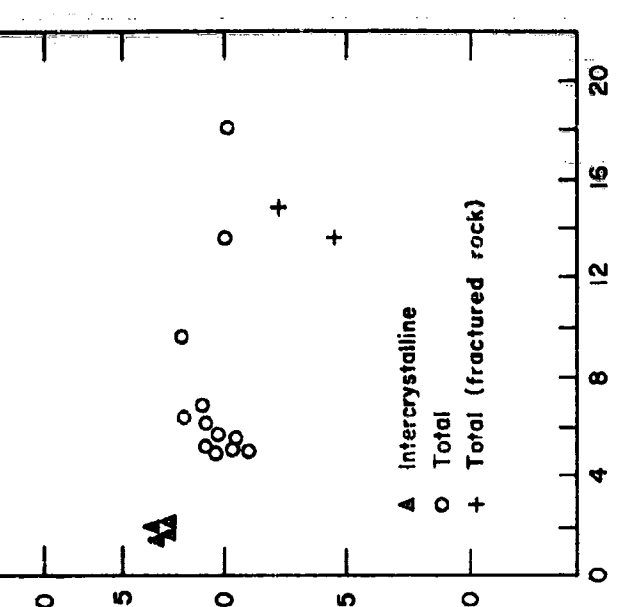


Figure 1.17. Longitudinal velocity vs. porosity for dolomite. (36)

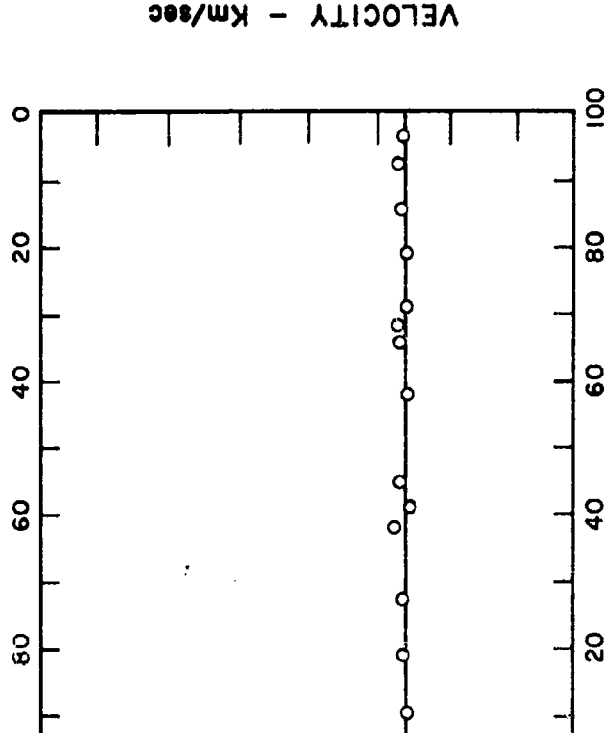


Figure 1.16. Longitudinal wave velocity as a function of water saturation at 350 bars. (36)

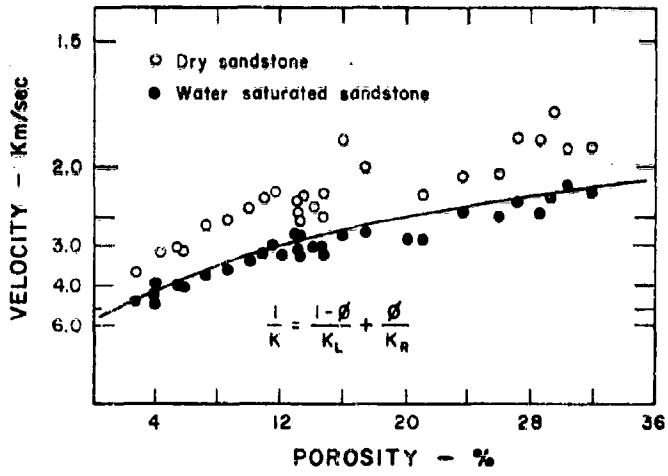


Figure 1.18. Deduced curve for longitudinal wave velocity vs. porosity for sandstone cores. (36)

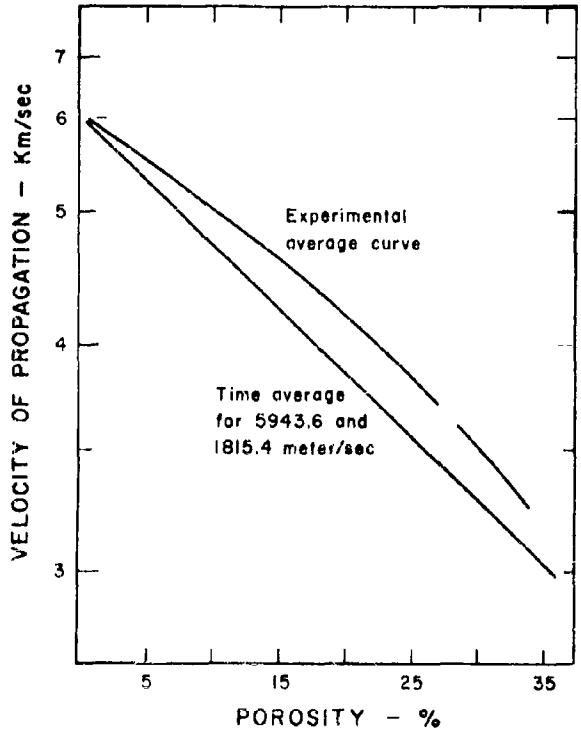


Figure 1.19. Longitudinal wave velocity vs. porosity. Experimental average curve compared with time average formula (36)

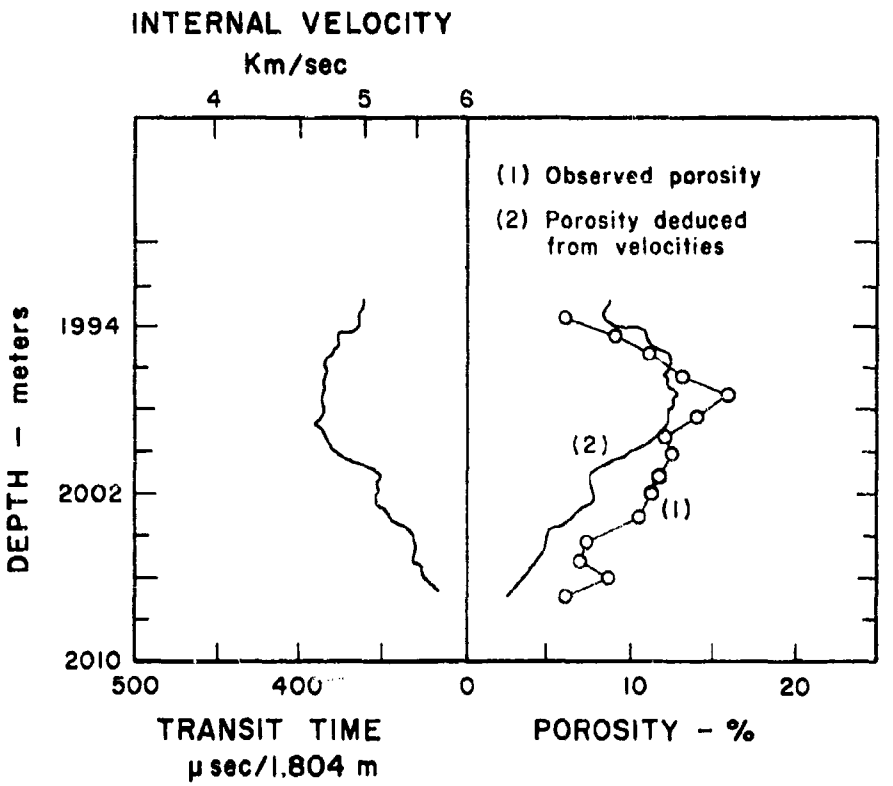


Figure 1.20. Comparison between measured porosity and porosity deduced from the value of measure velocity and the experimental average curve of Figure 1.19. (36)

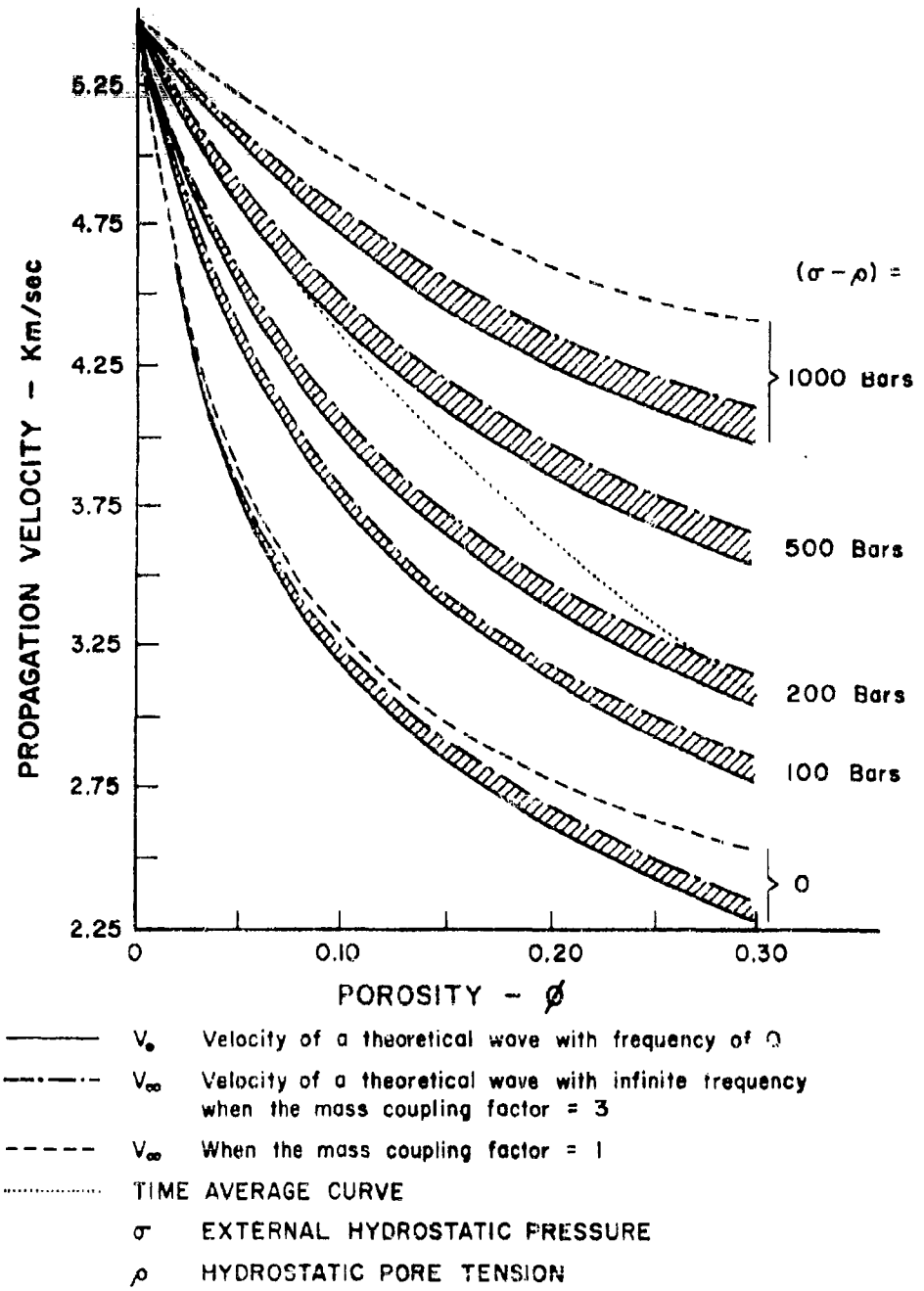


Figure 1.21. Longitudinal velocity as function of porosity in sandstone for different value of σ-ρ. (38)

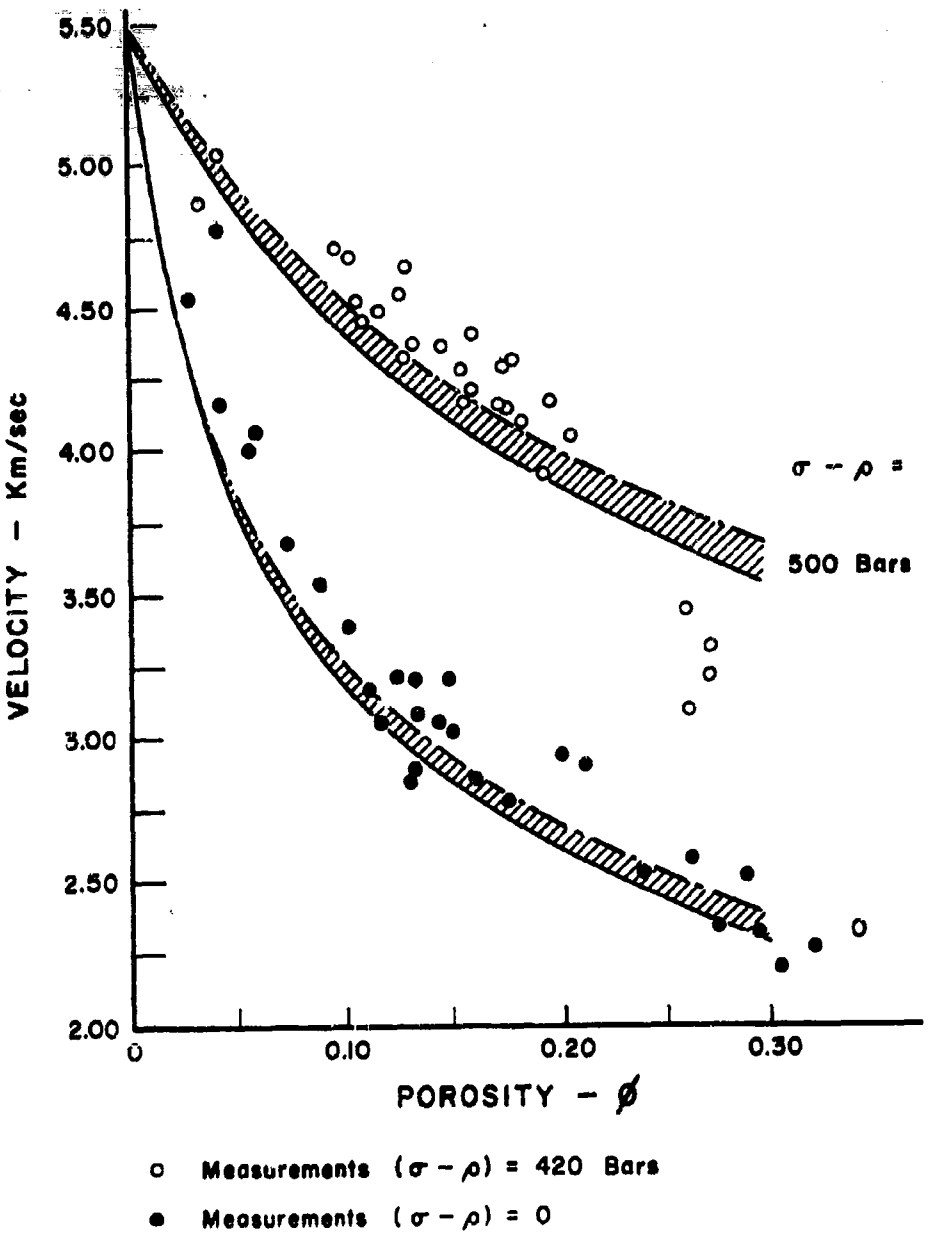


Figure 1.22. Longitudinal velocity vs. porosity. Comparison between results given by Biot's theory and experimental results for sandstone. (38)

Rock	Anisotropy Factor	Reference
Austin chalk	1.17	31
Homogeneous anhydrite	1.16	40
Anhydrite with intercalated limestones	1.12 to 1.14	40
Limestone	1.08 to 1.10	40
Arbuke limestone	1.3	36
Salt	no anisotropy	40
Sandstone	no anisotropy	40
Eagle Ford shale	1.33	36
Pierre shale (Limon, Colo.)	1.18	36
Pierre shale (Last Chance, Colo.)	1.14	36
Cambridge slate	1.07	31
Lorraine shale	1.4	31
Gneiss, Hell Gate, N.Y.	1.2	28
Micaschist, Woodsville, Vt.	1.36	28
Granodiorite gneiss, Bethlehem, N.H.	1.33	28
Gneiss, Pelham, Mass.	1.27	28

Rock Texture and Velocity. The relation of rock texture to velocity has been investigated, but limited largely to porosity studies described above. Birch[41] has indicated a possible relationship of average velocity in rock with the velocities of the mineral components. It is assumed that over a path L, reasonably long compared to the mean crystal diameter, that a pulse traverses each mineral in ratio to its proportion by volume in the rock. Thus the travel time is:

$$T = \frac{L}{V} = \frac{Lx_1}{V_1} + \frac{Lx_2}{V_2} + \ldots + \frac{Lx_i}{V_i} \qquad (1.10)$$

where:

T = travel time
L = path length
V = velocity in rock
$V_1, V_2 .. V_i$ = velocities in minerals 1, 2, ...i
$x_1, x_2 = x_i$ proportion by volume of minerals 1, 2, ...i

The velocity is then expressed by:

$$V = \frac{1}{\sum \frac{x_i}{V_i}} \qquad (1.11)$$

This development takes into account only the composition of the rock and gives satisfactory results at high pressure. It does not account for such factors as grain size, or preferred orientation of crystals which may be significant.

The importance of the rock texture is illustrated[31] (Figure 1.23) in its effect on pulses in a sample of Pittsford marble under uniaxial pressure. A first arrival of a wave with a very gradual rise time was observed, followed by a much sharper wave of higher energy. It was

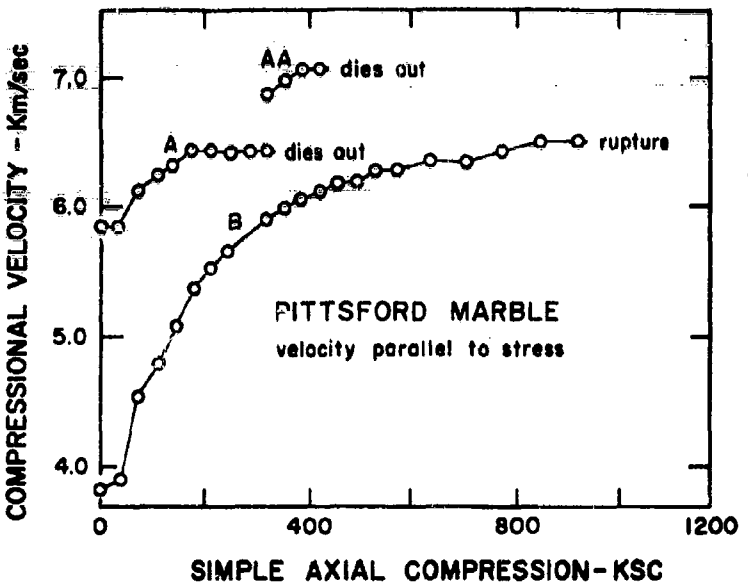


Figure 1.23. Slow and fast arrival pulses for Pittsford marble. (31)

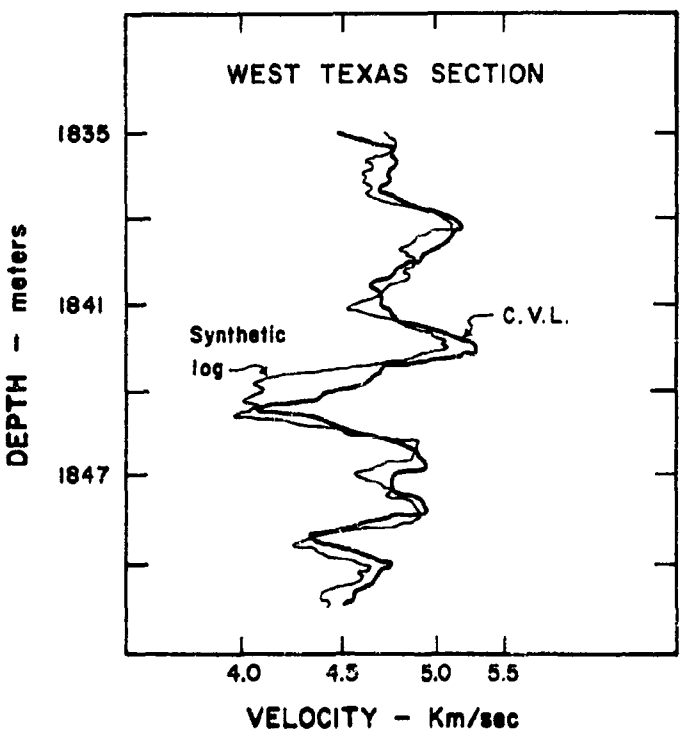


Figure 1.24. Comparison of field continuous velocity log with synthetic laboratory log. (36)

assumed that the fast wave was transmitted via a gross elastic structure inherited from the parent limestone, while the speed of the slower, large energy wave was due to the fine grains of the marble. If this explanation is valid, the rock texture is of ultimate importance in both velocity and energy effects.

Field and Laboratory Measurements. The apparent discrepancies between field and laboratory measurements arise principally from differences in environmental conditions in the field and in the laboratory as well as size and shape of specimen. Some effects of environment have been demonstrated by Wyllie[41], who measured the velocities in well cores and compared them with the velocities obtained *in situ* by a continuous velocity log. An *in situ* environment was similated by subjecting the samples to a uniaxial pressure and saturating them with brine which had the same velocity as the drill mud (Figure 1.24).

Correlation of Physical Properties.

Judd[42] has devised a statistical approach for correlating physical properties of rocks in which geological considerations were minimized and the analysis was based upon a comparison of fourteen physical properties of rocks: apparent specific gravity, percent porosity, shore hardness, abrasive hardness, specific damping capacity, moduli of rigidity and rupture, static and dynamic moduli of elasticity, compressive strength, impact toughness, longitudinal velocity of sonic wave propagation, tensile strength, and Poisson's ratio. Tensile strength was not included because of a lack of data, as well as the results of laboratory triaxial load tests because of a lack of standardization of the test methods used, and the results did not lend themselves easily to statistical analysis. Poisson's ratio data were also omitted because values were mathematically obtained from the other properties studied.

Judd's studies were prompted by the lack of usable quantitative values for rock properties needed in the proper design of foundations and tunnels. Secondly, discrepancies are usually found between geophysical measurement of rock properties and those obtained by static test methods. For example, Young's modulus measured by sonic wave propagation through laboratory specimens or by similar but *in situ* tests of rock is not in agreement with that obtained by static load tests in the field or laboratory (Figure 1.25). This presents a problem in the design of an arch dam where Young's modulus of elasticity for the rocks against which the dam abuts must be known, i.e., whether the value obtained by geophysical methods is the same Young's modulus required in dam design formulae. An almost instantaneous stress applied by an explosive generated wave (used in geophysical field tests) does not cause the rock to react similarly to the slowly applied static load (such as the thrust of the arch of the dam on rock abutments). This conclusion is supported by results (Figure 1.26) obtained from concrete cylinders tested with varying static load rates. The dependency of elastic parameter values upon the method of testing assumes vital importance in design of conventional civil engineering structures, and is equally important in the design of underground protective installations where such parameters are involved.

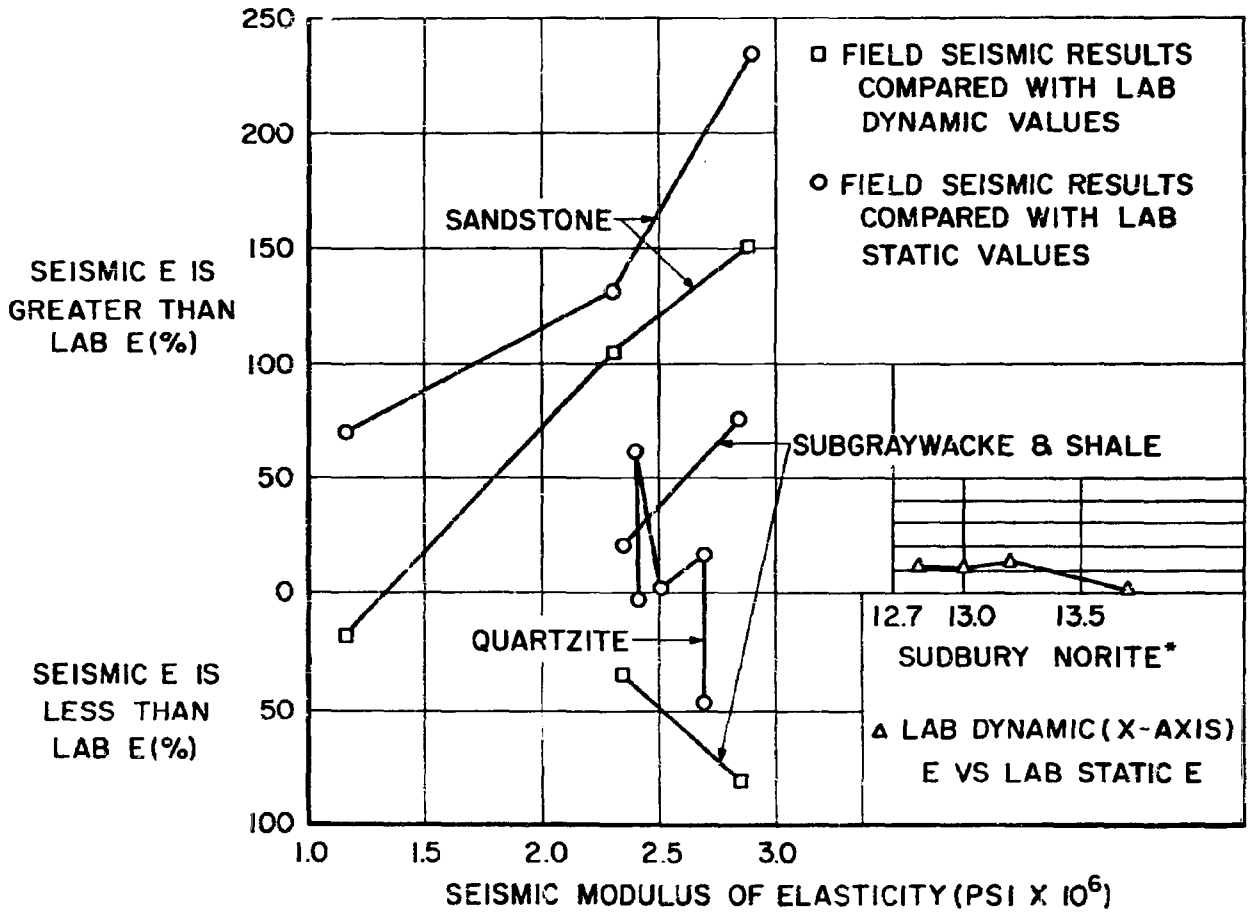


Figure 1.25. Comparison between laboratory and field values of Young's modulus. (42)

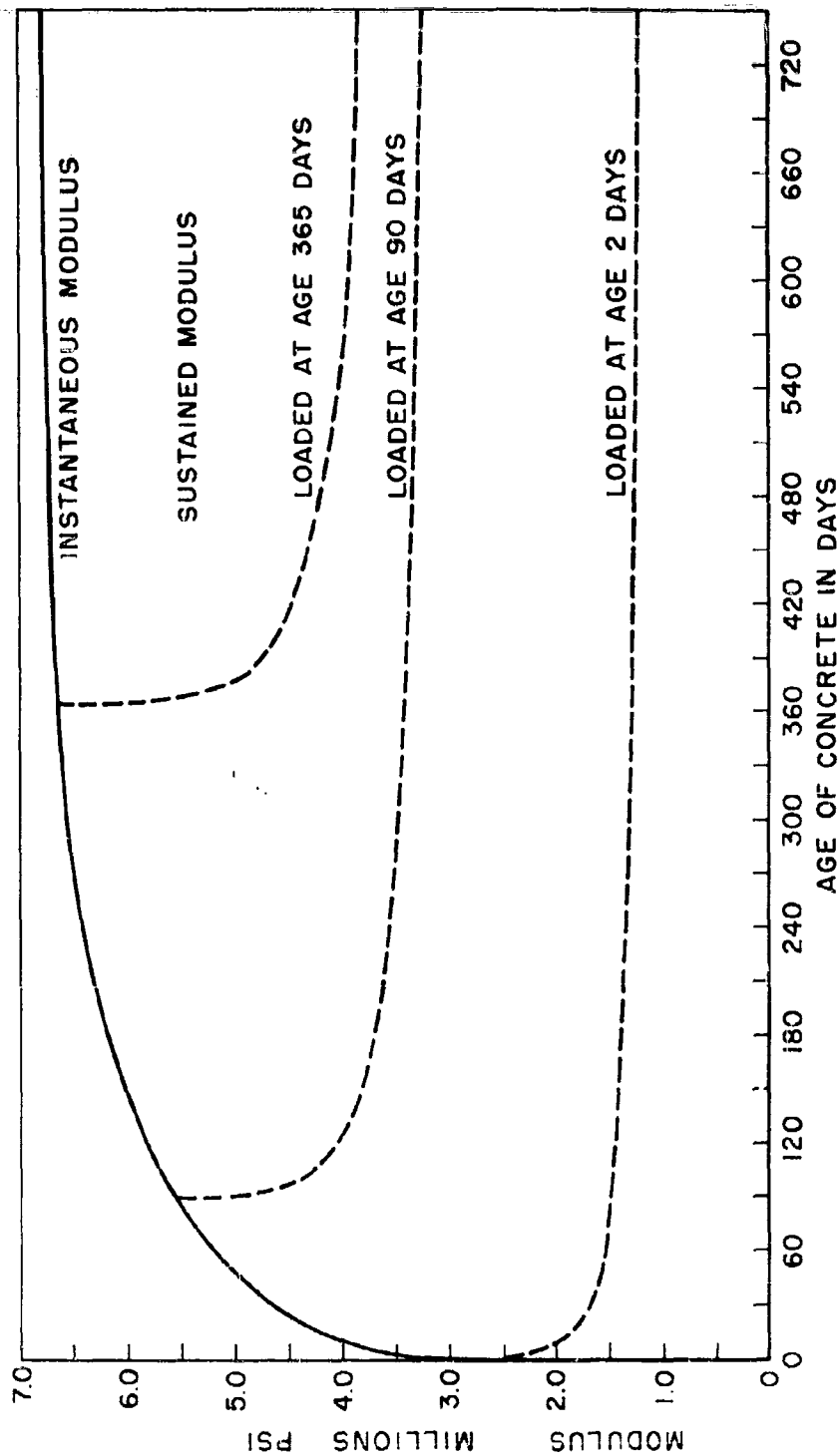


Figure 1.26. Instantaneous and sustained modulus of elasticity of concrete. (42)

Judd states that the unqualified acceptance of currently available geophysical data on elastic properties necessary in engineering design is inadvisable because of the questionable validity of the assumptions used to derive the basic formula for geophysical measurements of Young's modulus. Theoretically, this is valid if the transmitting medium is assumed to be homogeneous, isotropic, elastic and of infinite extent. However, experience has shown that these assumptions generally are invalid when applied to rock.

Also, it is questionable whether rock will act elastically at great depths or in areas of high residual tectonic stresses. At relatively shallow depths, the formula might be adapted to a rock medium if a presently unknown "X" adjustment factor was introduced. A statistical study was designed to determine whether such analysis of thousands of sets of data on physical properties of rocks could provide such a factor.

At present, competent engineering design procedures require comprehensive and costly preliminary testing whose results leave enough doubt to require the use of large safety factors. Statistical studies might be used to reduce the number of tests now necessary to evaluate rock reactions under engineering loads. Thus, if dependable correlative factors exist, the results of the relatively simple and economical determinations of apparent specific gravity, porosity, or compressive strength could be used to calculate the values of the elastic moduli. Such tests might also be used in computations to determine effects of nuclear weapons from H.E. tests.

Judd's approach was by means of linear regression on the IBM 7090 with results plotted by the Johnniac. The fourteen variables were compared with each other by pairs and then in increasing combinations; there was no experience to indicate if any one of the variables could be considered as completely independent or dependent of the others.

The data most nearly satisfying the necessary criteria of homogeneity of preparation were those of the U.S. Bureau of Mines and contained in the following references: 37, 43, 44, 45 and 46.

Another advantage of these data was the detailed petrographic descriptions supplied. Initially, however, no attempt was made to correlate on the basis of rock names because of a lack of petrographic standards for such descriptions. If in its further development the statistical approach proves sufficiently successful to be used on data from other sources, it would not be necessary to depend upon petrographic descriptions. However, a plot of rock descriptions against Young's modulus values obtained by static load tests was inconclusive as can be seen on Figure 1.27. However, in a plot of some results as cumulative percentages, sufficient discernable trends develop (Figure 1.28) to warrant further future study. (For details of computer programming see Judd's paper).

The x-y plots or scattergrams of pairs of data were visually compared permitting a rough match of as many as 4 pairs of data (Figure 1.29) even though all ordinates were not of the same magnitude. Some of the plots, indicating apparently definite linear relationships were discarded because the x-values were derived from the y-values.

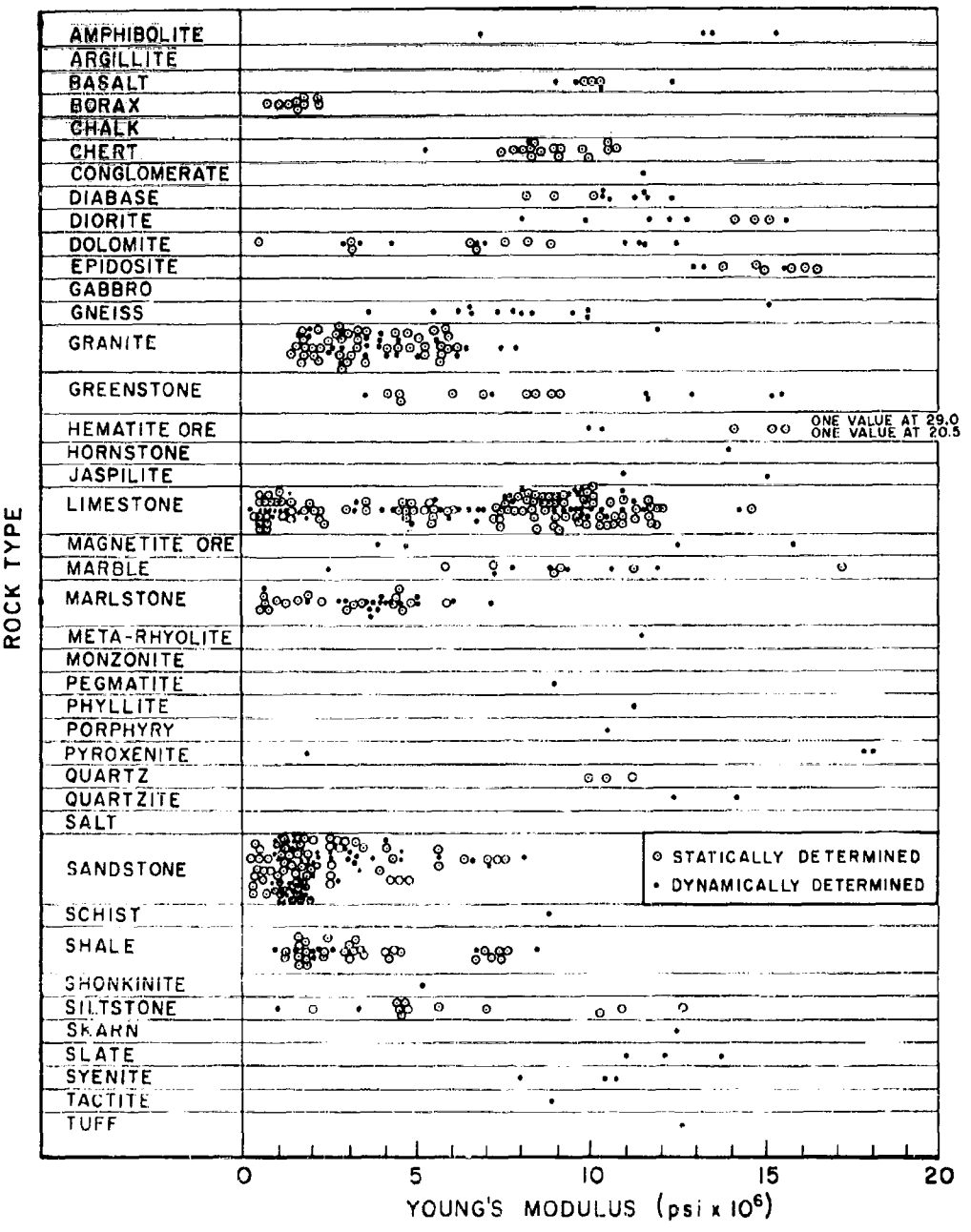


Figure 1.27. Relationship between rock type and Young's modulus. (42)

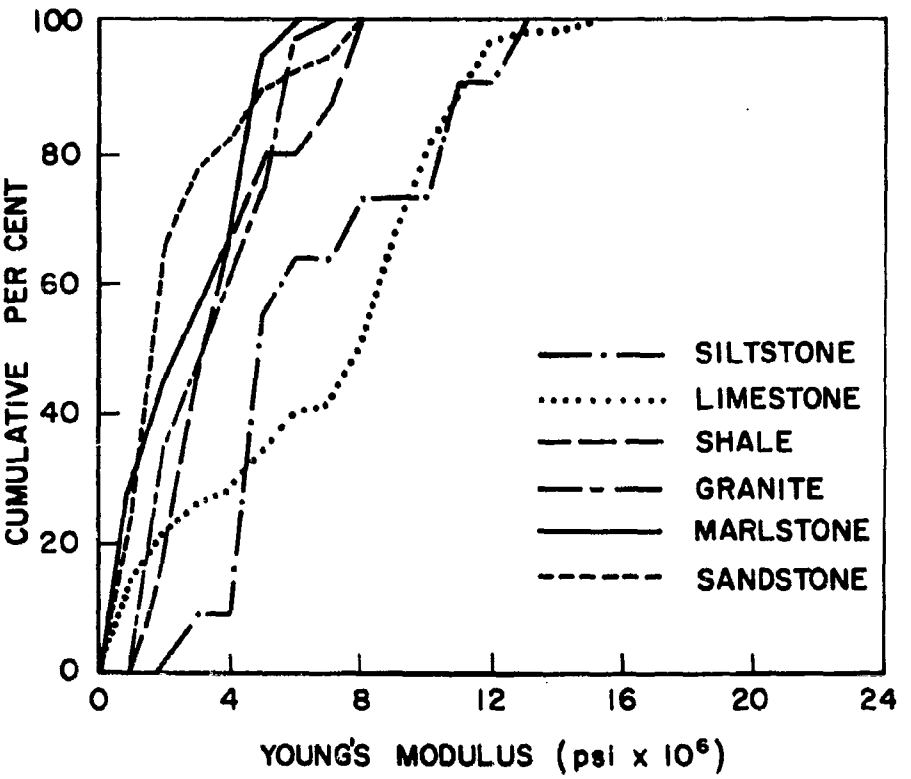


Figure 1.28. Relationship between certain rock types and statically determined values of Young's modulus. (42)

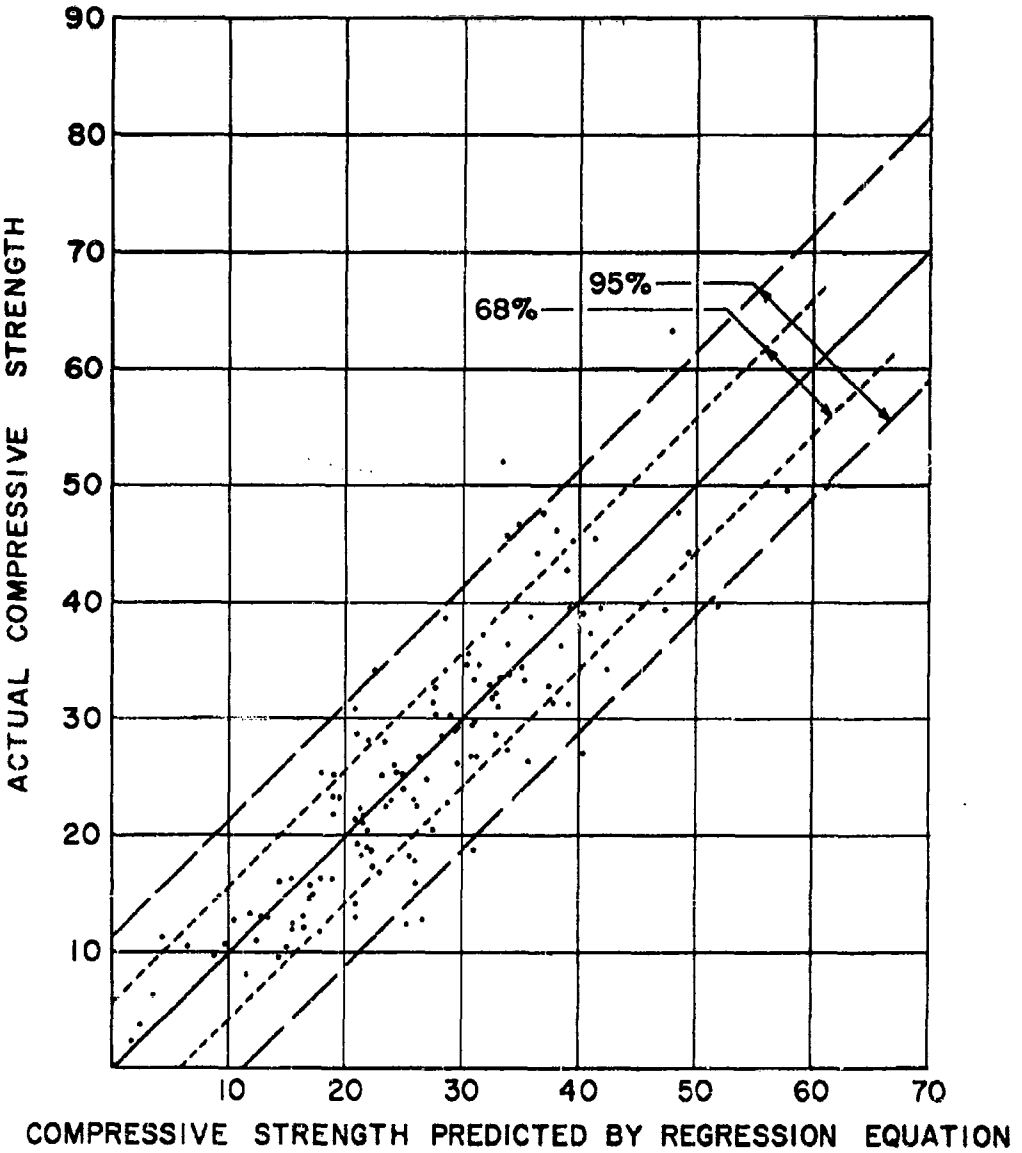


Figure 1.29. Relationship of actual to predicted compressive strength. (42)

Judd's analysis of mathematical dependency led to consideration of two categories or species (A and B) of properties. By logical reasoning it would appear that certain rock properties were related, whereas others should be completely unrelated. For example, one species A might be considered as impact toughness, scleroscope hardness, rigidity, rupture, and compressive strength, and all of these appear to provide a measure of the inherent strength of a rock and thus would depend upon the resistance of the "fibers" in the rock to the same methods of destruction when tested. Specific gravity and porosity, or longitudinal wave velocity and specific damping capacity were assumed to measure completely different rock characteristics and thus might be regarded as a second species B. Thus, it does not seem logical that species A could be linearly correlated with B, but there might exist linear correlations within one species.

However, as shown in Figure 1.30, some individual plots in one category have a distribution somewhat similar to those in the other. For example, longitudinal velocity versus impact toughness yields a distribution similar to shore hardness plotted against modulus of rupture or impact toughness. Comparable anomalies also appear in Figure 1.30k where specific damping capacity distributes similarly to some of the opposite specie values; and in Figure 1.30d rigidity and Young's modulus compare to the dissimilar characteristic of specific gravity. The similarity in distributions between dissimilar rock characteristics is a hopeful indication that correlations can be obtained, although apparently not necessarily by linear regression analysis.

The computer was asked to find which properties were most related and compressive strength was compared with all of the other properties, first in all possible combinations of two, then three, and finally eight variables. On a purely linear basis, the best relationship was between compressive strength and the combination of impact toughness, scleroscope hardness, and modulus of rigidity (note that all of these are A values). This computation resulted in Equation 1.12.

$$y = 0.672\ X_4 + 0.288\ X_5 + 2.878\ X_7 - 4.477 \qquad (1.12)$$

As can be seen in Figure 1.29, however, the deviation is too large for practical application. A least squares relationship has the disadvantage that undesirable weight is given to extreme values. Thus, the constant deviation shown in Figure 1.30, while acceptable at the middle and upper ranges, is valueless for low values of compressive strength. To avoid this in future studies, it is possible to weight data lines with low values of compressive strength. These conclusions further indicate that a more useful relationship may be curvilinear.

The best indications of linearity of results are in the scattergrams of Figure 1.31 which demonstrates that the dynamic modulus of elasticity varies directly as the static modulus of elasticity when both are obtained by laboratory methods. However, it is recommended additional data from other sources should be tested for final proof of this correlation.

On the basis of his somewhat limited study, Judd came to the following general conclusions:

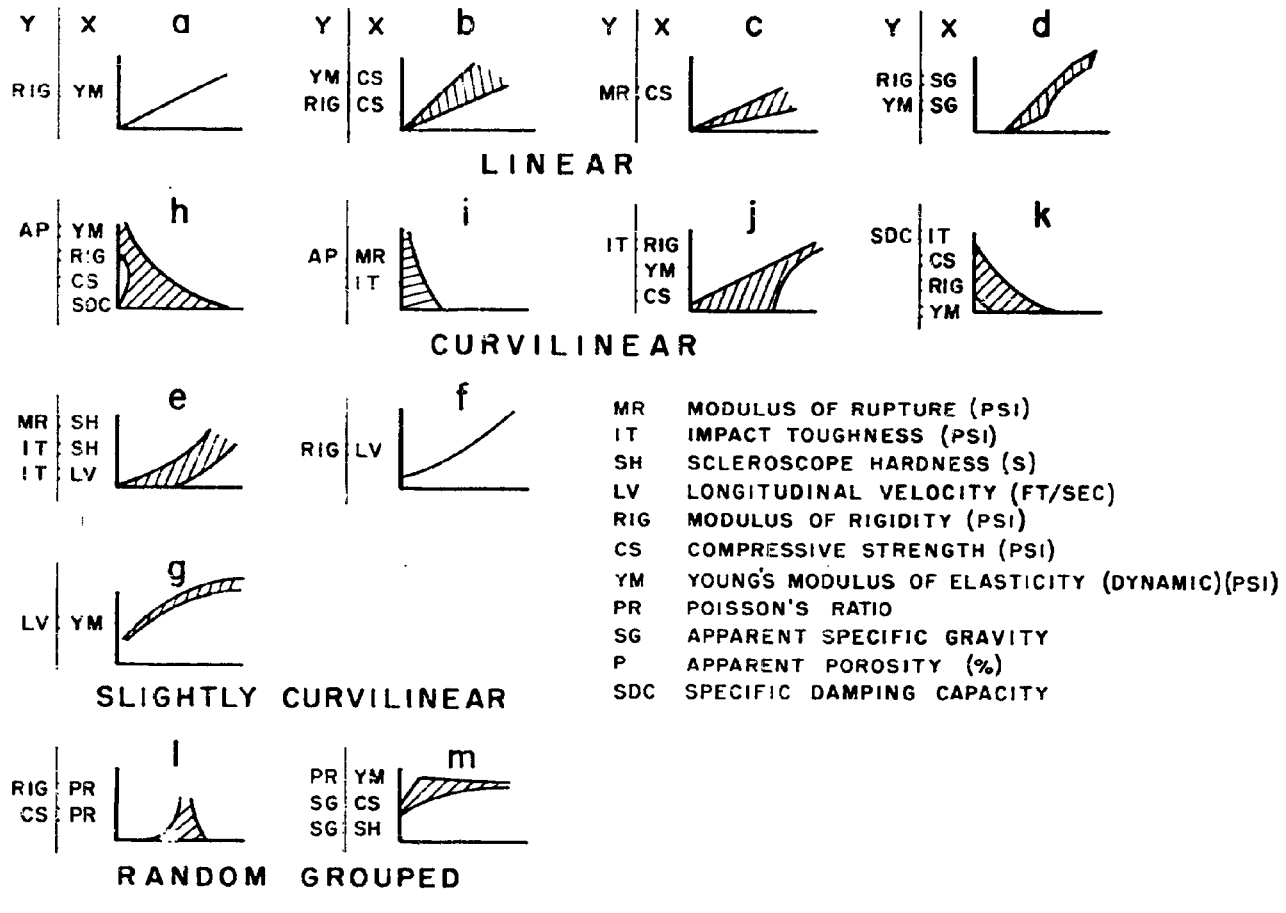


Figure 1.30. Sketches of comparative scattergrams. (42)

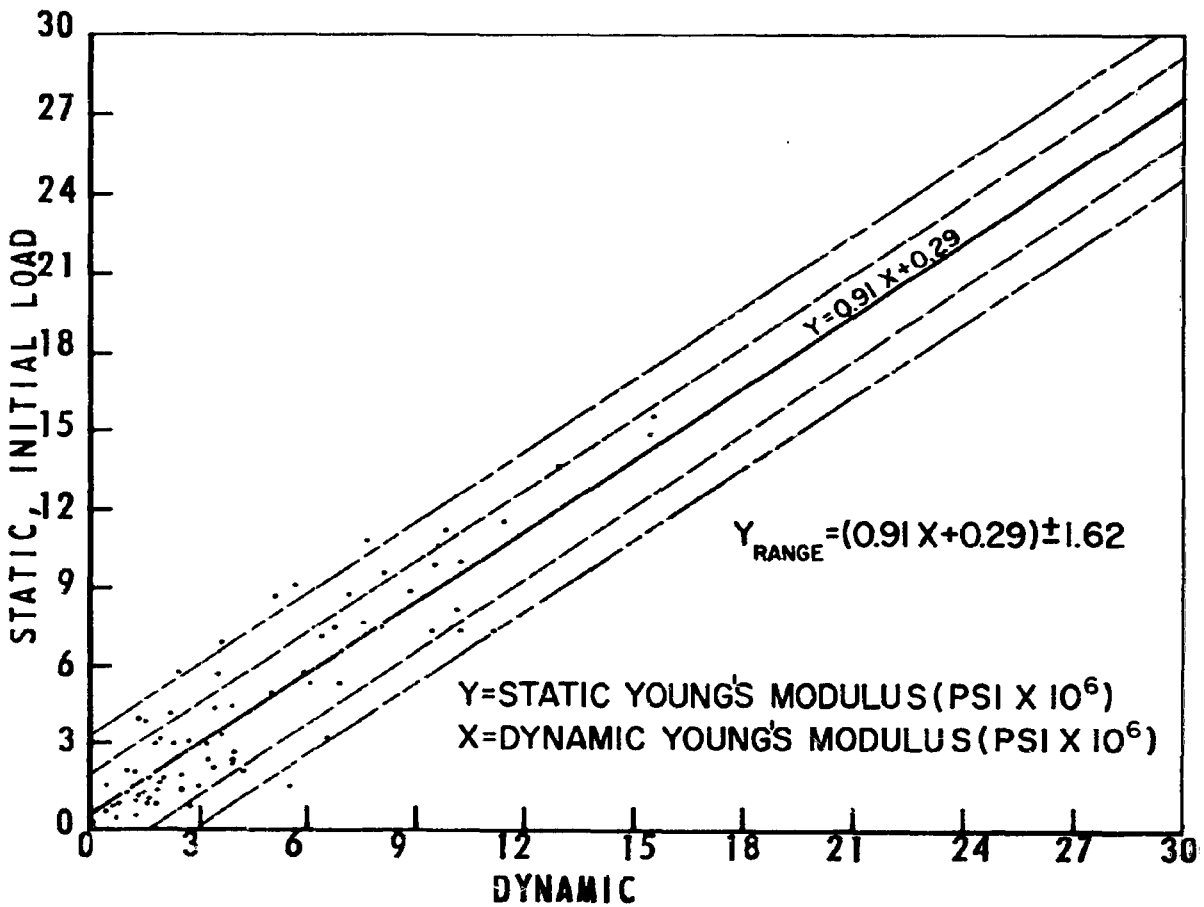


Figure 1.31. Correlation between dynamic and static E. (Laboratory determination). (42)

1. There appears to be a direct linear relationship between modulus of rigidity and Young's modulus, between compressive strength and Young's modulus, modulus of rigidity and modulus of rupture, and between the laboratory values of the static and dynamic moduli of elasticity.

2. There is also a direct curvilinear relationship between modulus of rupture and impact toughness with scleroscope hardness and longitudinal velocity.

3. Specific damping capacity possesses an inverse curvilinear relationship with impact toughness, compressive strength, modulus of rigidity and Young's modulus.

4. A direct slightly curvilinear relationship between specific gravity and modulus of rigidity and Young's modulus, and between modulus of rigidity and longitudinal velocity is indicated.

5. Other comparisons indicate possible trends but additional data will be required for more complete definition.

Finally, Judd concludes that there is increasingly overwhelming statistical evidence that prediction of rock properties cannot be based entirely on existing and conventional theories of elasticity. Further, statistical methods show definite promise of ultimately providing engineers and geologists with equations to predict rock properties within a relatively narrow and, thus, useful range.

CHAPTER I

REFERENCES

1. Nadai, A., Theory of Flow and Fracture of Solids, McGraw-Hill, 1950.

2. Eirich, F.R., Rheology Theory and Applications, vol. I, Academic Press, Inc. 1956, New York.

3. Spaulding, Jack, Deep Mining, Mining Publications, Ltd., London, 1949.

4. Isaacson, E. de St. Q , Rock Pressure in Mines, Mining Publications, Ltd., London, 1958.

5. Bureau of Reclamation, Physical Properties of Some Typical Foundation Rocks, Engineering Laboratories Branch, Concrete Laboratory Report No. SP-39.

6. Warner, Stanley E., and Violet, Charles E., Properties of the Environment of Underground Nuclear Detonations at the Nevada Test Site, Rainier Event, Lawrence Radiation Laboratory, University of California, UCRL 5542, Rev., April 1959.

7. Birch, F., Handbook of Physical Constants, Section 5, G.S.A. Spec. Paper No. 36.

8. Nicholls, H.R., In Situ Determination of Dynamic Elastic Constants of Rock. In. Symp. on Mining Research, Mo. School of Mines, Feb. 1961.

9. Zisman, W.A., Comparison of the Statically and Seismologically Determined Elastic Constants of Rocks. Nat. Acad. Sci. Proc., Vol. 19, pp. 680-686.

10. Ide, J.M., Comparison of Statically and Dynamically Determined Young's Modulus of Rocks. Nat. Acad. Sci. Proc., Vol. 22, pp. 81-92.

11. U.S. Bureau of Reclamation, Effect of Cracks in Concrete upon Dynamic Measurements of Elastic Modulus. Materials Lab. Report No. C-383, 1948.

12. Dvorak, A., Field Test of Rocks on Dam Sites. Proc. Fourth Intl. Conf. on Soil Mech. and Found. Eng., Vol. 1. Butterworths.

13. Rinehart, J.S., Propagation Velocity of Longitudinal Waves in Rocks, Effect of State of Stress, Stress Level of the Wave, Water Content, Porosity, Temperature, Stratification and Texture. Colo. School of Mines Res. Found. Report, Jan. 1961.

14. U.S. Bureau of Reclamation, Physical Properties of Some Typical Foundation Rocks. Concrete Lab. Report No. SP-39, 1953.

REFERENCES (Continued)

15. Bruckshaw, J.M., and Mahanta, P.C., The Variation of the Elastic Constants of Rock with Frequency. Petroleum. Vol. 17, No. 1.

16. Birch, F. and Bancroft, D., Elasticity and Internal Friction in a Long Column of Granite. Seis. Soc. America Bull., Vol. 28, 1938.

17. Philips, D.W., Tectonics of Mining. Sheffield Mining Magazine, 1948, p. 47.

18. Griggs, D., Creep of Rocks, Journal of Geology, Vol. 47, April-May 1939, p. 225.

19. Kessler, D.W., and Sligh, W.H., Physical Properties of the Principal Limestones Used for Building Construction in the United States, U.S. Bureau of Standards Tech. Paper 349, 1927.

20. Gutenberg, B., Internal Constitution of the Earth, McGraw-Hill, 1939.

21. Rove, Olaf N., Some Physical Characteristics of Certain Favorable and Unfavorable Ore Horizons, Econ. Geol., Vol. 42, 1947, p. 57, 161.

22. Griggs, D.T., and Bill, J.F., Experiments Bearing on the Orientation of Quartz in Deformed Rocks, Bull. Geol. Soc. Amer., Vol. 49, 1938, p. 1723.

23. Griggs, D.T., Deformation of Rocks under High Confining Pressures, Jl. of Geology, Vol. 44, July-Aug., 1936, p. 541-547.

24. Wright, F.D., and Bucky, P.H., Determination of Room and Pillar Dimensions for the Oil Shale Mine at Rifle, Colo., Trans. A.I.M.E., Vol. 8, p. 352.

25. Sipprelli, E.M., and Teichman, H.L., Roof Studies and Mine Structure Stress Analysis, Bureau of Mines Oil-Shale Mine, Rifle, Colorado.

26. Billings, M.P., Structural Geology. Prentice-Hall, 1947.

27. Loofbourow, R.L., Design of Underground Mines. Paper presented at A.I.M.E. meeting, St. Louis, Feb. 1951.

28. Birch, F., Velocity of Compressional Waves in Rocks at 10 Kilobars. Jl. Geoph. Res., Vol. 65, 1960.

29. Birch, F., Handbook of Physical Constants, Geol. Soc. America Sp. Paper 36.

30. Jakosky, J.J., Exploration Geophysics. Times Mirror Press, 1950.

31. Toucher, D., Anisotropy in Rocks under Simple Compression. Am. Geoph. Union Trans., Vol. 38, 1957.

REFERENCES (Continued)

32. Wyllie, M.R.J., et al., Elastic Wave Velocities in Heterogeneous and Porous Media, Geophysics, Vol. 21., 1956.

33. Wyllie, M.R.J., An Experimental Investigation of Factors Affecting Elastic Wave Velocities in Porous Media, Geophysics, Vol. 23, 1958.

34. Hicks, W.G., and Berry, J.E., Application of Continuous Velocity Logs to Determination of Fluid Saturation of Reservoir Rocks, Geophysics, Vol. 21, 1956.

35. Hughs, D.S., Elastic Wave Velocities of Sedimentary Rocks, Am. Geoph. Union, Vol. 32, 1951.

36. Uhrig, L.F., and Van Melle, F.A., Velocity Anisotropy in Stratified Media, Geophysics, Vol. 20, 1955.

37. Obert, L., et al., Standardized Tests for Determining the Physical Properties of Mine Rock, Bur. of Mines RI 3891, 1946.

38. Geertsma, J., Velocity Log Interpretation; Effect of Rock Bulk Compressibility, Soc. of Petr. Engr., Paper No. 1535-G, Oct. 1960.

39. Paterson, N.R., Seismic Wave Propagation in Porous Granular Media, Geophysics, Vol. 21, 1956.

40. Dunoyer de Segonzac, Ph., and Laherrere, J., Application of the Continuous Velocity Log to Anisotropy Measurements in Northern Sahara, Results and Consequences, Geoph. Prosp., Vol. 7, 1959.

41. Birch, F., Elasticity of Igneous Rocks at High Temperatures and Pressures, Bull. Geol. Soc. Am., Vol. 54, 1943.

42. Judd, W.R., and Huber, C., Correlation of Rock Properties by Statistical Methods, Int. Symp. on Mining Research, Mo. School of Mines, 1961.

43. Windes, S.L., Physical Properties of Mine Rocks, USBM RI 4459, 1959.

44. Windes, S.L., Physical Properties of Mine Rock, Part II, USBM RI 4727, 1950.

45. Blair, B.E., Physical Properties of Mine Rock, Part III, USBM RI 5130, 1955.

46. Blair, B.E., Physical Properties of Mine Rock, Part IV, USBM RI 5244, 1956.

CHAPTER II

STRUCTURAL ENGINEERING GEOLOGY

Introduction

The extreme variability of the physical character of the earth materials in which it is necessary to construct protective installations is the source of many of the major problems in their design. The soils in the mantle of the earth vary in their physical character as do the underlying rocks. Soil characteristics and soil mechanics will be dealt with only briefly in this study, however, insofar as their properties affect the response of underlying rock masses to static and impact loads to which both are subjected. The features of rocks of importance in the design of underground openings are those which are usually dealt with in studies of physical properties of rock (Chapter I) and in engineering structural geology with which this chapter is concerned.

In the construction of a building an engineer may choose the materials which will compose the final structure. On the other extreme a mining engineer has very little choice in the location of mine openings and the materials in which he must construct them. The ore must be excavated from the position where natural processes have placed it. The choice of a site and consequent earth material environment for an underground protective installation is not so restricted as a mining project, but regardless of the choice of site a wide variety of conditions may be encountered. In addition to the physical properties of solid rock, it is necessary to evaluate the overall rock mass as structural material to minimize the problems of engineering design.

Geological Engineering Structures

Structural elements of importance in the stability of *in situ* rock structures are folds, fractures, faults, bedding planes, joints, sheeting, secondary foliation and lineation, unconformities, contacts, igneous intrusions, dikes, sills, and surface flows. Superimposed on these are the effects of chemical alteration which may be a result of weathering, subsurface water flow, hot solutions, heat or deformation, a combination of these agents; or healing and strengthening (by silicification for example).

Folds[1]

Folds are wave-like structures in rock and are best exhibited in stratified formations, such as sedimentary or volcanic rocks, their metamorphic equivalents, or any layered rock, such as banded gabbro. They vary from inches to miles in lateral, longitudinal, and vertical

dimensions. Folds which are convex downward are termed synclines, upward are anticlines; they may be inclines, overturned, be in multiple or single form and also may develop into overthrusts or other complex structures. Various types of folds are illustrated in Figures 2.1 to 2.2. It has been observed that most folding is disharmonic, i.e., that the form of the fold is not uniform throughout the stratigraphic column in which it occurs.

Folds are not always readily recognizable from surface evidence. Their occurrence, dimensions, and other features can be determined in many cases only after careful geologic mapping both of surface outcrops and underground structure exposed by drilling or excavation. In complex or eroded folds the sequence of beds is fixed by study of paleontology, ripple marks, drag folds or other geologic occurrences.

Four principle types of folding are recognized by geologists[1]: (1) flexure folding, (2) flow folding, (3) shear folding, and (4) folding due to vertical movements.

Flexure folding may hypothetically be caused by either lateral compressive forces or couples (Figure 2.3). When several beds are folded they may slip past one another and the beds change shape by plastic deformation. The relative competence of the beds determines the amount of flowage and fracture. Competent beds transmit forces over long distances and dominate the movement of less competent associated beds. Fractures may heal, depending on the type of rock.

Flow folding is believed to exist when competent beds are absent and all rocks are plastic because of their physical properties, high temperatures or high confining pressures. Individual strata may not transmit forces over great distances, and minor folds may be more abundant.

Shear folding or slip folding is described as that resulting from minute displacements along closely spaced fractures. This is illustrated in Figures 2.4 and 2.5. The small fractures accompanying this process may be eliminated later by recrystallization.

Folds due to vertical movement of underlying material may be created and this type of folding is classed as one type of flexure folding.

Folds are believed to be caused by: (1) horizontal compression, (2) horizontal couples, or (3) convection currents under the earth's crust; some are dome shaped due to (4) intrusion of igneous rock, (5) intrusion of rock salt, (6) differential compaction or (7) changes in chemical composition. Thus, if the forces which caused the formation of a fold were not relieved, residual stresses of considerable magnitude from this source could be expected in constituent rocks.

Folding, with its accompanying processes, would almost invariably create problems in the design of underground installations because it involves weakening of rock structures through the processes enumerated above, and may cause anomalous stress conditions to exist. Examples in underground openings are treated in Chapter III.

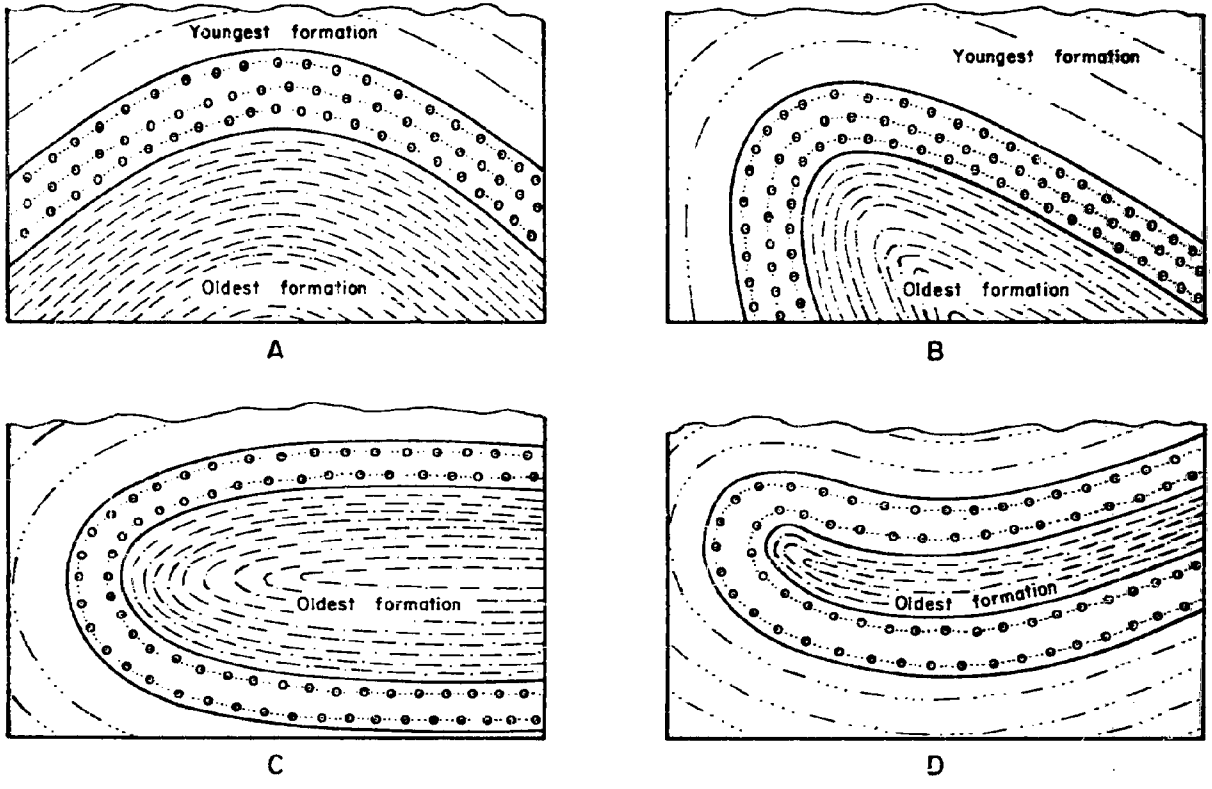


Figure 2.1. Types of anticlines[1].

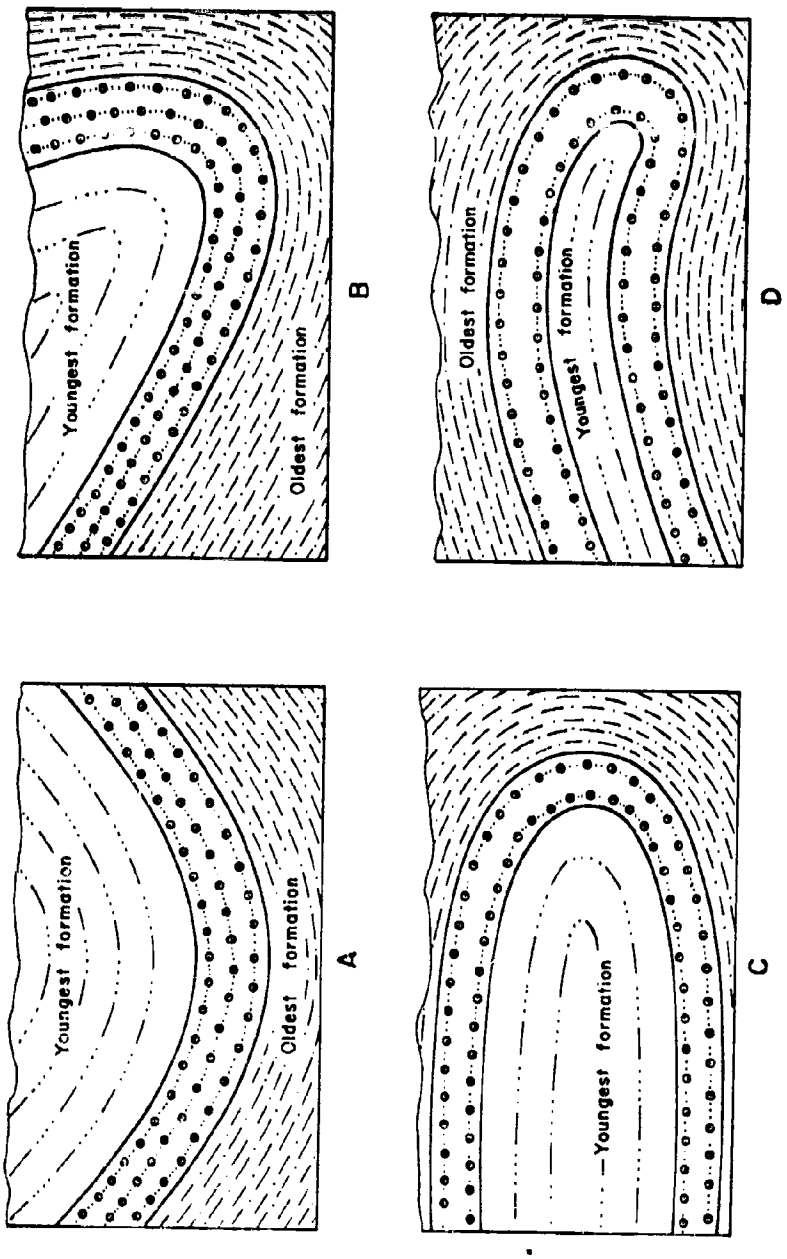


Figure 2.2. Types of synclines[1].

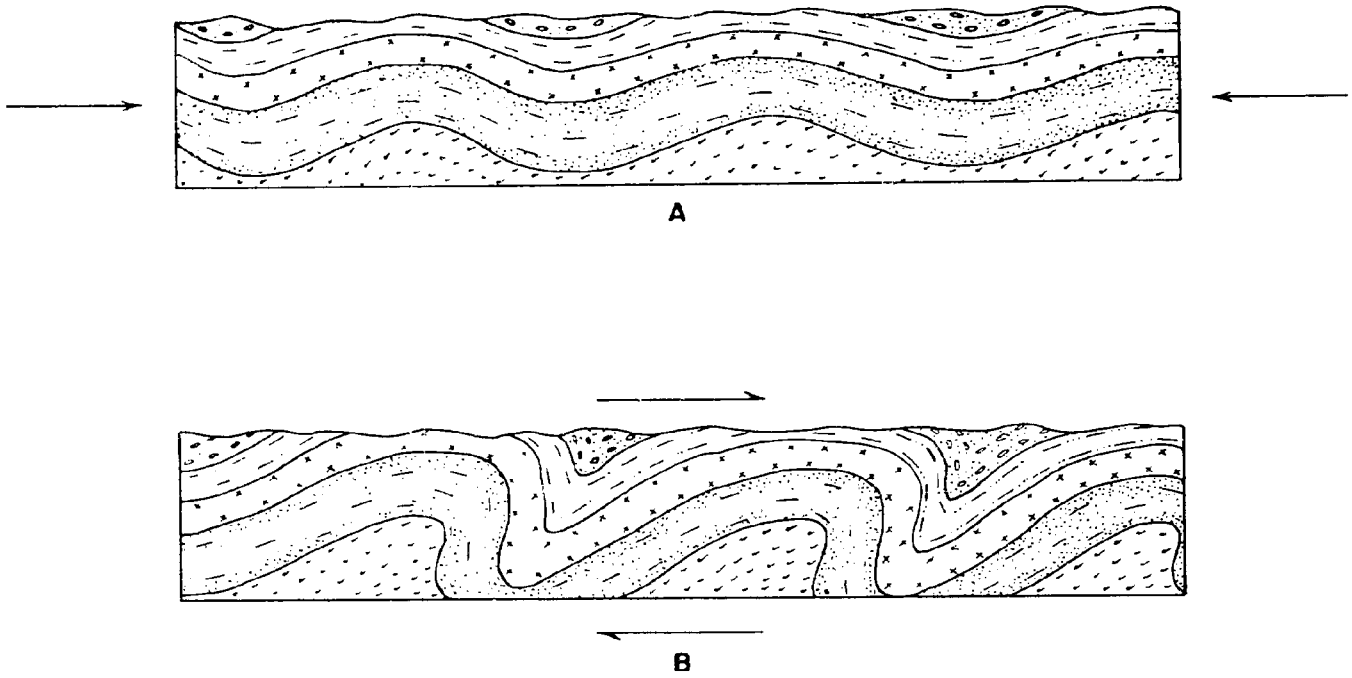


Figure 2.3. Flexure folding. A- Folds resulting from simple comparison. B- Folds developed by (1) a couple or (2) compression and a couple combined[1].

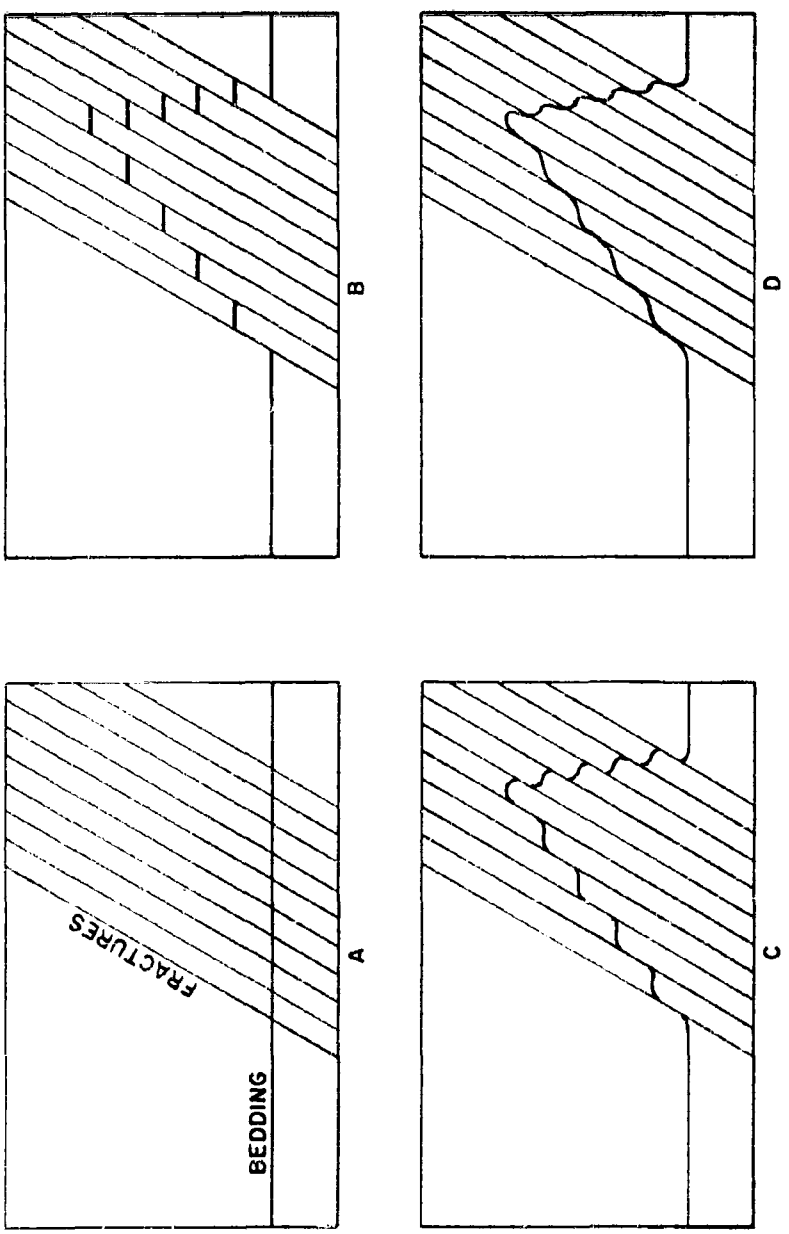
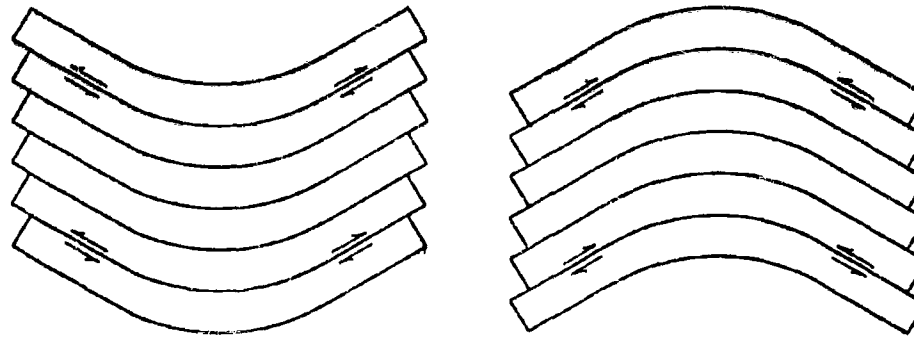


Figure 2.4. Shear folding before and during displacement along fractures[1].



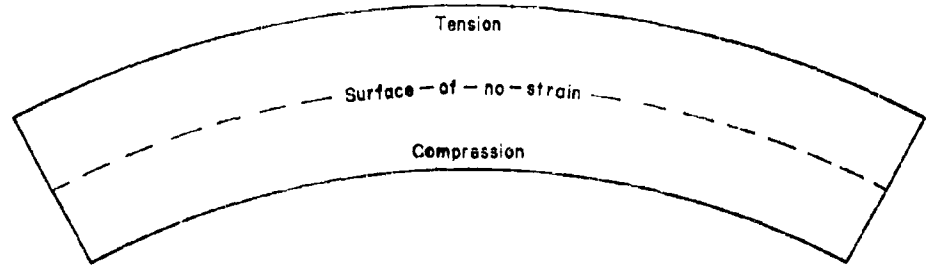


Figure 2.5. Regions of tension and shear in flexure folding[1].

All types of rock failure may be expected to be found in folds (Figure 2.6). Tension and shear stresses may be the dominant cause of failure, although crushing of porous rocks by compression may also be present. Such failure is expressed in rocks of the earth's crust by joints, faults, fractures, and some types of cleavage. Many fractures may subsequently be healed by physiochemical processes, or may be filled by veins or dikes.

Joints

Joints are defined as surfaces that divide rocks, along which there has been no visible movement parallel to the surface. Their strike and dip may be measured in the same manner as on faults. They vary in size from inches to hundreds of feet along both strike and dip. They never occur singly, and may be spaced only inches apart in which case they are called fracture cleavage. Joints may be classified either geometrically or genetically. Both classifications are useful in evaluating certain of the structural characteristics of rock segments or masses.

Strike joints are those parallel to the strike of bedding, schistosity, etc., dip joints are parallel to the dip while oblique joints lie between the other two (See Figure 2.7). In many rocks a large portion of the joints are parallel. Thus, a joint set consists of a group of more or less parallel joints, while a joint system consists of two or more joint sets with a characteristic pattern. Sets of joints which are perpendicular are referred to as a conjugate joint system. One method of portraying the intensity and attitude of joints is given in Figures 2.8 and 2.9. Strikes and dips for a given area are plotted in two semicircles, the intensity scaled along the radius for the given direction.

Another more precise method is to plot the poles of perpendiculars to the joints. All joints for a given area are assumed to be at the center of a hemisphere, the points where the perpendiculars intersect the surface of one half of the sphere are plotted. The equal area method, Figure 2.10 consists of plotting a line from the center of a circle normal to the strike of the joint with the dip scaled along the radius from the center where one degree of dip equals 1/90th of the radius. From this point diagram a contour sketch may be prepared to show the concentration of points. Most methods such as the above do not show the actual area or volumetric distribution of joints, their size or curvature.

Genetically, joints are classed as shear joints or tension joints. Often if the type of joint can be recognized it is possible to define the force which caused its formation. They are caused by tension, shear, shrinkage in volume and other processes of similar nature. They may occur in all types of rocks, but their best development occurs when a rock has a relatively homogeneous structure. Thus, even-grained rocks such as granite, syenite, basalt, limestone, shale and slate may be well jointed. Joints of various types may also occur in cooling magmas, and are very common in such masses as granite intrusions (Figure 2.11). As in the case of faults and other types of fractures, joints may serve as channels for mineralizing solutions. Where they occur in the wall rocks of mineral deposits they also furnish means of access for solutions for

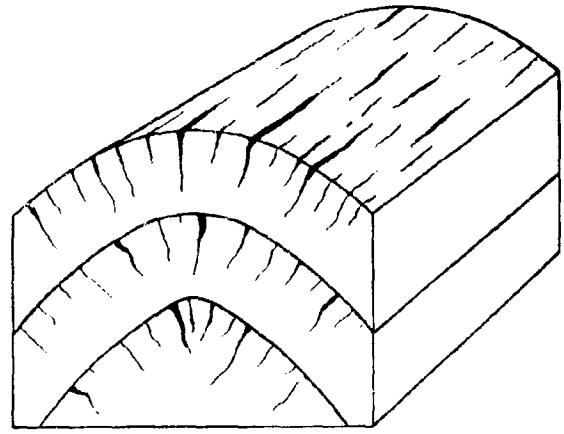


Figure 2.6. Simple fold showing tension joints.

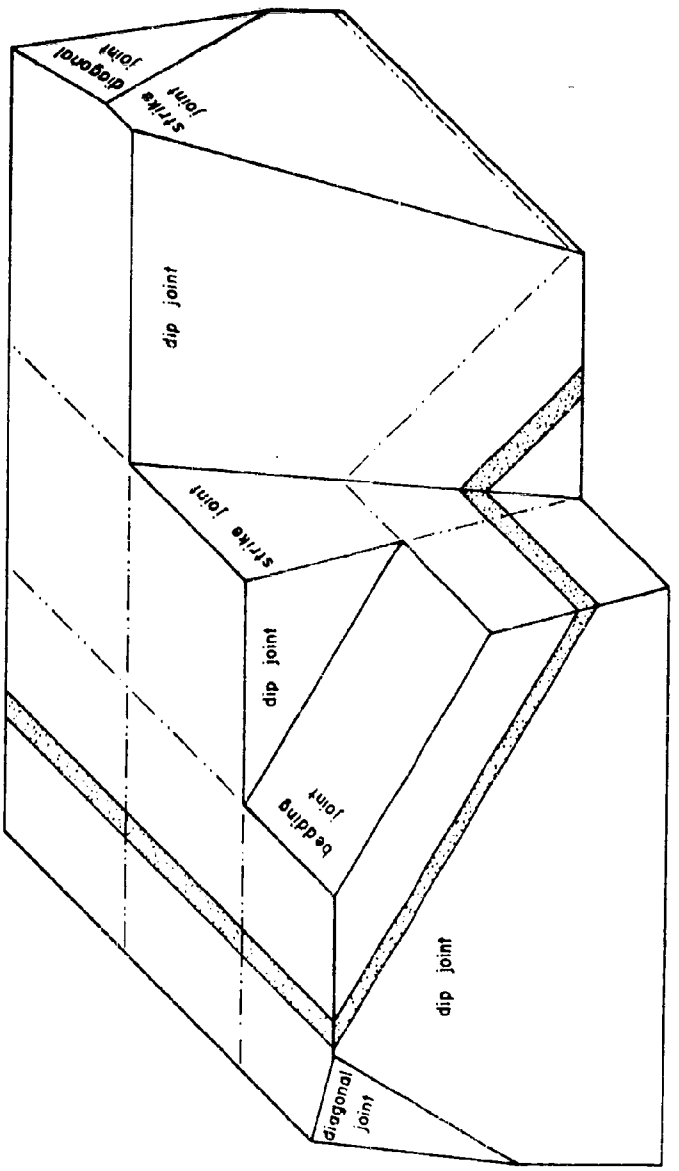


Figure 2.7. Geometric classification of joints[1].

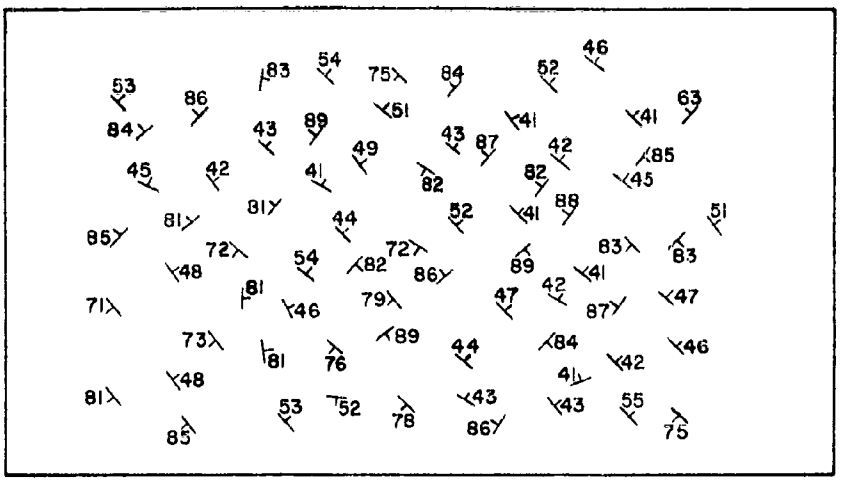


Figure 2.8. Joint map of a hypothetical area. Attitude of individual joints shown by dip-strike symbols[1].

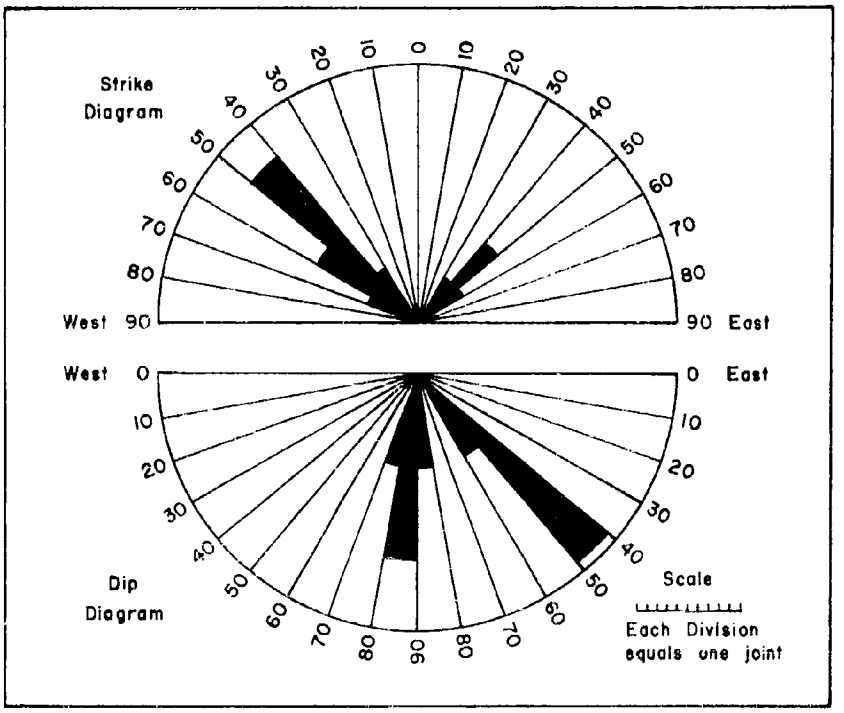


Figure 2.9. Joint diagrams of area shown in Figure 2.8[1].

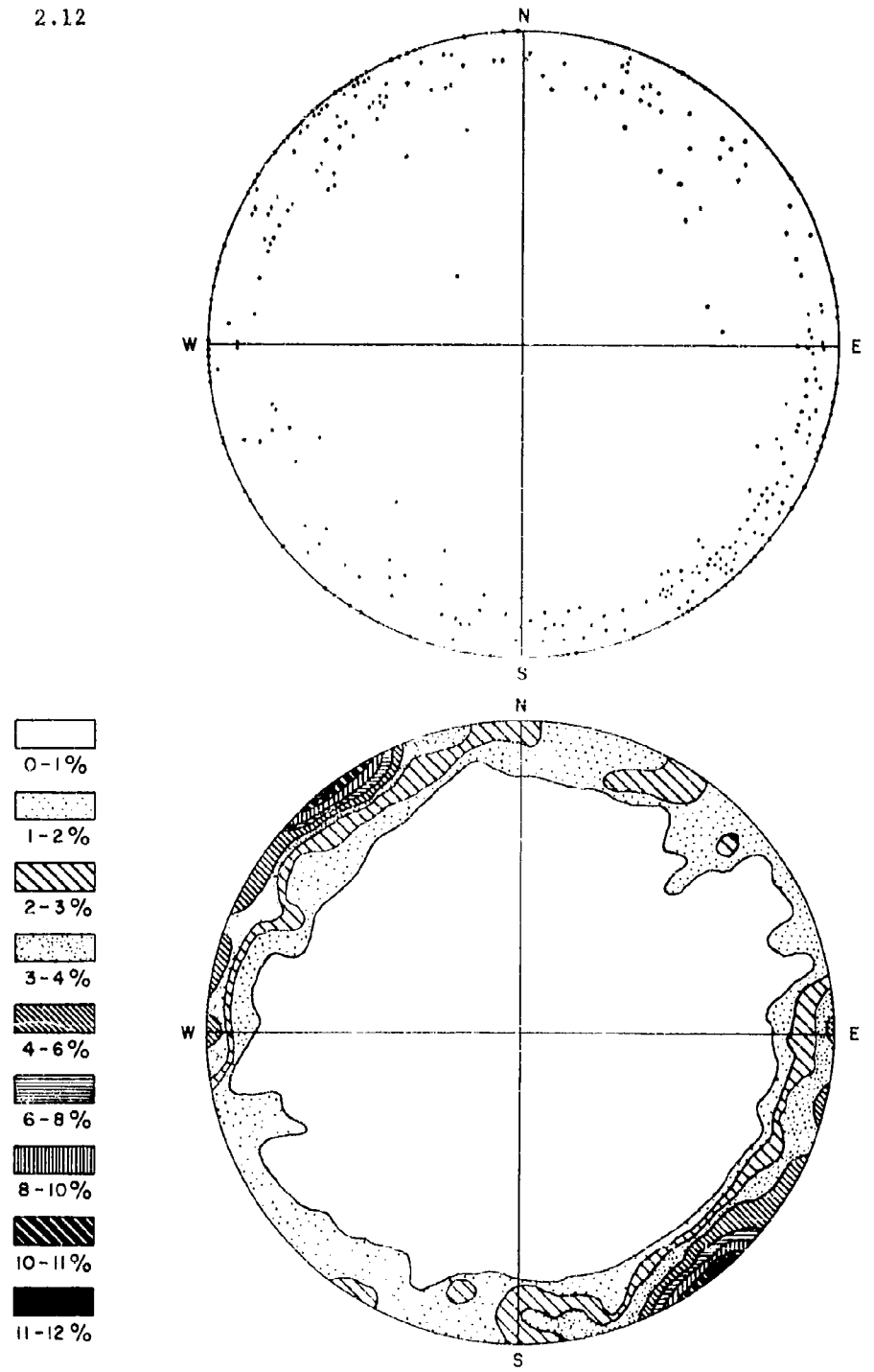


Figure 2.10. Point and contour diagrams of 311 joints in Adirondack Mountains[1].

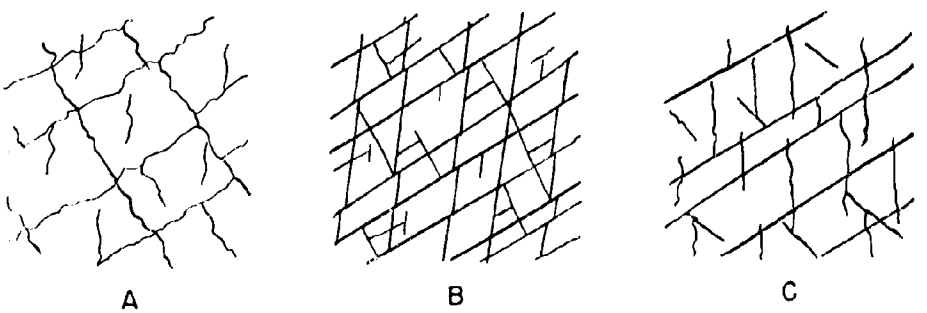


Figure 2.11. Typical joint patterns. A - Rough and irregular minimum caving. B - Smooth surface, maximum caving. C - Smooth and rough, considerable caving.

either replacement or alteration. Unless the alteration is of such a nature as to heal the rock (e.g., silicification) it may weaken it and cause problems of support in excavating operations.

Bedding Planes

The partings or planes which mark the boundaries between the various strata in sedimentary rocks may or may not represent effective planes of weakness. In certain coal mines the planes between the roof shale and the overlying rock, or bedding planes in the shale itself are largely responsible for "falls of roof" in coal mines. This is the cause of many of the fatalities which occur in bituminous coal mines.

Genetically, these planes represent interruptions or changes in the processes which were responsible for deposition of the rocks in their original position. The character of these interruptions determined in general whether the rocks on either side of the plane were to adhere closely to each other, or whether a parting between the strata resulted. In the latter case, a structural discontinuity was produced and a structural weakness incurred which could make a particular bed a weak member in a rock structure.

Sheeting, a form of fracture similar to jointing, is found in granites and other types of rock. It may be due to cooling, release of load by erosion, or combination of release of vertical load and force of residual lateral pressure.

Joints, of course, constitute fractures in rock and as such represent sources of rock weakness. Rocks with a high density of joints or joint configurations which tend to weaken rock structure should be avoided. Spacing of joints would appear to be one of the more critical factors in evaluating their effects.

Faults

Faults are rock fractures along which the opposite walls have moved relative to each other. Strike and dip are measured in the same manner as for bedding or joints. The block above the plane of the fault is the hanging wall and the block below the footwall. Faults may consist of a single fracture plane or a fault zone may be hundreds of feet wide. Distributive faulting is indicated where differential movement is in the form of small displacements along closely spaced fractures. Where a fault intersects the surface of the earth, the intersection is known as a fault trace or a fault outcrop. These may be straight, but are most often sinuous and may show high topographic relief which is important in various aspects of surface geologic mapping. The movement along faults may be translatory or rotational, the movement being relative with no evidence along the fault as to which block moved.

In underground structures such as mines, tunnels, and protective installations the relative position of rock masses displaced by faults

may become critical. In mining operations the position of beds favorable for deposition of valuable minerals is of vital importance as well as choice of competent rock for permanent openings such as haulage ways. Stable opening design for protection against attack by nuclear weapons involves many of the same basic principles of selection of position in the stratigraphic column and geologic structure as does the selection of locations for stable mine openings, although in the majority of cases only static forces are involved in stability of mine openings.

Faults may be recognized by: (1) discontinuity of geologic structures, (2) repetition or omission of strata, (3) physical features characteristic of fault planes, (4) silicification and mineralization, (5) sudden changes in sedimentary facies, and (6) physiographic features.

Only part of the above factors are of primary importance in studies of rock mass stability. The discontinuity of structures at a fault plane contributes, in the great majority of mine and tunnel openings, to greater instability. This is true not only becuase of the presence of the fault fracture itself, but because of secondary fractures and brecciation which accompany many types of faulting. (Breccia is the mass of subangular fragments of crushed rock along the fault plane.)

Silicification and mineralization may tend to heal the fractures in a fault zone or may further weaken the rock structure. Silicification, in addition to furnishing evidence of the presence of faults, usually results in strengthening of the fractured rocks in a fault zone.

Where a downthrow block near a fault is not completely covered by alluvium the topographic features may indicate the presence of a fault. (See Figures 2.12, 2.13 and 2.14). Such fault scarps owe their relief to the movement along the fault. Various types of fault structures are similarly indicated by surface relief, which plays an important part in predicting subsurface geology by means of topographic maps and aerial photographs.

Thrust faults are usually indicated where older rocks are found above younger ones in the stratigraphic column. The mechanics of thrust faulting may be worked out on an idealized basis, as well as the mechanics of gravity and shear or tear faulting.

The result of faulting is to relieve stress and to make the conditions within the rock approach what has been called the standard state, i.e., where the three mutually perpendicular pressures at a point are equal. From the above, Anderson reasons that the fault traces of tear faults and thrust faults should be straight while those of normal faults might be sinuous. This was borne out in observations on a number of faults in the British Isles.

Faults constitute one of the most significant types of tectonic geologic structures. They may (1) act as channels for water, (2) serve as hosts for deposition of valuable minerals, (3) act as a control for deposition elsewhere by damming mineralizing solutions and diverting them to favorable beds for replacement, (4) may serve as loci for stress

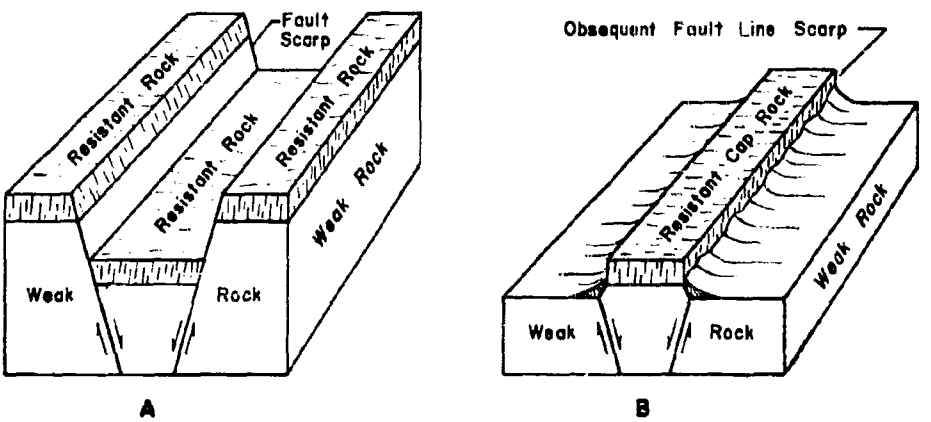


Figure 2.12. Diagram of block faulting with topographic results.

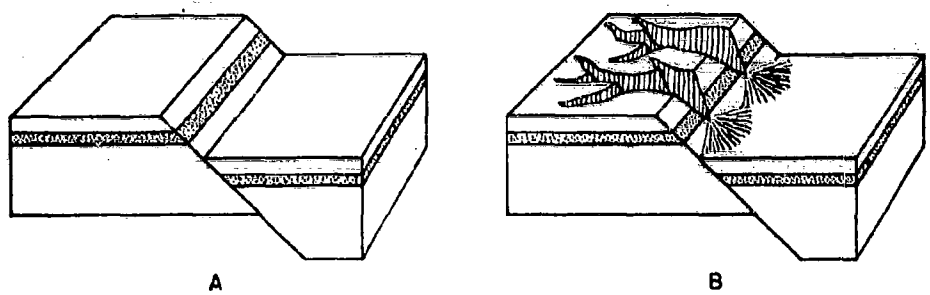


Figure 2.13. Fault scarp before and after erosion[1].

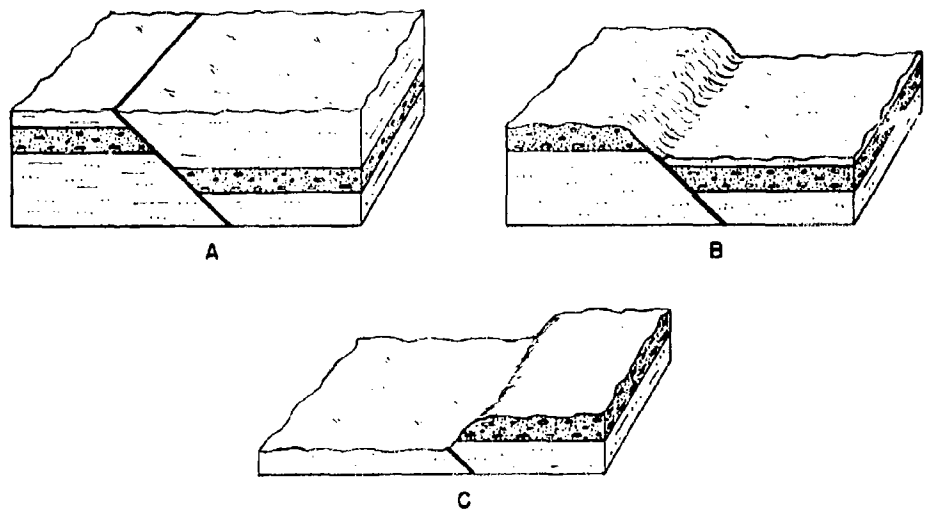


Figure 2.14. A- Fault-line without scarp, formations resistant to erosion. B- Fault scarp down throw formations easily eroded. C- Scarp due to greater resistance of down throw block[1].

relief or stress concentration, and (5) may create diverse mining problems in the prospecting, exploration, development, and exploitation stages of mining. Likewise, their effects are of primary significance in relation to stability of rock structures around protective underground installations.

Faults have been defined above as ruptures in the earth's crust along which the opposite walls have moved past each other parallel to the interfaces of the fracture. Although many faults are relatively clean breaks between rock blocks, in other cases the movement has resulted in the creation of a fault zone (Figures 2.15 and 2.16). This consists of a number of interweaving small faults or fractures or a brecciated zone. In many cases the fracturing which accompanies fault movement is transmitted to a large extent to the surrounding rock, usually diminishing in intensity and size with distance from the main fault zone. This type of fracturing plus that due to slumping of leached and mineralized rock masses have a marked effect in support problems.

Post-Mineral Movement. The movement along a fault may pulverize some of the rock into a fine-grained gouge, which often looks and feels like clay. Post-mineral movement along a mineralized zone forms a gouge containing pulverized minerals from the vein itself. The "planes" thus formed constitute structural weaknesses in the rock, which in turn result in a condition of instability when openings are made in or near them. In general, it appears that post-mineral faulting more seriously affects the choice of correct mining methods than pre-mineral faulting when the choice of a mining method depends primarily upon the support problems involved. Post-mineral faulting usually decreases the strength of both the ore body and the wall rock. (See Chapter III.)

As pointed out above mineralizing solutions may heal the fractures along a pre-mineral fault and strengthen the structure to such an extent that no support is required during mining. On the other hand, pre-mineral faults and their incident fractures may provide escape channels for solutions which have deposited their valuable minerals, and these solutions may alter the wall rock to such an extent that it becomes weak. Once a plane of weakness has been established by a fault or a fracture, the original zone of attrition may also serve as a plane of relief for subsequent stresses. Even when a fissure has been completely healed by mineralization, the resulting vein, if incompetent, is less resistant to fracture than the stronger enclosing rock. Post-mineral movement along well developed fault zones may be expected as a common occurrence if the vein is composed of friable materials or filled with unmineralized gouge.

Photoelastic studies and mathematical analysis can provide some solutions to stress problems in homogeneous materials, and much work has been done along with these and other methods to explain rock failure and phenomena such as rock bursts. More critically important than studies of stress distribution around openings in ideal materials are those investigations which will take into account the presence of the discontinuities and irregularities which must be ignored in usual methods of analysis, but which are of vital importance in a dependable solution of the problem. A study of geologic structures and their effect upon rock pressures and

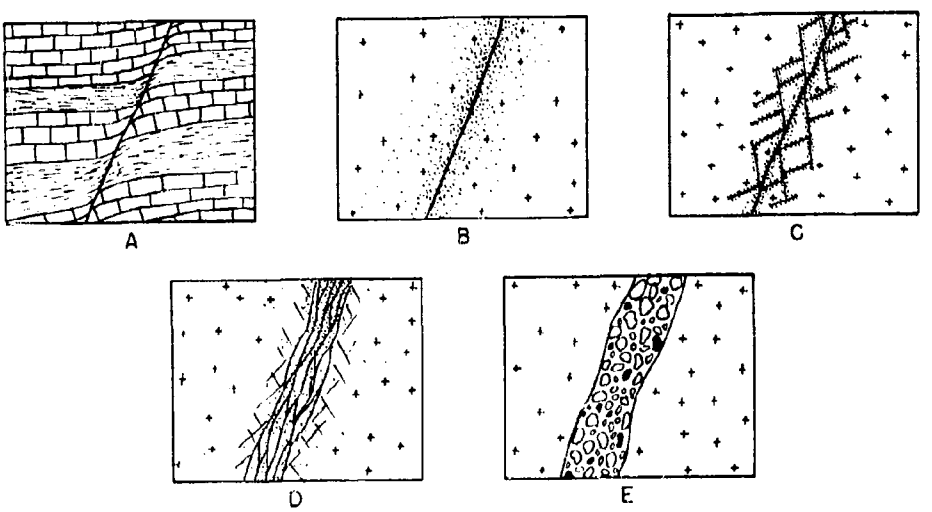


Figure 2.15. Types of faults. A - Clean sharp break, no alteration of wall rocks. B - Sharply defined, no subsidiary fractures, pervasive alteration. C - Sharply defined, with subsidiary fractures, localized alteration. D - Braided, with subsidiary fractures, general alteration. E - Open, porous, filled with breccia.

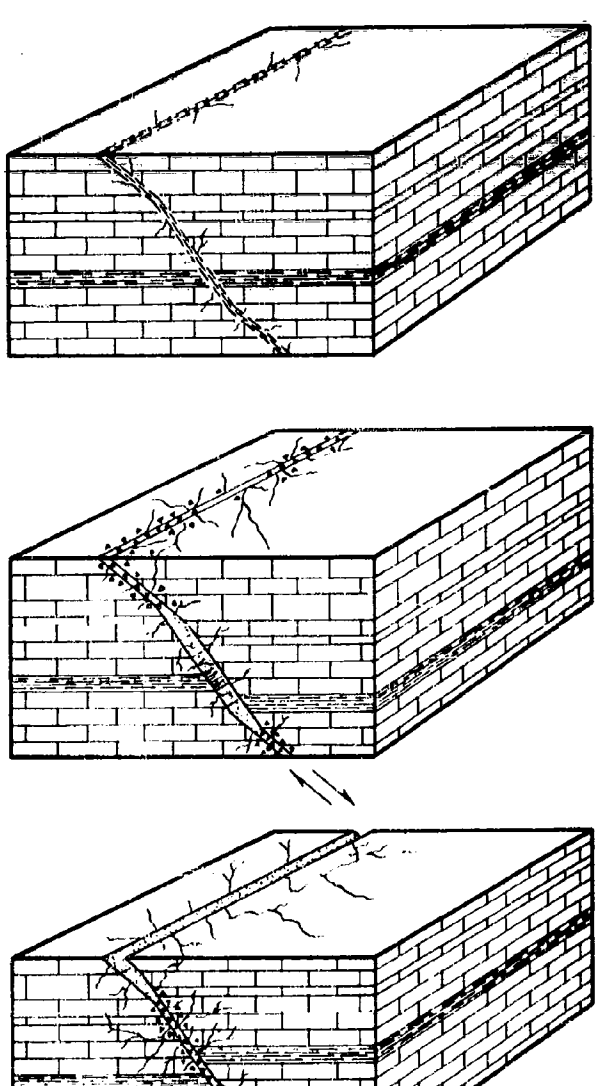


Figure 2.16. Fault movement with fractures induced by irregularities along the fault plane.

stress distribution in a majority of cases may be virtually the whole problem.

Secondary Foliation and Lineation

The ability of certain rocks to fracture along parallel surfaces is termed foliation, resulting in foliate structure. It may be primary features resulting from formation processes. For example, many fine-grained sedimentary rocks tend to break parallel to bedding planes producing bedding fissility. This may be due to differences in grain size, composition of layers or platy grains oriented parallel to the stratification. Also, certain igneous rocks of both intrusive and extrusive origin, possess primary foliation.

Rock cleavage is the term, distinguished from mineral cleavage, applied to the capability of rocks to break along parallel surfaces of secondary origin, either parallel or inclined to the bedding. (Figure 2.17). Schistosity is a form of rock cleavage formed in recrystallized rocks such as schist or gneiss. Foliation may be classified as follows:

Table 2.1

Classification of Types of Foliation[1]

A. Primary

1. Sedimentary rocks - bedding fissility
2. Plutonic rocks - primary foliation
3. Extrusive rocks - flow structure

B. Secondary: in both sedimentary and igneous rocks

1. Flow cleavage (also called slaty cleavage)
2. Fracture cleavage (essentially closely spaced joints)
3. Shear cleavage (slip cleavage)
4. Bedding cleavage - (cleavage parallel to bedding of metamorphic rocks)

Lineation (Figure 2.18) is the parallelism of some directional property of rock, such as the orientation of crystals, elongated pebbles, parallel crests of corrugations of similar small scale occurrences. Lineation usually lies in the plane of foliation and geologic map symbols for the two are usually combined. Both cleavage and lineation may be related to the major structure in which they occur. Flow fracture and shear cleavage are often associated with folds in alternating competent and incompetent beds.

Unconformities

Unconformities are surfaces of erosion or non-deposition which separate younger rocks from older ones. They are formed by: (1) the

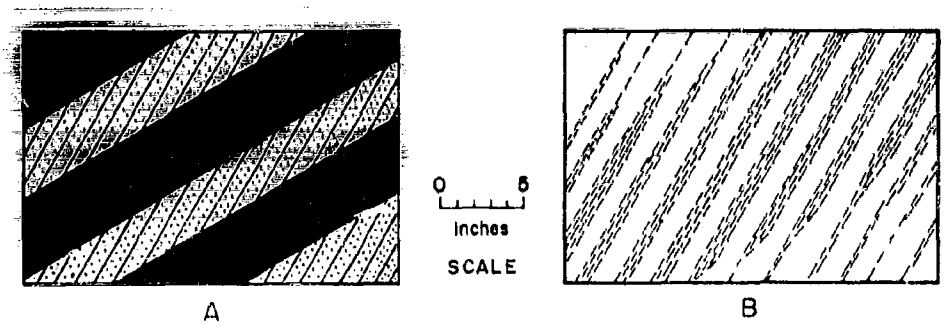


Figure 2.17. Cleavage banding and segregation banding.[1]

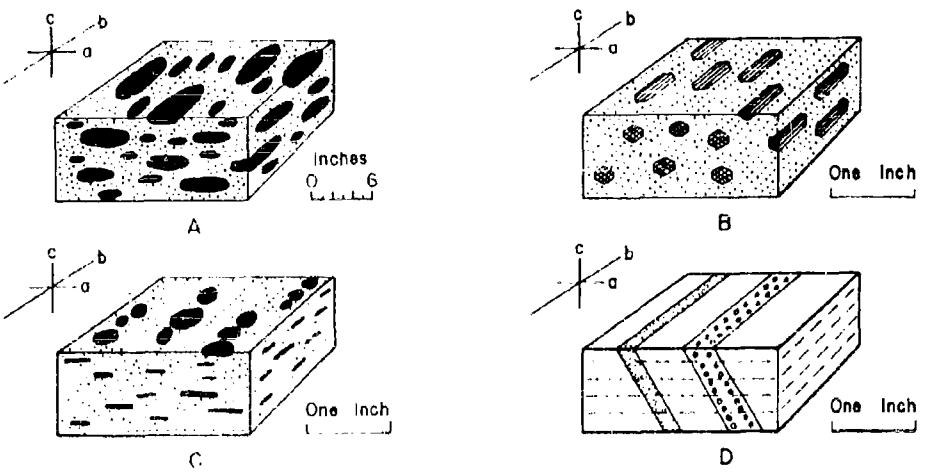


Figure 2.18. Lineation. A- Elongated pebbles. B- Elongated crystals of hornblende. C- Lineation caused by circular plates of mica. D- Cleavage represented by top of block and planes shown by dotted lines.[1]

deposition of older rocks, (2) uplift, erosion and movement, and (3) deposition of younger strata. They may be parallel (disconformities) or angular. (Figures 2.19 and 2.20). They constitute important structural surfaces of weakness and in many cases are confused with faults in aerial and other types of mapping of geologic structures.

Lava Flows

Extrusive igneous flows result in the formation of tabular igneous bodies which are thin relative to their horizontal extent. Their structure is quite variable. Tumuli are low, small dome-like hills; pressure ridges are long sharp ridges a few feet to several hundred feet in length; and squeeze-ups are small extrusions through the crust of the lava itself. Lava tunnels are long caverns beneath the surface of a lava flow. Flows are distinguished from sills in that the latter have smooth, fine-grained tops.

Pyroclastic rocks, also of volcanic origin, are those broken up into fragments into dust, ash, cinders, blocks, etc. These may be cemented to form tuff, tuff-breccia, volcanic conglomerates and agglomerates.

Rock Types

In most mining and excavation problems, the sequence of geological formations in the district is one of the first things which must be learned, together with the types of rock which form the column. In general, the earth's mantle is composed of three types of rock (See Chapter I) which have been classified geologically as: (1) sedimentary, (2) igneous, and (3) metamorphic. For the outer ten miles of the earth's crust, it has been estimated that the composition is as follows[2]: igneous rocks, 95.0 percent; shales, 4.0 percent; sandstone 0.75 percent; and limestones, 0.25 percent. Although there are over 1,000 different known minerals, 99 percent of the igneous rocks is made up of about 12 rock-forming minerals.

Economically valuable mineral deposits are found closely associated with all three types, both with respect to origin and deposition. Many important metallic mineral deposits are found in connection with igneous rocks. Consequently, for a mining engineer to obtain an understanding of the factors which influence the efficient mining of these deposits, it is necessary for him to possess an understanding of the geologic processes which may have resulted in their formation. In addition, geologic processes which may have altered the physical or chemical character of the deposit or enclosing rocks subsequent to mineralization may also have a marked effect upon mining planning and layout. Inasmuch as the original structure and composition of a rock mass may govern its structure after it has been altered or deformed, it is expedient to appraise certain of the genetic features of the three types of rock.

Sedimentary Rocks. The arrangement of sedimentary rocks in layers or strata is one of their most characteristic features. The strata, which

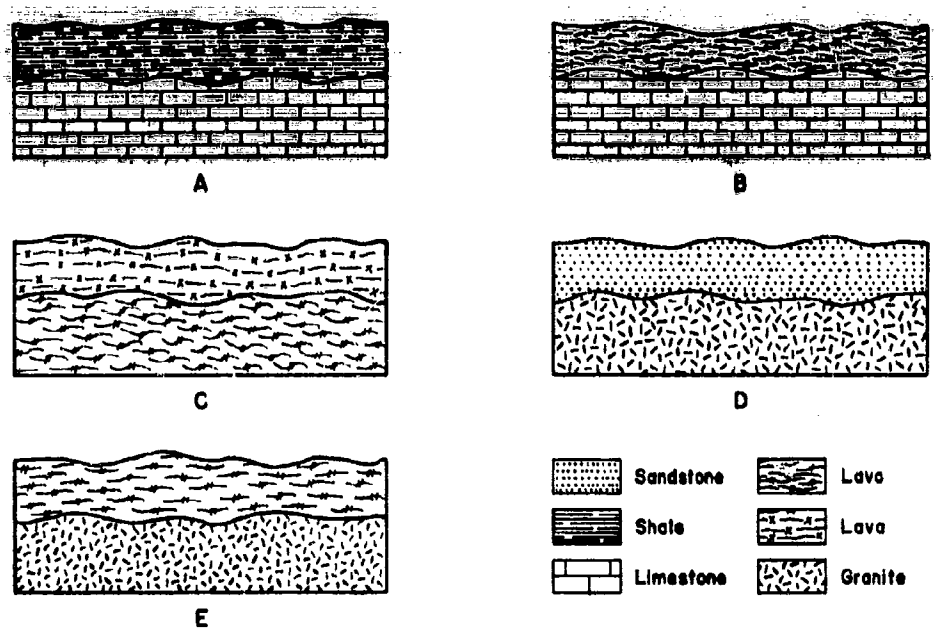


Figure 2.19. Various types of unconformities.[1]

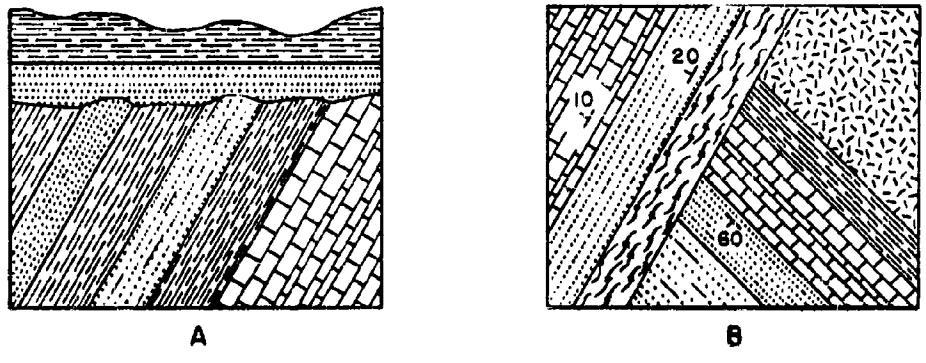


Figure 2.20. Angular unconformities.[1]

are separated by bedding planes, can usually be distinguished one from another by differences in composition, texture, hardness, cohesion, strength, color, and other physical and chemical properties. A bed or stratum is usually considered to be a layer which is composed throughout of similar material. Sedimentary rocks can often be split easily along the bedding planes, and in some types of shales, the orientation of minerals may produce a definite cleavage. Although bedding is a geologic feature peculiar to sedimentary rocks, it must be kept in mind that all sedimentary rocks do not exhibit this feature. Also, some extrusive igneous rocks frequently evidence layers which are crudely similar, but which were formed parallel to the surface of successive flows. The original attitude of stratification planes is usually horizontal, but cross bedding, nonconformities and disconformities are common features in variance to the generality.

All of these features play an important part in the formation of mineral deposits where sedimentary rocks are the host rock for mineralizing solutions. The relationship between beds in the stratigraphical column, the presence of bedding planes, joints or cleavage, and the composition of individual layers have an ultimate effect upon problems involved in mining deposits found in this type of rock. Their physical characteristics and the manner in which they deform under stress also have an important bearing upon their structural stability.

Igneous Rocks. When a liquid magma reaches a position in or on the earth's crust where temperatures and pressures are low enough, the molten material will solidify. Those magmas which solidify after entering rocks in the earth's surface are called intrusions, and those which break through the earth's crust to the surface are termed flows or extrusions. The texture or grain size of an igneous rock is governed largely by the rate of cooling. If a melt cools slowly, large crystals may be formed, but when it is cooled rapidly a glassy or fine-grained material is formed. Contacts between igneous and other types of rocks may be sharp or gradational. Pegmatite dikes or sills, which are formed by a melt flowing and solidifying along a fracture of bedding plane, are important because of their association with valuable minerals. (Figures 2.21 and 2.22). Mineral deposits formed by magmatic segregation also are important in their relation to the formation of igneous rocks and valuable mineral deposits.

Igneous rocks may exhibit a flow structure (Figure 2.23) due to a difference in viscosity of the magma from point to point, which creates either a laminar or a platy flow structure. Fault and joints can occur in igneous rocks only when they have cooled and attained a solid state. It may be that many of the joints and minor faults in large granite masses occur during the later stages in the intrusion, owing to the persistence of forces which cause the magma to rise in the earth's crust. Large intrusions may also be fractured and then intruded by subsidiary magmas, adding to the complexity of the structure. In addition to the occurrence of primary structures other phenomena are often observed such as the contact metamorphic effects imposed upon contiguous rocks.

For structural purposes, three major realms or zones of igneous activity are recognized by Hills[2]:

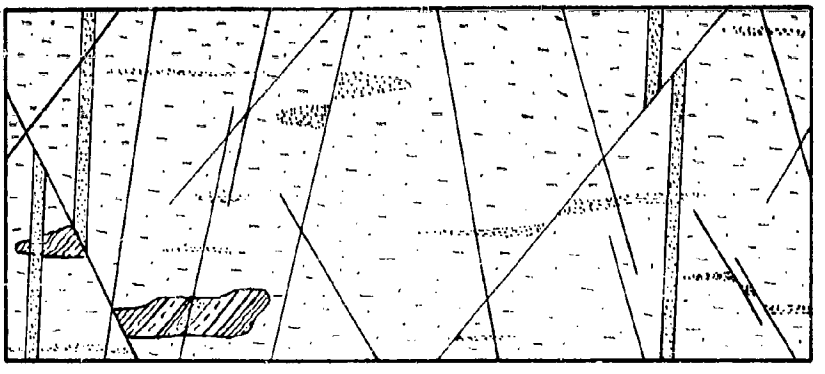


Figure 2.21. Plan view of an igneous rock with flow lines and diagonal faults and joints.[3]

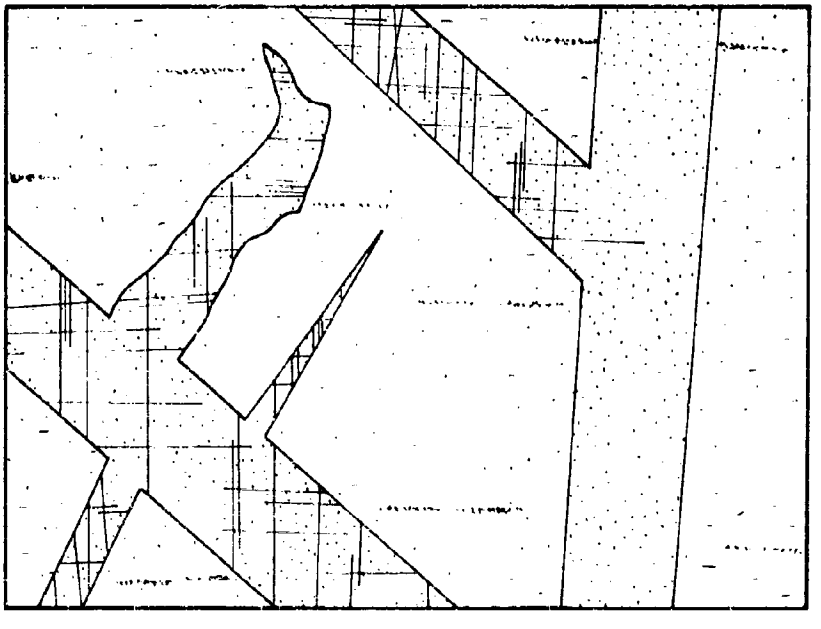


Figure 2.22. Diagonal joints in dikes. Fractures in dikes represent either diagonal joints in dikes or cross joints in enclosing syenite.[3]

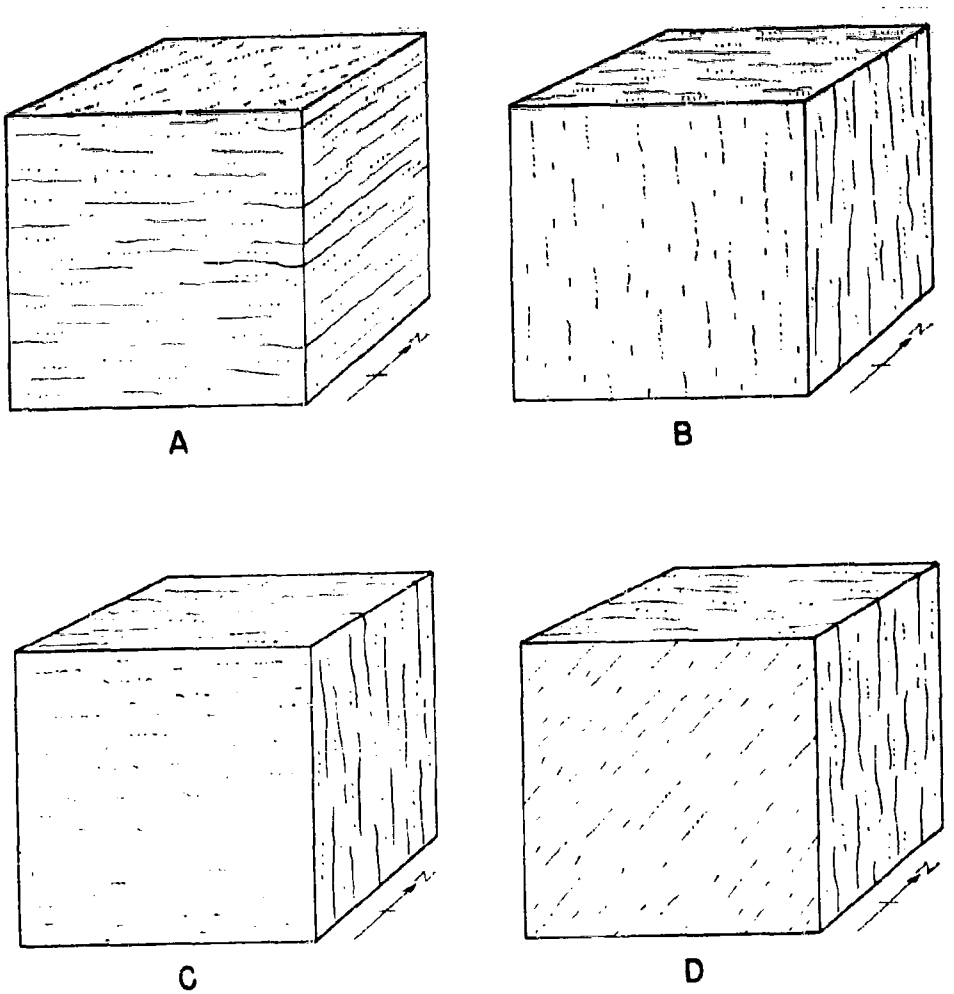


Figure 2.23. A - Horizontal flow layers; B - Vertical flow layers and vertical flow lines; C - Vertical flow layers with horizontal flow lines; D - Vertical flow layers with pitching flow lines[3].

1. Ultra-plutonic intrusions in the lowest levels of the earth's crust which are characterized by dominance of structure due to flow, both in the intrusions and their wall rocks, fracture phenomena being almost entirely absent. The injection of magmatic material occurs along zones of weakness, or by assimilation, and replacement or even actual melting of the country rock is widespread.

2. An intermediate zone where the effects of flow together with those of fracture are exhibited by both the intrusion and its wall rock.

3. The tectonic features of intrusions in the superficial crust zone show that fracture predominates over plastic or viscous flow in the walls of the intrusions. Roof rocks are dislocated by the rising magma and contacts are blocky.

Butler[4] also recognizes three zones of deformation of rocks where rock structure is related to mineralization and consequently to structural stability. These are characterized by (1) brecciation at shallow depths, (2) brecciation and shear in an intermediate zone, and (3) shear only at great depths. Failure by shear is postulated also as evidence of failure under heavy load and at shallow depth. It might also be noted that a large percentage of igneous rocks found in the crustal zone contains from 45 to 80 percent total silica and these rocks range from gabbros and basalts to quartz diorite (Figure 2.24). The percentage of quartz has a marked effect upon such physical properties as strength, creep, compressibility, and such processes as re-cementing of rock fractures by silicification which materially affect the strength of rock masses.

Primary structures of igneous rocks[3] are those which develop during their formation. Most igneous rocks possess flow structure of either a linear of platy character, although some are massive, compact, and virtually "structureless" after their initial consolidation. Crystalline flow structure is believed to be due to suspension of crystals in a partly solidified magma and orientation by subsequent flow. Platy structure may be formed by alignment of phenocrysts, local irregularities in composition, parallelism of xenoliths or by segregation of minerals. Biotite grains are particularly conducive to platy structure.

The term <u>rift</u> is the ability of granitic rocks to split in a direction other than that of the "bedding", i.e., the latter being parallel to the earth's surface. Massive gabbro, diabase, nirite, and similar rocks do not seem to possess this characteristic. In granite quarries it has been found that blocks are cut by three sets of planes: flat lying planes, rift, and the "hardway". The latter two are vertical and normal to each other.

There are several types of platy parallelism found in igneous rocks. (1) In uniform granular rocks the crystals may be elongated and the plane of such structure is observable. In quarries it has been found that "rift" planes follow parallel microscopic cracks and bubbles. (2) Phenocrysts may be arranged with their largest crystal faces in parallel planes. (3) Where these are numerous they form layers which are parallel to the phenocrysts. (4) Segregations and xenoliths may also form layers by accumulation. Flow layers are also formed with the length, thickness, and gen-

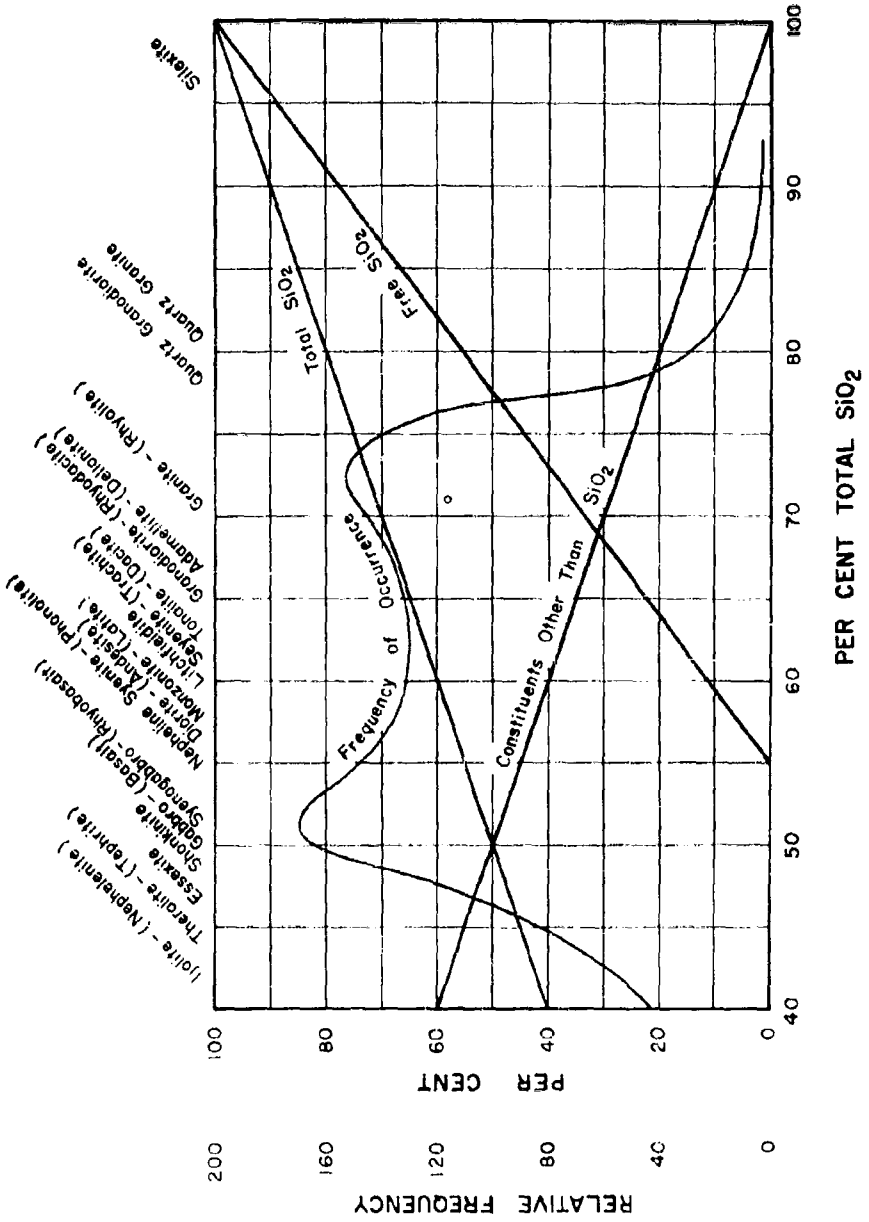


Figure 2.24. Relative frequency of occurrence of SiO_2 in igneous rocks in the earth's crust.

eral features varying greatly. In most of the cases of platy structures the surfaces so formed constitute potential fracture surfaces.

Balk[3] classified joints in igneous rocks as functions of flow structure: (1) cross joints, (2) longitudinal joints, (3) diagonal joints, and (4) primary flat joints. Cross joints are those that lie perpendicular to flow lines. They are usually straighter than other types, are equivalent of tension joints, being formed during the very early stages of magma consolidation. Longitudinal joints lie parallel to flow lines, some caused by the cooling of a magma. Diagonal joints are those which occur at 45° to the flow lines and are caused by shear. In some types of igneous rocks there has been a tendency to flat lying joints. Their origin is somewhat uncertain. (See Figures 2.25 and 2.26).

Diagonal joints are believed to represent shear planes which are dominate over cross joints if the mass is so constrained that slippage is prevented. Dikes themselves are common in igneous rocks and may weaken the overall structure if they are not firmly welded to the walls.

Large quarries in the Strehlen granite in eastern Germany have permitted an extensive study of its structure. Throughout this mass a linear parallelism of structure trends east and west forming an arch. The rift and flow lines in this rock coincide. (See Figure 2.27).

Figure 2.28 is based on the results of experiments with wet clay which created fissures and flow lines as shown.

The examples given indicate that masses of igneous rock have structures which are related to an observable geological system of flows, joints, fissures, etc., which would be of basic design value in locating protective construction installations within them.

Metamorphic Rocks. These may be classed in two categories: (1) contact rocks produced by igneous intrusions along their contacts or walls, and (2) regionally metamorphic types which may cover a large area.

Contact rocks include both the border rocks of the intrusion and the metamorphosed or recrystallized portions of the intruded rocks, such as products from shales, slates, or limestones; sandstones are less influenced by intrusions. The term hornfels is generally applied to densely crystalline, altered shales. Alteration of limestones on contacts usually results in the formation of a series of lime-silicates such as garnet, pyroxene, epidote, and vesuvianite.

Regionally metamorphic rocks may be representative of either sedimentary or igneous types. Gneisses are usually banded or foliated rocks of granitoid texture, and often have the appearance of granite (Figure 2.29). Schists including mica-, hornblende-, quartz-, and chlorite schists are usually foliated with the characteristic mineral well developed. Quartzites are sandstones which have been hardened and solidified with the addition of new silica. Slates are derived from shales or clays, and usually show a prominent cleavage structure which has no definite relation to the original bedding, the cleavage having been produced by

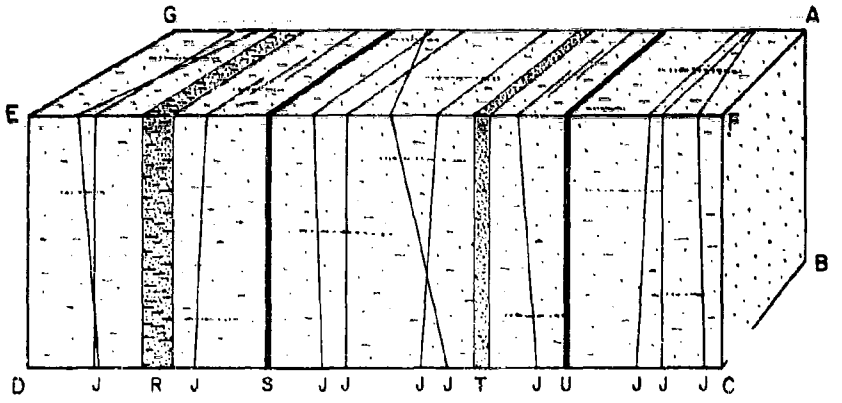


Figure 2.25. Idealized relations between flow lines in igneous rock and artificial parting. (ABCF, CFED, AFGE.) Cross joints are given by (J) and dikes by (R,S,T,U). Horizontal flow lines tend from left to right and rift planes (C,F,E,D) as a rule trend the same. Hardway planes (A,B,C,F) are perpendicular to the flow lines, and the primary "bedding" planes (A,F,G,E) include the flow lines. They may, or may not coincide with exfoliation planes caused by weathering. Cross joints (J) and dikes (U) are normal to flow lines.

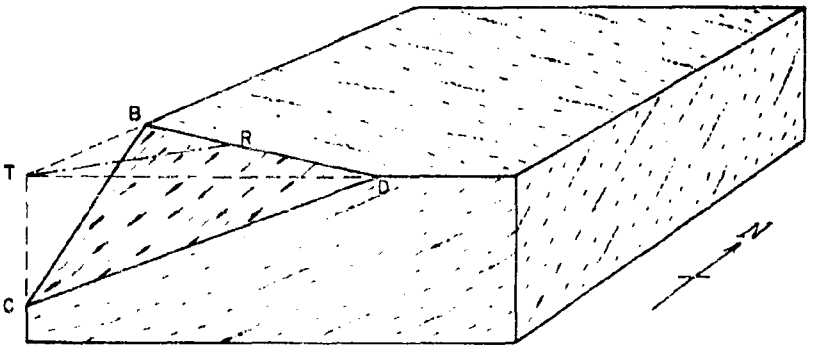


Figure 2.26. Idealized relations between flow lines in igneous rock and artificial parting.[3]

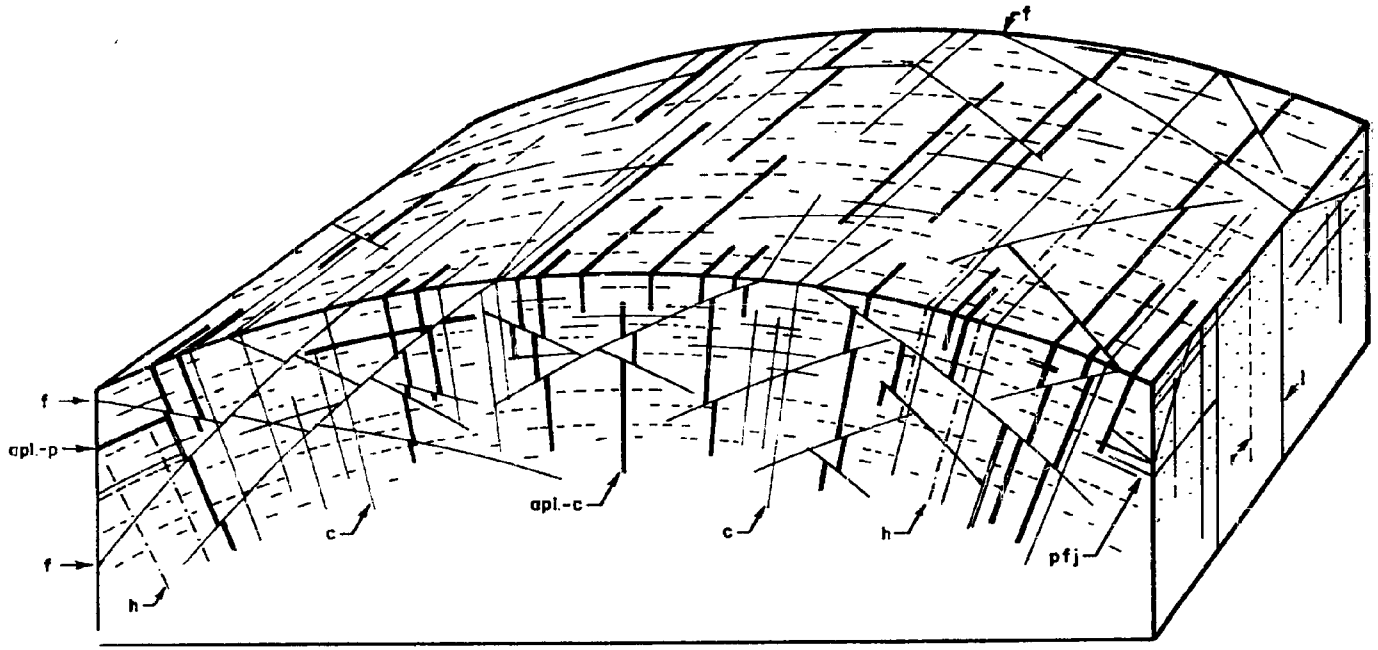


Figure 2.27. Primary structural elements and directions of parting in granite map, Strehlen, Germany. (f) Flat-lying normal faults; (c) cross joints, (l) longitudinal joints; (pf) primary flat-lying joints; (apl-p) aplites on primary flat-lying joints; (h) hardway planes (dots and dashes); rift planes (rows of dashes).[3]

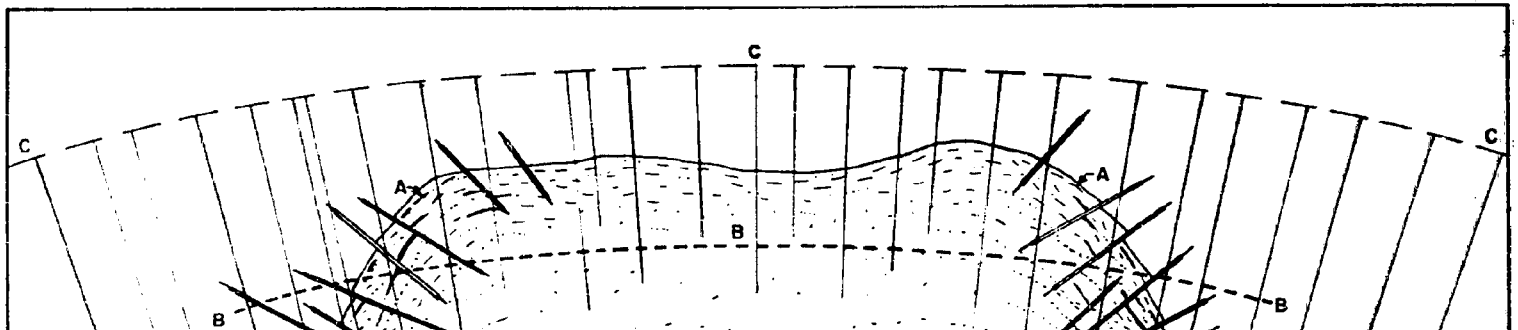


Figure 2.28. Idealized superposition of flow structures and fracture systems in a massive intrusive and surrounding rocks. The oldest structure is a dome of flow layers (a) next younger are marginal fissures, with or without upthrusts, frequently accompanied by dikes (double lines). B is the arch of flow lines with cross joints perpendicular to it or the larger arch C.[3]

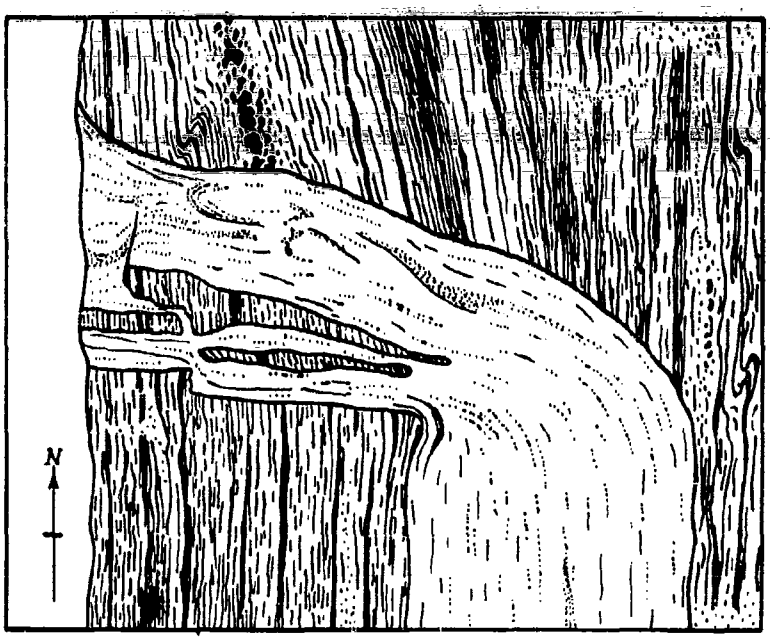


Figure 2.29. Plan view of a ledge of granite gneiss, foliated north-south, taverned by a 6-foot dike of foliated granite. This is illustrative of complicated structures which might occur in igneous and metamorphic rocks.[3]

pressure. Graywackes are irregularly breaking, sandy metamorphosed shales or volcanic tuffs and breccias. Marbles are recrystallized limestones.

The long-continued stress and recrystallization which accompany regional metamorphism and "rock flowage" usually result in a banded structure in rocks produced from both sedimentary and igneous rocks. Various minerals in the rock are oriented with their longer axes parallel. This produces planes of weakness when the rocks are subjected to fracture stresses that differ from those which caused the cleavage. Rocks which have been metamorphosed in this manner are said to possess a schistose structure. In addition, schists may exhibit cleavage which is independent of their schistosity, with occasional traces of the original stratification. If schistose structure of rocks is coarse in character, the rocks grade into gneisses. Here the bands may be more prominently developed than in the schists, but they do not fracture so easily.

Products of weathering include surface materials which are subject to weathering processes, whose end products are usually soils. These also might be considered as products of metamorphic processes.

Primary Metamorphism

Metamorphism may be defined as the change in a rock either in physical form or chemical composition due to pressure, heat, solutions or other causes. Metasomatism is metamorphism which involves a change in the chemical composition of rocks by the addition or subtraction of one or more of the constituents, elements or compounds. Dynamic-regional metamorphism usually results in the formation of metamorphic rocks such as schist, gneisses, etc. (See Metamorphic Rocks).

Of equal significance are secondary types of metamorphism which are caused by the action of solutions which may be associated with primary ore deposition. (See below). These serve not only as valuable guides in prospecting for ore, but they vitally affect the structural strength of the ore and the enclosing rock during mining. U.S. Bureau of Mines tests[5,6] have shown that even slight degrees of alteration materially affect the elastic properties of rock.

One of the common types of rock alteration is contact metamorphism, which is the change in structure and composition of the enclosing rocks immediately in the vicinity of igneous intrusions. The types of rocks which are most commonly affected by intrusives are limestone, which is changed to marble, shale, which is changed to hornfels, and sandstone, which is changed to quartzite, all with the addition of new minerals. Igneous rocks are affected less by contact metamorphism inasmuch as they were formed under igneous conditions themselves. Certain minerals are characteristic, though not necessarily diagnostic, of contact metamorphism. These are garnet, wollastonite, epidote, pyroxene, amphibole, magnetite, quartz, and certain sulphides. The distance to which this process may penetrate invaded rocks varies greatly in different localities and also in different rocks. Certain beds may be altered for long distances from the contact while others remain unchanged within a short distance of the intrusive. Contact metamorphic rocks and minerals are commonly tough

and resistant to erosion. Structurally they might be expected to be competent unless subjected to later faulting or destructive alteration.

Secondary Metamorphism

Hydrothermal alteration is a metasomatic process which involves the alteration of rocks by hot ascending solutions; it frequently accompanies the process of primary ore deposition. The wall rocks of veins are commonly fractured by fault movement, and these fractures afford ready access to solutions which alter the rock if conditions such as chemical composition, temperature, etc., are suitable. Alteration is usually more intense near the vein and is likely to diminish rapidly with the distance from the vein. Most alteration seems to be carried out by depleted solutions which have already deposited the heavier base minerals along the vein.

Where there is a tightness of fractures at considerable depth because of pressure, the alteration of wall rocks is likely to be less intense along deep-seated fractures than in shallow deposits. It also may be less intensely developed in relation to deposits which were formed in open spaces, but of considerable intensity around replacement deposits. Some of the most common effects of intense alteration along veins are sericitization and the introduction of pyrite (pyritization) which may grade into propylitization at greater distances from the deposit. In basic rocks the tendency is for propylitization to persist close up to veins and perhaps give way there to sericitization.

Sericitization is the type of hydrothermal alteration which results in a complete loss of soda and a large gain in silica, potash, perhaps pyrite and other substances. The typical product of complete sericitization is a finely granular aggregate of sericite, quartz, pyrite and calcite, which usually forms a very incompetent rock. Sericitized rocks are often white to light yellow in color and are usually soft. Minute scales of sericite are distinguishable megascopically and are often the means of distinguishing between sericitization and kaolinization. Both types of alteration are destructive in character as far as rock strength is concerned.

Silicification of mine rock by processes of hydrothermal alteration is also frequently encountered. According to chemical laws the tendency toward silicification is usually greater in acid rocks (of high silica content) than in basic rocks (of low silica content). The formation of a reticulated structure is common in limestones where siliceous seams may be formed which enclose partly altered or fresh fragments of limestone. Quartz which is formed in this manner is often cherty in character, whereas the replacement of calcium by silica may reproduce the original structure. As the name of the process implies, it involves the addition of silica to the rocks through which solutions move. The silica is usually fine-grained or amorphous in character and may be deposited along the cracks or by replacement. A hardening effect normally results when quartz becomes part of a rock, with an accompanying increase in structural strength. Fissures are often "healed" by silicification, which may lessen the problems of support when rocks associated with such fissures are excavated.

Kaolinization may occur as a result of either hydrothermal alteration, or by weathering, alteration of rocks, ores, and minerals by atmospheric waters. It is typically a result of surface agencies, but may also occur where hydrothermal solutions are acid in character. This process involves the decomposition and solution of hard feldspars and other minerals and the formation of kaolin, which is soft and friable in character. Consequently, rocks and ores which have been subject to kaolinization are likely to be structurally weak and will not stand pressure long, especially when exposed to air.

As pointed out previously, the walls of deep-seated veins are not as extensively altered as veins formed at shallow depths. In veins nearer the surface where the hanging wall has been subjected to fracture, brecciation and mineralization, hydrothermal alteration will extend farther into it than into the foot wall, giving rise to a "heavy" hanging wall. This may come about as a result of a greater resistance of the foot wall to fracturing relative to that of the hanging wall. The hanging wall rocks can readily adjust themselves to geologic stresses through fracturing, while the foot wall, which may be under stresses of equal magnitude, remains massive and unbroken due to the reinforcement of the underlying rock.

Argillic-clay minerals occur in sulphide ore and are characteristically of earlier formation than sericite. Chemical data indicate that calcium and sodium are generally removed from the rock to a significant degree, whereas potassium and silica remain constant or increase slightly.

The complexity of hydrothermal alteration is illustrated by the following list of products and the minerals from which they may have been formed or by which may have replaced.

Plagioclase: Sericite, kaolinite, other silicates, sulphides and quartz.

Orthoclase: More resistant to alteration, but excessive alteration may form same minerals as for plagioclase.

Biotite: Secondary biotite, chlorite, calcite, and other silicates with some sulphides.

Augite: Horneblende, biotite, chlorite, and others.

Quartz: Resistant to alteration, but may be replaced to a small degree by sericite, orthoclase, and others.

Magnetite: Hematite.

Illmenite: Leucoxene.

Zircon: Unaltered.

Apatite: Unaltered in some cases, destroyed in others.

Strength of Ore. In general, the structural strength of ore is affected by the same factors as the surrounding rock. The composition of the ore may make it very competent or very weak. Massive sulphides, for example, will stand in very large arches, whereas softer, more friable mineral complexes are weak.

Geology and Underground Water

Where water is found in the underground zone, the substrata and geologic structure govern its movement and distribution. Most water is of atmospheric (meteoric) origin although small amounts of connate (entrapped) water is found in some types of rocks. The latter and magmatic water (volcanic) are usually highly mineralized.

Large amounts of ground water occur in permeable geologic formations known as aquifers, which allow water to move through them under natural conditions. An aquilude is an impermeable formation which contains but does not transmit water, while an aquifuge is an impermeable rock which neither contains nor transmits water. Fault zones and interconnected fractures may provide water channels, which may be enlarged by solution.

Approximately 90 percent of all aquifers consist of unconsolidated rocks, chiefly sand and gravel.[7] Limestones vary widely in porosity and permeability, those acting as important aquifers containing large solution channels. Volcanic rocks, such as basalt, may form permeable aquifers, rhyolites are less permeable, while intrusive rocks are impermeable. Sandstone and conglomerate usually are made up of cemented grains, the cementation reducing the flow. The best sandstone aquifers are those which are only partially cemented, or those which permit flow of water through joints. Crystalline and metamorphic rocks are relatively impermeable.

An ideal underground protection site would be free from groundwater. Such water would cause construction or operation problems and usually is a source of maintenance difficulties. Aside from the problem of pumping volumes of water, a significant portion of underground water is corrosive because of dissolved minerals. Hence, while an overlying aquifer may be desirable for water supply purposes, the accompanying problems may offset this advantage. Conceivably a large surface blast could disturb the rock structure above an underground opening sufficiently to open channel ways from the aquifer to the opening.

For effects of water on mechanical properties of rock see Chapter I.

CHAPTER II

REFERENCES

1. Billings, M.P., Structural Geology, Prentice-Hall, 1942.

2. Hills, E.S., Outlines of Structural Geology, 1940.

3. Balk, R., Structural Behavior of Igneous Rocks, GSA, memoir 5, 1937.

4. Newhouse, W.H., Ore Deposits as Related to Structural Features, Princeton University Press, 1942.

5. Obert, L., Windes, S.L., and Duvall, W.I., Standardized Tests for Determining the Physical Properties of Mine Rock, USBM RI 3891, August 1946.

6. Obert, L., Windes, S.L., Physical Properties of Mine Rock, Unpublished paper, AIME Meeting, New York, March 1947.

7. Todd, D.K., Ground Water Hydrology, Wiley, 1959.

CHAPTER III

GEOLOGY AND UNDERGROUND STRUCTURE STABILITY

Introduction

The problems involved in the stability of mines and those in the stability of underground protective excavations are identical for static conditions, and most of the factors which contribute to static stability are also likely to contribute to strength under dynamic loading. A wealth of data is available on underground mining conditions, and while it is largely descriptive in character it is the most reliable guide that is currently available for overall evaluation of underground opening stability problems.

In mining processes a method of mining ore is employed which will yield the largest net return on a given deposit. The method employed must be safe and must also permit optimum extraction of valuable minerals under the particular geological conditions encountered. The classification of stoping methods adapted by the Bureau of Mines[1] was devised largely on the basis of rock stability. The best method of stoping depends upon the geological characteristics that determine the area of back or walls that will be self-supporting during the removal of ore; the nature and size of supports required; and the support required for permanent openings to prevent subsidence. More specifically, geology must be studied in detail so that: (1) Preliminary openings may be placed to best advantage; (2) permanent openings may be placed in solid stable rock; (3) stopes may be planned for optimum stability and ground control; (4) mine openings may be maintained at minimum cost; (5) openings may be located to avoid water; (6) overall mining methods may be planned; and (7) maximum safety can be achieved.

Mining Methods - Classification

The features of ore deposits and their environment which dictate a given mining method may be created before, during, or after mineralization takes place. From a structural engineering point of view the following characteristics are important: (1) The size and shape of the ore body; (2) the depth and type of overburden; (3) the location, strike and dip of the deposit; (4) the strength and physical character of the ore; (5) the strength and physical character of the surrounding rock; (6) water and drainage, i.e., the presence or absence of aquifers; (7) grade and type of ore and other economic factors. Of these only the last has little parallel importance in underground protective structures. (An exception would exist, for example, where excavation was being made in a marketable rock such as limestone suitable for agricultural or other purposes.) The above factors can be readily interpreted in terms of geological entities, some of a quantitative and others of a purely qualitative nature. As part of the background for a geological analysis of stoping

methods and related rock mechanics, a classification of mining methods will illustrate many of the principles of rock stability involved:

Classification of Stoping Methods[1]

A. Stopes naturally supported.

1. Open stoping.
   (a) Open stopes in small ore bodies.
   (b) Sublevel stoping.

2. Open stopes with pillar supports.
   (a) Casual pillars.
   (b) Room (or stope) and pillar (regular arrangement).

B. Stopes artificially supported.

3. Shrinkage stoping.
   (a) With pillars.
   (b) Without pillars.
   (c) With subsequent waste filling.

4. Cut-and-fill stoping.

5. Stulled stopes in narrow veins.

6. Square-set stoping.

C. Caved stopes.

7. Caving (ore broken by induced caving).
   (a) Block caving; including caving to main levels and caving to chutes or branched raises.
   (b) Sublevel caving.

8. Top slicing (Mining under a mat which, together with caved capping, follows the mining downward in successive stages).

D. Combination of supported and caved stopes. (As shrinkage stoping with pillar caving, cut-and-fill stoping with top slicing of pillars, etc.).

Physical Factors and Selection of Stoping Methods

The physical characteristics which dictate the choice of a stoping method might be grouped from a different point of view as follows: (1) strength of ore and wall rocks, (2) shape, horizontal area, volume, and regularity of the boundaries of the ore body, and the thickness, dip and/or pitch of the deposit and individual ore shoots, (3) continuity of the ore within the boundaries of the deposit, (4) depth below the surface and nature of the capping or overburden, and (5) position of the deposit relative to surface improvements, drainage and other mine openings.

In the selection of a stoping method it is usually necessary to consider the influence of several factors and then in the final analysis minimize or disregard those of lesser importance in order to satisfy the requirements of the more important ones. Similar principles will govern in the selection and construction of protective installations.

Strength of Ore and Wall Rocks

The structural strength of both the ore and wall rocks is one of the first of the characteristics of an ore deposit which is appraised before mining operations have opened up large sections of a deposit, as it determines the safe size of excavations, the length of time that they may be left open with safety, or the support which will be required.

The structural strength of the ore and rock mass depends not only upon the inherent strength of the solid rock itself, but upon the existence of fractures and planes of weakness and their geometric arrangement, bedding planes, and schistosity, as well as upon the element of time. A small block of rock of uniform texture and structure which is not cut by fractures or joint planes is almost invariably a stronger structural unit than a larger mass lacking uniformity and cut by planes of weakness. However, very large pillars may show greater strength than laboratory test specimens due to the effect of confinement of the central core, even though some fracturing and variation of properties exist. The arrangement and distance between fractures and other planes of weakness has a profound effect upon the overall strength of a rock mass. For example, if a series of joints or bedding planes all trend in the same direction, i.e., if they are approximately parallel, the mass may be weak in resistance to stresses in one direction while it is strongly resistant to stresses normal to the first.

Frequently, fresh, newly-exposed rock (shale and others) is strong, but after it has been exposed to air for a period of time, it may slough or swell and become difficult to support. In other cases, the stresses imposed upon a strong rock arch may weaken it gradually until it fails. Thus, the element of time must be regarded as important in its chemical and mechanical effects upon the support of underground openings.

The strength of the ore and walls in relation to the size of a deposit, particularly the horizontal area, is of major importance. For example, a caving method cannot be employed in a deposit if its horizontal area is so small in proportion to its mass strength that it will not cave when the ore is undercut. On the other hand, providing temporary or permanent support even in a firm ore body of large horizontal extent becomes increasingly difficult as stopes are increased in size, and some type of support such as pillars, filling or timbering is needed if a supported-stope method is indicated. Inasmuch as dry filling will usually provide only side support to the walls and cannot be placed so that it will afford close support to the back, the lateral dimensions of a stope back which will stand undisturbed over a filled excavation are limited by the weakness of the overlying rocks. The larger the area is, the less the probability that filling will support it adequately. For example, filled

square sets which support the back of a stope are much more effective than filling or square-setting used independently. Hydraulic or sand filling may not have these deficiencies.

Shape, Size, and Dip of Deposit.

The shape of ore bodies varies from massive to tabular, and from bedded deposits to pipes, shoots, dikes, and sills, depending upon their genetic history and the character of the host rocks in which they are formed. The attitude of a deposit will directly influence the method chosen to mine it. For example, the ore in a tabular deposit dipping at a high angle may be completely removed without use of supports if the walls are moderately strong A similar deposit dipping at a low angle, however, may possess a horizontal span so great that it is necessary to support the hanging wall with natural pillars or timbers.

A deposit which is regular in shape may require less support during stoping operations than one which is very irregular, other physical characteristics being identical. Thus, mining operations in an irregular deposit will produce stopes with uneven walls overhanging slabs or projecting columns of wall rock. These irregularities may require support, especially if the rock is fractured or broken, but if the walls are smooth and regular and of uniform strength they may stand without support This factor is of particular importance in very deep workings where, in the deep or "rockburst" zone, it has been found that concentration of stresses at corners and around projections relates them closely to the occurrence of rockbursts.

A small ore body in firm rock often can be mined entirely without any support other than that of the walls themselves. If larger ore bodies are found in the same kind of ground mass, it usually is necessary to provide support in the form of pillars, filling or timber because greater sections of backs and walls are left unsupported when the ore is removed In other words, there is a limit to the length or width of an un-supported arch or span that will possess sufficient structural strength to resist the pressures of the overlying rock masses. It is obvious, therefore, that the size of a mineral deposit is another of the fundamental features which must be considered when a mining method is to be applied to an ore body The size of openings relative to fracture spacing is an obvious strength factor, (See Chapter VIII), but requires evaluation for each particular case

Depth Below Surface and Character of Overburden.

Frequently, as depth of mining operations increases the mining method must be changed because the openings require more support to keep them open. Deposits near the surface do not have a large column of rocks above them and consequently they are subject to the relatively low lithostatic pressures The pressure on mine openings other than residual or tectonic stresses, increases proportionately with the depth below the surface.

The character of the overburden and the physical condition of the rock mass above the deposit may have an important effect upon rock stresses at depth. Relative magnitudes of pressures in the three directions will depend upon the state of the overlying material, i.e., whether it is elastic, plastic, or viscous in character. The weight of a thick mass of unconsolidated overburden is sustained by the underlying rock, and if mine openings are made in the latter, the total weight is transmitted to the pillars, walls or other supports, either directly or by thrust of rock arches, etc. Similarly, if a separated block or "pressure block" is formed over the workings by huge masses of rock being severed from the surrounding formations, these pressures are transmitted to the supports in the mine. Pressure blocks of tremendous size may be present as a result of natural geological phenomena, such as faults, or may occur as a result of mining operations. Thus, the direction of pressure may be governed largely by geological structure, particularly in the vicinity of faults, folds or jointed structures.

The direction in which pressure is exerted upon the walls or roofs of an underground excavation depends largely upon the attitude of the deposits and must be taken into account when a mine operator is deciding upon a method of stope support. In a steeply dipping tabular deposit, waste filling will furnish adequate support against side pressure from the walls, whereas in a wide deposit, in which the greatest pressure acts vertically downward on the backs of stopes, filling cannot be relied upon to prevent damaging movement. In wide stopes, waste rock cannot be back-filled or packed tightly enough against the back or roof to support firmly the weight that may come upon it, while sand (hydraulic) fill has better packing and support characteristics. Furthermore, filling usually shrinks in volume after it has been placed in a stope, leaving open spaces and consequent unsupported sections of roof. It is logical, then, that a cut-and-fill method, for example, can be employed where the pressure is from the sides and the back is strong and self-supporting, while, on the other hand, if the pressure is vertical, square-setting supplemented by filling or some other method of supporting the back is necessary.

If the earth's surface were made up of homogeneous elastic material with no faults or fractures in it, the horizontal pressure at depths would be found equal to a function of Poisson's ratio for the material and the weight and depth involved. If it were plastic, and homogeneously so, the condition of the material would approach hydraulic behavior, in which the magnitudes of pressures are equal in all directions. Unfortunately, none of these conditions attain in a predictable manner under normal circumstances because of the heterogeneity of the earth's crust, both with respect to its composition and structure.

Influence of Geology on Rock Structure and Geometry

It has been shown how the size, shape, regularity of outline, continuity, and other geometric characteristics of ore deposits have a controlling influence upon the support problems involved in their exploitation. Aside from the various theories of the genesis of mineral

deposits, such as structural control, etc., the association of geologic structures with and their influence upon ore deposition are also of prime importance in the mining operations of development and exploitation. Further, many of the same basic elements of rock structure stability are found in tunneling and protective excavations.

The structural features of ore deposits influence all four phases of mining operations, i.e., (1) prospecting, (2) exploration, (3) development, and (4) exploitation. In the first phase of the mining process, geology is the most important tool which is employed in the finding of new ore bodies, and is most effective in the hands of an experienced mining geologist. In the second and third phases of a mining operation, however, it is essential for the mine engineer with a knowledge of strength of materials to have as complete a knowledge as possible of the structural features of the deposit which will affect the production of ore, and which will, in turn, affect the margin of profit. These features fall into the categories of: (1) attitude, size, and shape, as well as (2) planes of weakness, (3) zones of alteration, (4) zones of strong and weak mineralization, (5) competent and incompetent beds, and (6) inherently strong and weak igneous rocks, etc. At present most of these must be dealt with in a qualitative manner, because the structure of the earth's crust is so complex that it yields to a quantitative analysis only in a general way. The structural features of ore deposits may well be considered in relation to three general types of deposits: (1) bedded deposits, (2) veins, and (3) massive deposits.

Bedded and Sedimentary Deposits. Deposits of this type which have not been disturbed by faulting, folding, or other dynamic action, are, like flat-lying beds of coal, very simple to mine. Support problems are often non-existent or a systematic method of pillar support is employed to hold the roof and the overlying rock. Poor rock in the immediate roof, however, such as shale, immediately creates hazardous conditions.

Good examples of this type of deposit are the ores in southeast Missouri, the Tri-State District, Silver King Mine at Park City, Utah, and numerous limestone mines. Coal mines of similar character are very numerous. In each of these the geometry of the deposit is controlled primarily by the thickness and character of the favorable bed which was mineralized, replaced, or deposited. One of the most serious problems in this type of mine may be that of determining the number of pillars which must be left to support the roof.

Veins in Fracture, Shear, and Fault Zones. A large portion of commercial mineral deposits are found in or closely associated with these structural features. The most favorable rocks for mineralization are often those which were originally relatively strong, brittle, and competent. These favorable rocks fracture without notable flow and are strong enough to maintain openings for deposition of minerals. Deposits formed in these structures vary from tabular veins to pipe-like bodies and shoots, and may be regular or irregular, wide or narrow, continuous or discontinuous. Therefore, it could logically be expected to find all types of mining methods used in vein, fissure or shoot deposits. Only in very wide veins does the size have an important influence upon mining. (Figure 3.1)

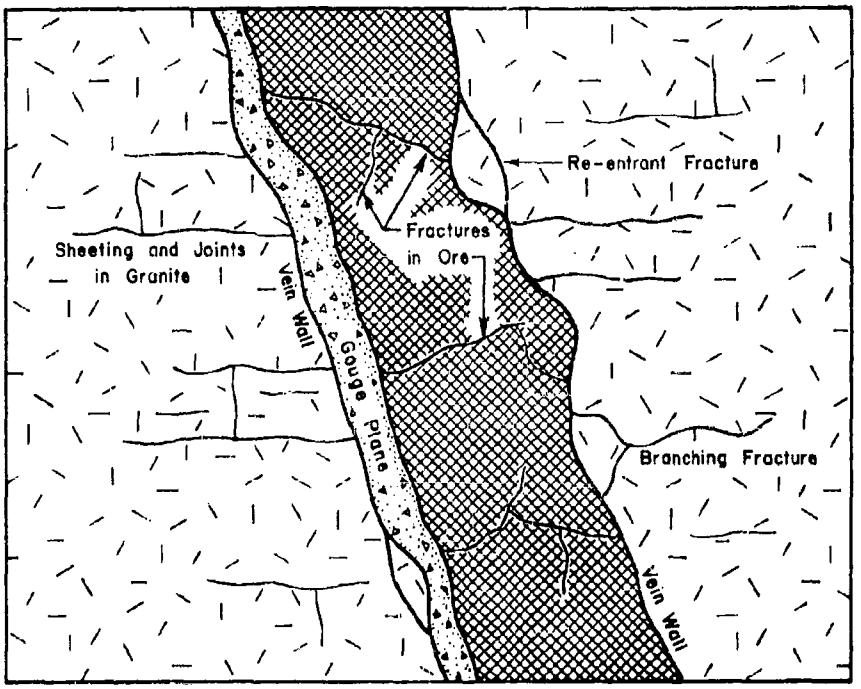


Figure 3.1. Diagrammatic sketch of cross section of vein in granite showing types of fractures and other structure.

The structural formation of veins is employed by Gunther and Fleming[2] as a basis for defining different vein types, and is useful in examining their structural characteristics.

A fissure vein is a mineral mass, which is generally tabular in form with local irregularities. It fills or accompanies a fissure, or a series of closely set and intimately related parallel fractures in the enclosing rock, the mineral mass having been formed later than both the rock and the fracture, either by filling of open spaces in the fracture zone or by chemical alteration of the fractured rock.

Pipes or chimneys are formed where the structural control guides the mineralization along channels of marked vertical continuity, but of relatively small horizontal dimensions. Fault intersections are typical.

Branching veins may extend from the main vein either into the hanging wall or the footwall. The mining of such deposits in the wrong sequence may result in a high concentration of stresses in pillars near the intersections of vein branches.

Conjugate joint systems are often mineralized to form vein systems. Joint patterns such as these are believed to be the result of compressive stresses which were relieved by joint formation rather than the formation of single fissure.

It will be noted that all types of veins are formed along existing planes of weakness in the rock mass. Where a fissure has been completely healed by subsequent mineralization, the resulting vein is often likely to be less resistant than the enclosing rock. Consequently, post-mineral movement may find stress relief through fracturing or crushing of the vein material. Thus, the type of mineralization and its tendency to strengthen or weaken an existing rock structure is of ultimate importance in determining the manner in which subsequent rock stresses in the vicinity of the original fracture will be relieved by further movement or fracturing. In the event that a vein complex is formed by strong, coherent minerals, it would be reasonable to expect the wall rock to relieve or absorb some of the unbalanced post-mineral stresses. Similar fault movement and fracturing to that which has been observed in mines is also found in non-mineralized rocks in which underground installations might be established.

Massive Deposits. The massive disseminated copper ore bodies of the western states are typical of this type of deposit, although other structural classes are mined by the same methods. Those which have enough overburden or capping to prohibit mining by open pit methods are usually mined by block caving. The porphyry coppers are usually massive, flat-lying and relatively regular in outline. They are low-grade but their reserves are measured in millions of tons. The concentration of valuable minerals has been due to secondary enrichment, which in turn generally means a weak, leached capping. Other massive deposits are the molybdenum ore bodies at Climax, Colorado, the Sunrise iron mine in Wyoming, and asbestos mines in Canada.

In each of the above categories, the mineral deposit takes the general form of the host rock or structure, as the case may be, thus controlling the size and shape of the deposit as well as its attitude, location, strike, and dip. As will be seen later, each of these items has its own particular effect upon mining operations, some more important than others, with the importance of each varying from mine to mine.

Mining Methods, Geology and Rock Stability

The history of the development of underground openings in mining and other types of underground excavations, such as tunnels, serves as one of the most reliable current (1961) guides in the appraisal of rock structure stability. Hence, a brief review of the engineering principles and methods employed in the mining of deposits and excavation of other openings in various rock masses encountered will aid materially in establishing the current status of applied rock mechanics.

Although mine openings which are left with natural pillars are often classed as belonging to supported stoping methods, the geology and general stability of rock masses in which room and pillar methods of mining are adaptable are the types which may be most desirable, in general, for construction of underground installations. There are some exceptions to this general rule, but usually the geology of deposits mined by this method is simple. The faulting, jointing, and other weakening processes are little in evidence or are lacking entirely. The complexity of geologic structure usually increases with the increase in complexity of mining methods. The description of mining methods and geologic factors governing the choice of mining methods and the case histories which follow and are given in Appendix III will be discussed in the following order: (1) open stopes with pillars, (2) sublevel stoping, (3) shrinkage stoping, (4) cut-and-fill stoping, (5) square-set stoping, (6) top slicing and sublevel caving, and (7) block caving. The essential details of these methods as related to rock stability are outlined to serve as a basis for a more thorough understanding of the many qualitative and few quantitative aspects of geologic structure as they are related to mining methods in current engineering practice. Detailed examples of geologic case histories are given in Appendix III-A. Summaries of geologic factors for several representative mines are itemized in tables accompanying the description of each method.

Open Stopes with Pillars.

These methods are applicable in general to geologic conditions which are desirable for protective construction. Little or no artificial support is required, and the walls and roof are self-supporting. Small ore bodies may be mined from wall to wall without any pillars being left. Where ore bodies are larger pillars of ore are left to keep the roof span to a safe dimension. Pillars may be regularly or randomly spaced (Figures 3.2 and 3.3), and the method may be applied to either horizontal or inclined deposits. It finds its greatest application in flat-lying, bedded type deposits.

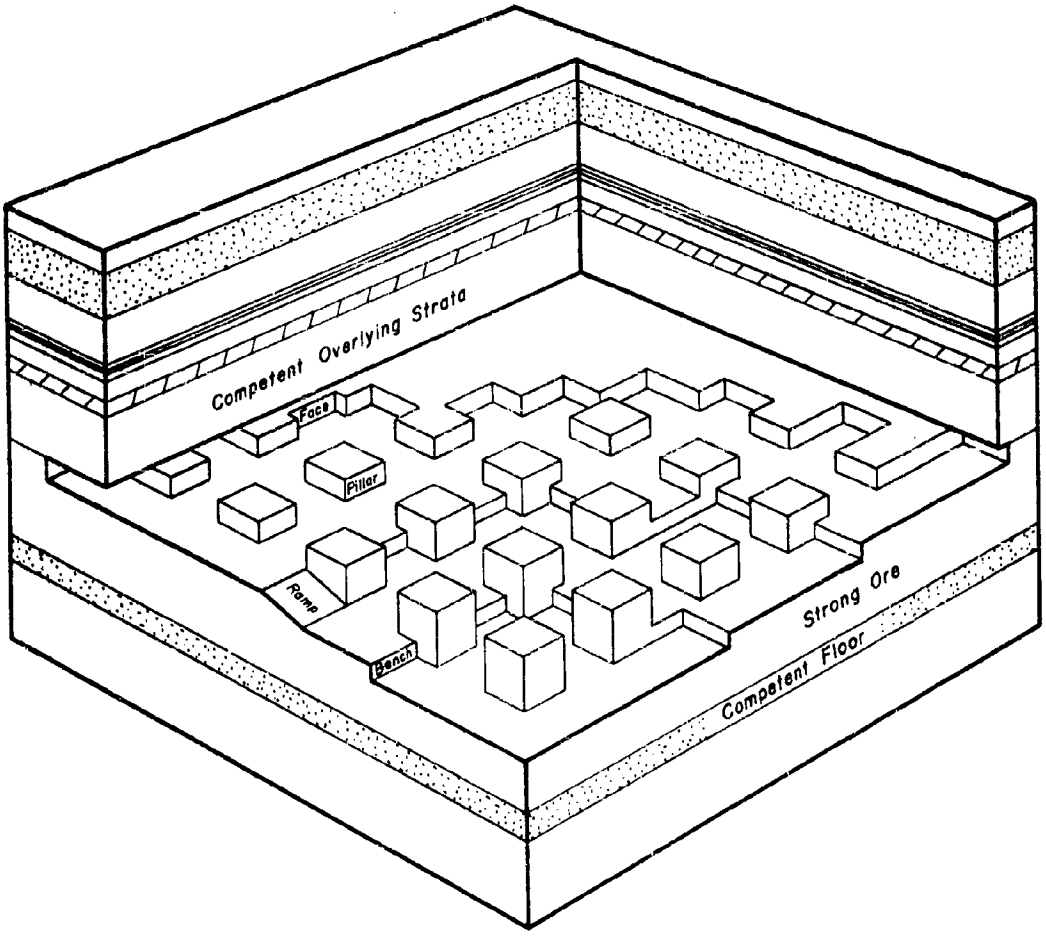


Figure 3.2. Room and pillar method with regular pillars.

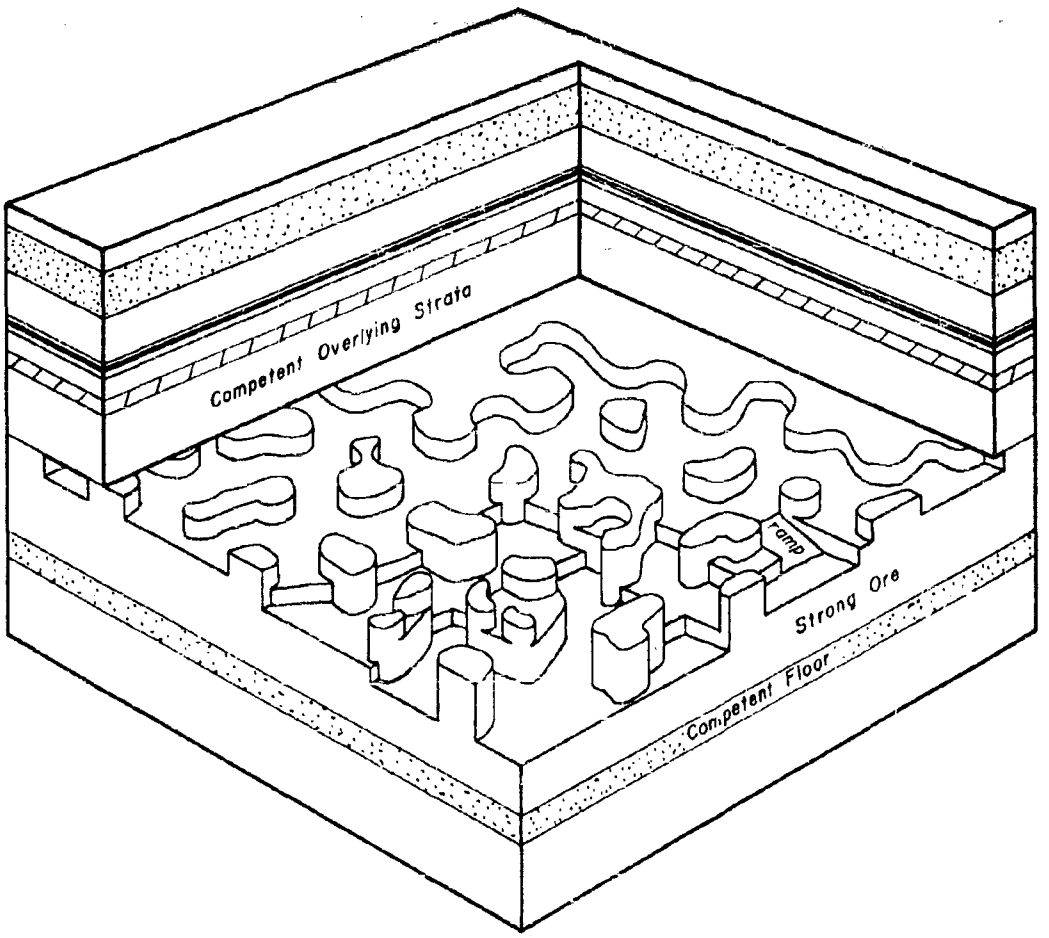


Figure 3.3. Room and pillar method with random pillars.

This method of mining is commonly employed in the extraction of bedded type deposits such as bituminous coal, limestone, phosphate, and deposits of similar geologic character. In non-metallic mines particularly, a regular system of room and pillars is often employed and approximately 50 percent of the valuable mineral is mined, the other 50 percent being left in pillars for support. In other mines, such as the lead mines in southeast Missouri, casual pillars are left to support the roof as required by local geology.

While pillar support may also be used in steeply inclined deposits only deposits of a flat line character will be considered here.

The method of development, and mining of a characteristic flat lying deposit is illustrated in Figure 3.3. One or more development openings are driven in a selected direction and rooms are excavated usually at 90° to the development openings. However, the pattern of layout of rooms in development openings may vary considerably. Pillar heights vary from a few feet in the case of many coal mines to as high as 200 feet in certain lead mines.

Methods of excavating development openings and rooms are quite variable. The principle concern in excavation processes in relation to stability is usually care in blasting. That is, holes should be placed in a proper manner and only an optimum amount of explosives used so that a minimum of overbreak or fracturing beyond the desired surface is caused.

The mine structures of example mines (Table 3.1) are representative of the application of room and pillar type of mining to bedded deposits. These deposits are notable for their simplicity of structure, lack of faulting, both pre-mineral and post-mineral, lack of alteration, and for the competency of the beds and the strength of the overall geologic structure. In spite of the fact that dimensions of the deposits are variable, the method has uniform application throughout the deposits as long as the ore and rock are strong enough to support large openings. The placing of pillars is governed almost entirely by the presence of faults, fractures of weak beds. Where these planes of weakness do not occur, the pillars may be spaced regularly.

It is also noteworthy that many of these deposits occur in sedimentary rocks or in sedimentary rocks which have been metamorphosed. In the case of the deposits in the Tri-State District, the rock was strengthened considerably by the addition of silica which converted the limestone to chert and flint. In most cases the bedding planes, although inherent weaknesses of sedimentary rocks, do not cause problems of support unless they are accompanied by faults and fractures.

Wherever it is encountered, shale almost invariably causes the mine openings to require timber. If water is present, the shale becomes muddy with the consistency of soft clay. If it is dried out by air it tends to slough and spall. Water courses are also a consistent source of trouble. Even if they are dry they represent planes of weakness. If they are active, they create pumping problems.

Table 1.1

Open Stoping with Pillars

Mine	Geological Type of Ore Body	Dimensions	Country Rock	Faulting, Folding, Fractures, etc.	Alteration of Ore and Rock	Type of Mineralization	Geological (Stability) Factors
[illegible]	[illegible]	[illegible]	[illegible]	Nothing to show vertical fracture	None reported	Shale containing "Kerogen"	Flat bedded deposit in undisturbed strata. Shale not subject to sloughing on contact with air.
[illegible]	[illegible]	[illegible]	[illegible]	No [illegible] & are washed out [illegible]	None reported.	Deposit of high calcium limestone	Flat bedded deposit, relatively strong overlying shale strata which remained strong when not exposed to air.
[illegible]	[illegible]	[illegible]	[illegible]	Fine [illegible]	Little local alteration	Disseminated galena in limestone and shale	1. Flat bedded deposit 2. Simple undisturbed structure 3. Strong ore and rock.
[illegible]	[illegible]	[illegible]	Overlying & [illegible] ually strong & plant, standing well; pillars heavily fractured, explosive close pressure of pillars	Local fracture & [illegible] ssp ciant fault.	original limestone converted to lime, dolomite & massive	Sphalerite & galena in flint and chert	1. Flat bedded deposit 2. Simple relatively undisturbed structure.
Mill Shale Mine	Dipping Bedded Deposit	Thickness 5 feet [illegible] 15 feet	Limestone and quartzite	Some post-mineral faulting, has little effect upon mining method	Local oxidation of ore by meteoric water	Sulphides, some oxidized	Simple, relatively thin bedded deposit, roof requires stull support.
[illegible] Mine	Flat [illegible]	[illegible] ft. thick, 75 ft. [illegible]	Interbedded lime and shale	No marked faulting. Overlying beds easily jointed.	Some weathering.	Sedimentary deposit.	Presence of shales and jointing seriously weaken overlying beds. Roof stable when top 12 ft. of mined bed left for roof.

Sublevel Stoping

Sublevel stoping is best adapted to steeply inclined deposits which have strong ore and strong walls. The ore is usually blocked out by two horizontal drifts separated vertically by 100 to 200 feet and raises between the two horizontal drifts, the latter separated by comparable distances. (Figure 3.4). An inspection of the accompanying sketch will show why the ore must be strong as well as the wall of the stope after the ore is excavated. The ore in place must serve as a footing for men who are mining the same and must be sufficiently strong to support the sublevel drifts which are driven at intermediate intervals between the two main haulage levels. Although moderately weak ore may be worked by sublevel stoping if the working faces are kept in the same vertical plane throughout the vertical extent of the stope, this is not usually a safe practice. Vertical pillars may be left between stopes on the same level, and horizontal ones to support the main haulage levels. After the main blocks of ore have been completely mined it is often a practice to rob the pillars, and the walls of the stope may collapse after the pillars have been robbed. In some mines large stopes created by the sublevel method of stoping have remained open for very extended periods of time.

The stress distribution around inclined openings in homogeneous rock has been studied by photoelastic methods and results of these studies are given later in this report. The sublevel method is used to mine both shallow and deep deposits and deposits of a wide variety of dimensions. It is applicable to deposits of small dimensions which are relatively weak, but the method would not be applicable to deposits with the same ore and wall strength if the dimensions were larger and consequently required larger roof spans or larger openings in general.

The employment of the sublevel method of stoping requires, among other characteristics, strong ore which will both serve as a strong roof and offer safe footing for men and equipment on benches which have been undercut by mining. (See Table 3.2). Massive sulphide ore which has not been subjected to fracturing or alteration processes such as oxidation is almost ideal for this type of mining. The sulphide minerals seem to have a capacity for filling small fractures as well as large ones, providing a mineral complex, even in complete replacement processes, which is very competent and strong. The healed fractures vary from those of microscopic size to faults and even cavities of fairly large dimensions.

Strong walls are found in rocks of all three genetic types. Fine-grained rocks are very competent, even when slightly fractured. In all of the examples given, there is a lack of extensive post mineral faulting, fracturing, and alteration processes which tend to weaken the rock structure.

The large size of the ore deposits is a desirable feature, as in the case of the Lower H ore body is the Horne mine, which is massive and irregular in outline, and the walls of the stope are constituted of massive sulphide ore itself. In this deposit, the silicification of the rhyolite breccias has played an important part in strengthening the enclosing rock structure which was fractured by pre-mineral stresses.

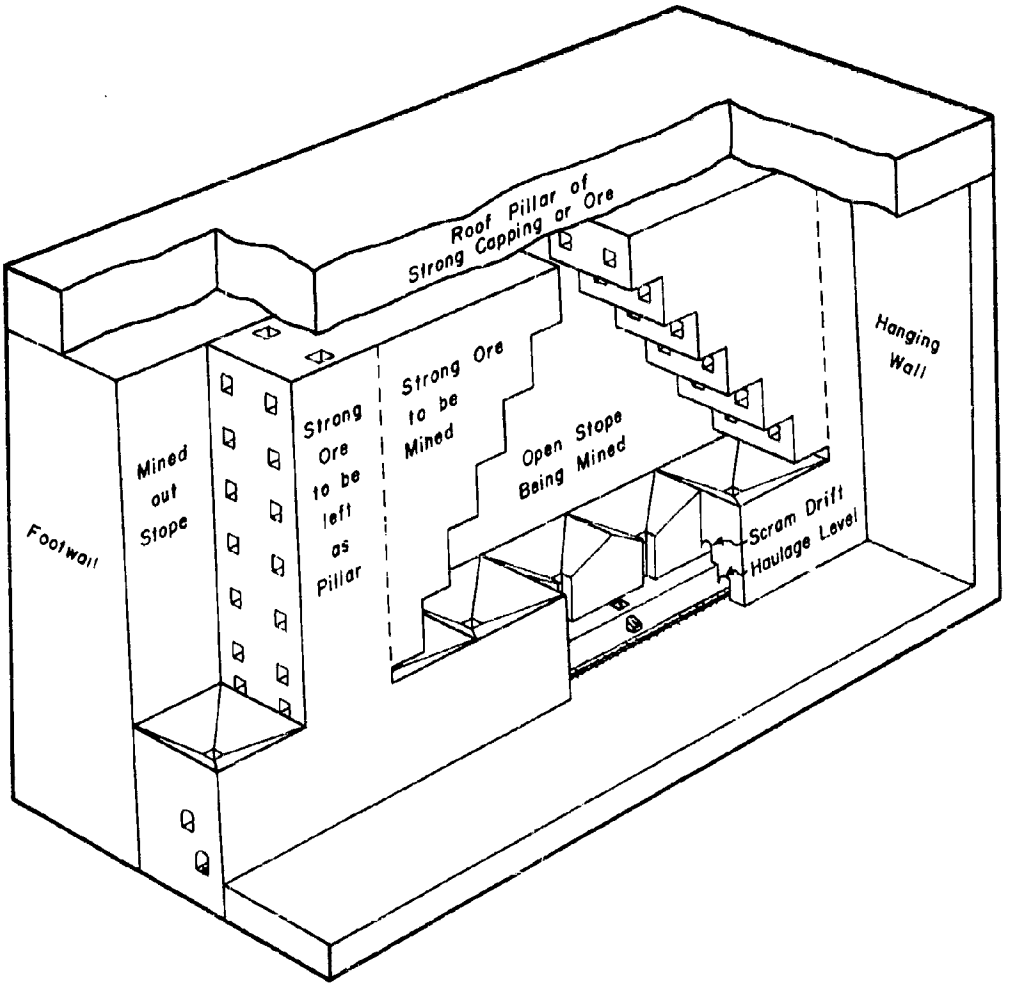


Figure 3.4. Schematic of sublevel stoping which is adapted to strong ore and strong wall configurations.

Table 3.2

Sublevel Stoping

Mine	Structural Type of Ore Body	Dimensions	Country Rock	Faulting, Folding, Fracturing, etc.	Alteration of Ore and Rock	Type of Mineralization	Geological (Stability) Factors
Horne Mine	Large, irregular nearly vertical body of massive sulphides, occurring as a replacement of brecciated	"B" ore body: length --6 ft. width = ft. to 5 ft. Stoping width---6 ft	Rhyolite, brecciated, tuffs and agglomerates	Faults of small displacement, & shear zone - faulting are of varying intensity	Silicification of breccias. Sericitization - Chloritization are minor	Massive sulphides carrying Cu & Au Ore is unusually strong & compact in character & stands well. Occasional slips in ore,-little gangue material.	1. Silicification of breccias, strong rocks 2. Massive sulphide ore has but few slips 3. Destructive alteration has minor effect 4. Minor post-ore faulting.
Flin Flon Mine	Massive sulphides in a shear zone to irregular lenses & irregularities in connected lenses	Width ft. to ft. Depth ft. to ft. Length	Rhyolite--hard fine-grained, different from rocks and schistose areas. Footwalls from qtz. porphyry to soft talc schist somewhat flatter than hw, firm under schist	None recorded.	1. Silicification-producing a quartz chlorite schist. 2. Chloritization producing a black, slabby schist	Massive sulphides--Au, Ag, Cu, Zn. Ore very heavy and hard three types: 1. Massive sulphide 2. Disseminated 3. Banded ore	Both ore and hanging wall are strong and firm; footwall is reasonably strong.
Mine Island Mine	Ore deposits occur as replacement lenses in shear zones and folds in a thick series of shales dipping 35° to 90°	Length ft. to Depth ft. to Min. thickness stope ft. to ft. ft. bands in hw & fw to 70 ft. band in hw	Shales	Folding and faulting assoc. with all ore bodies, faults usually inconspicuous slips cause weak hw & use of sq. sets, slumping has occurred due to structural weakness of hw caused by faulting. Ground weakness due to pre-ore folding & faulting.	Oxidized ore in some areas,-mined by square sets and cut-and-fill where weak.	~.6 oz Ag, 8.2% Pb, 8.12 Zn. Valuable sulphides usually interbanded with pyrite and pyrrhotite. Oxidized ore is weak and friable	1. Low grade of ore 2. Desirability of allowing development and exploitation to go on concurrently 3. Ore oxidizes rapidly 4. Ore breaks in blocks making caving unsuitable
Kam Antelope Mine	Mineralized band of argillaceous ss and shales. Deposit is an asymmetrical plunging syncline Dips: flat to 90°	to feet thick	Hw shades into lean shales, qtz. ss & dol.; band of schist on fw on top of qtz. and congl.	No major faults which affect stability	Metamorphosed argillaceous sandstone and shale.	Disseminated Cu sulphide in ss & shale	1. Openings can always be barred down and made safe 2. Working conditions are always uniform 3. Pillar spacing can be varied as conditions demand 4. No major faults or destructive alteration.
Burra Burra Mine	Irregular lenticular mass of iron sulphides as repl. of limestone	.5 mile long Few ft. to 180 ft. wide, dips 35 to ~°	Highly metamorphosed schists, graywacke and slate stand unsupported over 100 ft. span. Walls firmer than ore, schistosity parallel bedding, breaks at bedding	Walls stand well ex. where fract. by folding ore has few hor. slips & joints, faults are of small displ.	Minor alteration of graywacke and schist	Iron sulphides carrying 1.6% Cu in chalcopyrite Ore does not break free from walls	1. Massive, strong ore with few fractures 2. Strong wall rock--few prominent fractures 3. Steep dips 4. Minor vertical joints 5. Premineral faulting and folding has minor effect on stability. Probably largely compensated by strength of rock.

Shrinkage Stoping

The characteristic feature of shrinkage stoping is that broken ore is left in the stope to support the walls while the remainder of the stope is mined. The broken ore also serves as a floor on which the miners may stand while mining the ore above them. A block of ore is developed in a manner similar to that employed for sublevel stoping in the preliminary stages. No sublevels are driven, however, and the ore is mined from the bottom upward. (Figure 3.5). Because the ore expands when it is broken, about 35 percent of it must be drawn off at the bottom during the mining process. After a stope is completed the ore is drawn out and the space is left open. If pillars are left at the ends of the stope or the top or bottom they are often robbed when that part of the mine is to be abandoned.

Since the ore must stand by itself during the whole process of mining, over the width and length of the stope it must be strong. The walls may be somewhat fractured but may not be excessively weak because they will then slough off as the ore is withdrawn, and the ore will be diluted. Hence, in deposits which are mineable by the shrinkage methods, the overall structure is one degree weaker geologically than the structures to which sublevel stoping is applicable. In the latter both the ore and walls must be strong while in shrinkage stoping the walls may be somewhat weaker.

Shrinkage stoping is classified by some as an open stope method of mining, and by others as a supported stope method. Each classification is probably justified because the back of the stope, which is usually ore, is unsupported during the process of mining, while the walls are supported by broken ore whether they need support or not. Deposits mined by this method are, then, more or less on the border-line between those which require support during mining and those which do not. In terms of strength of ore and walls, it means that the ore should be strong in any case, while the walls may be weaker than the walls of deposits mined by sublevel stoping.

A comparison of Table 3.2 and Table 3.3 shows that there has been little, if any, significant alteration of the ore or rock in either type of mining. But there is more evidence of dynamic movement of the rock in the deposits mined by shrinkage stoping, especially post-mineral faulting.

In some cases, as at the Hollinger and Wright Hargreaves mines, the size of the veins was the determining factor, only narrow veins being mined by this method. At the United Verde mine a massive sulphide body, non-ore, serves as the host rock for the ore deposits. Unless disturbed by faulting and fracturing it is very competent as are similar bodies (ore) at the Tennessee Copper Company (sublevel stoping).

As in the case of the other methods of mining studies, almost any of the genetic types of rock may prove structurally strong if they are fresh and unfractured.

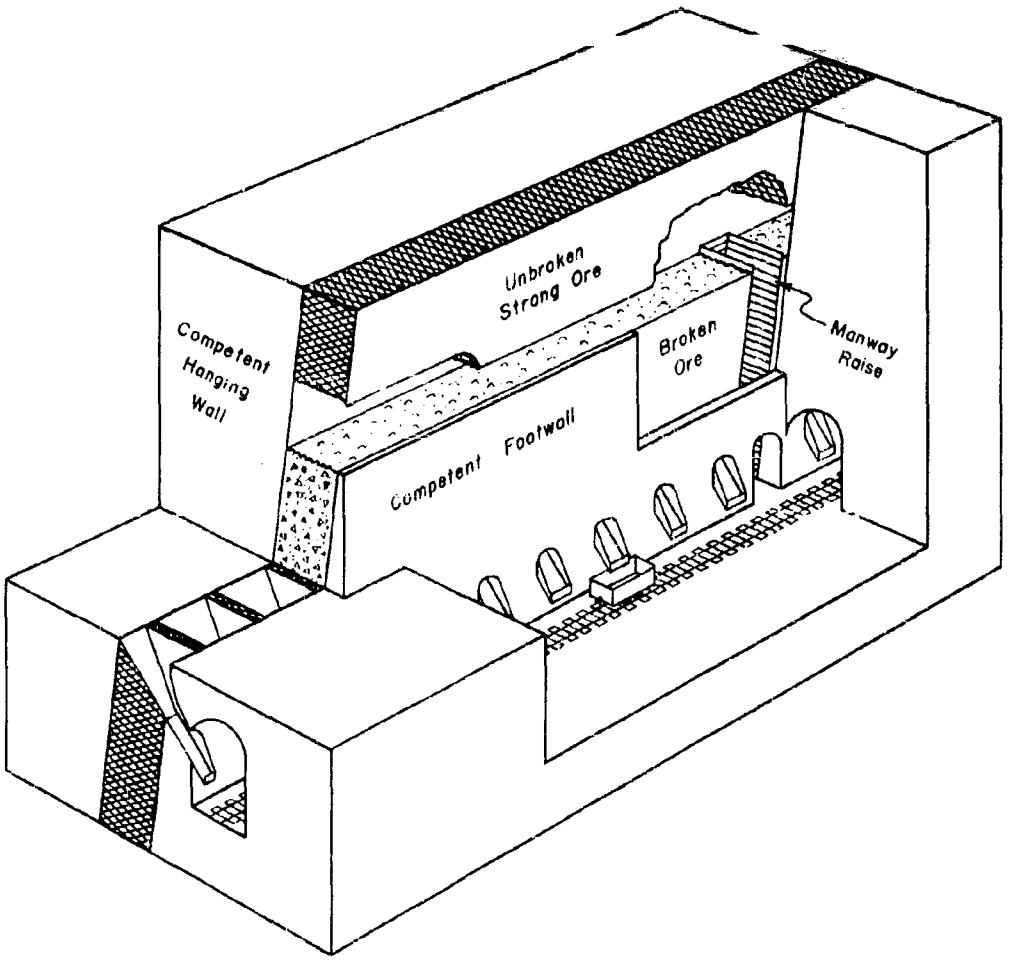


Figure 3.5. Diagrammatic sketch illustrating principles of shrinkage stoping method.

					Geological (Stability) Factors
					ore because of lack of faulting and alteration. Steep dip.
					Strong, walls are ore, steep dip.
					Strong ore and all with minor fracturing, ste dip.
					Strong ore and all, steep dip.
					Solid ore and lls due to lack of faults and alte ation, steep dip having in gabbr and slate, shrinkage an cubic.
					Strong ore and lls with numerous faults which ... minor effect on stability.
					Strong ore and lls with minor faulting, fractu ing and alteration, steep dip, few ker than 8m.
					Shrinkage stoping use where ore and walls are strong; oth methods used in w ak ore and rock; steep dips; mineral cemented by m neralization.
					Relatively strong ore ad wall rock, ste p dips.

Table [illegible]

Summary Section

Mine	Structural Features of Ore Zone	Size of Ore Zone	Ore Body Shape	Faulting, Folding, Fracturing, etc.	Alteration of Ore and Rock	Type of Mineralization	Geological (Stability) Factors
[illegible]	[illegible]	[illegible]	[illegible]	[illegible]	[illegible]	Au & sulphides in pyrite	Relatively strong ore & walls, with steep dips, weak schist on fw.
[illegible]	[illegible]	[illegible]	[illegible]	[illegible]	[illegible]	[illegible]	Strong ore and walls.
[illegible]	[illegible]	[illegible]	[illegible]	[illegible]	[illegible]	[illegible]	Only minor post-mineral faulting and hydro-thermal alteration. Shrinkage stoping used only in veins thinner than 8 feet and with strong walls.
[illegible] Pittsburg-Idaho, Pittsburg Idaho	Numerous veins, width and continuity variable	Veins of 1 to 12 ft. width, narrower and less persistent	Porphyry and brecciated porphyry dominated by quartz veinlets	Several strong post-mineral faults, whose complexity diminishes rock stability.	Porphyry altered & weak in local areas	Pyrite, tellurides, chalcopyrite, free gold & molybdenite in quartz	Shrinkage stoping used where ore is 6 ft. or more wide with strong walls. Porphyry breccia strengthened by mineralization.
Nevada-Mass. Co.	Tungsten ore in thin limestone beds	Average = 5 feet	Limestone beds dipping 7° to 75°	Beds displaced by post-mineral faults	None reported.	Scheelite (?)	Steeply dipping deposit with strong ore and walls.
United Verde Mine	Massive type-schist replacement as "fingers" in schist and porphyry	Large horizontal area	Schist, porphyry and massive sulphide	Not described	None reported.	Sulphides	Massive sulphide-strong permits shrinkage stoping, schist varies in strength, - requires support.

Cut-and-Fill Stoping

The development work, that is, drifts and raises driven preliminary to actual mining by cut-and-fill stoping, proceeds in principle in much the same manner as that for sublevel stoping and shrinkage stoping. The cut-and-fill method, as the name implies, employs a sequence in which the ore is removed in a series of parallel slices and as each slice is removed a layer of waste fill is placed in the stope leaving sufficient working headroom in which to drill the ore. The applicability of this method is much the same as that of shrinkage stoping. The ore must be strong since the miners work under an overhanging back of ore. The walls may be weaker since they are supported almost immediately by filling. Fill may be broken rock from other parts of the mine, or more recent developments have utilized hydraulic filling by means of pumping of slurries through pipe lines into the stopes and draining the water off. The latter method creates a more satisfactory fill usually than a fill composed of large fragments of broken material because the latter settles more. The walls can be weaker than those which would be found in shrinkage stopes, and the ore may be of such a type that dilution cannot be allowed. Also, if the ore is of such a character that it might oxidize readily and cause difficulty in later concentration processes shrinkage stoping cannot be employed. Cut-and-fill method of mining is illustrated in Figure 3.6. Its applicability in addition to the above factors is greatest in steeply inclined deposits where ore may be removed by gravity after it is blasted and the stopes may also be filled by gravity from above. The overall structure in deposits commonly mined by this method is usually quite weak. However, mining methods demand that minimum subsidence occur adjacent to the ore body and hence immediate filling usually will give a reasonably strong support and maintain a stable overall structure to the mine locale.

Cut-and-fill stoping (Table 3.4) is employed successfully in those deposits which display a degree of structural weakness just one step farther removed from those which are fairly strong and may be mined by shrinkage methods. It is common to find both of these methods of mining used in the same mine to extract the ore from different sections of the same deposit, as well as to find that many mines use three methods of mining in the same deposit, i.e., square-set stoping in addition to the two noted above.

Cut-and-fill stoping requires relatively strong ore which will require no support during stoping operations. It is used to advantage where the ore is strong but the walls are so weak that shrinkage methods cannot be used or dilution of ore results.

This method is essentially a selective method of mining, and consequently can be used in irregular deposits. It also will permit some storing in stopes.

The geological reasons for use of cut-and-fill are summarized as follows:

1. Weakening of rock structure by pre-mineral faulting.

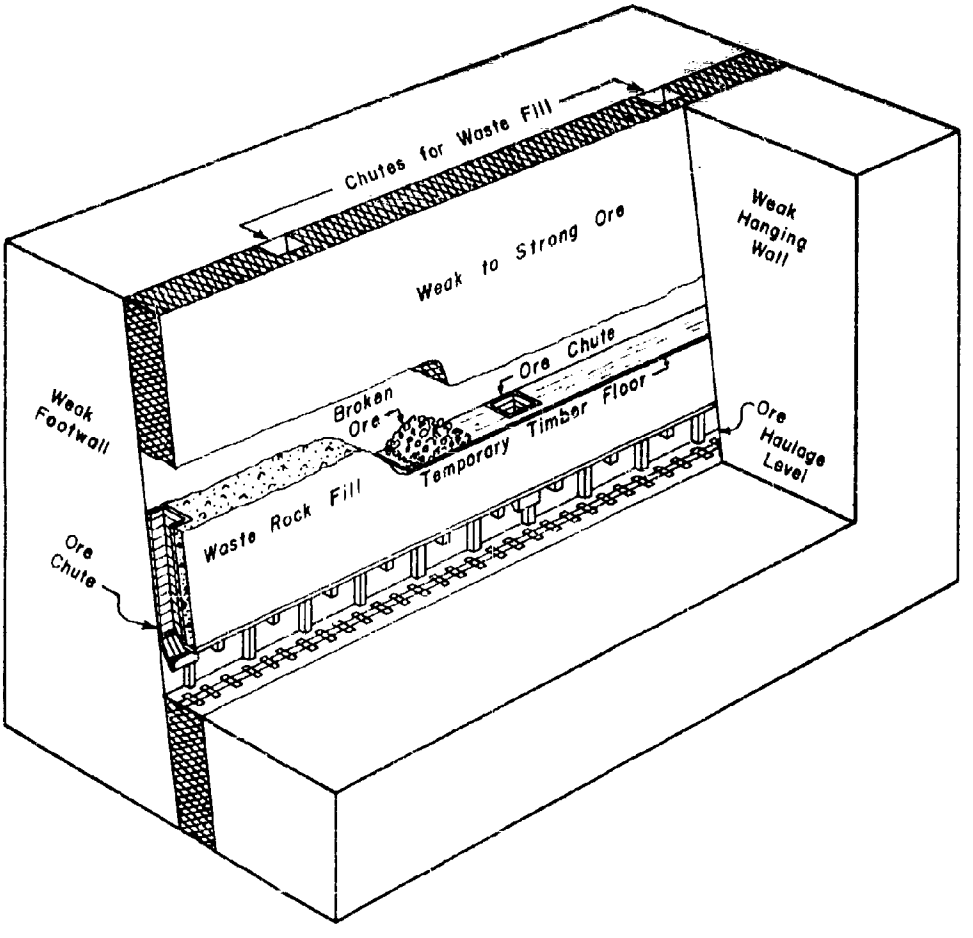


Figure 3.6. Method of cut-and-fill stoping is adapted to moderately weak ore and wall structures.

Mine	Alteration of Ore and Rock	Type of Mineralization	Geological (Stability) Factors
		Quartz vein	Weak walls and ore on lower levels where pressure is greater due to depth.
		Ore is in quartz vein	Cut-and-fill used where ore is strong enough that it does not require immediate support, but where walls are weak due to faulting and alteration. Cut-and-fill in narrow veins only.
		Quartz, pyrite and "Flinty"	Fracturing and alteration of rock causes the walls to require close support. Only narrow veins mined by cut-and-fill stoping.
		Quartz, pyrite and small amount of galena	1. Vein system very complex 2. Fractures and schisting create local weakened structure 3. Wide variations in the width of vein 4. Variations in the strength of vein filling.
		Native copper in lava flows	1. Ore is persistent but varies greatly in width. 2. Copper is irregular and patchy, -requires sorting. 3. Badly broken ore.
	Intense silicification	Massive & disseminated sulphides in norite and granite	Cut-and-fill used where: 1. There is weakness due to shear 2. Ore bodies are irregular 3. Rock bursts in granite 4. Pressure due to depth of mining operations 5. Highgrade ore requiring selective method.
	Porphyry highly altered to "fruitland & molybdenite in quartz	Pyrite, tellurides, chalcopyrite, fine gold & molybdenite in quartz	Method used on North and South veins where walls are brecciated or crushed and silicified.
	Intense silicification	Sulphide replacement and dissemination	Walls weak and slabby due to faulting and lack of silicification.
		Hard quartz, sugar quartz or conglomerate-like material	Blocky quartzite or porphyry walls tend to slough.

2. Weakening of rock structure by post-mineral faulting.

3. Further weakening of rock by hydrothermal and hydro-metamorphic processes.

4. Lack of silicification in certain areas of a deposit.

5. Lack of other types of "healing" mineralization.

6. Irregularity of outline of deposit, which requires a selective method of mining.

7. Irregularity of grade or lack of uniformity of grade of ore, which also requires a selective method.

8. Ore oxidizes rapidly, preventing use of shrinkage stoping which "stores" ore in stopes for long periods of time. This is true for ore which is to be treated by flotation.

Square-Set Stoping

This method is most applicable in mining deposits in which the ore is structurally weak. Also the surrounding rock may be fractured, faulted, and altered to such an extent that it also is very weak. The geometry of the deposit may be such, and the value of the ore of sufficient magnitude that caving methods may not be employed. The method is very flexible in that sets can be extended in any direction or can be terminated as irregularities in the shape of the ore body are encountered. Development takes place in much the same manner as that in the methods previously described. In stoping one small block of ore is removed sufficiently large to allow replacement of a set of timber, which is immediately set in place. (Figure 3.7). The primary function of the square sets is to furnish only temporary support for loose fragments of rock and to offer a passageway to the working face. Permanent support for the stope walls is supplied by filling the sets with broken waste rock. This is placed as soon as possible after a tier of sets is worked out, especially if the ground is heavy.

In many geological settings in which a square set method of mining is employed the ore and rock structure actually approach being unconsolidated materials. As will be noted in the examples given below the instability is caused by faulting, fracturing, and folding, and destructive alteration which accompanies mineralizing processes.

The factors affecting the use of square-sets are as follows:

1. Grade of ore - the ore must be high enough in grade to pay for the use of the large amount of timber required.

2. Physical character of ore and rocks - in nearly all of the mines using this method, the enclosing rocks are broken and altered. Structurally weak ore and rocks usually go together, although this is not always the case.

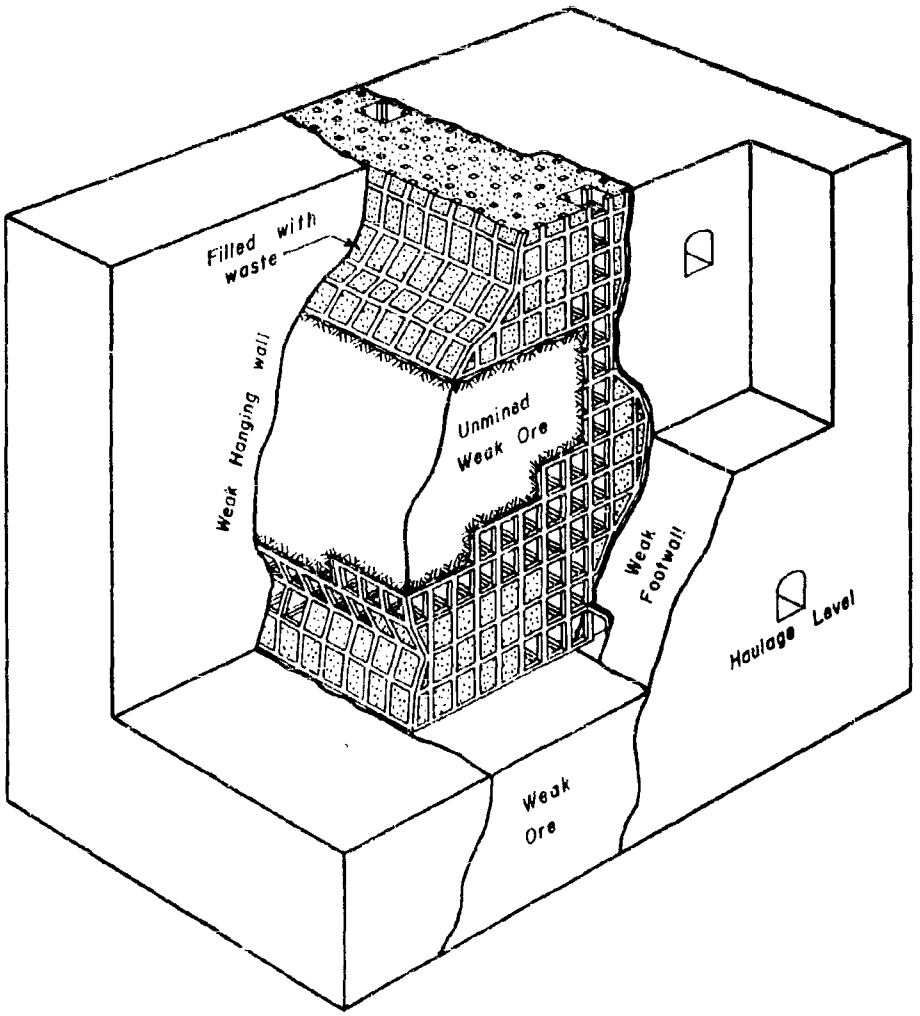


Figure 3.7. Square set method is used under conditions requiring maximum support for ore and walls.

3. Size, shape, and dip of deposit - the method is very flexible and can be used in almost any size of deposit regardless of its shape and dip.

4. Effect of ground movement - may be some settling in the fill, and there is squeezing and subsidence of country rock.

The square-set method is the one which is employed when all other methods, exclusive of caving methods are not applicable because of support problems involved or the need for selective mining. (Table 3.5).

Top Slicing and Sublevel Caving

The top slicing and sublevel caving methods of mining are similar in development and in many aspects of ore removal.

In the top slicing method the ore is removed in a series of horizontal slices beginning at the top of the orebody immediately beneath the capping. The latter is allowed to cave after each slice of ore is mined. As each horizontal section of ore is removed the ground above is temporarily supported by timber. (Figure 3.8).

The most suitable type of deposit for mining by top slicing is ore of large horizontal extent in which the ore is too weak to stand without support except over a short span. The most vital requirement is a weak capping which will cave when it is undermined.

Development for top slicing consists of driving a series of drifts and crosscuts at some distance below the mining level and then raising to the top of the ore for mining.

Sublevel caving is very similar to top slicing. The general plan of operations is to mine every other slice, permitting the weight of the capping to assist in mining of the ore. The capping should be somewhat stronger than that in which top slicing is applicable.

For both top slicing and sublevel methods of mining, the most necessary requirement of the structure is a weak capping that will cave when it is undermined. This feature is found in the given examples and is due either to the presence of weak members in the overlying formation or to the presence of planes of weakness. (Table 3.6). In either case the caving formations should not "key" and arch to such an extent that sudden collapses will create dangerous mining conditions. Top slicing is more readily adaptable to deposits of large horizontal extent, while sublevel caving can be employed to mine deposits which are more irregular in outline. In both cases the ore should be moderately weak, but strong enough to stand temporarily. This characteristic may be due to the inherent character of the mineral complex itself or due to alteration and fractures.

Mine					Geological (Stability) Factors
Arimetco Mining					Fracturing and alteration of rock cause the veins to require close timbering in wider veins.
Bunker Hill / Sullivan Mine				Irregular masses of ore with siderite in quartz gangue	Close timbering required because of fracturing of rock and ore, size of ore bodies and need for high percentage extraction of ore.
McIntyre Mines / Silverbell					Square setting used because of friable char. of rock, presence of slips, contacts and general irregularity of ore.
[illegible] Mine / Sedalia				Irregular, pinching and swelling veins. Mineralization intensifies with depth. Ore consists of: 1. base-sulphides of zinc, iron and lead 2. lead-sulphides 3. lead	Close Square set timbering required because of cross fractures in ore in some areas. Cut-and-fill is also used.
[illegible] Mine / Gardiner					Joints and fractures of deposit constitute planes of weakness which require close support; silicified areas require less support.
[illegible]					Fractures of ore and walls cause openings to require close timber support
[illegible]					Intense fracturing, alteration and mineralization weakened structure so that immediate support is required.
[illegible]					Fracturing and alteration of rock cause openings to require support.

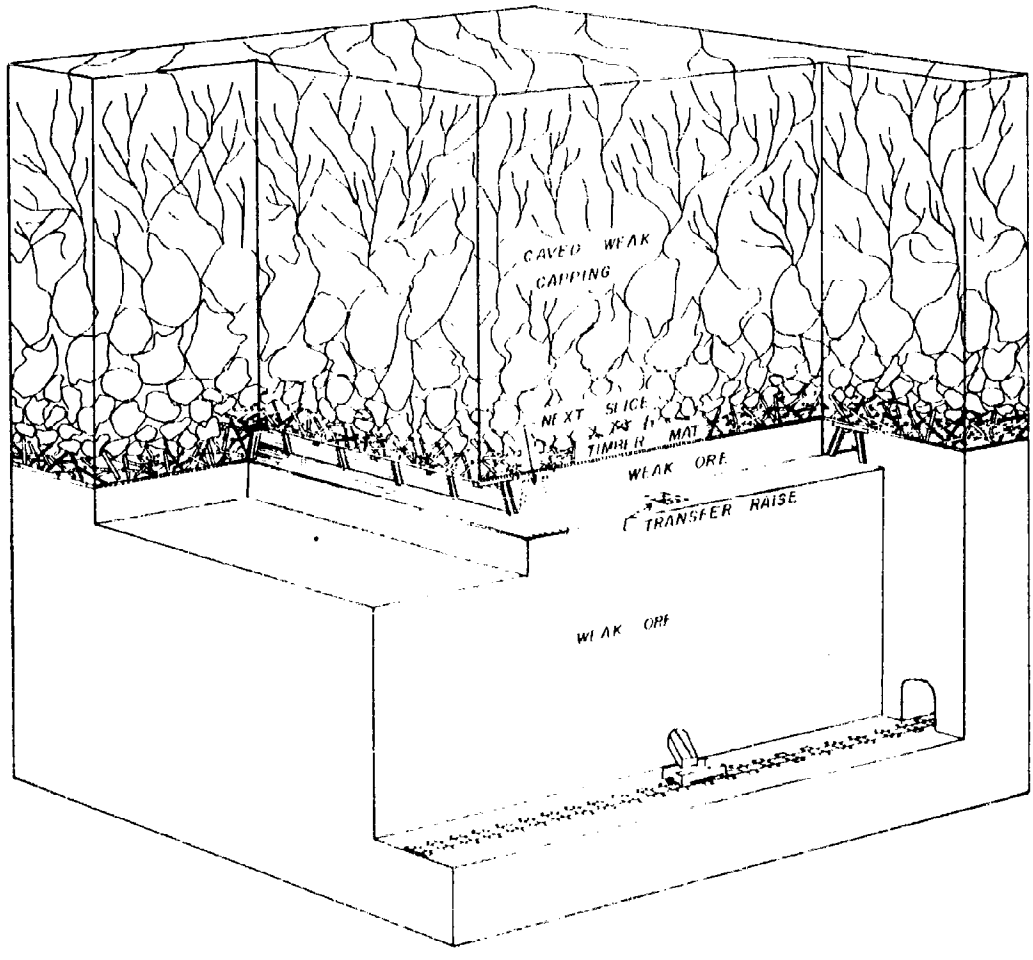


Figure 3.8. Block diagram illustrating principles involved in application of top slicing method.

Mine					Type of Mineralization	Geological (Stability) Factors
						Much wet shale ore, method also applicable to wide fissures.
					Massive sulfide impregnation in schists	Broken condition of ore body and walls made most other systems unsafe.
				Oxidation by meteoric water in upper part of ore body and fissure	Hematite ores, secondary concentration in residual zone of iron bearing sediment	Top slicing used in wide ore, otherwise mined by sublevel stoping.
Typical Mines of Pyritic Ore Bodies	Pyrite, pyrrhotite, chalcopyrite, sphalerite, galena, gold, silver, tin, bismuth, tellurium, selenium, cadmium, indium, gallium, germanium, thallium, arsenic, antimony, cobalt, nickel, molybdenum, tungsten, uranium, vanadium, platinum group metals	Massive, stratiform, lenticular, tabular, irregular, pipe, veins, stockwork, replacement, disseminated, massive sulfide, gossan, supergene enrichment, oxidation, leaching, metamorphism, deformation, folding, faulting, fracturing, schistosity, foliation, lineation, lithology, stratigraphy, host rocks, wall rocks, footwall, hanging wall, ore zones, ore shoots, ore controls, structural controls, lithologic controls, stratigraphic controls		Sedimentary, metamorphic, volcanic, igneous, hydrothermal, exhalative, sedimentary exhalative, volcanogenic, syngenetic, epigenetic, Kuroko, Besshi, Cyprus, Noranda, Mount Lyell, Rammelsberg, Sullivan, Tharsis, Iberian Pyrite Belt, Appalachian, Canadian Shield, Scandinavian, Urals, Australian, Japanese, Philippine, Indonesian, Papua New Guinea, Solomon Islands, Fiji, New Zealand, Chilean, Peruvian, Bolivian, Mexican, Cuban, Dominican Republic, Haitian, Jamaican, Puerto Rican, Virgin Islands, Bahamian, Caribbean, Central American, South American, North American, European, Asian, African, Australian, Oceanian, Antarctic, Arctic, Subarctic, Temperate, Tropical, Subtropical, Desert, Arid, Semi-arid, Humid, Subhumid, Mediterranean, Continental, Maritime, Coastal, Inland, Island, Peninsular, Archipelagic, Oceanic, Continental, Shelf, Slope, Rise, Abyssal, Trench, Ridge, Seamount, Guyot, Atoll, Reef, Lagoon, Beach, Dune, Estuary, Delta, River, Lake, Swamp, Marsh, Bog, Fen, Peat, Coal, Lignite, Bituminous, Anthracite, Graphite, Diamond, Gold, Silver, Platinum, Copper, Lead, Zinc, Tin, Nickel, Cobalt, Molybdenum, Tungsten, Uranium, Vanadium, Iron, Manganese, Chromium, Titanium, Aluminum, Magnesium, Sodium, Potassium, Calcium, Barium, Strontium, Lithium, Beryllium, Boron, Fluorine, Chlorine, Bromine, Iodine, Sulfur, Phosphorus, Arsenic, Antimony, Bismuth, Selenium, Tellurium, Cadmium, Indium, Gallium, Germanium, Thallium, Rhenium, Hafnium, Zirconium, Niobium, Tantalum, Rare Earths, Yttrium, Scandium, Actinium, Thorium, Protactinium, Uranium, Neptunium, Plutonium, Americium, Curium, Berkelium, Californium, Einsteinium, Fermium, Mendelevium, Nobelium, Lawrencium, Rutherfordium, Dubnium, Seaborgium, Bohrium, Hassium, Meitnerium, Darmstadtium, Roentgenium, Copernicium, Ununtrium, Ununquadium, Ununpentium, Ununhexium, Ununseptium, Ununoctium	Concentration of hematite in pitcher and trough	1. Triangular shape of ore bodies 2. Soft weak ore 3. Fairly strong capping which slabs when unsupported.

Block Caving.

Block caving is most applicable to large orebodies which have a capping which may be caved. Development consists of driving a series of evenly spaced crosscuts below the bottom of the ore, from which main, branch, and finger raises are driven up to the ore. The ore is then undercut and the weight of the ore plus the capping is employed to force the ore to crush, run down through the raises and thus mine itself. The most ideal conditions for block caving are found in the porphyry copper deposits where both the ore and capping are weak. However, large deposits of relatively strong ore with strong capping are also mined by block caving. In this case it may be necessary to completely undercut a section of the ore and isolate it on one or more sides with shrinkage stopes. (Figure 3.9).

Use of block caving resulted from a gradual development of methods wherein the pillars left in rooms were mined in Lake Superior iron mines. The mechanics of block caving involve first, the weakening of a mass of rock by undercutting, second, further breakage of the ore just above the draw points, usually by blasting, and finally crushing of the ore by the mass of overlying material so that it may be drawn off through "finger" raises. The results of the process are the production of a large mass of unconsolidated material above the draw points and a more competent mass below this elevation to the haulage level. The strength and stability of the lower mass is often affected by the movement of the upper. The creation of such large unconsolidated masses of rock has been proposed by some as a means of providing protection for underground installations. The presence of a blanket of unconsolidated material is suggested as a means of damping shock or stress waves from large scale explosions at or near the surface.

The work of King at the Climax Molybdenum mine is one of the few published attempts to evaluate the strength of block caving mine rock in a quasi-quantitative manner (Table 3.7). The strength of the rock and the ore are defined in terms of the spacing of fractures, type of mineralization in the fractures, silicification, and alteration of the constituent minerals. The original composition of the rock and the type of alteration are also important. Silicification and kaolinization almost universally indicate weak rock structure. Strength and composition of mineralizing solutions, pre-mineral and post-mineral faulting, composition of the local rocks all contribute to strengthening or weakening the rock structure as the case may be.

At Climax (Appendix III) the rock formations are strong as compared with those of other block caving mines. However, the relative positions of the four classes of rock, plus the fact that the ore is not very strong, make the deposit adaptable to block caving methods.

In the "porphyry coppers" the alteration and mineralization processes are of such a nature that they create favorable conditions for block caving methods, both in the ore and the capping rocks. Close fracturing is a universal characteristic in this type of deposit and also in the asbestos, iron, and limestone mines utilizing this method.

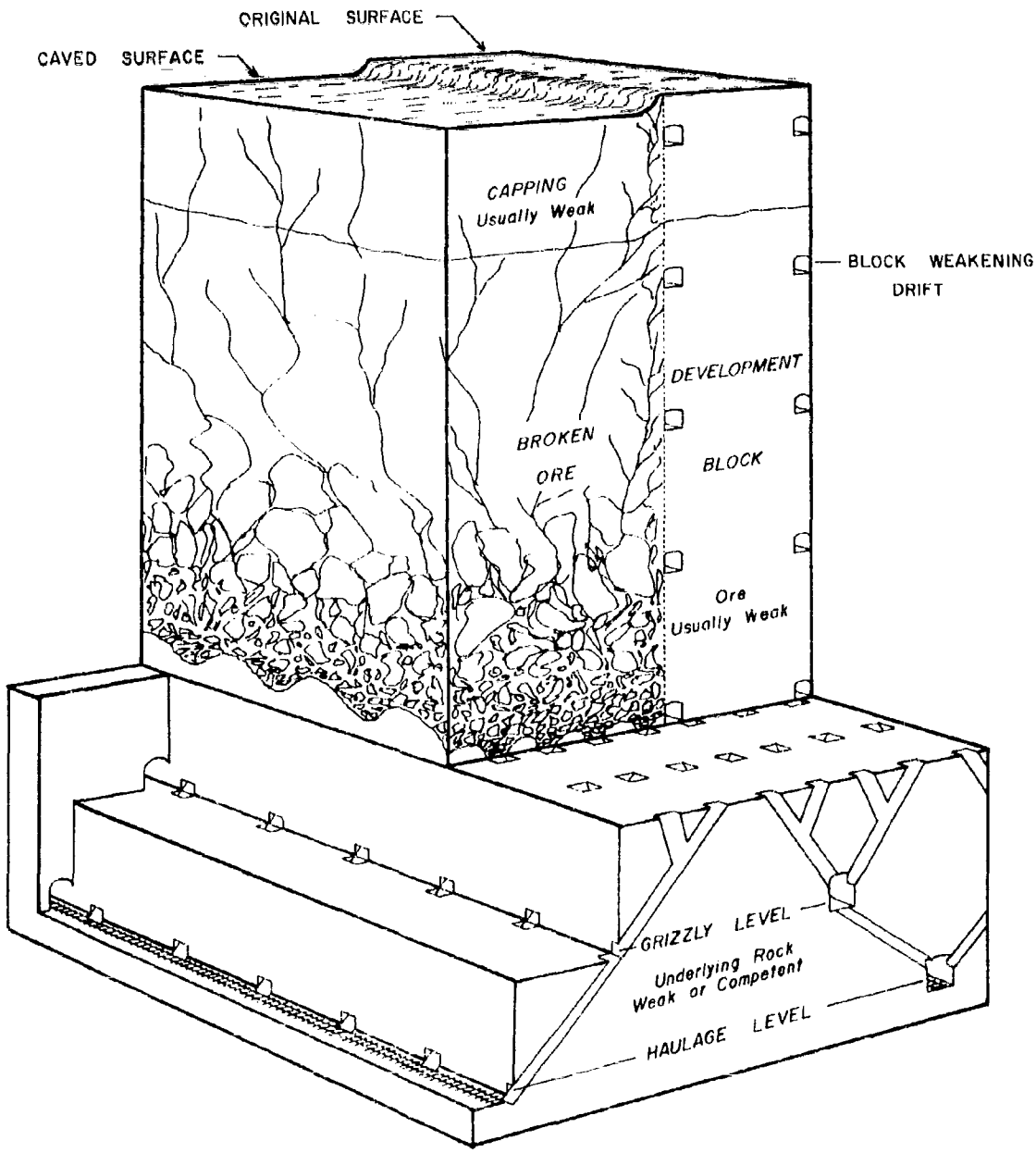


Figure 3.9. Block diagram illustrating principles involved in application of block caving method.

Table 3.7

River Covers

Mine				Faulting, Folding, Fracturing, etc.	Alteration of Ore and Rock	Type of Mineralization	Geological (Stability) Factors
Mine Name Mine Name					Ore most altered and fractured	Replacement of country rock by chalcocite, in seams or disseminated	Both ore and capping weakened by alteration and fractures. Ore body of massive type.
Mine Name Mine Name					Kaolinized slides in quartz. Silicification intense at fault. Slight at the capping. Gives surface alteration & is then silicified	Molybdenite in fractures & disseminated in quartz veinlets	Massive ore body and capping are fractured, altered and weak enough to cave; ore varies from weak to moderately strong.
						Chalcocite, molarite, azurite & chrysocolla in cracks. Some disseminated chalcocite	Massive ore body thoroughly fractured and weak.
						Asbestos & chrysotile as small veins on cleavage planes	Massive ore body well fractured, shattered and sheared.
						Mainly red hematite	Ore is weak and earthy. Schist is weak and tends to dilute ore. Lms and qs are strong and break into large slabs.
						Disseminated chalcocite with minor	Massive deposit with both weak ore and capping due to fractures and alteration.
Name Mine Name of Area Name of Co.					Kaolinized, silicified and sericitized	Irregular replacing pyrite disseminated in veinlets.	Fracturing of both ore and capping plus alteration make suitable conditions for block caving.
Porphyry Mine Porphyry Copper					Lms metamorphosed and recrystallized	Mineralized & recrystallized lms	Solution fissures in lms & and fact that the hw breaks well and can be blended with the lms permits the use of block caving.

Summary and Conclusions

Numerous basic facts concerning geological data and their relation to mining methods particularly with reference to stability and support requirements have been described in the foregoing pages, and the most important may be summarized under three general headings:

1. Planes of Weakness:

a. Open stopes with pillars are generally used in deposits which are notable for their simplicity of structure, lack of faulting, and alteration, and for competency of rock and ore. Bedding planes may or may not be important causes of rock failure or weakness, depending upon the nature of partings and type of rock.

b. Complexity of structure may or may not contribute to critical weakening of ore and rocks, depending upon the nature of contacts and component members of the geologic mass.

c. Rock weakness may be caused by either pre-ore or post-ore faulting, the latter being the more common cause. Even slight post-mineral movement may cause failure in a brittle ore complex. Joints, faults, contacts, bedding planes, etc., relieve stresses which would otherwise be built up in the rock. Pre-ore fractures are often healed by mineralization but also serve as loci of alteration and further weakening.

d. Schistosity, particularly in relatively fine-grained rocks, does not seem to be a serious source of planes of weakness in rocks.

e. Contacts between ore and wall rocks often form important planes of weakness.

f. Intersections of shear zones may cause prominent irregularities which create mining problems.

g. Internal gouge slips in the ore affect its strength, the stability of rock and ore, and consequently the method of mining.

2. Effects of Mineralization and Alteration:

a. The conversion of limestone to chert and flint in the Tri-State district strengthened the rocks. The strengthening effect of silicification apparently may more than offset the weakening effects of sericitization. A high silica content of the original rocks is often essential to silicification.

b. At both the Horne mine, Norwanda, Quebec, and at Ducktown, Tennessee, the massive sulphide ores are very strong. Microscopic studies of sulphide ore show that even very small cracks are healed by mineralization, which contributes materially to the strength of the ore.

c. Silicification and mineralization of rhyolite breccias has strengthened them sufficiently so that they will support themselves in large openings.

d. Variation in the type of wall rock, or in the degree of faulting or alteration may alter support requirements and thus permit the use of different types of mining in the same deposit.

e. Where the mineralization has tended to follow joint planes and fractures into the walls of replacement veins, close wall support is necessary for complete extraction and clean mining.

3. Other Characteristics:

a. Strong rocks are found among igneous, sedimentary, and metamorphic types. Shale is almost universally weak.

b. A study of the history of the Hollinger deposit shows that a majority of the geologic events had an important effect upon the final structural strength of the ore and rock.

c. At the United Verde mine the rocks are strong to weak in the following order: massive, sulphide (non-ore), porphyry, and schist. At the Frood mine, Sudbury, Ontario, the rhyolite is brittle, well jointed and has a high rock burst potential. Quartzite and cemented breccia are reasonably firm, and gabbro and greenstone (fine to medium-grained) are firm except where loosened along joints. At the Creighton mine the rocks are strong to relatively weak in the order named: norite, gabbro, and granite. Rockbursts are more common in the granite.

d. Alteration of rocks in the Butte area was influenced by (1) temperature of the solutions, (2) their chemical composition, and (3) their concentration. Degree of alteration is apparently not entirely dependent upon the degree of crushing or fracturing of the rock.

e. In certain cases slates and graphitic rocks may act as lubricants along slip planes and facilitate adjustments of rock pressures and stresses.

f. Hard, brittle rocks are more susceptible to bursting than soft, weak ones.

g. At the Tintic Standard mine the choice of mining method (square-set) was controlled by: (1) size of ore body, (2) post-mineral crushing and fracturing, (3) degree of alteration of ore and country rock, (4) sequence of interbedded limestones and shales in geologic column, (5) slumping of ground over replacement deposit, (6) lack of sufficient silicification to strengthen structure, and (7) inherent weakness of ores themselves.

h. The factors influencing the incidence and severity of rockbursts are: (1) depth of workings, (2) structural features of ore and enclosing rocks, (3) dip of ore body, (4) concentration of mining operations, and (5) rate of mining.

i. In deposits employing caving methods a weak capping is an important requisite. Weakness is generally due to fracturing, alteration, leaching, or to the presence of inherently weak rocks.

j. Drying of mine rock by pumping or ventilation often causes certain types of rocks to slack, slough or crumble.

Of all of the causes of weak mine rock structures, post-mineral faulting and "destructive" alteration are the most important. Pre-mineral faulting has resulted in the weakening of rocks and ores, but to a lesser degree than the first two causes, usually because many mineralization processes tended to heal the fractures caused by previous dynamic movement. Alteration resulting in formation of sericite or kaolin is invariably "destructive".

Both silicification and certain types of mineralization have a strengthening effect upon rock structures. They may come about as a result of either primary or secondary processes.

There appears to be no direct correlation between genetic rock types and their tendency toward being strong or weak. Their strength is a function not only of the physical properties of the rocks themselves, but of their environment and geologic history.

If a scale of comparative indices is set up for the four factors in the table below, an interesting comparison can be drawn. Let the numbers from 0 to 4 represent increasing degrees of intensity as follows:

ROCK STABILITY INTENSITY FACTORS FOR NON-CAVING METHODS

Stoping Method	Pre-mineral faulting, etc.	Post-mineral faulting, etc.	Rock alteration	Silicification or Strenghtening min.
Open Stopes	0-2	0-1	0-1	0-3
Sublevel	0-3	0-1	0-1	0-4
Shrinkage	1-3	0-1	0-2	0-4
Cut-and-fill	2-4	2-4	2-4	0-4
Square-set	2-4	2-4	2-4	0-4

0 . . . . Negligible
1 . . . . Moderately weak
2 . . . . Moderately strong
3 . . . . Strong
4 . . . . Very intense

There is considerable overlapping of the effects of the more crucial geologic factors which affect rock strength. And the effects of one may be offset by one of the others. For example, silicification may create a very strong but brittle rock structure which may be easily weakened by further dynamic movement of the rocks.

It is noted that underground works (power stations) can be designed and constructed with confidence and efficiency if considerable preliminary investigation and research is undertaken. Recommended items are as follows:

1. The in situ state of stress of the rock should be determined possibly in connection with diamond drilling and this should be correlated with geology and topography of a given site.

2. A direction type of geophone for detection of sub-audible rock noise should be employed to locate centers of disturbance or failure.

3. The depth of penetration of blasting effects into wall rocks should be determined.

4. The behavior of rough and smooth jointed rock in situ should be investigated.

5. Investigation should be made of the effect of rock bolts and cementing in stabilizing jointed rocks of various types.

The experience acquired in the construction of the Snowy Mountain power station has shown that conventional methods of geological mapping and careful diamond drilling programs were adequate to avoid gross weaknesses which may be encountered, particularly those associated with major faulting. However, these methods were inadequate to determine with sufficient accuracy the characteristics of the jointing of the rock mass at depth, or to identify with ease geologic or rock structure which is important in determining the stability of underground openings. It was concluded that only by direct exploration by tunneling can such details be determined. Experience has also dictated the desirability for design characteristics so that a maximum degree of flexibility can be employed to permit adjustments of location to take advantage of geologic conditions revealed by exploratory openings.

Geology and Protective Construction

The geological characteristics within a given geographical strategic area will be the determining factors which will govern the choice of a site as being suitable for protective purposes. The geological features of the earth's crust which have proven important in the stability of mines, tunnels and power stations will be equally critical in determining the stability of protective installations. With the exception of experience in mines which have high order rock bursts, however, additional design criteria for protective cover must be ascertained to incorporate resistance factors for dynamic loads. Resistance to bomb penetration, attenuation, refraction and reflection of stress waves, as well as the strength of the local rock structure around the openings must be considered. Obviously, some of these do not have parallel significance in the static stability of mine openings.

Favorable Overlying Geological Configurations. Genensky and Loofbourow[3] have made a study of twelve geological configurations in the United States. They conclude that "the material which lies between the roof of the installation and the surface of the earth need not necessarily be composed of hard competent rock. Broken rock, shale and other uncompacted rock may be more effective as blast-wave attenuators." In addition to certain geologic structures they also suggest the use of broken rock or "umbrellas" to provide optimum attenuation. The term "umbrella" is applied to openings in the rock above the protective installation. It is also concluded that further experimental data are required to predict the reaction of various combinations of rock to nuclear blasts. Also, it is emphasized that definite conclusions in the reaction of various combinations of rock cannot be drawn without further experimentation.

The following configurations were considered by Genensky and Loofbourow: (1) glaciers, (2) masses of plastic rock, (3) cellular rock, (4) a great thickness of cellular rock, (5) a great thickness of cellular and thin-bedded rock, and (6) a combination of thin-bedded cellular and plastic rock. Further consideration was given to existing mines in certain formations and openings under caved and broken ground. The studies by Genensky and Loofbourow are quite general and inconclusive.

Favorable Local Geology. For reasons which are discussed more in detail in later chapters of this report, it is believed that it will be necessary that the immediate rock in which an installation is to be located should be strong and competent. As pointed out in the chapter on artificial support, steel, concrete, and timber will support only the weight of an assumed arch of rock a few feet in depth around an opening. Hence, the natural rock structure itself should be capable, with some local support, of carrying a very large percentage of static and dynamic loads imposed upon it.

Thus, a local rock structure should have a minimum of fractures and alteration. Fault zones are usually areas of critical stress. Certain types of joint patterns are difficult to support, and the spacing of planes of weakness relative to the size of the opening is one critical measure of structural strength. (See also Chapters on static and dynamic stresses.) The value of types of rock as "attenuators" for high level stress waves of large geometry has not been determined.

CHAPTER III

REFERENCES

1. Jackson, C.F., and Gardner, E.D., Stoping Methods and Costs, USBM Bull. 390, 1936.

2. Gunther, G.C., and Fleming, R.S., The Examination of Deposits, McGraw Hill, 1932.

3. Genensky, S.M., and Loofbourow, R.L., Geological Covering Materials for Deep Underground Installations, Project Rand RM-2617, August 1960.

CHAPTER IV

WAVE MECHANICS AND INSTRUMENTATION

Introduction

The response of an underground structure situated within a semi-infinite (half-space) rock medium to a high-intensity impact loading is a function of the impact time history, the rock medium, and the underground structure configuration. The theoretical analyses of rock media responses to dynamic loads have been limited for the most part to mathematical derivations of ideal elastic half-space response to concentrated or distributed loads at the free boundary. Any attempt to improve the similarity between the theoretical model and actuality is accomplished only at the expense of increasing the complexity of the mathematics. The degree to which the theoretical results correspond to field conditions can only be determined by field measurements.

Instrumentation is a necessity for the acquisition of data for checking theoretical formulations as well as to aid in originating new concepts. Wave mechanics instrumentation may be applied in the laboratory as well as in the field and may include accelerometers, velocity gages, strain gages, displacement gages, pressure gages, high speed cameras and other types of devices. In regions of intense dynamic loading, properties of rock other than the purely mechanical properties, such as luminescence, etc., may give pertinent information. The principal types of instrumentation which have been utilized and an evaluation of their application is presented.

Propagation in an Extended Medium

The manner of propagation of stress waves within extended solids is dependent upon the nature of the medium within which they are developed. In extended isotropic elastic solids, two types of elastic waves may be propagated, dilatational waves which travel with the velocity,

$$c_1 = \left[\left(K + \frac{4}{3}\mu\right)/\rho\right]^{\frac{1}{2}} \tag{4.1}$$

where K is bulk modulus

μ is rigidity modulus

ρ is density

and distortional waves which travel with the velocity,

$$c_2 = (\mu/\rho)^{\frac{1}{2}} \tag{4.2}$$

another type of stress wave, propagated at the surface of an elastic medium, is known as a Raleigh wave. The disturbances associated with this particular type of wave decrease with depth.

Kolsky[1] points out that real solids are never perfectly elastic. Solids which exhibit a hysteresis loop in the stress-strain curve may attenuate transient pulses traveling through them to a great degree. The velocity gradients set up by the stress wave may result in a second type of attenuation, associated with the viscosity of the material. In both cases these losses are attributed to internal friction of the material, resulting in a conversion of mechanical energy to heat. Materials may also exhibit mechanical relaxation or the increase of strain asymptotically with time under a fixed stress. Where stress wave periods are close to media relaxation times, attenuation of the stress waves is severe. Finally the compressions and dilatations produced by the stress transfer of energy from the strain wave to the material in the form of heat, produces additional attenuation.

Two other types of stress waves must be considered here, which are of importance in the study of the response of rock masses. Shock and plastic waves both may occur in the case of media whose stress-strain relations have ceased to be linear. Shock waves are formed in media in which the velocity of propagation of large amplitude disturbances is greater than that of smaller ones. This behavior may be exhibited above a certain threshold amplitude. As a result any pulse above the threshold value develops a steeper and steeper front as it penetrates the medium, the thickness of the front being determined by the molecular arrangement of the medium. Plastic waves are developed in media which are linear up to a given stress, but for stresses greater than this, flow occurs. This behavior results in an elastic wave being propagated through the medium, with a plastic wave following in its path at a lower velocity.[1]

Propagation in an Extended Elastic Medium

If an elastic solid is unbounded only two types of waves can be propagated through it, dilatational and distortional waves. The equations of motion for these waves are derived by means of well-known theory of elasticity relationships, and, therefore, only the results will be presented here. The equations of motion take the form

$$\rho \frac{\partial^2 \Delta}{\partial t^2} = (\lambda + 2\mu)\nabla^2 \Delta \tag{4.3}$$

$$\rho \frac{\partial^2 \bar{\omega}x}{\partial t^2} = \mu \nabla^2 \bar{\omega}x; \quad \rho \frac{\partial^2 \bar{\omega}y}{\partial t^2} = \mu \nabla^2 \bar{\omega}y; \quad \rho \frac{\partial^2 \bar{\omega}z}{\partial t^2} = \mu \nabla^2 \bar{\omega}z \tag{4.4}$$

where λ and μ are Lame's constants

∇^2 is the operator $\left(\frac{\partial^2}{\partial x^2} + \frac{\partial^2}{\partial y^2} + \frac{\partial^2}{\partial z^2}\right)$

Δ is $(\epsilon_{xx} + \epsilon_{yy} + \epsilon_{zz})$

$\bar{\omega}$ is a rotation component

Equation 4.3 is the wave equation of a dilatation Δ propagated through the medium with velocity $[(\lambda + 2\mu)/\rho]^{\frac{1}{2}}$. Equations 4.4 represent the wave equations of rotation (shear) propagated at a velocity of $(\mu/\rho)^{\frac{1}{2}}$.

It can be shown that any plane wave propagated with an extended elastic isotropic medium must travel at one of these two velocities. From the above discussion it can be seen that the velocity of distortional waves depends only on the density and shear modulus of the medium, whereas the velocity of dilatational waves is a function of bulk modulus as well as shear modulus. This behavior is explained by the fact that in the case of a dilatational wave the medium is subjected to both compression and shear.

The general form of the solution to differential equations of motion of the dilatational and distortional waves, Equations 4.3 and 4.4, respectively is

$$\alpha = f(x - ct) + F(x + ct) \tag{4.5}$$

where f is an arbitrary function corresponding to a plane wave along the x-axis in a positive direction, and F to one in the opposite direction. It can be seen that the effect of time is merely to displace the wave a distance along the x-axis without altering its shape.

If a stress wave originates at a point in an unbounded medium, the differential equation of motion may be represented by the equation

$$\frac{\partial^2 \alpha}{\partial t^2} = c^2 \left(\frac{\partial^2 \alpha}{\partial r^2} + \frac{2}{r} \frac{\partial \alpha}{\partial r}\right) \tag{4.6}$$

This equation may be placed in the same form as Equations 4.3 and 4.4,

$$\frac{\partial^2 (r\alpha)}{\partial t^2} = c^2 \frac{\partial^2 (r\alpha)}{\partial r^2} \tag{4.7}$$

The solution of this equation is

$$\alpha = \frac{1}{r} \left[f(r - ct) + F(r + ct)\right] \tag{4.8}$$

Equation 4.8 representing a spherical wave differs from Equation 4.5 representing a plane wave in that the spherical wave amplitude is inversely proportional to the distance r from the source of disturbance.

Rayleigh Waves. In an elastic isotropic solid where there is a bounding surface elastic surface waves may occur in addition to the two types of waves discussed above. Lord Rayleigh showed that their effect decreases rapidly with depth and that their velocity of propagation is smaller than that of body waves. The velocity of propagation of surface waves is independent of the imposed frequency and dependent only on the elastic constants of the material. For this reason these waves do not change in form as they travel. Rayleigh waves of high frequency are attenuated more rapidly with depth than those of low frequency. In any case the disturbance is insignificant at depths greater than one wave length. These surface waves are of importance in seismic phenomena since they spread only in two directions and thus fall off more slowly than elastic body waves.

Love Waves. The direction of vibration of the horizontal components of Rayleigh waves is parallel to the direction of propagation. Surface waves encountered in seismic investigations where the horizontal components vibrate parallel to the wave front are known as Love waves. Love suggested that these waves can be accounted for by assuming that the elasticity and density of the outer layer of the earth differs from that in the interior. Thus transverse waves can be propagated through the outer layer without penetrating the interior.

Reflection and Refraction. Any wave which is incident upon the interface of two elastic media will produce compressional (P) and distortional (SV) waves in both media. Thus, an incident P wave (Figure 4.1) will result in reflected and transmitted P waves, and reflected and transmitted SV waves. Similarly, an incident SV wave will result in four transmitted and reflected waves. (Figure 4.2).

Figure 4.3[2] gives the square root values of ratios of transmitted to incident energy between two strata for certain ratios of density, longitudinal (α) and distortional (β) velocity and for Poisson's ratio where the reflected and transmitted waves are of the same type. This shows that refracted waves of the same kind do not lose an appreciable amount of energy in passing discontinuities, except for near-grazing incidence. Figure 4.4[2] is a comparable plot of waves which changes type at an interface. Gutenberg[2] points out that: "From the theory, it follows that except for signs the distribution of energy is the same for incident P and SV waves if one compares refracted waves of the same kind, refracted transformed waves, etc.".

Muskat and Meres[3] calculated the reflected energy of P waves for normal and near normal incidence. The results of some of their calculations for waves of normal incidence are shown in Figures 4.5 to 4.8 for specific examples of low and high speed strata configurations. These show that a high velocity contrast is desirable for reflection, while strata whose velocities increase monotonically with depth gives the smallest reflection.

Hence, in the selection of a site for a deep installation, the reflecting capabilities of the geologic structure should be considered, as well as the attenuating properties.

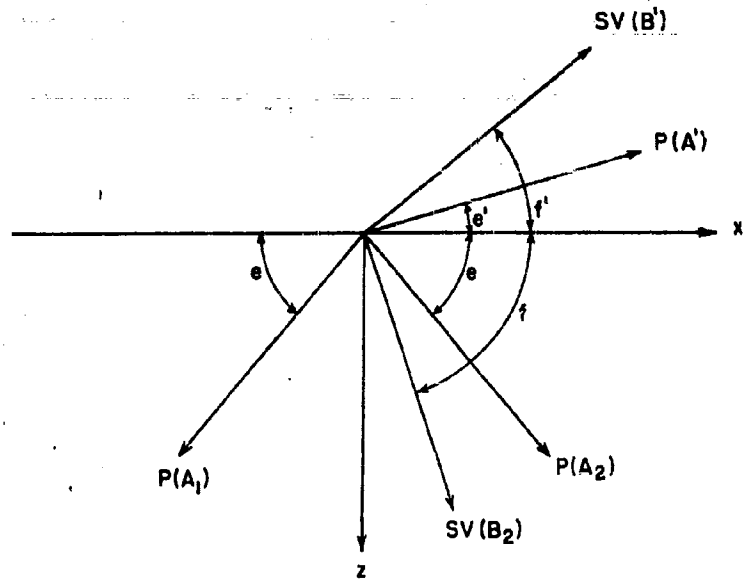


Figure 4.1. Reflection of P waves at an interface between two elastic solids.

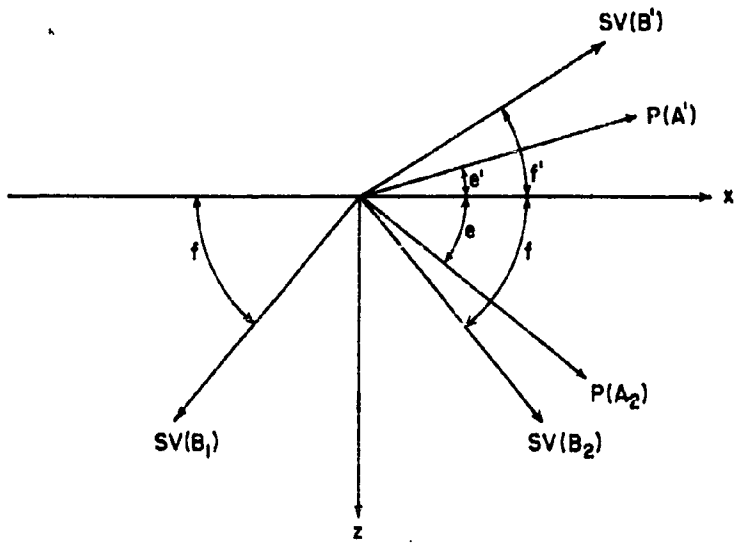


Figure 4.2. Reflection of SV waves at an interface between two elastic solids.

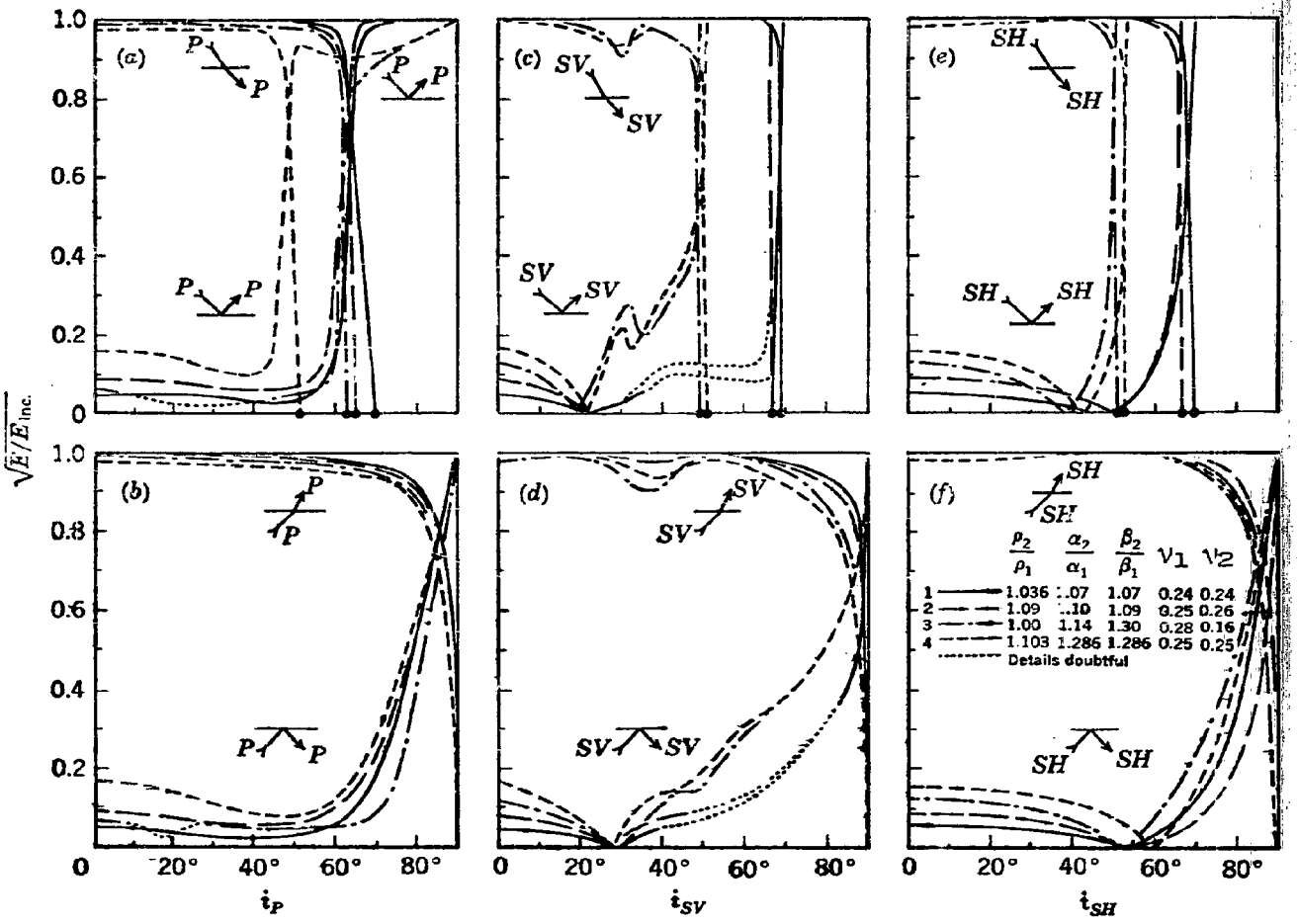


Figure 4.3. Square roots of ratio of reflected or transmitted to incident energy if no change in wave type occurs. (After Gutenberg.) Subscript 1 refers to upper layer, subscript 2 to lower layer.

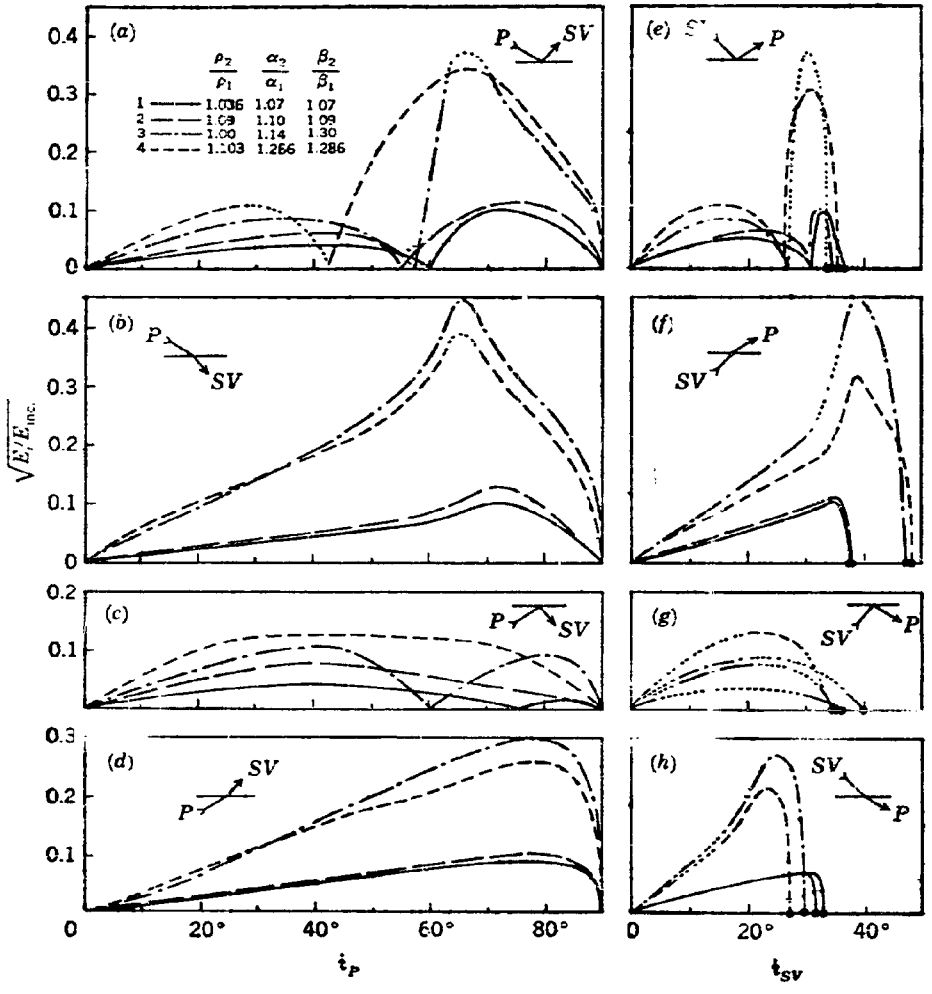


Figure 4.4. Square roots of ratio of reflected or transmitted to incident energy if incident and reflected or transmitted waves are of different type. (After Gutenberg) Subscript 1 refers to upper layer, subscript 2 to lower layer.

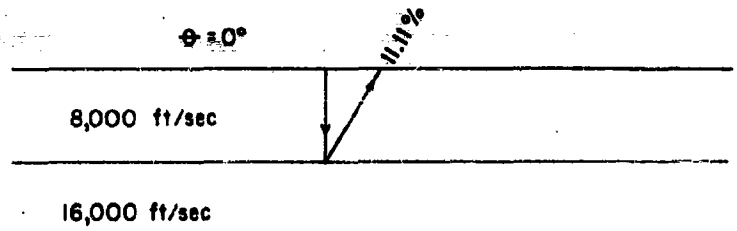


Figure 4.5. Normal incidence on an interface separating an incident bed with velocity 8000 ft./sec. from a refracting bed of velocity 16,000 ft./sec. 11.1% of the incident energy will be reflected to the surface from the interface as a longitudinal wave.

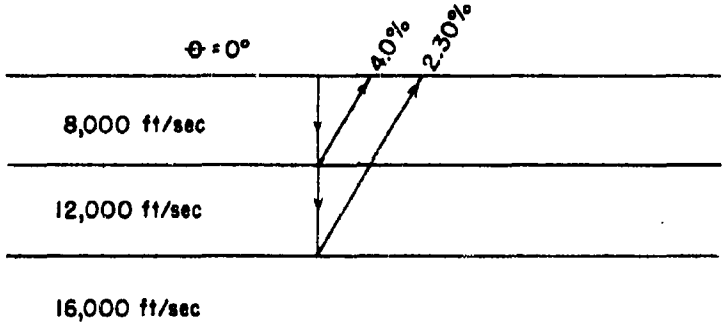


Figure 4.6. A two interface system in which the incident stratum of velocity 8000 ft./sec. is separated from the final reflecting stratum of velocity 16,000 ft./sec. by a bed of intermediate velocity, 12,000 ft./sec. The angle of incidence = 0°. Energy reflected from first interface equals 4% of incident energy; energy returning from the highest speed layer = 2.3% of incident energy.

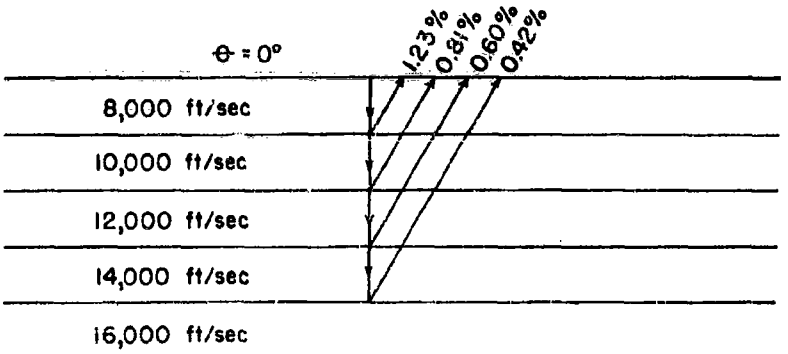


Figure 4.7. A 4-interface system in which the highest and lowest velocity beds are separated by three intermediate layers with equal velocity increments. The angle of incidence = 0°. Energy reflected from 10,000 ft. bed = 1.2% of incident energy; energy reflected from 12,000 ft. bed = 0.8% of incident energy; energy reflected from 14,000 ft. bed = 0.6% of incident energy; energy reflected from highest speed bed = 0.4% of incident energy.

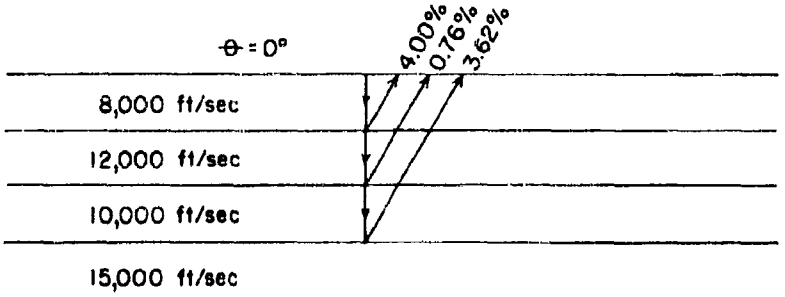


Figure 4.8. The reflections at normal incidence from a typical sedimentary section with a low velocity intermediate stratum. Energy reflected from first interface = 4% of incident energy; energy reflected from intermediate low velocity bed = 0.8% of incident energy; energy reflected from deepest and highest speed bed = 3.6% of incident energy.

Propagation in an Extended Anelastic Medium. When solid materials are set into vibration some of the elastic energy is always converted into heat (the various mechanisms by which this takes place are collectively termed internal friction). There is at present no satisfactory explanation for internal friction in solids, and more experimental data are required.

The dynamic viscoelastic behavior of solids has been represented by a number of idealized models, the simplest of which are the Voigt and Maxwell solids, Figures 4.9a and 4.9b, respectively. In the figures, the springs represent linear internal resisting stresses of an elastic body, that is, in which $\sigma = E\epsilon$, whereas the viscous elements represent behavior in which the resistive stress is directly proportional to the strain rate, $\sigma = \eta \frac{d\epsilon}{dt}$.

A Voigt solid is based upon the assumption that the resisting stress within a solid can be represented as the sum of two sets of terms, one proportional to the strain and the other to the rate of change of strain, or

$$\sigma = E\epsilon + \eta\frac{d\epsilon}{dt} \tag{4.9}$$

This equation may be represented by a viscous and an elastic model element in parallel.

A Maxwell model is based on the assumption that the strain developed in a solid as the result of an externally applied stress can be represented as the sum of two terms, one proportional to the applied stress and the other proportional to the time integral of the applied stress, or

$$\epsilon = \frac{\sigma}{E} + \frac{1}{\eta}\int \sigma dt \tag{4.10}$$

This behavior may be represented by a linear elastic element and a viscous element in series.

An interesting aspect of the behavior of these two hypothetical materials is that the logarithmic decrement of damping is inversely proportional to frequency for Maxwell solids and directly proportional to frequency for Voigt solids. Unfortunately, for most solids the measured logarithmic decrement does not follow either model, suggesting that a more complicated arrangement is required. The arrangement of Figure 4.9c, sometimes identified as Berger's model, gives results more in accordance with the behavior of real solids.

More complicated models have been considered to account for the fact that a number of different relaxation phenomena may take place simultaneously in a solid. This has resulted in models consisting of multiple series and parallel combinations of the basic Maxwell and Voigt models. Such a treatment is mathematically equivalent to a superposition approach postulated by Boltzmann. The basic models have also

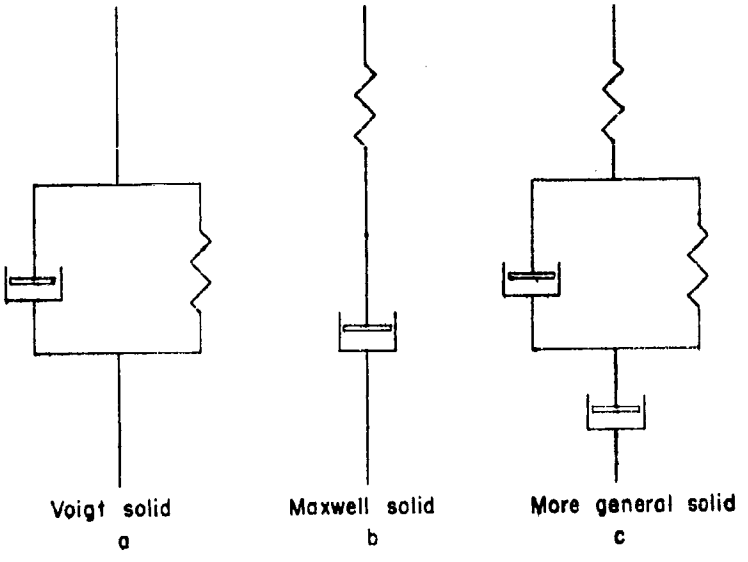


Figure 4.9. Models of visco-elastic solids (after Kolsky).

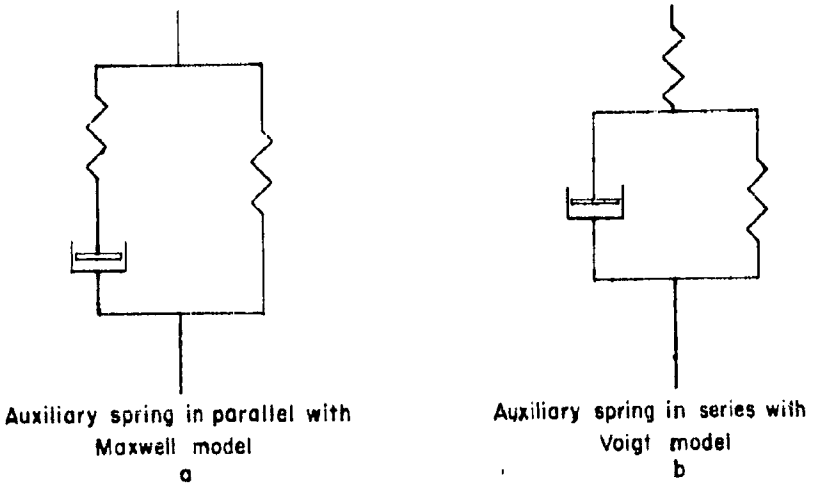


Figure 4.10. Two equivalent mechanical models (after Kolsky).

been modified as shown in Figure 4.10 to better describe relaxation phenomena. The theory of vibrations in a Boltzmann solid results in extremely complicated mathematical analysis, and the results have so far found very little application in the study of the dynamic behavior of visco-elastic materials.

The equations of wave motion in a Voigt solid are derived in the same form as for an elastic solid. Thus, the equation for the plane displacement of a dilatational wave becomes

$$\rho \frac{\partial^2 u}{\partial t^2} = (\lambda + 2u)\nabla^2 u + (\lambda^1 + 2u^1)\nabla^2(\frac{\partial u}{\partial t}) \qquad (4.11)$$

where λ and u are two viscous constants corresponding to Lame's constants, and for a distortional wave

$$\rho \frac{\partial^2 u}{\partial t^2} = u\nabla^2 u + u^1\nabla^2 (\frac{\partial u}{\partial t}) \qquad (4.12)$$

A plane distortional wave which is propagated in the x-direction has a particle motion in the z-direction (amplitude w) is represented by the following solution of Equation 4.12:

$$w = e^{qx} \cos (pt - fx) \qquad (4.13)$$

where q is a dissipative factor, p is the angular frequency of the stress wave, and f is 2π divided by the wavelength λ.

This equation indicates that the wave is damped exponentially as it proceeds through the solid. For small amounts of damping the phase velocity is the same as for an elastic solid. The treatment of dilatational waves in a Voigt solid is essentially the same as that presented for distortional waves.

Although very few solids behave, even approximately, like either the Maxwell or the Voigt model, when the dynamic mechanical behavior of a visco-elastic solid is required for only a restricted region of frequencies the "elasticity" and "viscosity" obtained from these simplifications is convenient for the description of its mechanical properties. This may be particularly true in the case of dynamic studies of underground structures.

Wave Attenuation in Rock. Dobrin[4] points out that the energy of a wave is proportional to the square of its amplitude. However, as a spherical wave spreads out from its source the energy is distributed over an area which increases as the square of the radius of the sphere, and thus the specific energy varies as the inverse square of the radius. The amplitude theoretically varies as the inverse of the radius. In addition to a decrease in energy due to dispersion inherent in spherical geometry of the wave, it suffers a loss due to internal friction and absorption approximately defined by

$$I = I_o \frac{e^{-qr}}{r} \qquad (4.14)$$

where I is the amplitude at a distance r from the source, I_o the initial amplitude and q a constant depending upon the material.

This equation has been found to approximate quite closely the behavior of seismic waves at some distance from an exploding charge. Some additional data and observations are available from underground nuclear detonations and large scale HE explosions.

Swift, et al[5], report in connection with the Rainier event that the peak vertical acceleration decays with distance from the charge and accelerations were measured at distances of 580, 650 and 720 ft. from the charge. At distances closer to the surface, accelerations deviated markedly from those closer to the explosive chamber. The decay was not found to obey a well defined law. Particle velocity and displacement were determined by integrating acceleration time records, but results were not conclusive.

Perret and Preston[6] report that in a horizontal direction from the detonation of Rainier the highest peak accelerations decayed approximately as the inverse fourth power of the range. Below 10 g, attenuation of peak acceleration approached the inverse square power of the range.

Subsurfaces stresses and strains associated with the Tamalpais event by Adams, et al[7], showed that stresses measured at five stations between 100 and 425 feet radial distance varied as the inverse cube of the radial range. Plotted data for strain indicates that strain attenuated at a rate between the inverse cube and the inverse square. In general, the results of Plumbbob and Hardtack operations are somewhat inconclusive and can be applied only to the tuff at NTS.

For small scale charges[8] the rate of decay of peak strain is plotted against scaled distance for four types of rocks in Chapter V. The type of rock not only has an effect upon the attenuation of strain with distance, but on the magnitude of strain as well. The rate of attenuation varies inversely as the distance from the charge to exponential values of from 1.5 to 2, except close to the explosive where the attenuation may be less. This is not comparable to the results recorded from nuclear explosions where the attenuation was much higher at shorter distances.

Extrapolation of wave attenuation effects apparently may not be made in accordance with scaling laws. That is, some of the effects such as friction losses are functions of distance only and not of scaled distance. This is particularly emphasized where attempts have been made to scale from results of HE shots to NE explosions in terms of cratering and the parameters which govern the mechanism of formation of both true and apparent craters. The rate of attenuation of wave parameters in badly broken or altered rock does not appear to have

been evaluated. A few measurements have been made in sandstone in connection with the UET program, and some in limestone. It would be of primary interest to learn the effects of attenuation upon stress waves in large masses of competent granitic rock which might be employed for underground protective cover.

Plastic Waves. The propagation of a plastic deformation is essentially a non-linear phenomenon. Problems of strain which is linear with stress up to a proportional limit, one univalued function above the proportional limit with increasing stress and another function for decreasing stress have been considered by a number of investigators including Taylor[9] and von Karman[10]. The solution for a semi-infinite bar loaded by a suddenly imposed velocity at one end, involving Lagrangean coordinates is shown schematic representation of the distribution of strain in a bar, (Figure 4.11). The elastic wave front moves at the same velocity as in the purely elastic case; the velocity of propagation of the intermediate portion of the curve is $c = (S/\rho_o)^{\frac{1}{2}}$, where $S = \frac{d\sigma^1}{d\epsilon}$, the modulus of deformation at a particular strain ϵ, and ρ_o is the density of the unstretched bar; and the velocity of the plastic wave front depends upon the maximum strain. For most solids $\frac{d\sigma^1}{d\epsilon}$ is constant for stresses up to the elastic limit and then decreases, so that large strains are propagated with velocities lower than that of elastic waves and the distribution of strain is similar to that shown in Figure 4.11. If $d\sigma^1/d\epsilon$ increases with increasing strain, any large pulse traveling through the medium will acquire a steep front, the gradient of which is limited by dissipation through viscosity and thermal conduction. (See shock waves below).

The discussion of plastic waves above has been concerned only with the loading of a semi-infinite bar. When a stressed bar is suddenly released a wave of unloading travels down the bar. The front of this wave travels with a velocity corresponding to the velocity of elastic waves in the material. It consequently overtakes the plastic wave front which was induced during loading. Plastic and elastic response of the material becomes quite complex as repeated reflections take place.

Very little consideration has been given in the literature to the propagation of plastic waves in extended media.

Shock Waves. The velocity of propagation of a disturbance in a plastic material, where the elastic modulus $S = d\sigma^1/d\epsilon$ is constant, will be greater for large compressive disturbances than for smaller ones. Thus any finite compression pulse will eventually acquire a steep front as it travels through the medium. In solids, particle velocities are very small compared to propagation velocities so that if S is constant, stress pulses can travel for considerable distances without change in form. As mentioned previously S usually decreases beyond the elastic limit, and plastic rather than shock waves are generated in most solids.

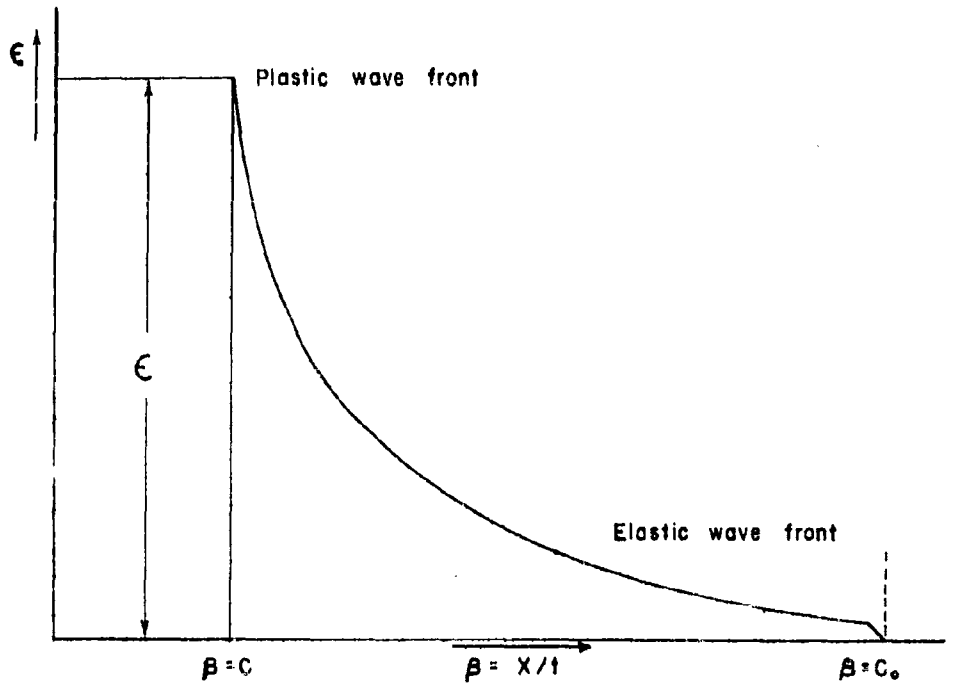


Figure 4.11. Schematic representation of distribution of strain in a plastic wave (after Kolsky).

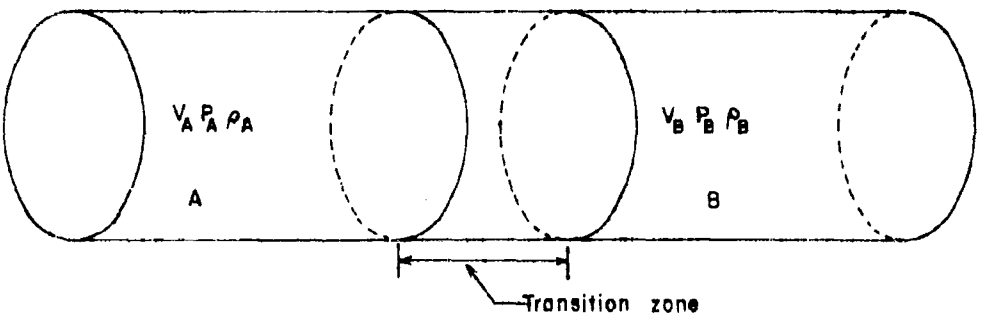


Figure 4.12. A cylindrical mass of material of unit cross-section passing from right to left through a shock front. Reference system fixed in the transition zone (after Kolsky).

Shock waves may also be set up in solids when dilatational waves of sufficiently large amplitude are propagated through them. The velocity of elastic waves of dilatation in a solid is $c = [(K + 2/3\mu)/\rho]^{\frac{1}{2}}$. Since the compressibility K of solids increases at high pressures, the velocity of waves of large amplitude may be expected to be greater than that of waves of small amplitude.

Bridgman has shown that the volume v and the hydrostatic pressure P in a solid can be related by

$$\frac{v_o - v}{v_o} = aP + bP^2 \qquad (4.15)$$

The bulk modulus K is given by $v \frac{\partial P}{\partial v}$. In the case of metals a pressure on the order of 1000 kg./sq. cm. results in a change in the bulk modulus of approximately one percent, with a resulting change in velocity of propagation of ½ percent. The influence of compressibility of the material upon dilatational velocity is therefore significant only at extremely high pressures, and shock waves are likely to be produced in a solid only when it is intimately associated with a detonating explosive or when a high speed projectile is fired at it.

A brief account of the fundamental shock wave equation derivation is included here. These relations, known as the Rankine-Hugoniot equations, are based on conservation of mass, momentum and energy in the medium. The equations are derived utilizing the assumptions that a plane shock wave has been set up and is traveling through the material with a velocity $\underline{c}$; the particle velocity, pressure, and density behind the shock wave are constant; there is a transition zone at the front of the shock in which conditions are steady; and ahead of the transition zone the material is undisturbed.

Figure 4.12 shows a cylindrical element of material of unit cross-section containing the transition zone. The coordinate system is fixed relative to the transition zone. Pressure, density, and particle velocity behind the transition zone are denoted by P_A, ρ_A, and V_A, respectively, and in the undisturbed material by P_B, ρ_B, and V_B. The mass $\underline{m}$ is the material entering the transition zone per unit time.

Since matter and momentum are conserved,

$$m = \rho_A V_A = \rho_B V_B, \qquad (4.16)$$

and

$$m(V_B - V_A) = P_A - P_B \qquad (4.17)$$

The rate of work being done by the element is $P_A V_A - P_B V_B$ per unit time which is equal to the change in kinetic energy and internal energy of

the material passing through the transition zone. Thus

$$P_A V_A - P_B V_B = m \left[\tfrac{1}{2} (V_B^2 - V_A^2) + \Delta U \right] \qquad (4.18)$$

where ΔU is the change in internal energy per unit mass.

By means of these three equations one may derive the velocity of propagation of the shock front

$$c = V_B = \frac{1}{\rho_B} \left[(P_A - P_B)/(\rho_A \rho_B)/(\rho_A - \rho_B) \right]^{\frac{1}{2}} \qquad (4.19)$$

The particle velocity of material behind the shock front relative to the undisturbed material is given by

$$V = V_B - V_A = \left[(P_A - P_B)\ (\rho_A - \rho_B)/\rho_A \rho_B \right]^{\frac{1}{2}} \qquad (4.20)$$

and the change in internal energy per unit mass is

$$\Delta U = \tfrac{1}{2} (P_A + P_B)\ (\rho_A - \rho_B)/\rho_A \rho_B \qquad (4.21)$$

It can be shown that the shock front velocity given in Equation 4.19 approaches the velocity of sound in the medium for very small pressure differences. Kolsky indicates that the thickness of the shock front depends upon the characteristics of the medium. Little research has been performed in measuring of depth of shock waves in solid media.

Wave Mechanics and Crater Formation

If the limits of a true crater can be defined within reasonable limits for rocks of given characteristics this should offer one reliable means of predicting safe survival depths for installations. One approach to this problem has been made by Brode and Bjork[11] on a mathematical basis. A hydrodynamic model is assumed and the early motions associated with the burst are calculated for tuff. The results demonstrate that the problem is essentially a two-dimensional one, and furnish preliminary values of pressures and motions involved. Excavating action is due to direct shock from the bomb. Brode and Bjork also state that "In protective construction for the military, the crater boundaries define a sensible if perhaps extreme limit inside which survival cannot be expected".

Assumptions made involve a knowledge of the early history of the bomb explosion, that pressures are far in excess of shear or viscosity characteristics of natural materials and hence a hydrodynamic model is the most suited for the early stages. At the stress level below which hydrodynamics can be applied, calculations should embrace appropriate features of plasticity and elasticity.

A set of equations in Eulerian variables is set up, ignoring effects of viscosity and heat conduction. The solution of the equations is accomplished by computer in a series of two step processes in which the transport terms are first neglected and then later taken into account. An equation of state for the tuff relating pressure P, internal energy E and the ratio of density to initial density $\eta = \rho/\rho_o$ is as follows:

$$P = 0.425\eta E + 0.113\eta^{3/2}E + 5.30\eta E^{\frac{1}{2}} + 0.707\eta E^{2}/(10^{5} + E) \quad (4.22)$$

This does not cover the solids state properties of rock which become important where pressures dimish to about 10 Kbars.

Several isobar maps for a 2 megaton burst at various times after a detonation are given by Brode and Bjork. At 50 ms and a depth of 70 m the crater bottoms, with the material above this point moving up, and that below moving down. The crater thus predicted is approximately equal to that predicted by conventional scaling laws (cube root scaling). Some adjustments must be made in calculations to maintain a proper energy balance.

Figure 4.13 shows the calculated pressure distribution in the crater at 105 ms when a maximum pressure of 3+ Kbars exists at 250 ±m and is ½ Kbar at 350 meters.

Brode and Bjork conclude that the kinetic energy of the bomb debris as it reaches the ground is the most important mechanism in inducing ground motion below the crater, as well as on the formation of the crater itself. The crater size and ground shock are thus very sensitive to height of burst. Also shallow burial or a denser bomb case should enhance cratering efficiency. It is also noted that the presence of a nearly free surface causes stress patterns below the burst to be elongated along the vertical axis.

Making an approximation from the data in Reference 5 it appears that at a depth of 2000 ft. an overpressure of about ½ Kbar could be expected to exist as the dynamic free field stress. With a lithostatic pressure of 2000 psi (minimum) the total field would approximate 10,000 psi. The stress concentration factor for a circular tunnel in a unidirectional field is 3+ and hence, the stress concentration at the rib of a tunnel at this depth would be 30,000 psi, which exceeds the compressive strength of many common rocks.

Instrumentation for Dynamic Response

The instrumentation required for the measurement of the dynamic response of underground rock structures and surrounding rock media to impact loadings such as produced by HE or NE explosives has consisted primarily of displacement, acceleration, pressure and strain measuring devices. The philosophy of instrumentation of these various types of measurements has several common features: (1) the measuring technique should not unduly alter the phenomena being measured, i.e , the instrument should not seriously interrupt the continuity of material, (2) the instrument readings should directly measure the phenomena which it is desired to record and be capable of calibration, (3) it is a requisite

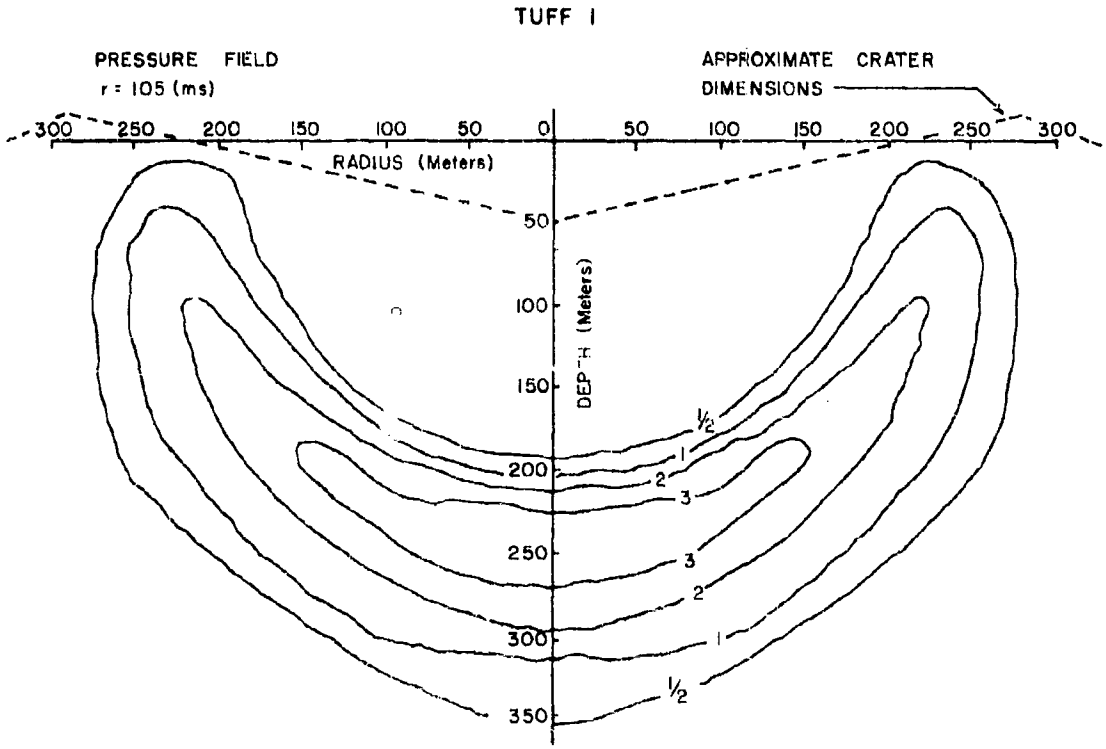


Figure 4.13. Calculated Pressure Distribution under 2 Megaton Surface Shot at 105 Milliseconds.

that the gage length of the sensing device be sufficiently small to permit detection of the highest effective frequency dynamic phenomena present; and (4) the instruments used for data acquisition shall preferably be of a remote-recording type.

A complete success of measuring a phenomena in a rock medium such as strain, without altering the strain field or presenting a discontinuity has not been achieved. The first requirement is a strain sensing device in intimate contact with the surrounding rock which has a modulus of elasticity equal to that of the surrounding medium. In addition, the strength of the gage and bonding material should be greater than that of the medium. However, if data are required above the proportional limit of the medium, similar stress-strain curves of gage and medium are desirable. This is important where strain readings are made in the vicinity of underground openings. If the strain measurements are to include dynamic responses, the question of reflection and refraction of strain waves at the gage-medium interfaces is often critical, and an impedance match between gage and medium is expedient. An impedance match is made most frequently by adjusting the gage density to be equal to that of the surrounding rock. In certain instances the presence of lead wires or other connections may disrupt the continuity of the rock and invalidate the results. Miniaturization of transducer components has been undertaken as one means of reducing the anomalous effects on the rock body.

Transducers used in the near vicinity of a strong dynamic disturbance may register effects other than those desired. Extraneous effects may result from unnecessary sensitivity to strains along other axes, or may be the result of response to accompanying phenomena. The design of transducers for measurement under these conditions requires detailed attention to the behavior of the medium and to the sensitivities of the measuring technique itself.

The necessity for proper choice of gage length in measuring dynamic phenomena has received considerable attention. It is generally agreed that the gage length of the transducer should be on the order of one-tenth of the wavelength of the highest frequency component it is desired to record. Relatively little attention has been given, however, to a study of which type of record is more representative of the actual response in rock, the measurement of grain-by-grain phenomena or response on a larger scale.

Strain Instrumentation. Strain measurements have been made in the field by a number of methods, most of which have utilized bonded electrical resistance gages. The U.S. Bureau of Mines[12] has utilized such gages, cemented in copper boxes for shielding purposes, attached to rock cores which were then placed in drill holes and grouted to the media.

The Corps of Engineers[13] has improved on this technique by mounting strain gages in laminated plastic sandwiches and molding them into 5-inch diameter hydrostone cylinders which were in turn cemented into drill holes. The density and static modulus of elasticity of the hydrostone closely approximated that of the surrounding rock. Cements can

be molded as carriers for strain gages, which would provide a satisfactory match for most rock media.

Acceleration Measurements. Acceleration transducers are relatively bulky and little effort has been made to date to match them to their surroundings. Discontinuities and mismatches should be of less significance for accelerations than for strain measurements. Accelerometers of a piezoelectric type have been used for accelerations up to 40,000 g's. They may be mounted in cased holes, uncased holes, or on mounts on the inside of underground tunnels.

Pressure Measurements. Pressure measurements have been made in rock media of response to explosive loadings using both piezoelectric and diaphragm type transducers. Walsh[14] has added a cautionary note in the use of piezoelectric transducers that the lead wires must be carefully placed so that any change in lead wire capacitance during the test does not obscure the results.

Durelli and Riley[15] also report on a barium titanate gage 5/16 inch diameter by 1/4 inch long with a wall thickness of 20 mils. The surfaces are silvered to establish polarizing fields. The gage delivers 3 to 5 millivolts per psi which makes it adequate for oscillograph recording. It is also insensitive to acceleration effects. Calibration is accomplished by checking recorded outputs against calculated overpressures in a shock tube. This device has the disadvantage that it will not survive overpressures in the 1000 psi range.

Little attention appears to have been given in past investigations to the use of so-called "rigid inclusions" to directly record stress within the rock masses. More study of this factor would appear to be warranted.

Durelli and Riley describe a type of cylindrical diaphragm gage which employs a Baldwin SR-4 type A-19 strain gage as a sensing element. The device was embedded in Hysol 8530/CH_2 and tested statically and dynamically. The gage was subject to "arching", and gave erratic readings for static and dynamic loading.

Promising results were also reported for a foil type gage embedded directly in the Hysol. Results were the same for both static and dynamic loading, as well as the gage being of high sensitivity. Further research was recommended on this type of gage.

Displacement Instrumentation[13]. Relative displacement versus time measurements have been made within tunnels during explosive loading tests utilizing linear potentiometers having strokes of ± 1.250 inches. These instruments are limited to use at medium frequencies due to the inertia of the components.

CHAPTER IV

REFERENCES

1. Kolsky, H., Stress Waves in Solids, Oxford University Press, Amen House, London, 1953.

2. Gutenberg, B., Energy Ratio of Reflected and Refracted Seismic Waves, Bull. Seism. Sec. of Am. Vol. 34, p. 85, 1944.

3. Muskat, M., and Meres, M.W., The Seismic Wave Energy Reflected from Various Types of Horizons. Geophysics, Vol. 5, p. 149, 1940.

4. Dorbin, M.B., Introduction to Geophysical Prospecting. McGraw-Hill, 1960.

5. Swift, L.M., et al., Surface Motion from an Underground Detonation, ITR-1528, Oct. 1957.

6. Perrett, W.R., Preston, R.G., Preliminary Summary Report of Strong-Motion Measurements from a Confined Underground Nuclear Detonation, ITR-1499, June 1958.

7. Adams, W.M., et al., Summary Report of Strong Motion Measurements, Underground Nuclear Detonations, ITR-1711, January 1960.

8. Duvall, W.E., and Atchison, T.C., Rock Breakage by Explosives U.S. Bureau of Mines, R.I. 5356, 1957.

9. Taylor, G.I., James Forrest Lecture, J.Inst. Civil Engrs., Vol. 26, p. 486, 1946.

10. von Kármán, T. and Duwez, P., J. Appl. Phys., Vol. 21, p. 987, 1950.

11. Brode, H.L., and Bjork, R.L., Cratering from a Megaton Surface Burst. Project Rand RM2600, June 30, 1960.

12. Atchison, T.C., et al., Mobile Laboratory for Recording Blasting and Other Transient Phenomena. USBM TI 5197, June 1956.

13. Ehlers, O.K., et al., High Explosive Equivalence for Underground Detonation of Operation Plumbob, ERDL Tech. Rept. 1625-TR, April 1960.

14. Walsh, H.R., An Experiment on Soils Loaded Dynamically by a Shock Tube, AFSWC-TN-60-39, December, 1960.

15. Durelli, A.J., and Riley, W.F., Research Studies of Stress Waves in Earth and Model Earth Media. Arm. Res. Found. Ill. Inst. of Tech. AFSWC-TR-60-4, October 1959.

CHAPTER V

ROCK FAILURE

Introduction

The majority of available data on the behavior of materials under load is concerned with metals and the theories developed have been applied primarily to metals and glasses. Most explanations of the behavior of rock materials are made by means of the theory of elasticity, at least as a first approximation. Of the theories and data which are applicable to rock a very large percentage is concerned with response to static loading only. The investigation of response of rock to impact loading has been conducted both on laboratory and field scale with a view to check the applicability of the tensile (Hopkinson bar) theory of slabbing. Much of the research performed by the U.S. Bureau of Mines, for example, has dealt with the mechanism of true crater formation by high explosives in solid rock. Laboratory tests of rock materials strained in flexure by transient loads shows a high degree of time dependency of fracture strain. Ground motion initiated by surface and underground nuclear detonations have been theoretically investigated both with respect to surface soil response and the reactions of deep underground rock structures.

Criteria of Failure

Many of the classical and modern theories of limiting states of stress and conditions of mechanical behavior of solids are reviewed by Nadai[1]. Such criteria are based largely on the conditions which cause materials (1) to deform permanently or (2) to fail by fracture.

As a generalization, the state of stress of a body may be determined by six quantities, the principal stresses σ_1, σ_2, and σ_3, and the direction of the principal axes. The state of stress necessary to cause flow may be described in terms of the principal stresses, i.e.

$$f_1 (\sigma_1, \sigma_2, \sigma_3) = 0 \qquad (5.1)$$

which represents a surface in terms of these three coordinates, known as the limiting surface of yielding. Limited features of the shape of this surface may be determined from observations of the behavior of materials. For a state of hydrostatic stress, i.e., $\sigma_1 = \sigma_2 = \sigma_3 = p$ $(p > 0)$ failure or flow does not occur for compact crystalline solids. Hence, the deduction can be made that the limiting surface of yielding cannot intersect the line $\sigma_1 = \sigma_2 = \sigma_3$. Similarly, it may be deduced that another surface exists if one or more of the three principal stresses are tensile such that it represents the limiting states of stress which may cause rupture:

$$f_2 (\sigma_1, \sigma_2, \sigma_3) \quad 0 \qquad (5.2)$$

and is termed the limiting surface of rupture. While the exact form of this surface ordinarily cannot be established, some plausible assumptions may be made concerning it. For a series of metals which were investigated with $\sigma_2 = \sigma_3$ the shape of the limiting curve in two coordinates is shown

in Figure 5.1 which represents the results for brittle metals and has considerable applicability to rocks. The tests were either simple tension (A), simple compression (B), a tension test with superposed lateral hydrostatic pressure (branch AC) or by rupturing round notched bars (branch AD of curve a and branch DE of curve b). In the latter tensile tests σ_1 is the axial stress and $\sigma_2 = \sigma_3$ the radial stresses at the minimum section of a notch. Data point C resulted from a hydrostatic pressure on the surface of a cylindrical bar with no axial stress, and point D to state of equal triaxial tension, i.e., test point D resulted from a state of equal triaxial tension stresses, i.e., $\sigma_1 = \sigma_2 = \sigma_3$. If a brittle material should rupture when one of the stresses reaches a certain value in tension independently of the other principal stresses the test points would fall along either of the lines c or d. These lines represent the theory of maximum stress which will be discussed below. Experimental work by McAdams[1] thus does not verify the theory of maximum stress since fracture may occur in a state of pure triaxial tension where a and d intersect at a stress (point D)

$$\sigma_1 = \sigma_2 = \sigma_3 > 0 \qquad (5.3)$$

which is almost twice as large as the stress in simple tension. The curve in the positive quadrant represents fracture conditions when all three principal stresses are in tension, and is different in character than when all three are compressional. In many materials under biaxial compression oblique shear fractures are predominant. It would also appear that the distances OA and OE should be equal. The above theory is not incompatible with the Mohr theory of strength under certain assumptions.

Theories of Strength

The principal theories of strength which have found some degree of substantiation are as follows[1]:

1. Maximum Stress Theory.
2. Maximum Elastic Strain Theory (St. Venant's "Equivalent" Stress Theory).
3. Theory of Constant Elastic Energy of Deformation.
4. Theory of Constant Elastic Strain Energy of Distortion or of Constant Octahedral Shearing Stress.
5. Maximum Shearing Stress Theory.
6. Mohr's Theory of Strength.
7. Griffith's Theory of Fracture.
8. Slip of Loose Granular Material.
9. Octahedral Stress as a Function of Mean Normal Stress.

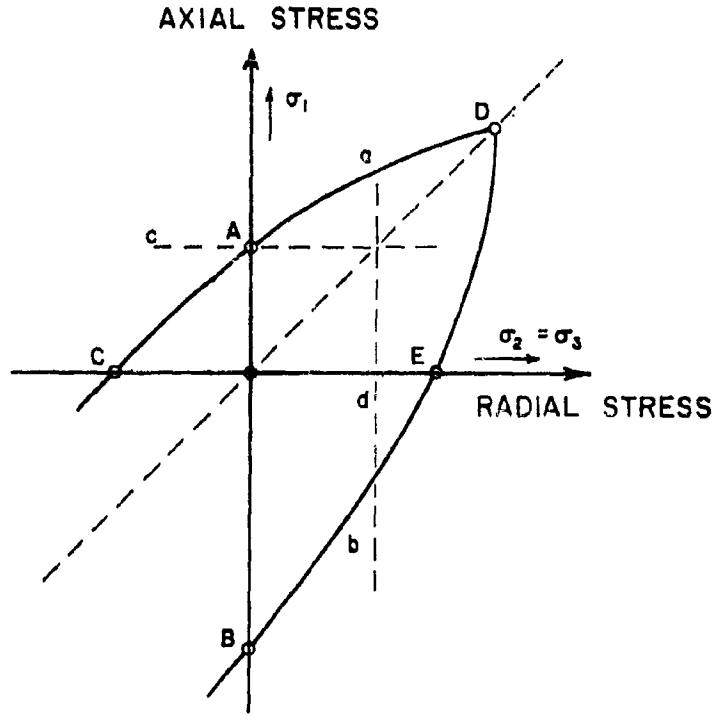


Figure 5.1. Limiting states of stress for fracture of brittle metals according to D. J. McAdam.

A consideration of mechanisms of fracture involves distinguishing between cleavage and shear fracture, which does not necessarily correspond with the classification of materials being either "ductile" or "brittle". Under conditions of high hydrostatic pressure even brittle materials become plastic.

Maximum Stress Theory. The basis of this theory is that the maximum principle stress causes failure if its absolute value is larger than those of the other principal stresses. Nadai points out that this theory cannot be applied as a criterion of yielding, because these equal tensile or compressive principal stresses should cause failure, which is contrary to observed experimental results. That is, in compact materials three equal compressive stresses may cause only elastic distortion. The surface (yielding or failure) represented is a cube, the faces of which are spaced symmetrically around the origin of the σ_1, σ_2, σ_3 system of coordinates. Modified forms of the theory give cubes as failure surfaces which are displaced along one of the diagonals of the coordinate system. The maximum stress theory has been employed by the Bureau of Mines in evaluating both static and dynamic rock failure.

Maximum Elastic Strain Theory. This hypothesis states that the maximum possible elastic strain causes material to either yield or fracture. Mathematically, if the elastic strain is positive, then the expression in

$$\epsilon_1 = \frac{1}{E}\left[\sigma_1 - \nu(\sigma_2 + \sigma_3)\right] \leq \frac{\sigma_1}{E} \qquad (5.4)$$

the brackets should be smaller than the positive limiting "equivalent" stress σ_0, i.e.,

$$\sigma_1 - \nu(\sigma_2 + \sigma_3) \leq \sigma_0 \qquad (5.5)$$

For simple uniaxial tension the lateral strains are equal to $\nu\sigma/E$, and where $\nu = 1/3$ the yield stress in pure compression should be three times that in tension. This does not correspond with the observed behavior of metals. Further, the theory does not hold for equal triaxial stresses. The limiting surface for this theory is two inverted three sided pyramids.

Theory of Constant Elastic Energy of Deformation. With respect to this theory Nadai points out that the total elastic energy at transition to the plastic state can have no significance as a limiting pressure because large amounts of elastic energy may be stored without causing either fracture or permanent deformation.

Theory of Constant Distortion Elastic Strain Energy. (Constant Octahedral Shearing Stress). The strain energy of distortion is equal to the total elastic energy minus the elastic energy of volume dilatation. From Hooke's law:

$$\begin{aligned} E\epsilon_1 &= \sigma_1 - \nu(\sigma_2 + \sigma_1) \\ E\epsilon_2 &= \sigma_2 - \nu(\sigma_3 + \sigma_1) \\ E\epsilon_3 &= \sigma_3 - \nu(\sigma_1 + \sigma_2) \end{aligned} \qquad (5.6)$$

The total strain energy is

$$1/2\ (\sigma_1\epsilon_1 + \sigma_2\epsilon_2 + \sigma_3\epsilon_3) =$$

$$\frac{1}{2E}\left[\sigma_1^2 + \sigma_2^2 + \sigma_3^2 - 2\nu(\sigma_1\sigma_2 + \sigma_2\sigma + \sigma_1\sigma_3)\right] \tag{5.7}$$

The energy due to change in volume is

$$1/6(\sigma_1 + \sigma_2 + \sigma_3)(\epsilon_1 + \epsilon_2 + \epsilon_3) = \frac{1 - 2\nu}{6G}(\sigma_1 + \sigma_2 + \sigma_3)^2 \tag{5.8}$$

From these the strain energy of distortion per unit volume is:

$$W = \frac{1}{6G}(\sigma_1^2 + \sigma_2^2 + \sigma_3^2 - \sigma_1\sigma_2 - \sigma_2\sigma_3 - \sigma_1\sigma_3)$$

$$= \frac{1}{12G}\left[(\sigma_1 - \sigma_2)^2 + (\sigma_2 - \sigma_3)^2 + (\sigma_3 - \sigma_1)^2\right] \tag{5.9}$$

For the case of simple tension, i.e., for $\sigma_1 = \sigma_o$, $\sigma_2 = \sigma_3 = o$, $W = \sigma_o^2/6G$, or for constant elastic energy of distortion $2\sigma_o^2 = \text{const.}$ The octahedral shearing stress is also

$$\tau o = 1/3\left[(\sigma_1 - \sigma_2)^2 + (\sigma_2 - \sigma_3)^2 + (\sigma_3 - \sigma_1)^2\right]^{\frac{1}{2}} \tag{5.10}$$

By comparing with the previous equations it is seen that the theory of constant elastic distortion strain requires that the octahedral shearing stress be constant. This represents a limiting surface of yielding which is a circular cylinder whose axis corresponds with the space diagonal in the positive quadrant. It does not intersect the line $\sigma_1 = \sigma_2 = \sigma_3$, which excludes states of hydrostatic stress from causing plastic deformation. Its applicability to rock materials has not been determined.

Theory of Maximum Shearing Stress. Some observations of extrusion of metals led to the assumption that the plastic state is created in them when the maximum shearing stress just reaches the internal resistance of the metal to shear. The slip planes in certain materials were found to be inclined at 45° to the principal stresses. If it is assumed that $\sigma_1 > \sigma_2 > \sigma_3$, the yield condition is given by

$$\tau \text{ max} = \frac{\sigma_1 - \sigma_3}{2} \quad \text{const.} \tag{5.11}$$

The behavior of certain metals under triaxial unequal compression stresses is found to comply fairly well with the maximum stress theory, but experimental results are often represented more satisfactorily by the theory of constant octahedral stress. Both of these theories predict that the yield stress for uniaxial tension and compression should be the same. If one of the principal stresses is zero, both the octahedral and the maximum shearing theory may be represented by the same plane figure in the σ_1, σ_2 plane.

Isaacson[2] has proposed the theory of maximum shearing stress as a criterion for the behavior of rocks around deep mine openings in India.

Mohr's Theory of Failure. Mohr's theory, which utilizes the well known stress circle and the envelope to a family of circles as criteria of failure of materials subject to biaxial or triaxial stress has been applied to an analysis of data obtained for rocks by Balmer[3]. The empirical equations which result offer only one analytical approach to an evaluation of failure parameters. The envelope may be fitted to experimental data by the method of least squares or other methods of curve fitting. The following development is by Balmer[3].

Mohr's circles are of radius $\frac{\sigma_y - \sigma_x}{2}$ located at coordinates $(\frac{\sigma_y + \sigma_x}{2}, 0)$ and the system of equations are represented by the equation:

$$\left[\sigma - \frac{(\sigma_y + \sigma_x)}{2}\right]^2 + \tau^2 = \left(\frac{\sigma_y - \sigma_x}{2}\right)^2 \qquad (5.12)$$

where σ and τ are the normal and shearing stress at failure.

For triaxial tests Mohr's assumption that the intermediate stress has no influence on failure is followed, and cylinders which are stressed axially and normal to their circumference may be treated as if stressed biaxially. The parametric equations for the envelope are obtained in the usual manner by differentiating σ_y with respect to σ_x and solving the resulting equation and equation (5.12) for σ and τ. The results are:

$$\sigma = \sigma_x + \frac{\sigma_y - \sigma_x}{\frac{\partial \sigma_y}{\partial \sigma_x} + 1} \qquad (5.13)$$

and

$$\tau = \frac{\sigma_y - \sigma_x}{\frac{\partial \sigma_y}{\partial \sigma_x} + 1} \sqrt{\frac{\partial \sigma_y}{\partial \sigma_x}} \qquad (5.14)$$

These two equations give the normal shear stresses at failure and the slope of the curve relating the stresses. These are represented graphically in Figure 5.2. From Mohr's diagram the angle of failure α is given by:

$$\tan \alpha = \sqrt{\frac{\partial \sigma_y}{\partial \sigma_x}} \qquad (5.15)$$

It is also noted that

$$2\alpha = \phi + 90^\circ \qquad (5.16)$$

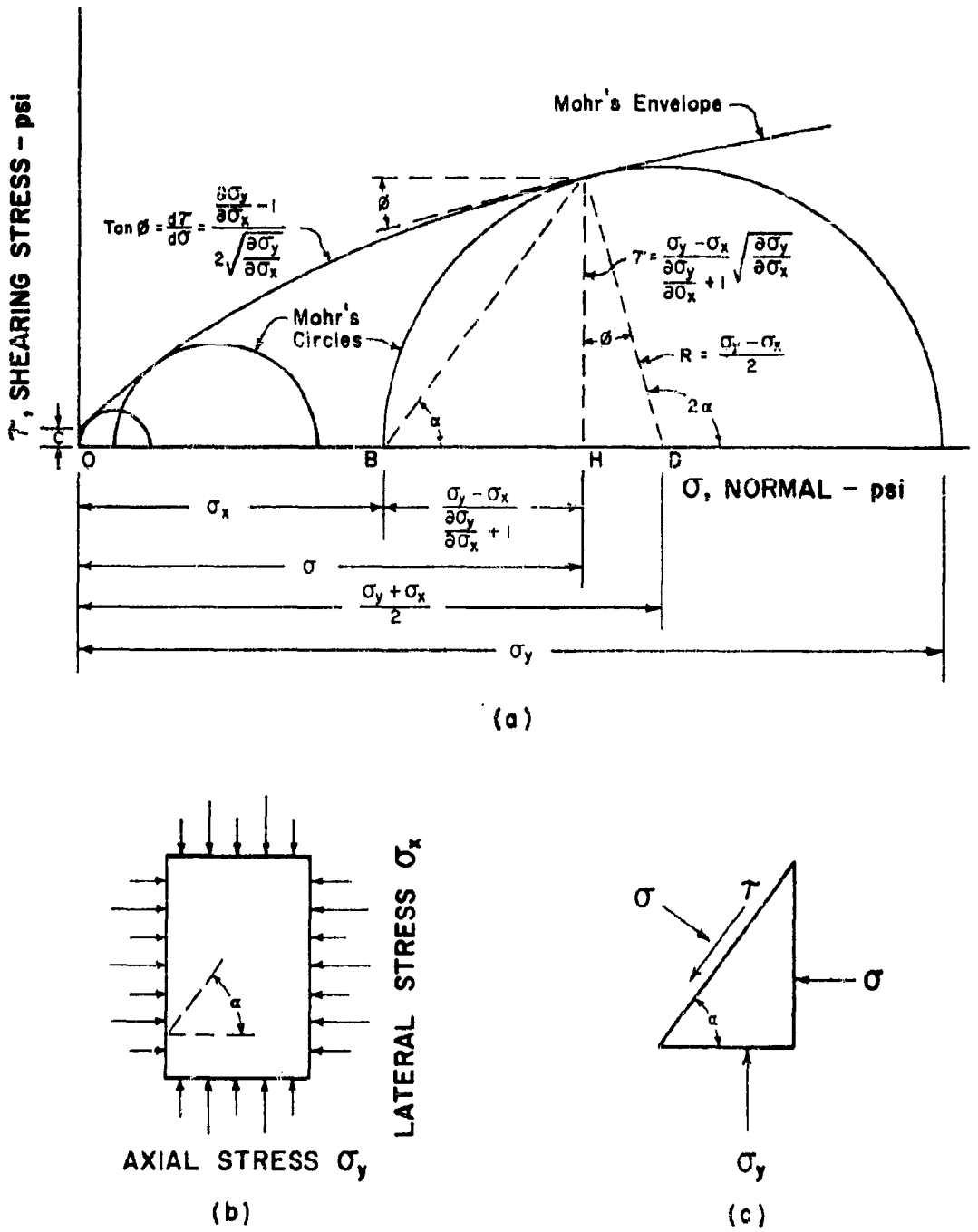


Figure 5.2. Mohr's diagram.

Also

$$\frac{d\tau}{d\sigma} = \tan \phi = \frac{\frac{\partial \sigma_y}{\partial \sigma_x} - 1}{2\sqrt{\frac{\partial \sigma_y}{\partial \sigma_x}}} \qquad (5.17)$$

which gives the mathematical relationship between the slope of the stress curve $\frac{\partial \sigma_y}{\partial \sigma_x}$ and that of Mohr's envelope.

Balmer suggests two methods of applying the above theory to a particular set of data: (1) select a function for Mohr's envelope which fits the data, or (2) select a function which describes the relation between the axial and lateral stresses. The required function in either case is determined by curve fitting, usually by the method of least squares: Both straight and curved line envelopes are suggested, i.e.:

$$\tau = C + \sigma \tan \phi \qquad (5.18)$$

or

$$\sigma_x = b\,(\sigma_y)^c + a \qquad (5.19)$$

Of these, the curvilinear analysis is the simpler and is preferable for those data which can be represented by a straight line.

Physical property tests by the Bureau of Reclamation[4], based partially on the work by Balmer, have employed Mohr's envelope as a means of evaluating the shear strength of rock, which is difficult to obtain by direct means. The envelope gives the relationship between shearing and normal stress at failure. In the results reported by the Bureau of Reclamation the envelope is assumed to be linear and its equation is determined by the method of least squares. The intercept C (equation 5.18) is called the unit cohesive strength or the shear stress at zero normal stress, and its slope tan ϕ is the coefficient of internal friction. The increase of compressive strength with lateral restraint is also plotted to yield a visual relationship between these two quantities.

The computed Mohr's envelope is taken as the limiting value of the shearing stress on the plane of failure for a corresponding normal stress. Confidence limits are established to take into account the dispersion of laboratory test data. The confidence limits diverge as they approach the upper and lower limits of recorded data indicating that extrapolation is not reliable.

When the envelope is considered to be a curve, the coefficient of internal friction is variable and the values of the unit cohesive strength are lower.

Griffith's Theory of Fracture.[5] Experience has shown that isotropic brittle materials break in uniaxial tension when the tensile stress reaches a critical value, that of the brittle (tensile) strength. In very thin fibers the strength usually increases with decreasing diameter. On the other hand, the tensile fracture surface of crystals is frequently a crystallographic plane of low index and high atomic density ("cleavage plane"); in many crystals such as quartz, however, the surface of fracture is non-crystallographic and has the same appearance as that in glass. Crystallographic fractures obey Sohncke's law[6], that is, it occurs when the normal tensile stress to the cleavage plane attains a critical value. It has been found that in alkali halides, for example, the fracture cleavage plane is (100)*, and the critical normal stress is in the order of 20 bars. One of the simplest ways of obtaining a rough estimate of the molecular cohesion of the solid is found in surface energy, and the elastic energy in the stressed specimen provides the surface energy for the surfaces of fracture. This amounts to 2α for a specimen of unit cross section where α is the specific surface energy. It is postulated that a large fraction of the energy 2α must be present at the moment of fracture between the molecules immediately adjacent to the surface of fracture. That is, if σ_m is a fracture stress, and $\sigma_m^2/2E$ is the energy density (Hooke's law) the total energy $a\sigma^2_m/2E$ between two neighboring atomic planes of spacing $\underline{a}$ should be of the order of magnitude of α.

Solving for σ_m yields mathematical equation

$$\sigma_m = (2\alpha E/a)^{\frac{1}{2}} \tag{5.20}$$

For certain metals, minerals, and glasses of similar materials E is of the order of 10^5 or 10^6 bars, while the corresponding α is 10^3 ergs/cm^2 and that of $\underline{a}$, 3×10^{-8} cm. The critical stress for these materials must therefore be of the order of 10^{11} dynes/cm^2 or 10^5 bars. Tensile stresses of this order have been measured in especially prepared glasses, mica, and thin tungsten wires, but for ordinary materials such as window glass the stress is only 1000 bars, and the tensile stress of common steels and other metals or of a much lower order of magnitude than those predicted by the estimated values of molecular cohesion.

Griffith's theory of failure[6] is based upon the assumption that the low order of tensile strength in common materials is due to the presence of small cracks or flaws. Actual stresses may occur around these flaws which are of the order of magnitude of molecular cohesion values, while the average tensile strength may be quite low. Based upon the developments made by Inglis[7] of the stress distribution around an elliptical hole in a stressed plate, the major axis being 2c and with a stress σ perpendicular to the major axis, the highest stress occurs at the ends of the major axis and is equal to

$$\sigma_m = 2\sigma(c/\rho)^{\frac{1}{2}} \tag{5.21}$$

in which ρ is the radius of curvature of the ellipse at the ends of the major axis. It will be noted that the maximum stress goes to infinity as ρ is decreased to 0. Utilizing energy relationships Griffith assumed that the crack would lengthen and would lead to fracture if, for a small increase of its length equal to 2c, the work of the external forces were equal to the increase of the elastic energy around the crack plus its surface energy. It can be readily seen that specimen surface cracks of

*Crystallographic direction.

depth c, which were the type with which Griffith worked experimentally, will produce the same stress concentration as internal cracks of lengths to c. It can be shown that the elastic energy in a plate due to an elliptical crack is given by the following:

$$W_e = \pi c^2 \sigma^2 / E \qquad (5.22)$$

this holds for the conditions where the thickness is small compared with the length to c of the crack, that is, if there is a state of plane stress. On the other hand, if the thickness is large compared to c, a condition of plane strain, the elastic energy due to the presence of the crack is given by:

$$W_e = (1 - \nu^2)\pi c^2 \sigma^2 / E \qquad (5.23)$$

where ν is Poisson's ratio. The work of the external forces when the crack in introduced is found to be twice the excess elastic energy, W_e, while the surface energy of the crack is:

$$W_s = 4\alpha c \qquad (5.24)$$

The crack is said to be in unstable equilibrium with the external forces if, for a small increase of its length, the increase of the surface energy of the crack and of the excess elastic energy is just equal to the work done by the external forces, this may be expressed mathematically by:

$$\frac{d}{dc}(W_e - W_s) = \frac{2\pi c}{E}\sigma^2 - 4\alpha = 0 \qquad \text{or} \qquad \sigma = (2\alpha E/\pi c)^{\frac{1}{2}} \qquad (5.25)$$

This holds for a thin plate and the corresponding equation for a thick plate is

$$\sigma = [2\alpha E/\pi c(1 - \nu^2)]^{\frac{1}{2}} \qquad (5.26)$$

Cracks will then occur and fracture processes take place as soon as the actual stress exceeds the values given in Equation 5.25 or 5.26.

The Griffith fracture condition may also be derived from atomic considerations. The smallest radius that the end of a crack may have is the interatomic distance $\underline{a}$. Hence, if ρ is replaced by $\underline{a}$ in Equation 5.21 and it is divided by Equation 5.20, the value of the mean applied stress at which the crack of atomic dimensions equals molecular cohesion is

$$\sigma = (\alpha E/2c)^{\frac{1}{2}} \qquad (5.27)$$

This differs from Griffith's condition (Equation 5.25) by a factor of $\frac{1}{2}$ compared to $2/\pi$.

Griffith's experiments showed that the dangerous cracks in glass occurred at the surface, and this has been found to be true for many cases of brittle fracture. The theory does not appear to be applicable in the case of ductile failure.

One important question related to the Griffith theory is whether the number of dangerous (effective) cracks must be large. It is reasoned that the scatter of values of measured strengths of brittle materials indicates that the number cannot be large.

Orowan[5] points out that in polycrystalline metals which contain two textural elements, crystal grains and grain boundaries, the mechanical behavior of the two is fundamentally different. Plastic slip in the grains begins when the shear stress in the slip plane reaches a well defined critical value. Critical shear stress does not change rapidly with temperature and remains finite up to the melting point. On the other hand the grain boundaries show all the characteristic features of viscosity as produced by a disorderly arrangement of atoms or molecules. Boundaries show no yield stress, and the rate of sliding of adjacent grains would probably be proportional to the shear stress if the surfaces were even and the grains could slide without geometrical nonconformity. Due to the "keying" of grains the rate of boundary sliding diminishes after a small deformation and disappears. If the intercrystalline cohesion is low, the boundaries may become the weakest element in the solid. When fracture occurs it runs along them. This is characteristic of brittle fracture.

As outlined above the basic hypotheses of the Griffith[8] failure theory utilize the evaluation of potential strain energy and surface energy of cracks. The energy of a crack is proportional to its surface energy and results in equal reduction of strain energy about the crack when fracture takes place. That is, an increase of potential energy due to the surface tension of the crack must be balanced by the decrease in the potential of the strain energy and the applied forces. Disparity between observed theoretical rupture stresses and strength observed in ordinary tensile stresses leads one to seek for a reason for the low order of observed rupture stress. Griffith attributes these to three possible reasons: (1) In heterogeneous materials a mutual surface tension may excess between different constituents to cause concentrations of energy. (2) The material may possess high order residual stresses. (3) It may contain small cracks due to manufacturing processes or other reasons.

The latter reason seems to offer the most fruitful avenue for investigation of possible cause of defect of strength. The application of Hooke's law to an analysis of stresses about small elliptical cracks was made by Inglis[7] for a two dimensional elastic case. The equation was solved by a means of elliptic coordinates in α and β obtained by the conformal transformation:

$$x + iy = c \cos (\alpha + i\beta) \qquad (5.28)$$

A condition that a crack in a thin plate (See Figure 5.3) may be extended, that is, that a rupture may occur, is found by making a stipulation that the total energy remain unchanged by small variations in the length of the crack. The equation for this condition is as follows:

$$\sigma = \sqrt{\frac{2\,ET}{\pi\, c}} \qquad (5.29)$$

where σ is the component of the applied force or stress normal to the direction of the crack, 2c is the length of the crack, and E and T are respectively Young's modulus and the surface tension of the material. The component of the applied force S parallel to the crack has no influence on the rupture stress. A maximum stress, σ_m, at the ends of the crack has been given by Equation 5.21.

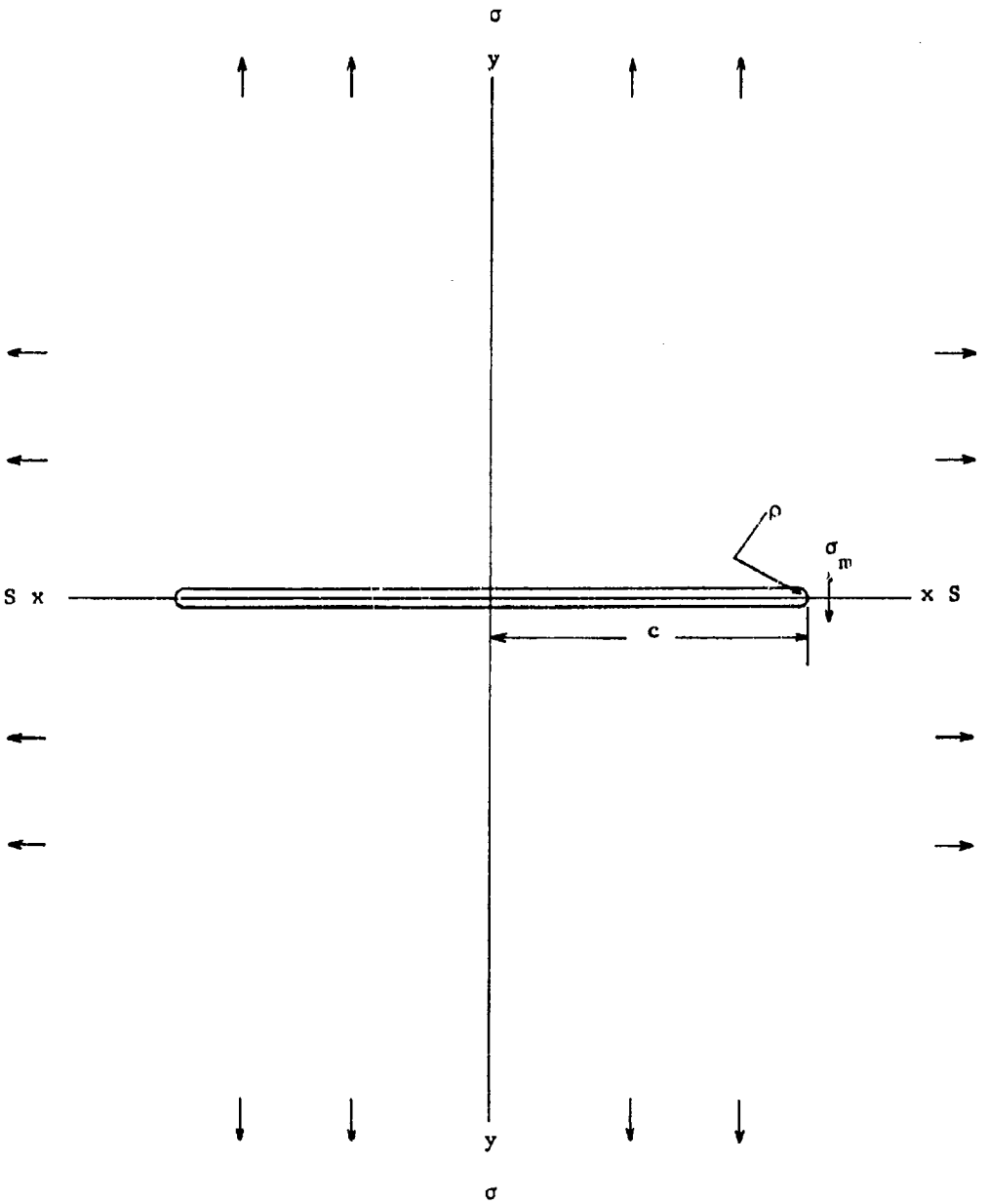


Figure 5.3. Diagrammatic representation of crack and stress system for normal orientation - Griffith theory.

$$\sigma_m = 2\sigma\sqrt{\frac{c}{\rho}} \tag{5.30}$$

where ρ is the radius of curvature of the corners of the crack, provided ρ is small compared with c. This follows from the expression derived by Inglis:

$$\sigma_m = \sigma(1 + 2\frac{a}{b}) \tag{5.31}$$

which holds for an elliptic hole of semi-axes a and b. Equation 5.30 indicates that the rupture stress of the material is constant if ρ and c are constant.

For the case of plane strain the force necessary to cause rupture is:

$$R_1 = \sqrt{\frac{2E\ (1 - \nu^2)T}{\pi c}} \tag{5.32}$$

where ν is Poisson's ratio.

The strain energy of the material at the point of rupture may be calculated easily as follows:

$$\frac{\sigma_m^2}{2E} = \frac{\sigma_1^2}{2E\ (1 - \nu^2)} = \frac{4T}{\pi\rho} \tag{5.33}$$

that is, the same amount of energy is required for rupture in both the cases of plane stress and plane strain. To ascertain the effect of a number of cracks randomly oriented in a given material, it is assumed first that the cracks are so far apart that the maximum stress due to any crack is not seriously affected by the adjacent cracks. This follows directly from an application of de St.-Venant's theory. It cannot be applied to determine absolute strength unless the sizes of the cracks are known. However, it can be employed to give a close approximation. Thus, for a crack which is oriented at an angle θ to the horizontal, the expression for the stress at the ends of the crack for a plate which has forces Q and P applied at the outer edges is given by:

$$R_{\beta\beta} = \frac{(P + Q)\sinh 2\alpha_o + (P-Q)(e^{2ao}\cos 2\beta - 1)\cos 2\theta + (P-Q)e^{2ao}\sin 2\beta \sin 2\theta}{\cosh 2a_o - \cos 2\beta} \tag{5.34}$$

where α_o is the parameter of the ellipse corresponding with the edge of the crack, and θ is the coordinate which specifies the position of points on the ellipse. The direction $R_{\beta\beta}$ is parallel to the edge of the crack. It is postulated that tensile stresses are positive and that P is algebraically greater than Q. For values of θ and β for which $R_{\beta\beta}$ is a maximum, it is found that in general, $R_{\beta\beta}$ is a maximum at two pairs of points in each crack. If $\theta = 0$ or $\frac{\pi}{2}$, these points occur at the ends of the major and minor axes respectively. However, for all other values of θ both pairs are very near the ends of the major axis. Also, one pair of maximum stresses is usually tensile and the other compressive. By imposing the condition that the maximum tensile stress so found is constant it follows that the required laws of rupture are as follows: (Figure 5.4)

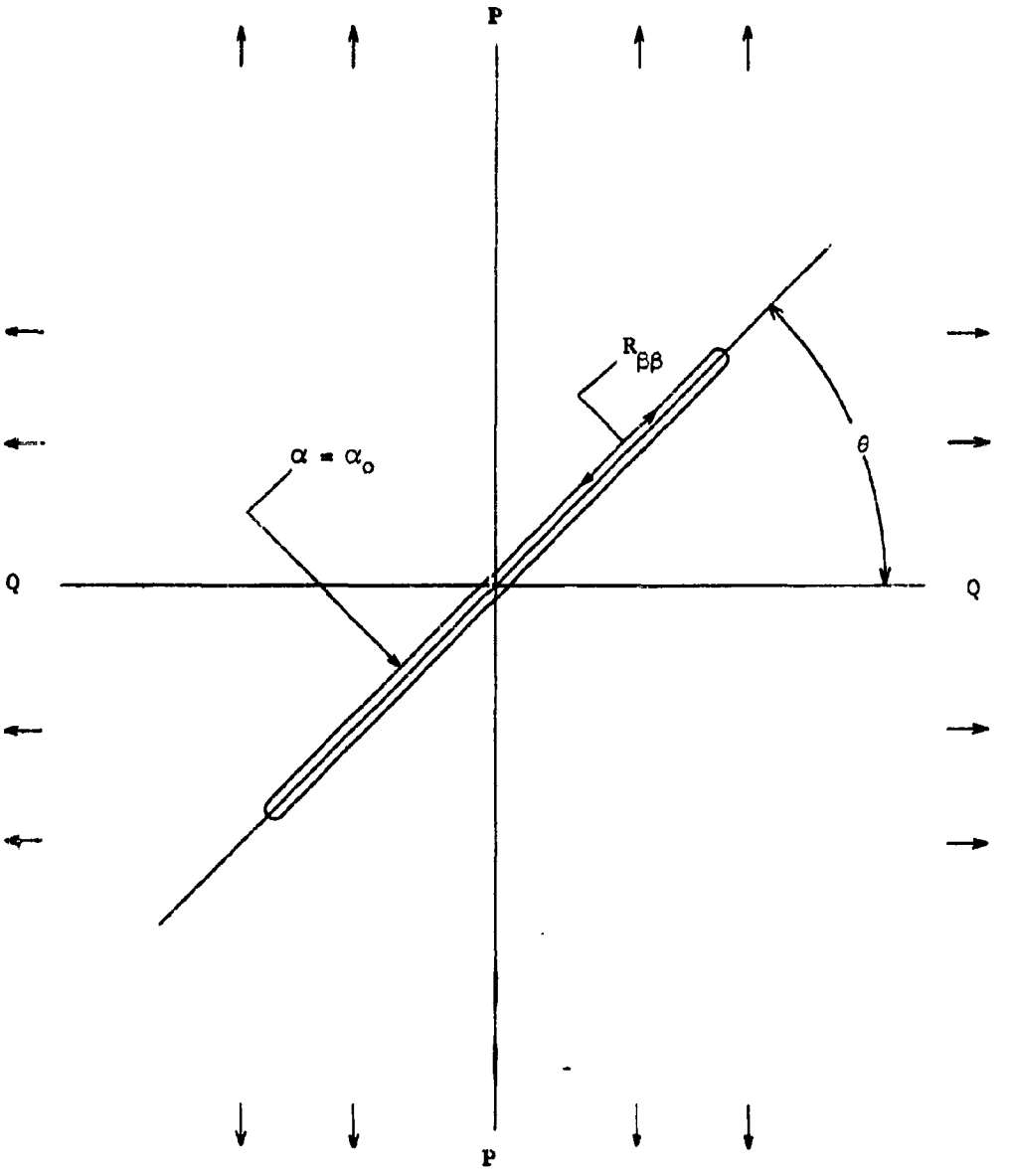


Figure 5.4. Diagrammatic representation of crack and stress system for angular orientation - Griffith theory.

(1) If 3P + Q is positive, the condition for rupture is:

$$P = K, \tag{5.35}$$

where K is a constant which depends on the properties of the material and the dimensions of the cracks.

(2) If 3P + Q is negative, the rupture condition is given by the equation:

$$(P - Q)^2 + 8K(P + Q) = o \tag{5.36}$$

For oblique fracture the equation for the angle of fracture is given by:

$$\cos 2\theta = -\frac{1}{2}(P - Q)/(P + Q) \tag{5.37}$$

Griffith notes further that in comparative tensile and compressive tests of stone and light materials that the crushing (compressive) strength is from 7 to 11 times the tensile strength, and that the angle of fracture is oblique.

A comparison of Mohr's and Griffith's theories of failure has been made by Clausing[9]. He shows that the relationship between the principle stresses and failure given by Griffith's theory are as depicted in Figure 5.5 and those given by Mohr's theory are given in Figure 5.6. For each case it can be shown, for certain conditions, that the angle of failure is given by the expression:

$$\tan\theta = \frac{1}{\sqrt{\frac{dp}{dQ}}} \tag{5.38}$$

Thus, Mohr's theory predicts that fialure of materials is due to failure in shear while Griffith's theory postulates that it is due to failure at crack tips. But each theory may lead to the same conclusion concerning the angle of failure. Thus, if it can be postulated that the friction angle utilized in the Mohr's theory may not be constant, the two theories are in practical agreement. If on the other hand the angle of friction in the Mohr theory must be held constant then the two theories are not in agreement in that the slope of the tangent to Mohr's circles is not constant for all materials as predicted by a constant friction angle and should not be represented by a straight line.

Nadai[1] points out that the great value and importance of the Griffith theory are in having shown that the tensile strength σ_1 of amorphous solids depends on a few physical parameters such as the "average" length 2c of the hypothetical flaws or cracks, the modulus of elasticity E, and the surface tension T. Further, the conditions for fracture in certain cases can be understood by investigating the equilibrium of the stresses about such weakened regions of small but finite size in which an exchange of energies of different characters takes place which causes the propagation of growth of weaker regions. Thus, the phenomena of fracture might be investigated from the point of view of separation of crystal lattices, or the mechanical equilibrium of forces in finite regions where one type of energy may change to another, which weakens the material and may lead to rupture.

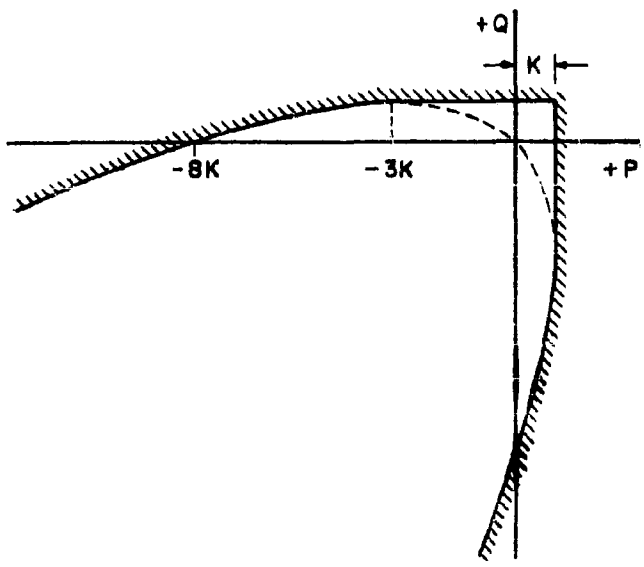


Figure 5.5. Geometrical representation of the biaxial fracture criterion of Griffith.

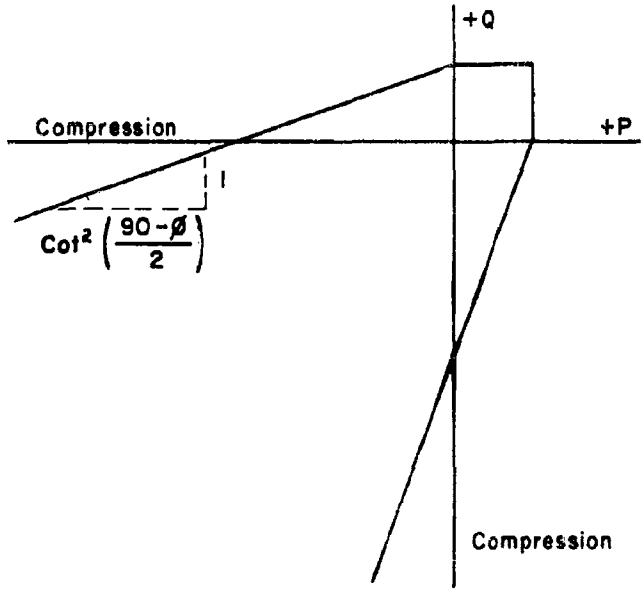


Figure 5.6. Principal stress at failure -- Mohr's Theory.

Rock Bursts

The phenomena of rock bursts are analogous in many respects to those failures which might be expected to occur when rock structures close to an underground protective installation are subjected to the overpressures induced by a nuclear explosion at the surface over the installation. The primary differences are related to the time to build up critical stresses in the rock, i.e., pressure rise times, accelerations, particle velocities, etc. Failure theories are explanatory only.

In mining experience a rock burst is the occurrence of the rupture of a mass of strained rock in such a manner that a portion of the accumulated strain energy is released in a short period of time. Types of failures vary from splitting off of small slabs of rock from a mine well or face to the collapse of large pillars, roofs, or other massive portions of the mine structure. The build-up of strain energy above those existing prior to excavation may have taken months to accomplish and it continues to accumulate until some critical area of the rock is strained to failure.

On the other hand, the build-up of total strain energy found in rock strained by transient loads is characterized by three separate states of stress, the first two of which are common with rock burst phenomena. The first is the stressed condition of the rock in its natural state before any openings are made in it. These stresses are due to the weight of overlying rock and to any residual tectonic stresses which may have caused deformation. Included also would be certain stress concentrations due to structural discontinuities in the rock, chemical processes, etc. The second type of stress is that which is induced by the introduction of openings into the rock. These have an effect of further distorting the natural static stress field and of creating stress concentrations, usually at or near the periphry of the opening (See Chapter VI). Intersection of an opening with structural discontinuities of the rock may create areas of high local stress concentration. The ratio of the latter to an ideal free stress field may be viewed as a stress multiplication factor which in many cases will increase the effect of a third type, or transient field, due to a surface explosion. One may conclude, therefore, that many of the criteria for failure of rock structures under rock burst conditions will be similar to those of failure in underground protective structures.

Some observations by Morrison[10] are based on the concept of a "pressure ring" about a large excavated area. This is evidenced by distortion of the openings near the main excavation. Shear cracks appear and minor slabbing of rock takes place. Thus, it is postulated that the stress concentration at the surface of the opening is relieved and the areas of higher stress move back into the surrounding rock where stability is re-established. This new area is referred to as a dome. On the basis of this analogy the following is postulated by Morrison:

1. When the excavation has been made stability is re-established in the rock by the formation of a new stress zone which results from an elastic movement of rock toward the excavation. The rock within this zone is likely to fail and form a fracture zone. The surface between the

fracture zone and the area of maximum stress is referred to as a dome, the stress being a function of the shape of the dome.

2. The size of the excavation is the controlling factor in the formation of the dome. Under otherwise similar conditions the shortest span controls the depth into the walls to which doming takes place as well as the magnitude and distribution of stress.

3. The stress pattern resulting from the excavation of an opening is a composite of all other stress fields in the locality.

The existence of such fracture zones in mine rock subject to rock bursts is generally conceded to exist and the energy which is released by rock bursts is that associated with the sudden transition from a solid strained state to a fractured constrained state.

Rock Burst Energy. Only estimates of the energy released by rock bursts are available. The seismic waves associated with the burst of a shaft pillar at the Lake Shore Mine in Canada were picked up at Weston, Massachusetts, 580 miles away[11]. Estimates of seismic wave energy on the Kolar Gold Fields in India have been estimated as being in the order of 15 million foot tons. Leet[12] has estimated a figure of 50 million foot tons for certain bursts in South Africa, while Morrison suggests that major bursts result in the release of as much as 500 million foot tons of energy. The latter figure implies that about 250 million cubic feet of rock would be relieved of its strain energy.

The conditions which influence rock bursts in mines are (1) the area of the excavation, (2) the shortest roof span, (3) stress pattern and concentration, (4) types of rock involved, (5) directions of planes of weakness in the rock, and (6) the dip of the mineral deposit.

The heaviest rock bursts are attributable to pillar failure. Where zones of weakness cross a working area or a drift (tunnel) these may form unstable structures. Multiple stress zones created by multiple adjacent openings should be avoided at all costs because they create overlapping stress zones, the effect of which is usually additive.

It is further noted by Roux and Denkhaus[13] that when an excavation is made at great depth failure planes appear at its surfaces, extending into the walls. In drifts (tunnels) of 7 x 8 feet cross section the fracture zone may extend as far as 20 feet into the surrounding rock. The fractured ground within the fracture zone is called intradosal and that outside of the fracture zone extradosal. In many mines extradosal bursts occur more frequently than intradosal. That is, the extradosal ground ahead of the working face serves as an abutment which supports the superincumbent rock to the surface. (Figures 5.7 and 5.8).

Distressing of working faces, which moves the zones of high stress back into the rock mass is practiced in many deep South African mines. It is accomplished by drilling holes 10 feet deep into the rock on 5 foot centers and fracturing the rock, in place, by moderate size charges of H.E.

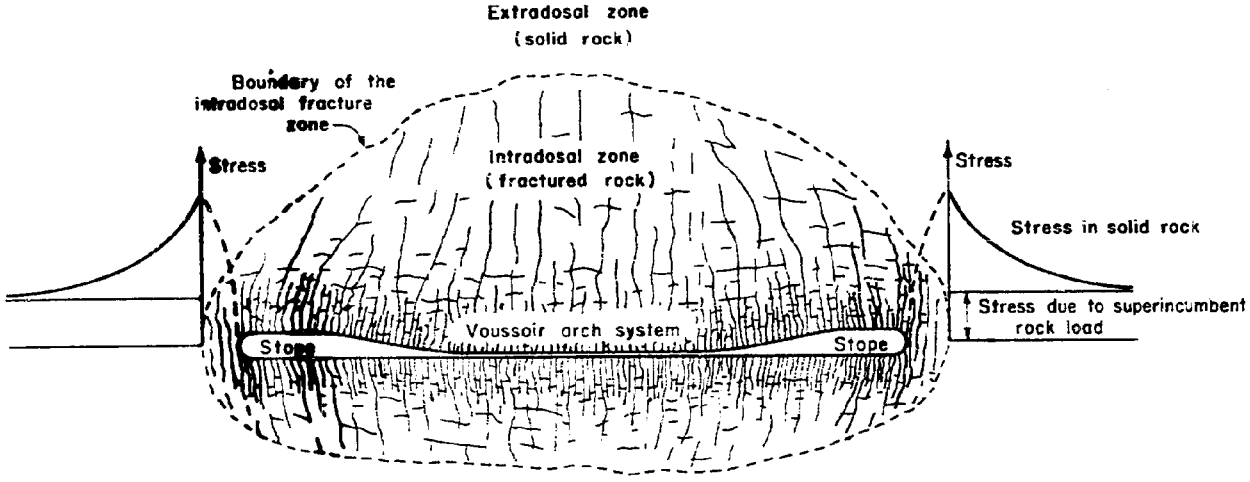


Figure 5.7. The conditions prevailing in the ground around an excavation at depth.

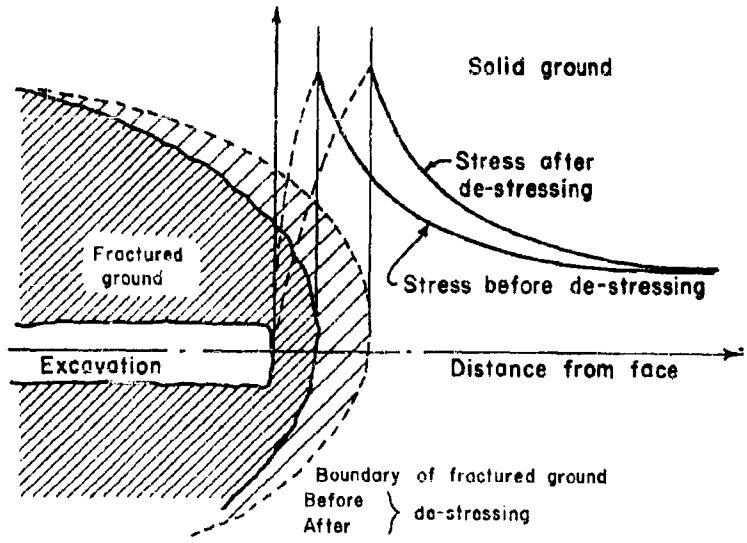


Figure 5.8a. Probable effect of artificial de-stressing on the stress distribution ahead of the face.

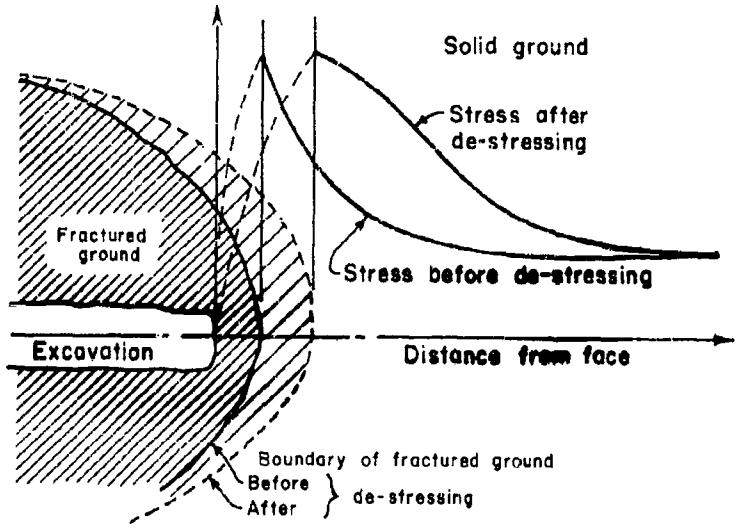


Figure 5.8b. Probable effect of natural de-stressing on the stress distribution ahead of the face.

In general, it has been found necessary to avoid creating such underground structures as small pillars, pillars with acute angles in horizontal cross section, or in fact, any type of structure which will permit the occurrence of high stress concentrations. Thus, drifts (tunnels) should not be driven parallel and within critical distances of faults. When faults or similar structure are to be crossed the underground opening should be driven at right angles to the structure.

The effect on stress concentration of decreasing the size of remnants is shown in Figure 5.9, where the P represents the peak stresses and the C the core stresses.

Mechanisms of Dynamic Failure

General

The mechanism of failure of rock is very closely associated with the environment which causes failure. Of these, the geometry of the body loaded as well as the geometry of the loading force are primary factors. In addition, the type of stresses created, confinement, magnitude and time distribution of the loading force may have controlling effects. For example, a semi-infinite medium may be loaded at essentially a surface point, or it may be loaded internally at varying distances from its free surface. Quite different results are observed for a finite body, such as a beam, which is loaded in bending. As is the case for compact solids failure under dynamic loading is usually due to tension or shear stresses. Porous media may apparently fail in compression, but the basic failure of constituent grains or the binding material is due to tension or shear. These concepts appear to be applicable whether failure occurs in the elastic range as a fracture, as plastic flow or plastic flow and subsequent fracture.

Failure Due to Plane Tension Waves. One of the most widely used mechanisms employed to explain failure of rock in many blasting processes is the "Hopkinson bar" principle. In the original Hopkinson experiment a compressive wave in a steel bar was permitted to reflect as a tension wave from a free end of the bar, causing a glued segment on the free end to fly off when the magnitude of the tension in the reflected wave became large enough to break the bond. This principle for massive solids is illustrated in Figure 5.10 in its application to slabbing of rock at a free surface by a compression wave impinging on that surface. The manner of slabbing is determined largely by the rise and fall times of the pulse, and the Bureau of Mines[14] utilizes the static breaking strain in tension as a criterion for evaluating the control factor in slab formation. That is, it was assumed that the fracture strain under dynamic loading could be approximated by that which caused fracture under static conditions. This mechanism was also employed to account for a large part of the breakage which occurs in the formation of craters in rock by means of buried HE charges of small sizes.

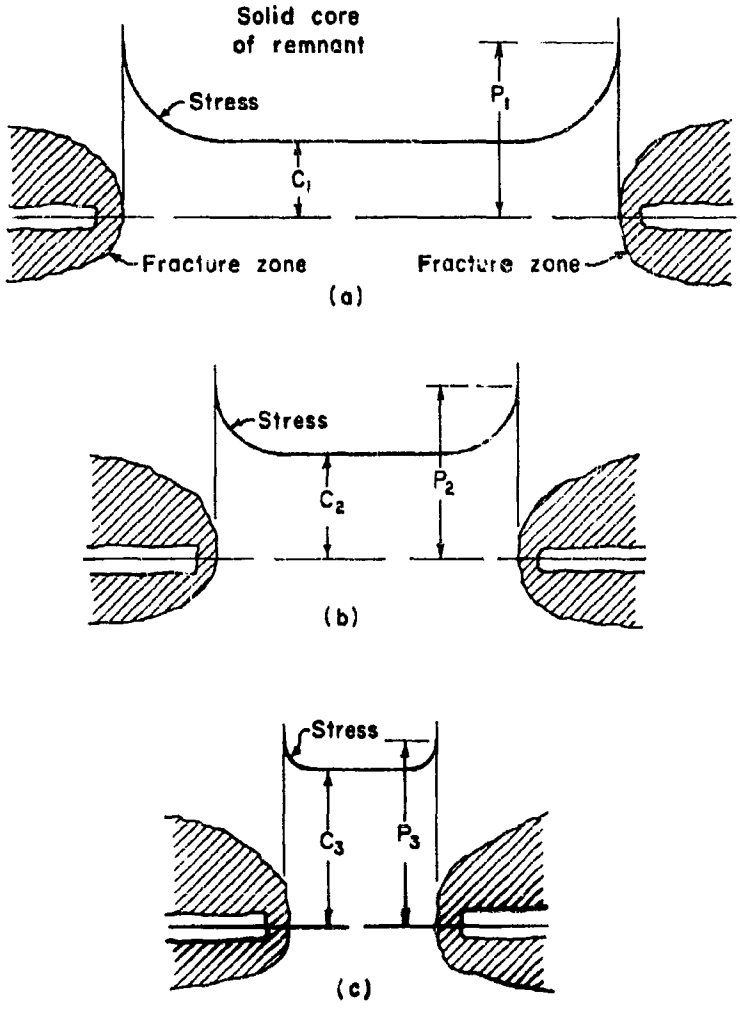


Figure 5.9. The distribution of stress in the solid core of a remnant as it becomes worked out.

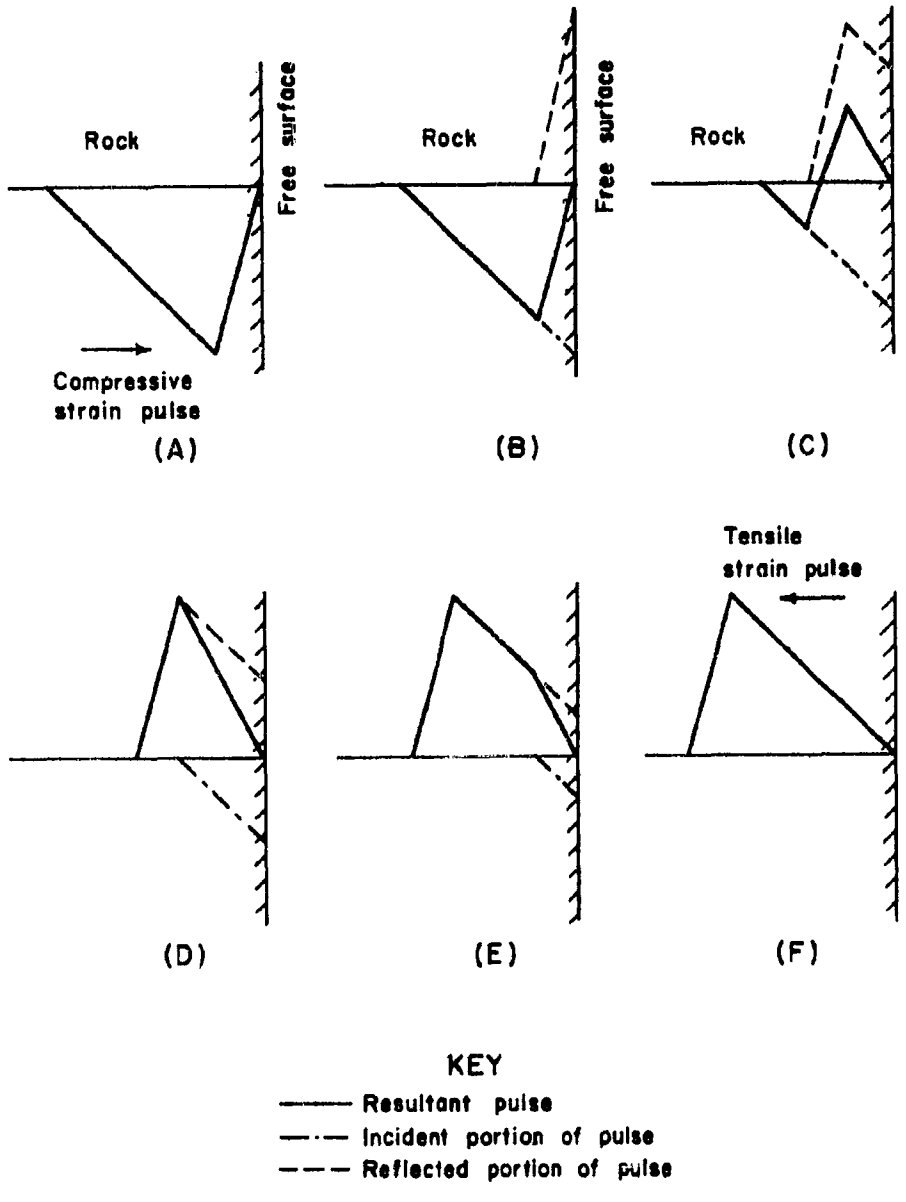


Figure 5.10. Tensile fracture by reflection of a compressive strain pulse.

Breakage Processes. In underground explosion tests damage may be analyzed on the basis that (1) the tunnel is small compared to the length of the strain wave or pulse and that failure occurs in much the same manner as in a static stress field, or (2) that the tunnel is large compared to the length of the strain pulse and damage is caused largely by reflection from free surfaces of the tunnel. Where the explosive cavity and tunnel are relatively close together and the explosive cavity is not less than about one-fourth the diameter of the tunnel, recent research with burn cut rounds indicates that shear mechanisms may also be of importance on a very small scale.[15]

The reflection mechanism and the mechanism of shattering may be of importance in damage to tunnels or other openings because the relationship between pulse magnitude, pulse length, geologic structure and the size of opening may be in a critical range.

Strain Reflection.[14] When a longitudinal compressive wave in solid media is incident upon a free boundary both a longitudinal and a transverse wave are reflected. For angles of incidence of less than 50° a compressive wave is reflected as a tensile wave and most of the energy is contained in this wave. Figure 5.11 shows a simplified triangular strain wave impinging on a free surface at normal incidence. The dotted lines below the coordinate line represent the cancelled portion of the incident compression pulse and the dotted line above represents the cancelled portion of the reflection tension pulse and the solid line represents the resultant or actual pulse. Inasmuch as rock is much weaker in tension than in compression or shear the reflected tensile pulse may break the rock. A study of Figure 5.11 shows that the tensile strain rises to its maximum value at a distance from the free surface equal to half the length of the incident compressive pulse. Before it reaches this maximum the magnitude of the tensile strain developed during reflection depends primarily upon the shape of the decay portion of the incident compressive pulse. The shape of the rising portion of the pulse does not affect the magnitude or location of the peak tensile strain but it may affect the position where breaking strain is initially developed.

The process of tensile slab fracturing is illustrated in Figure 5.10. A compressive pulse impinges on a free surface and is reflected as a tensile pulse. After a given time the tensile strain developed becomes equal to the dynamic tensile breaking strain of the rock and a crack develops at the point of maximum strain. The surface of this crack acts as a new face from which the remainder of the impinging wave will reflect. The slab thus formed will move forward because of the entrapped energy in the form of particle velocity. This process continues until the tensile strain developed is less than the tensile breaking strain of the rock. In general, the number of slabs produced in such a reflection process equals the first whole number less than the ratio of the magnitude of the fall strain pulse to that of the breaking strain of the rock.

This theory predicts that the depth of a crater broken by a sperical charge should equal approximately half of the fall length of the strain pulse, provided that half of the fall length of the strain pulse is less than the charge depth and the charge is sufficiently large to

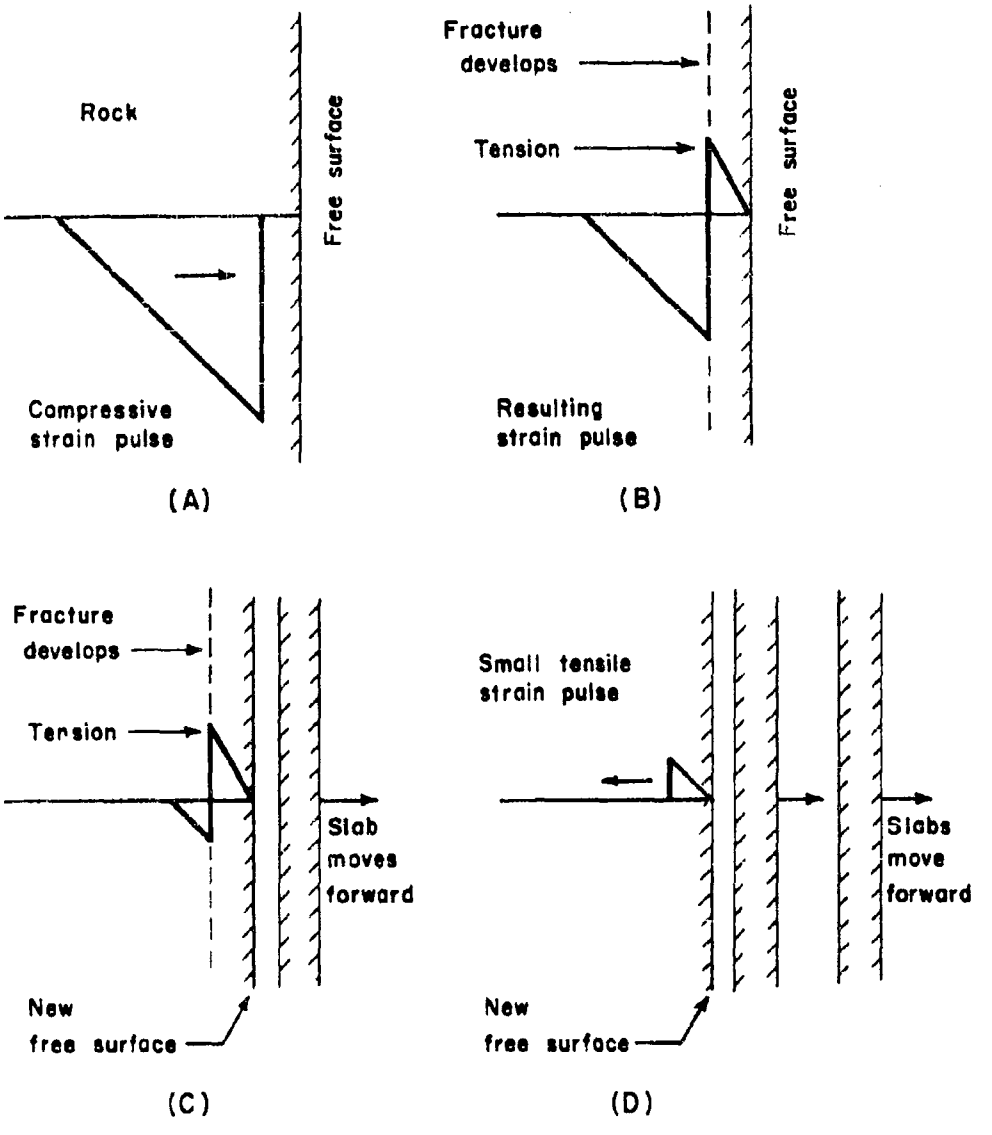


Figure 5.11. Reflection of a triangular compressive strain pulse.

produce a fall strain several times larger than the breaking strain of the rock. However, if half of the fall length of the strain pulse is greater than the charge depth the rock will break only to the crushed zone around the charge. If approximately horizontal slabs develop near the crushed zone the curvature of the remaining wave causes it to reflect from the new free surface at large angles and it can develop only small tensile strains at large horizontal distances. Experimental crater data illustrate the limitations on crater depth and crater radius by these two factors.

Theory and field results were found to agree[14] in four types of rock within reasonable limits. When the fall strain is only slightly greater than the tensile breaking strain of the rock, one slab is formed, when twice as great two slabs, etc., until the crater depth D_k equals the charge depth D. Quantitatively, however, the reflection theory predicts greater crater depths than are obtained experimentally.

Crater Tests - USA CE[16] and USBM[14]

General. The results of crater tests performed by the Corps of Engineers and the Bureau of Mines provide the only relatively complete data in the literature which are related to damage of tunnels in solid rock by HE. Certain experiments were carried out primarily to determine the critical scaled distances between charges and underground openings where damage would not occur. These tests included a large range of charge sizes of TNT and a whole range of scaled distances, charge to tunnel, from those causing no damage to those causing maximum damage. The Bureau of Mines tests were designed to verify the reflection theory of rock breakage and to define critical parameters in blasting of rock. The first group of tests were made in Navajo sandstone, Unaweep granite and limestone at Dugway Proving Grounds, and the second in Lithonia granite, Green River Marlstone, Kanawha sandstone and Niobara chalk.

Nomenclature of Crater Tests. The nomenclature employed by the Bureau of Mines is given below. Figure 5.12 illustrates some of the dimensions of a crater formed by a confined explosive charge. Applicable definitions are as follows:

A_k = Area of crater at surface

R_k = Radius of crater at surface = $A_k\sqrt{\pi}$

D = Depth to center of gravity of charge

W = Weight of explosive in pounds

V_k = Volume of crater computed by rotating each quadrant through 90°, i.e.

$$V_k = \frac{\pi}{2}\,(r_1A_1 + r_2A_2 + r_3A_3 + r_4A_4)$$

where A_1, A_2, A_3, A_4 are the areas of each half cross sections, and r_1, r_2, r_3 and r_4 are the radii of their respective centers of gravity.

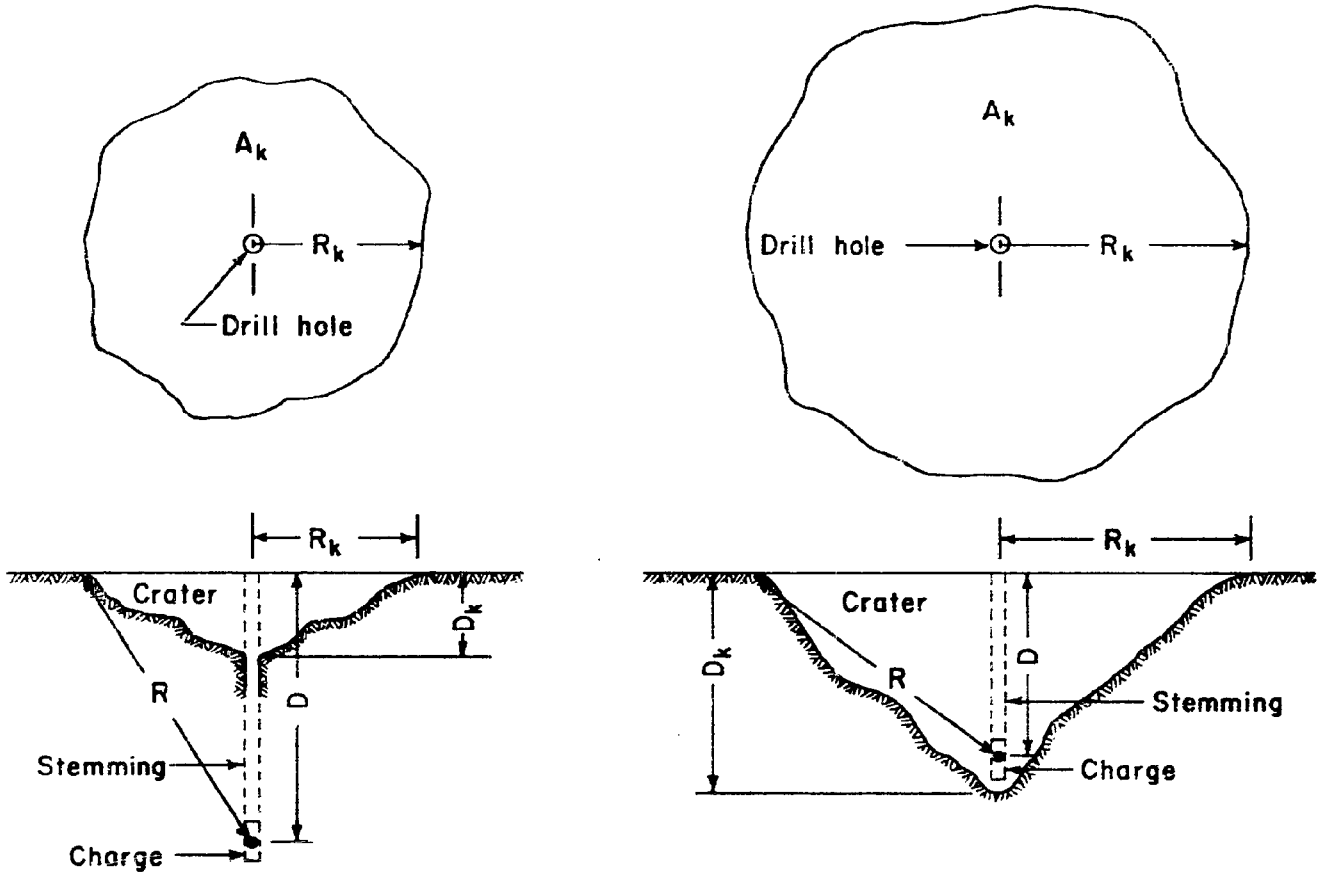


Figure 5.12. Plan and section drawings illustrating crater tests variables.

R = Radius of rupture = $\sqrt{D^2 + R_k^2}$

F = Scale factor = $\sqrt[3]{W}$, defined in feet

The scale factor $\bar{r}$ as a standard practice is defined as a length in feet which is numerically equal to the cube root of the charge weight in pounds. Thus linear dimensions are scaled by dividing by $\bar{r}$, areas by $\bar{r}^2$ and volumes $\bar{r}^3$. Strain is a length ratio and is consequently a scaled quantity. Time is also scaled by dividing by $\bar{r}$ and thus scaled time multiplied by velocity yields scaled distance.

Critical Factors in Effective Breakage. The critical factors in effective breakage can be defined in terms of scaled crater dimensions. They are scaled charge depth $D/\bar{r}$, scaled crater depth $D_k/\bar{r}$, scaled crater volume V_k/W, and scaled crater radius of rupture $R/\bar{r}$.

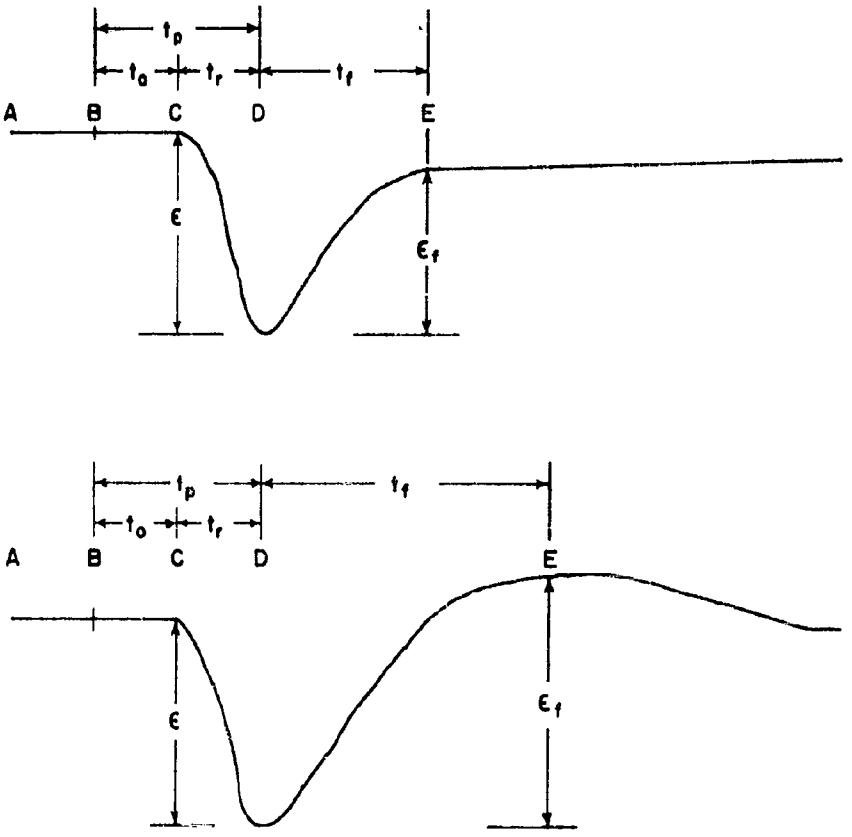
In the large majority of efficient blasting processes it is believed necessary that the rock break approximately to the explosive charge position. This would require for effective blasting of craters that $D_k/D = 1.00$. The allowable variation from this ideal condition is discussed in connection with types of rock in a later section. Effective scaled charge depths lie in the range of 0.9 to 1.6 and are of approximately the same magnitude for rocks of similar physical properties. The corresponding scaled crater radii vary from 2 to 4, scaled radii of rupture from 2.2 to 4.5, all depending upon the type of rock, and to a limited extent on the type of explosive, diameter of charge hole, geologic structure of the rock, and related factors. Scaled crater volume, whose units are cu ft/lb, is one of the best measures of the efficiency of a single blast. The best criteria for determining size and depth of charges appears at present to be a combination of values of scaled charge depth, scaled crater depth and scaled crater volume. Scaled crater radius and scaled radius of rupture are similarly the best means of fixing the optimum value for charge spacing.

Of the above parameters the only one which the reflection mechanism predicts directly is the crater depth. The reflection theory has been employed successfully in predicting crater depths to a reasonable degree of accuracy and critical depths at which confined charges must be placed in order that surface damage will be caused by the detonation. If the theoretical crater depth is equal to half the fall length (See Figure 5.13) of the strain pulse, then,

$$\frac{D}{\bar{r}} = \frac{ct_f}{2\bar{r}} \tag{5.39}$$

The total distance L travelled by the strain pulse for a full crater is the charge depth plus one-half the fall length. Thus,

$$\frac{D}{\bar{r}} = \frac{L}{\bar{r}} - \frac{ct_f}{2\bar{r}} \tag{5.40}$$



A = Start of trace
B = Detonation of charge
C = Start of strain pulse
D = Peak of compressive strain
E = End of fall strain
t_o = Arrival time for start of pulse
t_r = Rise time
t_f = Fall time
t_p = Arrival time for peak strain
ϵ = Peak compressive strain
ϵ_f = Fall strain

Figure 5.13. Strain Record Measurements.[14]

From these two equations the relation between charge depth and crater depth may be calculated. This was done in the USBM tests for four rock types and it was found that the average observed experimental depths were always less than those computed from the above equation.

Rocks Tested. Physical properties of the rock-types in which USA CE and USBM crater tests were made are given in Table 5.1. Data on crater tests are given in Tables 5.2 and 5.3.

As stated above three types of rock were tested in the UET program and four by the USBM. Shots in granite produced a wide shallow crater, while the others formed deeper, more irregular craters. The breakage in the last three (sedimentary rocks) was controlled to a certain extent by bedding.

Figures 5.14 to 5.17 depict the strain data for the four types of rock.[14] Of the scaled values plotted, the fall time and the fall strain are the most important in predicting crater formation. Within the range of size of shots fired the various factors "scaled" within reasonable limits which indicates that model laws may be employed with assurance.

Figures 5.18 to 5.25 show the relationships between various scaled dimensions of craters for USBM tests and Figures 5.26 to 5.33 the scaled dimensions for preliminary UET tests.

A comparison of crater dimensions data for the six types of rock yields several pertinent facts. The UET tests were designed to ascertain the safe scaled charge depth beyond which breakage at a free surface would not occur in rocks appropriate for protective underground installations. Preliminary UET tests utilized charges of weights from 0.5 lb to 2560 lb. USBM tests utilized charges from 0.4 to 32 lb. The USBM tests were designed to test the applicability of the reflection theory over the whole range of scaled charge depths which result in crater formation in four rock types of widely different physical properties for four explosives. The majority of the detonations in the UET tests are at a large range of scaled depths for two similar explosives, while those in the USBM tests are more evenly distributed with respect to scaled charge depth.

Granite. The shape of the curves for $D_k/\sqrt{r}$ vs $D/\sqrt{r}$ for the two types of granite (Unaweep and Lithonia) are very similar, although crater depths for Unaweep granite are greater for a larger range of charge depths. The same holds true for $R_k/\sqrt{r}$ vs $D/\sqrt{r}$ curves and the V_k/W curves. It appears that perhaps the curves plotted by USBM may not be based upon a sufficiently large number of shots at scaled charge depths greater than 2. The $R/\sqrt{r}$ vs $D/\sqrt{r}$ plots on log-log paper yield,

$$\frac{R}{\sqrt{r}} = 2.9 \left(\frac{D}{\sqrt{r}}\right)^{0.17} \qquad (5.41)$$

for Lithonia granite and

$$\frac{R}{\sqrt{r}} = 2.41 \left(\frac{D}{\sqrt{r}}\right)^{0.34} \qquad (5.42)$$

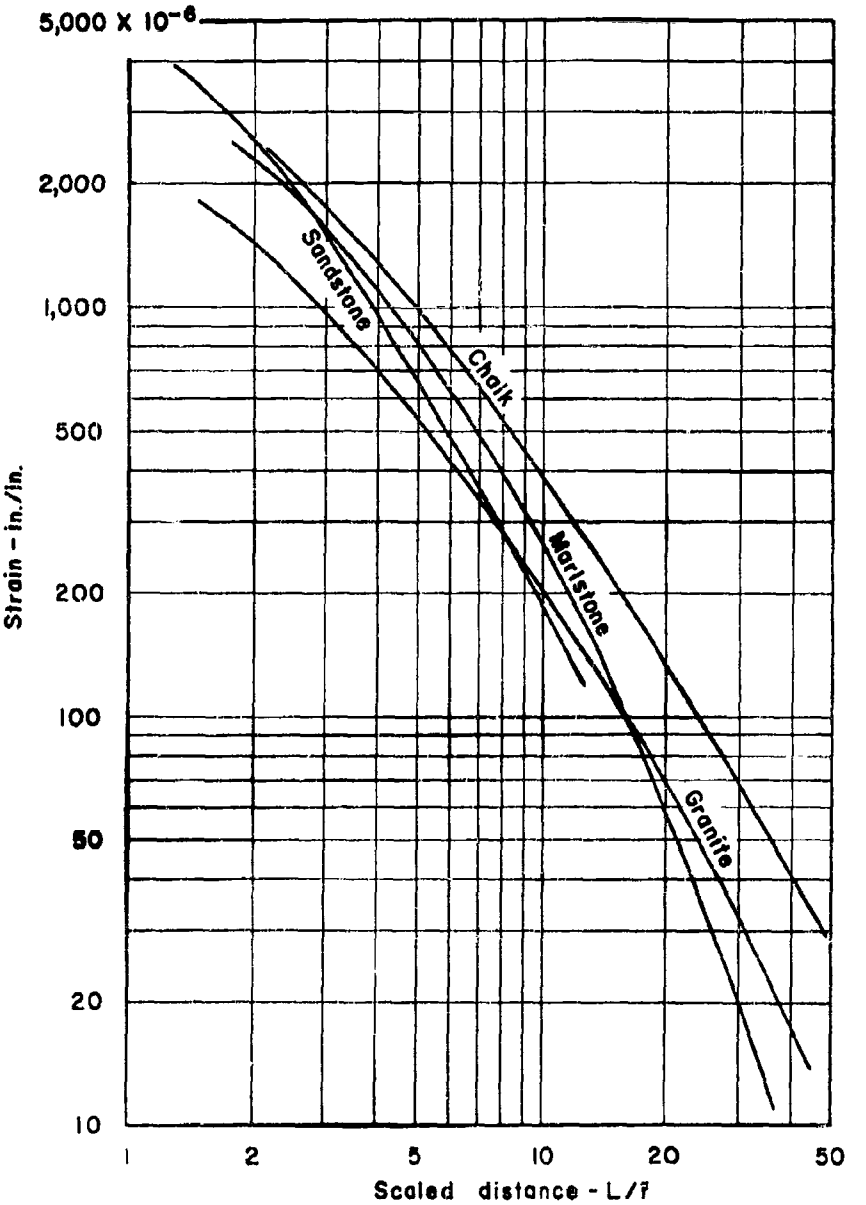


Figure 5.14. Decrease of peak strain with scaled distance from small HE charges in four different types of rock[14].

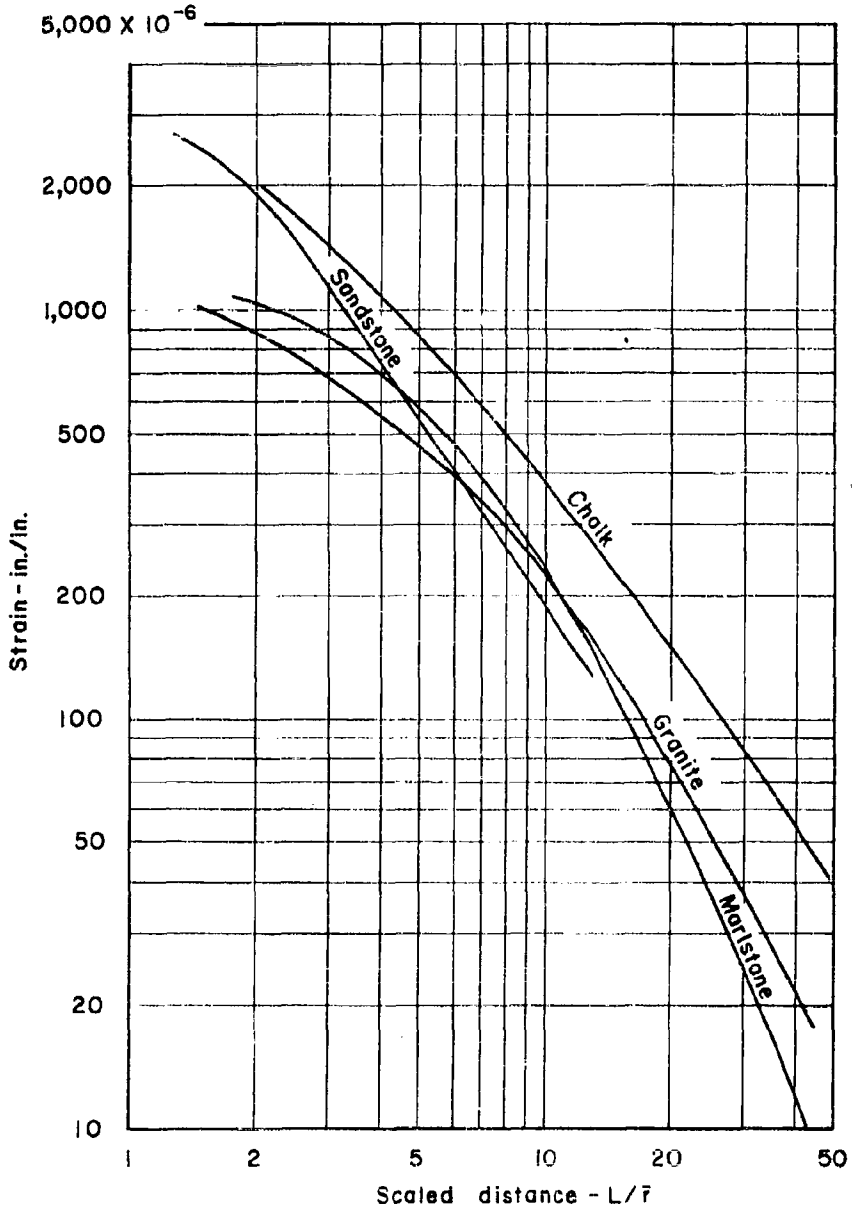


Figure 5.15. Decrease of fall strain with scaled distance from small HE charges in four different types of rock[14].

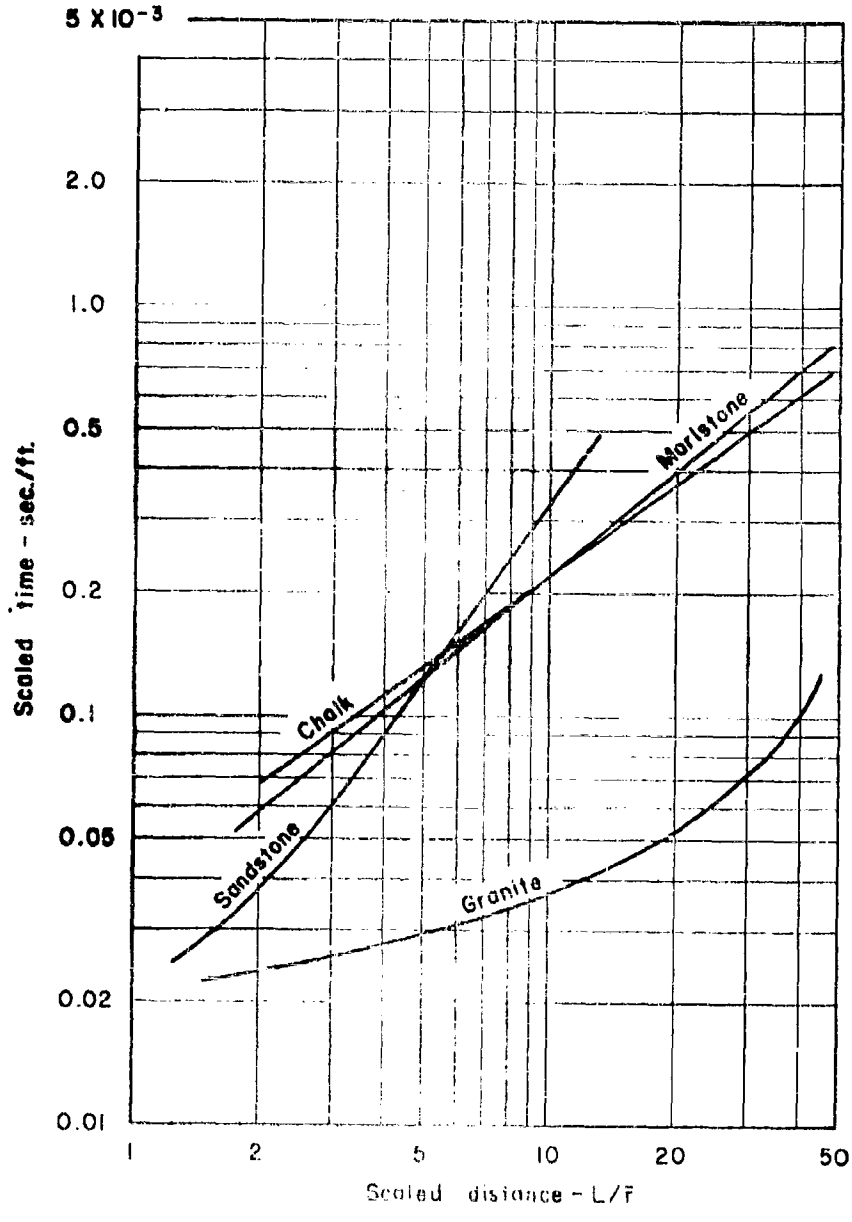


Figure 5.16. Change of rise time with scaled distance from small HE charges in four different types of rock[14].

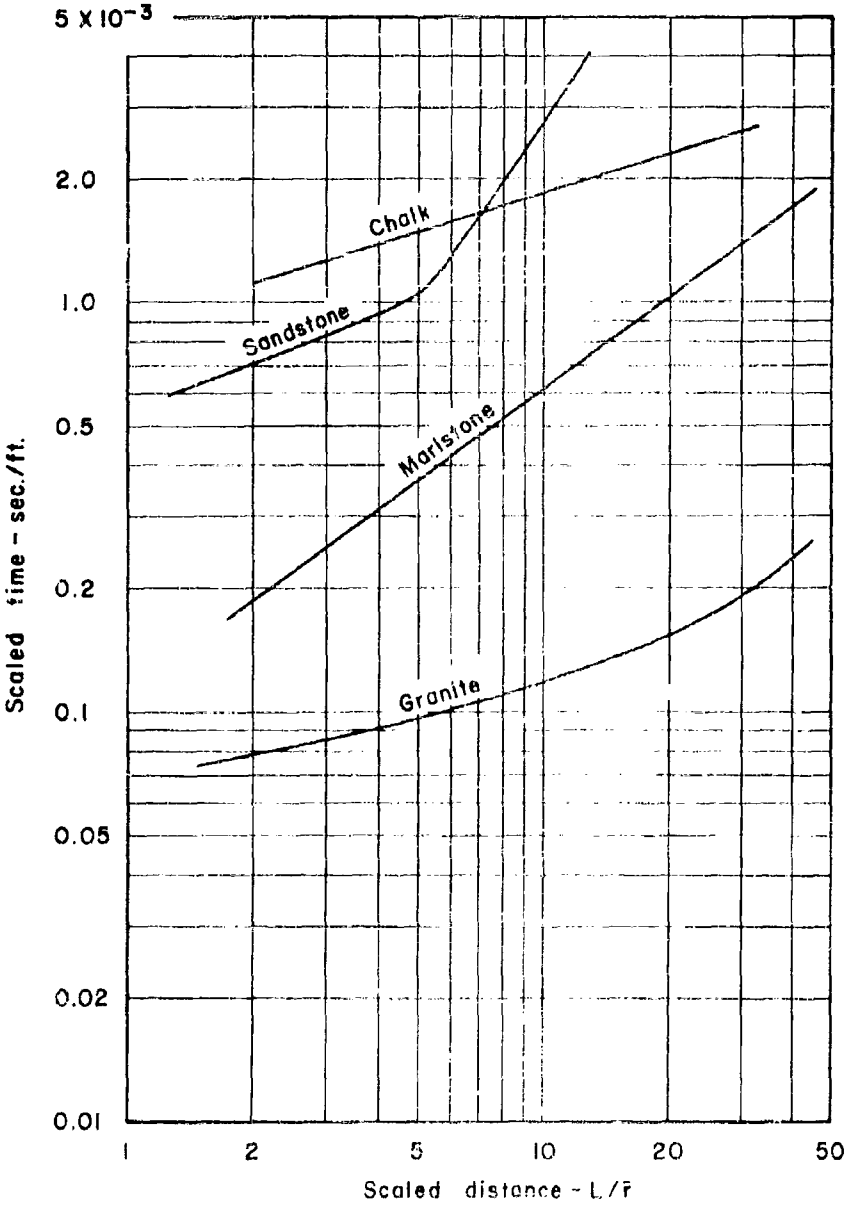


Figure 5.17. Change of fall time with scaled distance from small HE charges in four different types of rock[17].

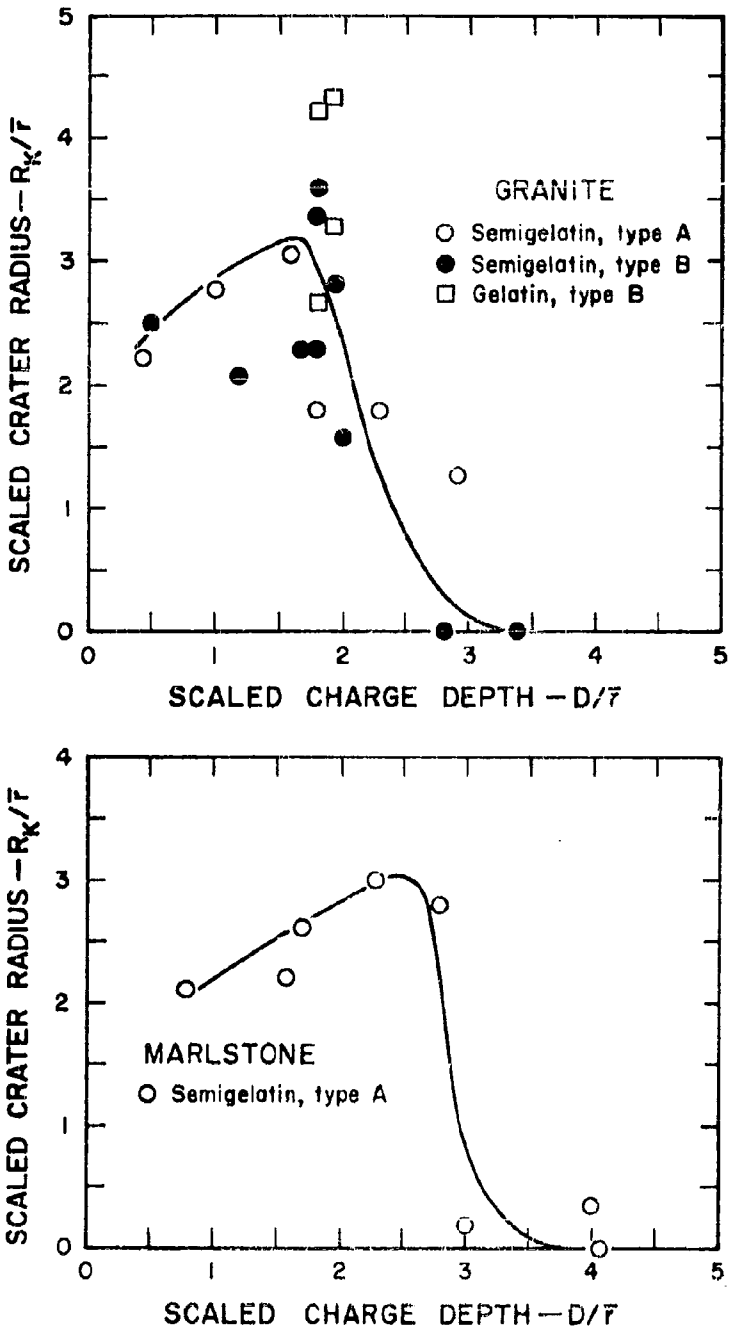


Figure 5.18. Scaled crater radius vs. scaled charge depth--granite and marlstone.[14]

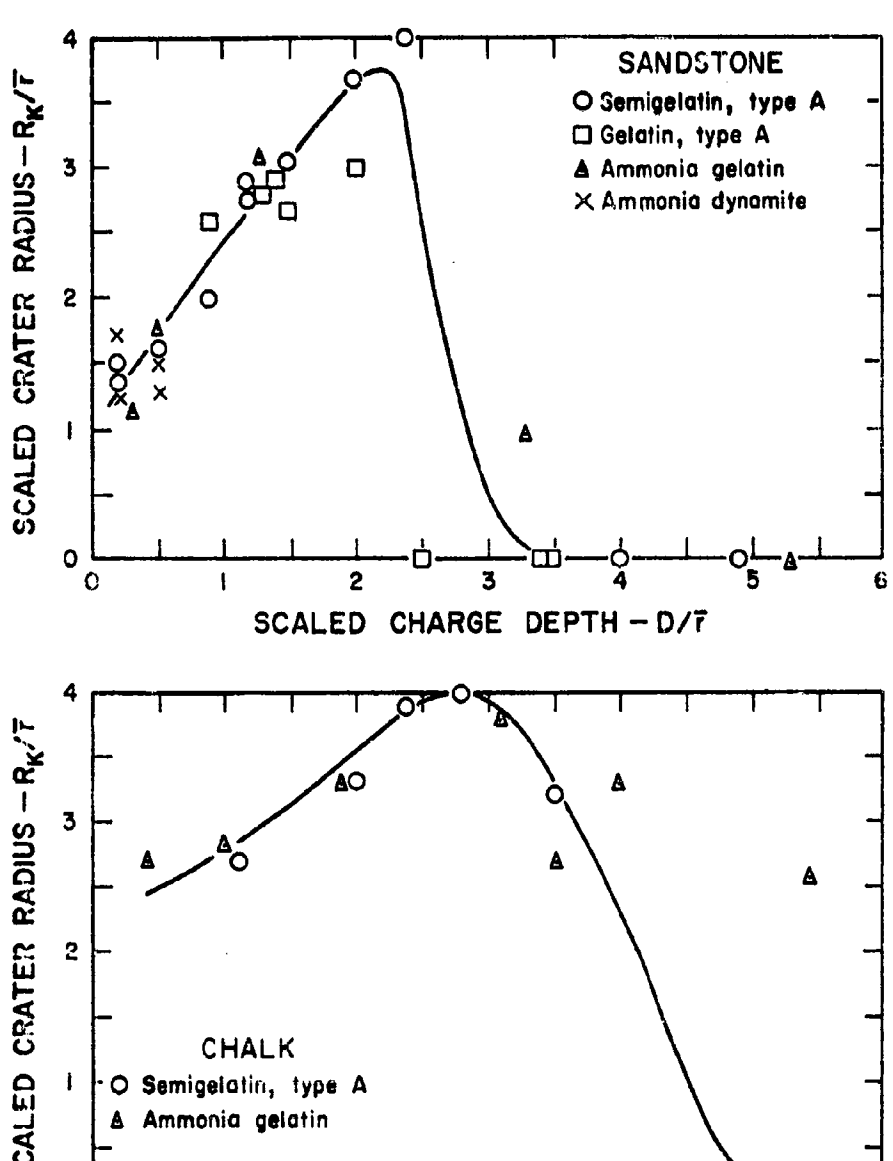
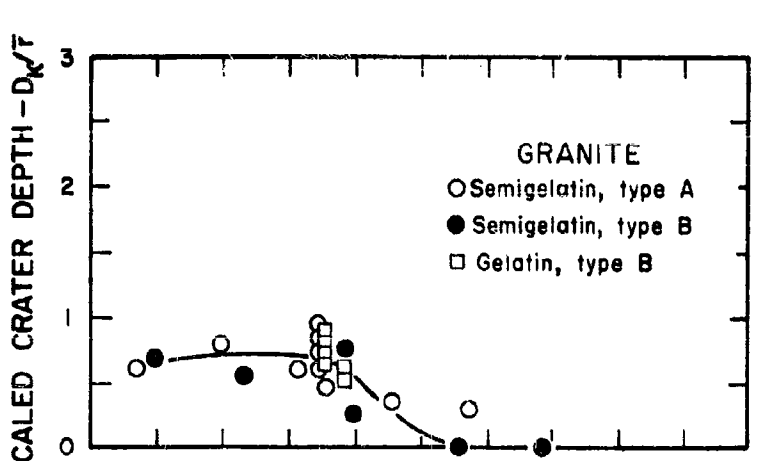


Figure 5.19. Scaled crater radius vs. scaled charge depth--sandstone and chalk.[14]



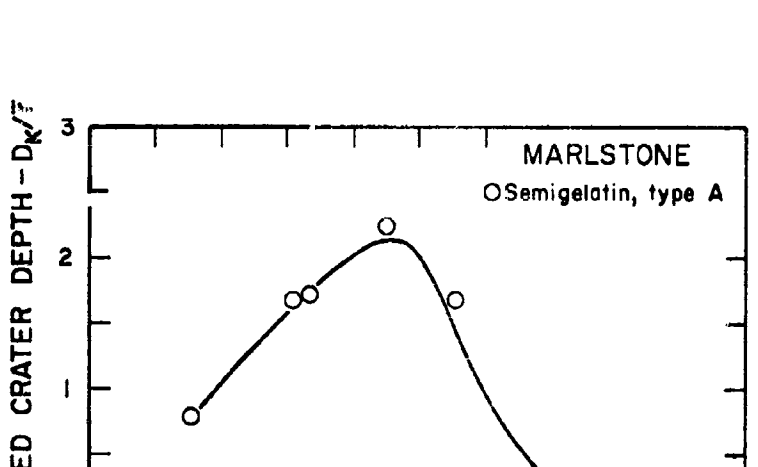


Figure 5.20. Scaled crater depth vs. scaled charge depth--granite and marlstone.[14]

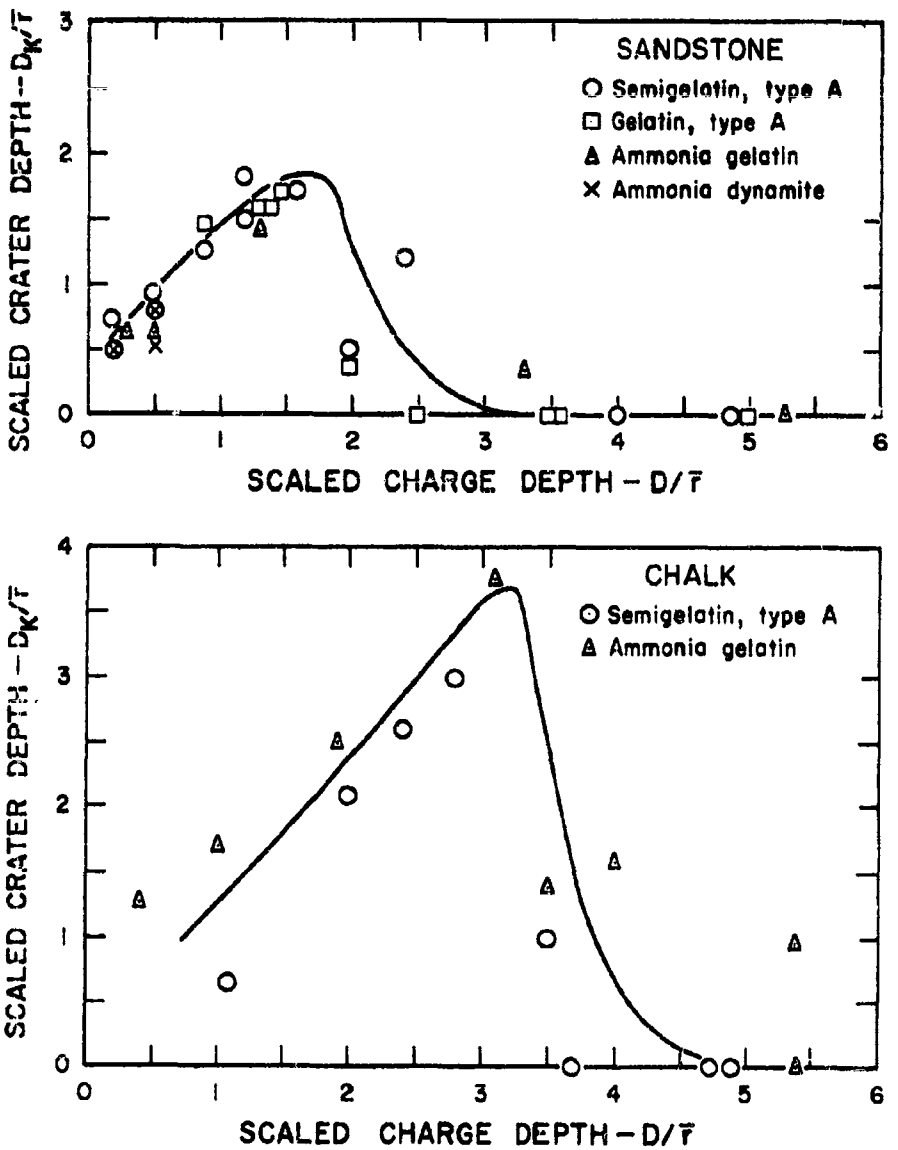


Figure 5.21. Scaled crater depth vs. scaled charge depth--sandstone and chalk.[14]

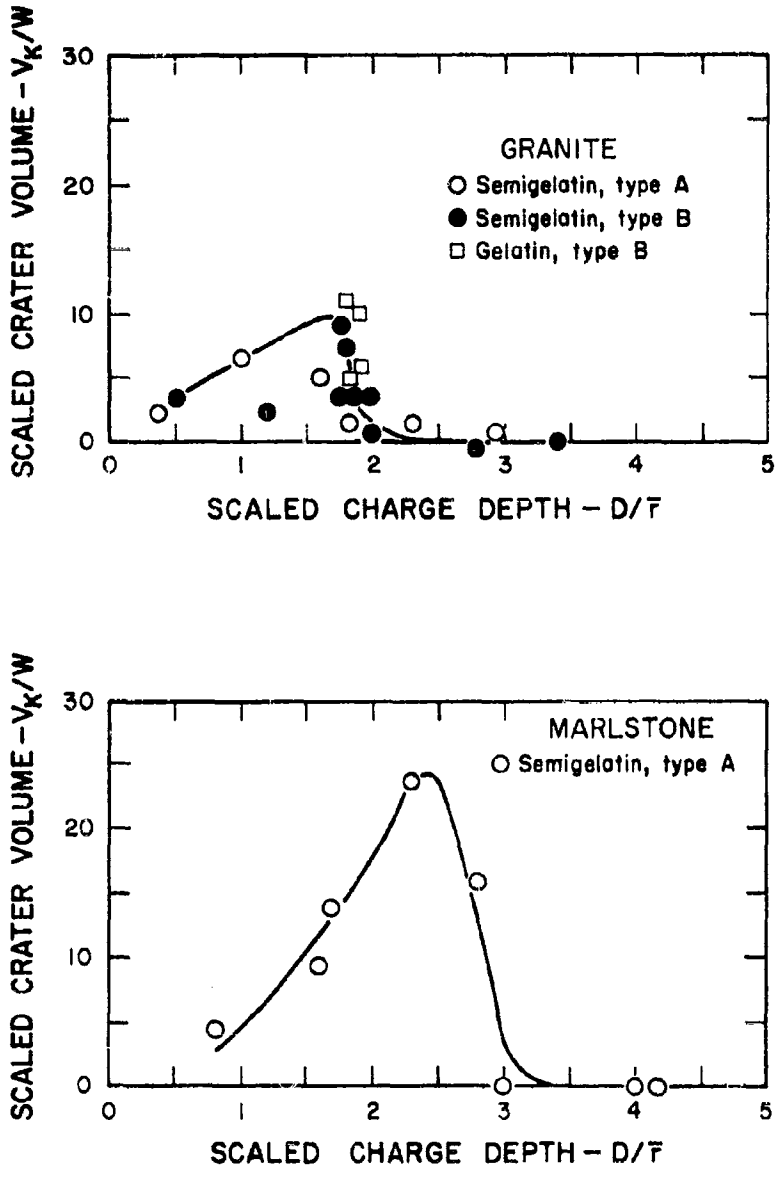


Figure 5.22. Scaled crater volume vs. scaled charge depth--granite and marlstone.[14]

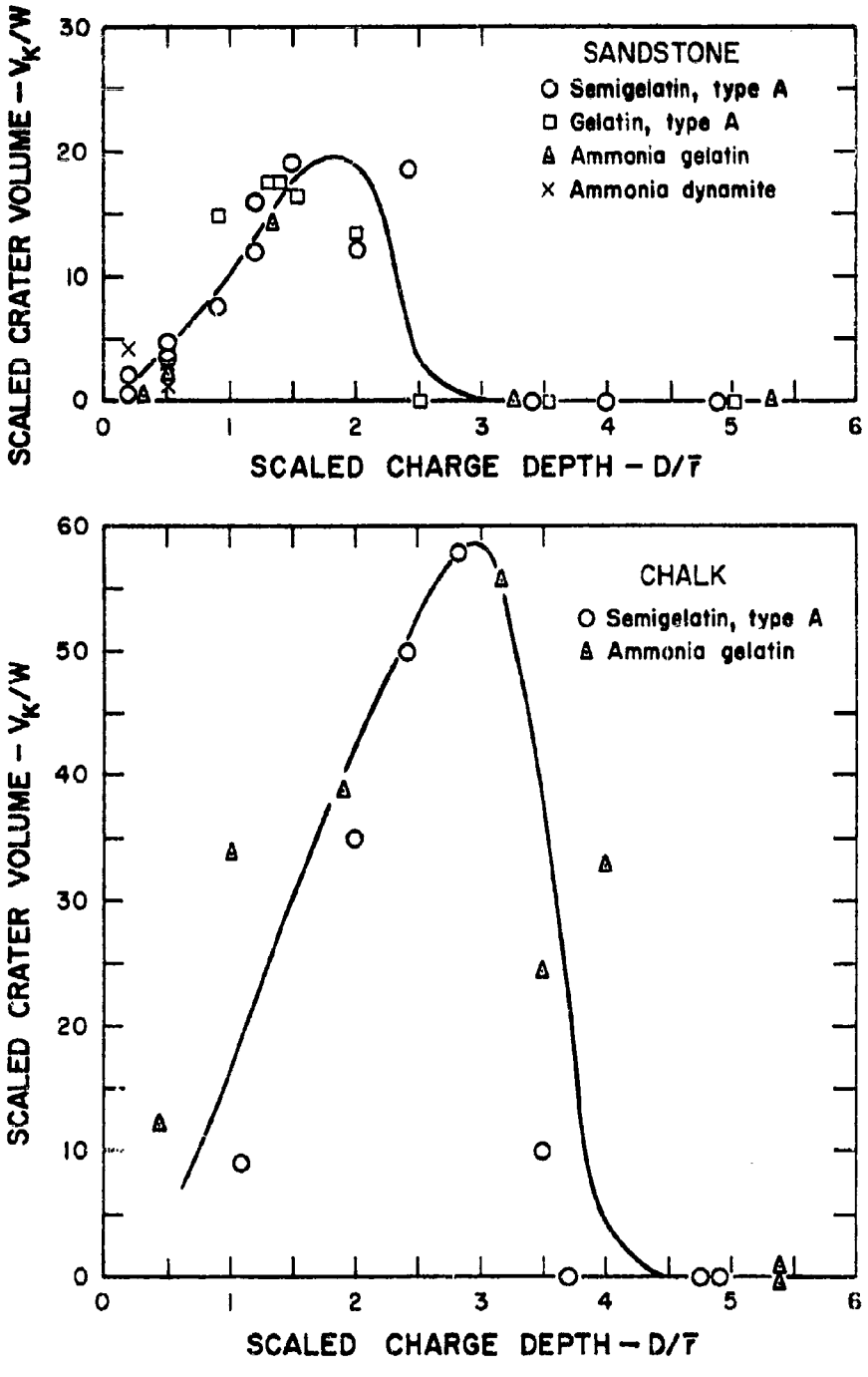


Figure 5.23. Scaled crater volume vs. scaled charge depth--sandstone and chalk.[14]

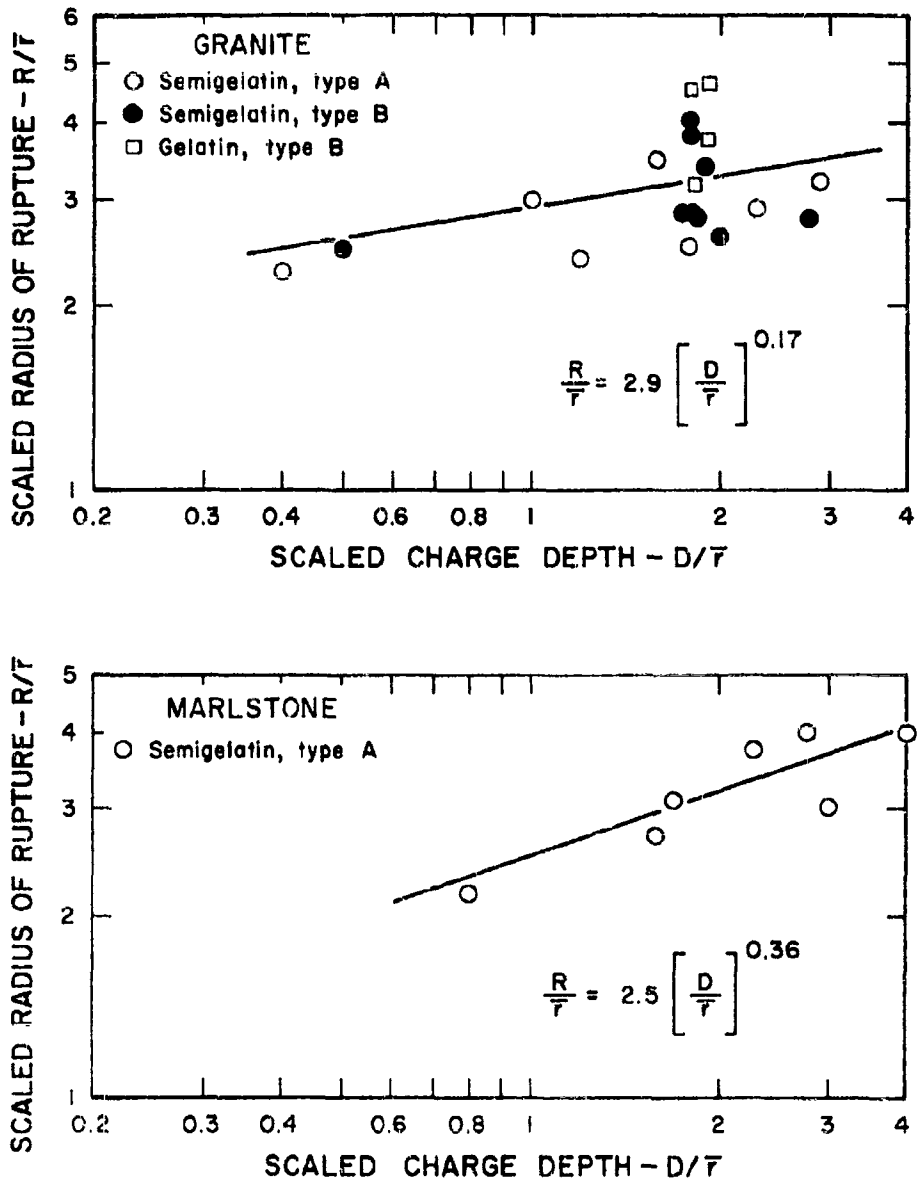


Figure 5.24. Scaled radius of rupture vs. scaled charge depth--granite and marlstone.[14]

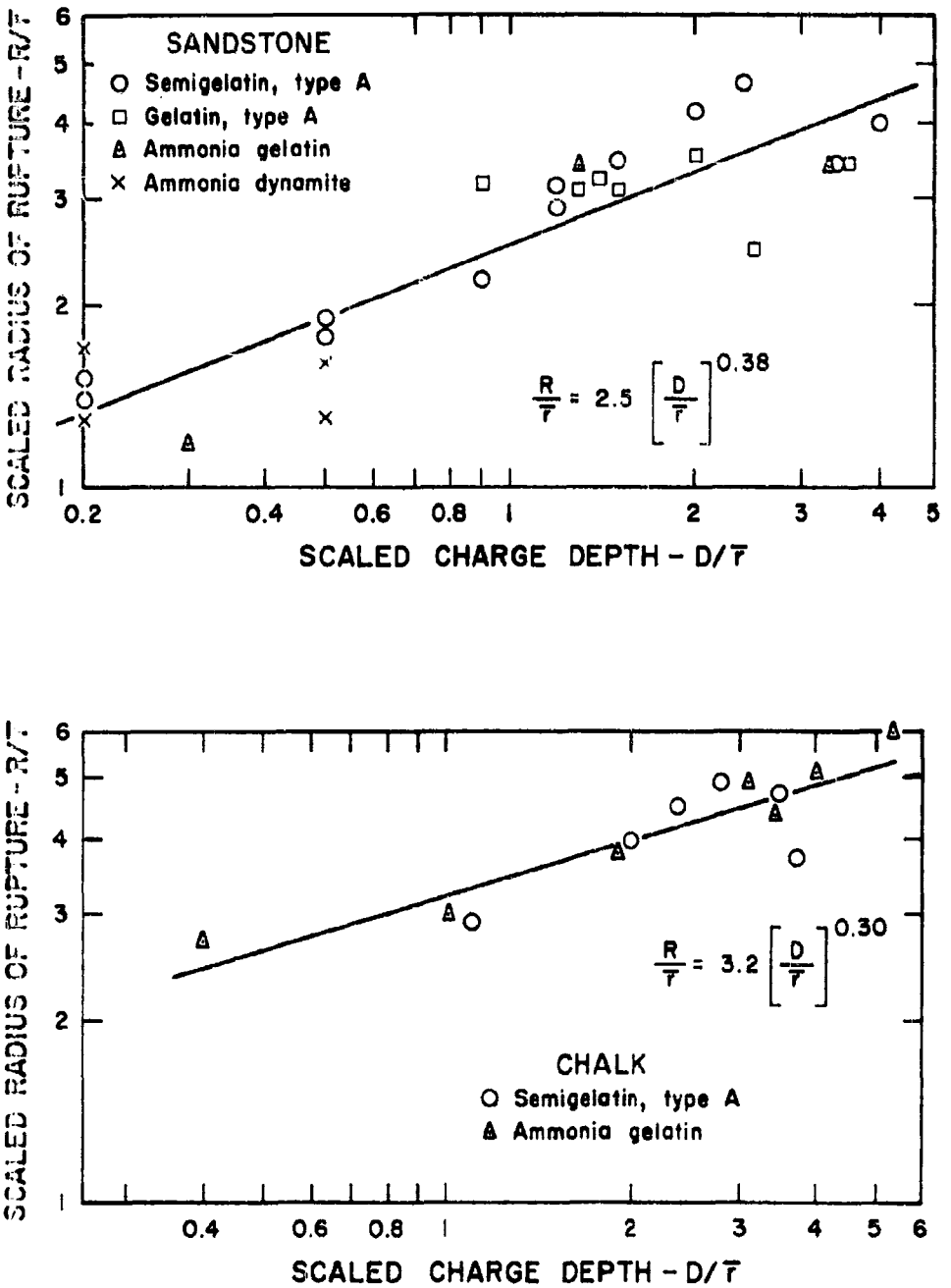


Figure 5.25. Scaled radius of rupture vs. scaled charge depth--sandstone and chalk.[14]

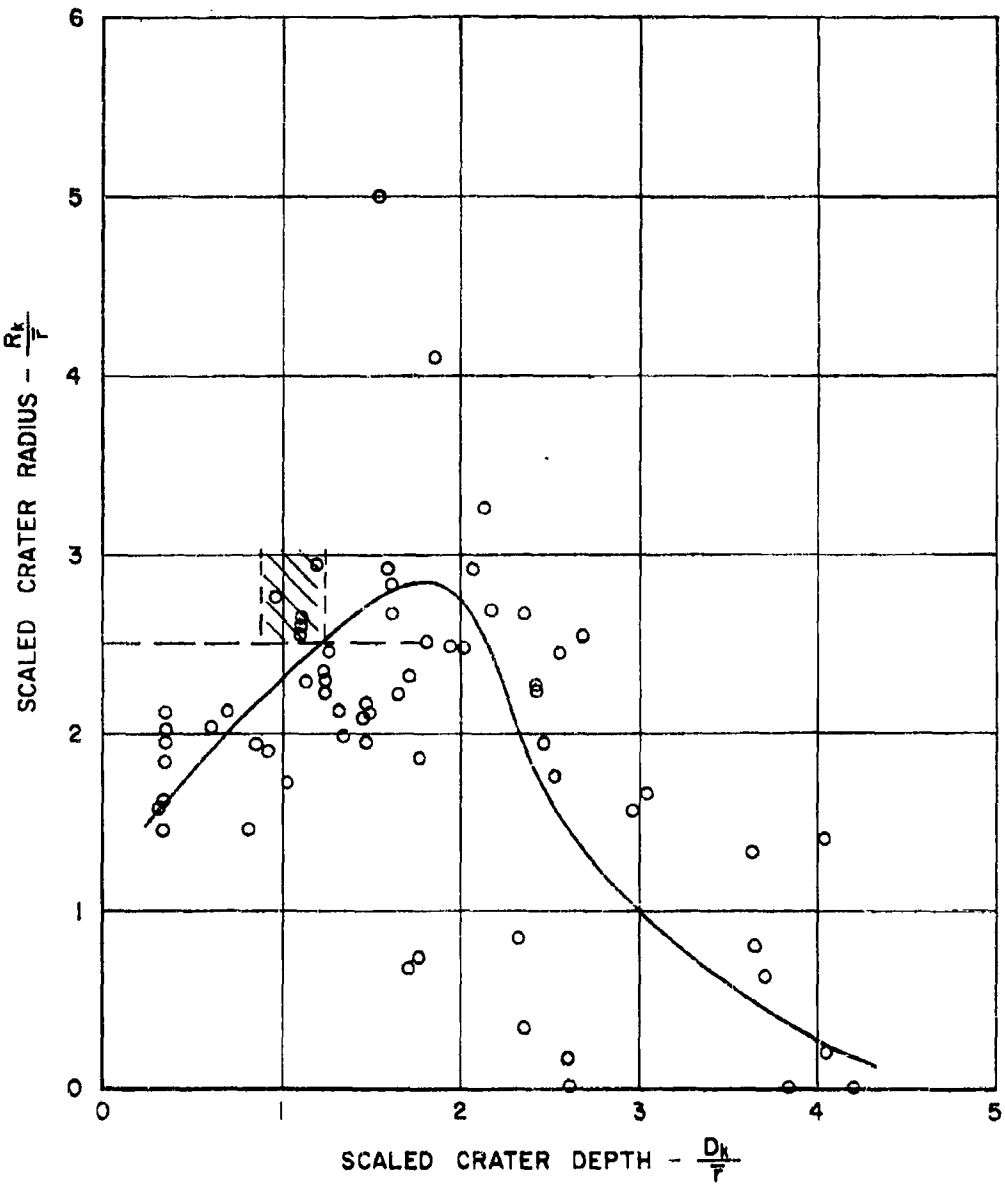


Figure 5.26. Scaled crater radius vs. scaled crater depth--Unaweep Granite.[14]

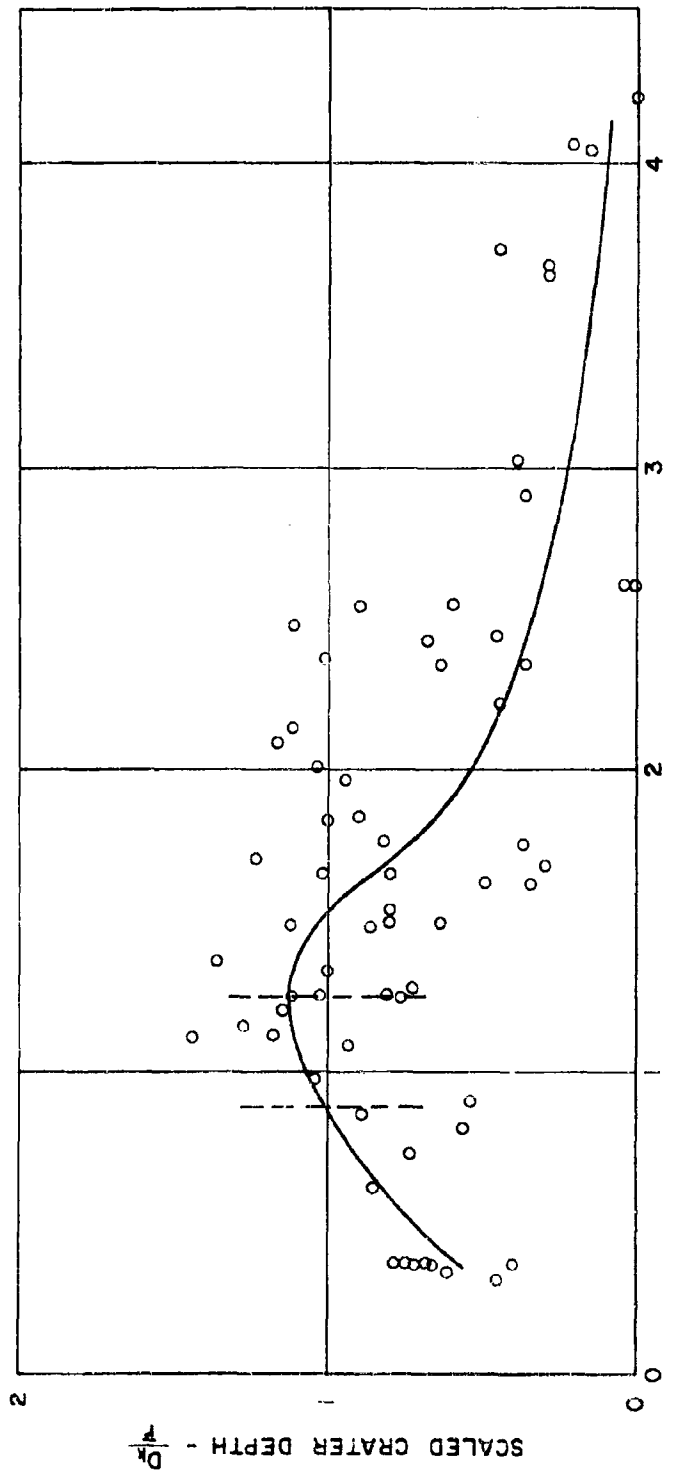


Figure 5.27. Scaled crater depth vs. scaled charge depth--Unaweep Granite.

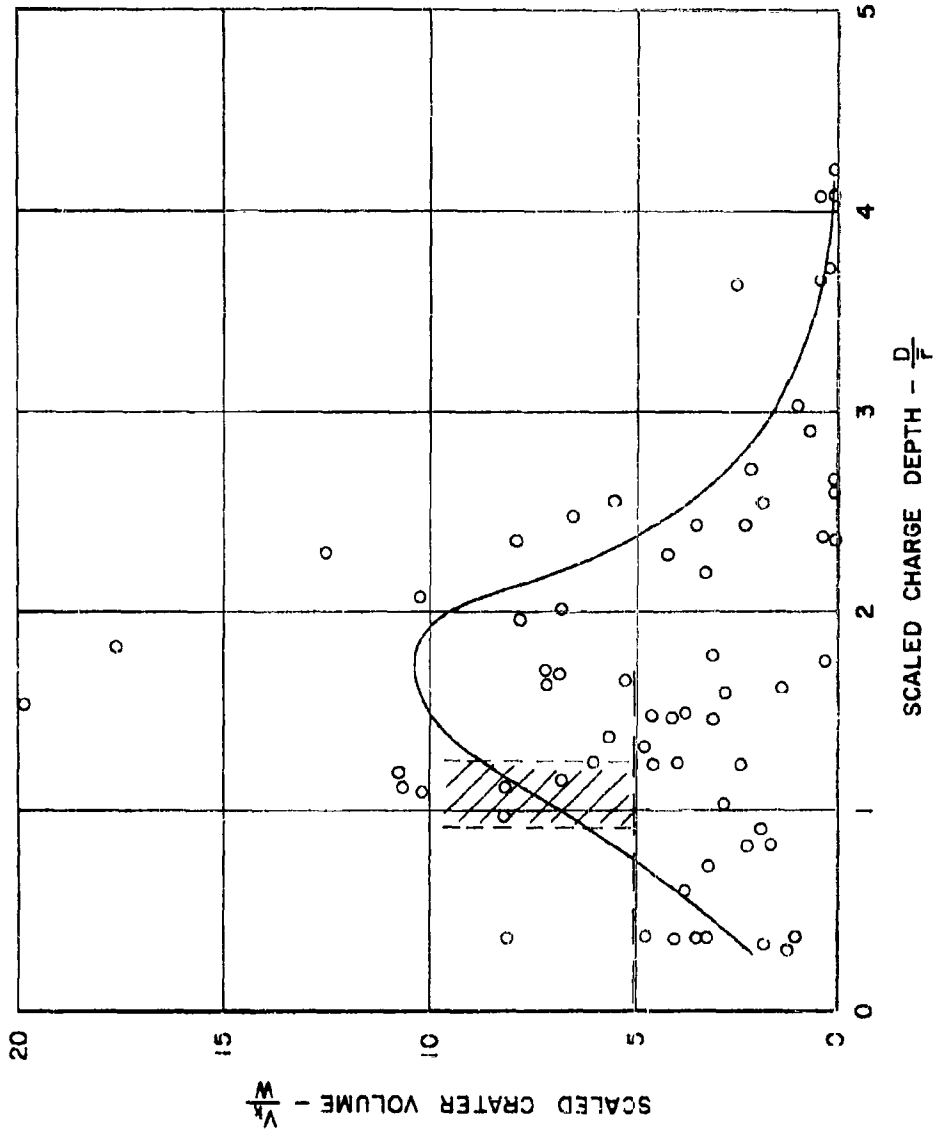


Figure 5.28. Scaled crater volume vs. scaled charge depth--Unaweep Granite.

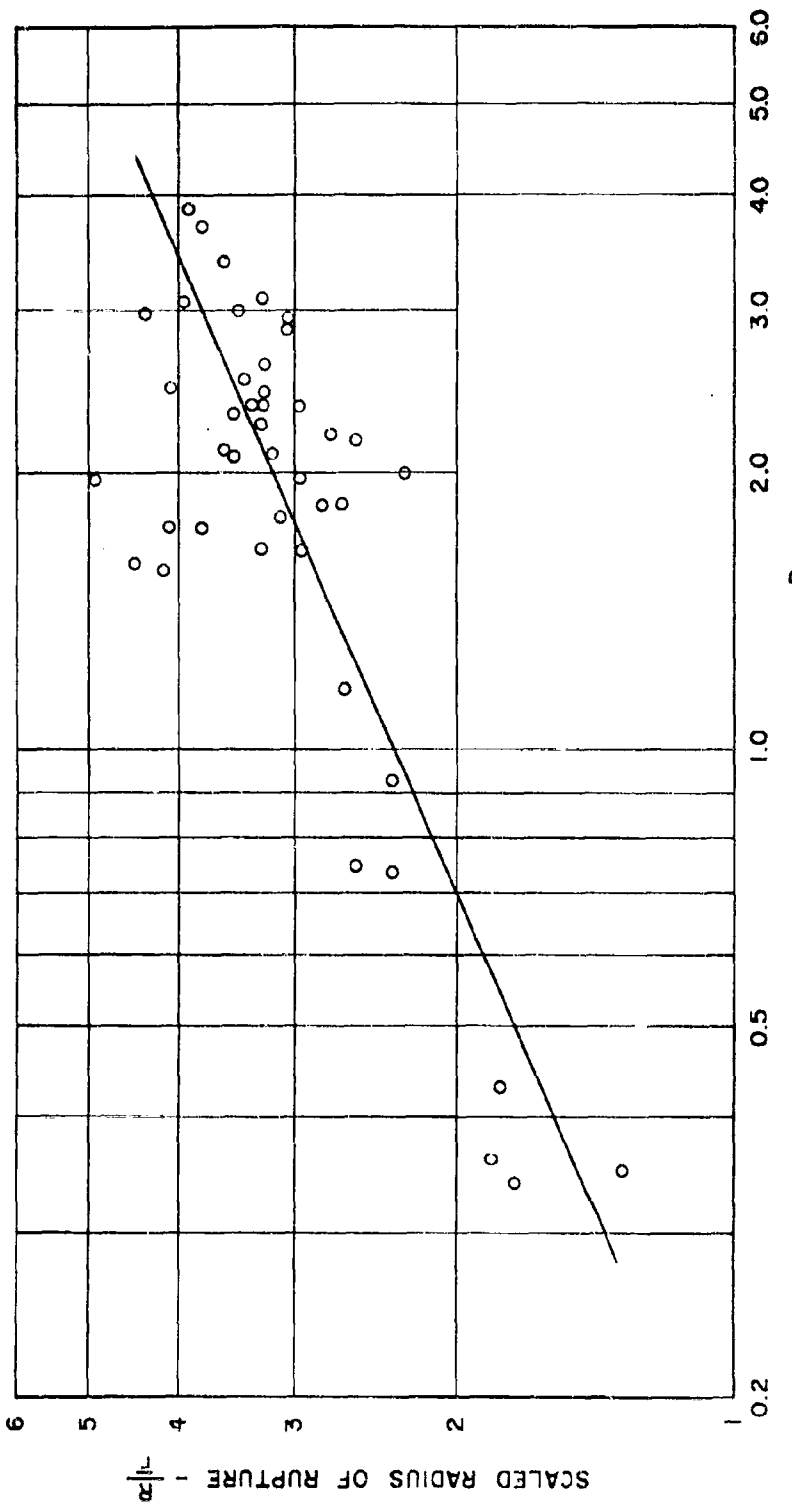


Figure 5.29. Scaled radius of rupture vs. scaled charge depth--Unaweep Granite.

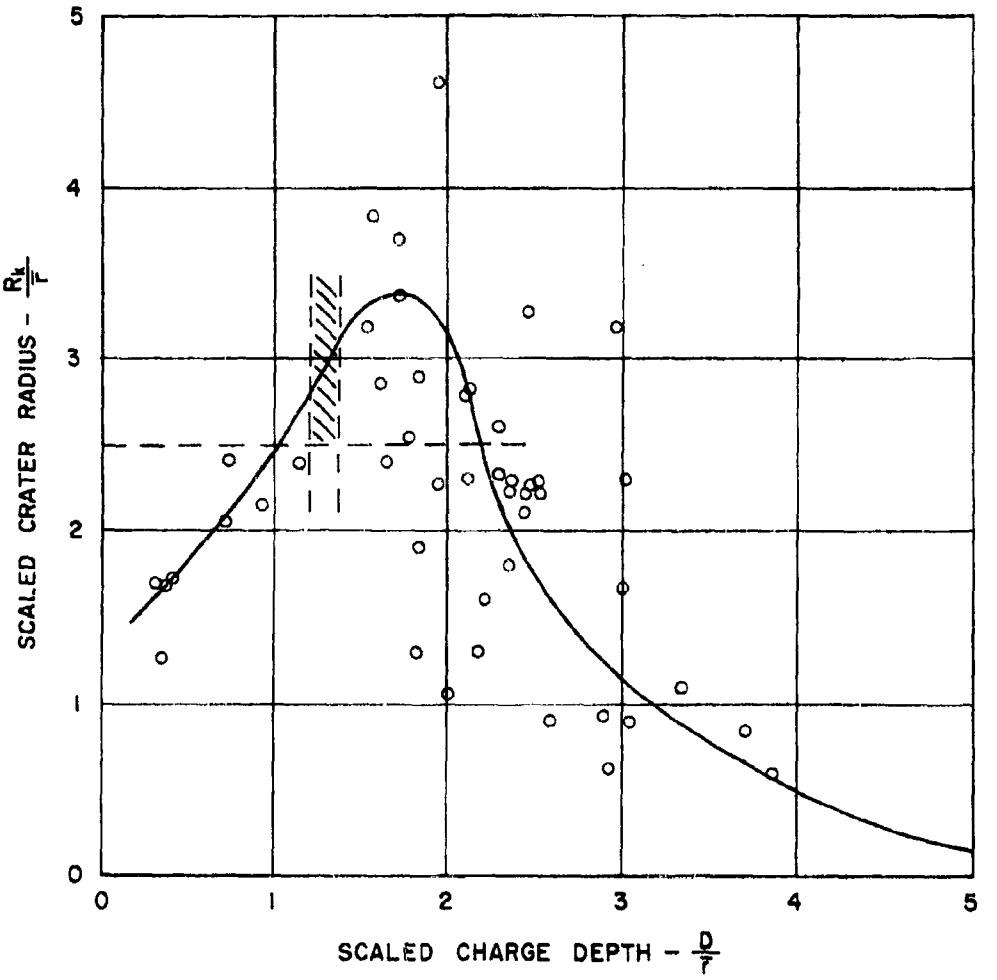


Figure 5.30. Scaled crater radius vs. scaled charge depth-- Navajo Sandstone.

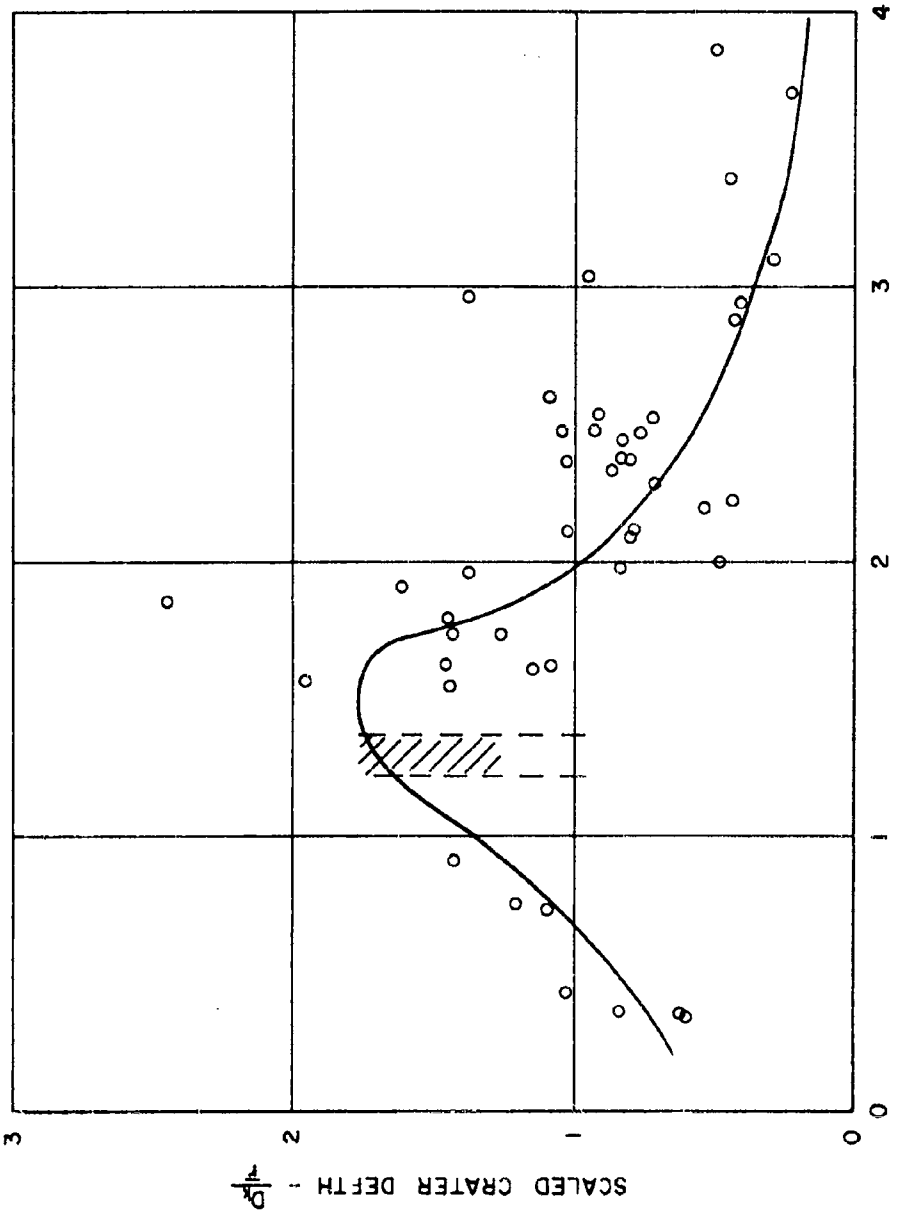


Figure 5.31. Scaled crater depth vs. scaled charge depth--Navajo Sandstone.

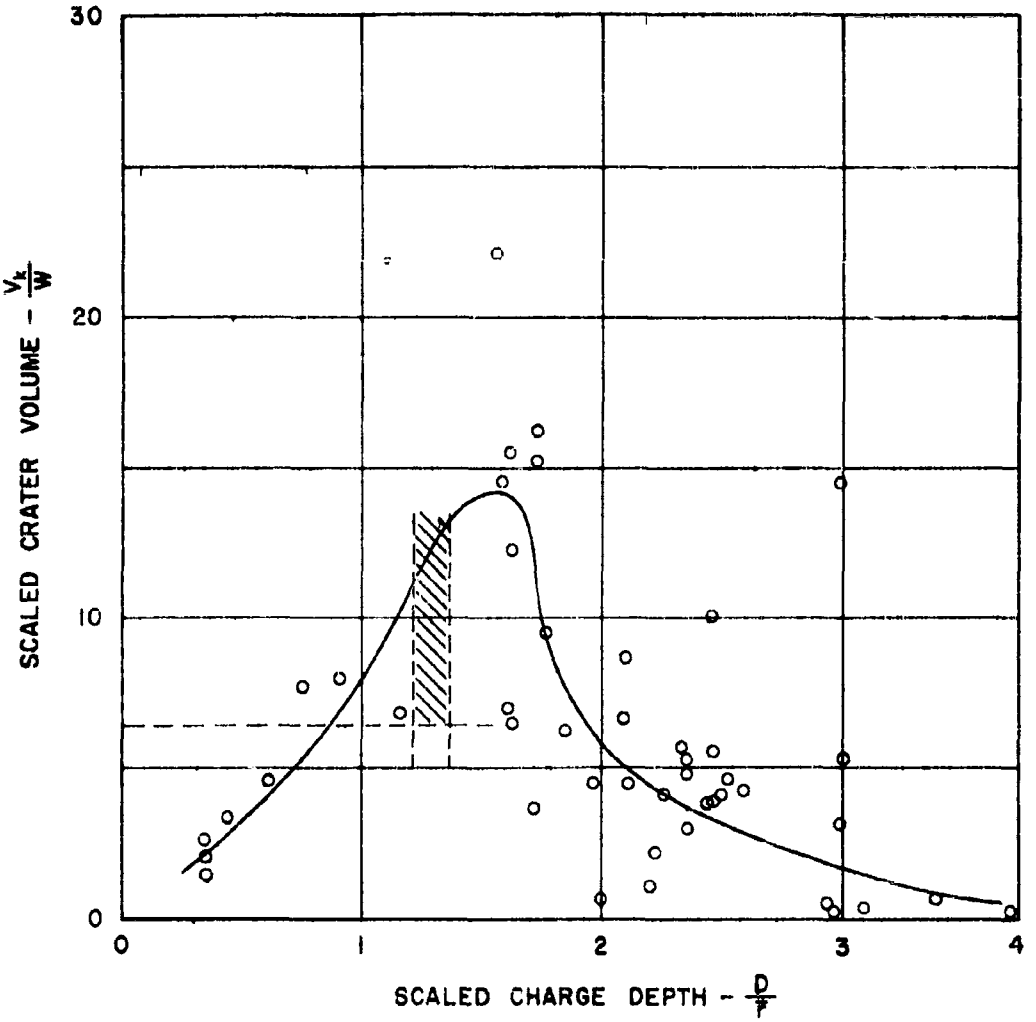


Figure 5.32. Scaled crater volume vs. scaled charge depth--Navajo Sandstone.

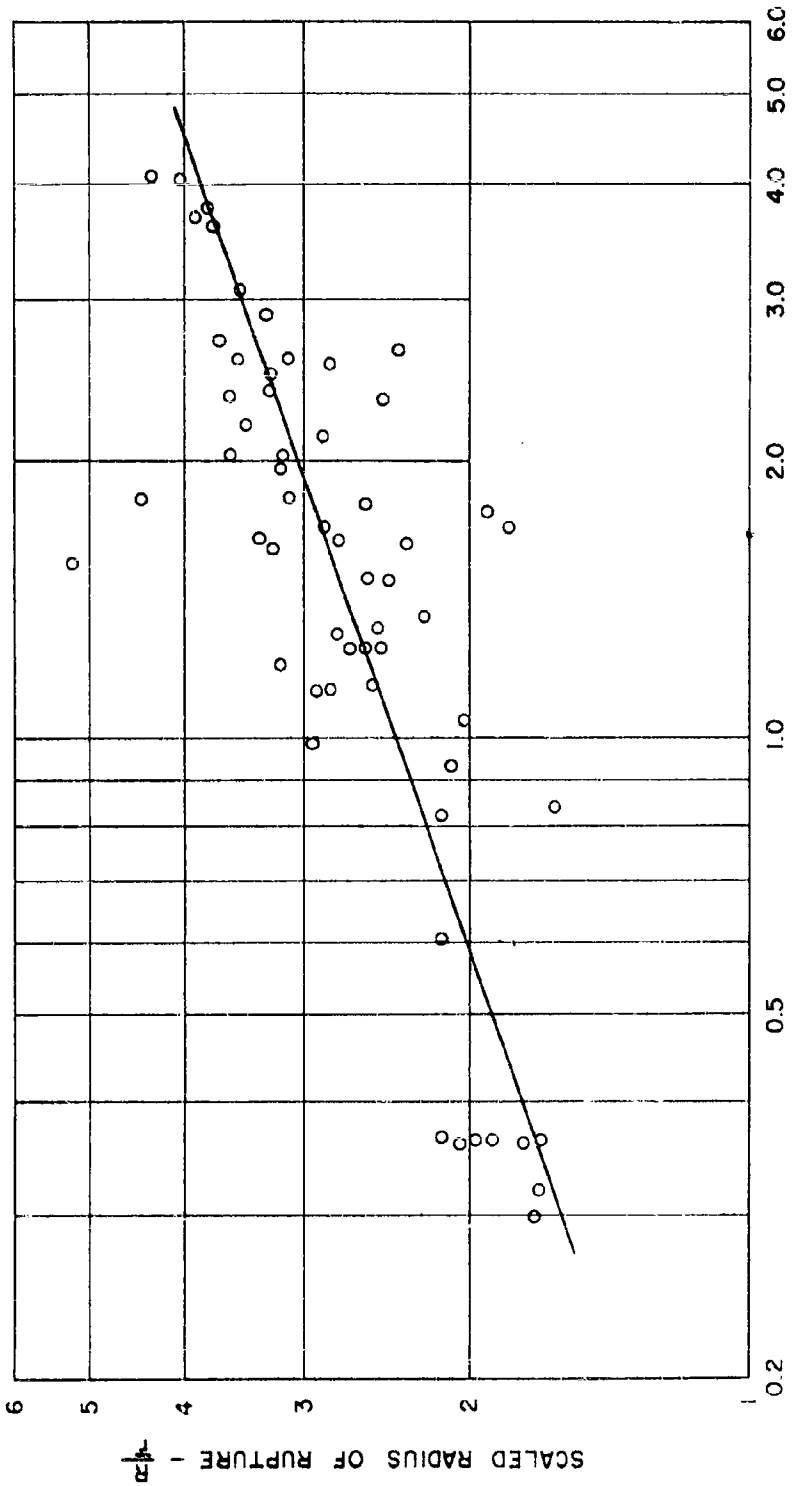


Figure 5.33. Scaled radius of rupture vs. scaled charge depth--Navajo Sandstone.

TABLE 5.1[14,16]

Physical Properties of Rocks (UET & USBM)

Rock Type	Navajo Sandstone	Unaweep Granite	Limestone	Lithonia Granite	Green River Marlstone	Kanawha Sandstone	Niobara Chalk
Description				gneissic	oil shale	coarse grained	chalky limestone
App. spec. gr.	2.25	2.25	2.68	2.6	2.1	2.2	2.0
Comp. Str. psi	11700	24300	30400	30000	10000	10000	2000
Tensile Strength psi	240	640	not measured	450	not measured	70	not measured
Dynamic Tensile br. strain μ in/in	480	370		380	310	560	400
Mod. of rupture, psi	884	3640	3060	2000	400	400	300
Scler. hardness	39	49	--	85	45	30	10
Dynamic E, psi	2.56×10^6	4.89×10^6	10.8×10^6	3.0×10^6	1.2×10^6	1.0×10^6	0.75×10^6
Mod. of rigidity, psi	1.34×10^6	2.56×10^6	--	1.5×10^6	0.5×10^6	0.5×10^6	0.5×10^6
Long. bar vel., ft/sec	9000	11500	17400	9000	6000	5000	5000
Long. field vel. ft/sec	6000-9000±	15200	11000	18500	13000	5000	7500

TABLE 5.2[16]

Crater Test Data

UNAWEEP GRANITE[1]

No.	a	W	D	R_k	D_k	V_k	$\bar{r}$	$D/\bar{r}$	$R_k/\bar{r}$	$D_k/\bar{r}$	$R/\bar{r}$	V_k/W	Expl.
A-1	2 5/8"	0.40	1.70	0.25	0.25	0.09	0.74	2.16	0.34	0.34	2.38	0.23	C-2
3	2 5/8"	1.00	1.83	4.10	1.00	17.81	1.00	1.83	4.10	1.00	4.49	17.8	C-2
4	2 5/8"	2.20	1.63	2.86	1.00	8.7	1.30	1.25	2.20	0.76	2.53	4.0	C-2
6	2 5/8"	0.62	1.82	2.77	0.95	7.8	0.85	2.14	3.25	1.12	3.89	12.5	TNT
7	2 5/8"	1.62	1.46	2.50	1.30	8.7	1.17	1.25	2.14	1.11	2.48	5.4	TNT
8	2 5/8"	2.62	1.28	2.56	0.75	5.3	1.38	0.93	1.86	0.54	2.08	2.0	TNT
9	2 5/8"	0.50	1.90	1.76	0.35	1.2	0.79	2.41	2.22	0.44	3.28	2.3	C-2
10	2 5/8"	1.12	1.68	1.73	0.50	1.6	1.03	1.63	1.67	0.48	2.33	1.4	TNT
11A	2 5/8"	1.50	2.25	2.83	1.05	9.0	1.14	1.97	2.48	0.92	3.17	7.9	C-2
12	2 5/8"	1.10	2.69	0.17	0.10	-	1.03	2.61	0.16	0.09	-	-	C-2
13	2 5/8"	2.60	2.42	1.02	0.50	0.55	1.37	1.76	0.74	0.36	1.90	0.21	C-2
14	2 5/8"	4.50	2.18	3.49	1.65	21.5	1.65	1.32	2.12	1.00	2.50	4.8	C-2
17	2 5/8"	1.12	1.60	5.10	0.80	22.2	1.03	1.55	5.00	0.78	5.23	19.8	C-2
18	2 5/8"	0.20	0.94	1.64	0.20	0.57	0.58	1.62	2.82	0.34	3.25	2.85	C-2
39	4 1/2"	2.53	3.73	5.48	0.45	5.8	1.38	2.70	2.52	0.12	3.69	2.20	TNT
40	4 1/2"	5.13	3.79	4.64	0.75	17.2	1.72	2.20	2.69	0.43	3.47	3.3	TNT
41	4 1/2"	10.13	3.20	4.50	1.45	31.3	2.16	1.48	2.08	0.67	2.55	3.1	TNT
42	4 1/2"	18.00	3.29	6.00	2.80	109.5	2.62	1.25	2.31	1.06	2.63	6.1	C-2
B-1	4 1/2"	2.13	5.20	0.25	0.20	-	1.28	4.06	0.19	0.15	4.06	-	TNT
2	4 1/2"	7.12	4.50	1.63	1.20	3.4	1.92	2.34	0.84	0.62	2.49	0.5	TNT
3	4 1/2"	20.00	4.06	5.35	3.05	93.9	2.21	1.49	1.97	1.12	2.47	4.7	C-2
5	4 1/2"	15.00	4.19	4.59	2.05	45.9	2.46	1.78	1.86	0.83	2.57	3.1	C-2
6	4 1/2"	7.00	4.96	4.60	1.70	38.4	1.91	2.59	2.41	0.89	3.54	5.5	C-2
10	4 1/2"	30.00	3.75	9.24	3.60	3.24	3.11	1.20	2.97	1.15	3.20	10.8	C-2
11	9"	4.63	6.83	2.31	0.35	2.02	1.67	4.08	1.39	0.20	4.31	0.44	TNT
12	9"	15.12	7.17	3.84	0.90	13.9	2.47	2.90	1.55	0.36	3.28	0.92	TNT
13	9"	60.00	6.50	8.63	4.00	313.5	3.91	1.66	2.21	1.02	2.76	5.2	C-2
14	9"	7.50	7.25	2.55	0.55	3.7	1.96	1.69	1.30	0.28	3.91	0.49	C-2
15	9"	75.00	5.38	10.32	3.02	321.0	4.21	1.28	2.45	0.71	2.76	4.3	C-2
15A	9"	100.00	3.92	6.41	4.10	177.2	4.66	0.84	1.38	0.88	1.62	1.8	TNT
16	9"	30.00	6.80	8.40	3.55	263.4	3.39	2.01	2.47	1.04	4.18	6.8	C-2
17	9"	23.81	6.80	7.74	2.90	182.8	2.87	2.36	2.69	1.01	3.58	7.7	C-2
19A	9"	20.00	6.52	6.08	1.80	70.1	2.71	2.41	2.24	0.66	3.29	3.5	C-2
21	9"	215.00	8.15	11.95	8.15	1206.3	5.99	1.36	1.99	1.36	2.41	5.6	C-2
22	9"	250.00	7.10	16.20	7.50	2063.2	6.30	1.13	2.57	1.19	2.80	8.3	C-2
C-1	4 1/2"	10.00	2.40	5.80	3.00	107.1	2.15	1.12	2.69	1.39	2.91	10.7	C-2
2	4 1/2"	10.00	3.55	6.34	1.70	71.9	2.15	1.65	2.94	0.79	3.37	7.2	C-2
3	4 1/2"	10.00	4.50	6.37	2.50	101.6	2.15	2.09	2.91	1.16	4.58	10.4	C-2
4	4 1/2"	10.00	5.52	3.77	1.25	18.7	2.15	2.56	1.75	0.58	4.10	1.9	C-2
5	4 1/2"	10.0	6.52	3.63	0.82	11.1	2.15	3.04	1.68	0.38	3.46	1.1	C-2
6	4 1/2"	10.00	7.70	-	-	-	2.15	-	-	-	-	-	C-2
7	4 1/2"	45.00	5.34	7.52	2.85	169.5	3.56	1.50	2.11	0.80	2.58	3.8	C-2
8	4 1/2"	40.12	5.66	7.30	2.95	165.4	3.42	1.65	2.13	0.86	2.59	4.1	TNT
9	4 1/2"	25.12	5.01	6.71	3.65	173.2	2.93	1.70	2.29	1.24	2.85	6.9	TNT
11	9"	25.00	11.29	-	-	-	2.92	3.86	-	-	-	-	C-2

TABLE 5.2 (Cont.)[16]

Crater Test Data

UNAWEEP GRANITE[1]

No.	a	W	D	R_k	D_k	V_k	$\bar{r}$	$D/\bar{r}$	$R_k/\bar{r}$	$D_k/\bar{r}$	$R/\bar{r}$	V_k/W	Expl.
12	9"	70.00	13.50	2.68	1.50	11.3	4.12	1.70	0.65	0.36	1.82	0.16	C-2
13	9"	40.00	14.29	-	-	-	3.41	4.19	-	-	-	-	TNT
14	9"	50.12	13.79	2.35	1.65	9.6	3.69	3.73	0.63	0.44	3.78	0.19	TNT
16	9"	14.12	2.65	4.16	2.20	40.1	2.41	1.09	1.72	0.91	2.04	2.8	TNT
17	9"	25.12	3.66	6.83	2.35	115.3	2.93	1.24	2.33	0.80	2.63	4.6	TNT
18	9"	50.12	4.08	9.70	5.25	519.6	3.69	1.11	2.62	1.42	2.85	10.3	TNT
19	9"	70.12	4.12	11.40	4.30	587.6	4.13	0.99	2.76	1.04	2.93	8.4	TNT
20	9"	100.00	5.33	10.49	5.90	684.1	4.64	1.14	2.26	1.27	2.53	6.8	C-2
II C-1	9"	70.50	3.40	1.96	2.38	164.7	4.14	0.82	1.96	0.57	2.12	2.3	TNT
II C-2	18"	320.00	4.17	13.98	5.87	1200.8	6.84	0.61	2.04	0.85	2.13	3.8	C-2
II D-1	36"	1080.00	7.31	16.70	6.80	1989.0	10.26	0.32	1.63	0.66	1.66	1.8	C-2
II D-2	52 1/2"	2560.0	4.17	22.68	5.95	3199.0	13.68	0.30	1.66	0.43	1.69	1.3	C-2

TABLE 5.2 (Cont.)[16]

Crater Test Data
NAVAJO SANDSTONE[1]

No.	a	$\bar{W}$	$\bar{D}$	$\bar{R}_k$	$\bar{D}_k$	$\bar{V}_k$	$\bar{r}$	$\bar{D}/\bar{r}$	$\bar{R}_k/\bar{r}$	$\bar{D}/\bar{W}$	$\bar{R}/r$	V_k/W	Expl.
A-1	1 3/8"	0.50	1.58	0.84	0.38	0.28	0.79	2.00	1.06	0.48	2.26	0.6	C-2
19	1 3/8"	1.20	2.50	2.38	1.05	6.2	1.06	2.36	2.24	1.05	3.25	5.2	C-2
21	1 3/8"	1.40	2.66	2.62	0.90	6.5	1.12	2.37	2.33	0.80	3.32	4.6	C-2
22	1 3/8"	1.50	2.41	3.22	1.20	13.0	1.14	2.11	2.82	1.05	3.52	8.7	C-2
30	2 5/8"	3.28	3.50	2.68	1.25	9.5	1.48	2.36	1.81	0.84	2.97	2.9	C-2
32	2 5/8"	3.00	3.53	2.11	1.18	11.5	1.44	2.45	2.11	0.82	3.23	3.8	C-2
33	2 5/8"	2.80	3.55	2.28	1.03	11.2	1.41	2.52	2.28	0.73	3.39	4.0	C-2
34	2 5/8"	6.00	3.15	6.15	2.30	91.2	1.82	1.73	3.37	1.26	3.78	15.2	C-2
35	2 5/8"	4.12	2.87	4.05	2.32	39.0	1.60	1.79	2.53	1.45	3.10	9.5	TNT
36	2 5/8"	6.00	2.90	5.76	3.57	89.2	1.82	1.59	3.16	1.96	4.46	14.5	C-2
37	2 5/8"	4.62	2.75	4.00	1.90	31.8	1.66	1.65	2.40	1.14	2.91	6.9	TNT
40	2 5/8"	2.75	3.21	3.26	1.00	11.1	1.40	2.29	2.32	0.71	3.25	4.0	TNT
43	2 5/8"	0.65	1.92	1.39	0.35	0.73	0.87	2.21	1.60	0.40	2.73	2.1	TNT
44	2 5/8"	0.65	1.84	2.00	0.68	2.86	0.87	2.12	2.31	0.78	3.14	4.4	TNT
45	2 5/8"	1.42	2.46	1.47	0.60	1.35	1.12	2.19	1.31	0.54	2.55	1.0	TNT
47	4 1/2"	6.50	4.60	4.09	1.42	24.9	1.86	2.47	2.20	0.76	3.30	3.8	C-2
48	4 1/2"	4.50	4.85	1.12	0.68	0.89	1.65	2.94	0.68	0.41	3.02	0.2	TNT
B-1	4 1/2"	6.00	4.75	3.46	2.00	25.1	1.82	2.61	1.90	1.10	3.22	4.2	C-2
5	4 1/2"	8.38	4.00	9.27	2.80	251.8	2.03	1.97	4.57	1.38	4.97	30.1	TNT
8	4 1/2"	18.38	4.14	10.11	3.80	407.1	2.66	1.57	3.83	1.44	4.14	22.1	C-2
10	4 1/2"	14.00	4.30	8.92	3.45	226.5	2.41	1.74	3.70	1.43	4.09	16.2	C-2
11	9"	11.00	6.85	2.04	0.65	2.8	2.22	3.08	0.92	0.29	3.21	0.3	C-2
14	9"	106.00	3.50	2.45	5.65	788.4	4.70	0.75	2.45	1.20	2.56	7.6	TNT
16	9"	10.62	6.62	3.69	2.28	32.6	2.20	3.00	1.68	1.04	3.44	3.1	TNT
17	9"	17.62	6.42	3.27	2.35	177.2	2.60	2.47	3.27	0.90	4.09	10.0	TNT
18	9"	12.75	5.75	5.24	2.45	70.4	2.33	2.47	2.25	1.05	3.34	5.5	TNT
19	9"	38.12	6.20	6.41	5.40	232.0	3.36	1.85	1.91	1.61	2.65	6.1	TNT
20	9"	12.00	6.91	5.23	2.20	63.0	2.28	3.03	2.29	0.96	3.79	5.3	C-2
NX	9"	10.00	3.50	5.15	2.32	64.4	2.15	1.63	2.39	1.08	2.89	6.4	C-2
C-1	4 1/2"	10.00	2.50	5.11	2.48	63.4	2.15	1.16	2.38	1.15	2.64	6.8	C-2
2	4 1/2"	10.00	3.50	2.81	3.17	121.5	2.15	1.63	2.81	1.47	3.24	12.2	C-2
2a	4 1/2"	10.00	3.50	5.70	4.57	155.2	2.15	1.63	2.65	2.12	3.11	15.5	C-2
3	4 1/2"	10.00	4.50	5.98	1.77	66.4	2.15	2.09	2.78	0.82	3.47	6.6	C-2
C-4	4 1/2"	10.00	5.50	4.82	1.90	46.3	2.15	2.55	2.24	0.88	3.39	4.6	C-2
6	4 1/2"	21.00	5.45	6.25	2.28	93.3	2.76	1.97	2.26	0.83	2.99	4.4	C-2
7	4 1/2"	8.12	5.80	1.88	0.80	5.0	2.01	2.89	0.94	0.40	3.03	0.6	TNT
9	4 1/2"	12.12	5.31	5.97	1.85	69.1	2.29	2.32	2.61	0.81	3.49	5.7	TNT
10	4 1/2"	6.00	6.17	2.01	0.80	4.6	1.82	3.39	1.10	0.48	3.56	0.6	C-2
11	9"	33.62	11.95	2.61	0.75	5.3	3.23	3.70	0.81	0.23	3.78	0.2	TNT
13	9"	70.00	12.27	13.02	5.72	1015.7	4.12	2.98	3.16	1.38	4.34	14.5	C-2
14	9"	35.00	12.62	3.92	1.65	6.4	3.27	3.86	0.54	0.50	3.90	2.0	C-2
11 C-1	9"	70.00	3.84	8.85	5.91	485.2	4.12	0.93	2.15	1.43	2.34	6.9	C-2
C-2	18"	320.00	2.96	11.92	7.10	1057.0	6.84	0.43	1.74	1.03	1.79	3.3	C-2
D-1	18"	1080.00	3.60	13.11	6.42	1518.0	10.26	0.35	1.27	0.82	1.31	1.4	C-2
D-2	36"	2560.00	4.71	23.37	9.00	5148.0	13.68	0.34	1.71	0.65	1.74	2.0	C-2

TABLE 5.3[17]

Tunnel Demolition Shots in Basalt

ERDL[2]

No.	Tunnel	W	$\bar{r}$	D	$D/\bar{r}$	$R_k/\bar{r}$	Remarks
6	22	4 x 750*	9.08	15-20	1.65-2.21	3.31	Charges spaced 30'.20' burden too much.
A-1	22	4000**	15.9	12.5	0.79	--	Demolition effective
B-1	22	500**	7.94	15.7	1.98	--	No break through
B-2	22	500**	7.94	15.0	1.89	--	not stemmed, spalling only
B-4 & 8	22	2 x 750	9.08	15.0	1.65	2.21	Charges spaced 20',100' damaged.
B-5	22	750	9.08	15.0	1.65	?	Broke through

* C-2 and C-3
** Nitrostarch

for Unaweep granite. The first equation was determined by the method of squares, the latter by the authors of this report by the method averages.

For Lithonia granite the probability of achieving an effective crater radius or volume drops off very rapidly for $\frac{D}{\sqrt[3]{Y}} > 1.6$. Applying the criterion that probability of producing an effective crater should be statistically nearly equal to one, and choosing values of scaled depths from each curve which is well below possible camouflet depth, for Lithonia granite, this yields a range of scaled charge depths of

$$0.75 < \frac{D}{\sqrt[3]{Y}} < 1.00$$

to assure positive crater formation, the limits being governed largely by crater depth.

For Unaweep granite the corresponding limits are, again choosing values of scaled depth from the curves smaller than camouflet depths,

$$0.90 < \frac{D}{\sqrt[3]{Y}} < 1.25$$

for successful cratering.

Reference to physical properties of the two types of granite shows that they have about the same dynamic breaking strain. The density of Lithonia granite (2.60) is greater than that of Unaweep granite (2.25). The corresponding Young's Moduli are 3.0×10^6 and 4.89×10^6. While E is greater for Unaweep granite, its density is less. The correlation between these properties and the difference in breakage properties is not well defined.

If the same procedure is applied to the other types of rock, the results listed in Table 5.4 are obtained.

Discussion. No single criterion seems to satisfy the conditions of efficient breakage for all types of rock on which data are available. A combination of crater dimensions was used to fix the lower limit of charge depth, while the upper limit of charge depth value was chosen so that the majority of shots in this range gave satisfactory values for other crater dimensions and was well below the critical point on curves where crater dimensions dropped rapidly with further increase of charge depth.

The limits of scaled charge depth for efficient breakage vary considerably. Lithonia granite appears to be the most difficult rock to break. This is due to the very short fall length of the strain curve. The scaled volume of craters varies widely even for one rock type. However, the values tabulated in Table 5.4 for scaled charge depths are believed to give safe limits for crater breakage to an "infinite" free face.

TABLE 5.4

Summary of Effective Breakage Criteria - Surface Craters

Rock Type	V_k/W	$D_k/\bar{r}$	$R_k/\bar{r}$	D_k/D	$D/\bar{r}$
Lithonia Granite	+5.00	+0.60	+2.5	+0.75	0.75 - 1.00
Unaweep Granite	+5.00	+0.90	+2.50	+0.85	0.90 - 1.25
Kanawha Sandstone	+7.00	+1.20	+2.50	+1.00	0.90 - 1.50
Navajo Sandstone	+6.50	+1.20	+2.50	+1.00	1.20 - 1.35
Green River Marlstone	+7.00	+1.25	+2.40	+0.95	1.25 - 1.75
Niobara Chalk	+10.00	+1.00	+2.65	+1.00	0.80 - 2.50

Tunnel demolition tests by ERDL[17] also tabulated in Table 5.1 show that breakage was unsuccessful in basalt with a scaled depth of 1.89 using nitro-starch. A scaled depth of 1.65 with Comp C-2 and C-3 was successful, while a scaled depth of 2.21 using the same explosive was not. Comparable figures for surface crater depths in basalt are not available. This series of tests was conducted at full scale with charges placed in chambers in the walls of the tunnels at the spring line. Charges varied in size from 500 to 4000 lb.

Failure in Flexure. A series of experiments was designed by Clark and Caudle[18] to test the response of rock-like materials to transverse impact. Small simply supported beams of hydrostone (gypsum cement) were subjected to impact by drop weights and the shock loading from No. 6 blasting caps upon and just above the beam. One of the primary objectives of the investigation was to determine any possible relationship between rate of strain and fracture strain. Many of the beams impacted by drop weights broke on a second or third peak of one of their natural frequencies. The beams subjected to blast load from a No. 6 blasting cap broke on the first rise. Some typical strain-time histories are given in Figure 5.34. The strain necessary to fracture appears to increase almost as the inverse expotential of the rise time.

While the geometrical configuration of the above tests is somewhat similar to the possible loading of stratified members of underground roof structures, the model beams were subjected only to concentrated loads. The type of loading of a full scale underground structure will be quite different. The load will not be concentrated and the load pulse length will be much longer.

Thus, an underground structure may be subjected to several g's acceleration with a resultant downward velocity, a subsequent retardation and a damping out of the motion. Also, the whole stress field about the structure will have been altered and increased. If a segment of the immediate stratum over an opening can be regarded as a restrained beam initially loaded by its own weight only, an analysis could be made of the response of the beam to the acceleration, resulting velocity, deceleration and superposed stress field.

Rock Failure and Nuclear Bursts

Brode[19] indicates that cratering by nuclear weapons and the rupture and ground shock associated therewith are the primary phenomena of importance to deep underground installations. The air blast furnishes an appreciable load at the surface, and these pressures are transmitted downward at seismic velocities. Added to these pressures are those transmitted by the expanding bomb vapors. Brode states further that the survival of an underground structure is quite likely only a short distance outside of the crater.

Beyond the true crater will be a zone of crushing, plastic flow, and permanent deformation. It is postulated[19] that small resistant structures can roll with the ground shock and can survive in spite of high acceleration forces and permanent displacement in the soil. The shock, having

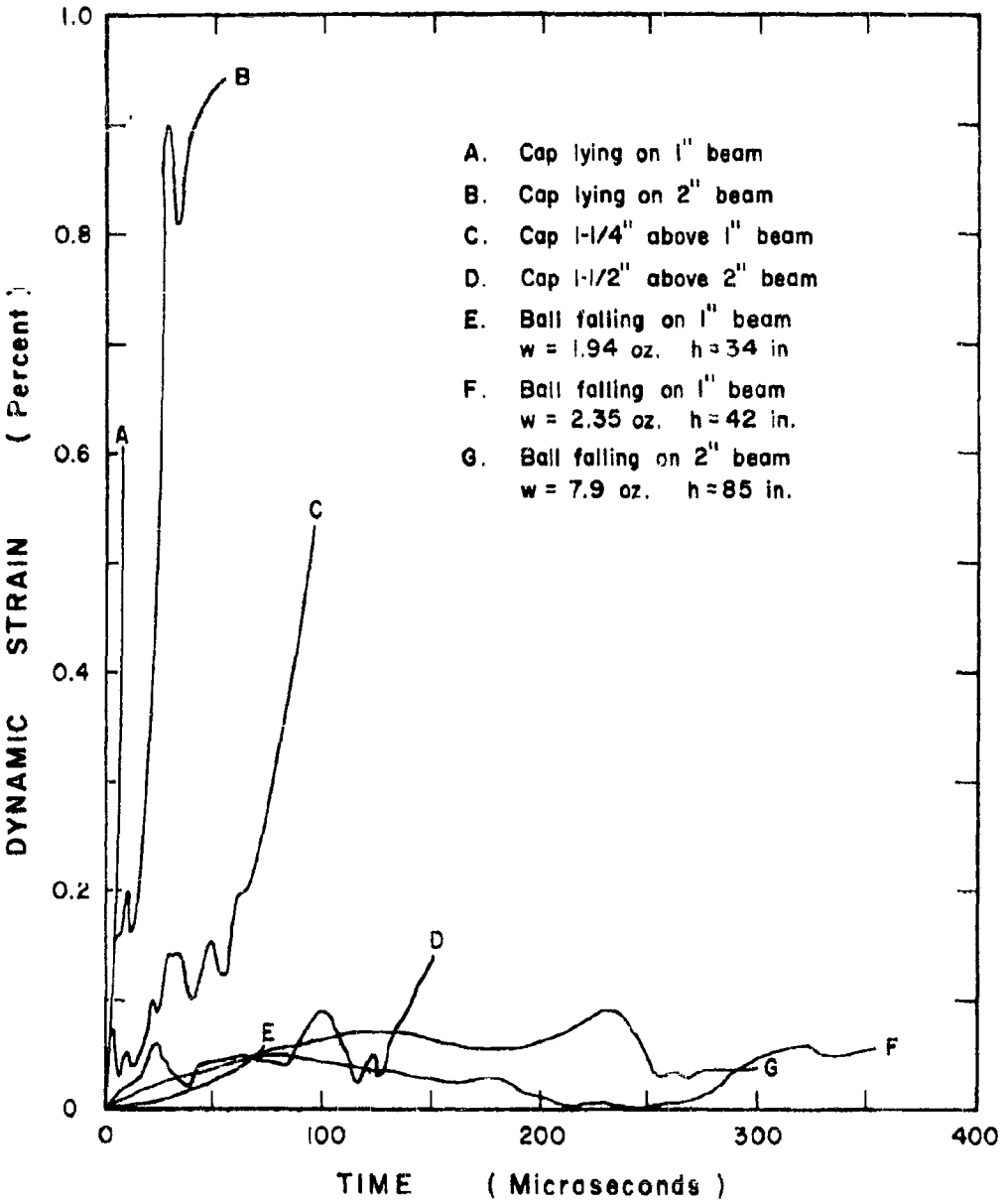


Figure 5.34. Comparison of response of rock beams to impact loading by drop weight and No. 6 blasting caps.[23]

lost some of its sharpness, is likened to an ocean swell of long wave length, which neither tears or crushes the material with high local stresses. Further, a deep tunnel or cavity might be damaged only by spalling if any high frequency components are present in the shock.

The failure of rock subjected to nuclear blasts is of interest for engineering design purposes both with respect to gross or large scale phenomena, and those of local character, the latter being concerned with those parameters which influence the ground behavior at distances from the blast beyond which rock may be considered stable for protective construction. Few of the available records of surface bursts indicate efforts to measure the deep rock response to these bursts.

Detailed studies of Rainier and Neptune shots[20,21,22,23] offer some data which are pertinent, however, and available results, many of which are qualitative are summarized here.

There were nine major shots detonated in the underground program (Table 5.5). The geologic locale in which these events took place is a geologic column of 250 feet of welded tuff which is underlain by 1700 feet of bedded tuffs and a thick bed of dolomite (Figure 5.35). The weakly cemented granular tuff Tos_7 is considered to be a stratigraphic feature of some importance in interpretation in its relation to the Rainier, Evans, Tamalpais ard Neptune events which occurred about 100 feet below this formation. Blanca and Logan were detonated in Tos_8 about 600 feet below this horizon. Values of compressive strength of the tuff of 1200 psi and tensile strength of 165 psi are reported. The seismic velocities above Rainier are given in Table 5.6.

The scaled depth is defined (Table 5.7) as $D/W^{\frac{1}{3}}$ where D is the actual depth in feet and W is the energy release in kilotons of TNT equivalent. One kiloton of TNT equivalent is taken as equal to 10^{12} calories of prompt release energy.

Earth motion measurements indicated that a large earth cap beginning about 180 feet below the mesa surface separated from the mesa over the Rainier charge and then fell back into place. The most significant verticle displacement was one foot at ground zero, while the peak surface acceleration was 6 g at 186 milliseconds after zero time.

For specific local results the Rainier event has been studied in most detail. The drifts and drill holes in the shot zone are shown in Figures 5.35 to 5.37. While temperature distribution and radioactivity studies were made, the effects on the physical properties of the rock mass are of most interest in stability studies. It was found that the temperature and radioactivity were concentrated within shells and that within these shells the rock was generally permeable to drill water. Based on these observations it was concluded that the explosions produced cavities of radius $R = 50\ W^{\frac{1}{3}}$ feet, which stood for a short period of time and then collapsed.

TABLE 5.5

Major Features of Underground Nuclear Explosives

Event	Yield (W) kt	Medium	Depth (D) feet	Scaled Depth $D/W^{1/3}$	Measured radioactivity deposited on surface %	Crater volume yd^3	Crater volume/kt yd^3
Jangle-S	1.2±0.1	Alluvium	-3.5*	-3.3*	>65	1,650	1,400
Jangle-U	1.2±0.1	"	17	16	>80	37,000	31,000
Teapot-Ess	1.2±0.1	"	67	63	90	96,000	80,000
Neptune	0.090±.020	Bedded Tuff	99	220	1-2	33,000	370,000**
Blanca	19.0±1.5	" "	835	310	<0.5	0	0
Logan	$5.0^{+0.2}_{-0.4}$	" "	830	485	0	0	0
Rainier	1.7±0.1	" "	790	670	0	0	0
Tamalpais	0.072±.010	" "	330	780	0+	0	0
Evans	0.055±.030	" "	840	[illegible]	0++	0	0

*3.5 feet above surface.
**This explosion took place in bedded tuff under a sloping surface 1:3 so the crater is probably larger than would be expected on a level surface.
+No breakthrough to surface but radioactive gases in large quantities leaked into the tunnel.
++No breakthrough to surface but stemming failed, releasing gross fission activity into the tunnel.

TABLE 5.6

Seismic Velocity, Vertical Distribution over Rainier

Interval depth below surface, feet	Interval velocity, ft/sec	Distance above Rainier shot room, feet
230-270	7,150	665-625
270-310	13,700	625-585
310-395	6,650	585-500
395-525	7,070	500-370
525-675	7,180	370-220
675-775	5,850	220-120

(Shot room at depth 895 feet.)

TABLE 5.7

Radii of Radioactive Shells

Event	Radius (feet)	Scaled radius ($R/W^{1/3}$ feet/$kt^{1/3}$)
Neptune	21	47*
Blanca	130	48
Logan	85	50
Rainier	62	52
Tamalpais	30	73**

*Cratering shot

**Fired in a large room

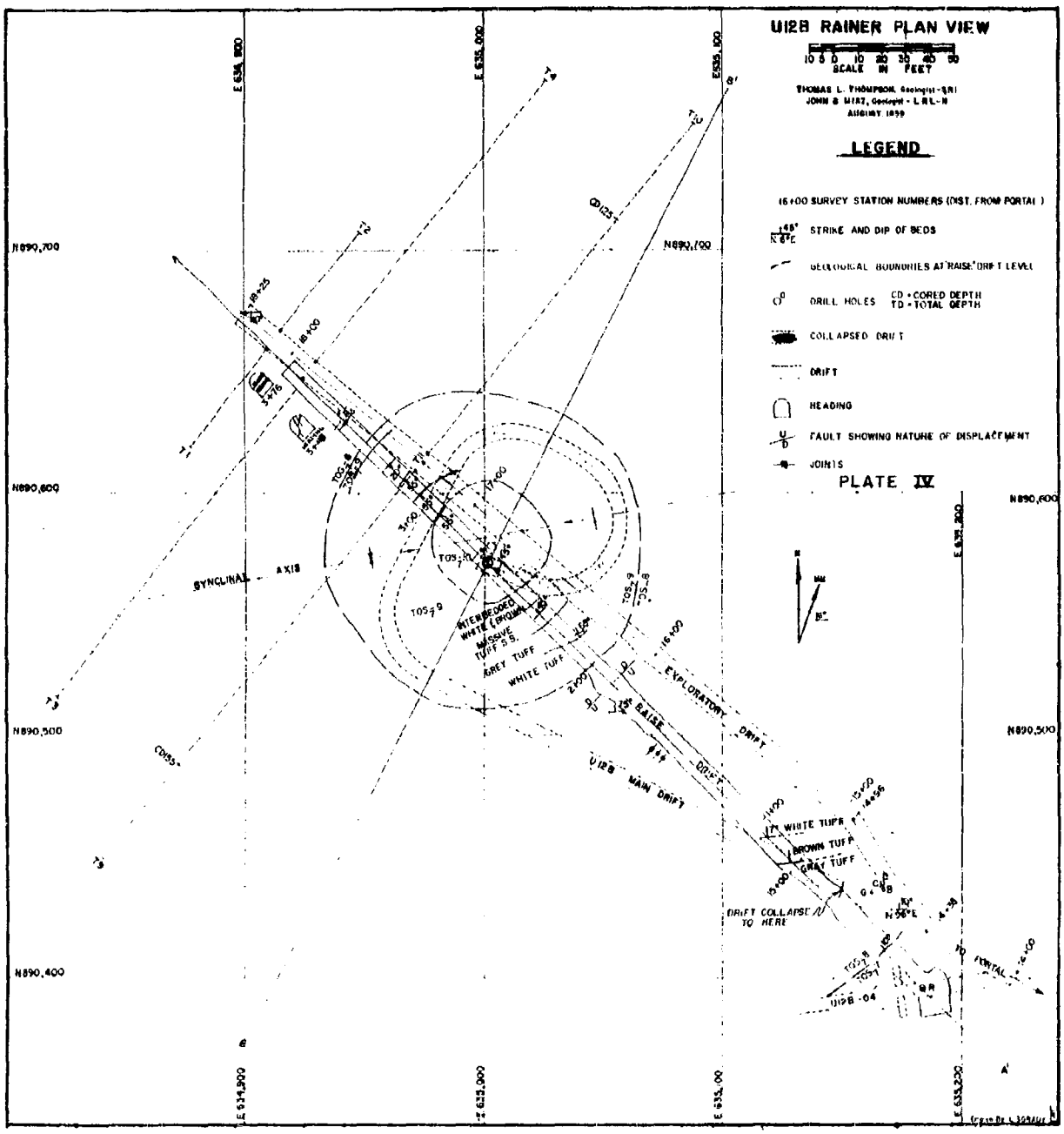

U12B RAINER PLAN VIEW
SCALE IN FEET
LEGEND
(6+00 SURVEY STATION NUMBERS (DIST. FROM PORTAL)
STRIKE AND DIP OF BEDS
GEOLOGICAL BOUNDRIES AT RAISE/DRIFT LEVEL
DRILL HOLES CD = CORED DEPTH TD = TOTAL DEPTH
COLLAPSED DRIFT
DRIFT
HEADING
FAULT SHOWING NATURE OF DISPLACEMENT
JOINTS
PLATE IV
SYNCLINAL AXIS
INTERBEDDED WHITE (BROWN) MASSIVE TUFF S.S.
GREY TUFF
WHITE TUFF
EXPLORATORY DRIFT
U12B MAIN DRIFT
WHITE TUFF
BROWN TUFF
GRAY TUFF
DRIFT COLLAPSED TO HERE
PORTAL
U12B-04
N890,700
N890,600
N890,500
N890,400
E634,800
E635,000
E635,100
E635,200

Figure 5.35.

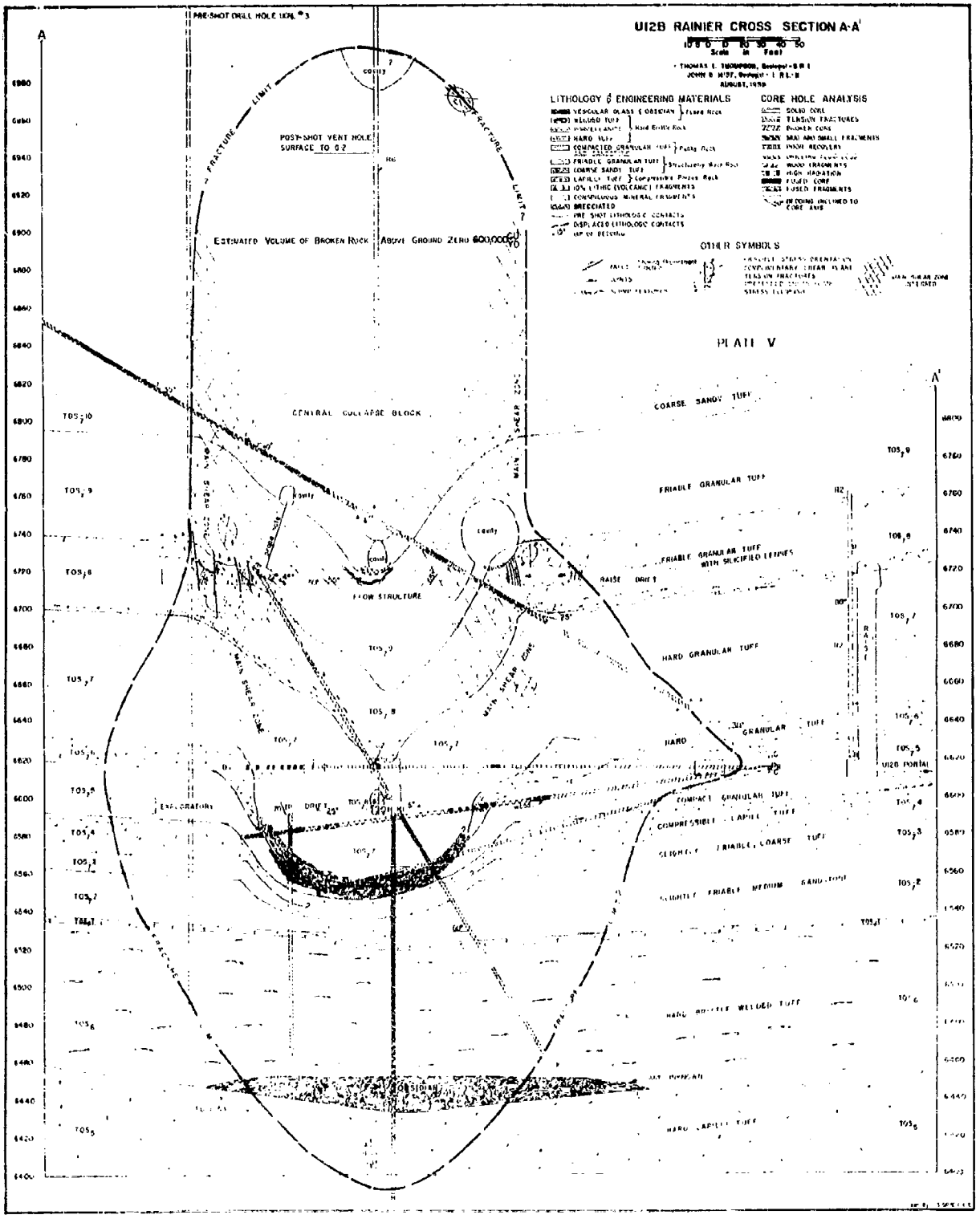

U12B RAINIER CROSS SECTION A-A'
LITHOLOGY & ENGINEERING MATERIALS
CORE HOLE ANALYSIS
OTHER SYMBOLS
PLATE V
POST-SHOT VENT HOLE SURFACE TO 0.2
Estimated Volume of Broken Rock Above Ground Zero 600,000 CY
CENTRAL COLLAPSE BLOCK
MAIN SHEAR ZONE
FRACTURE LIMIT
FLOW STRUCTURE
COARSE SANDY TUFF
FRIABLE GRANULAR TUFF
HARD GRANULAR TUFF
COMPACT GRANULAR TUFF
U12B PORTAL
EXPLORATORY

Figure 5.36.

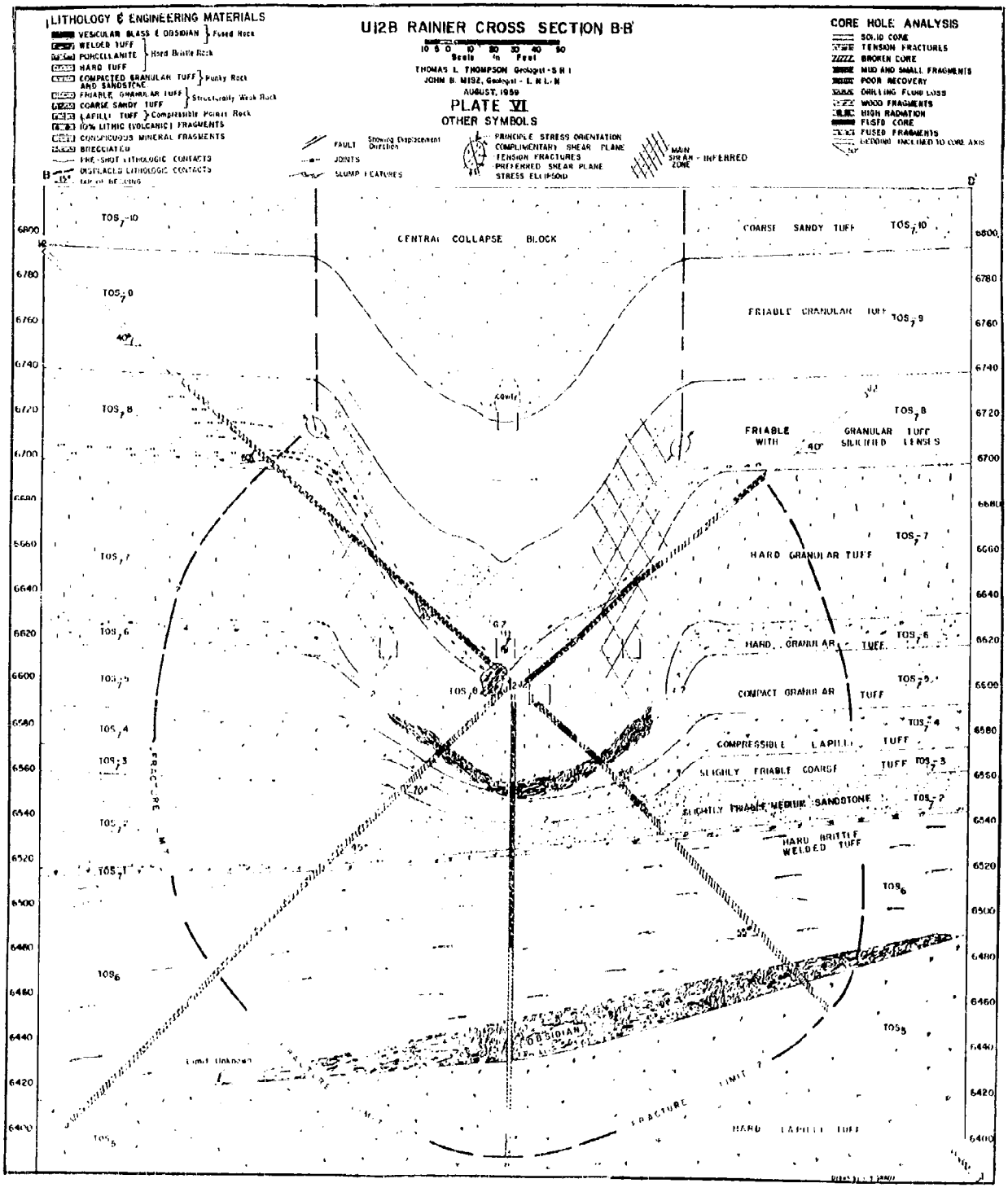

U12B RAINIER CROSS SECTION B-B'
Scale
Feet
THOMAS L. THOMPSON Geologist - S.R.I.
JOHN B. MISE, Geologist - L.N.L.-N
AUGUST, 1969
PLATE VI
OTHER SYMBOLS
LITHOLOGY & ENGINEERING MATERIALS
VESICULAR GLASS & OBSIDIAN
WELDED TUFF
PORCELANITE
HARD TUFF
Fused Rock
Hard Brittle Rock
COMPACTED GRANULAR TUFF AND SANDSTONE
FRIABLE GRANULAR TUFF
COARSE SANDY TUFF
LAPILLI TUFF
Punky Rock
Structurally Weak Rock
Compressible Porous Rock
10% LITHIC (VOLCANIC) FRAGMENTS
CONSPICUOUS MINERAL FRAGMENTS
BRECCIATED
PRE-SHOT LITHOLOGIC CONTACTS
DISPLACED LITHOLOGIC CONTACTS
FAULT
JOINTS
SLUMP FEATURES
PRINCIPLE STRESS ORIENTATION
COMPLIMENTARY SHEAR PLANE
TENSION FRACTURES
PREFERRED SHEAR PLANE
STRESS ELLIPSOID
MAIN SHEAR ZONE - INFERRED
CORE HOLE ANALYSIS
SOLID CORE
TENSION FRACTURES
BROKEN CORE
MUD AND SMALL FRAGMENTS
POOR RECOVERY
DRILLING FLUID LOSS
WOOD FRAGMENTS
HIGH RADIATION
FUSED CORE
FUSED FRAGMENTS
CENTRAL COLLAPSE BLOCK
COARSE SANDY TUFF
FRIABLE GRANULAR TUFF
FRIABLE WITH SILICIFIED LENSES
HARD GRANULAR TUFF
HARD GRANULAR TUFF
COMPACT GRANULAR TUFF
COMPRESSIBLE LAPILLI TUFF
SLIGHTLY FRIABLE COARSE TUFF
SLIGHTLY FRIABLE MEDIUM SANDSTONE
HARD BRITTLE WELDED TUFF
OBSIDIAN
HARD LAPILLI TUFF
FRACTURE
Limit Unknown
B
B'
6800
6780
6760
6740
6720
6700
6680
6660
6640
6620
6600
6580
6560
6540
6520
6500
6480
6460
6440
6420
6400

Figure 5.37.

The Rainier cavity, when it was first formed, was lined with about 4 inches of melted rock. Inspection of the collapsed zone showed blocks from a few inches in diameter up to several feet. The regions between the blocks were filled with pulverized material which had resolidified probably due to the high clay content. The upper post-shot exploratory drift, 100 feet above the zero point, encountered blocks a few inches to a few feet in diameter with open cracks, as well as a large cavity.

It is approximated that the temperature a few microseconds after detonation was $10^{6°}$ K and the pressure 7×10^6 atmospheres. Calculation of the behavior of the medium by Nuckolls[24] by means of a computer program, from a few microseconds to 100 milliseconds is as follows: it was assumed that the rock mass of tuff has a negligible large scale tensile strength, and that it behaves as a linear elastic solid as long as the tension does not exceed the stress due to overburden pressure. The values of elastic constants used were measured values for bulk modulus, shear modulus, and sound velocity. When tension in the spherical shell becomes greater than the lithostatic stress, the components of the stress tensor are equated to a pressure (shear modulus equal to zero) which is related to the volume by a bulk modulus type of equation of state. Calculated results and measured values of arrival-time of shocks were found to be in good agreement (Figure 5.38). The peak shock pressure as a function of distance is given in Figure 5.39, and decreases as $r^{-2.35}$ out to about 10 meters. The tuff was vaporized to 2.3 meters in 0.2 milliseconds at a peak pressure of 1.0 megabar and melted by shock pressure to 3.3 meters at a peak pressure of 0.4 mb. Enough energy was consumed by the shock in the first 4.6 meters to melt all the tuff included within this spherical volume (660 tons). It was calculated that the total melted by fission decay energy was 1.2 times this amount (880 tons).

As the shock wave progressed outward it crushed the rock to a radius of 130 feet where the pressure was 1.4 kilobars, or twice the measured static compressive strength. The energy distribution of the Rainier shot is given in Table 5.8.

TABLE 5.8

Rainier Energy Distribution

State	Radii	Percentage of prompt energy
Gas	0 - 62 ft	8.2
Liquid	62 ft - 62-1/4 ft	19.1
Crushed	62-1/4 ft - 130 ft	47.0
Fractured	130 ft - 280 ft	21.2
Elastic	280 ft	4.5

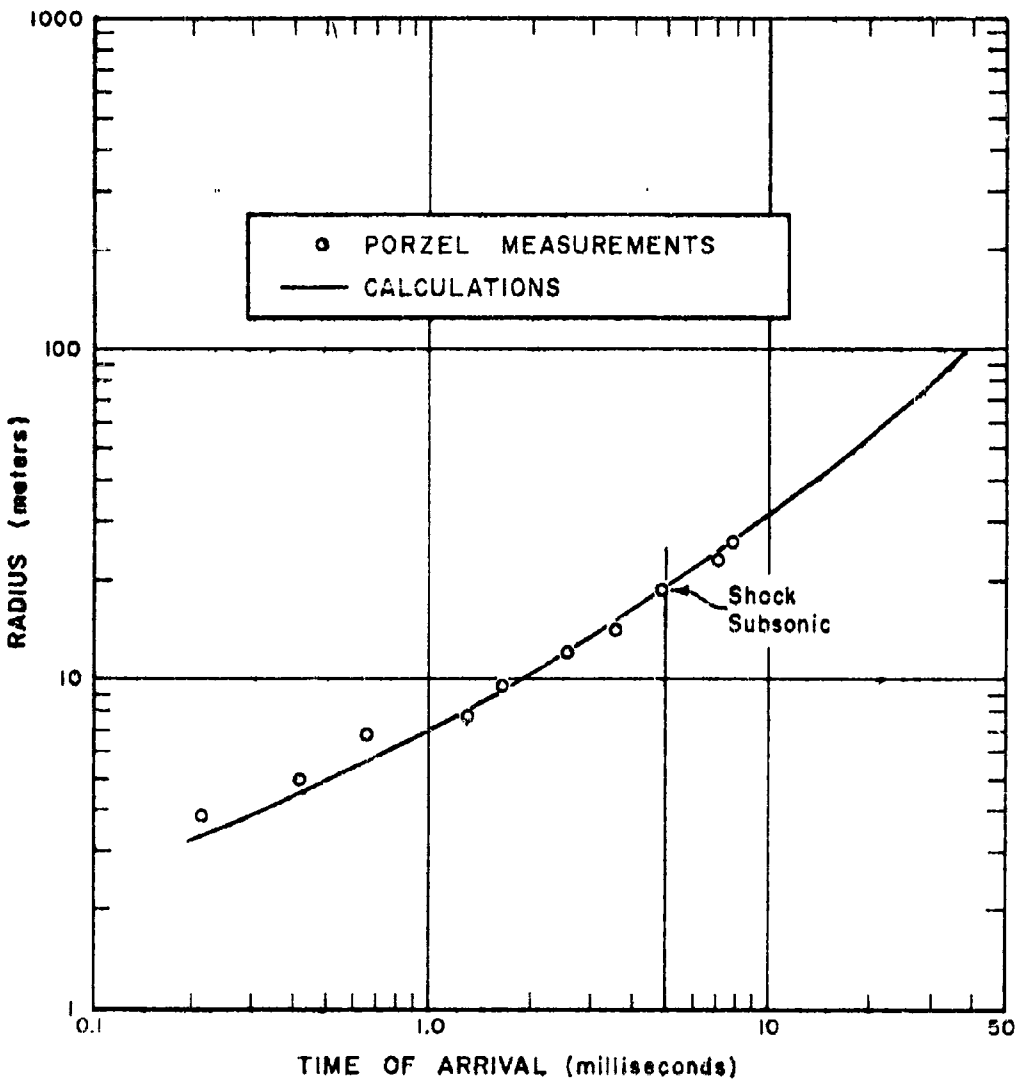


Figure 5.38. Shock time-of-arrival--Rainier event.

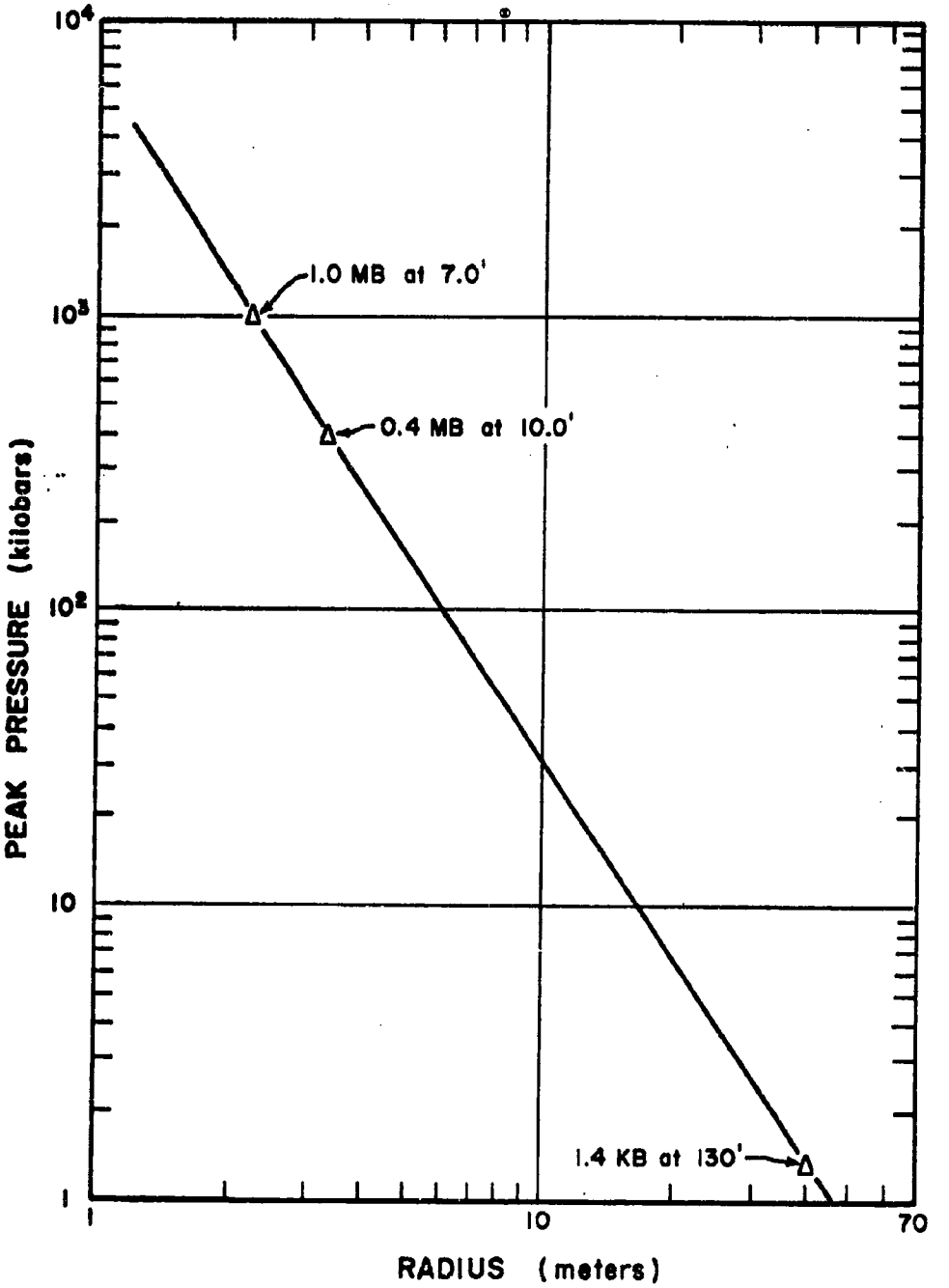


Figure 5.39. Peak shock pressure--Rainier event.

The conclusions reached by Johnson, et al.[23], are:

1. Radioactivity of nuclear explosions in the kiloton range of tuff can be completely contained at depths of $D = 400\ W^3$ feet.

2. The initial cavity formed has a radius of $R = 50\ W^3$.

3. The melted rock, which is converted to glass on cooling amounts to 500 ± 15 tons per kiloton of energy release.

4. The collapse of the cavity produced a zone of about 70,000 yds^3/kt (120,000 tons/kt.).

5. About 30 percent of the total energy release was deposited in steam and hot rock at a temperature in excess of 1200° C.

The Neptune event, as described by Shelton, et al.[22] is of interest because it approximates some of the phenomena which might be expected if a weapon were to penetrate the overburden before detonating. The distance to the nearest point on the surface was 100 feet. The yield of the shot was 115 ± 15 tons. When the shot was fired the surface bulged upward 25-35 ft., followed by venting. Eleven preshot holes were drilled into the shot area (Figures 5.35 to 5.37). Preliminary studies indicate that several layers of tuff and sandstone had retained their continuity, but had fallen into the cavity created by the detonation. Crushing of the tuff occurred 40 feet downward and 50 feet laterally except in the direction of the original drift where it extends 80 feet. The extent of the crushing appears to have been influenced by bedding plane weaknesses. Fracturing also extends 70 feet below the zero point, according to interpretation of drill cores, and to the surface, the boundary of the latter fracturing lying on a core. Downhill at the surface the fracture limit lays at the interface of the brittle Tos_6 and the more "punky" Tos_5.

The detailed history of the Neptune event[22] is given as follows: All of the material around the device was vaporized in a few microseconds. The temperature and pressure were about 150,000° K and 25,000 atmosphere, respectively, which are much smaller than those for the Rainier event. The 25 kilobar pressure did not generate a shock strong enough to melt or vaporize the rock, but crushed the rock, allowing the cavity to expand. The shock wave decreased in strength, finally propagating as an elastic wave. The reflected wave (tensile) plus the rarefaction tail of the outgoing wave fractured the surface by spalling and created a crater on the slope of the mesa. Estimates based on the $50\ W^3$ formula for Rainier and other shots predicted a 50 foot radius cavity, however, 70% of the energy was believed lost to the atmosphere due to venting. The crater was thus formed due to three processes, (1) the breakage of the rock between the crater and the detonation point by spalling, (2) acceleration of broken rock by venting gases, and (3) collapse of the cavity. (See Figures 5.40 to 5.42).

Shelton further points out that test results from HE charges (TNT) of 256 lb. to 20 tons that the basic scaling law of $W^{\frac{1}{3}}$ is correct for cratering. Considering gravity effects a scaling law of $W^{\frac{1}{3.4}}$ has been found to give a better empirical fit.

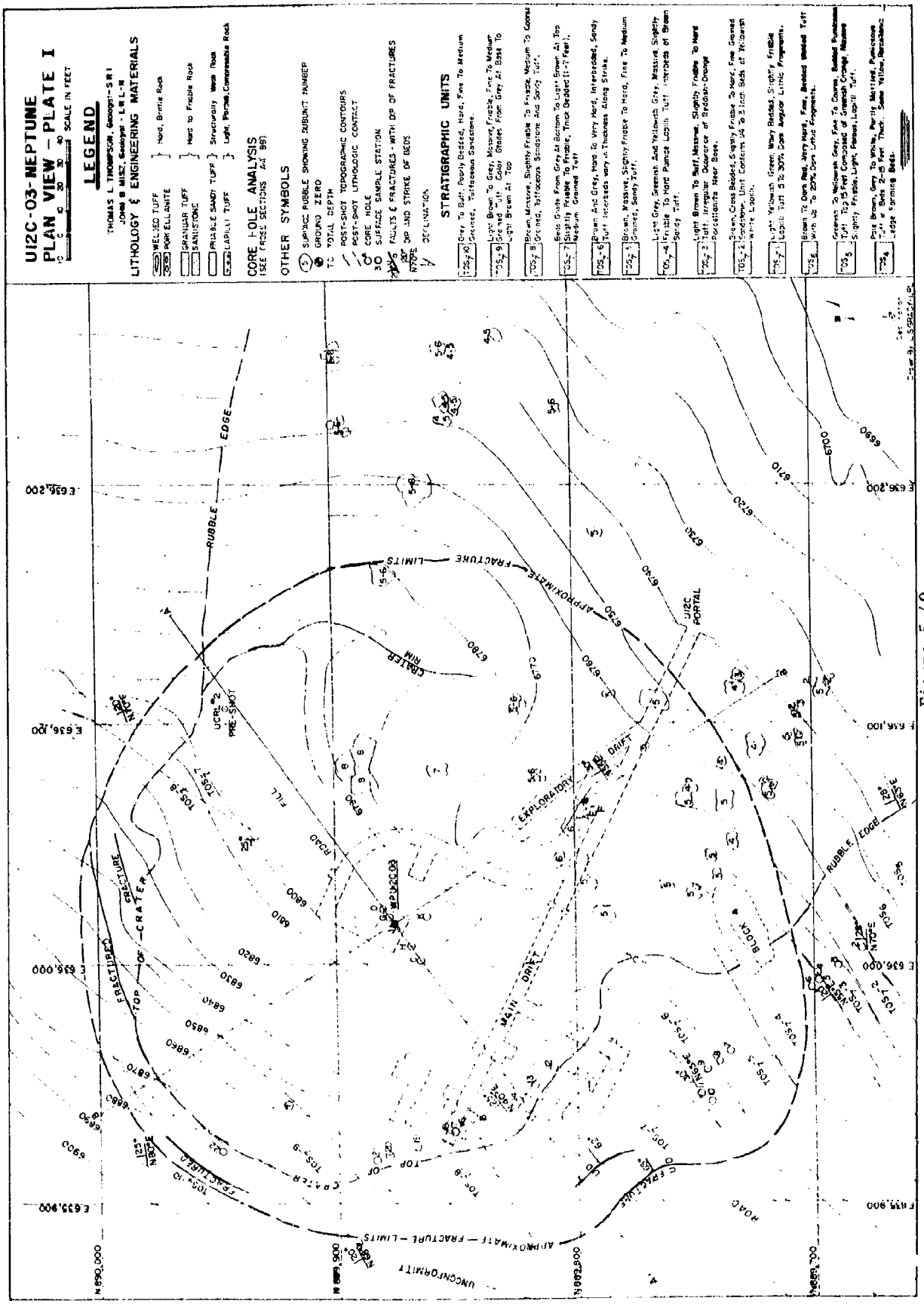

U12C-03-NEPTUNE
PLAN VIEW – PLATE I
SCALE IN FEET
LEGEND
THOMAS L THOMPSON, Geologist-SRI
JOHN B MILEY, Geologist - LASL-N
LITHOLOGY & ENGINEERING MATERIALS
WELDED TUFF
PORPHYRITIC ANDESITE
GRANULAR TUFF
SANDSTONE
FRIABLE SANDY TUFF
LAPILLI TUFF
Hard, Brittle Rock
Hard To Friable Rock
Structurally Weak Rock
Light, Porous, Compressible Rock
CORE HOLE ANALYSIS
(SEE CROSS SECTIONS Apr 85)
OTHER SYMBOLS
SURFACE RUBBLE SHOWING RUBBLE NUMBER
GROUND ZERO
TD TOTAL DEPTH
POST-SHOT TOPOGRAPHIC CONTOURS
POST-SHOT LITHOLOGIC CONTACT
CORE HOLE
SURFACE SAMPLE STATION
FAULTS & FRACTURES - WITH DIP OF FRACTURES
DIP AND STRIKE OF BEDS
DECLINATION
STRATIGRAPHIC UNITS
Grey To Buff, Poorly Bedded, Hard, Fine To Medium Grained, Tuffaceous Sandstone.
Light Brown To Grey, Massive, Friable, Fine To Medium Grained with Color Grades From Grey At Base To Light Brown At Top
Brown Massive, Slightly Friable To Friable, Medium To Coarse Grained, Tuffaceous Sandstone And Sandy Tuff.
Basic Grade From Grey At Bottom To Light Brown At Top Slightly Friable To Friable, Thick Bedded (5-7 Feet), Medium Grained Tuff
Brown And Grey, Hard To Very Hard, Interbedded, Sandy Tuff Interbeds vary in Thickness Along Strike.
Brown, Massive, Slightly Friable To Hard, Fine To Medium Grained, Sandy Tuff.
Light Grey, Greenish And Yellowish Grey, Massive Slightly Friable To Hard Pumice Lapilli Tuff Interbeds of Brown Sandy Tuff.
Light Brown To Buff, Massive, Slightly Friable To Hard Tuff, Irregular Deposits of Reddish-Orange Porcellanite Near Base.
Brown, Cross Bedded, Slightly Friable To Hard, Fine Grained Sandstone. Unit Contains 1/4 To 2 Inch Beds of Yellowish White Lapilli.
Light Yellowish Green, Wavy Bedded, Slightly Friable Lapilli Tuff 5 To 30% Open Angular Lithic Fragments.
Brown To Dark Red, Very Hard, Fine, Banded Welded Tuff With Up To 25% Open Lithic Fragments.
Greenish To Yellowish Grey, Fine To Coarse, Bedded Pumiceous Tuff, 10 Feet Consolidated Lapilli Tuff.
Slightly Friable, Light, Porous, Lapilli Tuff.
Pale Brown, Grey To White, Partly Laminated, Pumiceous Tuff in Beds 2-15 Feet Thick. Some Yellow, Resistance Ledge Forming Beds.
RUBBLE EDGE
APPROXIMATE FRACTURE LIMITS
CRATER RIM
U12C PORTAL
EXPLORATORY DRIFT
MAIN DRIFT
FRACTURED TOP OF CRATER
UNCONFORMITY
ROAD
BLOCK

Figure 5.40.

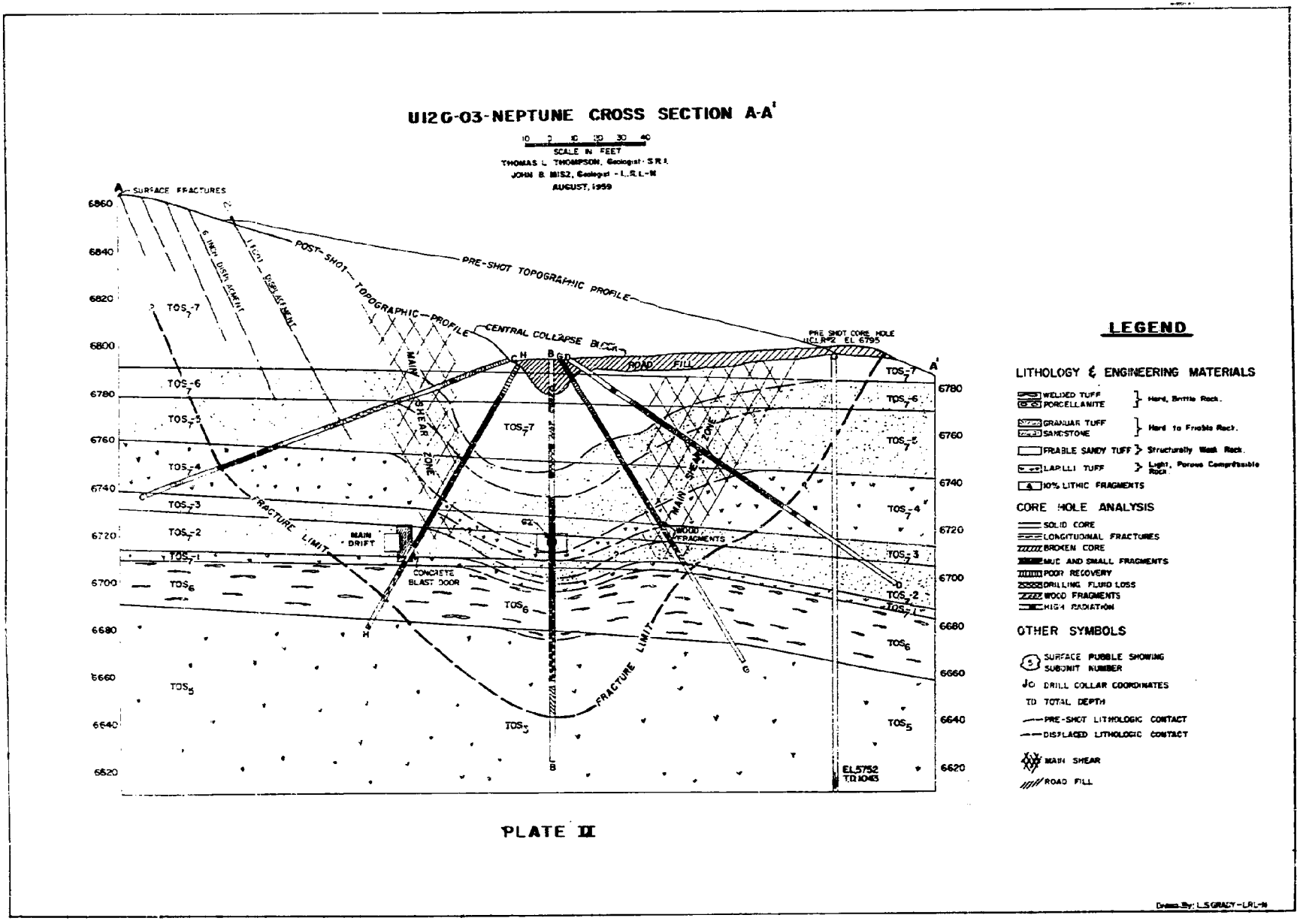


PLATE II

Figure 5.41.

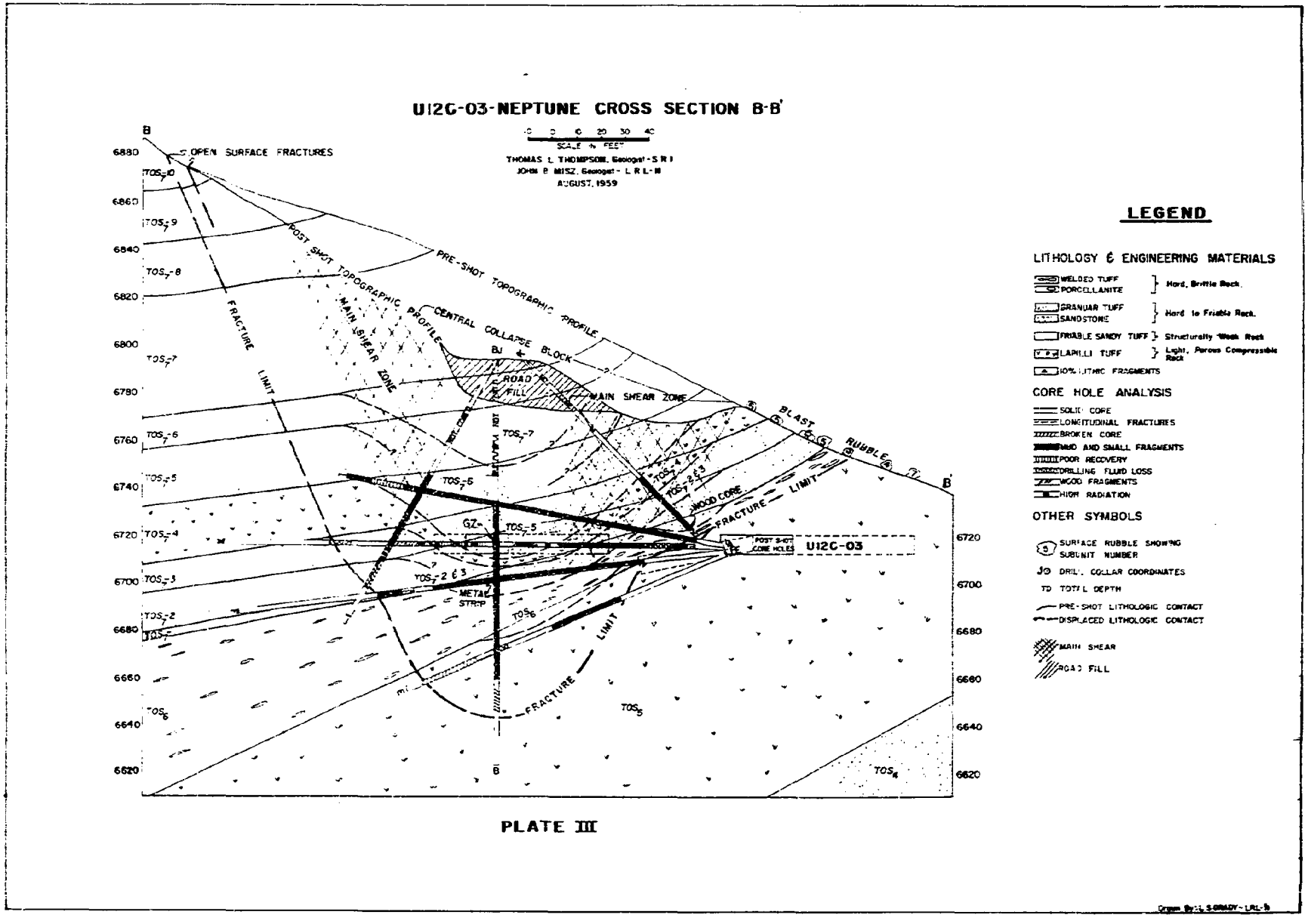


PLATE III

Figure 5.42.

CHAPTER V

REFERENCES

1. Nadai, A., Theory of Flow and Fracture of Solids, McGraw-Hill, 1950.

2. Isaacson, E. de St. Q., Rock Pressure in Mines, Mining Publications, Ltd., 1958.

3. Balmer, G., A General Analytic Solution for Mohr's Envelope, ASTM Proceedings, Vol. 52, pp. 1260-1271, 1952.

4. Balmer, G., Physical Properties of Some Typical Foundation Rocks, Concrete Laboratory Report No. SP-39, Bureau of Reclamation, August 1953.

5. Orowan, E., Fracture and Strength of Solids, Reports on Progress in Physics, Vol. XII, 1948-1949, pp. 185-232.

6. Griffith, A.A., The Phenomena of Rupture and Flow in Solids, Phil. Trans. Roy. Soc. London, A, Vol. 221, pp. 163, 1921.

7. Inglis, C.E., Stresses in a Plate Due to the Presence of Cracks and Sharp Corners, Trans. Inst. Naval Architects, London, Vol. LV, pt. I, pp. 219, 1913.

8. Griffith, A.A., Theory of Rupture, First International Congress of Applied Mechanics (Delft), Vol. 55, 1924.

9. Clausing, D.P., Comparison of Griffith's Theory with Mohr's Failure Criteria, Quarterly of Colorado School of Mines, Vol. 54, July 1959.

10. Morrison, R.G.K., A Theory of Rockbursts, So. African Mining Jl., Vol. 63, 43-45, 1952.

11. Hodgson, E.A., Velocity of Elastic Waves, Bull. Seism. Soc. of Am., Vol. 32, October 1942.

12. Leet, D.L., Vibration Studies - Blasting and Rock Bursts, Trans. CIM, Vol. 54, 1951.

13. Roux, A.F.A. and Denkhaus, H.G., An Investigation Into the Problem of Rockbursts, Jl. Chem. M & M Soc. South Africa, Vol. 55, pp. 103-124, November 1954.

14. Duvall, W.I. and Atchison, T.C., Rock Breakage by Explosives, U.S. Bureau of Mines, RI 5356, 1957.

15. Bullock, R.L., Experimentation With Shatter-Cut Rounds, Univ. of Mo. School of Mines and Metallurgy Technical Series No. 95, Third Annual Symposium on Mining Research, 1957.

REFERENCES (cont.)

16. Colorado School of Mines, Underground Explosion Test Program, Series I and Series II Experiments, December 1948.

17. Mason, R.M. and Crossley, C.H., Hasty and Deliberate Tunnel Demolition Tests Conducted Near Senic, Washington, and Maupin and Madras, Oregon, ERDL Report 1408, 1 June 1955.

18. Clark, G.B., and Caudle, R.D., Brittle Fracture of Small Short Rock Beams Under Central Transverse Impact Loading, Fourth Symposium on Rock Mechanics, Penn State U., March 1961.

19. Brode, H.L., Nuclear Burst Phenomena Pertinent to Deep Underground Structures, Protective Construction Symposium, Rand Corp., 1959.

20. Thompson, T.L., and Misz, J.B., Geologic Studies of Underground Nuclear Explosions Rainier and Neptune, UCRL 5757.

21. Warner, S.E., and Violet, C.E., Properties of the Environment of Underground Nuclear Detonations at the Nevada Test Site, UCRL 5542 Rev.

22. Shelton, A.V., et al., The Neptune Event-A Nuclear Explosive Cratering Experiment, UCRL 5766.

23. Johnson, G.W., et al., Underground Nuclear Detonations, UCRL 5626.

24. Nuckolls, J., Computer Calculation of Rainier, Plowshare Symposium, San Francisco, May 13-15, 1959.

CHAPTER VI

STATIC STRESSES AND DESIGN OF OPENINGS

Introduction *

The problem of accurately determining the stresses which exist in massive rocks in the earth's crust has long been of interest to engineers and geologists. Many mining problems are directly concerned with the stresses which may cause mine openings to collapse during the course of their usage. This chapter is concerned with two phases of occurrence of rock stresses: (1) the stresses existing in the rock before the introduction of mine openings, i.e., the free-field stress, and (2) the induced rock stresses due to the introduction of mine openings. The investigation of rock stresses has to the present been largely limited to simple analytical geological structures.

There have been many hypotheses formulated to explain the stressed state of the earth's crust and its causes, but it has been very difficult to measure the free field earth stresses without changing them in the process, and thus invalidating the results. Many reliable qualitative evaluations have been made of the initial earth stresses from observation of the effect of stresses upon mine openings, and upon geologic structures.

General practice has been for the design of mine structures (width, height, and contour of mine openings, and the size and shape of pillars) to be determined upon an empirical basis because (1) the effects of making an underground mine opening upon the pre-existing stresses within the surrounding rock were not known, (2) the concepts of pre-existing stresses has been expressed in an inexact manner, and (3) the varying effects of complex geologic conditions are not subject to exact analysis. Thus, mine structures have been designed from formulae for which there is no complete theoretical foundation (except whether they succeed or fail). To insure the stability of the mine structures designed in this manner, it has been necessary to apply large safety factors. Research concerned with the stresses around mine openings may be classified in three general categories: (1) theoretical studies of a purely mathematical character, (2) studies of models intended to duplicate the stress conditions existing in the prototype mine opening, and (3) observation and measurement of the stress conditions in an actual mine opening.

Theoretical studies differ widely in the basic assumptions made about the physical properties of the rock. Some solutions of problems in underground stress analysis assume that rock is elastic, homogeneous, and isotropic in character; others assume that rock possesses plastic, viscous, elastic-viscous properties, or a combination of them. There have been some trends toward the application of soil mechanics to underground mining problems. As yet, there has not been conclusive evidence presented to indicate which of the particular methods of solution has the greatest applicability.

---

* pp. 6.1 to 6.52 condensed from Ref. 20.

Experimentation with full-scale rock structures such as those which are found in underground mine openings has, with few exceptions, proven too impractical and too costly to be worthwhile. If exact results are to be obtained, it is more economical to conduct tests in a laboratory where conditions can be closely controlled. Inasmuch as full-scale models of mine structures cannot be constructed in the laboratory, however, the most feasible approach to the problem is to resort to the use of small scale models. In general, model studies are divided into two categories, those involving photoelastic principles, and those concerned with testing models made of rock from the prototype. The stress concentrations which are found by means of polarized light are then compared with those in the prototype. In the second method, models made of rock from the prototype are stressed in a manner which will give an approximation of the stresses applied to the prototype; the stresses developed within the model are measured with strain gages, or the model is stressed to the failure point. Several methods of applying stress to a rock model have been attempted. One of the most successful methods has been that of applying a centrifugal force to the model in order to simulate stresses due to the model's own weight.

It should be emphasized that none of the methods for solution of underground stresses explains all stress phenomena observed because of the lack of accurate knowledge of the physical properties of rocks under field conditions, and the great complexity of these conditions due to inhomogeneity of the rock, geologic discontinuities, and many other factors.

Obert, et al.[1], of the Bureau of Mines has discussed a number of the factors involved in the design of openings in competent rock. Their design procedures can be applied not only to the openings created in mining processes, but in tunnels, underground storage chambers for petroleum products, underground air-raid shelters and military protective structures. Design principles are more widely applicable in cases other than mining because a greater latitude of site choice is possible where location of openings is not dictated by the location and environment of a mineral deposit.

The problem of designing a stable underground opening involves two basic elements: (1) the maximum stress in the rock and (2) the strength of the in situ rock. This is true whether the stresses are static in character or are caused by a transient pulse. Even for the most simple cases the stress patterns are complicated by the heterogeneity of the rock, discontinuities and irregularities in both openings and rock structure.

Obert[1] has defined competent rock as that which, because of its physical and geological characteristics, is capable of sustaining an underground opening as walls, roof, pillars, etc., without the use of any substantial type of artificial support. For the purpose of design of openings in competent rock, it is classed as being either massive or bedded. Massive rocks include many igneous rocks and some metamorphic rocks. Bedded rocks are those which have strata whose thickness is small compared to the roof span. Effects of time, including chemical alteration are not evaluated quantitatively. Safety factors of 2 to 4 are usually employed in walls and pillars, and 4 to 8 in

members such as bedded roofs in tension.

Initial Stresses and Stress Concentrations in the Earth's Crust

Several interpretations have been made of the stresses existing underground before a mine opening has been introduced. In general, these stresses are known to be influenced primarily by the weight of the overlying material, the relation of the opening of the rock masses around it (depth of over-burden, etc.), geologic discontinuities (faulting, bedding planes, etc.), the physical characteristics of the surrounding rock, and tectonic forces.

A reasonable hypothesis for the stress fields existing in underground rock before a mine opening has been introduced was proposed by Mindlin in 1939[2]. It is assumed that stresses within the earth at different depths may be approximated by one of three stress fields, as shown in Figure 6.1. They are (1) hydrostatic stresses acting on each unit of the solid, a state of materials at depth probably greater than those now mined, (2) lateral restraint accompanying the application of the gravitational field, an approximation of the forces acting at an intermediate depth within the earth, and (3) no appreciable lateral restraint on a unit of the solid, the state of some materials in the immediate vicinity of the surface. These cases represent the range of variation of earth stresses. The actual stress condition existing underground before a mine opening is introduced generally lies between the two extremes of (1) and (3). For this reason, these three conditions have been widely used in solutions by photoelastic and elastic analytical methods.

From observation of the phenomena which occur in all types of underground mine workings, it is apparent that these three conditions are not always sufficient to account for all possible initial earth stresses. Beyl[3] has pointed out that the effect of overbridging beds and the lateral transmission of stress, which occurs in pulverulent matter, partly relieve the excavations of vertical stress caused by the weight of the rock. In some cases erosion relieves some of the vertical stress while the lateral (tectonic) pressure remains constant. Furthermore, where excavations are made at great depth, lateral pressures are sometimes observed which are higher than would be predicted for that depth. In some areas of uniform horizontal stratification, one can notice traces of horizontal thrusts which are indications of appreciable orogenetic (mountain building) pressure in a horizontal direction. Beyl lists another pressure with a thermic origin. This pressure is multilateral and may be due to the exothermic transformation of peat into lignite and coal, the intrusion of magma, or the occurrence of metamorphism.

Beyl obtained the state of stress in the rock mass at the surface and at depth by the superposition of three fields of pressure: (1) a horizontal force due to orogenetic pressure which is often the largest component, (2) a vertical force resulting from the weight and repre-

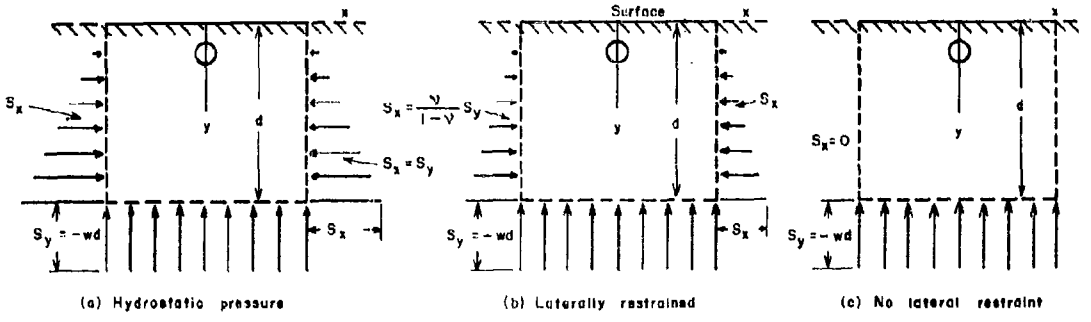


Figure 6.1 Assumed states of stress in the earth at a great distance from any disturbing influence.

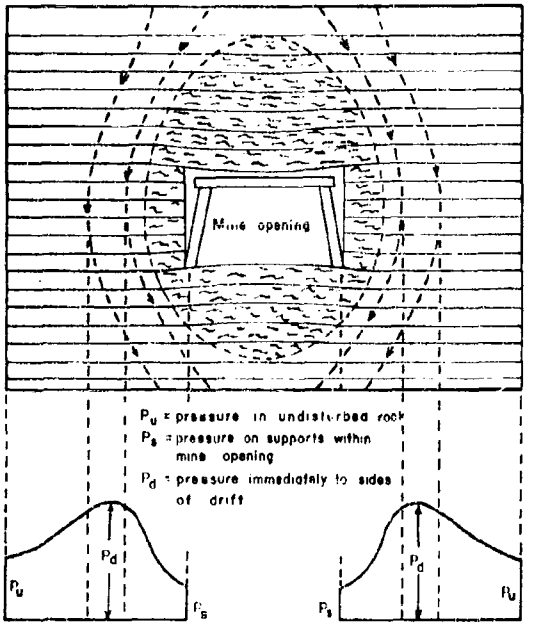


Figure 6.2 Pressure dome and stress trajectories around a drift.

senting part of the weight of overlying deposits, (3) a hydrostatic pressure equal in all directions. He made use of these concepts to explain on a qualitative basis some of the conditions observed in rock formations under high pressures. The solutions based upon these suppositions require a knowledge of the orogenetic pressure and the vertical forces transferred by the layers of rock to lower layers (Beyl's theory of the effect of overbridging beds) which has not been evaluated. For that reason the three conditions postulated by Mindlin which cover most of the static conditions encountered except when lateral pressures are greater than vertical pressures are employed. For this latter case, it is only necessary to superimpose a horizontal stress of the desired magnitude upon the stresses given for the case of no lateral restraint. The primary difficulty is in accurately predicting the required magnitude of the horizontal stress. If a method can be devised for measuring the existing free field stresses in the earth's crust without disturbing them, the possibilities of expressing those stresses mathematically with a reliable degree of accuracy will be greatly increased.

Stresses Around Openings in Solid Homogeneous Materials

The immediate purpose of stress analysis of underground mine structures is essentially twofold: (1) to obtain a concept of the effect of the size and shape of a single mine opening upon the stresses existing initially within the surrounding rock, and (2) to determine the effect of a group of mine openings upon the stresses the size, shape, number, and relative positions of the openings are varied. The ultimate purpose is to apply the results of these analyses to achieve more economical and safe design of underground openings.

Stress analyses of underground mine openings for many simple cases have been performed by mathematical analysis and an analysis of models in the laboratory. These results cannot always be applied directly to obtain quantitative applications for general underground problems because they are solutions of cases which were chosen for the simplicity of the concepts and mathematics involved, and thus their field of application is limited. This is one aspect of stress analysis which necessitates the development of a mode of investigation in which the theoretical and model studies are checked or supplemented by field studies and experimental laboratory work. In this manner, the fullest benefit of the laboratory work as well as the field work may be obtained.

Early Underground Stress Analysis

Early investigators assumed that the rock surrounding mine openings approximated some solvable, fundamental structural unit, primarily because of the manner in which failure was observed to occur at the mine opening. Many investigations were centered upon the observation that a dome-shaped space forms around certain collapsing underground openings. The rock in the top of the original opening failed, leaving a dome-shaped structure or opening which apparently re-established equilibrium[4]. In most instances this attempt to relate underground structures with some known structural unit was only an approximation,

primarily because of the assumption that the rock at some distance from the mine opening had no effect upon the stresses in its immediate vicinity.

During the period 1881 to 1885, two investigators, Fayol and Rizha[5], proposed theories with similar content. These theories were the forerunners of the "dome" theories. The mine opening was assumed to be surrounded by a roughly spherical shell within which the rock was loaded by its own weight. Thus, the rock within the dome collapsed when the pull of gravity exceeded the cohesion with the surrounding rock.

In 1935, the dome theory was extended in an article by Dinsdale[6]. In essence, he assumed an egg-shaped pressure ring surrounding the mine opening, and within this ring the hanging wall was separated from the external rock by shearing action and rested upon the supports within the opening. Figure 6.2 represents a cross-section of the mine opening, illustrating the proposed dome. The conclusions reached by Dinsdale were that the pressure on the immediate ribs and supports within the opening is small in comparison to the stresses a short distance from the sides of the opening. He showed, in a simple static analysis, that the height of the dome increased with depth; thus, the pressure on the supports was proportional to depth. The value of this analysis is doubtful since the basis for the assumptions leading to its solution are subject to question.

A general criticism of the dome theory has been given by Shoemaker[4]. His objections are: (1) the occurrence of the pressure dome itself is assumed but not explained; (2) the theory takes no account of forces outside of the dome acting on the rock within the dome; (3) the magnitude of forces assumed is not sufficient to account for the observed effects; and (4) the theory is based on the assumption that the rock is stressed within its elastic range. (This last assumption can be justified in many cases, however).

Other theories have been presented which treat layers of rock immediately overlying the mine opening as beams loaded by their own weight. These theories have differed only in the manner in which the beams were considered to be restrained and in the manner of their failure. One of the most advanced hypotheses of this type was published by Rice[5] in 1923; he assumed that when failure of the beam occurs inward shearing at the ends causes the formation of a dome-shaped space. The concepts are subject to criticism since the beams were assumed to be loaded only by their own weight, and no consideration was made of an external load on them.

Theoretical research upon the problem of underground mine structures has advanced rapidly in the last twenty years, particularly with the application of the theory of elasticity and photoelasticity to the problem.

Theory of Elasticity Applied to Underground Mine Structures

A solution of the problem of the distribution of stress around a mine opening by the theory of elasticity requires some basic generalizations and assumptions; it involves solving a stress function for the problems which is related to the existing stress conditions by the boundary stresses and stress-strain relationships. The assumptions to affect a solution are (1) the rock is of a homogeneous isotropic nature; (2) the mine opening is approximated by a definite geometrical figure; (3) the mine opening is horizontal throughout its length and very long in comparison to its cross-section; (4) the stresses along the length of the opening are uniform; (5) the underground mine consists of an opening or a series of openings in an infinite or semi-infinite (bounded only by the earth's surface) mass; and (6) the stresses encountered lie within the elastic limits of the materials. These assumptions are necessary both to permit the application of the theory of elasticity to the problem and to simplify the mathematics of the analysis. They usually cause a loss of generality and narrow the field of application of the results, but do give an approximation of the stresses which may be expected under conditions approaching the ideal case. In addition, they form a basis for more advanced theory in which it is not necessary to make such confining assumptions. A justification of these assumptions has been given by several authors. Duvall[7,8] in particular has made a relatively complete study of them.

Photoelasticity Applied to Underground Mine Structures

In the case of simple ideal problems, theoretical analysis is perhaps the most satisfactory since it provides an exact solution. In most instances, however, underground openings do not have simple boundaries. They are often of large number, and so arranged in a manner which is difficult to analyze mathematically. It is in the approximate solution of these more difficult problems that photoelasticity has its best application.

The assumptions in applying the photoelastic method to stresses around mine openings are: (1) those made for the solution by the theory of elasticity, and (2) the postulate that the stresses about a mine opening may be approximated by the stresses about a similarly shaped opening in a plate under the same load as exists on a cross-section of the mine opening. The error involved in making the latter assumption is very negligible for depths greater than about 2.5 times the diameter of the hole, as shown by Panek[9].

Results obtained by use of a photoelastic model serve as a solution for the prototype, because it can be shown mathematically that for a prototype opening at a considerable distance from the surface the prototype is approximately in a state of plane stress. Thus, the model stresses are for practical purposes directly proportional to the corresponding prototype stresses, because the mathematical solution of the two problems is identical if certain negligible terms are omitted. In model and in prototype, the stress distribution depends only upon the shapes of the openings and their orientation in respect

to the applied stresses. Therefore, the scale ratio (ratio of a linear model dimension to the corresponding linear prototype dimension) may be chosen at will. The only requirement is that the model be geometrically similar to its prototype[9].

The photoelastic method is not an exact method of solution, since it is subject to the errors inherent in experimental analysis. It has been shown by Duvall that these errors do not cause a difference from the theoretical value in the simple cases of more than six percent[8].

The primary objective in most early analyses was the determination of the stress distribution around a tunnel or shaft, or in pillars or arches. Only recently has attention been directed toward determination of the stresses in a mine as a unit, that is, the stress concentrations due to a number of underground openings.

Stress Distribution Around a Single Opening

The effect of making openings of different shapes upon the stresses existing in rock masses before the openings are made is of fundamental interest. A series of geometrical shapes has been chosen by various investigators which are relatively simple to solve mathematically and which also approximate certain typical underground openings.

Solutions to these problems have three immediate objectives: (1) to determine the effect of the different shapes upon the stress concentrations at the boundaries of the openings for different states of initial stress in the rock; (2) to determine the shape best suited (smallest stress concentration induced in the surrounding rock) for each of the stress field conditions within the earth; and (3) to determine approximately the stress which exists around actual mine openings.

Circular Openings. A complete work on the stresses existing around a circular tunnel was published by Mindlin in 1939[2]. By means of the theory of elasticity he solved the problem of stresses around a horizontal cylindrical hole of circular cross-section in a semi-infinite elastic solid stressed by gravity. He assumed that stresses within the earth at different depths may be approximated by three states of pressure which existed before the opening was made, as shown in Figure 6.1. The problem is one of mathematical complexity. By introduction of a bi-polar coorinate system[10], it is greatly simplified, and an exact solution of the classical elasticity equations can be obtained. The length of the tunnel is considered to be large in comparison to its diameter. This and the fact that the body force is assumed to be uniform permits the treatment of the problem as one in plane strain.

Panek[9] has made a further development in Mindlin's analysis and its application. The zone of stress caused by the introduction of an opening is confined to a small area about the opening, and the maximum tensile and compressive stresses occur on the boundary of the opening. In general, the back (roof) and floor of the opening are in tension and the ribs (walls) are in compression, with the exception that, when the lateral initial earth pressure is increased to more than about one-half the vertical pressure, the tangential stress on the entire boun-

dary of the opening becomes compressive. The critical tensile stress seldom exceeds in magnitude the vertical pressure and is only slightly affected by the size of opening, but it is highly sensitive to the ratio of lateral to vertical initial pressure. Thus, the value of Poisson's ratio for rock is very important in the intermediate case, since it determines the lateral stress field,

The critical values (on the horizontal and vertical diameters of the circle at the boundary) of the tangential stress are shown in Figure 6.3 for the three different pressure states. In these cases, the vertical stress field is taken to have a magnitude of -1, i.e., it is compressive. There is little change in magnitude of the stress concentration factor for a depth of hole to hole diameter ratio (d/h) of greater than 2.5. This does not mean that the actual stress does not increase with depth but indicates that the stress concentration factor remains constant.

For a hole at a considerable distance from the surface, the size of the opening has little effect upon the critical stresses. The tangential stress is shown as a dimensionless ratio and may be converted to a stress in pounds per square inch by multiplying by 1.2d, where d is depth from the surface in feet. This is equivalent to assuming a specific gravity of 2.77 for the rock encountered in the homogeneous mass.

In his analysis, Panek compared the stresses obtained by Mindlin with stresses for three cases analogous to those solved by Mindlin. The latter were obtained by assuming the circular opening to exist in a plate in a uniform-stress field. The problem becomes one of plane stress rather than plane strain, simplifying it considerably.

The initial stresses, applied to the edges of a plate, are (Figure 6.4):

(a) Uniform compressive stress $S_y = S_x$

(b) Uniform compressive stress S_y; a uniform compressive stress $S_x = \frac{\nu}{1 - \nu} S_y$.

(c) Uniform compressive stress S_y, $S_x = 0$.

The solution of the stresses around a circular opening for these stress fields is accomplished by use of polar coorinates with origin at the center of the opening, and a solution for the radial, tangential and shearing stresses may be obtained for the three cases. The stresses are independent of the size of the hole, and are also independent of the elastic moduli of the material. Figures 6.5 and 6.6 show that the zone of stress concentration is localized in the neighborhood of the opening, that is, within a distance of three radii of the center of the circular opening.

As is the case in the analysis by Mindlin, the critical stresses occur on the edge of the hole on the vertical and horizontal diameters, and they act parallel to the boundary of the hole. Figure 6.7 illustrates the variation in tangential stress around the perimeter of the opening for the three different cases. If it is desired to find the

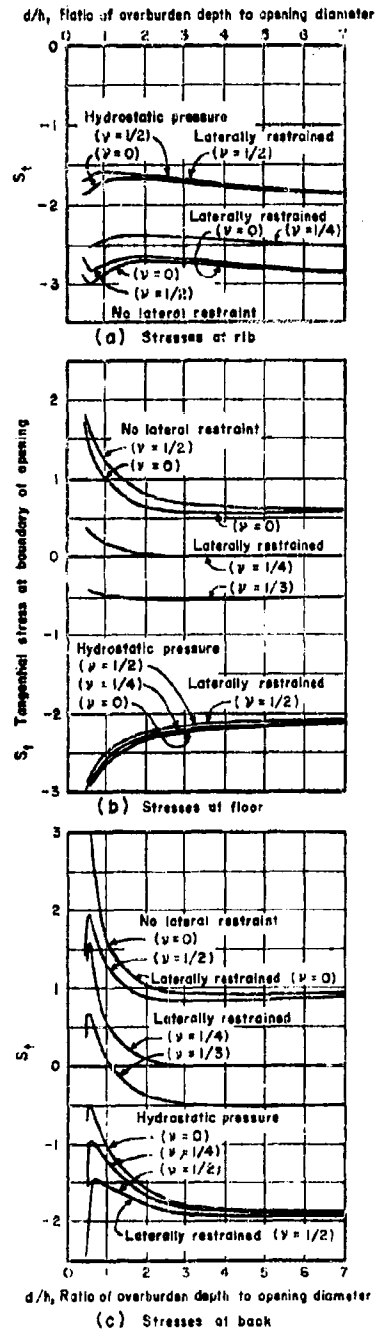


Figure 6.3 Tangential stresses for a circular cylindrical opening in a semi-infinite mass as affected by increasing depth.

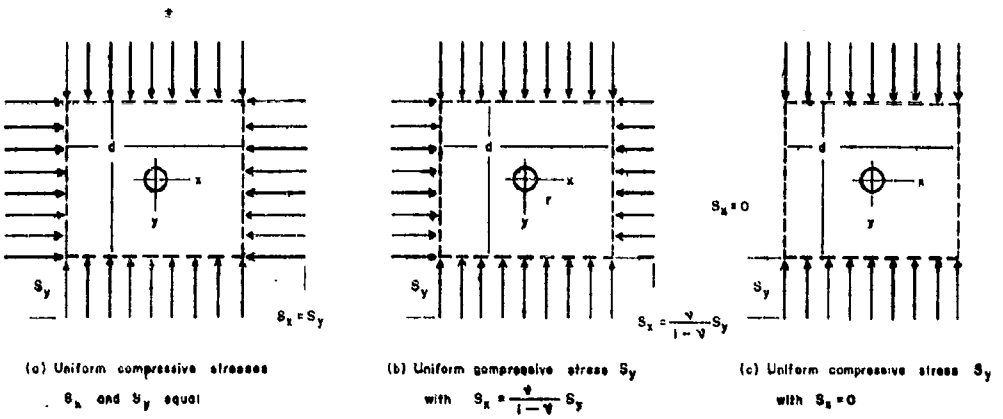


Figure 6.4 Uniform compressive stresses in an infinite plate at a great distance from any disturbing influence.

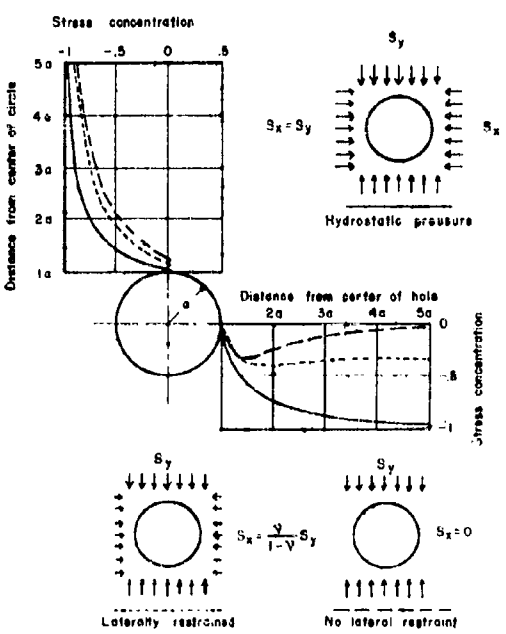


Figure 6.5 Areal distribution of radial stress along the horizontal and vertical axes of symmetry for a circular hole in an infinite plate.

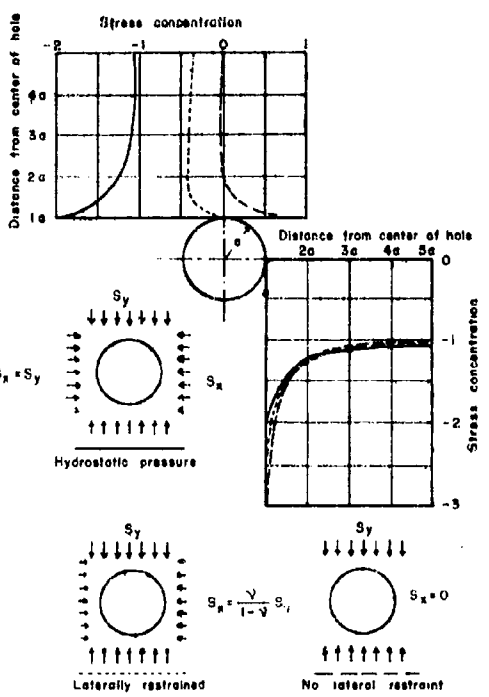


Figure 6.6 Areal distribution of tangential stress along the horizontal and vertical axes of symmetry for a circular hole in an infinite plate.

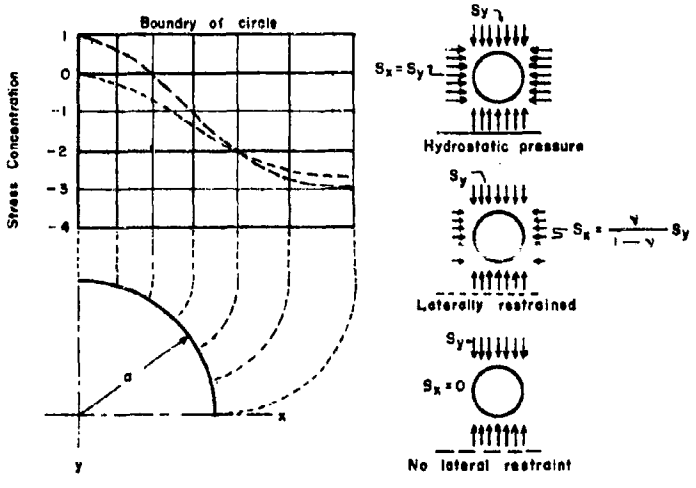


Figure 6.7 Tangential stress concentration on the boundary of a circular opening in an infinite plate.

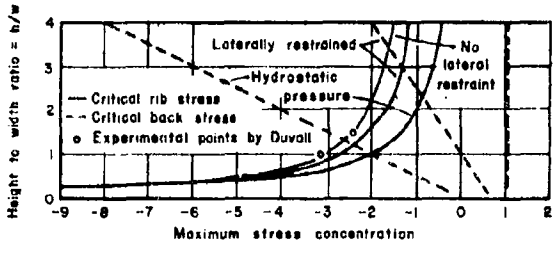


Figure 6.8 Stress concentration on the boundary of an ellipse at the major and minor axes as the height-to-width ratio varies.

shearing stress acting at any point upon the boundary, it is merely one-half the tengential stress. One can show that the maximum shearing stress also varies from point to point, reaching its greatest value on the edge of the opening.

When the opening is far from the surface (for large d/h), the values of the tengential stress for the three respective cases, as determined by Mindlin's analysis, are found to approach the corresponding values as given by Panek for the uniform stress field. Thus, the simpler solution may be used to determine the stress concentration due to a circular opening when it is far from the surface of the rock mass (when the roof of the hole is at a distance below the surface equal to more than twice the hole diameter). This is important because it greatly simplifies the testing of experimental models, such as plastic plate models for photoelastic studies. The use of uniform-stress fields permits the solution of problems, such as the introduction of openings of geometrical shape other than circles, which would be difficult and tedious to solve by the theory of elasticity.

The problem of a circular opening in a uniform stress field has also been solved photoelastically by several investigators, and the results have been found to be comparable to the theoretical results. In most instances, the case of a plate in a vertical uniform stress field with no lateral restraint has been solved, and from this, the other two cases have been obtained by superposition[10]. In addition, numerous problems of more complex nature have been solved by use of circular openings in a plate, using photoelastic methods. An example is the case of a circular opening very close to a free boundary[11].

Elliptical Openings. The problem of stresses around an elliptical opening introduced in a uniform stress field has been solved by C. E. Inglis[12], the solution being effected by the use of curvilinear coordinates. Table 6.1 indicates the values of the critical boundary stresses for ratios of major to minor axes (w/h), for the angle of inclination (δ) of the major axis of the ellipse with a horizontal plane and with the magnitude of the initial horizontal stress (S_x).

A number of important facts may be established from the data given for an elliptical opening: (1) In the case of hydrostatic pressure, critical compressive stress is always on the major axis, being independend of δ, and the entire boundary is in compression. The minimum stress occurs on the minor axis, (2) For a horizontal stress field (S_x) less than the vertical stress field (S_y), the critical compressive stress occurs at the sides of the opening and the critical tensile stress at the top and bottom, (3) For a given S_x and w/h, the critical compressive stress is greatest at δ = 0 deg. and smallest at δ = deg, (4) Critical compressive stress increases linearly with increasing w/h when δ is small.

Some interesting results may be obtained by altering the shape of the ellipse. Starting with a circular shape and elongating the horizontal diameter, the rib compression increases, and the back stress concentration factor becomes more tensile, never exceeding +1, however. Start-

TABLE 6.1[9]

Critical Values of Tangential Stress on an Elliptical Boundary

($S_y = -1$)

w/h	δ	Critical Value of σ_t				
		$S_x = 0$		$S_x = S_y/3$		$S_x = S_y$
1		1.0	-3.0	0	-2.7	-2.0
2	0	1.0	-5.0	0.33	-4.7	-4.0
	22½	1.0	-4.6	0.29	-4.3	-4.0
	45	1.1	-3.7	0.13	-3.5	-4.0
	67½	1.1	-2.5	(-0.25)	-2.4	-4.0
	90	1.0	-2.0	(-0.67)	-1.7	-4.0
3	0	1.0	-7.0	0.44	-6.7	-6.0
	22½	1.1	-6.3	0.43	-6.1	-6.0
	45	1.3	-4.6	0.29	-4.7	-6.0
	67½	1.2	-2.7	(-0.23)	-3.0	-6.0
	90	1.0	-1.7	-1.33	-1.3	-6.0
4	0	1.0	-9.0	0.50	-8.7	-8.0
	22½	1.2	-8.0	0.52	-8.0	-8.0
	45	1.5	-5.8	0.42	-6.1	-8.0
	67½	1.4	-3.0	(-0.14)	-3.7	-8.0
	90	1.0	-1.5	-2.00	(-1.2)	-8.0

Parentheses indicate that the value is not actually a critical one.
w/h = the ratio of the major to minor axis
δ = the angle of inclination of the major axis with the horizontal.

ing with a circular shape and elongating the vertical diameter, the rib compression decreases slightly and the back stress becomes more compressive for most values of S_x (Figure 6.8).

Variation of the lateral pressure S_x has little effect on the critical rib stress, but is a major factor in determining the critical back stress. The critical stresses are at a minimum when the maximum rib stress is equal to the maximum back stress. This is true only when δ = 90 deg., or when w/h = 1 (a circle)[9]. By use of the equation determining the tangential stresses around an elliptical opening, and the fact that the minimum critical stresses occur at δ = 90 deg., it can be shown that the shape of the ellipse for which the critical stresses are a minimum is given by $w/h = S_y S_x$, from which it can be seen that the larger $S_y S_x$ the more elongated the ellipse. When the shape of the ellipse is given by the above formula, the ellipse having its major axis vertical, it can also be shown that the magnitude of minimum critical stress is given by $\sigma = S_y + S_x$, a compression equal to the sum of the initial vertical and horizontal earth pressures.

Ovaloidal Openings. The case of an ovaloid hole in a uniformly loaded plate was investigated by Greenspan[13] first as an ovaloid which was a square with a semi-circle erected on each of two opposite sides. A solution of this problem was obtained by approximating a true ovaloid with a figure which could be represented by a simple set of parametric equations. A plate was considered to be in a state of generalized plane stress, the stress at points remote from the hole having the constant normal components in the horizontal direction $\sigma_x = S_x$ and in the vertical direction $\sigma_y = S_y$; the constant shearing stress was $\tau_{xy} = T_{xy}$. By making use of a curvilinear coorinate system, an equation for the tangential stress about the opening was obtained. As examples of this solution, two complete calculations were obtained, one considering a tension applied to the plate as parallel to the long axis of the ovaloid, and the other considering a tension applied parallel to the short axis as ovaloid. To apply these results to an underground opening it is necessary to compare the solution for the stresses in a plate with an ovaloid-shape hold, which is in a state of plane stress, with that of stresses around a horizontal cylindrical opening with an ovaloid cross-section in a semi-infinite mass, which is in a state of plane strain. This comparison is justified, as the difference in magnitudes of the solutions for plane stress and plane strain is negligible.

By the principle of superposition the results may be added to obtain the stress conditions existing around the ovaloid opening for any of the three basic stress fields. Figure 6.9 illustrates the tangential stress existing around a square with semi-circular ends and with the major axis vertical or horizontal, respectively, for the three states of stress.

Duvall[8] employed the photoelastic method for a series of ovaloidal openings with axes parallel and perpendicular to an applied unidirectional stress field; he determined the maximum stress concentration on the boundary, as well as the stress concentrations at the ends of each axis. (Table 6.2). As the height-to-width ratio decreases, the

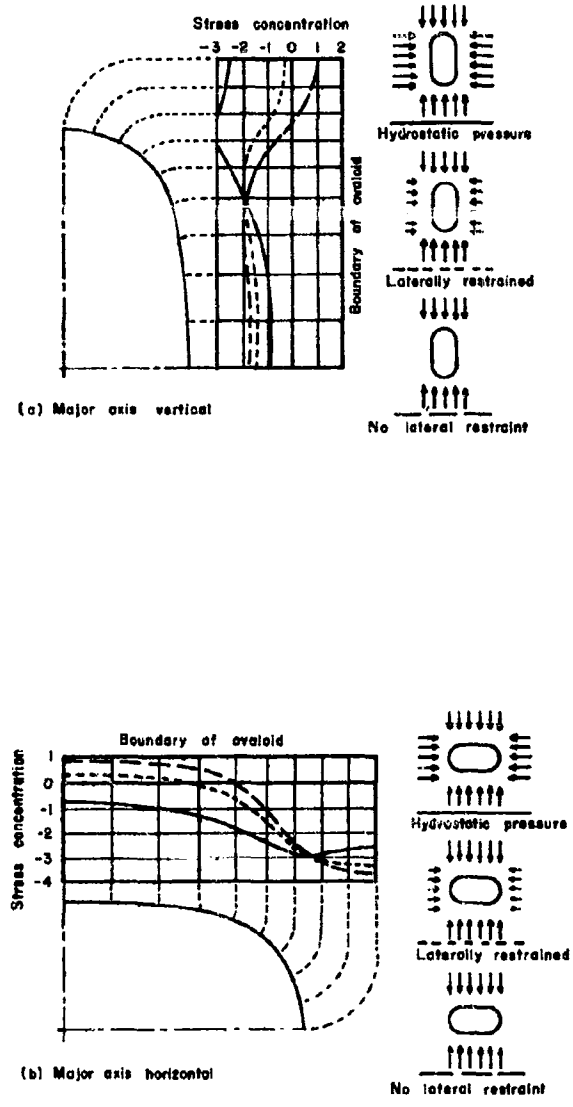


Figure 6.9 Tangential stress concentration on the boundary of an ovaloidal opening (square with semi-circles attached to opposite ends).

TABLE 6.2[7]

Ovaloidal Openings - Unidirectional Stress Field

Height of Opening h (in.)	Width of Opening w (in.)	Ratio of h/w	Stress Concentration at End of Vertical Axis	at End of Horizontal Axis	Maximum
0.388	1.504	0.258	-0.93	5.35	5.35
.389	1.141	.341	-1.07	4.75	4.75
.764	1.500	.509	-1.01	4.14	4.14
.389	.761	.512	-0.92	4.02	4.02
.391	.391	1.000	-1.09	3.17	3.17
.767	.767	1.000	-1.14	3.05	3.05
1.511	.764	1.98	-1.20	1.90	2.64
2.262	.765	2.96	-1.17	1.72	2.40
2.512	.765	3.29	-1.28	1.6	2.35
3.015	.765	3.94	-1.17	1.65	2.33

TABLE 6.3[7]

Stress Concentration for Ovaloids - Hydrostatic Stress Field

Ratio of Minor Axis to Major Axis	Stress Concentration* at End of Major Axis	at End of Minor Axis
1.00	2.10	2.10
1.00	1.98	1.98
.51	2.95	.83
.34	3.68	.65
.257	4.28	.58

* Computed from unidirectional stress field data.

maximum stress concentration increases without limit. (See Figure 6.10). The experimental points were obtained by means of the photoelastic method.

The relation between the height-to-width ratio and the stress concentration on the horizontal axis of an ovaloid at its boundary is given in Figure 6.11, as compared to corresponding data for an elliptical opening. From a comparison of Figures 6.10 and 6.11, it can be seen that the maximum stress concentration at the boundary of an ovaloid does not necessarily exist on the horizontal axis of the ovaloid, and may differ considerably from the stress concentration on the horizontal axis. The stress concentration produced on the ends of the vertical axis of an ovaloid in a unidirectional stress field is approximately equal in magnitude, but opposite in sign, to the applied stress field and is practically independent of the height-to-width ratio. From data obtained for ovaloidal openings in thin plates subjected to a unidirectional stress field, the boundary stresses for a hydrostatic stress field are obtained by algebraic addition of stresses. Table 6.3 indicates the stress concentration at the ends of the major and minor axes of an ovaloid in a hydrostatic stress field. The stress concentrations are compressive at the ends of both axes of the ovaloid regardless of the major to minor axis ratio. As the major to minor axis ratio increases, the stress concentration at the end of the major axis increases, and that at the end of the minor axis decreases in a like manner.

Rectangular Openings. Studies have been made of the influence of a rectangular opening with a short dimension h, a long dimension w, and a small fillet of radius of curvature r at the corners upon the stresses in a plate[8] subjected to the three aforementioned states of stress. Panek[9] and Duvall[8] have furnished considerable information, largely from photoelastic experiments, about the stress concentrations existing around rectangles with dimensions of varying proportions. Interest lies primarily in the effects upon the maximum stress concentration of varying the long-to-short dimension ratio (w/h), the radius of curvature-to-short dimension ratio (r/h) or the angle δ which the long dimension w makes with the horizontal.

Consider an opening of rectangular cross-section in a plate in a two-dimensional stress field, where S_y is the applied vertical stress and S_x is the applied horizontal stress. S_x is permitted to possess all values between zero and S_y. For small S_x/S_y there will be a tensile boundary tangential stress on the top and bottom of the opening. With the major dimension of the rectangle horizontal, the critical tensile stress occurs at the center of the back and floor. As the angle of the major dimension of the rectangle with the horizontal increases, the critical compressive stress moves from the intersection of the fillets with the vertical sides to the lateral fillets, and the critical tensile stress shifts to the highest and lowest both occurring at or close to the ribs. After a 90 deg. rotation, the critical stresses are again tensile at the center of the top and bottom and compressive at the ribs near the fillets.

For values of S_x near zero (no lateral restraint) and between 30 and 80 deg., the critical tensile stress becomes excessively high; under other conditions it does not exceed +1. The value of the critical tensile stress is sensitive to the value of S_x, decreasing as the

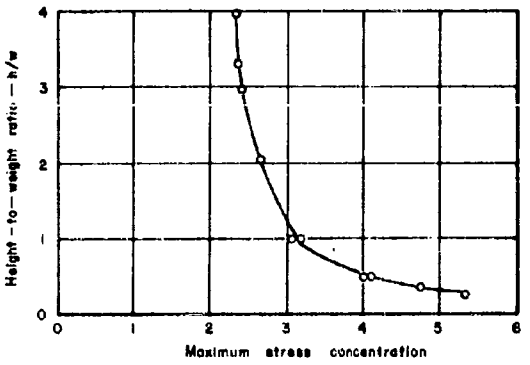


Figure 6.10 Maximum stress concentration as a function of height-to-width ratio for ovaloidal opening - unidirectional stress field.

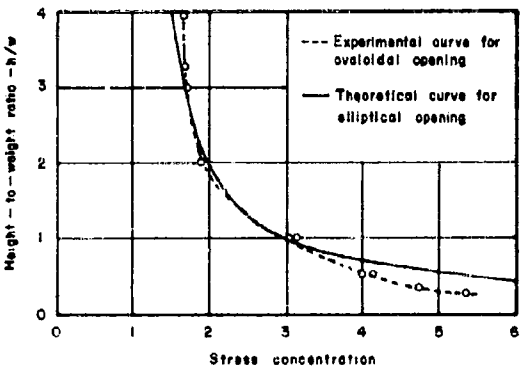


Figure 6.11 Stress concentration at end of axis perpendicular to the direction of applied stress as a function of height-to-width ratio - unidirectional stress field.

ratio of S_x/S_y increases. For values of S_x greater than $S_y/2$, the stress on the boundary of the rectangle becomes wholly compressive in nature. The critical compressive stress increases linearly with increasing w/h, and is not altered to any extent by increase in the lateral pressure for small values of δ. For values of δ less than 80 deg., the critical tensile stress decreases slightly with an increase in w/h.

Figure 6.12 gives the relation between the maximum stress concentration and the height-to-width ratio (h/w) for a rectangular opening in a plate placed in a unidirectional stress field. The maximum stress concentration increases without limit as h/w decreases, but the rate of increase is not as great as for ovaloidal or elliptical openings. As the fillet radius decreases from r/h = 1/4 to r/h = 1/12, the critical compressive stress increases; the stress at r/h = 1/12 is only 1.5 times greater than for r/h = 1/4. The smaller the radius of curvature of the fillet, the nearer the critical compressive stress is located toward the center of the fillet.

The tangential boundary stresses occurring on the perimeter of a square (a special case of a rectangle) for the three types of initial stress, were also developed by Greenspan[13], (Figure 6.13). The maximum compressive stress on the boundary occurs at the filleted corner, and for hydrostatic pressure the maximum stress concentration has a value of 4.57 as compared to 1.0 for a circle under the same conditions. As the applied horizontal stress decreases, the roof stress becomes more tensile but is never greater than about +0.8.

Summary

In order to apply the results obtained to long single openings in underground mines where the rock formations approach being a homogeneous elastic medium, it is necessary to compare the stress concentrations for the different shapes of opening for each of the three states of rock pressure.

No Lateral Restraint. For an opening introduced in a unidirectional force field (no lateral restraint), two important facts can be determined. (1) To reduce the maximum stress concentration around an opening having a height-to-width ratio greater than unity, the opening should approximate an ellipse. (2) To reduce the maximum stress concentration around an opening having height-to-width ratio less than unity, the opening should approximate a rectangle with rounded corners. Figure 6.14 gives a comparison of stress concentrations for different shape openings in a unidirectional field. Stress concentration decreases with an increase in h/w. It is observed that when h/w = 1, an ellipse becomes a circle and a rectangle becomes a square. A rectangle with r/h = ½ is an ovaloid; and when h/w = 1, this also becomes a circle. Figure 6.15 illustrates the shape of opening which is most favorable for a given condition of major-to-minor axis ratio and angle of inclination (δ) of the major axis with the horizontal where $S_y = -1$ and $S_x = S_y/3$ (σ_t for $S_x = 0$ differs very little from σ_t for $S_x = S_y/3$). This conclusion agrees with that obtained from Figure 6.14.

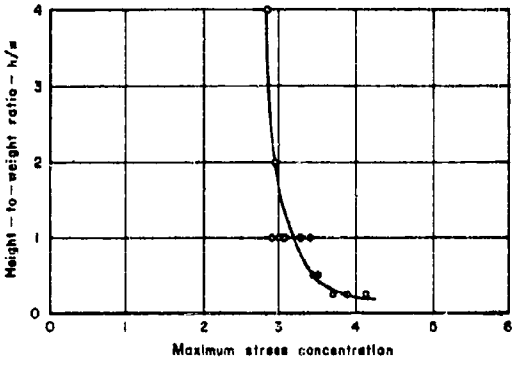


Figure 6.12 Maximum stress concentration as a function of height-to-width ratio for rectangular openings having slightly rounded corners - unidirectional stress field.

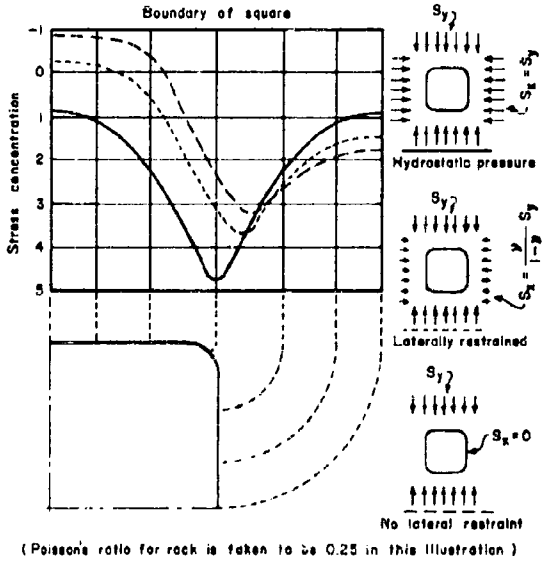


Figure 6.13 Tangential stress concentration on the boundary of a square opening in an infinite plate for the three initial states of stress.

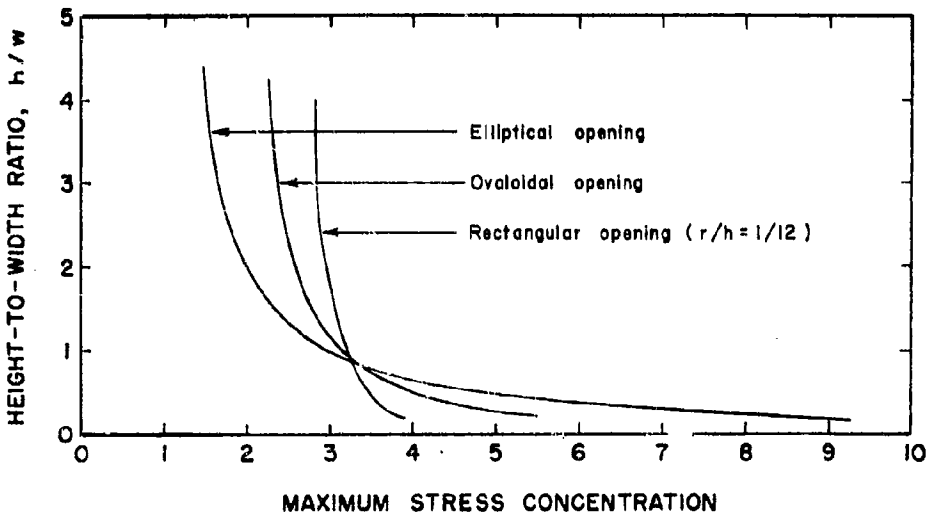


Figure 6.14 Effect of shape of opening on maximum stress concentration - unidirectional stress field.

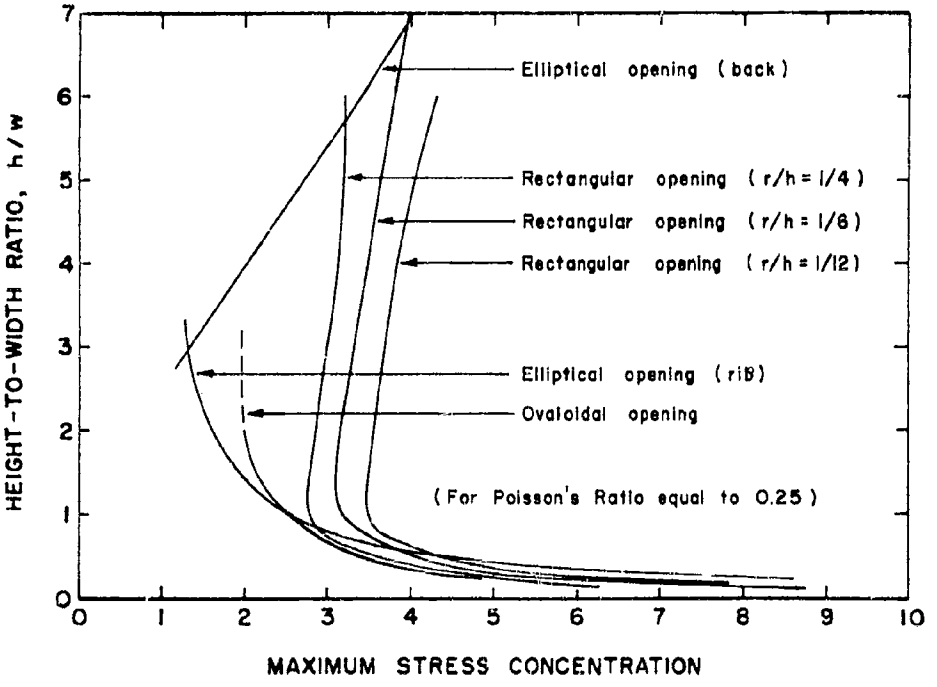


Figure 6.15 Comparison of critical compressive tangential stress for rectangles and ellipse.

The two important factors that cause high stress concentrations around openings in a unidirectional stress field are a height-to-width ratio less than unity and sharp corners on the horizontal axis of the hole. The maximum stress concentration is related to the maximum compressive stress which exists in the vicinity of the opening, in general found in some portion of the immediate ribs. It is necessary to choose a shape of opening such that the compressive stresses induced are not sufficient to cause crushing of the ribs or other type of failure of the opening such as shearing.

A stress concentration occurs at the middle of the back and floor which is tensile in nature. It is approximately equal in magnitude to the initial verticle pressure for the different shapes of openings. This stress may cause roof failures in many instances where the strength of the roof as a unit is less than the tensile stress concentration. In the choice of openings, the shape which induces the least critical compressive stress is usually preferred for design purposes. This choice is based not only on the qualification that the critical compressive stresses be minimized, but also on the fact that the shape which induces the least critical compressive stress generally induces the least critical tensile stress. The least critical compressive stress induced by an opening in a unidirectional stress field occurs in the case of an ellipse with h/w greater than 5.

Laterally Restrained. In choosing the most desirable shape of opening for a laterally restrained plate in a uniform stress field, we assume that $S_x = S_y/3$. This is equivalent to assuming that $\nu = 0.25$ for the rock in the vicinity of the hole, since $S_x = \frac{\nu}{1 - \nu} S_y$ in the case of a laterally restrained plate. The tangential stress pattern around an opening is a laterally restrained plate does not differ greatly from the tangential stress for a plate without lateral restraint, but the magnitude of the tensile stress is decreased markedly.

The trends of the critical compressive stress with the height-to-width ratios are plotted in Figure 6.15. Ovaloids (rectangles where $r/h = \frac{1}{2}$) have not been included. It can be seen by interpolation, noting that an ellipse and ovaloid are equivalent when $w = h$, that for height-to-width ratios less than about 1, the ovaloids (rectangles with maximum radius fillets) are the preferred shape. For h/w between 1 and 4, the most favorable shape is that of an ellipse. For h/w greater than 4, ovaloids are again the most favorable shape. The lowest possible critical compressive stress is induced by an ellipse $h/w = 3$.

Hydrostatic Pressure. Under conditions of hydrostatic pressure the ovaloid induces the smallest critical stress throughout the ranges of h/w considered. Next best shapes are an ellipse for h/w less than 2, and a rectangle with large radius fillet for h/w greater than 2 (Figure 6.16). The least possible critical compressive stress is induced by an opening of circular cross section.

Stress Distribution around Multiple Openings

Often openings may occur sufficiently close together that the introduction of one opening affects the stress concentrations around

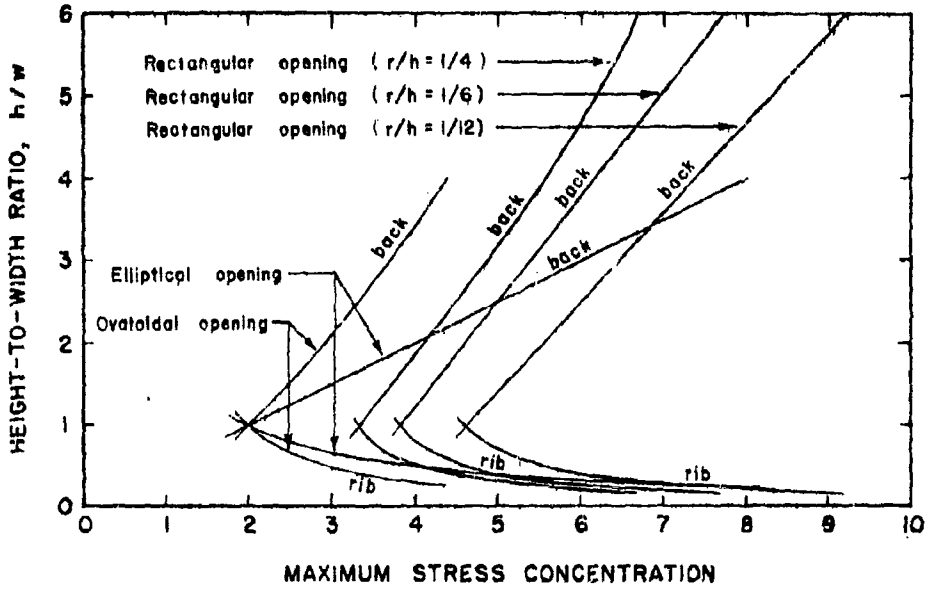


Figure 6.16 Comparison of critical compressive tangential stress for rectangles and ellipse under conditions of hydrostatic pressure.

another. This condition is of primary importance, because stress concentrations are increased when two or more openings are in close proximity. In the case of multiple openings, interest is again centered upon the points of maximum stress concentration, as well as the stress distribution in pillars formed by two or more openings, the relationships between stress concentrations, and the size and shape of pillars.

In specific applications to mining operations or protective construction the results from a study of multiple openings may be used to estimate the stress distribution in pillars to show what factors cause high local stresses and how local stresses may be reduced by the proper design of openings. There have been only a few mathematical solutions of the problems of stress distribution around multiple openings. Solving these problems by the theory of elasticity involves very complex equations for the most simple geometric shapes; thus only a few have been made. The photoelastic method, however, lends itself readily to the solution of these problems.

In addition to the simplifying assumption made above the further assumption is made for multiple openings that each pillar is uniform in width and height and is long in comparison to its width and height. In these problems solutions were obtained assuming a condition of plane stress. This produced results which are approximately equal to the actual conditions existing around openings which are in a state of plane strain. (The equations differ only by infinitesmals).

Only two types of stress fields are considered here. They are that of (1) hydrostatic pressure, and (2) no lateral restraint. These two states represent the hypothetical limits of stress expected underground and the stresses existing within the earth where openings are introduced should fall between these extremes.

Circular Openings. The problem of two circular openings and the pillar left between them was solved by Ling[14] analytically. He determined the critical compressive stresses within the pillar (on horizontal diameters at the boundary of the holes). For a ratio of pillar width to opening height P/h = 2, these stresses differ little from those for a single opening. The differences in σ_c between small P/h and large P/h is less than 1 (see Table 6.4). The critical compressive stresses range between -3.26 and -2.99 for the case of no lateral restraint, and between -2.89 and -2.05 for hydrostatic pressures; (S_y -1).

Duvall[8] solved the problem of two circular openings which were placed in a unidirectional stress field supplied perpendicular to the line of centers of the two holes, as indicated in Figure 6.17. The stress concentrations were determined photoelastically at points A, B and C, as the opening-to-pillar width ratio was varied. The stress concentration at position B (pillar rib) proved to be the maximum. The stresses noted at A and B are tangent to the boundary of the opening and are compressive in nature. The stress at position C is tangent to the boundary, equal in magnitude to the applied stress field (S_y), and of opposite sign. An increase in the ratio of opening-to-pillar width causes an increase of stress concentration at A and B. The

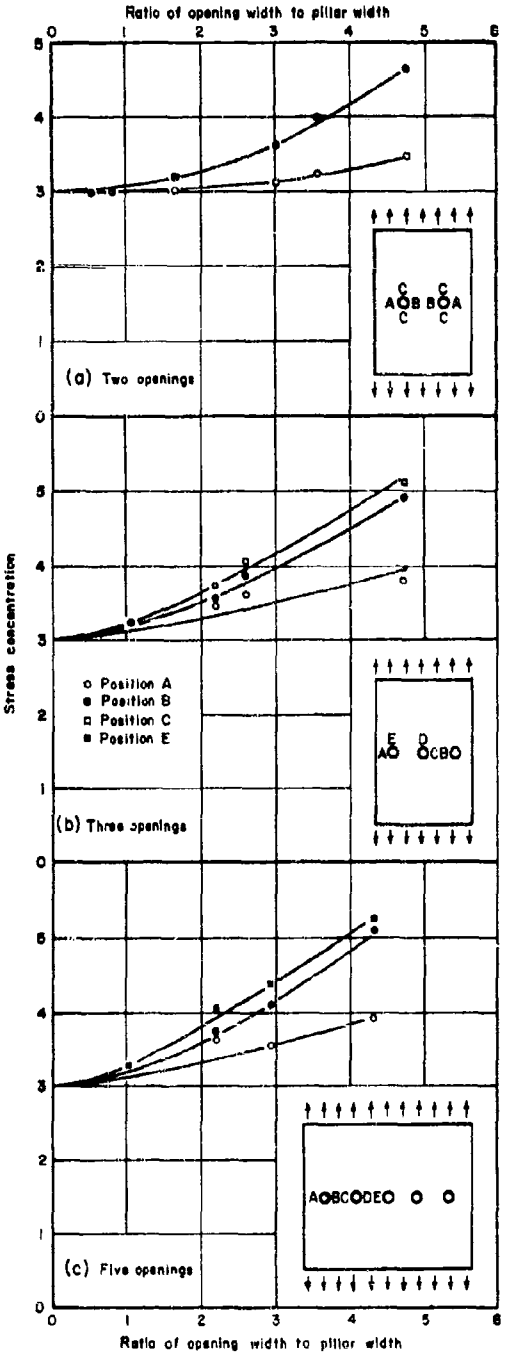


Figure 6.17 Stress concentration as a function of the ratio of opening width to pillar width in an applied stress field perpendicular to line of centers.

TABLE 6.4[9]

Critical Compressive Tangential Stress for a Pair of Circular Holes

(S_y = 1; Solution by Theory of Elasticity)

P/h	Critical S_t	
	$S_x = 0$	$S_x = S_y$
½	-3.26	-2.89
1	-3.02	-2.41
2	-2.99	-2.16
4	-3.00	-2.05

P/h = the ratio of pillar width to opening height. Applied stress field is perpendicular to the line of centers of the holes.

stress concentration is always greater at B than at A, and the rate of increase with greater opening-to-pillar width is also greater at B than at A. Table 6.5 lists the results of photoelastic studies with two circular openings. These results compare favorably with those given by mathematical analysis. In addition, they show that for P/h less than ½, a width of opening-to-pillar width ratio of greater than 2, the stress concentration at the pillar rib increases very rapidly.

The distribution of shear stress in the pillar (Figure 6.18) becomes more nearly uniform as the opening-to-width ratio becomes large. This indicates that for a small pillar formed by two large openings, the average stress in the pillar is almost as large as the maximum stress.

Stress concentrations caused by three circular openings (centers lying on a straight line) were also evaluated by Duvall[8] using photoelastic methods for the condition of no lateral restraint. The stress concentrations were determined at points A, B, C, D and E (see Figure 6.17) as the ratio of opening width to pillar width was varied. Table 6.6 gives the data pertaining to this series. The stress concentration at position C (inner ribs of pillars) is the maximum which occurs within the plate. The stresses at A, B and C have the same sign as the applied stress, and the stresses at D and E have the opposite sign to the applied stress.

Figure 6.17 shows the relationship between the opening-to-pillar width ratio and the stress concentration at positions A, B and C for the three circular openings. The stress concentrations at C are not only largest, but also show the greatest increase with increase in the opening-to-pillar width ratio. Stress concentrations at C range from

TABLE 6.5[8]

Stress Concentration for a Plate Containing Two Circular Openings

(Solution by Photoelasticity)

Ratio of Opening Width to Pillar Width	Stress Concentration at Positions A	B	C
0.530	2.97	2.97	-0.97
.808	3.03	3.03	-0.91
1.66	3.08	3.20	-0.93
3.01	3.13	3.61	-0.96
3.56	3.27	3.97	-1.07
4.74	3.42	4.61	-1.04

Applied stress field is perpendicular to the line of centers of the holes.

TABLE 6.6[8]

Stress Concentration for a Plate Containing Three Circular Openings

(Solution by Photoelasticity)

Ratio of Opening Width to Pillar Width	Stress Concentration at Positions A	B	C	D	E
1.08	3.21	3.21	3.21	-0.81	-1.02
2.22	3.47	3.56	3.74	-0.93	-1.02
2.61	3.60	3.88	4.08	-0.94	-1.02
4.76	3.80	4.92	5.12	-1.05	-1.05

Applied stress field is perpendicular to the line of centers of the holes.

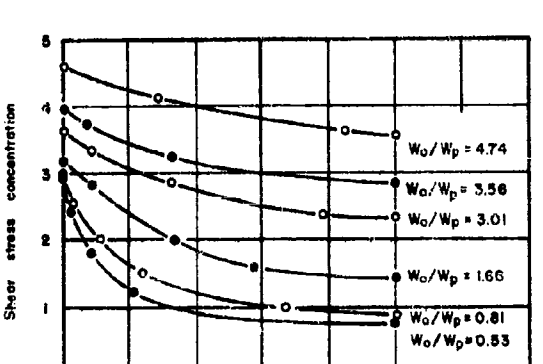


Figure 6.18 Distribution of shear stress in pillar formed by two circular holes - applied stress field perpendicular to line of centers.

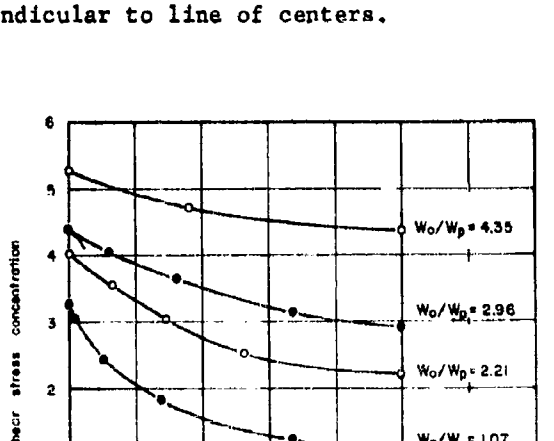


Figure 6.19 Shear stress distribution in central pillars - plate containing five circular openings in an applied stress field perpendicular to line of centers.

3.21 for opening-to-pillar width ratio of 1.08, to 5.12 for opening-to-pillar width ratio of 5.12. This is a sizeable increase over the stresses induced by two circular openings.

Capper[15] also studied by photoelastic methods the problem of three circular holes in a plate subjected to a stress perpendicular to their line of centers. The case of a plate whose edge was at a distance of two radii from the center of the outside hole was investigated. Green[16] solved a similar problem theoretically in which he assumed an infinitely wide plate. Duvall's photoelastic solutions utilized plates where the width was such that the distance from the edge of the plate to the center of the outside hole was equal to or greater than four times the radius of the outside opening. The three solutions are in reasonable agreement if the differences in edge conditions are taken into account.

The case of five circular holes, forming four pillars, (see Figure 6.17) was solved by Duvall[8]. The load was applied perpendicular to the line of centers, and the stress concentrations at positions A, B, C, D and E were determined photoelastically (Table 6.7). The stress concentrations produced on the boundary of the circles at the ends of the diameters perpendicular to the line of centers of the openings are approximately unity; they are of opposite sign to the applied stresses, that is, tension occurs when the applied stress is compression. Figure 6.17 shows the relation between the opening-to-pillar width ratio and the stress concentrations at positions A, B and E. The difference between the stress concentration for positions E, D, C and B is small, but between B and A it is large. Thus for a large number of openings the maximum stress concentrations in all but the outermost pillars is nearly uniform, being less in the pillars near the side walls than in the central pillars.

TABLE 6.7[8]

Stress Concentration for a Plate Containing Five Circular Openings

(Solution by Photoelasticity)

Ratio of Opening Width to Pillar Width	Stress Concentration at Positions				
	A	B	C	D	E
1.07	3.29	3.29	3.29	3.29	3.29
2.21	3.63	3.72	3.89	4.03	4.03
2.96	3.53	4.08	4.22	4.39	4.39
4.35	3.96	5.12	5.22	5.28	5.28

Applied stress field is perpendicular to the line of centers of five holes.

The distribution of shearing stress through the central pillars at the line of centers, Figure 6.19, indicates that the maximum stress concentration produced in the pillars does not increase as rapidly as the average pillar stress with an increase in room-to-pillar width. Therefore the average stress in the pillar is very close to the maximum stress for large ratios of room-to-pillar width.

The theoretical stress distribution was studied by Howland[17] for an infinitely wide plate containing an infinite row of circular holes, the plate being subjected to a uniform stress perpendicular to the lines of centers of the holes (no lateral restraint). Duvall's experimental photoelastic analysis of the stress distribution for five circular holes in a plate with edges a finite distance (4 times the radius of a hole) from the center of the outside hole, which was done under similar conditions, was found to be in close agreement with Howland's theoretical study. Howland found the stress concentration at the end of the horizontal hole diameters to be 3.24 when the ratio of opening width to pillar width was 1.0, and Duvall found that the stress concentration in the center pillars for five openings was 3.29 for opening-to-pillar width ratio of 1.07. This agreement indicates that five circular holes approach the condition of a row of an infinite number of holes in an infinite plate.

By plotting the maximum stress concentration against the number of pillars for a given ratio of opening-to-pillar width (Figure 6.20), it is observed that for five openings the maximum stress concentration in the pillars has reached an asymptotic value and the addition of similar openings would not increase the maximum stress concentration appreciably. The stress concentration in the central pillars (Figure 6.21) for five openings approaches the average stress concentration in the pillars for opening-to-pillar width ratios greater than 4.

Ovaloidal Openings. The stresses around two ovaloidal openings (height-to-width ratio of 0.5) were investigated by Duvall[18]. A load was applied perpendicular to the line of centers of the openings (Figure 6.22) and the stress concentrations produced were measured by means of the photoelastic method. The stress at position C (Table 6.8) is of opposite sign to the applied stress (that is, tension occurs if the applied stress is compression) and is somewhat less than the applied stress. The stresses at positions A and B are of the same sign as the applied stress. The stress concentration at point B is the maximum on the boundary of the openings. The relation between the opening-to-pillar width ratio and the stress concentrations at positions A and B is given in Figure 6.22. For small opening-to-pillar width ratios two circular openings produce a much smaller stress concentration than two ovaloidal openings, whereas for large opening-to-pillar width ratios the stress concentrations are almost the same as for two shapes of opening, although circular openings are still slightly favorable.

With five ovaloidal openings (height-to-width ratio of openings equal to 0.5), the stress concentrations produced were evaluated photoelastically. Figure 6.22 indicates the manner of loading and positions A, B, C, D and E where stress concentrations were determined. The stresses at positions A, B, C, D and E have the same sign as the applied

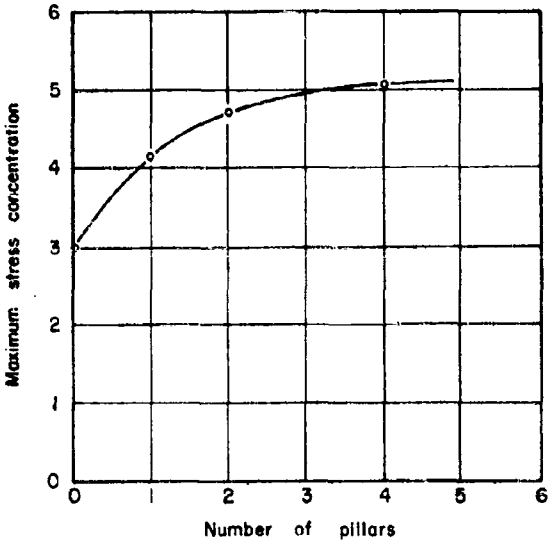


Figure 6.20 Relation between maximum stress concentration and number of pillars for ratio of opening width to pillar width of 4.0.

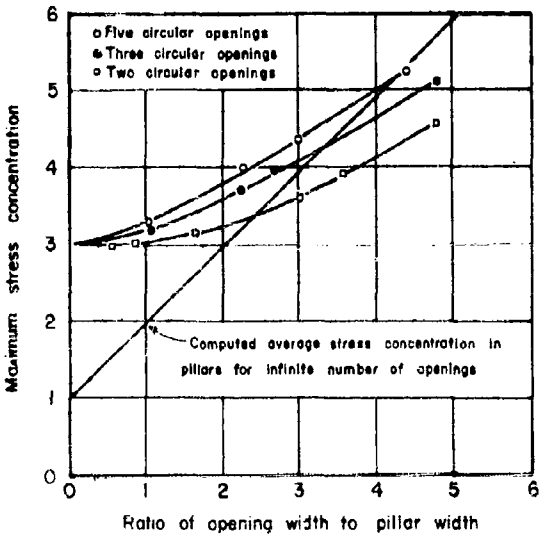


Figure 6.21 Maximum stress concentration in pillar formed by circular openings as a function of the ratio opening width to pillar width in an applied stress field perpendicular to line of centers.

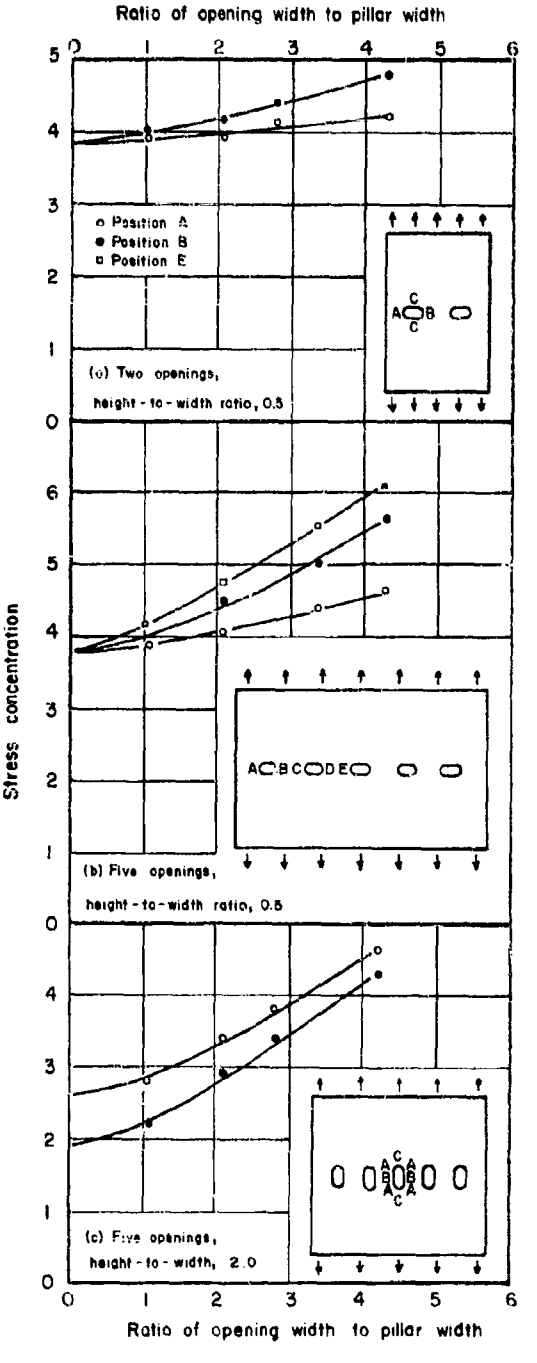


Figure 6.22 Stress concentration as a function of opening width to pillar width ratio in an applied stress field perpendicular to line of centers.

TABLE 6.8[8]

Stress Concentration for a Plate Containing Two Ovaloids

(h/w = 0.5; Solution by Photoelasticity)

Ratio of Opening Width to Pillar Width	Stress Concentration at Position A	B	C
1.01	3.94	4.00	-0.81
2.05	3.94	4.20	-0.73
2.76	4.19	4.43	-0.69
4.27	4.22	4.81	-0.70

Applied stress field is perpendicular to the line of centers of the holes.

TABLE 6.9[8]

Stress Concentration for a Plate Containing Five Ovaloids

(h/w = 0.5; Solution by Photoelasticity)

Ratio of Opening Width to Pillar Width	Stress Concentration at Position A	B	C	D	E
1.03	3.90	3.90	3.90	4.05	4.17
2.09	4.09	4.50	4.61	4.70	4.79
3.40	4.41	5.02	5.40	5.47	5.56
4.28	4.66	5.67	5.93	6.10	6.10

Applied stress field is perpendicular to the line of centers of the holes.

stress (Table 6.9) and the stresses on the boundary at the vertical axis of the opening are of slightly less magnitude and of opposite sign to the applied stress. Figure 6.23 illustrates the relationship between the opening-to-pillar width ratio and the stress concentrations at positions A, B, and E. The values of stress concentrations at positions C and D lie between those of the stress concentrations at B and E and are omitted. The maximum stress concentration occurs at position E, ranging from 4.17 for an opening-to-pillar width ratio of 1.03, to 6.10 for an opening-to-pillar width ratio of 4.28. This is considerably higher than for the case of five circular holes in the same situation.

The shear stress distribution through the central pillars along the line of centers of the openings were determined and plotted as a function of the distance from the edge of the pillar for the different opening-to-pillar width ratios. These curves (Figure 6.23) show that stress distribution in the pillars becomes more nearly uniform as the opening-to-pillar width ratio becomes larger; this was also true of circular openings.

For five ovaloidal openings (height-to-width ratio equal to 2.0), the load was applied as in previous experiments, and the stress concentrations produced at positions A, B and C (Figure 6.22) were determined photoelastically. At position C the stress is of slightly less magnitude than the applied stress, but of opposite sign. The stresses at points A and B are of the same sign as the applied stress. Maximum stress concentration occurs at A. The relations between the stress concentrations and the opening-to-pillar width ratio are shown in Figure 6.22 and in Table 6.10. The stress concentrations for five ovaloidal openings with height-to-width ratio of 2.0 are less than the corresponding stress concentrations for five circular openings when both are in a unidirectional stress field.

TABLE 6.10[8]

Stress Concentration for a Plate Containing Five Ovaloidal Openings

(h/w = 2.0; Solution by Photoelasticity)

Ratio of Opening Width to Pillar Width	Stress Concentration at Position A	B	C
1.04	2.81	2.21	-0.72
2.10	3.41	2.93	-0.84
2.79	3.83	3.41	-0.96
4.20	4.67	4.31	-1.02

Applied stress field is perpendicular to the line of centers of the openings.

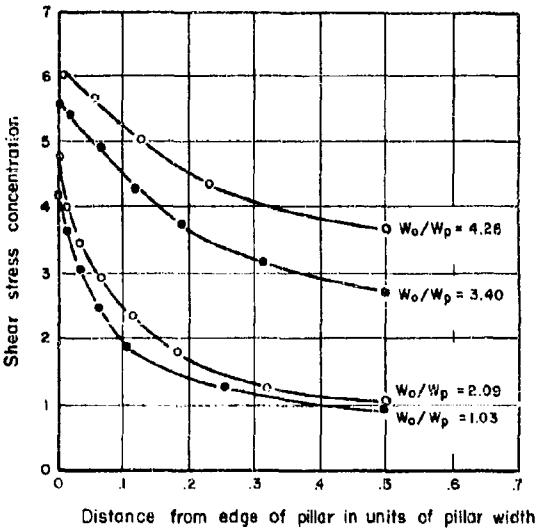


Figure 6.23 Shear stress distribution in central pillars - plate containing five ovaloidal openings (height-to-width ratio = 0.5) in an applied stress field perpendicular to line of centers.

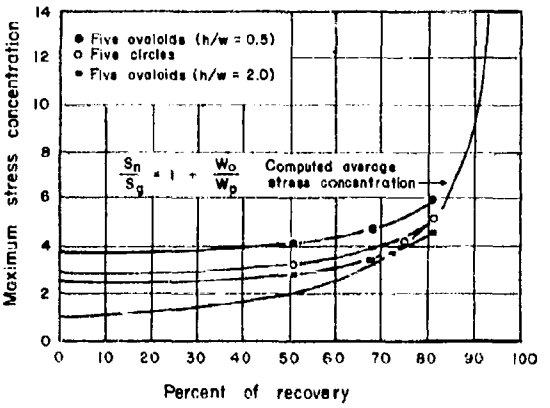


Figure 6.24 Maximum stress concentration as a function of percent of recovery for pillars formed by five openings.

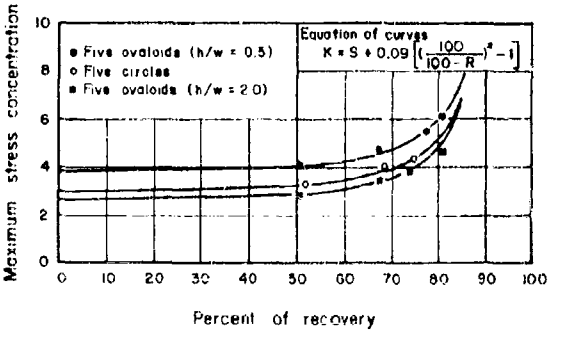


Figure 6.25 Comparison of the empirical equation and the experimental data.

Rectangular Openings. Panek[9] performed an extensive series of experiments with plates containing two rectangular openings with corner fillets. The ratio of the major to minor axis (R/h), the ratio of the radius of fillets to the minor axis (r/h), the angle of inclination of the major axis with the horizontal (δ), and the ratio of the pillar width to the minor axis (P/h) were all varied to determine their effects upon the stress concentrations around the openings; the photoelastic method was used.

It was found that the pillar width had comparatively little effect on the critical tensile stress. Decreasing the pillar width from P/h = α to P/h = 1 adds a critical compressive stress concentration of about 1.5 to the original stress concentration, when R/h = 3. The greater the value of R/h, the greater the increase in stress. R/h is the most important factor controlling the critical pillar stress when P/h is greater than 1. The stresses in the roof and floor of the openings appear to be little affected by either R/h or P/h. Hence, if the lateral pressure is small and the roof fails in tension, there will be practically no advantage to be gained by decreasing the roof span. Panek observed that the smaller the P/h, the more rapid increase of σ_t with R/h. When P/h is less than 1, the critical stress is influenced at least as much by the pillar width as by the room width; for pillars several times as high as they are wide, P/h is probably more important than R/h. Rectangles with large radius fillets were more satisfactory than those with small radius fillets.

Summary

It has been shown by investigators that the stress concentrations induced by a number of openings are greater than those induced by a single opening of a similar geometrical shape. In general, the stress concentrations increase with the addition of each opening up to about five; then the stress concentrations remain almost constant with the addition of more holes. It can be said that the stress conditions existing in the central pillars approximate those existing in the pillars formed by an infinite number of holes.

As the opening-to-pillar width ratio increases, the average stress concentration in the pillars increases at a faster rate than does the maximum stress concentration. This indicates that the average stress approaches the value of the maximum stress concentration within the pillar. At about 75 percent recovery (removal of material), the stress concentration and average stress within the pillar are nearly equal. In most instances a tensile stress is produced in the roof and floor of the mine openings, approximately of the magnitude of the applied stress. With the application of lateral confining pressures, these tensile stresses diminish very rapidly.

In an ore body, where pillars are all of the same height, the pillars in the center of the stope are indicated (theoretically) as being under more stress than those near the side walls of the stope. The maximum stress concentration in pillars is on or near the rib of the pillar, indicating that failure should occur first at the surface of the pillar.

For a ratio of pillar width to pillar height not less than one, it is more advantageous to decrease the long cross-sectional dimension of the openings rather than to widen the pillars if critical pillar stress is too high. If the ratio of the pillar width to pillar height is less than one, pillar width should be increased and possibly room width decreased if critical pillar stress is too high.

Duvall[8] gives a simple derivation of the stresses existing in the pillars formed by the introduction of an infinite number of holes in a plate of infinite extent. Holes were all of equal size (any geometrical shape), equally spaced. If the plate is stressed perpendicularly to the line of centers of the holes, so that the average stress in the plate at a great distance from the row of holes is S_y, then the load on any one pillar is given by

$$L_p = S_g t(W_o + W_p) \tag{6.1}$$

where

L_p = load supported by one pillar

S_g = average stress in plate at a distance from row of holes

W_o = width of opening

W_p = width of pillar

t = thickness of plate

If a uniform stress distribution in each pillar is assumed so that the average stress within the pillar is given by S_n, then the load on any pillar is given also by

$$L_p = S_n t W_p \tag{6.2}$$

From equations 1 and 2 the following relation can be derived

$$\frac{S_n}{S_g} = 1 + \frac{W_o}{W_p} \tag{6.3}$$

S_n/S_g is the stress concentration for the average stress in the pillars. This is approximately equal to the maximum stress concentration where the ratio of the opening-to-pillar width is large.

Insufficient data were obtained to compare the different shapes of openings for the hydrostatic loading. In the case where the earth stress field is one of no lateral restraint, a comparison of the maximum stress concentration produced in pillars formed by five ovaloids having a height-to-width ratio of 0.5, five ovaloids having a height-to-width ratio of 2.0, and five circles is of value. The maximum stress concentration for each of these three shapes has been plotted as a

function of the percent mined area or percent recovery (excavation) in Figure 6.24. Also shown is a plot of Equation 6.3 which gives the average stress concentration for an infinite number of pillars. Figure 6.24 shows that for less than 50 percent recovery the maximum stress concentration is not greatly affected by the percent recovery, but for recoveries greater than 50 percent the maximum stress concentration increases more rapidly with an increase in the percent excavation. The three curves for the circular and ovaloidal openings are similar in shape; thus the effect of percent recovery upon the change of maximum stress concentration in pillars is independent of the shape of the openings. The order of preference for underground mine openings with regard to stress concentration is (1) ovaloids with height-to-width ratio of 2.0, (2) circles, and (3) ovaloids with height-to-width ratio of 0.5.

From the experimental data contained in Figure 6.24, the following equation may be represented by:[8]

$$K = S + 0.09 \left[\left(\frac{100}{100 - R} \right)^2 - 1 \right] \qquad (6.4)$$

where

K = maximum stress concentration in pillars

S = maximum stress concentration around a simgle opening

R = percent recovery

Equation 6.4 can be made to fit data for openings of many shapes by proper choice of value of the maximum stress concentration. For example, in an unidirectional stress field (no lateral restraint) S = 3.0 for a circle, S = 3.9 for ovaloid having a height-to-width ratio of 0.5, and S = 2.64 for ovaloid having a height-to-width ratio of 2.0. Comparison of the experimental data and results obtained from the empirical equation are given in Figure 6.25. Curves are drawn from the equation; points are from the experimental data.

Equation 6.3 gives good results for percent recoveries greater than 75 percent, but Equation 6.4 gives a better approximation over a wider range.

Stresses in Simple Stratified Roofs

One of the principal difficulties in determining the stress distribution around actual mine openings lies in the evaluation of the effect of complex geologic conditions upon the stresses. In the previous section some solutions for the stress conditions existing around mine workings in solid homogeneous materials stressed within their elastic limit were given. It is apparent, however, that fissures, faults, bedding planes, intrusions, metamorphism of the rock, or any features which destroy the continuous homogeneous nature of the rock, alter the stresses

existing around the openings. Solutions taken from the previous chapter and applied under these conditions would thus be in error because of the discontinuities introduced by these geologic conditions.

In general, the effects of even simple geologic factors are not easily analyzed. The strengthening or weakening effects which they have upon rock and the included openings have not been evaluated quantitatively except for a few field correlations which have been of local nature. There is acute need for widespread field correlations of the different geologic factors to determine the effect of each factor upon the strength of rock and the stresses around underground openings. This would simplify efforts to express the effect of a specific geologic condition upon the local stress quantitatively and upon design criteria.

Some very simple geologic conditions have been approximated by mathematical analysis and in the laboratory and their effect upon the stress distribution around mine openings has been evaluated. One example is the case of mine openings existing in stratified materials which are uninterupted by faults or fissures, and the beds of which are homogeneous in character. Solutions of this problem have been obtained by the use of rock models taken from the site of the actual mine opening, and more recently, solutions for some simple specific cases were obtained using the theory of elasticity.

Centrifugal Testing to Simulate Stresses Occurring in Rock Beams Underground

An examination of Figure 6.2, which was used to illustrate the dome theory, indicates that the immediate roof of the opening, which is rectangular, may be considered as a beam or group of beams in layers loaded by the material above it and by its own weight. The material overlying the roof beams may apply a variable weight to the beam according to its rigidity and other properties. In ideal stratified materials, the immediate roof of a rectangular mine opening may be considered as a beam loaded by the overlying material and restrained between the pillars and the overlying material (the degree of restraint is also dependent upon the amount and character of overlying material).

One method of determining the stresses in these rock beams has been to make small-scale models from the rock and apply a load similar to that applied to the prototype. To be of benefit, it must be possible, by the laws to similitude, to calculate from the model what the results will be in the prototype. Thus, if the scale is one to ten, and the roof of the model to the weight of the prototype is equal to the same amount, all other properties of the two bodies being equivalent, the model will behave like the prototype if the density of effective weight of the model is increased in the same proportion that its linear dimensions are decreased. Bucky[18] published a paper in 1931 in which he described a centrifuge of

his own design which could be used to increase the effective weight of the rock model in the same proportion that its linear dimensions were decreased. A scale model built of the same material as the prototype was rotated in the centrifuge at such a speed that it exerted a force against the end plate of the centrifuge equal to its weight multiplied by the number of times it had been reduced in scale, giving results in the model similar to those in the prototype. The stresses in the model approximate those in the prototype due to a gravitational field if the model is subjected to an acceleration in the centrifuge equal (in units of gravity) inversely to the scale multiplier of the model (stress = force per unit area = density x acceleration x linear dimension). Density is the same constant for both the prototype and the model. The linear measurement has been reduced by the ratio stated previously, so that the acceleration must be increased by the same ratio to keep the stress in model and prototype the same. The number of times the effective weight of the model is increased is called the Model Ratio. The model dimension times the Model Ratio determines the dimension of the prototype that will behave in the same manner as the model being tested.

In order for this to be a successful method of testing, certain desirable characteristics are required of the rock models. These are (1) the model should be an exact scalar representation of the prototype; (2) the rock should be the same material as the prototype; (3) the model should be loaded in the same manner as the prototype; and (4) facilities must be available to observe and record the effects of the loading upon the model. The rock model tested in the centrifuge is loaded as nearly like the prototype as possible, since loads on rock beams due to their own weight and the weight of overlying materials are duplicated to a close approximation in the centrifuge. The specimen in the centrifuge is observed by use of stroboscopic light.

The use of the centrifuge employed by Bucky had certain distinct advantages over other methods of testing: (1) it was a source of information for mine openings stressed to failure; (2) it enabled the user to obtain solutions in a short period of time: (3) it may be applied in principle to many underground problems; and (4) it closely duplicated, in the model, the loading of the prototype. It also appears to have several disadvantages: (1) the grain structure of the rock may have little effect on the stress in the prototype, but the grains are not reduced in the model so that they become larger in relative size and might possibly have some effect upon the stress in the model; (2) rock being heterogeneous in character, it would appear difficult to obtain a specimen of rock for a model which would exhibit the overall properties of the prototype; (3) obtaining the correct amount of restraint at the ends of the beams is a problem, and (4) with the method outlined, it is possible to determine only certain maximum stresses which occur at the time of failure. The overall stress pattern obtainable by other methods is not easily obtained by centrifugal testing, particularly in the elastic range. This is important because a knowledge of the stress concentrations below the elastic limit permits the designing of structures in which stresses are below the elastic limit. Some attempts have been made to rectify this difficulty by using photoelastic models in the centrifuge, but the stresses were difficult to evaluate, due to

the photographic problems involved. A possible source of error in the first centrifuge used by Bucky was the fact that the lever arm of the centrifuge was only 8 to 8-3/4 in. long. For specimens more than a few inches in depth this means that the variation in effective weight of a specimen is considerable over its depth. In the case of a single beam this condition would not lead to difficulty since the error is small, but in the case of multiple beams it appears that larger error might be introduced. The centrifuge later used by Bucky had a 2-foot lever arm so that the variation of centrifugal force over the depth of a beam and its related load is not very large in comparison to the magnitude of the centrifugal forces.

It was found in a series of experiments by Bucky that below a certain thickness the beams failed by tensile fracture of the lower center section, but for greater thickness of beams made of certain types of rock an arch-like piece of rock separated from the center of the beam, leaving the remainder of the beam standing. Bucky explained this latter phenomena as a natural arching of the rock similar to that which occurs underground in the roof of the openings where the stresses are very high.

In general, the procedure was to cut single-beam models from the rock to be tested and run them to failure in the centrifuge. This determines their relative strengths. The beam simulating the prototypes are then tested in the centrifuge and also stressed to failure. It is comparatively simple to determine the load on the model beam simulating the prototype; and utilizing the previously determined strengths, it is possible to determine the maximum length of beam which can be used for a particular load.

A new manner of using the centrifuge has been introduced by the Applied Physics Laboratory of the U.S. Bureau of Mines at College Park, Maryland[19]. Strain gages are attached to the rock beams being tested to determine the actual strain up to the point of failure. This provides a means of determining the stress distribution in a rock model in the centrifuge.

Rock Beams with Three Types of Loads

The problem of stresses in stratified roof rock also lends itself to solution by the theory of elasticity. In the instance where the roof rock is assumed to consist of only a single stratum, the mathematics are not too involved. For a larger number of beams, the solutions become more complex. In the solutions given here, interest was centered around three questions: (1) Is it possible to approximate the stress existing in a rock roof by assuming that the load is equivalent to a uniform load on the top of the beam? (2) Does centrifugal testing give an accurate measurement of the stress within the roof members? (3) Is there enough difference between the stresses obtained by centrifugal testing and by applying a uniform load to warrant the use of a centrifuge? In addition, it was desired to obtain the fundamental concepts necessary to determine the effect of stratified layers over a mine working on the stresses in the mine roof.

Mathematical Analysis of Stresses in Simple Roof Strata

Where the dimensions of flat-lying openings underground are of proper magnitude, the roof may be considered to be composed of a plate. A very close approximation to this can be obtained by assuming that a section of the roof may be considered as a beam. Bucky made this assumption in much of his laboratory testing in the centrifuge, but stressed the beams to failure rather than analyzing the stress distribution on a fundamental basis to compare it with the prototype.

The following analyses were made to show the stress distribution which occurs in simple and restrained beams under the three different conditions which might be encountered underground or in laboratory testing, i.e., (1) uniformly loaded, (2) loaded by own weight, and (3) centrifugally loaded.

Simple Beams

Only in rare instances can the roof of an opening be represented by a simple supported beam. However, the stress analysis of this case serves as a basis for the solution of other problems directly concerned with roof support. The fundamental assumptions made previously for solutions by the theory of elasticity must be made also for the following.

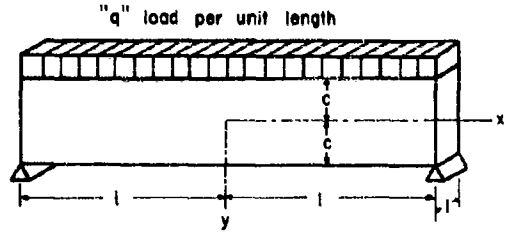
Uniform Load. The solution of the stress distribution in a beam subjected to a uniformly distributed load is treated by Timoshenko[20,21], whose notation is employed herein. It is assumed, together with the assumptions of elastic behavior indicated earlier, that a small rectangular beam can be taken as being representative of a section of a mine roof, that is, a solution in plane stress may be used to closely approximate the condition of plane strain.

Figure 6.26 illustrates the method of loading the beam and the coordinate system used. The stresses in a beam under uniform load are given in Table 6.11.

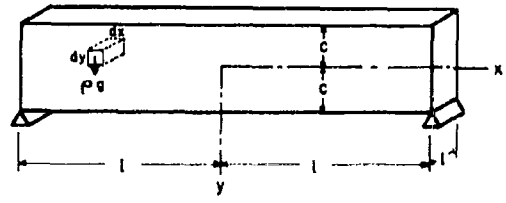
It can be clearly seen that the maximum tensile stress (σ_x) occurs at the midpoint of the beam in the lowermost fibers. It is important to note that both the magnitude and distribution of the stress is independent of the elastic constants of the material.

Loaded by Own Weight. Solutions of the stress distribution in a beam loaded by its own weight (weight per unit volume = ρg) involve the simultaneous solution of the differential equations of equilibrium, and the compatibility equation for plane stress, which must also satisfy the boundary conditions. The equilibrium equations are satisfied if the stresses conform to the equation relating the Airy stress function to the stresses and the Airy differential stress function.

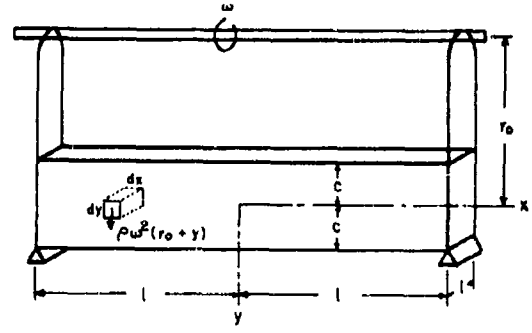
It is interesting to note that the σ_y force is very small, being zero at the bottom and top and also at the center of the beam. In the upper half of the beam σ_y is compressive, and in the bottom of the beam



(a) Uniform load



(b) Loaded by own weight



(c) Centrifugally loaded

Figure 6.26 Simple beams showing method of support, loads and coordinate systems.

TABLE 6.11[20]

Compilation of Stress Equations for Simple Beam Loaded by Three Type Loads

No.	Total Load	σ_x	σ_y	τ_{xy}
1A	Uniform Load	$\sigma_x = \frac{3qy(l^2-x^2)}{4c^3} + \frac{qy}{2c^3}\left(y^2-\frac{3c^2}{5}\right)$	$\sigma_y = \frac{qy}{4c^3}(3c^2-y^2) - \frac{q}{2}$	$\tau_{xy} = -\frac{3qx(c^2-y^2)}{4c^3}$
1B	Loaded by Own Weight	$\sigma_x = \frac{3\rho gy(l^2-x^2)}{2c^2} + \frac{\rho gy}{c^2}\left(y^2-\frac{3c^2}{5}\right)$	$\sigma_y = \frac{\rho gy(c^2-y^2)}{2c^2}$	$\tau_{xy} = -\frac{3\rho gx(c^2-y^2)}{2c^2}$
1C	Centrifugal Loading	$\sigma_x = \frac{3\rho\omega^2\gamma oy(l^2-x^2)}{2c^2} + \frac{\rho\omega^2\gamma oy}{c^2}\left(y^2-\frac{3c^2}{5}\right) + \frac{\nu\rho\omega^2}{2}\left(\frac{c^2}{3}-y^2\right)$	$\sigma_y = \frac{\rho\omega^2}{2}(c^2-y^2)\left(\frac{\gamma oy}{c^2}+1\right)$	$\tau_{xy} = -\frac{3\rho\omega^2\gamma ox(c^2-y^2)}{2c^2}$

σ_y is tensile. Figure 6.26 shows the manner of loading and the coordinate axes.

Centrifugal Loading. The case of a beam loaded centrifugally must be treated in a somewhat different manner to the case of a beam loaded by its own weight due to the fact that the load (body force Y) is a function of y.

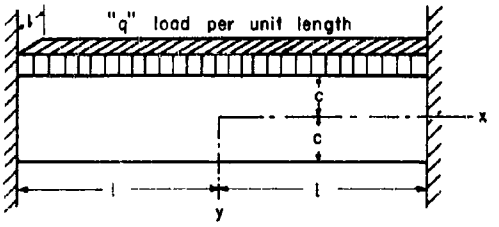
Writing the stresses in terms of the stress function and the body force potential, they can be evaluated at the boundaries, and the equations for stress throughout the body are obtained (Table 6.11).

It can be seen that these equations for stress are quite similar to those obtained for a uniform load and a gravitational load, with the exception of the final term in σ_x. The stress σ_y is found to be very small in comparison to the maximum σ_x, as would be expected.

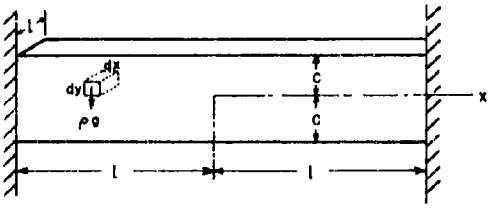
Restrained Beams.

The analysis of simply supported beams provides a basis for the examination of stresses in more complicated beam structures, a beam loaded by the same three types of loads but with restrained ends. This condition occurs over rectangular mine opening in stratified rock if the stresses are not so high that the ends of beams at the pillar are stressed beyond their elastic limit. Beams under thick cover may be thought of as completely restrained, that is, the end of the beam may be considered to lie at the edge of the pillars whereas beams under light cover may be considered to be only partially restrained, that is, the end of the beam lies somewhere over the interior of the pillar. Under some conditions, except for degree of restraint, both beams may be considered fully restrained with the lengths dependent upon the degree of restraint imposed by the overburden (Figure 6.27). The analysis may be made by two different methods. In both, the assumption is made (supported by St. Venant's Principle) that the stress σ_x at the ends of the beam may be replaced by the sum of two stresses -- a uniform normal stress and a stress due to a couple applied to the ends of the beam - without altering stresses from those actually existing in a restrained beam at distances a short distance away from the ends. This is another way of stating that to insure complete restraint a uniform normal stress (r) must be applied to the ends of the beam, so that there is no horizontal movement of the ends. A moment (M) must also be applied so that there is no rotation of the vertical fibers of the beam at the center point of the ends.

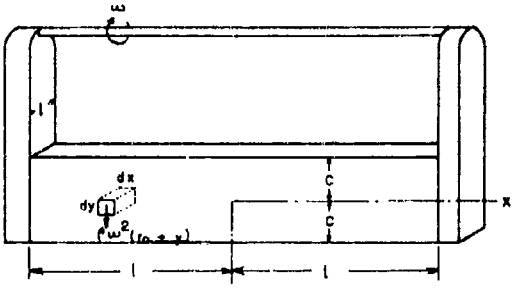
Following the first method, it is then necessary to add the boundary conditions to the boundary conditions for the previous beams and solve for the stress equations in a manner similar to that previously described. The stresses are evaluated at the boundaries, taking account of the two new boundary conditions, and an expression for σ_x involving r and M is determined.



(a) Uniform load



(b) Loaded by own weight



(c) Centrifugally Loaded

Figure 6.27 Restrained beams showing loads, restraints and coordinate systems.

In either method of investigation use of only the stress relationship involves indeterminate values. From a study of elementary stress solutions it is apparent that the only means of solution remaining is one involving strain relationships. Using appropriate strain relationships as properties of restrained beams it is possible to determine the unknowns r and M.

For plane stress differential equations define the strains in terms of the stresses, and are employed to obtain the solution of the problem. Substituting the values of σ_x, σ_y, and τ_{xy} into these equations, and integrating, expressions in u and v containing the terms r and M are obtained. Use is made of the strain relationships referred to previously to determine arbitrary constants of integration and the quantities r and M. The values for r and M when substituted into the stress equations give the results for three different load types shown in Table 6.11.

Summary

It has been previously noted that the stress σ_y induced in simple beams is very small in comparison to the stress σ_x at the center of the beam. The stress σ_y is also independent on the length of the beam.

In order to determine whether the stresses in simple beams loaded by three load types are comparable, the load per unit length of beam was made equal in all three cases. The loads, $2c\rho g$ and $2c\rho r_o\omega^2$, were set equal to the load per unit length q and the equations for the three cases were determined in terms of q, as is shown in Table 6.12. The shearing stresses in all three cases are equal. The σ_x stresses for a uniform load and for a beam loaded by its own weight are found to be the same, but the stress σ_x for the case of centrifugal loading differs from the other two cases by an additional term For beams of normal 1/c ratio, it is seen that this term is negligible in comparison to the other terms, and does not influence the σ_x forces measurably. Therefore, σ_x may be said to be equal for the three cases without introducing any measurable error. This is not true of σ_y, however; σ_y is small in the case of the centrifugal loading and in that of a beam loaded by its own weight, in both cases being only a small fraction of the load per unit length of beam. In the case of a beam loaded by a uniform load, σ_y ranges from a value equal to the load per unit length of beam at the top of the beam to a value of zero stress at the bottom surface of the beam.

The σ_y stresses are not large enough in any of the three cases to be directly responsible for failure of a beam because as the σ_y forces are increased to a critical value the σ_x forces have already exceeded this value because the relationship of the stresses is directly proportional.

In the case of restrained beams, it can be seen that σ_y and τ_{xy} remain the same as in the case of the simple beams (See Table 6.13). The additional terms which have been superimposed upon the original σ_x equations for the simple beams to obtain the σ_x stresses are different for the three different types of loading. To determine the magnitude of this difference it is necessary to assume that the load per unit length

TABLE 6.12[20]

Compilation of Analogous Stress Equations for Simple Beam Loaded by Three Type Loads

No.	Total Load	σ_x	σ_y	τ_{xy}
1A	Uniform Load	$\sigma_x = \frac{3qy}{4c^3}(l^2-x^2) + \frac{qy}{2c^3}\left(y^2 - \frac{3c^2}{5}\right)$	$\sigma_y = \frac{qy}{4c^3}(3c^2-y^2) - \frac{q}{2}$	$\tau_{xy} = -\frac{3qx}{4c^3}(c^2-y^2)$
1B	Loaded by Own Weight	$\sigma_x = \frac{3qy}{4c^3}(l^2-x^2) + \frac{qy}{2c^3}\left(y^2 - \frac{3c^2}{5}\right)$	$\sigma_y = \frac{qy}{4c^3}(c^2-y^2)$	$\tau_{xy} = -\frac{3qx}{4c^3}(c^2-y^2)$
1C**	Centri-fugal Loading	$\sigma_x = \frac{3qy}{4c^3}(l^2-x^2) + \frac{qy}{2c^3}\left(y^2 - \frac{3c^2}{5}\right) + \frac{vq}{4cr_o}\left(\frac{c^2}{3} - y^2\right)$	$\sigma_y = \frac{qy}{4c^3}\left(1+\frac{c^2}{r_o y}\right)(c^2-y^2)$	$\tau_{xy} = -\frac{3qx}{4c^3}(c^2-y^2)$

* Set 2 ρg equal to the load q to obtain a comparison of the magnitude of stresses.

** Set $2\rho r_o \omega^2$ equal to the load q to obtain a comparison of the magnitude of stresses.

TABLE 6.13[20]

Compilation of Stress Equations for Restrained Beam Loaded by Three Type Loads

No.		σ_x	σ_y	τ_{xy}
11A	Uniform Load	$\sigma_x = \frac{3qy}{4c^3}(l^2-x^2) + \frac{qy}{2c^3}\left(y^2-\frac{3c^2}{5}\right) - \frac{qy}{2c}\left(\frac{l^2}{2c} - \frac{3}{5} - \frac{3y}{2}\right)$	$\sigma_y = \frac{qy}{4c^3}(3c^2-y^2) - \frac{q}{2}$	$\tau_{xy} = -\frac{3qx}{4c^3}(c^2-y^2)$
11B	Loaded by Own Weight	$\sigma_x = \frac{3\rho gy}{2c^2}(l^2-x^2) + \frac{\rho gy}{c^2}\left(y^2-\frac{3c^2}{5}\right) - \rho gy\left(\frac{l^2}{c^2} - \frac{3}{5} - \frac{v}{2}\right)$	$\sigma_y = \frac{\rho gy}{2c^2}(c^2-y^2)$	$\tau_{xy} = -\frac{3\rho gx}{2c^2}(c^2-y^2)$
11C	Centri-fugal Loading	$\sigma_x = \frac{3\rho\omega^2 r_o y}{2c^2}(l^2-x^2) + \frac{\rho\omega^2 r_o y}{c^2}\left(y^2-\frac{3c^2}{5}\right) - \frac{v\rho\omega^2}{2}\left(\frac{c^2}{3} - y^2\right) - \rho r_o\omega^2 y\left(\frac{l^2}{c^2} - \frac{3}{5} - \frac{v}{2}\right)$	$\sigma_y = \frac{\rho\omega^2}{2}(c^2-y^2)\left(\frac{r_o y}{c^2} + 1\right)$	$\tau_{xy} = -\frac{3\rho\omega^2 r_o x}{2c^2}(c^2-y^2)$

for each of the three beams is the same, as was done in the case of simple beams. Substituting the values of the centrifugal load and gravitational load equal to the uniform load (per unit length of beam) into the stress equations for the respective beams, the stress equations for the three types of load are obtained considering an equal load on the three beams. These equations are shown in Table 6.14. A beam loaded centrifugally and a beam loaded by its own weight differ in σ_x only in an additional term in the equation for centrifugal loading. This term is so small as to be negligible. Similarly, the σ_y stresses differ in the case of uniform loading from the other two cases by a term, -- q/2.

Thus, it may be stated that the critical stresses within both simple and restrained beams loaded by (1) uniform loads, (2) gravitational loads, or (3) centrifugal loads are essentially the same, with the exception of certain terms of orders which may be neglected without appreciable error. Thus it is possible to approximate the stresses in a roof beam of rock in a mine, either by centrifugal loading or by uniform loading, if it may be considered as a simple beam or a restrained beam, and if the load is due to its own weight or a uniform load, or a combination of the two.

The design of underground structures has been limited by a lack of knowledge of (1) the stresses existing in rock underground before the introduction of an opening, (2) the effect of the introduction of an opening upon the pre-existing rock stresses, (3) the effect of complex geologic conditions, and (4) the physical properties of rock in situ.

Mining experience has shown that the stresses existing within rock underground may generally be thought of as intermediate between the stresses which would exist if there were no lateral restraint and those where hydrostatic pressures are found. In a few exceptional cases, it has been shown that the horizontal pressures may be greater than the vertical pressures, and compensation must be made for this fact.

The effect of introduction of mine and other type openings upon the stresses in rock underground has been solved for some of the simplest geologic conditions - homogeneous, isotropic, elastic material. The opening best suited for an opening (in regard to stress induced) is either (1) a circle, for hydrostatic pressures; (2) an ellipse with ratio of height-to-width equal to 3, for an opening in material which has been laterally restrained; or (3) an ellipse with height-to-width ratio greater than 5, for a mine opening in ground which has no lateral restraint.

In general, mines are composed of numerous adjacent openings underground rather than a single opening. The stresses in the pillars are found to increase with the addition of openings, until about five openings lie parallel to one another. Additional openings have no effect on the critical compressive stress in the pillars. The maximum stress concentration occurs in the centermost pillar on or near the rib of the pillar.

TABLE 6.14[20]

Compilation of Analogous Stress Equations for Restrained Beam Loaded by Three Type Loads

No.	Total Load	σ_x	σ_y	τ_{xy}
11A	Uniform Load	$\sigma_x = \frac{3qy}{4c^3}(l^2-x^2) + \frac{qy}{2c^3}\left(\frac{y^2}{5} - \frac{3c^2}{5}\right) - \frac{qy}{2c}\left(\frac{l^2}{c^2} - \frac{3}{5} - \frac{3v}{2}\right)$	$\sigma_y = \frac{qy}{4c^3}(3c^2-y^2) - \frac{q}{2}$	$\tau_{xy} = -\frac{3qx}{4c^3}(c^2-y^2)$
11B*	Loaded by Own Weight	$\sigma_x = \frac{3qy}{4c^3}(l^2-x^2) - \frac{qy}{2c^3}\left(y^2 - \frac{3c^2}{5}\right) - \frac{qy}{2c}\left(\frac{l^2}{c^2} - \frac{3}{5} - \frac{v}{2}\right)$	$\sigma_y = \frac{qy}{4c^3}(c^2-y^2)$	$\tau_{xy} = -\frac{3qx}{4c^3}(c^2-y^2)$
11C**	Centrifugal Loading	$\sigma_x = \frac{3qy}{4c^3}(l^2-x^2) + \frac{qy}{2c^3}\left(y^2 - \frac{3c^2}{5}\right) + \frac{vq}{4cr_o}\left(\frac{c^2}{3} - y^2\right) - \frac{qy}{2c}\left(\frac{l^2}{c^2} - \frac{3}{5} - \frac{v}{2}\right)$	$\sigma_y = \frac{qy}{4c^3}\left(1 - \frac{c^2}{r_o y}\right)(c^2-y^2)$	$\tau_{xy} = -\frac{3qx}{4c^3}(c^2-y^2)$

* Set $2c\rho g$ equal to the load q to obtain a comparison of the magnitude of stresses.

** Set $2c\rho r_o\omega^2$ equal to the load q to obtain a comparison of the magnitude of stresses.

Design of Openings in Bedded Rock

General

When the length of span of a roof is large compared to its thickness, the length of an opening is more than twice its width and there is no bend between the roof bed and the next above, a section of the roof may be considered as a simple clamped (restrained) beam loaded by its own weight. An inspection of the equation in Table 6.13 shows that σ_y is a maximum at $x = \pm l$, $y = +c$ and t_{xy} is a maximum at $x = \pm y$, $y = 0$. The shear stress is not uniform over the end of the beam. Thus, while the maximum deflection is at the center of the beam, failure would be expected at the ends.

The equations for the above parameters are, neglecting terms made small by large l/c ratios:

$$\Delta y = \frac{\rho g l^4}{128 E\ C^2} \tag{6.5}$$

$$\tau_{max} = \frac{3\rho g l}{8} \tag{6.6}$$

$$\sigma_{max} = \frac{\rho l^2}{4C} \tag{6.7}$$

The conditions set forth by Obert, et al.[21], are:

1. The strata thickness be uniform.
2. Flexure is caused by gravity, i.e., no end thrust.
3. Rock behaves elastically, is isotropic and homogeneous.
4. Ends of strata are "clamped" by superincumbent rock and opening walls.

Single Layer - Beams[22]

For roofs inclined at less than 10 degrees the above equations may be applied for design purposes. It can be seen that the maximum shear stress varies directly as the length of the span, while the maximum tensile stress varies as the square of the span. The ratio of the two is

$$\frac{\sigma_{y\ max}}{\tau_{max}} = \frac{21}{3c} \tag{6.8}$$

Equation 6.7 may be written for design purposes in the following form:

$$L = \sqrt{\frac{2Tt}{\rho g F}} \tag{6.9}$$

where L is the span length (equal to 21), t is the thickness (equal to 2C), T is the modulus of rupture and F is a safety factor. A plot of this equation is given in Figure 6.28 for a density of 0.09 lb/in^3.

Multiple Layer - Beams

The development of design criteria by Merrill[22] and Obert, et al.[21], for multiple layer roofs appears to be in error. In arriving at design equations, the maximum deflection of a thin beam lying upon and loading a thicker beam is equated to the maximum deflection of the thicker beams to obtain an equivalent weight density of the system. Except for beams of equal free deflection the deflections cannot be equated in terms of free beam deflection. That is, if a thin beam lies upon a thicker one, it will deflect less than predicted by the free beam equation, and the deflection of the lower beam will be greater. The equation for a clamped beam is, to a close approximation -

$$\Delta y = \frac{\rho g}{2EL\ bt^2} \cdot x^2\ (2Lx - L^2 - x^2) \qquad (6.10)$$

It can be readily seen that the total deflection of the system will depend upon the interaction of the two beams, which is not defined by the equation above for the maximum deflection (Equation 6.10).

Rectangular Roof - Plate

For comparison a roof may be considered as a plate. The values of maximum deflection and stress from the theory of plates are as follows:

$$\Delta y_{max} = \frac{A\rho g a^4}{Et^2} \qquad (6.11)$$

$$\sigma_{max} = \frac{6B\rho g a^2}{t} \qquad (6.12)$$

where

a = short dimension
b = long dimension
A, B = constants

Values of A and B for various values of b/a and Poisson's ratio equal to 0.3 are given in Table 6.15.

The maximum deflection for a rectangular plate occurs at the center and the maximum tensile stress at the end of the longer dimension in the upper fiber. For ratios of b/a greater than two the maximum stress is within 1 percent of that calculated from the beam formula and the maximum deflection is within 12 percent.

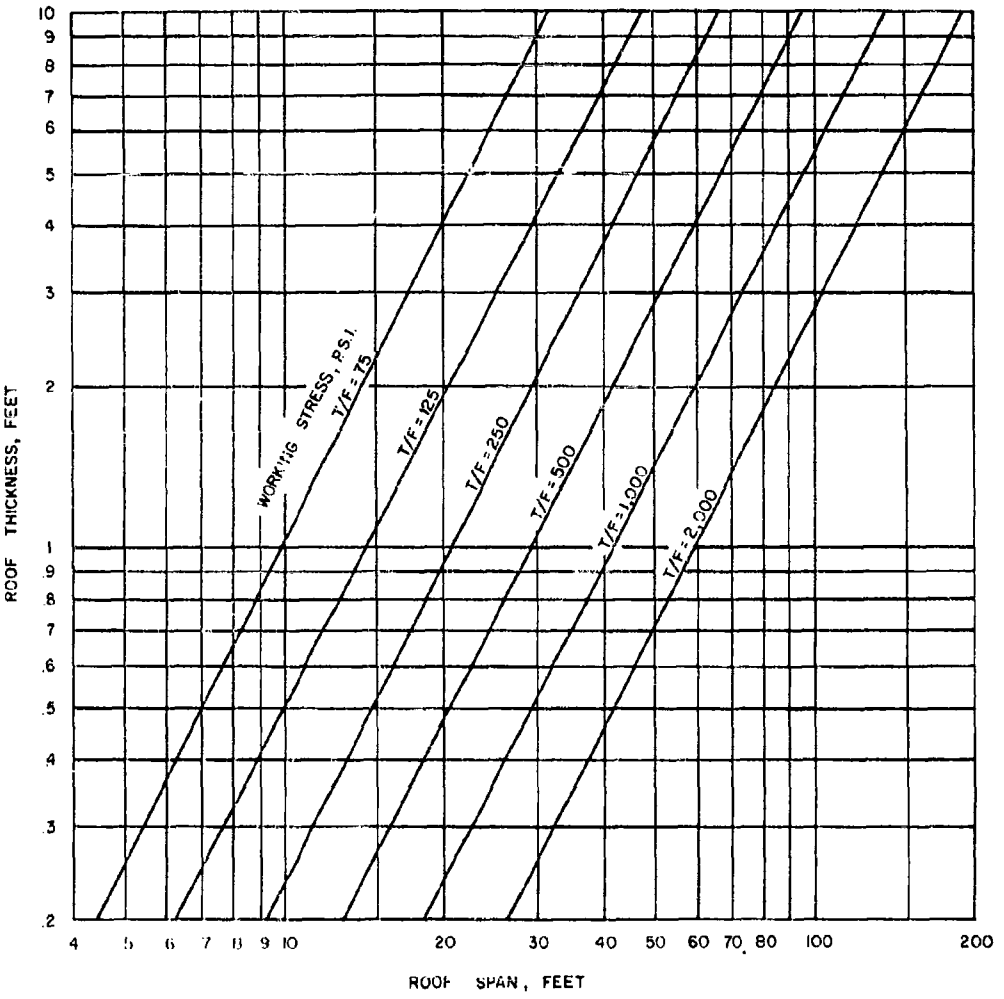


Figure 6.28 Roof span vs. roof thickness and working stress.

TABLE 6.15[1]

Constants for Use in Equations 11, 12, and 13

b/a	A	B	b/a	A	B
1.0	0.0138	0.0513	1.6	0.0261	0.0780
1.1	.0164	.0581	1.7	.0260	.0799
1.2	.0188	.0639	1.8	.0267	.0812
1.3	.0209	.0687	1.9	.0272	.0822
1.4	.0226	.0726	2.0	.0277	.0829
1.5	.0240	.0757			

The design equation is set up in the same manner as for a beam:

$$a = \sqrt{\frac{Tt}{6B\rho gF}} \qquad (6.13)$$

Inclined Roof

Where either the long dimension or the short one is inclined at an angle θ the stress is given by:

$$\sigma \text{ max} = \frac{\rho g L^2}{2t} \cos \theta \qquad (6.14)$$

and the design equation is

$$L = \sqrt{\frac{2\ Tt}{\rho g\ G \cos \theta}} \qquad (6.15)$$

Field Tests of Design

The equations given in the previous discussion were tested in the oil shale mine[22] and in a limestone mine[23]. In oil shale the predicted sag was 0.086 in for an 80 foot span, while the measured was 0.63 inches. The field behavior indicated either horizontal separations in the assumed 8 foot roof bed or the oil shale does not behave elastically.

Similar results were obtained in limestone[23, 24] where the roof sag was found to be much greater than that predicted by the theory of elasticity (Figure 6.29).

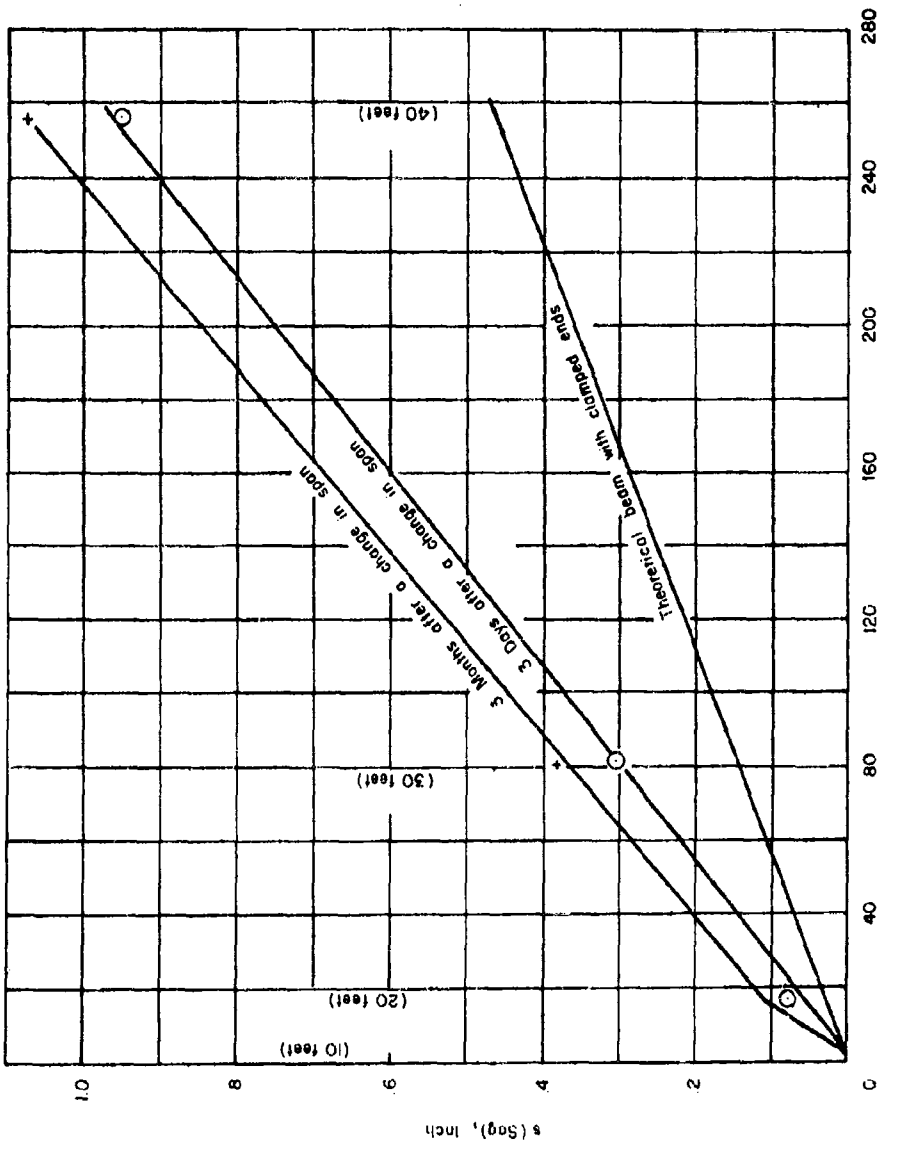


Figure 6.29 Relationship between sag and span from theory and measurements in place.

Failure Probability and Fracture Patterns

Experience and observation indicate that a large percentage of rock structures in which underground excavations have been made have been subjected to various degrees of fracturing of some type. Isaacson[25] states that "the ultimate answer to pressure control problems can only lie in the reasoned estimation of probabilities; the idea of certainty can never be achieved", That is, if the probability of failure for a given opening can be estimated, and it can be designed to restrict the probability of failure to a low lever, this should offer one of the most feasible approaches to the problem.

It is obvious that in fractured rock the larger the opening, the more fractures will be embraced in its periphery. The number of fractures, if randomly distributed, would increase as the first power of the radius of the opening. A linear relation between the number of fractures, depending upon their extent and pattern, could be taken as a first approximation of the minimum probability of failure.

Isaacson utilizes arguments from the theory of probability and assumptions outlined below to arrive at the following conclusions concerning circular shafts or tunnels of radius a in a hydrostatic stress field.

1. The most probable number of rockburst that will occur during the development of such an opening varies as the square of the radius.

2. The probability that no rockbursts will occur during excavation is equal to e^{-ka^2}, where k is a constant which depends upon the magnitude of the stress field and the character of the rock.

As a first approach consider a number of cubes placed in a testing maching and stressed to failure. If the probability of failure in shear in the range of τ, and $\tau + d\tau$ is $p(\tau)$. $d\tau$, then the probability that no failure will take place in a given specimen at or below a shear stress of τ is

$$\int_{\tau}^{\infty} p(\tau) \cdot d\tau \qquad (6.16)$$

The probability that there will be no failure in a rock mass of volume V subject to the same shearing stress is

$$\left[\int_{\tau}^{\infty} p(\tau) \cdot d\tau\right]^{V} \qquad (6.17)$$

on the basis that probabilities of independent events are compounded by multiplication.

The maximum shear stress at a point γ from a shaft or tunnel of radius a in a hydrostatic stress field P is $P\left(\frac{a}{\gamma}\right)^2$. The probability of no failure in an elementary ring Δr of unit length is

$$\left[\int_{P\left(\frac{a}{r}\right)^2}^{\infty} p(\tau) \cdot d\tau\right]^{2\pi r \cdot \Delta r} \tag{6.18}$$

The probability of no failure anywhere in a section of tunnel of unit length is, then

$$Q = \lim_{\substack{\Delta r \to 0 \\ r = a}}^{r = \infty} \left[\int_{P\left(\frac{a}{r}\right)^2}^{\infty} p(\tau) \cdot d\tau\right]^{2\pi r \cdot \Delta r} \tag{6.19}$$

or

$$\log Q = \int_a^{\infty} 2\pi r \left(\log \int_{P\left(\frac{a}{r}\right)^2}^{\infty} p(\tau) \cdot d\tau\right) \cdot dr \tag{6.20}$$

Assuming that the probability function $p(\tau)$ may be expanded in a power series the above equation may be evaluated to give

$$Q = e^{-2\pi A a^2} \tag{6.21}$$

where the constant A is some function of P and of the coefficients of the series for $p(\tau)$. The probability of no failure is e^{-ka^2} and the probability of at least one failure is $1 - e^{-ka^2}$. For small radii of openings the probability of failure increases very slowly with the increase of the size of the opening, increases very rapidly over a range of intermediate values and becomes asymptotic to a probability value of one at a value of which is dependent on k.

Isaacson points out that a large portion of the failures indicated by the above development will be small and localized. The probability of larger bursts may be considered as follows. In a unit cube of rock the probability of failure at or below a shear stress τ is

$$\int_0^{\tau} p(\tau) \cdot d\tau\tau \tag{6.22}$$

The most probable number of failures in a volume V will be given by

$$V \int_0^{\tau} p(\tau) \cdot d\tau \tag{6.23}$$

The most probable number of failures in a tunnel of radius a in a hydrostatic field of magnitude P will be

$$M = \int_a^{\infty} \int_0^{P\left(\frac{a}{r}\right)^2} 2\pi r \cdot p(\tau) \cdot d\tau \cdot dr \tag{6.24}$$

If $p(\tau)$, the probability function of the shear stress, is expanded as a power series and the necessary integrations are performed the following equation is obtained:

$$M = 2\pi Ba^2 \tag{6.25}$$

where B is a constant depending upon P and the coefficients in the expansion of $p(\tau)$. It follows, therefore, that the expected number of bursts increases as the square of the radius of the tunnel as the excavation is made.

The conclusion appears to be a logical one inasmuch as the weaknesses "exposed" by excavation are some function of volume rather than of surface area. On the basis of the above, which appear to be reliable conclusions in conformity with observed rock behavior in deep mines, it would also appear advisable to design protective construction openings as small as may be compatible with operational requirements.

Multiple Rock Cantilever Beams

A parallel of the case of multiple cantilevers of the general type created by excavation of openings in stratified rock have been analyzed[26] by means of the theory of elasticity for point loading in leaf spring design. Under ideal assumption of similar material and identical cross sections the pertinent formulae are quite simple. The theory is equally applicable to rock beams of similar dimensions and properties, as well as to some less ideal structures. Thus, for encastré rock beams which result from excavations in jointed strata the following development sheds some light upon the mechanics of stability and failure of such structures.

Landau and Parr[26] state in the case of a steel leaf spring, the laminae having equal or different thicknesses, under load each leaf touches the one above only at the point of encastriment and at its end. Further, any leaf of the spring may be considered as a cantilever beam having a flexible support somewhere between the fixed end and the point of application of the load. This assumption is the basis of the theoretical development.

Thus, if a weight or force acts at the end of the top of three stacked cantilever beams, it can be shown by integrating the moment equation

$$EI \frac{d2y}{dx2} = M \tag{6.26}$$

for each of the beams and utilizing appropriate boundary conditions that the relationship between the forces W_1, W_2 and W_3 is expressed by the following in generalized form

$$\delta_n = \frac{W_{n+1}[3(l_n)^2 l_{n+1} - (l_n)^3] - 2W_n(l_n)^3}{E_{n+1} I_{n+1}} = \frac{2W_n(l_n)^3 - W_{n-1}[3(l_{n-1})^2 l_{n-1}(l_{n-1})^3]}{E_n I_n} \tag{6.27}$$

Once the force at the end of a given beam is known it may be treated as a simple cantilever for solution of stresses and strains. Each side of Equation 6.2 is equal to six times the displacement of the end of the nth beam.

For two beams which are of the same material and equal cross sectional areas and $l_2 = 2\ l_1$ Equation 6.27 reduced to

$$W_2 = 4/5\ W_1 \tag{6.28}$$

The stress diagram for two beams is shown in Figure 6.30. The maximum horizontal stress in the longer beam is 4/5 of that in the shorter and the latter will fail first if the two are of equal strength. For a step structure of five beams increasing in length in equal increments the overall strength increases in the manner shown in Table 6.16.

TABLE 6.16

Relative Strength of Beams with Equal Spacing

Number of Beams	Relative Strength
1	1.00
2	1.60
3	2.21
4	2.81
5	3.41

Also, the greatest stress is found in the shortest leaf where they are all of the same thickness and material.

Voussoir Structures

When fractures are formed in a stratum in a roof rock member of an underground excavation a lateral unit section can no longer be considered either a simply supported beam or a simple restrained beam (encastre' at both ends). Evans[27] has proposed that the strength of such structures is due to their approximation of a voussoir arch type structure, the components of which are held in place by lateral as well as vertical pressure (See Figure 6.31). He assumes (1) elastic behavior, (2) no tensile stress, (3) adequate shear strength, (4) negligible verticle displacement, and (5) horizontal elastic strain of abutments is negligible. The mechanics of fabricated voussoir arches are discussed in detail by Pippard[28] who shows that the pin or contact on open joints may migrate with varying loads and failure may be predicted on model arches. However,

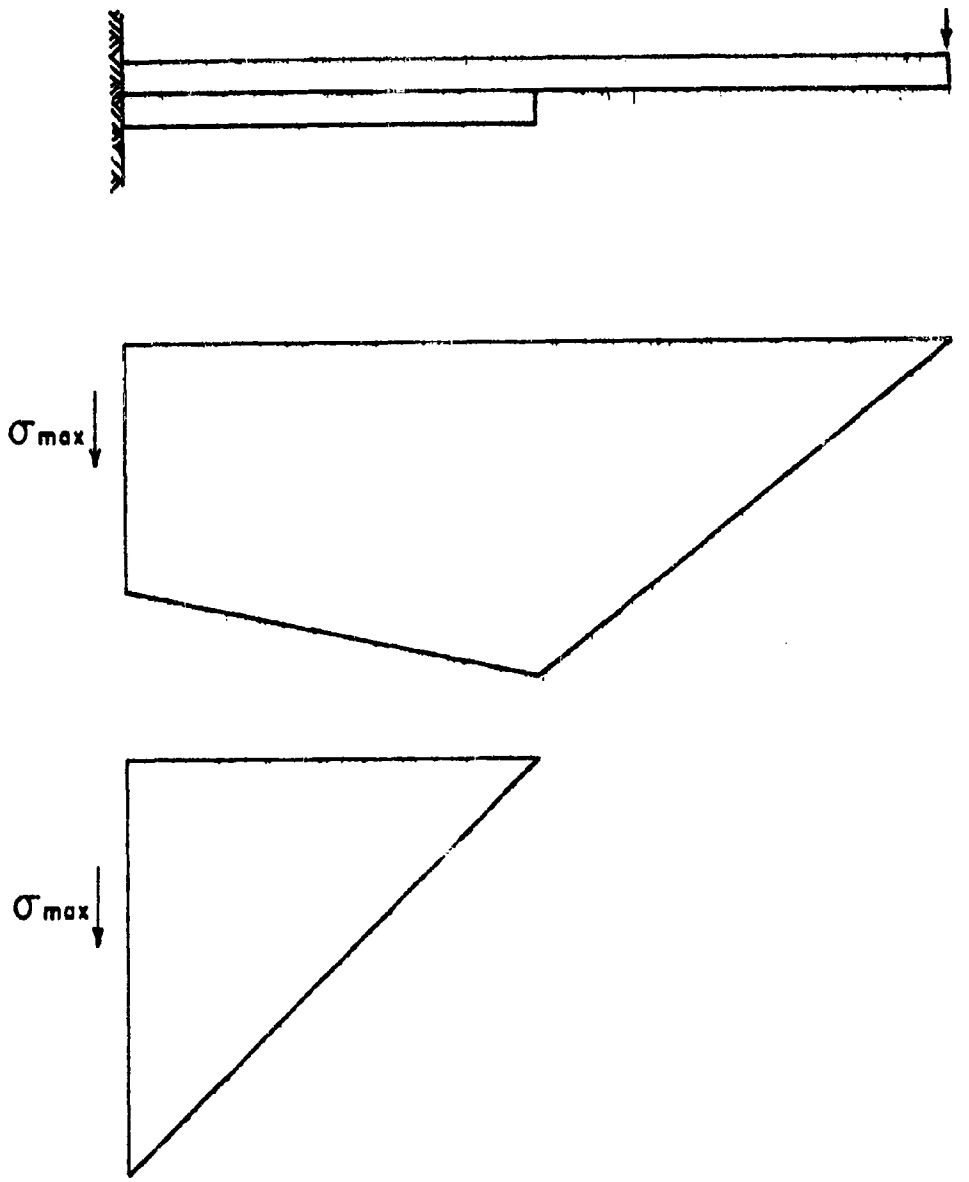


Figure 6.30 Stress distribution in two fixed cantilevers with a point load at the end of the large member.

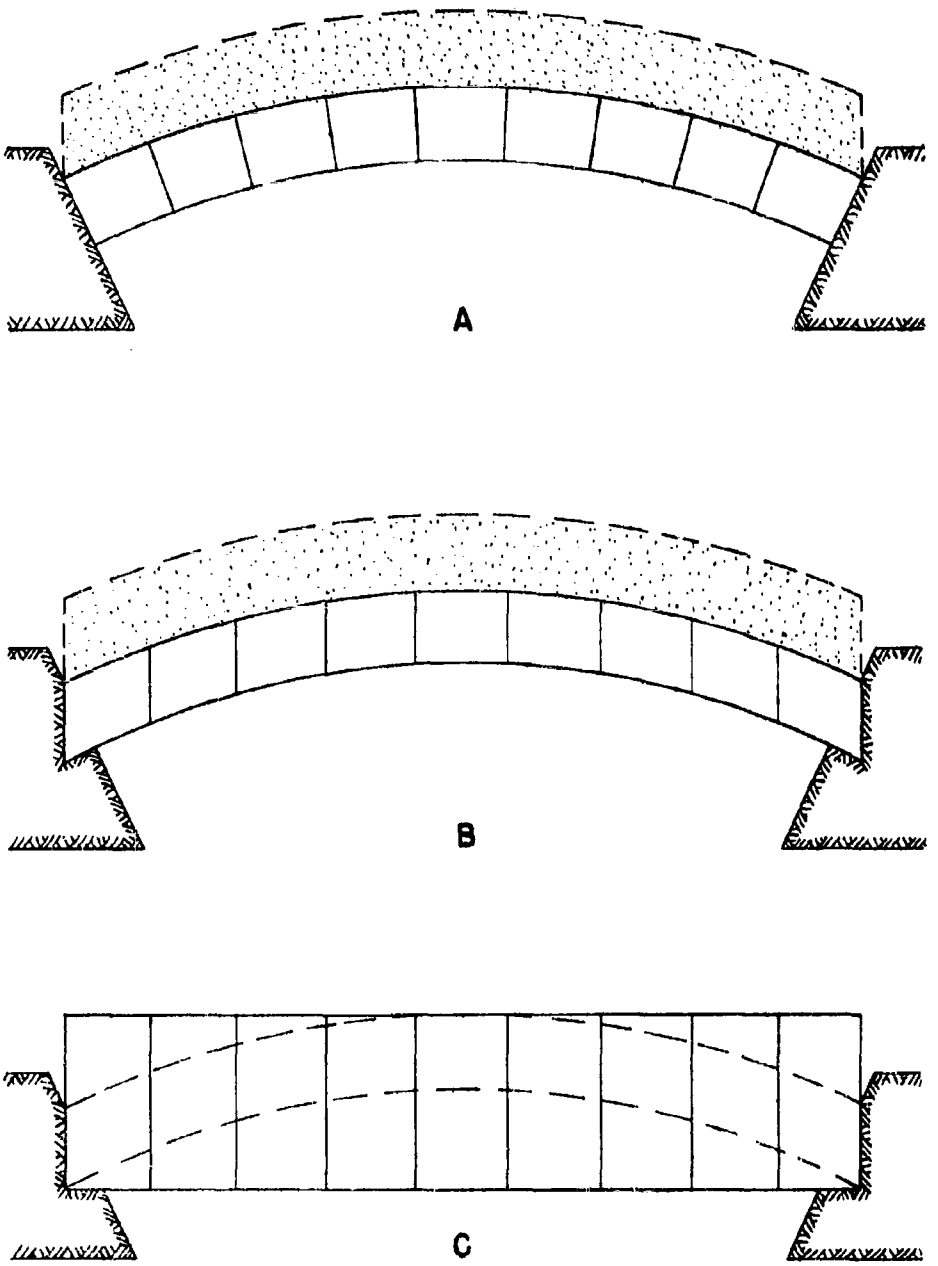


Figure 6.31 A, B, C. A. A normal voussoir arch with loose cover fill. B. The same as A with joints vertical. C. Similar to B, with all voussoirs equal but total load not increased.

similated rock arches underground and beams are never as geometrically symmetrical as fabricated arches and the principles involved are of restricted application. Evans assumes a fractured rock beam with a triangular stress distribution as shown in Figure 6.32.

T = thickness of the beam
nT = portion of section under stress
1/3nT = distance of centroid from surface
z = couple arm = T(1-2/3n)
H = thrust or effective compressive force = $\frac{fm}{2}$ -x nT

m2 = moment = Hz = $fmT^2 \left(\frac{n}{2} - \frac{n^2}{3}\right)$

However, there is some question as to the accuracy of Evan's assumption, in that in calculating the moments for the voussoir sections he neglects the shear force acting vertically at the end of the beam.

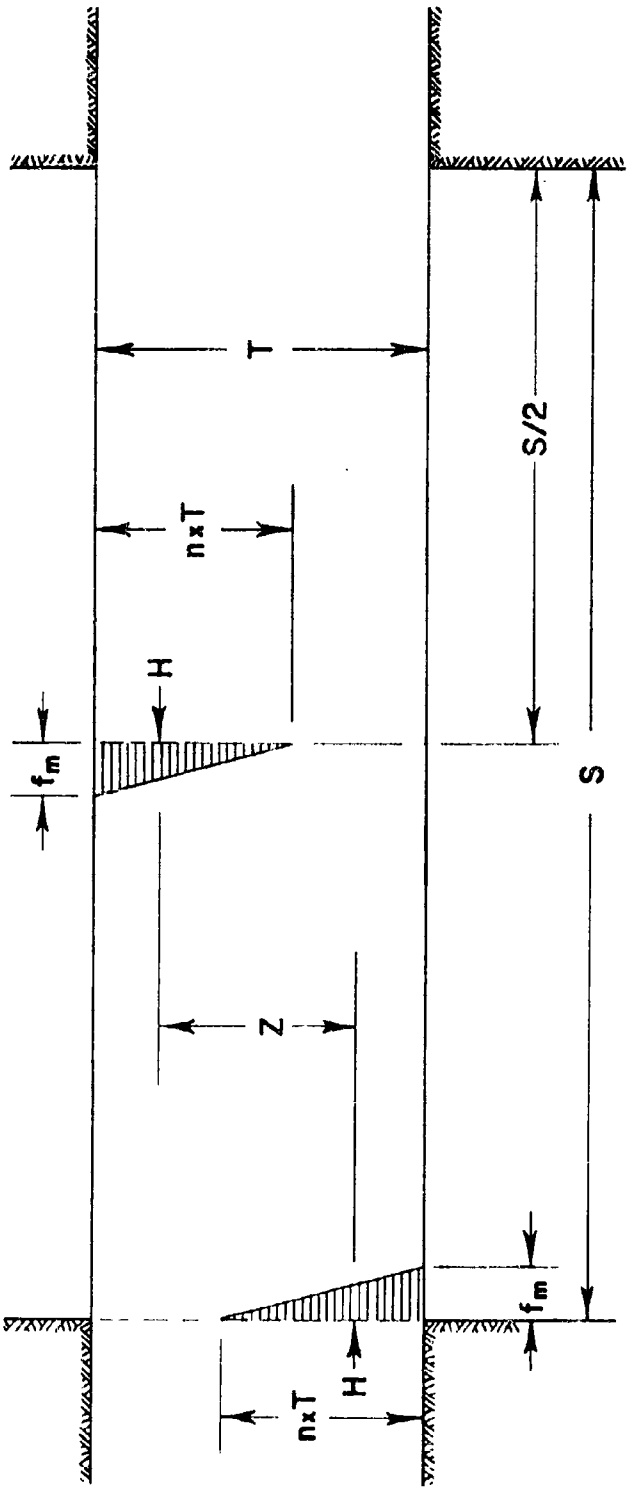


Figure 6.32 Evans' assumed stresses for simple voussoir analysis.

CHAPTER VI

REFERENCES

1. Obert, L., et al., Design of Underground Openings in Competent Rock, U.S. Bureau of Mines Bull. 587, 1960

2. Mindlin, Raymond D., Stress Distribution around a Tunnel, Proc. Am. Soc. Civil Eng., April 1939, pp. 619-642.

3. Beyl, Z.S., The Prestressed State of the Earth's Crust, Its Causes and Preservation, International Conference about Rock Pressure and Support in Workings, Liege, Belgium, April 24-28, 1951.

4. Shoemaker, R.P., A Review of Rock Pressure Problems, Am. Inst. Min. & Met. Engr., Tech. Pub. 2495, Mining Technology, Vol. 12, No. 6, Nov., 1948.

5. Rice, G.S., Some Problems in Ground Movement and Subsidence, Trans. Am. Inst. Min. & Met. Engr., Vol. LXIX, Feb. 1923, pp. 374-392.

6. Dinsdale, J.R., Ground Pressures and Pressure Profiles around Mining Excavations, Colliery Eng., Vol. 12, 1935, pp. 406-409.

7. Duvall, Wilbur I., Stress Analysis Applied to Underground Mining Problems, Part I - Stress Analysis Applied to Single Openings, U.S. Bureau of Mines Report of Invest. 4192, 1948.

8. Duvall, Wilbur I., Stress Analysis Applied to Underground Mining Problems, Part 2: Stress Analysis Applied to Multiple Openings and Pillars, U.S. Bureau of Mines Report of Invest. 4387, 1948.

9. Panek, Louis A., Stresses about Mine Openings in a Homogeneous Rock Body, Edwards Brothers, Inc., New York, 1951.

10. Frocht, Max Mark, Photoelasticity, Vols. 1 and 2, McGraw-Hill Book Company, Inc., New York.

11. Stresses and Pore Pressures around Circular Openings near a Boundary, U.S. Department of Interior, Bureau of Reclamation, Tech. Memo No. 597, Denver, Colo., Jan 12, 1940.

12. Inglis, C.E., Stresses in a Plate Due to the Presence of Cracks and Sharp Corners, Trans. Inst. Naval Arch., London, 1913, Part I, pp. 219-230.

13. Greenspan, Martin, Effect of a Small Hole on the Stresses in a Uniformly Loaded Plate, Quart. Applied Math., Vol. II, No. 6, 1944.

14. Ling, C.B., On the Stresses in a Plate Containing Two Circular Holes, Journ. App. Physics, Jan. 1948, pp. 77-82.

CHAPTER VI

REFERENCES (Continued)

15. Capper. P.L., Unpublished thesis, London 1927.

16. Green, A.E., General Bi-harmonic Analysis for a Plate Containing Circular Holes, Roy. Soc. Proc. 176A, Aug. 28, 1940, pp. 121-139.

17. Howland, R.C.U., Stresses in a Plate Containing an Infinite Row of Holes, Roy. Soc. Proc. 148A, Feb. 1, 1935, pp. 471-491.

18. Bucky, Philip B., Use of Models for the Study of Mining Problems, American Inst. of Mining & Met. Engr., Tech. Pub. 425, Feb. 1931.

19. Panek, Louis A., Centrifugal Testing Apparatus for Mine Structure Stress Analysis, U.S. Bureau of Mines Report of Invest., 4883, June, 1952.

20. Caudle, R.D., and Clark, G.B., Stresses around Mine Openings in Some Simple Geologic Structures, Univ. of Ill. Eng. Exp. Sta. Bull. 1430, Vol. 52, No. 69, May 1955.

21. Timoshenko, S., Theory of Elasticity, McGraw-Hill Book Co., Inc., New York.

22. Merrill, R.H., Design of Underground Mine Openings - Oil-Shale Mine, Rifle, Colo., Bureau of Mines RI 5089, 1954.

23. Merrill, R.H., Roof-Span Studies in Limestone, U.S. Bureau of Mines RI 5348, 1957.

24. Merrill, R.H., and Mongan, T.A., Method of Determining the Strength of a Mine Roof, U.S. Bureau of Mines RI 5406, 1958.

25. Isaacson, E. de St. Q., Rock Pressure in Mines, Mining Publications Ltd., Salisbury House, London, England, 1958.

26. Landau, D. and Parr, P.H., A New Theory of Plate Springs, Jl. of Franklin Inst., Vol. 185, pp. 418-508, Vol. 186, pp. 699-722, Vol. 187, pp. 65-98, 199-214.

27. Evans, W.H., The Strength of Undermined Strata, Trans. Inst. of M & M, Vol. 50, 1941.

28. Pippard, J.S., et al., The Mechanics of the Voussoir Arch, Jl. Inst. C.E., 1936-37.

CHAPTER VII

DYNAMIC STRESSES AND DESIGN OF OPENINGS

Introduction

Mathematical analysis of pertinent dymanic rock stresses resulting from surface or near surface detonations to the present has been concentrated on the effects of a step-type surface wave of limited horizontal extent applied to the surface of a half-space. Effect of such a stress wave of properly simulated duration and magnitude indicates that its effect upon the stress concentration at the surface of a cylindrical opening is to increase the effects of a free field by about 3.2 times, or a maximum of about 11 percent over a static field.

Analysis of effects of static stress indicates that an elliptical cross-section is the best design shape to use for most geologic structures which are suitable for protective construction, although a circular shape is most stable in a hydrostatic field. Cross-sections should be kept as small as possible because the total number of rock defects increases with the size of openings and consequently the probability of either limited failure or collapse of the opening under heavy stress loads.

Several bases are offered to serve for engineering design of underground openings to resist dynamic loads. These include (1) the application of theoretical multiplication of free stress field values by factors for the presence of the opening, (2) scaling from model crater studies in the particular type of rock, (3) extrapolation from model tunnel tests in similar types of rock, and (4) impact studies of the reaction of the structural segments of underground openings to blast loading.

At the present time design criteria are based primarily on the facts which have been learned from a small number of HE tests and a fewer number of underground measurements of phenomena induced by nuclear detonations. Also, theoretical studies have been described in two papers, one by Gilbert[1] and one by Baron, et al[2], and summarized by Pantall and Auld[3]. These deal with a mathematical analysis of the interaction in an elastic medium to a plane stress wave impinging on a circular cylindrical hole in a half-space.

Elastic Plane Stress and Cylindrical Openings. The static stress distribution around a circular opening in a plate has been treated in Chapter VI for three types of stress field conditions. For a unidirectional stress field the introduction of a circular opening creates a maximum stress which is three times that of the stress field. It acts on a plane normal to the stress field direction and is of the same sign as the free field

The pertinent results of the mathematical analysis in references 1 and 2 plus the results of experimental photoelastic research by Durell and Riley[4] have likewise been summarized by Pantall and Auld[3] and are briefly repeated here for purposes of further comparison and analysis.

In both theoretical and experimental analyses ideal elastic conditions are assumed. Gilbert and Baron, et al., assumed that an essentially plane wave was acting on one boundary of a half-space, and Gilbert that the incident pulse had a very short rise time and a slow decay. High frequency approximations from geometrical optics and utilization of the first two terms of a Fourier series offered a simplified approach. The maximum stress was found to be tangential, occurs at the hole surface at an angle of 60°, (Figure 7.1), and is twice the free field stress.

Baron, et al., solved the same problem by assuming that the components of the stress wave are $\sigma F(t)$ and $\nu\sigma F(t)$ parallel and normal to the direction of propagation respectively. A solution was obtained for a step pulse which would then be generalized for an appropriate F(t) by use of Duhamel s integral. Comparative results are given in Figure 7.1. Gilbert s results cannot be projected beyond 60° and it is noted the values obtained by the other method for a step pulse approach the static case.

Photoelastic experiments[4] were conducted with epoxy resin models impacted with a drop weight. The model, applied stress and results of stress analysis are shown in Figure 7.2 to 7.6. The resin used has the following properties:

$$E = 560 \text{ psi}$$

$$\nu = 0.46$$

$$\rho = 70 \text{ lb/ft}^3$$

For the created biaxial stress field, i.e., $\nu\sigma_A = -0.46\sigma_A$, the maximum static stress concentration would be 3.45 times the field stress, and the maximum dynamic stress was found to be 11.4 percent higher than this. Pantall and Auld conclude that the theoretical values of maximum stress and those determined experimentally are in reasonable agreement, and that it may be possible to use these solutions as first approximations to the design problems of underground protective installations.

The apparent weaknesses in the above approach are: (1) the assumption of ideal elastic rock (2) possible oversimplification of mathematical procedures, and (3) the assumptions concerning the nature and means of application of the forcing function, i.e., for air blast only. For a ground burst or detonation which occurs in a deep ravine or canyon, the partial confining effects of surface topography cannot be ignored, and geologic structure is probably more important than in static design.

Geologic Structure. Consider, for example, the case of an opening in a horizontally stratified medium. (Figure 7.7). It will necessarily approach being rectangular in shape and the roof strata may be the loci of high stress concentrations particularly near the ribs. As indicated in Chapter VI sections of such roofs may under certain conditions be

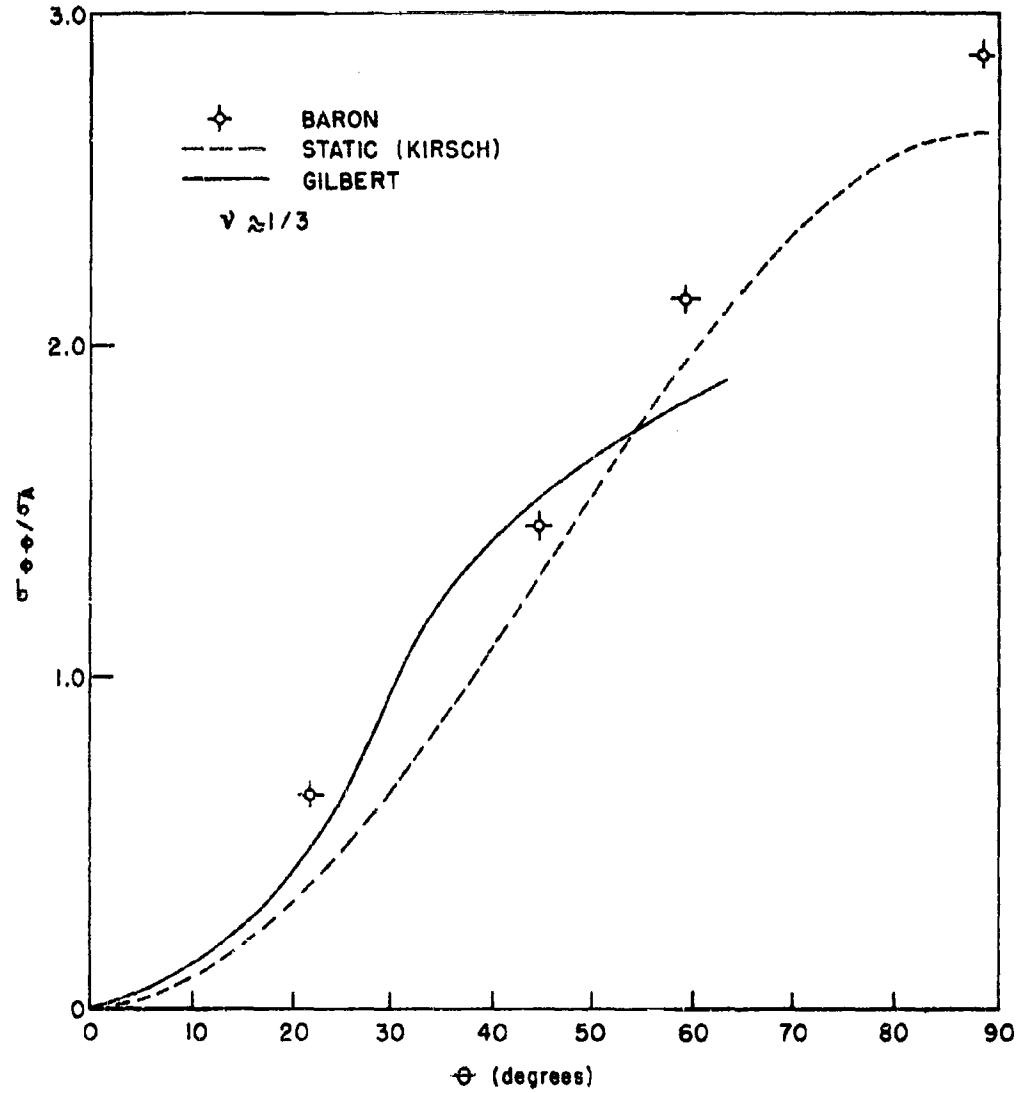


Figure 7.1. Hoop stress vs. central angle.[4]

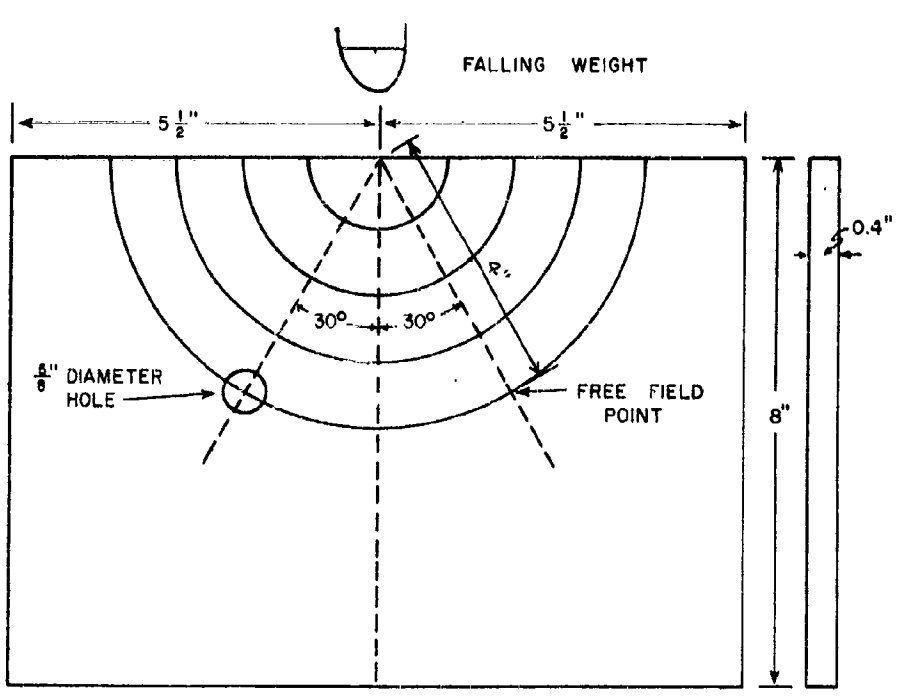


Figure 7.2. Sketch of model illustrating location of hole and symmetric free field point.[4]

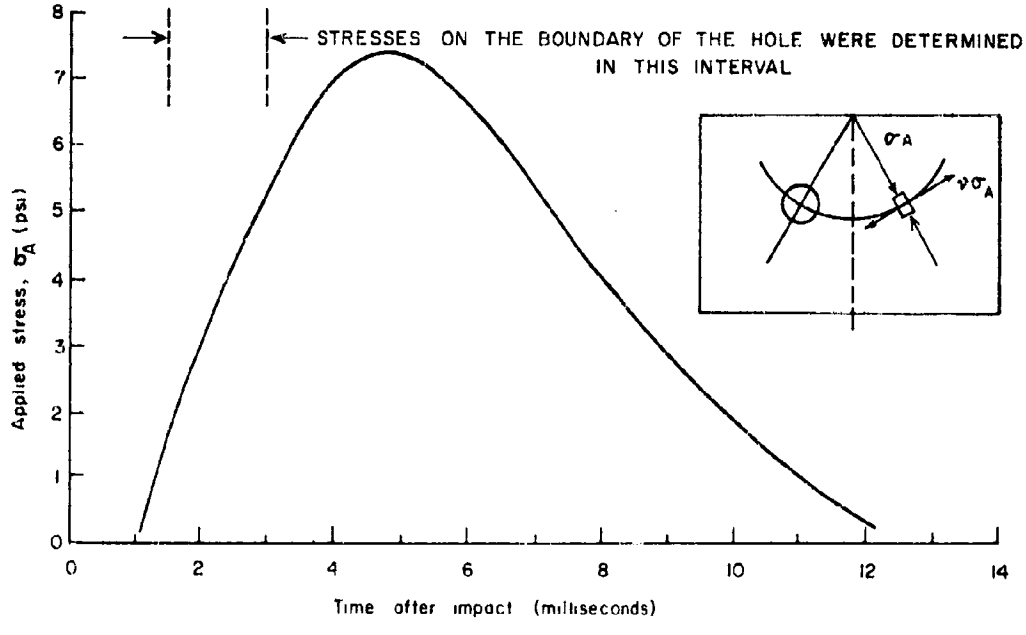


Figure 7.3. Applied stress as a function of time at the symmetric free field point.[4]

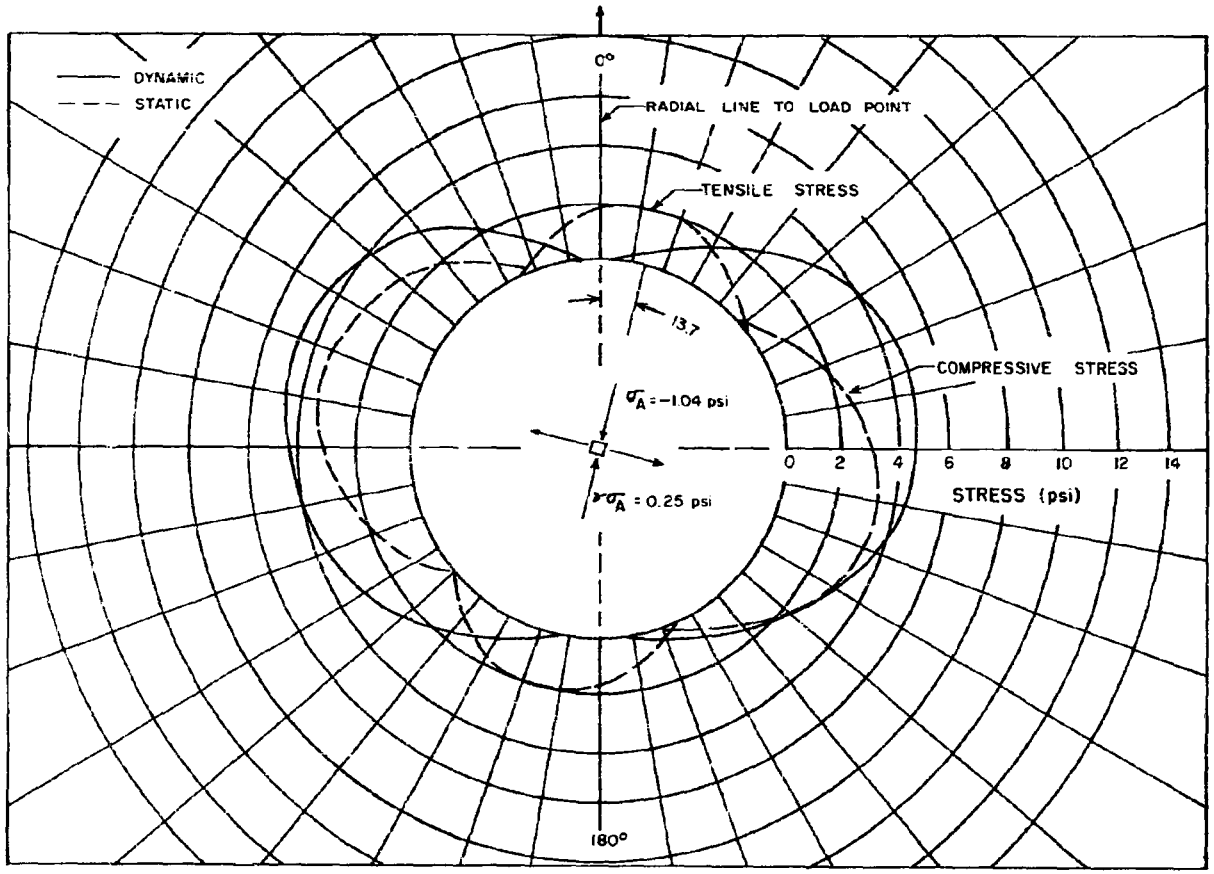


Figure 7.4. Static and dynamic stress distributions on the hole boundary - 1,320 microseconds after impact.[4]

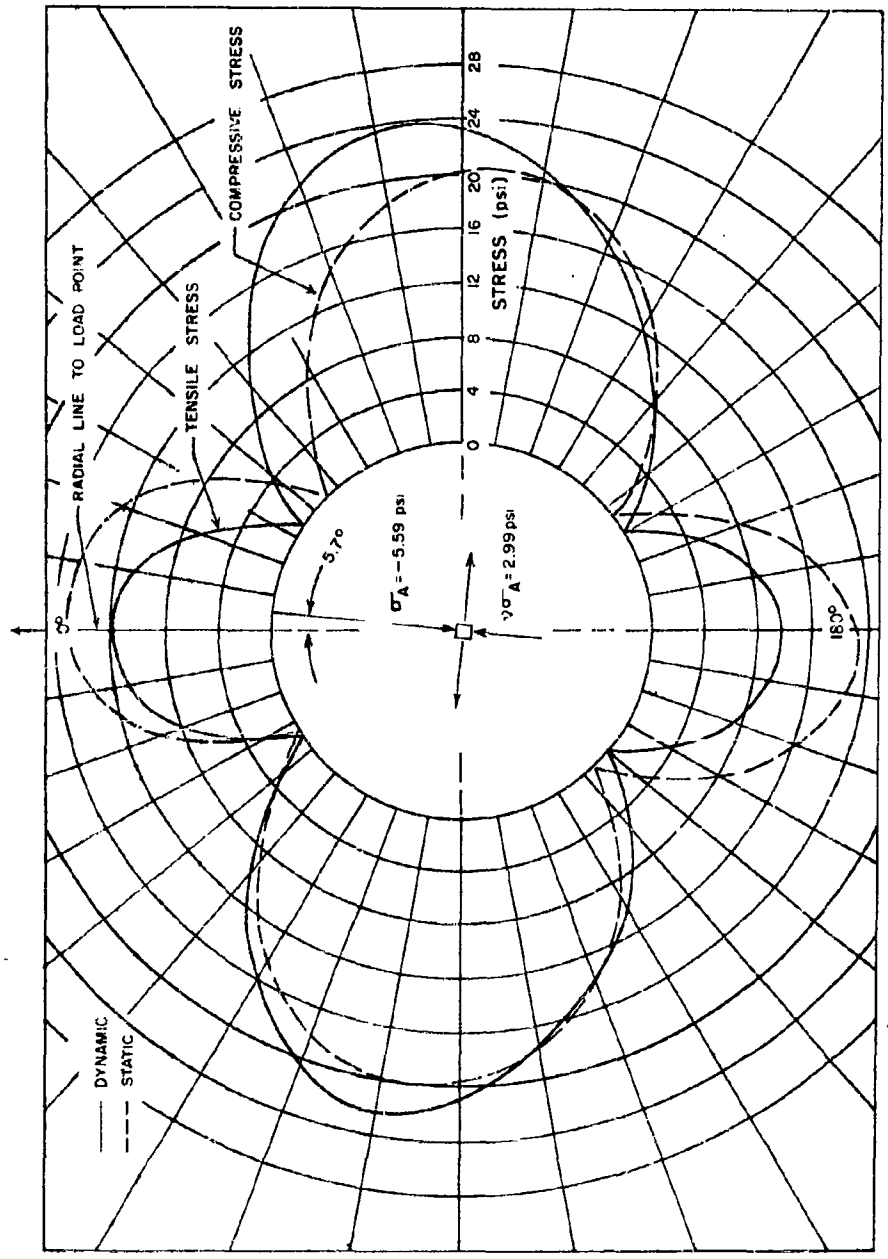


Figure 7.5. Static and dynamic stress distributions on the hole boundary - 3,075 microseconds after impact.[4]

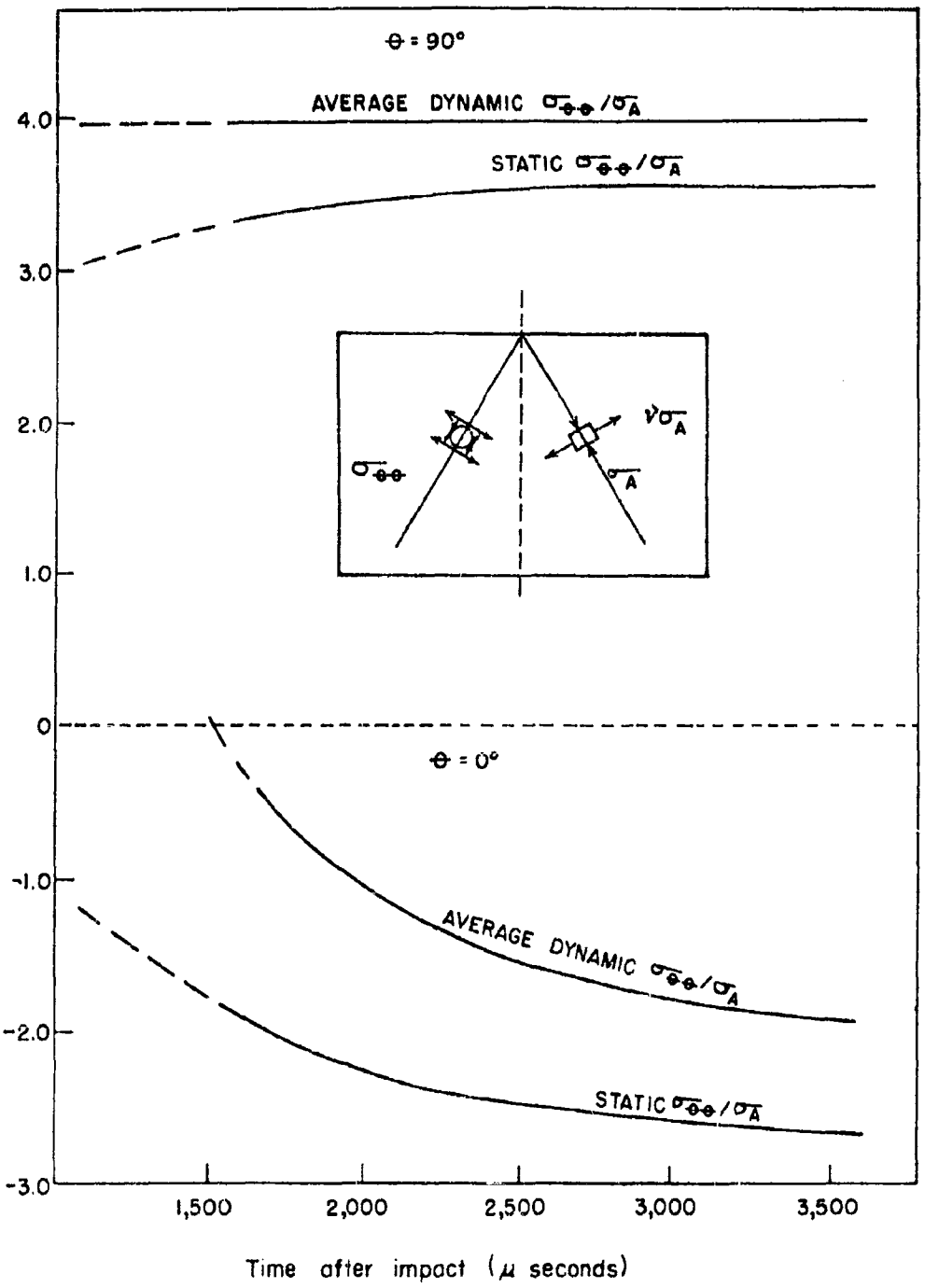


Figure 7.6. Hoop stress vs. time.[4]

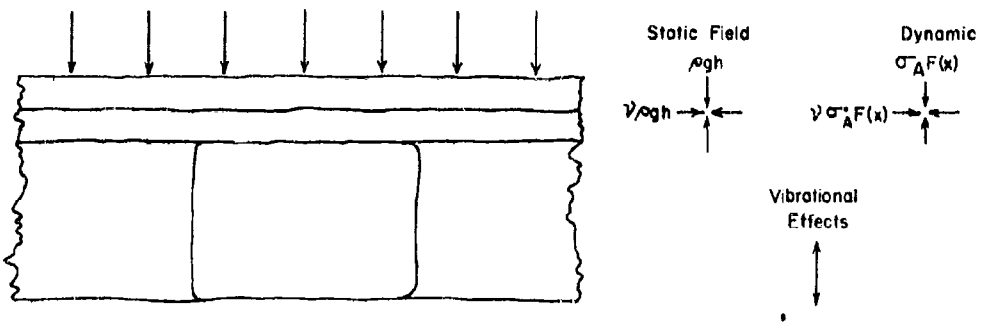


Figure 7.7. Rock strata would cause additional stresses due to vibration (inertia) effects in roof members.

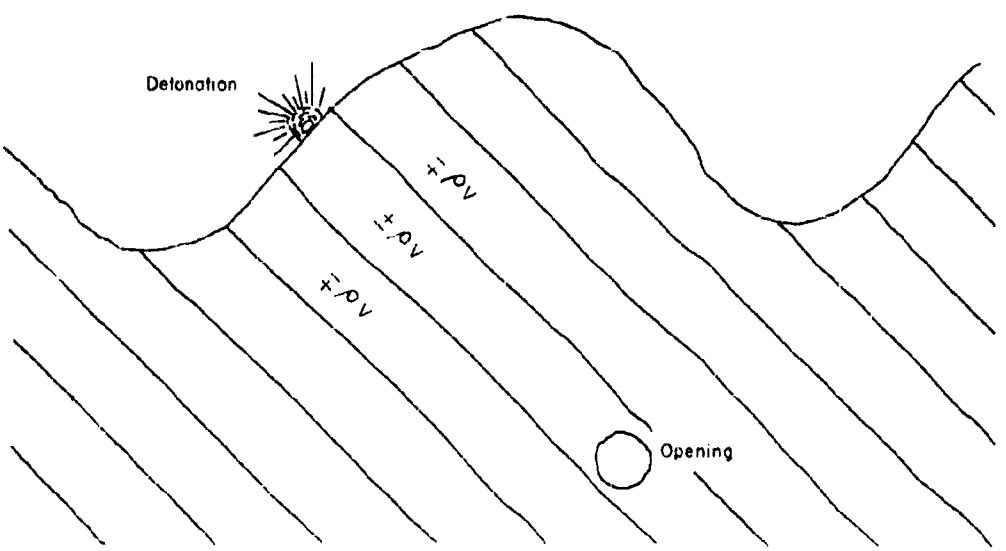


Figure 7.8. Diagramatic sketch of inclined strata with impedance condition which would tend to channelize wave energy, accentuated by detonation in deep ravine or canyon. Beds on above and below installation bed have significantly different ρv.

treated as restrained beams. In addition to the dynamic stress field which would be superposed on the existing static field, the beam would be subject to flexural vibrations. Accelerations of several g's may be experienced by the beam and the stresses induced due to vibration would be added to the direct effects of static and dynamic stress fields.

Figures 7.8 to 7.12 give other schematic examples of local geologic structures which may conceivably be encountered in underground openings. If there are vertical fractures present in a unidirectional field (vertical) the periphery of the tunnel would not support tension at the top or bottom of a circular opening, which would change the stress distribution about the opening. Also as a circular hole in a stressed plate is moved near a boundary, the stress concentration in the "pillar" between the hole and the boundary (fault) increases very rapidly[5]. Thus, openings should not be driven near and parallel to faults, or cross them at acute angles.

- Vertical or inclined joints, bedding planes or fractures of any type would affect the stress distribution in that they transmit no tensile stresses and very little shear stress. Also, as in the case of the roof beam considered above, inertial forces would be effective in dislodging broken segments of rock unless they were held in place by some type of support or rock bolt.

The effects that geologic structure may have upon stress distribution are indicated by results of an investigation by McHenry and Olsen of the Bureau of Reclamation as reported by Terzaghi and Richart[6].

The procedure employed is that of strain relief or stress relaxation. The strain relief is compared with the necessary stress to produce the same strain on laboratory specimens. The computation is based upon the assumption that the stress-strain relations governing the elastic expansion of the rock during strain relief are identical with those prevailing during the laboratory test. Terzaghi points out that this assumption is not necessarily justified, because the strain relief reduces the rock stresses to zero for the first time during the rock's history.

Subsequent to the performance of initial tests, strain relief techniques were improved and simplified, and Figure 7.13 gives the results of stress determinations made by the Bureau of Reclamation just prior to 1952 at the Gorge Powerhouse penstock (Seattle, Washington).[6] The tunnel is at a 200 foot depth beneath a ridge of sound granitic gneiss. The central vertical axis is the centerline of the roof, and the abscissae, measuring points on the tunnel profiles at the stations indicated.

The rock is described as being fairly intact and therefore the state of stress should be approximately the same at each station. However, the stress distribution varies in a somewhat erratic manner. Figure 7.14 shows a plotted stress diagram approximately compatible with computed stresses. The minimum stresses have a value of 1050 psi close to the top of the tunnel, and a maximum of 3750 psi close to the center of the rib. The initial horizontal pressure was initially smaller than the vertical, which is considerably different than the Hoover Dam Tunnel where the horizontal pressure was greater. The stresses measured correspond to

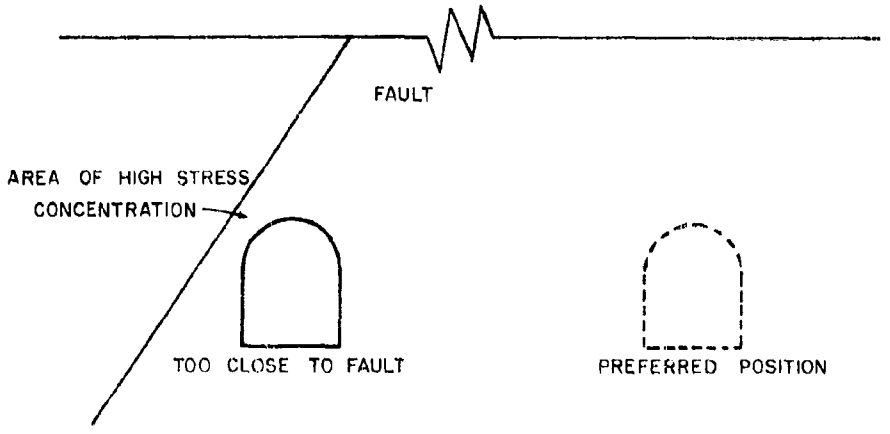


Figure 7.9. Placing of openings with long axis nearly parallel and too close to fault creates area of high stress concentration which may be critical in high magnitude stress field.

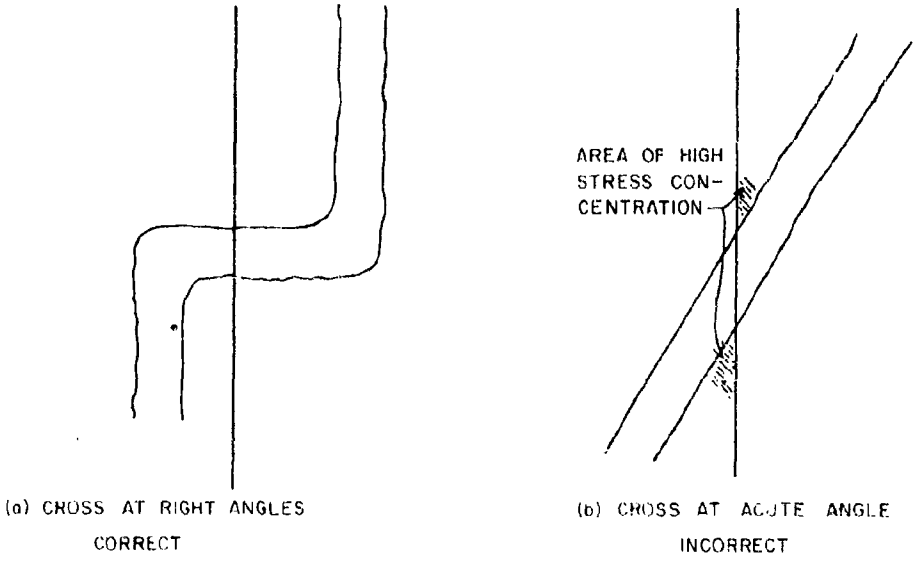


Figure 7.10. Faults should be crossed at 90° to minimize possibility of high stress concentration zones.

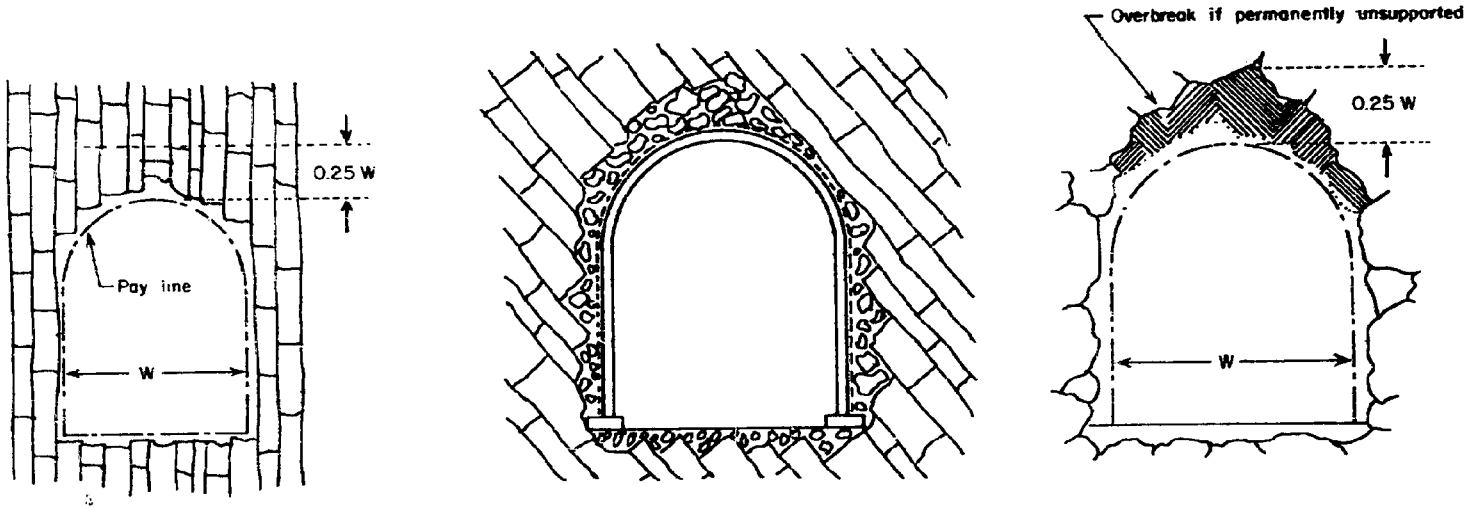


Figure 7.11. Openings in varied geologic structures.

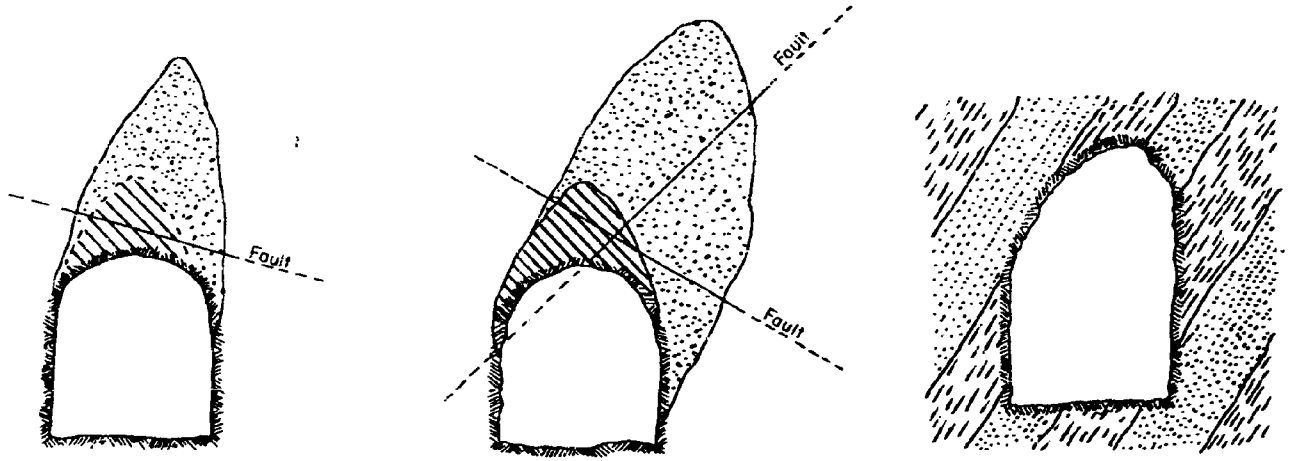


Figure 7.12. Openings in varied geologic structures.

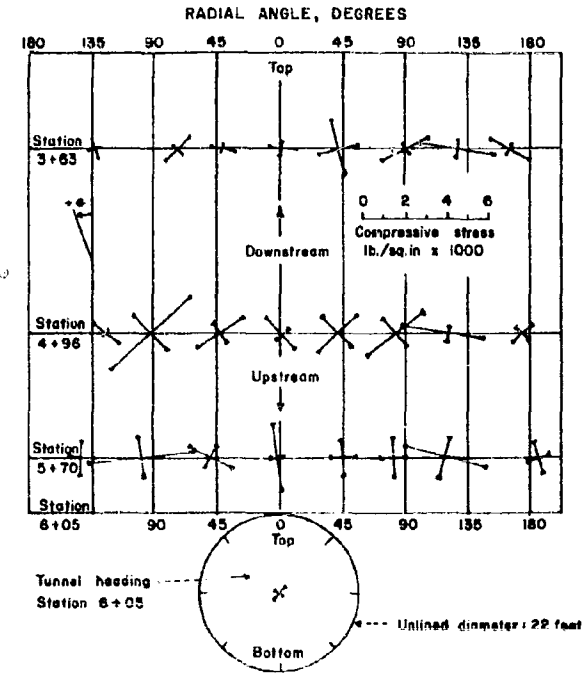


Figure 7.13. Residual principal stresses plotted upon developed inside surface of tunnel (after McHenry and Olsen, U.S. Bureau of Reclamation Report).[6]

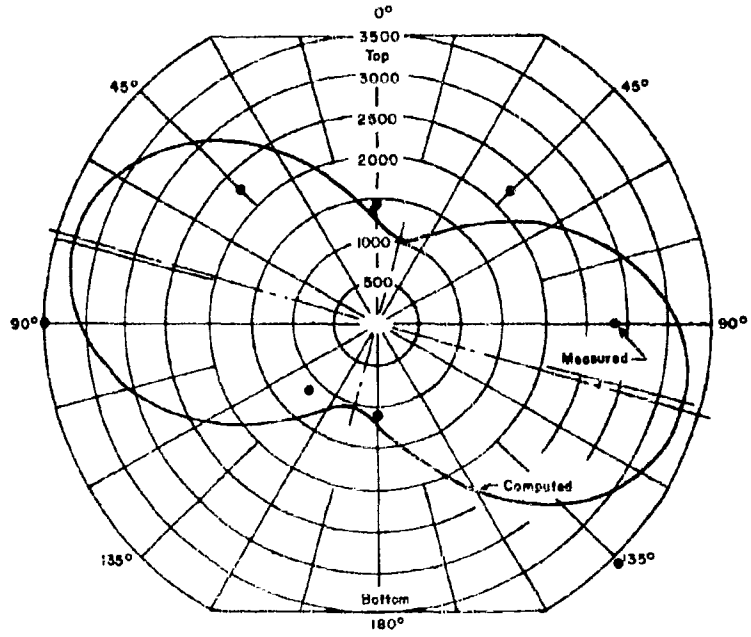


Figure 7.14. Residual tangential stress: station 4 + 96 (after McHenry and Olsen, U.S. Bureau of Reclamation Report).[6]

vertical free field stress of 1400 psi, whereas the depth of rock over the tunnel accounts for only 230 psi.

Thus, it can be readily seen that if dynamic stresses are superposed on existing static stresses, which in some cases may be much greater than would be expected from the vertical lithostatic pressure, failures may occur due to induced rock bursts very similar to those which occur in many operating mines where unfavorable stress conditions are created.

Transfer of Stresses - Rock Bursts. Isaacson[7] and others as well (see Chapter V - Rock Failure) have emphasized the principle of distressing of rock under critically high stress in deep underground workings where static stresses are of relatively high magnitudes because of depth or tectonic forces. This principle should be investigated with reference to its possible application to the problem of protective construction. The structure shown in Figure 7.15 has two advantages (1) it has moved the zone of major static stress away from the opening and (2) it furnishes a "buffer" between the "extradosal" rock and the "intradosal" rock which should increase probability of survival significantly for Zone 4* and possibly Zone 3* type damage. Such a method would probably not be effective in the NTS tuff, which rapidly re-cements and solidifies, but should be considered for rocks such as limestones and granites.

Artificial Support. Types of artificial support, i.e., timber and steel have been discussed in Chapter IX. It is not too clear at present which type of support is most desirable. Some hypothetical long time response curves for various types of support are given in Figure 7.16. Timber fails gradually, while rigid steel supports offer high initial resistance but fail rapidly. Bolted yielding arch supports offer virtually constant resistance to loading. It is suggested that some type of hydraulic support or damped elastic type support may offer some advantages. If the long period response can be approximated, a Berger's model or similar model may be devised to ascertain the response to a shorter period forcing function F(t).

In general, the principles of rock support which have been developed through experience in mines and tunnels may be employed as a basis for design of support under dynamic load. Much more must be known, however, regarding the nature of the loading function, rock reaction and the reaction of support members themselves to dynamic loads. Also, the nature of the dynamic stress field must be defined, and if equi-triaxial, a circular opening is indicated, or if the horizontal components are less than the vertical, an ellipse may be the better shape to use. In any event, shape of opening and support requirements will be governed in varying degrees by local geologic structure

* Zone 4: Slight spalling. Zone 3: Significant spalling.

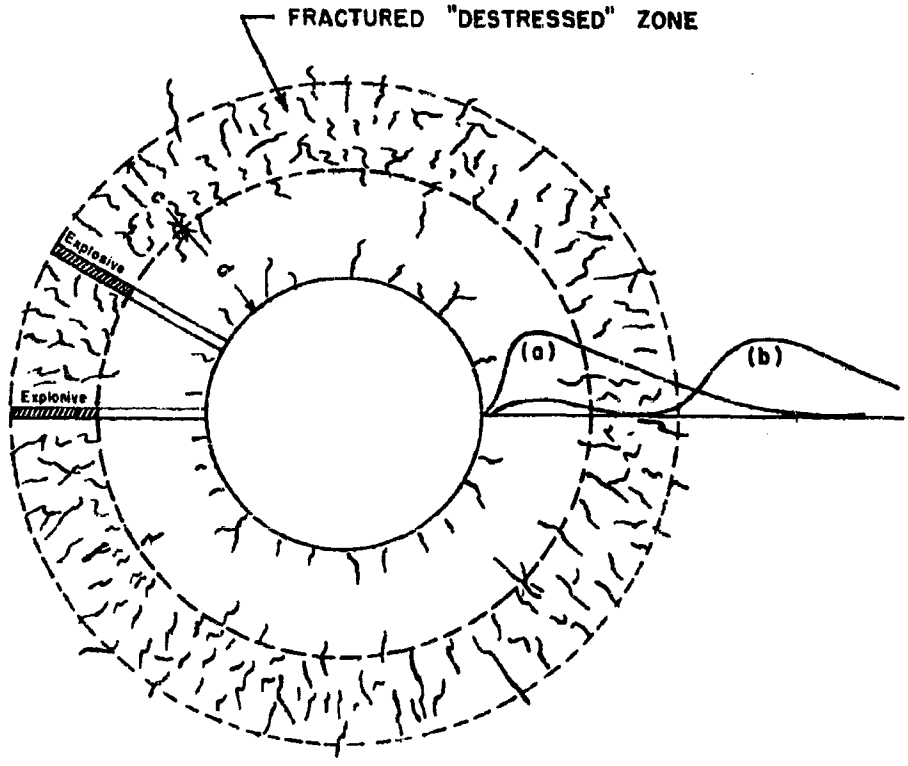


Figure 7.15. Formation of fractured or destressed zone by explosives around circular opening, leaving a ring of solid supporting rock, surrounded by a destressed zone of broken rock with the major static stresses transferred beyond the fracture zone. Curves represent (a) tangential stresses before destressing, and (b) after destressing. Principle offers some promise for protective design.

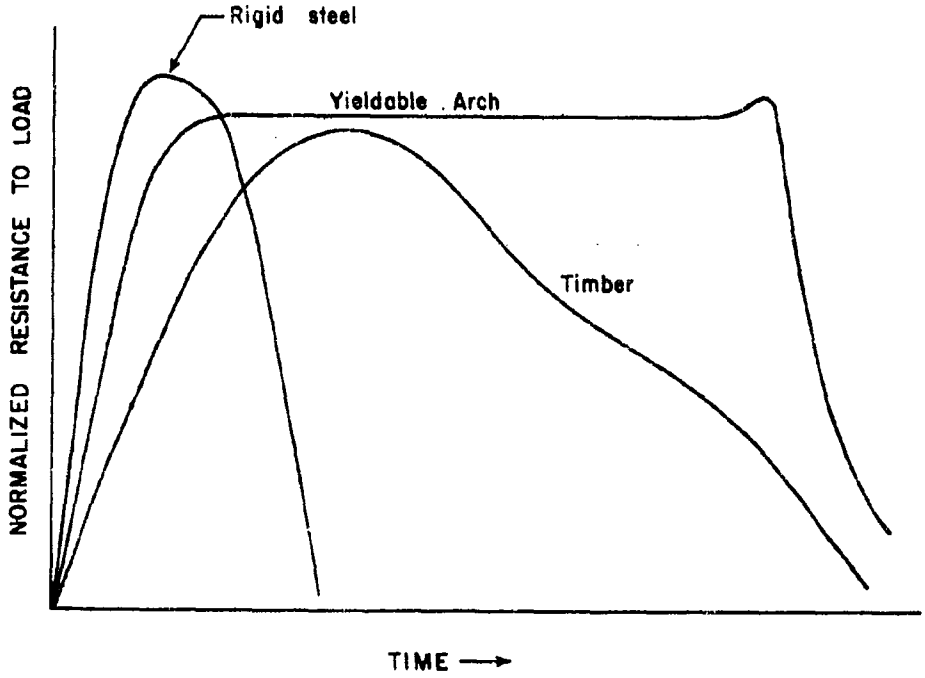


Figure 7.16. Hypothetical long time response curves for rigid steel, yieldable arches and timber. May be adapted to impact loading.

CHAPTER VII

REFERENCES

1. Gilbert, J.F., Elastic Wave Interaction with Cylindrical Cavity, E.H. Plesset Associates Inc., AF Bull. Div. Contract AF04(647)-342, December 1959.

2. Baron, M.L., et al., Theoretical Studies on Ground Shock Phenomena, The Mitre Corporation, October 1960.

3. Pantall, J.T., and Auld, H.E., Dynamic Stress Concentrations around Unlined Openings, AF SWC-TN-61-7, February 1961.

4. Durell, A.J., and Riley, W.F., Research Studies of Stress Waves in Earth and Model Earth Media, Armour Research Foundation, AFSWC-TR-60-4, October 1959.

5. Mindlin, R.D., Proc. Soc. Exp. Stress Anal., Vol. 5, 1948.

6. Terzaghi, K., and Richart, F.E., Stresses in Rock about Cavities, Geotechnique, Vol. 3, 1952.

7. Isaacson, E. de St. Q., Rock Pressure in Mines, Mining Publications, Ltd., London, 1958.

CHAPTER VIII

SIMILITUDE AND DEEP PROTECTIVE CONSTRUCTION

Introduction

If a strict application of mathematical theory were to be applied to treatment of scale factors for extrapolation of model blasting studies with a few pounds of HE to the effects of megaton size devices a large number of variables would of necessity enter into consideration. However, inasmuch as the effects of many variables such as mechanical and physical properties of rock, geologic structure, variation in pulse length, differences in explosive chamber size, magnitude of pressure, and others, cannot be evaluated and readily extrapolated by similitude, it is necessary to resort to gross effects and reasonable simplifications. By this means it appears to be possible, not only to make realistic approximations of the radius of probable survival of a deep installation, but to predict within a reasonable range pertinent safe design depths for various rocks of the types which would be recommended for protective installations.

For purposes of the following discussion it is assumed that the most damaging circumstances occur, i.e., that a bomb in the megaton range penetrates to sufficient depth, that it is sufficiently confined that a very large percentage of available detonation energy is transferred to the rock.

Similitude and Confined Explosives

The general scaling law for explosives may be stated in the following form:

$$S = \left(\frac{W_2}{W_1}\right)^{\frac{1}{3}} \qquad (8.1)$$

where

S = scale factor, i.e., the ratio between linear dimensions of model and prototype.

W_1 = weight of explosive for prototype.

W_2 = weight of explosive for model.

That is to say, the weight of explosive varies as the cube of the linear size of the model or prototype being tested. For example, according to theory if one pound of explosive is required to destroy a model tunnel, one thousand pounds would be required to cause the same degree of destruction in a tunnel ten times as large in all of its linear dimensions,

i.e., the linear dimensions of the explosive charge are increased in the same proportion as the increase in size of tunnel. This law of destruction by explosives is known as Hopkinson's rule[1]. It states that if all of the linear dimensions of a structure and the explosion to which it is subjected are scaled by a factor S, the resultant damage will be increased in the same scale or proportion. Cole[1] states that the rule is not known to be generally valid, but it was found to be true for the British "pot" gauge employed in testing the effect of underwater explosions.

The primary object of this analysis is to verify the fact that reaction of model and prototype tunnels and the parameters connected with explosive behavior obey this law, or to determine how much deviation may occur, its causes and how this may be taken into account in damage limit calculations.

In general, if it is assumed that the velocity of propagation depends upon stress and not the rate of strain then the scale factor S can be applied and the various factors of the model law may be tabulated as shown in Table 8.1. There was some indication that fracture may depend somewhat upon the rate of strain, but this apparently does not affect demolition results as much as other parameters such as confinement, strength of rock, etc.

Damage Scaling - Tuff. The damage-distance relationships for tunnel support tests were initially based on rock damage to tunnels in the Rainier event[2]. It was found in four subsequent detonations, however, that the closure effects upon access tunnels were greatly influenced by the tunnel configuration near the device. There is close agreement between the closure distances for the two tunnels with hooked ends, Rainier and Tamalpais. No correlation was indicated with the straight-end tunnels.

TABLE 8.2

Event and Tunnel	Tunnel configuration	Distance, zero point to closure	Angle of incidence zero point to closure	Yield	Distance to point of closure scaled to 1-kt	Outer limit zone 4, scaled to 1-kt
		feet	degrees	kt	feet	feet
Rainier, U-12b[a]	hooked	200	14	1.7	168	420
Tamalpais, U-12b.02	hooked	80	28	0.09	179	420
Logan, U-12e.02	straight	820	35	4.5	496	1190
Evans, U-12b.04	hooked	unknown	--	0.045	unknown	unknown
Blanca, U-12e.05	straight[b]	870	16	23.	306	690

[a] Information from Operation Plumbbob, included for comparison.
[b] With venting to the unusable portion of the drift beyond the zero point.

TABLE 8.1

Quantity (1)	Symbol (2)	Dimensions (3)	Diemnsions In New System (4)	Scale Factor (5)	Quantity In New System (6)	Quantities Comparable at a Constant Value of Distance r/S (7)
Length	L	L	SL	S	SL	L/S
Mass	M	pL^3	pS^3L^3	S^3	S^3M	M/S^3
Time	T	T	ST	S	ST	T/S
Force	F	MLT^{-2}	S^2LT^{-2}	S^2	S^2F	F/S^2
Energy	E	$ML^{-2}T^{-2}$	$ML^{-2}T^{-2}$	S^3	S^3E	E/S^3
Pressure	P	$ML^{-1}T^{-2}$	$ML^{-1}T^{-2}$	1	P	P
Velocity	v	LT^{-1}	LT^{-1}	1	v	v
Total Impulse	I'	MLT^{-1}	S^3MLT^{-1}	S^3	S^3I'	I'/S^3
Impulse per unit area	I	$ML^{-1}T^{-1}$	$SML^{-1}T^{-1}$	S	SI	I/S
Displacement	D	L	SL	S	SD	D/S
Acceleration	a	LT^{-2}	$S^{-1}LT^{-2}$	S^{-1}	$S^{-1}a$	Sa

TABLE 8.3

CRUSH AND FRACTURE ZONES - RAINIER & NEPTUNE

	Crushing - ft.	Scaled Distance	Fracture - ft.	Scaled Distance
Neptune	40 ft. down 50 - 80 ft. laterally	89 111-178	70 ft. downward	156
Rainier	80 - 130 ft.	67-108	220 ft. downward 280 ft. maximum	184 235

The size of the crush and fracture zones indicated by drilling the Rainier and Neptune sites (post-shot) have the distances and scaled distances in Table 8.3[3]. The scaled limit of the fracture zones for Rainier and Neptune corresponds quite closely to the closure distance for the Rainier tunnels. Hence, for tuff it appears that the fracture zone marks the limit beyond which survival might be expected and that support would be required for openings which approach this scaled distance. The scaled distance for other types of rock would not necessarily be of the same range of values.

Cratering and Scaling. Shelton, et al[4], in their studies of the possible uses of nuclear explosives for excavations state that HE test programs at NTS with charge weight ranging from 256 lbs. to 20 tons of TNT indicate from dimensional analysis that the basic scaling law based on $W^{1/3}$ is correct for true craters. (For apparent craters a scaling law closer to $W^{1/3.4}$ was found to apply due to gravity effects). Murphey and MacDougall[5], report that failure to eject material beyond the crater lip occurs at a scaled depth of burst of 2.5 (in lb.-ft. system) or 325 in the kiloton system (the multiplying factor being 130.1).

The major features of underground nuclear explosions conducted to date are given in Table 8.4. Neptune was the only one which broke through to the surface, and it was confined at a scaled depth of 220. Data for small scale cratering in various types of rock are given in Chapter V.

A comparison of the recorded fracture limits in UCRL 5757 and those tabulated in Table 8.3 agree very closely with the tunnel closure distances utilized by Lee and Wing given in Table 8.2.

ERDL Tunnel Demolition.[6] The Corps of Engineers conducted a series of tests to determine certain tunnel demolition criteria. Charges of HE were located in chambers in the rock (basalt) near the level of the spring line of full scale abandoned railroad tunnels. A summary of the shots fired is given in Table 8.5.

From the plots of scaled crater depths versus scaled charged depths (Chapter V) the indicated camouflet depths for the rocks are listed in Table 8.6, together with similar data from ERDL and NTS shots. The camouflet values for charges breaking to a free surface are undoubtedly too high for a tunnel target configuration. Comparable values to cause Zone 4* damage for openings are believed to occur well past the peak of the scaled charge depth versus scaled crater volume curve, but not at complete camouflet. The values so adjusted, selected somewhat arbitrarily, are included in Table 8.6. The values for Chalk may be anomalous at small scale because of its properties.

Scaled Cratering and Underground Damage Prediction. A plot of the results of numerous cratering experiments conducted in two types of granite, two types of sandstone, limestone, and tuff, and damage to target tunnels indicates scaling within reasonable limits for Zone 1 damage according to the cube root law. (Figure 8.1). Criteria for effective breakage is discussed in Chapter V, Rock Failure, utilizing data for crater radius, depth and volume.

* Zone 4 - Complete collapse.

TABLE 8.4

MAJOR FEATURES OF UNDERGROUND NUCLEAR EXPLOSIVES

Event	Yield (W) kt	Medium	Depth (D) feet	Scaled Depth $D/W^{1/3}$	Measured radioactivity deposited on surface %	Crater volume yd^3	Crater volume/kt yd^3
Jangle-S	1.2±0.1	Alluvium	-3.5*	-3.3*	65	1,650	1,400
Jangle-U	1.2±0.1	Alluvium	17	16	80	37,000	31,000
Teapot-Ess	1.2±0.1	Alluvium	67	63	90	96,000	80,000
Neptune	0.090±.020	Bedded Tuff	99	220	1-2	33,000	370,000**
Blanca	19.0±1.5	Bedded Tuff	835	310	0.5	0	0
Logan	$5.0^{+0.2}_{-0.4}$	Bedded Tuff	830	485	0	0	0
Rainier	1.7±0.1	Bedded Tuff	790	670	0	0	0
Tamalpais	0.072±.010	Bedded Tuff	330	780	0^{+}	0	0
Evans	0.055±.030	Bedded Tuff	840	2200	0^{++}	0	0

*3.5 feet above surface.

**This explosion took place in bedded tuff under a sloping surface 1:3 so the crater is probably larger than would be expected on a level surface.

+ No breakthrough to surface but radioactive gases in large quantities leaked into the tunnel.

++ No breakthrough to surface but stemming failed, releasing gross fission activity into the tunnel.

TABLE 8.5

ERDL TUNNEL DEMOLITION

Charge Size	Depth ft.	Scaled Depth-lb.	kt.	Results
500	15.7	1.97	256	Slight spalling
750	15	1.66	216	Broke through
750	15	1.66	216	Broke through
2-750*	15	1.66	216	Broke through
4-750	15-20	1.66	216	Broke through

* In coyote tunnels, unstemmed, charges fired simultaneously.

TABLE 8.6

CAMOUFLET SCALED DEPTHS AND FRACTURE ZONES FOR ROCKS

	Pound Base		Kitoton Base		
Rock Type	Camouflet	Adjusted Value	Camouflet	Adjusted Value	Remarks
Lithonia Granite	3.0	2.8	390	364	Free surface
Marlstone	4.0	3.2	520	416	Free surface
Kanawha Sandstone	3.5	2.7	465	351	Free surface
Niobara Chalk	4.8	4.0	624	520	Free surface
Unaweep Granite	4.3	3.3	559	429	Free surface
Navajo Sandstone	4.5	3.5	585	455	Free surface
Basalt (ERDL)	2.0	-	260	-	Tunnel target full scale
Tuff (NTS)	1.41-1.81	-	184-235	-	Tunnel target full scale
Limestone (MSM)	1.9	-	247	-	Tunnel target model scale

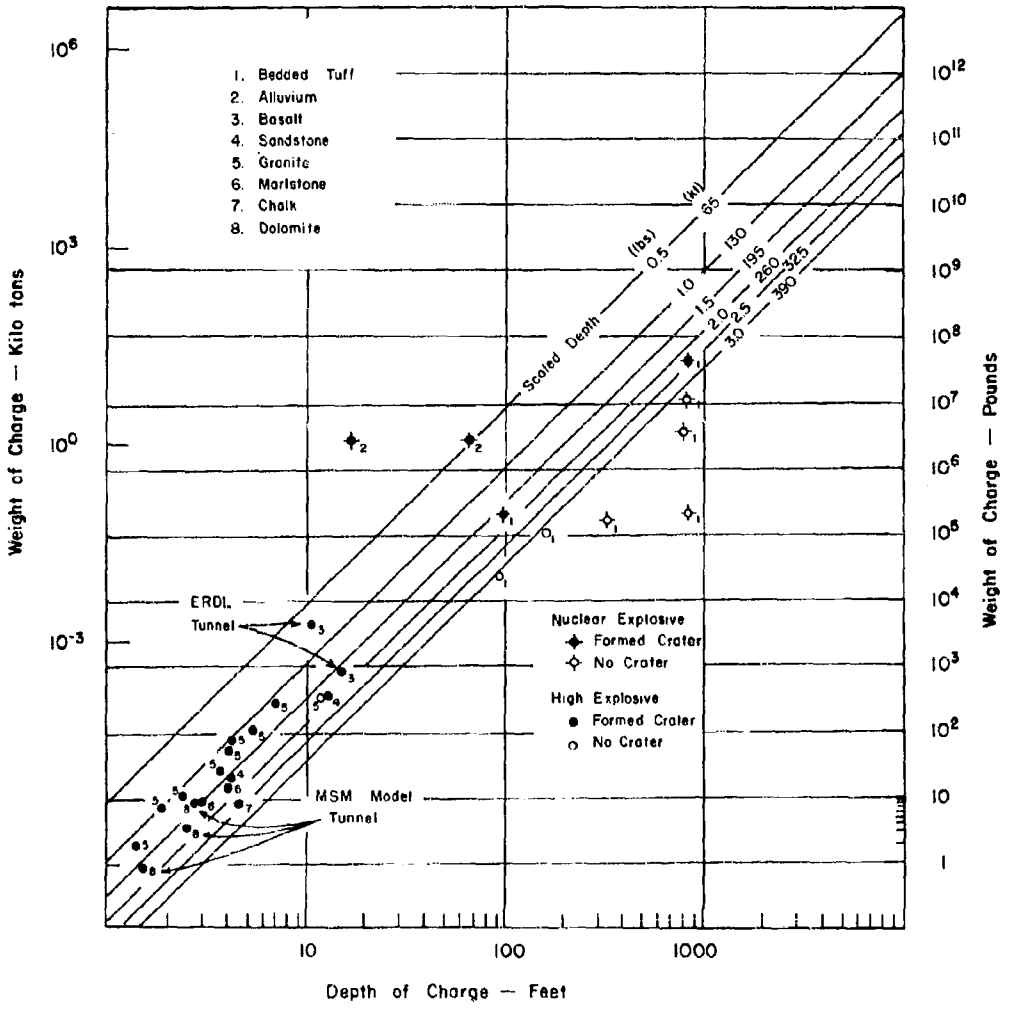


Figure 8.1a. Scaling of HE and Ne shots which were effective in cratering. All underground nuclear shots also included. Scaled distances are well-defined for Zone 1 damage.

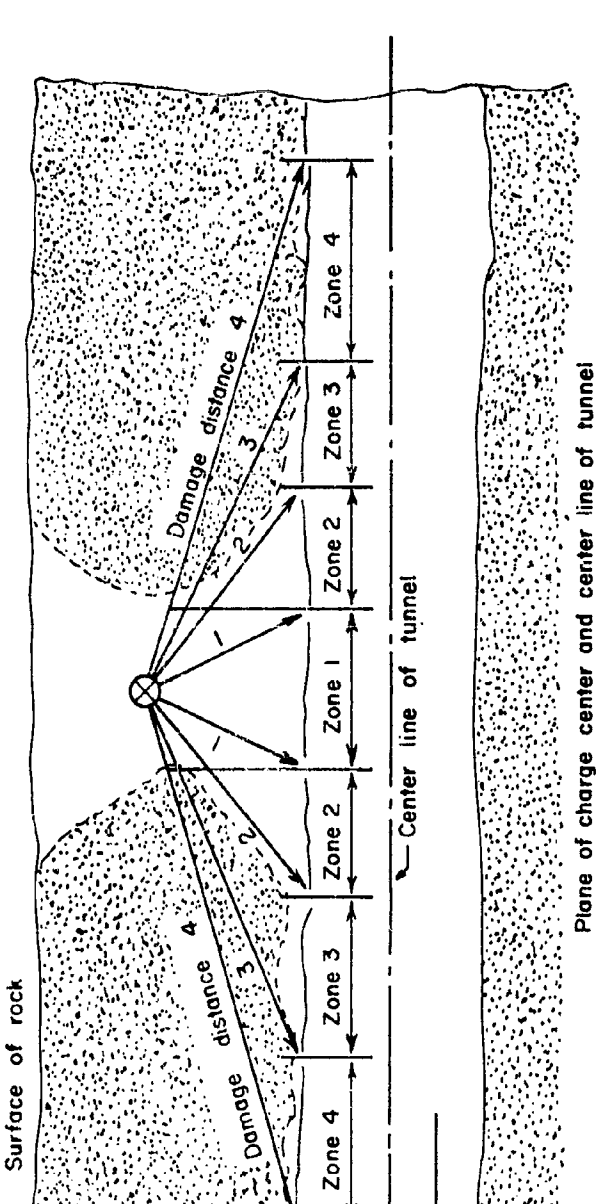


Figure 8.1b. Schematic diagram showing damage-distance notation and zones of damage. (2)

The most reliable single criterion appears to be a curve for crater volume because it is a measure of breakage energy (Figure 8.2). Proposed schematic sections for damage of Zone 1, 2, 3 and 4 types are indicated. Thus, if a series of crater experiments in the protective installation rock mass can be performed and the proper correlation is known between cratering and tunnel damage phenomena, the safe depth for the installation can be predicted quite accurately without a detailed knowledge of all of the physical properties of the rock. The geologic structure must, of course, also be known in detail, and the overlying rock have attenuating properties equal to or greater than that of the rock in which the installation is to be excavated. It is likely that where the target is the restricted surface of a tunnel that the curve would drop more rapidly on the right, depending on the spacing of geologic weaknesses relative to the size of the tunnel.

The determination of the correlation parameters for this type of extrapolation would appear to be a most fruitful field for research to furnish reliable data and criteria for engineering design.

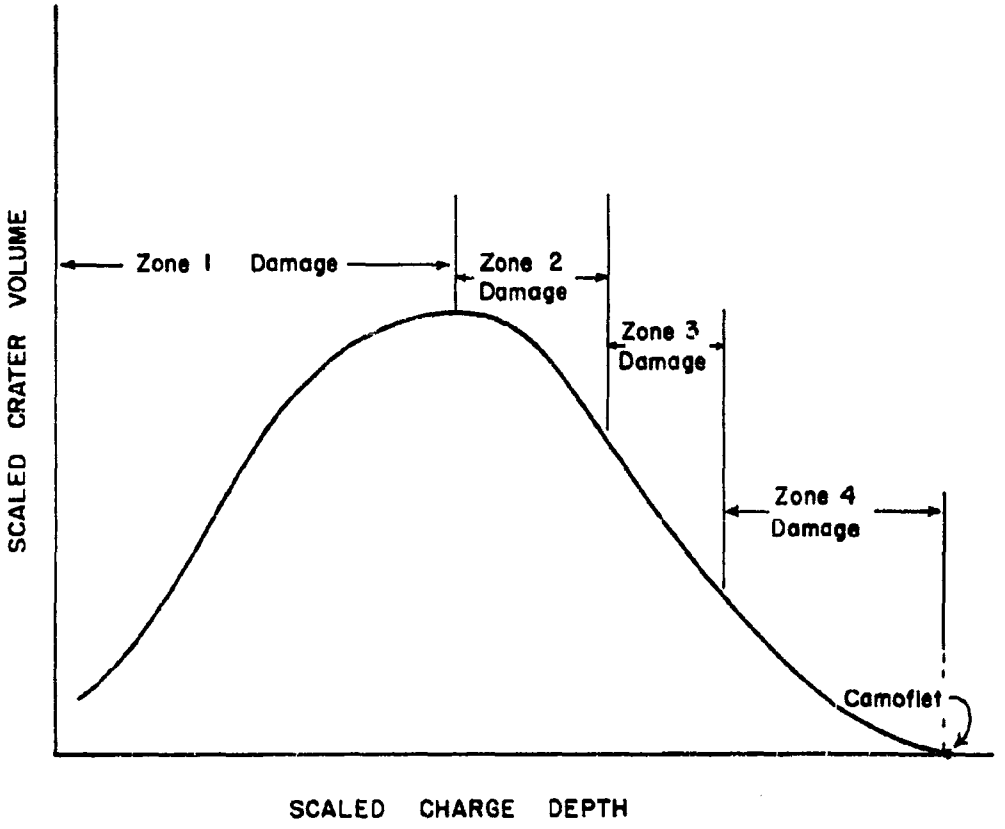


Figure 8.2. Schematic curve of scaled crater volume vs. scaled charge depth utilized to predict zonal damage to target underground openings.

CHAPTER VIII

REFERENCES

1. Cole, R. H., Underwater Explosions, Princeton University Press, 1948.

2. Lee, A. A., and Wing, E. Y., Evaluation of Blast and Shock Effects on Tunnel Support Structures, AED ITR-1714, May 1959.

3. Thompson, T. L., and Misz, J. B., Geologic Studies of Underground Nuclear Explosions Rainier and Neptune, Final Report UCRL-5757, Oct. 1959.

4. Shelton, A. V., Nordyke, M. D., and Goeckerman, R. H., The Neptune Event - A Nuclear Explosive Cratering Experiment, UCRL-5766, April 1960.

5. Murphey, B.F., and MacDougall, H. R., Crater Studies in Desert Alluvium, Sandia Corporation, SCTM 119-59, (51).

6. Mason, R. M., and Crossley, C. H., Hasty and Deliberate Tunnel Demoli-Tests Conducted Near Scenic, Wash., and Maupin and Madous, Ore., ERDL Report 1408, June 1955.

CHAPTER IX

SUPPORT OF UNDERGROUND OPENINGS

Introduction

Many of the sizes and shapes of openings that are proposed to be utilized for deep underground protective construction are the same as those which may be found in mines, tunnels and other types of man-made excavations. Consequently, the types of support required for quiescent conditions are identical for both types of openings under similar geologic conditions. No proven method of support has been devised for the loading conditions which would need to be resisted under high level impact loading.

If a site is chosen so that the majority of openings are in firm, strong rock, little or no artificial support will be required for stability under normal conditions. It is likely that in the most ideal rock, however, some support will be required in broken or faulted areas. Also, the proven methods of safe static support and support under "squeezing" conditions will provide the best basis for design of supports to resist transient or dynamic loads.

In either the case of static loading or dynamic loading, certain areas of an underground installation may require artificial support in areas of faulting, jointing, alteration, etc. For a large portion of openings in many mines timber support is employed. Timber is often chosen because of its lower cost and the relatively short period which is required for the mine openings to be kept operative. However, the properties of timber have been found to offer some advantages. First, timber usually fails slowly and is capable of supporting relatively large loads accompanied by large deflections. In squeezing ground timber will usually fail slowly and give adequate warning of high pressure from the rock which it is supporting. This quality may also be an advantageous one to utilize in protective construction to absorb a fraction of the shock and high velocity spallation from a high order impact load.

Static Support

Mine Timbering.[1] Some types of mine timbering are designed to support large openings (stopes) temporarily. That described below is adaptable largely to openings such as tunnels and large rooms which are approximately equi-dimensional in cross-section.

The simplest type of timbering is a one piece set composed of a single post, denoted stull or prop in mining terminology (Figure 9.1). It is placed primarily for support of loose slabs or where only a moderate amount of timber is required to hold the roof or wall. Two piece and three piece sets in Figures 9.2 to 9.4 are used where no timber sill

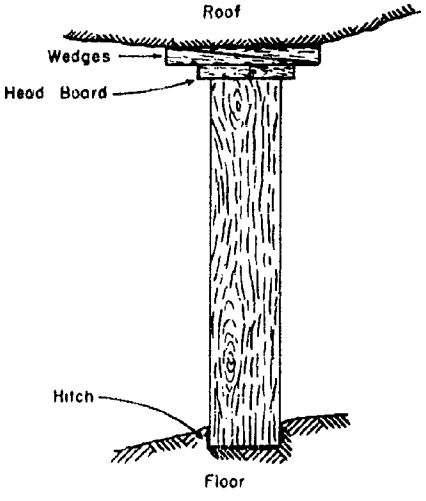


Figure 9.1. Post.

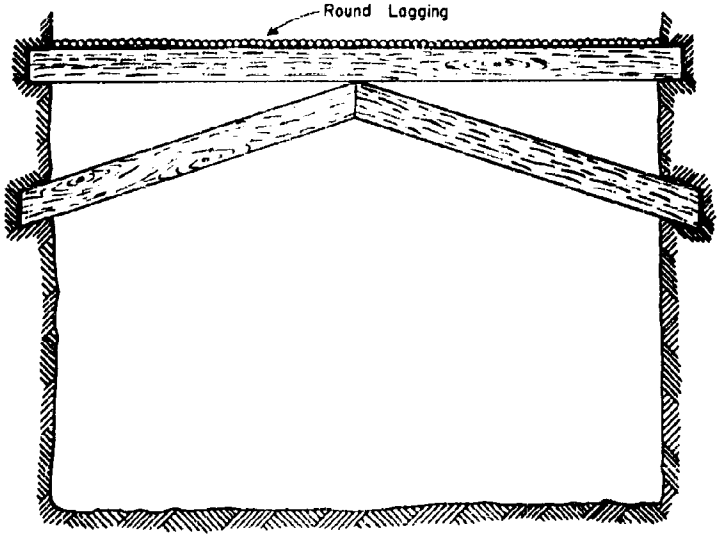


Figure 9.2. Reinforced stull.

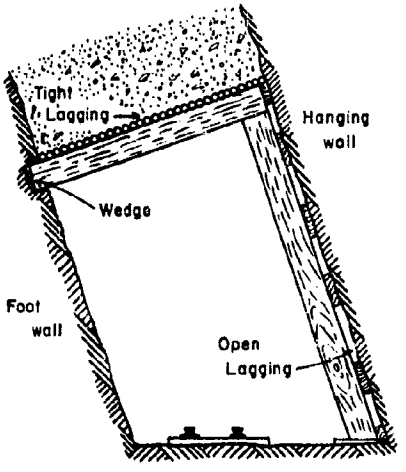


Figure 9.3. Two-piece stull set.

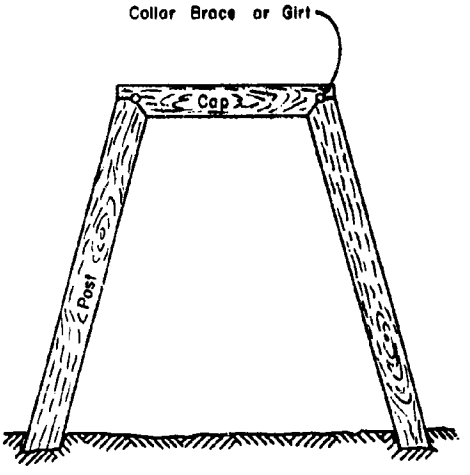


Figure 9.4. Three-piece set, inclined posts.

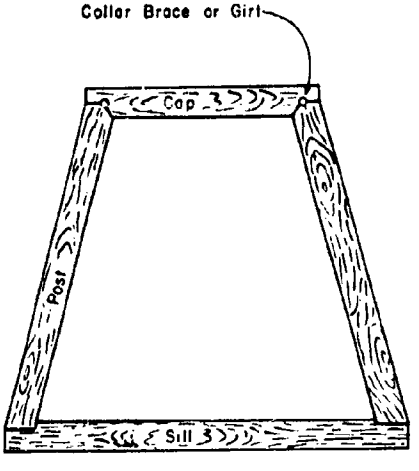


Figure 9.5. Four-piece set, sawed timber.

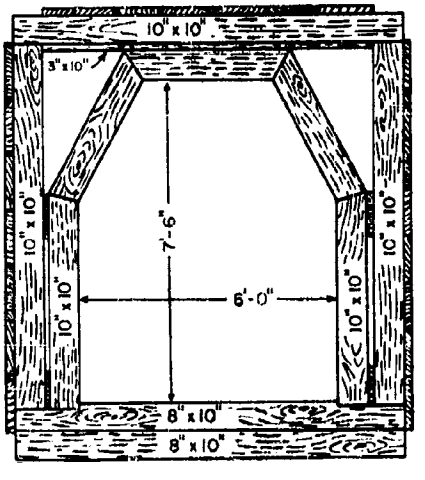


Figure 9.6. Heavy timbering at Broken Hill, N.S.W.

is required. For ground which requires still more support in drifts (tunnels) four-piece set designs are applicable as illustrated in Figures 9.5 and 9.6. For timbering of large stopes whose walls require close support, square sets are placed in excavations as soon as a sufficient amount of ore has been removed to make room for a timber set. This usually provides temporary support, however, and is filled with waste (broken rock) for permanent stability.

Cribbing offers a very strong type of timber support and its simplest form is fabricated by placing of lengths of square section timber at right angles to each other in successive layers. It may be built to any height and for stronger support may be filled with waste rock. A strong type of framing is made by dovetailing the timbers at the corners. (Figure 9.7)

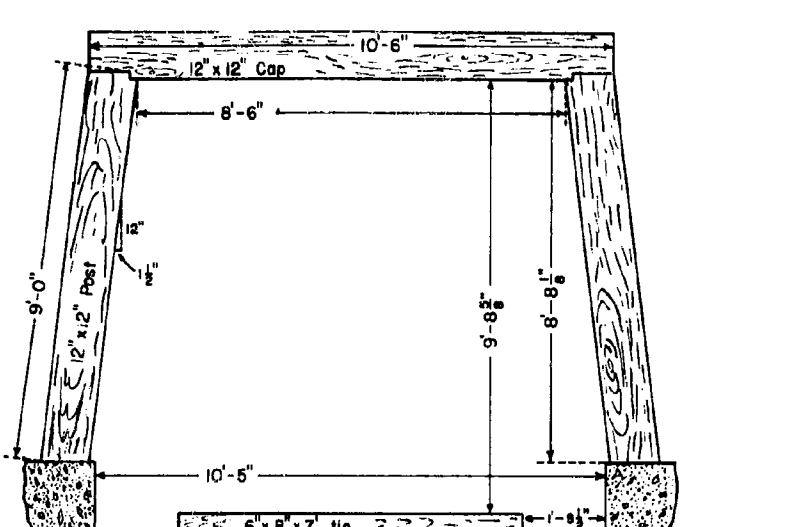
Steel Support

Proctor, White and Tergaghi[2] have offered a series of empirical formulas for the determination of loads on steel tunnel sets for various types of ground. The values employed are based on results of experiments in sand and observed behavior of timber in tunnels in the Alps. However, these design criteria are for the most part applicable to tunnels of shallow depth, or assume a limited amount of arching in the superincumbent rock which causes both a horizontal and a vertical load on the tunnel supports. In most cases the load is taken as a factor multiplied into the sum of the width and height of the tunnel. This appears to have some justification as a first approximation for static loads, particularly in sand or swelling ground, deteriorated rock or types of rock which slakes or swells on exposure to air.

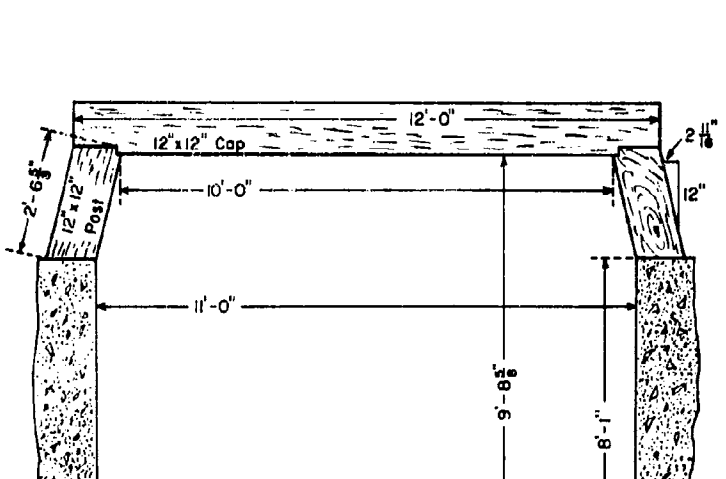
Steel can be erected in a shorter time and with fewer men than timber. The trend towards steel also has been because timber rots and decays behind the concrete lining which results in an uneven load on the framing or lining.

The first step in the design of a tunnel is the choice of cross sectional shape. Although upon first analysis it may appear that a circular cross section is the preferred design shape this does not automatically preclude others from consideration. Conventional cross sections (Figure 9.8) provide a horse shoe shape with a somewhat curved floor. Most shapes are adaptable to either timber or steel support (Figure 9.9).

Proctor, et al[2], point out that for tunnel support systems made of steel there are roughly five types: (1) continuous rib, (2) rib and post, (3) rib and wall plate, (4) rib, wall plate and post, and (5) full circle rib. These principle systems are shown in Figures 9.10 to 9.14. Figure 9.15 illustrates an invert truss type in combination with continuous ribs. The factors which must be considered in choice of a support system are (1) method of excavation, (2) rock behavior, and (3) the size and shape of the tunnel cross section. Methods include the full face method, top heading and various pilot drift methods. In protective construction, support requirements will be the primary consideration and the method of excavation will not necessarily govern the design of support members where they are required.

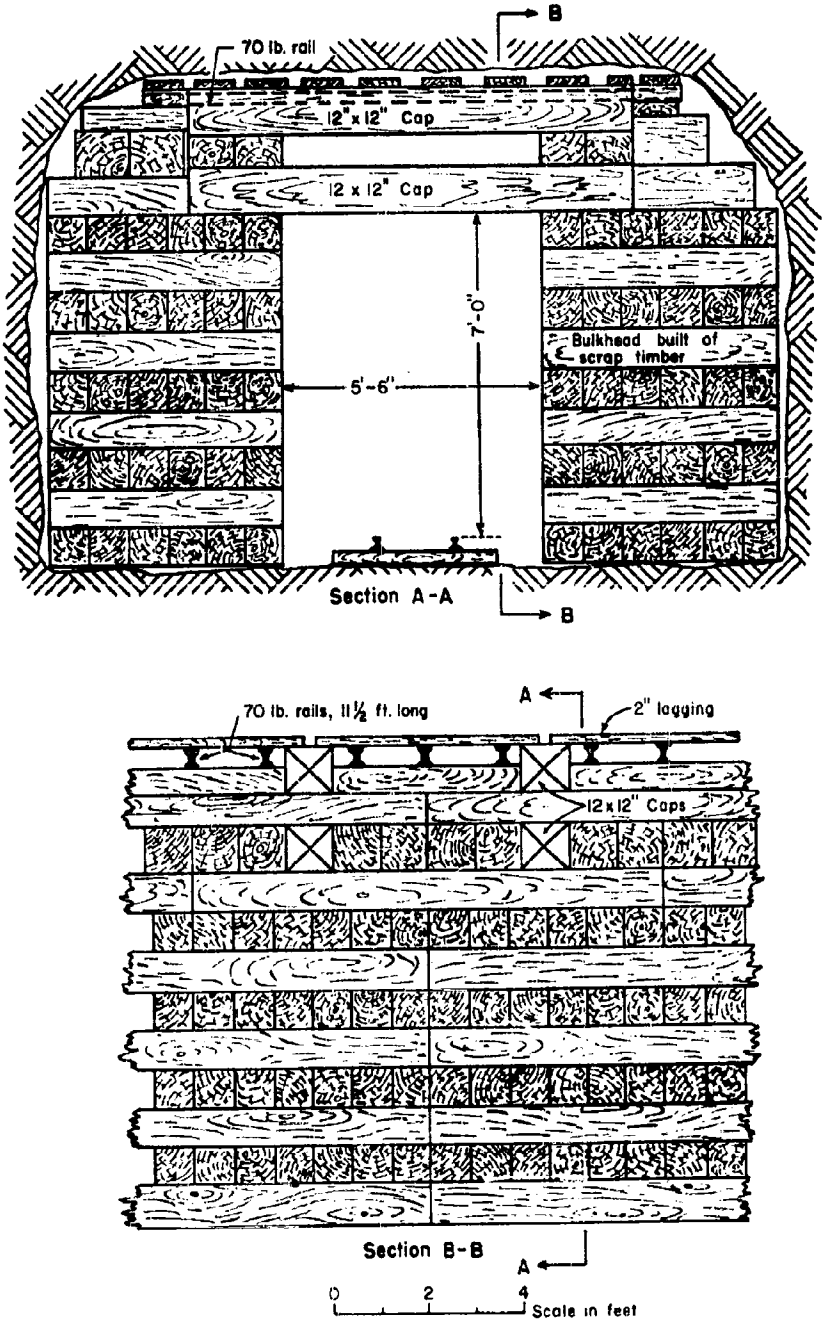


Standard 12" x 12" Tunnel Timber



Special 12" x 12" Tunnel Timber

Figure 9.7a. Support at United Verde mine.



Timber Bulkhead

Figure 9.7b. Support at United Verde mine.

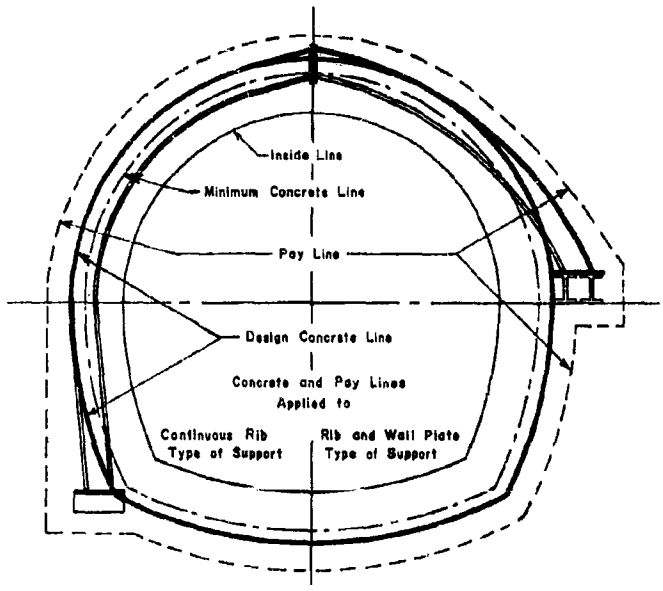


Figure 9.8. Tunnel cross-sections.

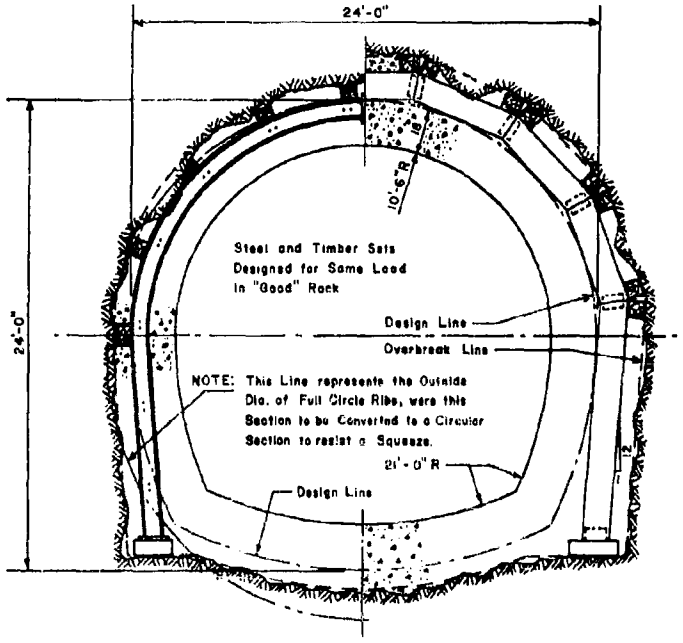


Figure 9.9. Comparison of steel and wood supports.

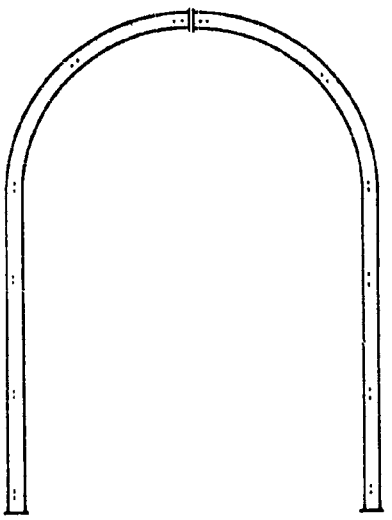


Figure 9.10.
Continuous rib type.

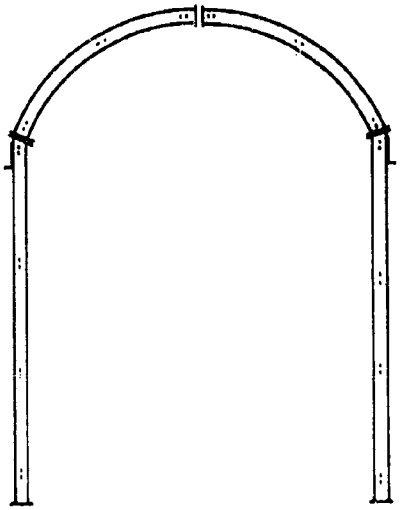


Figure 9.11.
Rib and post type.

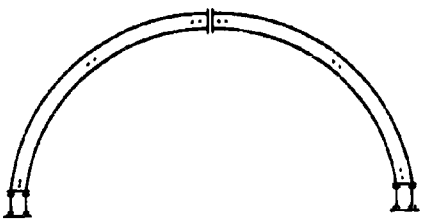


Figure 9.12.
Rib and wall plate type.

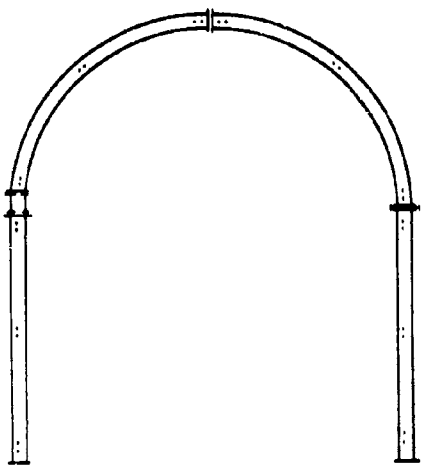


Figure 9.13.
Rib, wall plate and post type.

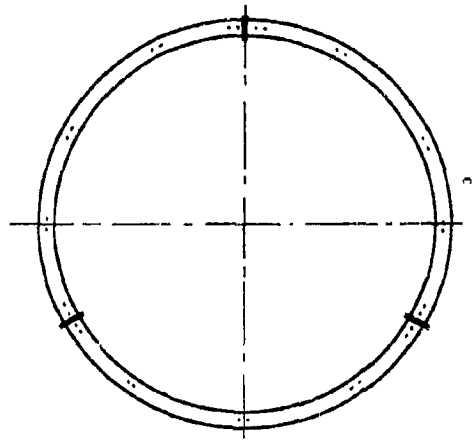


Figure 9.14. Full circle rib type.

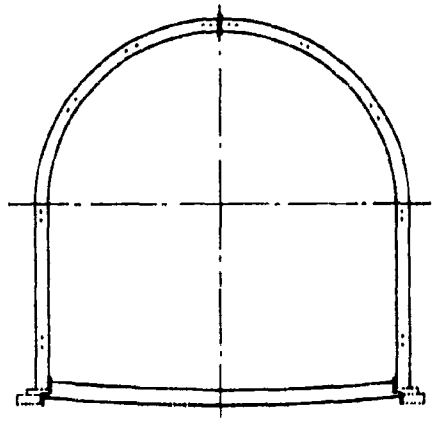


Figure 9.15. Invert strut.

A continuous rib type (Figure 9.10) is usually made in two pieces for maximum speed of erection, lowest first cost, and lowest erection cost. It is sometimes used in three or four pieces to meet special conditions and with the following methods of attack: (1) full face, (2) side drift, and (3) multiple drift. A rib and post type (Figure 9.11) is employed with the following methods of attack: (1) full face - in tunnels whose roof arch makes an angle with the side wall, (2) multiple drift and side drift - in tunnels of such large size that two-piece continuous ribs cannot be shipped and/or handled, (3) heading and bench and top heading - for support in the drift (with truss panels) for early support to roof. In the rib and wall plate type (Figure 9.12), the rib is also usually made in two pieces for maximum speed of erection, lowest first cost, and lowest erection cost. It is sometimes used in three or more pieces to meet special conditions and with the following methods of attack: (1) heading and bench, (2) top heading, and (3) full face. This type is especially applicable to circular and high sided tunnel sections where only a light roof support is needed. The rib, wall plate and post type (Figure 9.13) is used with the following methods of attack: (1) heading and bench and top heading - for quick support to roof, (2) side drift - in large tunnels with bad rock conditions requiring quick support, and (3) full face - for favorable rock where support is not needed tight to the face, for tunnels whose roof makes an angle with the side wall, and where post and rib spacing differ.

The full circle rib type (Figure 9.14) is used with the following methods of attack: (1) full face - in tunnels in squeezing, swelling and crushed rock, or any rock that imposes considerable side pressure, also where bottom conditions make it impossible to carry roof loads on foot blocks, and in earth tunnel conditions sometimes encountered in rock tunnels; (2) heading and bench - under earth tunnel conditions with joints at spring line. The invert strut (Figure 9.15) is used where mild side pressures are encountered, and also to prevent the bottom from heaving. A full circle with ribs closely spaced (Figure 9.16) is heavily lagged for heavy loads associated with squeezing conditions.

For a yielding lining for swelling rock (Figure 9.17) the squeeze is allowed to exhaust itself before placing the permanent lining, and the full circle type of steel support is used. The ribs are at wide spacing to permit the ground to extrude into the tunnel between them. Crush lattices of white pine are placed in the rib joints to permit shortening of the ribs to soften the ground. The ribs may be divided into any reasonable number of segments (3 shown in Figure 9.17) to provide the desired amount of shortening. When liner plates begin to buckle inward, they should be unbolted and allowed to rest on inner flanges of ribs above the spring line to protect from falls. Below the spring line they may be taken out permanently.

It is necessary to establish uniform contact between rib and rock to insure uniform loading of the ribs. Hence, a light gauge line plate lagging is used for erection and graveling purposes. The light liner plates offer little resistance to the squeezing ground and are removed as soon as distortion indicates the ground is being extruded between the ribs.

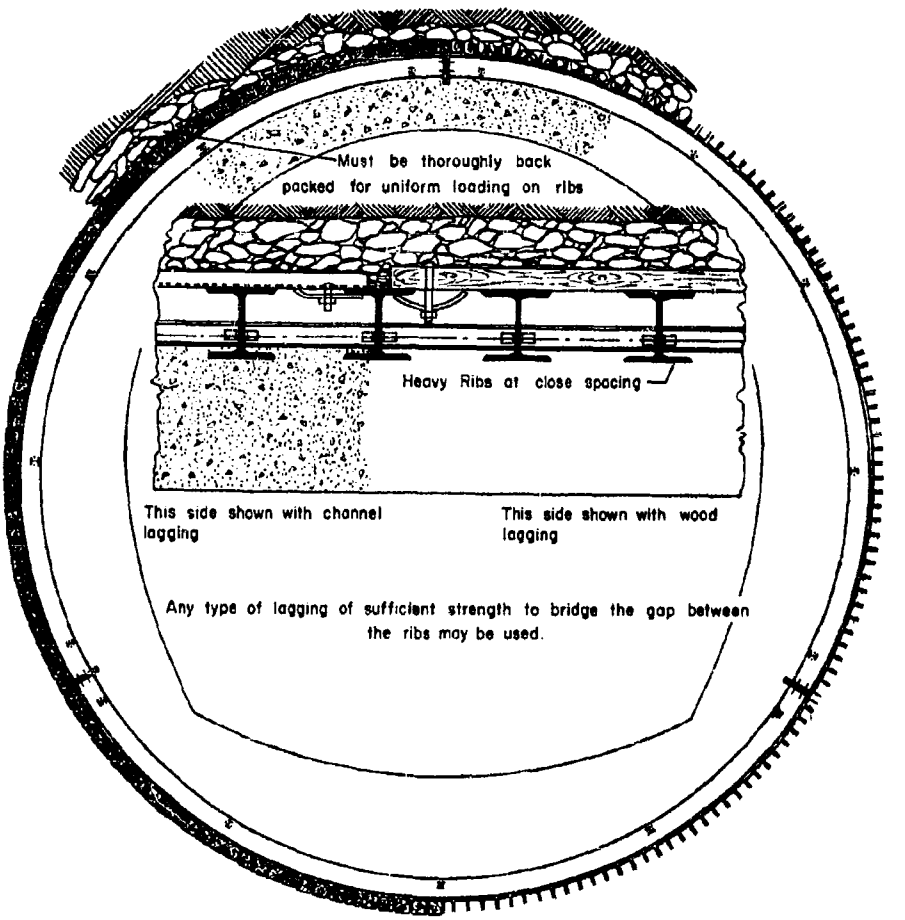


Figure 9.16. Full circle with ribs closely spaced.

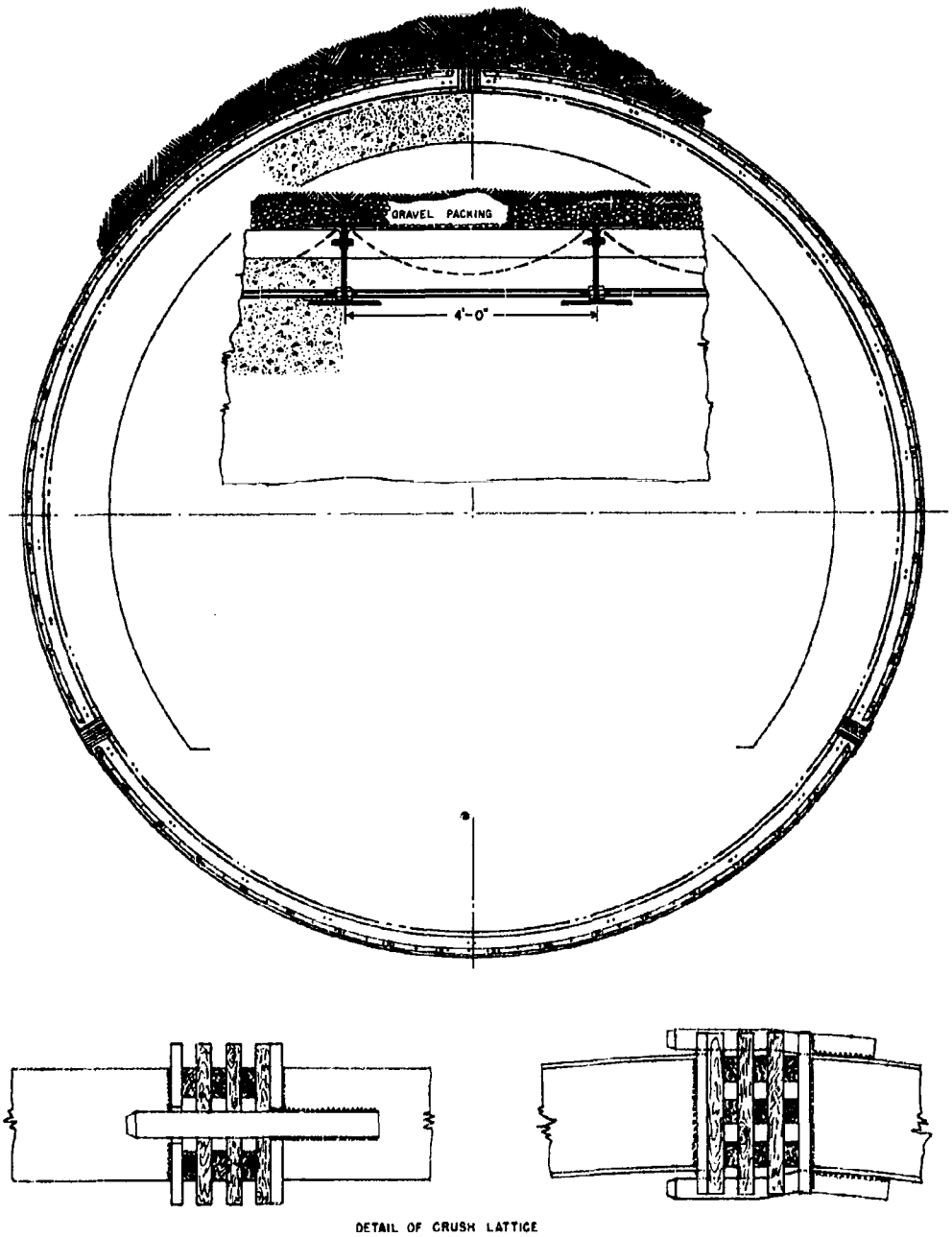


Figure 9.17. Yielding lining for swelling rock.

The pressures created on support members by squeezing and swelling ground approximate a hydrostatic field in plastic material and also represent some aspects of the critical stress conditions which would be imposed by the transients from a blast induced stress wave. It has been found that if swelling or squeezing ground is encountered it is highly desirable to convert the external cross-section of a tunnel to a full circle even if it means enlarging considerably to maintain the necessary internal clearances. Under squeezing conditions the steel ribs act as rings and are subject only to radial thrust without bending, thereby utilizing the greatest resistance per unit weight of steel. (Figures 9.16 and 9.17.).

One of the practices employed in swelling ground is to install full circle ribs at a wide spacing of about 4 feet and let the ground squeeze between the ribs until it reaches equilibrium. This method can be used in those cases where the strength of the rock is low enough to "flow" around the ribs without overstressing them (Figure 9.15).

Static Load Assumptions. According to Proctor, et al.,[2] a large portion of the overburden pressure is sustained by a rock or ground arch, which is assumed to develop under static conditions as a tunnel is excavated. The thickness of the effective arch varies with the type of overburden, the size and depth of the tunnel, method of excavation and the amount of support that is provided in the opening. An arch provides a natural shape for a tunnel roof and the design problem becomes one of providing a support system to stabilize the "keystone" of the arch. The arch rib is wedged against the rock and the procedure for its design is different from that of a free arch rib.

That is, in the open, the shape of the arch is adjusted to follow the thrust line from known loads, while underground the rib must follow the shape of the tunnel cross section and may depart widely from a thrust line determined by the assumed active loads. However, the thrust line can be made to follow the required arch contour, because the passive resistance of the rock resists forces tending to displace it. When the arch is properly blocked this passive force prevents the rib from changing shape.

Active loads are defined as those which tend to move or distort the rib, and are due to the weight of loose rock.

The rock load may closely approximate a uniform load if a tight, back-packed lagging is provided. However, in most cases the rock force is transferred to the ribs by a number of blocks inserted between the rib and the rock at blocking points. The force at the blocks are neglected and the active loads, usually vertical, may be resolved into two components, one of which is radial and is the only one considered.

The first step in design is to assume a type of active load and to apportion it among the blocks. It is also assumed that the steel will carry a certain arch thickness of the rock above the tunnel and that this weight of rock imposes a uniform vertical active load on the rib. If the load is not uniform the active force at some one blocking point will determine the thrust in the rib, which causes the rib to press against

The rock at all other blocking points with a force greater than the active rock forces at these points. Thus, in this case it is reasoned that the rib is actually proportioned for a single concentrated load on one block and all other loads can be neglected when this is found.

The point of maximum thrust is not predictable, however, and a uniform load is assumed equal to the weight of an inverted V or U of rock whose depth is one-half the width of the tunnel and whose length along the tunnel is equal to the width. Figures 9.18 to 9.21 illustrate various types of load assumptions. It will be noted that the sum of the active and passive forces which act on one blocking point (total length of arrow represents pressure in blocking point) is the same on all diagrams. Since the total external forces are the same in each case the internal stresses in the ribs for each type of loading are identical. In Figure 9.18 on the left is a uniform load distribution in which the shaded areas represent the rock which produces the loading. The height of the supported rock mass is H_1, the thin portions of the arrows representing active forces exerted on the rib and the wider portions the passive resistant forces. The right side represents a triangular loading based on a 45° break line which imposes the same total force on the ribs although the active and passive forces exist in different proportions.

Where there is a single active blocking point such as that shown at A in Figure 9.19 which is the same as the force at A in Figure 9.18, it is seen that the total force distribution is the same although the other forces are all passive. Figures 9.20 and 9.21 show other types of active loading conditions which may be made to similate uniform loading by controlling the amount of total active plus passive force exerted on each block. That is, by proper blocking the effective load is kept uniform providing the rib is not distorted.

Forces and Stresses in Blocked Ribs[2]

If the blocking points on a rib are too widely spaced bending stresses as well as thrusts are induced, which reduces the load carrying capacity of the rib. The bending moment varies as the square of the block spacing.

In design a layout is first made of one-half of a rib set. Blocking points are required close to the crown joint and one at the spring line or the junction between the arch and leg if the leg is battered. The intermediate blocking points are spaced according to the condition of the rock. The more firm the rock the greater the spacing can be. Because of irregularities in the rock surface a blocking point can be established only where suitable rock surface is available. Hence, block spacing will deviate widely from a given average.

Spacing of blocking points is governed by the following:

a. Cost of blocking varies with number of blocks required, but enough blocks should be placed, even against firm ground, to support the rib and give proper stress distribution.

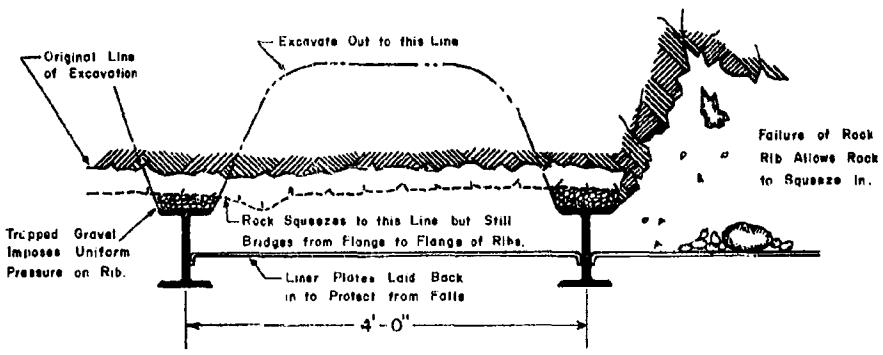


Figure 9.17a. Over-mining in stiff swelling ground to induce softening. The ground is allowed to squeeze to soften it. Slots may be excavated beyond the ribs in harder ground. This is repeated until the squeeze has run its course before concreting.

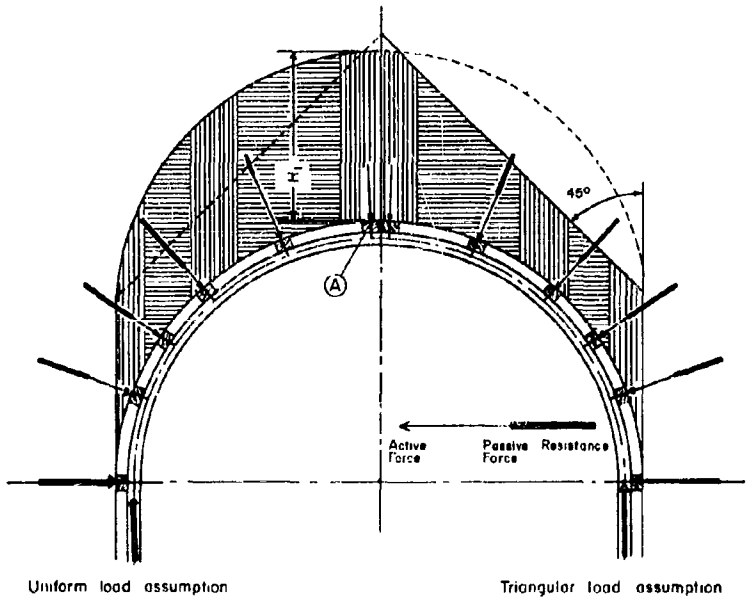


Figure 9.18.

The total combined active and passive forces at corresponding blocking points are the same in each loading assumption.

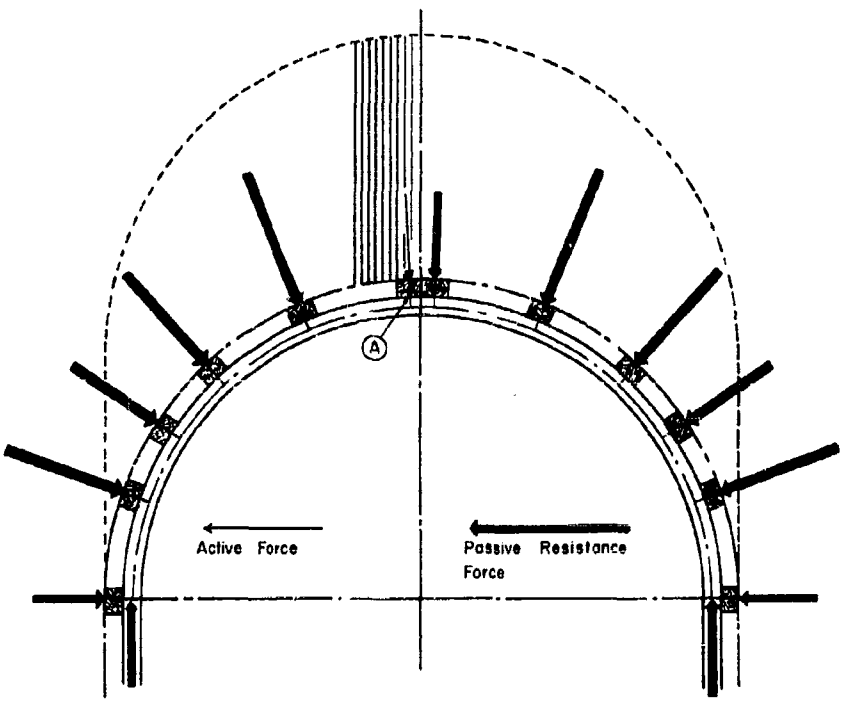


Figure 9.19. Concentrated load assumption. A concentrated active load at one blocking point induces passive forces at all the other blocking points. If the load at A is equal to the load at A in Figure 9.18, forces at all the other blocking points are the same as in Figure 9.18.

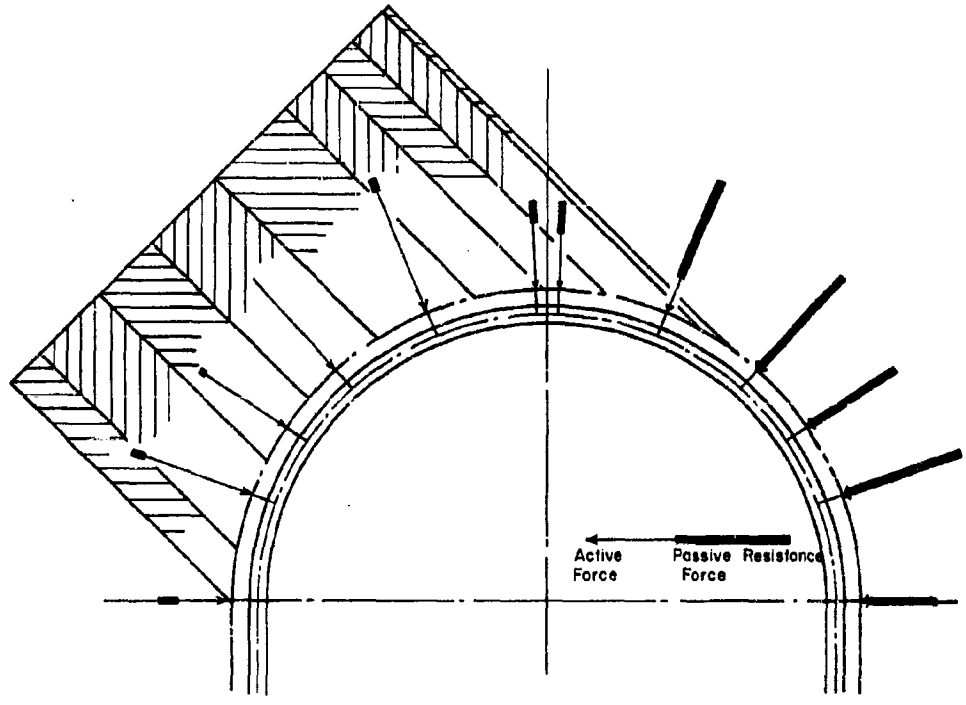


Figure 9.20. Oblique load assumption. When loads act obliquely they set up forces at the blocking points in the same manner as uniform vertical loads. The figure shows an assumption wherein the load is acting at 45° to the vertical. Such a condition might occur where the strata are inclined steeply or where a fault occurs at one side of the roof. Total forces set up at the blocking points are the same as for the uniform load assumption shown in Figure 9.18.

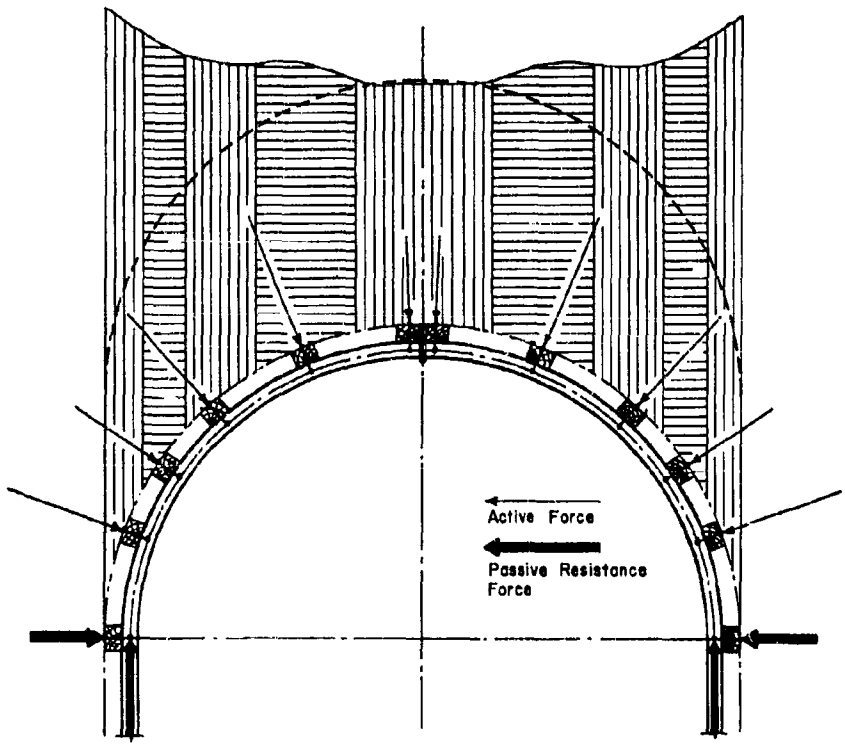


Figure 9.21. Where it is possible to apply the exact amount of active load to each blocking point to balance all forces, the loading diagram could be assumed as in this figure. All active forces are equal to the combined active and passive forces on the uniform load assumption, Figure 9.18.

b. For a given shape of rib and rock load the bending moments increase with increased spacing between blocks. The size of arc between blocks, and hence the bending moment, increases as the square of the distance between blocking points. The influence of rib spacing is indicated in Figure 9.22. (See Appendix 9-A for computations.) The reduction of stress for D (Figure 9.22) as compared to A is due to decreased spacing. The dimensions of the rib itself must be chosen on the basis of the greatest possible load effects. Therefore design is based on maximum tolerable spacing. Tables 9-B.1 and 9-B.2, Appendix 9-B, are used as guides in block spacing for static loading.

Blocking Points. Each block transfers part of the rock load to the rib, and the method of allocating the load is illustrated in Figure 9-A.1 in Appendix 9-A. The center of contact between the block and the rock surface is around the overbreak block point. Blocks transmit little or no shear and are oriented normal to a line tangent to the rib at the point of contact (Figure 9.23). The inner pin is assumed to be the neutral axis of the rib and is termed the neutral axis blocking point.

When a rib is installed there is no active rock force, otherwise a section of the rock would have fallen. It is postulated, therefore, that the rock load is supported by arch action of the rock, or by crown bars or temporary posts. Wedging of the block pre-stresses the rib and it in turn exerts an active force against the rock at each overbreak blocking point, represented by F_r in Figure 9.24a. The dash-dot lines represent the overbreak line and the small circles the overbreak blocking point. The rock resists by a passive force F_p, which establishes equilibrium. As temporary posts are removed or further excavation takes place, the rib begins to support the weight of the rock W, which acts in a vertical direction on the overbreak block point (Figure 9.24b). F_p hypothetically rotates and changes magnitude and direction as W increases until it may reach a maximum position tangent to the overbreak line.

Further increase in W changes part of the force F_r from active to passive. The rib no longer tends to displace the rock, but the rock deforms the rib which must exert a greater force to maintain equilibrium. In practice blocks should be wedged tightly so that F_r can never become passive.

Values of W are assigned from assumptions of active vertical loads. Ideally, it was assumed (Figure 9.18) that each block carried a rock load bounded by four vertical planes, and this prism is referred to as the active prism. An upper limiting value of F_r of the required rib force is obtained by assuming that the vertical sides of the active prism are frictionless. Based on this assumption the passive force F_p must act in a horizontal direction and the magnitude of the radial force F_r maximum is obtained by means of the force parallelogram in Figure 9.24f. The lower limiting value of F_r minimum is obtained by assuming that F_p acts tangent to the overbreak line (Figure 9.24g). The real value of F_r is somewhere between these two limits, depending upon the location of the real joints (fractures) in the rocks. It must also be recognized that real joints are not planes, and are seats of friction and interlock. Thus, it may be assumed that the adjacent rock can react on the active prism with a force applied at some angle, the vertical component of which is

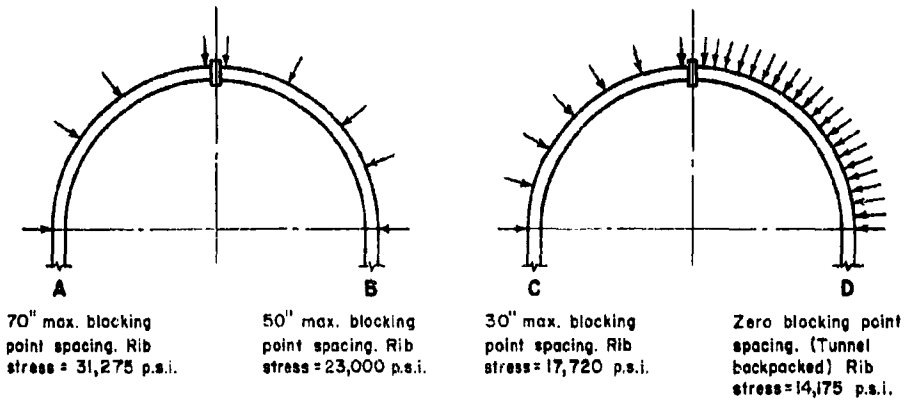


Figure 9.22. Effect on rib stress of changes in blocking point spacing.

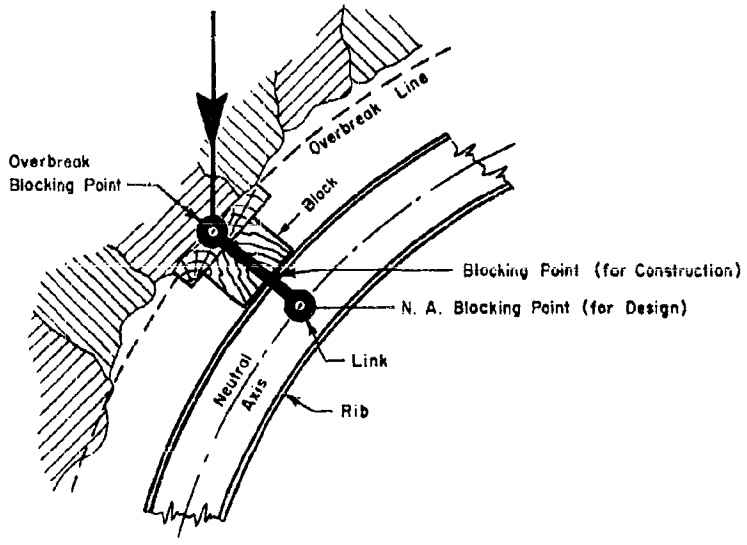
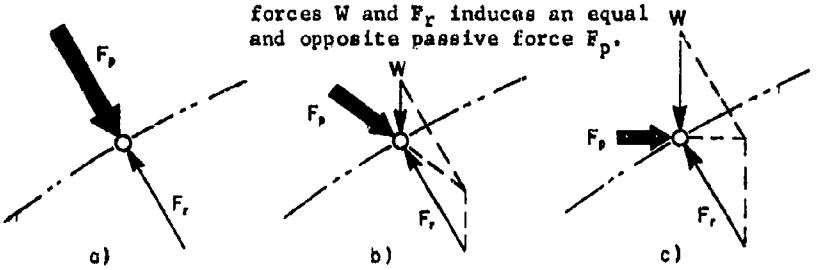


Figure 9.23. Transfer of force from rock to rib. Every block is considered to be a link as it has very little resistance to shear deformation. Forces are considered to be applied in a direction normal to the tangent of the rib at the neutral axis.

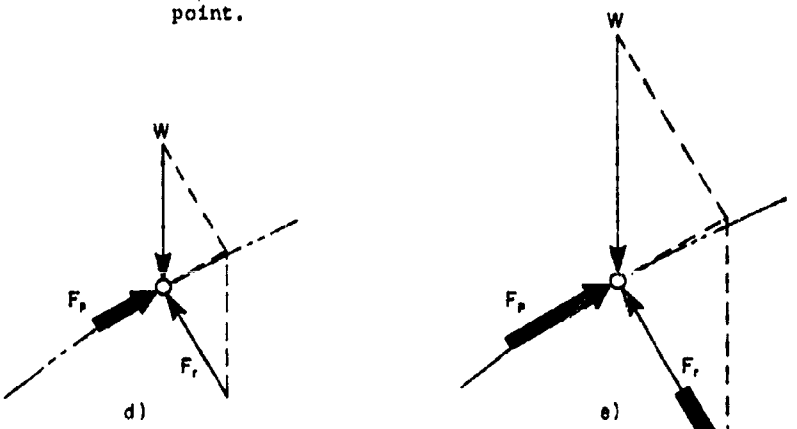
The rock begins to develop weight. It exerts an active vertical force W on to the block. The resultant of the two active forces W and F_r induces an equal and opposite passive force F_p.



The active force F_r exerted the prestressed rib is met by an equal and opposite passive force F_p induced in the rock.

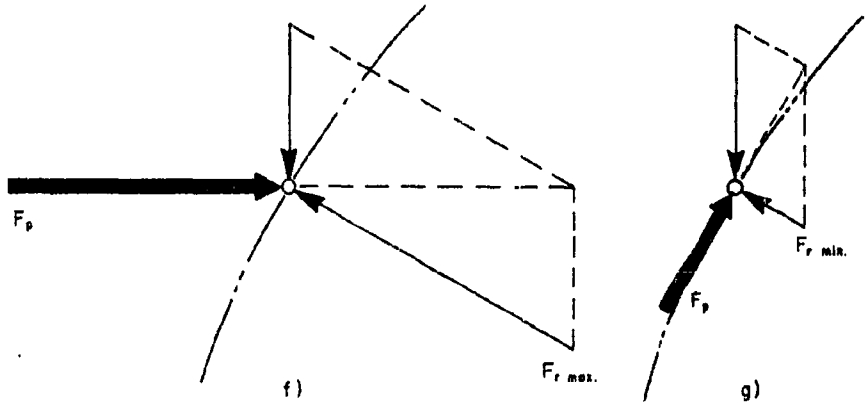
The active rock force W increases. Since the resultant of W and F_r induces an equal and opposite passive force, F_p, the magnitude of F_p changes and its direction passes through the horizontal.

Figure 9.24. Forces acting at overbreak blocking point.



With increasing active rock force W, the direction of F_p ultimately becomes parallel to the tangent. This is as far as it can rotate as the rock cannot supply a force whose line of action lies outside the rock.

With further increases of the active rock force W and the direction of passive force F_p fixed, F_r is not of sufficient magnitude to maintain the equilibrium. The blocking point then moves slightly toward the rib until the rib by deflecting slightly can mobilize a great enough Force F_r to establish equilibrium.



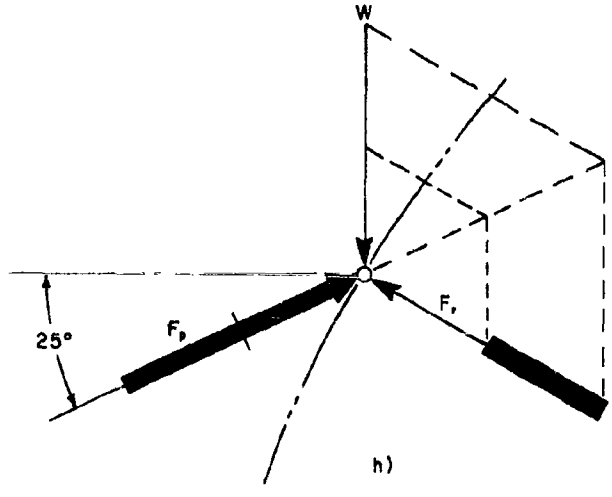


Figure 9.24. (cont.) It is assumed that because of friction, the rock can supply a force F_p whose direction is not more than 25° from the horizontal.

equal to the friction. The value for this angle is arbitrarily chosen as 25° from the horizontal (Figure 9.24b). The significance of this choice is that the active vertical force W increases from zero, while the active rib force F_r is "mobilized" by prestressing, remaining constant in value. The direction of the passive force F_p can rotate until it reaches the tangent line or the imposed limit of 25° below the horizontal. With a further increase in W the value of F_r, which is due to the elastic deformation of the rib caused by initial wedging, is no longer of sufficient magnitude to maintain equilibrium. This in turn results in an increase in F_r due to deformation of the rib, indicated by the heavy portion of the arrow F_r in Figure 9.24h. For semi-circular arches with the load assigned as shown in Figure 9.18 the slope angle of F_p does not exceed 25°.

Transfer of Forces. The scheme is shown for the neutral axis of one-half of a semi-circular rib with four blocking points and the center lines of the "pin-connected links" which transfer the loads. Blocks 2 to 4 are acted on by vertical forces W, which are resolved into two components F_t, and are neutralized by the passive forces F_p within the rock. Hence, only the normal forces are transmitted to the steel rib. (Figure 9.25). The assumption of pin joints means that there are no bending moments at the blocking points and the thrust acts in the direction of a straight line interconnecting adjacent blocking points.

Force and Stress Computation. Graphical representation of the thrust can be carried out with a polygon of forces treating the blocking points as panel points. Design procedures require the construction of a loading diagram and a force polygon, utilizing whatever passive force is required at each blocking point to establish equilibrium. The thrusts represented by the rays of the polygon act in the direction of the straight line connecting two adjacent blocking points. If the rib were made of straight sections the bending moment due to curvature would be eliminated.

The maximum bending moment M between blocking points is equal to the product of the thrust T and the rise h of the arc between them:

$$M = Th \tag{9.1}$$

Since the ribs are continuous there is a moment M_b at these points opposite to the thrust moment. Equilibrium requires that the moment M_m at the midpoint between blocks be approximately equal to the difference between the moment M_t and the average M_b at the blocking points:

$$M_m = M_t - M_b \tag{9.2}$$

The bending moments may be computed by the theory of curved bars, and the distribution of moments over the full arch is similar to that over a uniform, continuous beam. M_m is the maximum bending moment between supports and M_b at the supports. This gives an approximate maximum bending moment of

$$M_{max} = M_b = 0.67\ M_t = 0.67\ Th \tag{9.3}$$

for a continuous beam fixed at both ends.

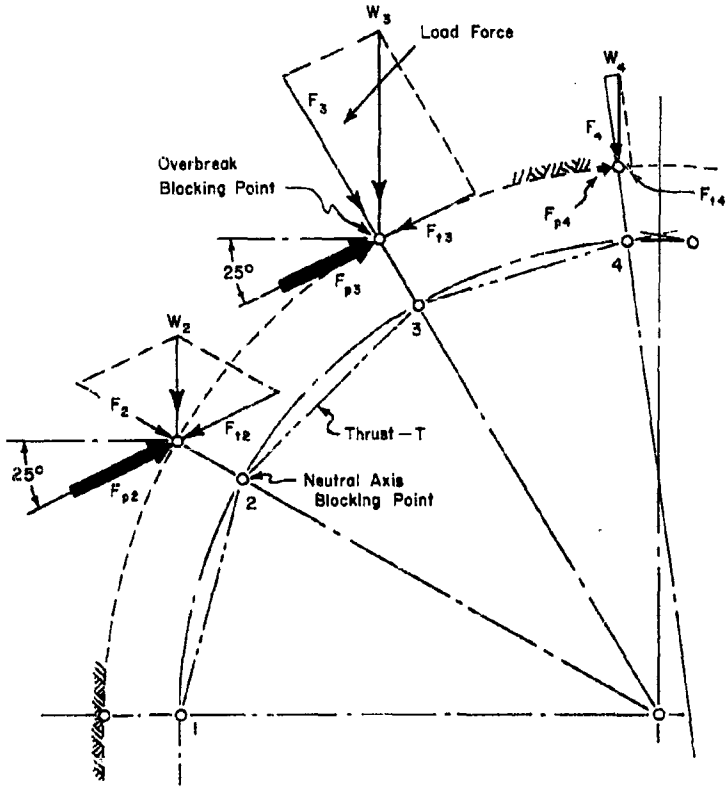


Figure 9.25. Resolution of forces at overbreak blocking points. The assumed active vertical force W at each blocking point is resolved into two components, a radial load force F and a component force F_t, acting at 25° to the horizontal or at the slope angle of the tangent, whichever is smaller. The force F_t induces an equal and opposite passive force F_p in the rock which can be of any required magnitude. Hence F_t is disregarded. The radial load force F either induces or opposes the rib force (F_r in Figure 9.24a) exerted through the block.

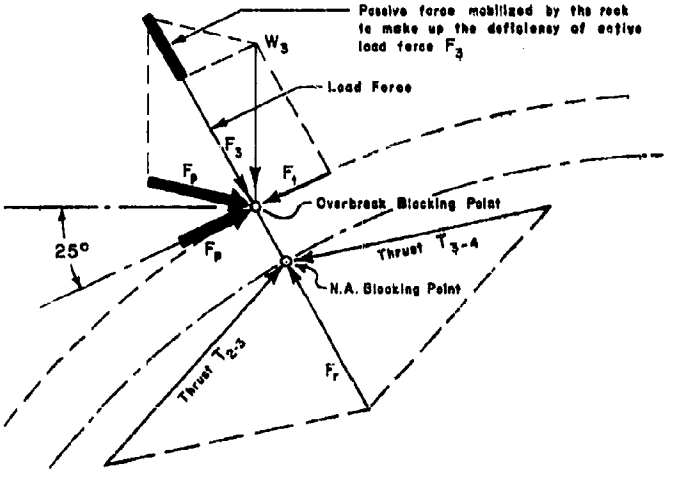


Figure 9.26. Action of forces at blocking point 3 (Figure 9,25), The rib force F_r is the resultant of the two thrust forces T. It is transmitted radially by the block to the rock where it is met by the active load force F. This in turn is the radial component of the active vertical load force W. If F is less than the rib force F_r, the rock mobilizes additional passive force by changing the direction and magnitude of passive force F_p so that the resultant of F_p and W is equal to F_r.

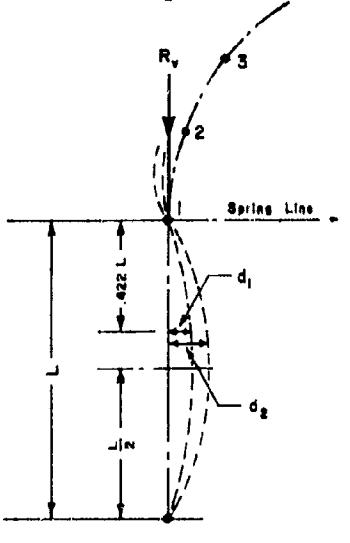


Figure 9.27. Deflection of leg.

If the rib is hinged the maximum is at the blocking point nearest the hinge and is equal to

$$M_{max} = M_b = 0.86\ M_t = 0.86\ Th \qquad (9.4)$$

This equation holds if the space between intermediate blocking points is less than that between a hinge and adjacent blocking point. The maximum fibre stress is equal to the sum of the compressive stress due to thrust and that due to bending.

The straight leg of a continuous rib consists of a slender column acted upon by the arch thrust and bending moment at the spring line. If the leg is rigid the moment may be approximated by

$$M_1 = 0.67\ M_t \qquad (9.5)$$

Due to the vertical thrust R_y and the deflection d_2 the total moment in the leg is (Figure 9.27):

$$M_c = (1.0 - 0.422) \times 0.67\ M + Td_2 \qquad (9.6)$$

or since

$$M_t = Th$$

$$M_c = 0.38\ Th + Td_2 \qquad (9.7)$$

If there is side pressure on the leg in addition to the arch forces, it is recommended that full circle ribs be used.

Examples of computations for the above theory are given in Appendix 9-A, taken directly from Proctor[2].

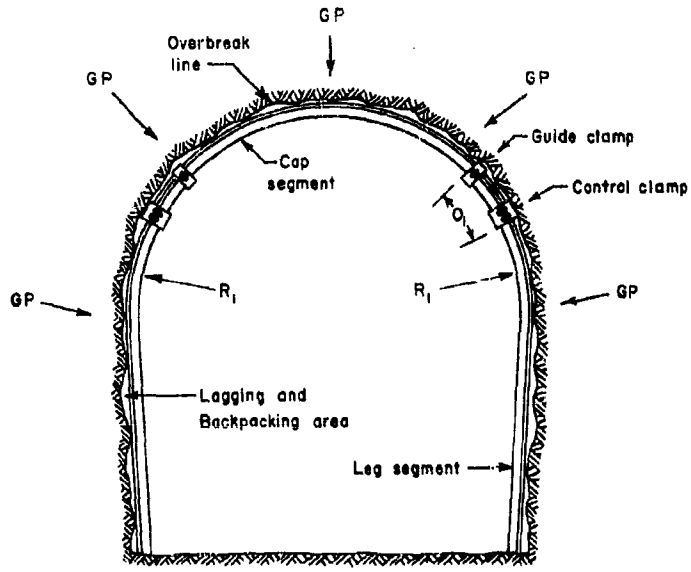
Evaluation of Proctor's Method

The above method has several obvious weaknesses. The first is concerned with the assumptions about load distribution and magnitude. These are highly idealized particularly the picture of frictionless prisms of rock above the arch. The height of the "rock arch" supported must also be a pure guess in most cases. Nevertheless, in spite of its weaknesses, the above method does represent a rational approach to a difficult problem.

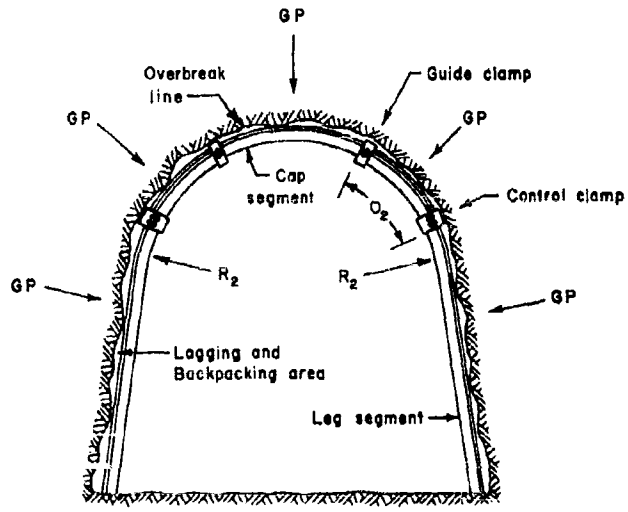
Based upon experience with this type of tunnel support, the type of support that would give maximum stability for underground protective openings is a full circle rib.

Yielding Arches. Yielding steel arches of several types have been employed [3] in Europe and England for support in roadways subject to collapse. Suncliffe reports field tests of three types of arches of which the Toussant-Heintzmann arch appeared to function most satisfactorily, although the tests were not conclusive. The loads to which these arches were subjected caused vertical displacements of more than 20 inches.

The principle of the arch is shown in Figure 9.28 on the basis of an American design by Commercial Shearing and Stamping Company[4]. The yieldable arches under normal usage are installed in underground openings as ground is removed. They are employed to support loads caused by



BEFORE YIELDING



AFTER YIELDING

Figure 9.28. Principle of yieldable arch.

changing ground movement or faulted and fractured rock. Arches are made of segments having identical cross section and a curvature of radius of R_1. They nest and overlap at the joints by a length O_1. When the ground load exceeds the design load of the arch as installed, yielding takes place at the joint until the overlap is O_2 and the radius of curvature shorten to R_2. During yielding, it is postulated that the overburden settles into a natural arch of its own, thus tending to bring all forces into equilibrium, the shortened arch having increased strength. The clamps are designed to slide along the arch members as the load increases beyond a certain critical design value. Types of yieldable connections are shown in Figure 9.29, and various types of arches for different ground pressures in Figure 9.30. It is suggested that the arch is stronger after it yields than before because of increased joint overlap.

The results of tests referred to above[3] indicated by strata dynamometer that the strata pressures were in the range of 1000 to 1300 psi. Some measurements indicated that the pressures might have reached values as high as 1900 psi. Under these pressures all types of yieldable arches collapsed, but the T-H type named above appeared to have more resistance and to yield in the manner for which it was designed.

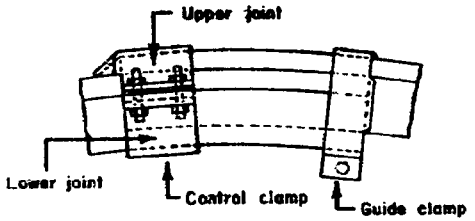
The principle of the yieldable arch, whether it possesses constant friction resistance or critically damped resistance of some type, appears to offer possibilities for support of underground protective installations. Portions of such installations subject to near detonations, particularly access openings, and also deep seated areas in fractured rock, would require stabilizing support to guarantee survival. This would vary from prevention or reduction of complete collapse to protection from spalling or simple dropping of large fragments from the roof and walls. In view of the fact that the direction of maximum pressure and the consequent location of critical stresses cannot be predicted, a complete circular ring would offer the most insurance of survival because of its greater structural stability under load.

Rock Bolts

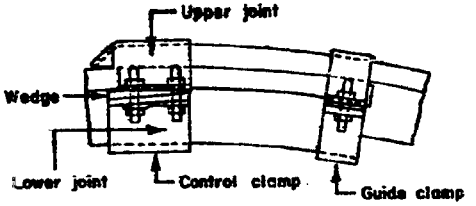
A quantitative description[5] of the engineering function of rock bolts is given by Schmuck[5]. The process of rock bolting consists of three steps, (1) anchoring the bolt in the hole, (2) applying tension to the bolt to place the rock under compression parallel to the bolt, and (3) placing the bolts in such a pattern that they will properly support the rock structure. The basic principle of bolting is that it should make the bolted rock an integral part of supporting structure. One exception is where bolts are employed for simple suspension.

Rock may be supported by bolts in five ways:

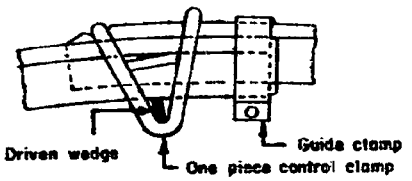
1. Suspension
2. Beam building
3. Reinforcement of arched opening requiring support
4. Reinforcement of an opening otherwise self supporting
5. Reinforcement of walls against shear and compressive action



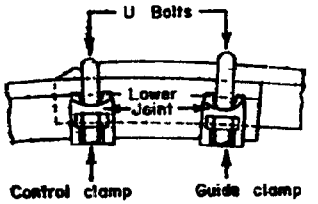
Type GB light duty connection - formed steel joint - bolted assembly - one piece guide clamp.



Type GF heavy duty connection - bolted wedged joint - two piece guide clamp.

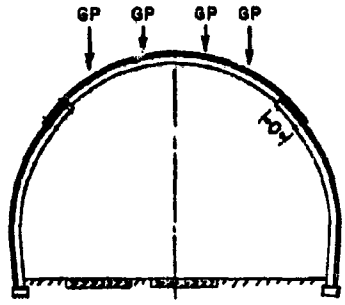


Type V quick assembly connection - driven wedge joint - one piece guide clamp.

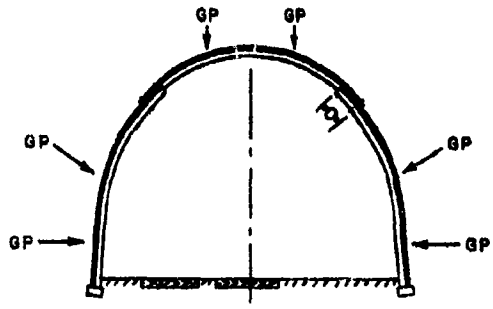


Type B limited yield connection - control and guide clamps assembled with U bolts.

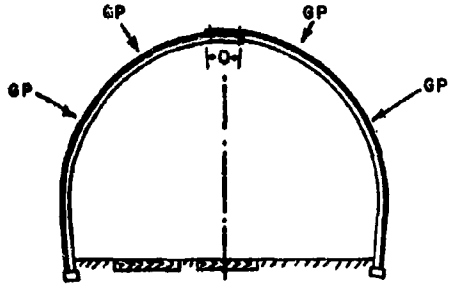
Figure 9.29. Yieldable connections.



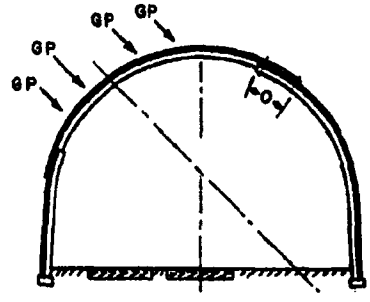
Symmetrical 3 segment arch with leg segments toed in. Used for predominantly vertical ground pressures.



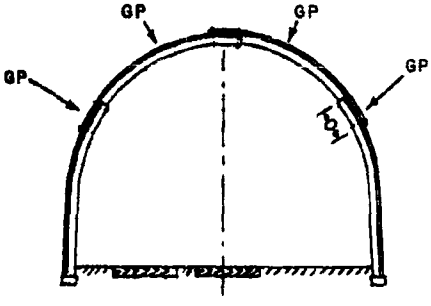
Symmetrical 3 segment arch with leg segments toed out. Used to resist vertical as well as lateral ground pressures.



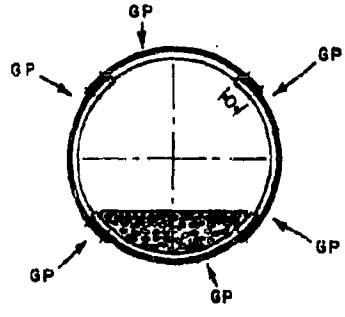
Symmetrical 2 segment arch. Rapid assembly characteristics. Used for moderate ground pressures.



Non-symmetrical 3 segment arch. Overlap located in plane at right angle to predominant direction of ground pressures.



Symmetrical 4 segment arch for special ground pressure patterns. Used in large sized openings to facilitate handling.



Symmetrical 4 segment ring to resist ground pressures from all directions. Rings can consist of 3 or more segments depending on diameter.

Figure 9.30. Typical yieldable arch shapes.

Suspension. This category includes those cases where bolts are employed to secure fragments or sections of rock which are loose and subject to dropping out of place. Small slabs or fragments are usually barred down after blasting when they would not constitute an integral part of the rock structure if bolted securely in place. Also included would be blocks of rock which are broken by fracture or joint patterns in such a manner that they may subsequently loosen and fall. Schmuck recommends that inasmuch as a bolt may be required to support the full load of the rock fragment it should have a sufficiently strong anchorage and overall strength to provide a safety factor of at least three.

Beam Building. A large portion of rock bolts has to date been used in stratified rock. In flat lying deposits the bolts are installed in bedded rock to bind the strata together to act as a single beam capable of supporting itself and thus stabilizing the overlying rock. The bolts should be long enough to form a "monolithic" beam which will be self-supporting and not be suspended from the stratum in which the bolts are anchored.

Panek[6,7,8] has made a detailed analysis of the effects of (1) bolt spacing, (2) bolt tension and (3) beam dimensions by use of model testing and similitude in evaluating their effects upon unfractured equal thickness multilayered rock mine roofs.

The notation used by Panek is as follows: (Notations at end of chapter).

For model testing of rock models subject to gravitational type body forces, the method of centrifugal testing has proven most useful[9]. In order that results of model tests simulate the prototype it is necessary to consider the mathematical relationships which will accomplish the extrapolation. A rather rigorous general equation is set up by Panek which, upon relaxation of some of the similarity requirements, becomes

$$\epsilon_x = f_3 \left(\frac{KwL}{E}, \frac{F}{EL^2}, \frac{L}{t}, \frac{L}{b}, \frac{b}{t}, N\right) \qquad (9.8)$$

This equation was written for strain because strain values were measured with SR-4 gages placed at suitable positions on the models. Also strain itself is a dimensionless quantity. The usual assumption of plane stress is included in the process of reduction of the above equation.

Panek's investigation was concerned with stratified roof consisting of beds of like material and equal thickness with no bond between them. These were held by bolts installed in straight lines across the opening, with the factor of suspension eliminated because the bolts did not extend into a thicker stratum above. It was assumed that the behavior of the lowest bed approximates that of a continuous rectangular plate clamped along two parallel lines.

This portion of the investigation resulted in the development of basic roof bolting design formulae for the conditions indicated above for model and prototype and the construction of a design chart (Figure 9.31) to determine bolt spacing, tension and length to provide a numerical value for increase of safety factor. These results were obtained partly by dimensional analysis and partly by factorial experimentation.

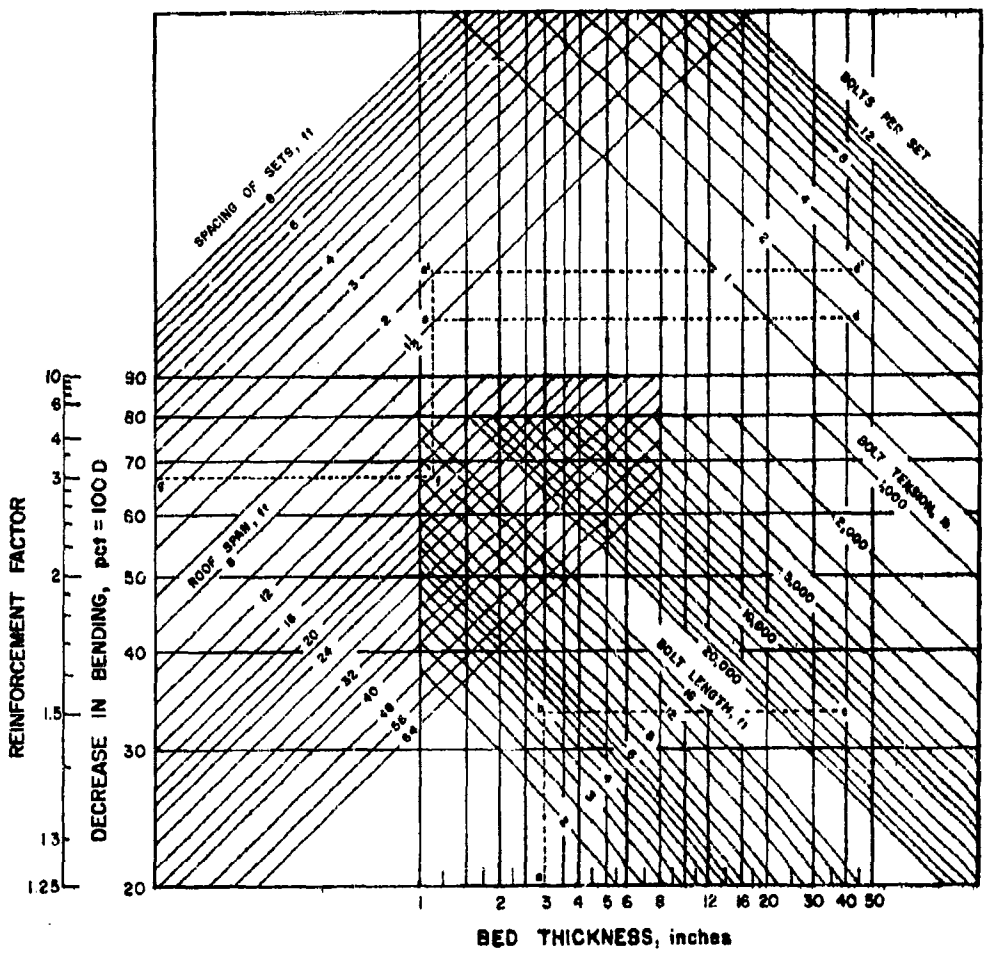


Figure 9.31. Roof-bolting design chart.

Based upon 92 model tests of over 600 strain measurements values of exponents and constants were determined for the model equation 9.9 which was found to have the following form for Indiana limestone:

$$\Delta\epsilon_{L/16} = 0.0858\left(\frac{WL}{E}\right)^{\frac{2}{3}}\left(\frac{L}{t}\right)\cdot\left(\frac{L}{b}\right)^{\frac{1}{2}}(N)^{\frac{1}{3}}\left(\frac{P}{EL^2}\right)^{\frac{1}{3}}\left(\frac{h}{t}-1\right)^{\frac{1}{3}} \qquad (9.9)$$

The standard error for this equation was 12.4×10^{-6} or 18.8 percent of the average observed $\Delta\epsilon_{L/16}$, some of which was attributed to instrument drift and changes in brush-contact resistance in the centrifuge.

Equation 9.9 should be applicable to any prototype, the characteristics of which fall within the same range as the models (Table 9.1).

TABLE 9.1

LIMITS WITHIN WHICH RESULTS OF FACTORIAL EXPERIMENT ARE APPLICABLE

Maximum KwL/E		24×10^{-6}	
Maximum L/t		64	
Maximum L/b		12	
Maximum N		12	
Maximum P/EL^2		17×10^{-8}	
Maximum h/L (h/L=h/t L/t)		3/8	
			For a 16-ft. span
Maximum span,	L	1066 in.(89 ft.)[1/]	-
Maximum spacing of sets,	b	L/12	16 in.
Maximum bolts per set,	N	12	12
Maximum bolt tension,	P	17×10^{-8} EL^2	25,000 lb.[2/]
Maximum bolt length,	h	3L/8	72 in.
Minimum bed thickness,	t	L/64	3 in.

1/ For $w = 0.09$, $E = 4 \times 10^6$
2/ For $E = 4 \times 10^6$

These results may be employed to obtain a relationship for the safety factor provided by rock bolts. By definition

$$SF = \frac{\text{Breaking strain for roof rock}}{(\epsilon_x)_{max} = \text{bending strain at rib, unbolted roof}} \qquad (9.10)$$

$$SF = \frac{\text{Breaking strain for roof rock}}{(\epsilon_x)'_{max} = \text{bending strain at rib, bolted roof}} \qquad (9.11)$$

From these, the reinforcing factor RF, due to bolting is defined by

$$RF = \frac{SF'}{SF} \qquad (9.12)$$

If the 1/16 point along the span is taken as representative, the percentage reduction in strain is the same at all points, and

$$RF = \frac{(\epsilon_x)_{max}}{(\epsilon'_x)_{max}} \tag{9.13}$$

Also

$$\epsilon'_{L/16} = \epsilon_{L/16} - \Delta\epsilon_{L/16} \tag{9.14}$$

hence

$$RF = \frac{1}{1 - \frac{\Delta\epsilon_{L/16}}{\epsilon L/16}}, \text{ or } \frac{1}{1 - D} \tag{9.15}$$

where

$$D = \frac{\Delta\epsilon_{L/16}}{\epsilon_{L/16}} \tag{9.16}$$

If is noted that 100D is the percentage decrease in strain, and for material which obeys Hooke's law also represents the percentage decrease in bending stress. The relationship between the top fibre bending strain and the stress at the 1/16-span point in a fixed-end beam supporting a uniformly distributed load equal to its own weight is

$$\epsilon_{L/16} = \frac{\sigma_{L/16}}{E} = \frac{0.324WL^2}{Et} \tag{9.17}$$

Substitution in the previous equations gives

$$D = 0.265\ (bL)^{-\frac{1}{2}}\ NP\ (\frac{h}{t} - 1)/W^{\frac{1}{2}} \tag{9.18}$$

If the safety factor of the unbolted roof is known, that for the bolted can be calculated. The above equations indicate how much support can be provided by a bolting system, but not how much is required. Also, the roof flexure can be decreased by increasing the number of bolts per set, the bolt tension, or by decreasing the spacing of the sets. An RF of two is proposed as a minimum, and if this value is not obtained the value of the bolting may be questioned. Solutions to the design formula for w = 0.09 are given by the roof bolting design chart in Figure 9.31. An example solution is indicated by dotted lines.

For an unbolted roof the following procedure is suggested, utilizing Figure 9.31.

1. Use the average thickness of beds, dividing the total thickness by the number of laminae, as a first approximation.
2. Select a bolt length to give firm rock at the anchorage horizon.
3. Test bolts for anchorage capacity.
4. Determine number of bolts so that spacing is reasonable.
5. Choose a trial value of set spacing not greater than the bolt spacing within sets.
6. Construct a-b-c-d-e-f-g in the design chart.
7. If the RF is less than 2, (a) decrease set spacing, and/or roof span, and/or (b) increase the number of bolts per set and/or the bolt length.

One basic difference between laminated beams and a solid beam of the same overall depth is the difference in shear stress distribution and its effect upon the principal stresses. A solid beam may support shear stresses anywhere in its interior, while laminated beams will only be able to support shear at the interfaces which are proportional to the friction between the laminae. Tests by Panek[8] indicate that the rock bolts do not resist distortion of the individual beds by shear in the bolts normal to their axes.

The strengthening of bedded structures by rock bolts may be determined by comparing the stresses in a single layer beam equal in depth to a composite beam of several beds where there is no friction between layers and no layer loads the one above or below it. It has been shown by Clark and Caudle[10] that the stresses in a simply restrained beam loaded by its own weight can be approximated by a uniformly loaded beam. (See Chapter VI). The coordinate system is chosen with the zero of the x-axis at the left end of the beam and y is positive downward. The maximum values of the shearing and bending stress occur at the ends of the beam (Figure 9.32) and have the following values:

$$(\sigma_x)\ \max = \frac{wL^2}{2t} \tag{9.19}$$

$$(\tau_{xy})\ \max = \frac{3wL}{4} \tag{9.20}$$

When the span, weight, and strength are critical the beam will fail along the cracks T, the beam becomes essentially a simply supported beam where maximum stress is transferred to the bottom fibre at midspan and would have a value of wL^2/t or twice that which causes failure at the ends but causes failure at T' when the stress reaches a value of $wL^2/2t$.

Horizontal and vertical displacements of beam sections for solid and laminated beams are shown in Figure 9.33. The vertical displacement at midspan is given by

$$\delta = \frac{qL^4}{384EI} \quad \frac{wL^4}{32Et^2} \tag{9.21}$$

The central and end cross sections remains vertical, but the remainder rotate about points on their neutral axes.

A comparison of the stress condition of a four member beam with a single member beam, Equation 9.21, shows that for beams of equal density and elastic modulus the maximum stress is four times as great for each member of the layered beam. If roof bolts could be made to create an effective thickness of the four-member beam equal to that of the single-member beam, the two would have equal strength. This would require, among other factors, that the bolts create sufficient friction between layers to resist any horizontal shearing forces which might exist in the monolithic beam.

While being subject to four times as much stress, the maximum deflection of a single thin beam is 16 times as great as that of a thick beam. The deflection can be reduced by mine prop support or by bolt suspension from a thicker overlying bed. For "beam building" the function of the bolts is only to increase friction between layers to resist shear.

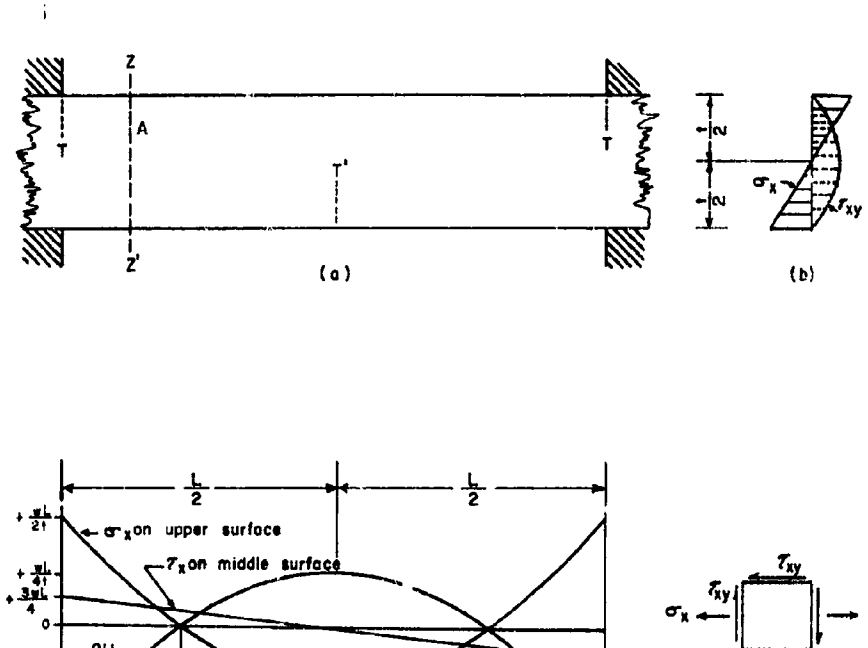


Figure 9.32. (a) Gravity-loaded beam. (b) Bending and shearing stresses on section Z-Z'. (c) Distribution of outer-fiber bending stress and middle-surface shearing stress across the span. (d) Stresses acting on element at A. Failure in flexure by tension cracks, T, T'.

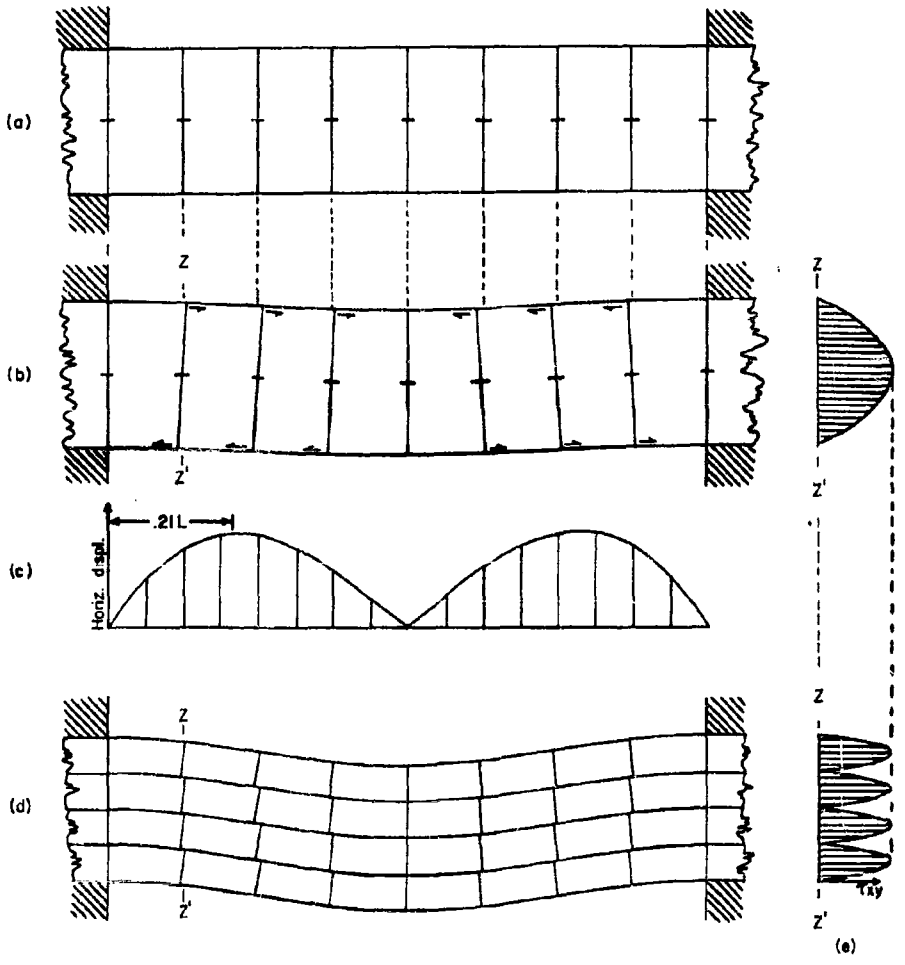


Figure 9.33. Flexure of gravity-loaded beams. (a) Plane cross sections of a beam before flexure. (b) Plane cross sections after flexure, showing directions of horizontal displacement. (c) Horizontal displacements of points on the upper and lower surfaces. (d) Flexure of a series of gravity-loaded beams, showing bedding-plane slip. (e) Distribution of shearing stress through sections Z-Z', comparing single beam to series of beams.

A series of tests using models of Indiana limestone was made in a centrifuge, creating comparable stresses to those in prototypes by placing the models in a high magnitude gravitational (centrifugal) field. The results indicated that a single layered bolted beam was not affected by the presence of the bolts. Similarly, multi-layered beams with bolts with no tension were not strengthened. The factors which contributed to strengthening were found to be the spacing and number of bolts and their tension. The results of model tests are shown in Figures 9.34 to 9.36 There was found to be no single neutral axis for any of the layered bolted beams, and they would approximate a single thick beam only at low loads or short spans.

The results of these tests indicated the necessity of proper bolt tension, proper spacing and a sufficient number of bolts. Even though some bolt configurations are preferable, patterns are not critical, although bolts should be installed as close to the working face as possible.

Reinforcement of Openings.[5,11] Methods 3 to 5 (concerning rock supported by bolts) may be considered collectively. Reinforcement of the skin area of an opening arises from two causes: (1) stresses in the rock (rocks are very weak in tension) and (2) the irregular shape of openings and fracturing caused by conventional excavation methods. If rock has enough so that it will support the loads on it and it were possible to blast exactly to the line "A" (Figure 9.37) no artificial support would be required. Because of irregularities and fracturing the actual arch must be considered to be outside of the overbreak line "B" and the rock between "A" and "B" must be supported, usually by bolts whose length is twice the depth AB.

Stress outside of the fractured rock diminishes rapidly until at one or two times the greatest cross-sectional dimension it approaches the value of the free field. (See Chapter VI). Hence, it has been found in large bore tunnels that rods of 6 to 8 feet in length are adequate to anchor any loose ground at the surface of the opening. Wherever sloughing or spalling occurs in an opening due either to excessive skin stress or to weathering, bolting has had a definite value in compacting and reinforcing this skin area.

Thomas[11] reports that in certain mines rock bolts are used to combat rock bursts. This is done by two means:

1. Compacting the skin areas of arched openings and attempting to supply enough additional reinforcement so that the opening itself is not the weakest portion of the rock mass subjected to extraordinary loads. (Figure 9.38).
2. Where a rock burst appears inevitable bolts are used to support a cushioning structure designed to restrain high velocity fragments.

In shafts or steeply dipping stopes bolts are used to constrain vertical movement and resist shear after movement has begun, as in the mines at Butte, Montana (Figure 9.39).

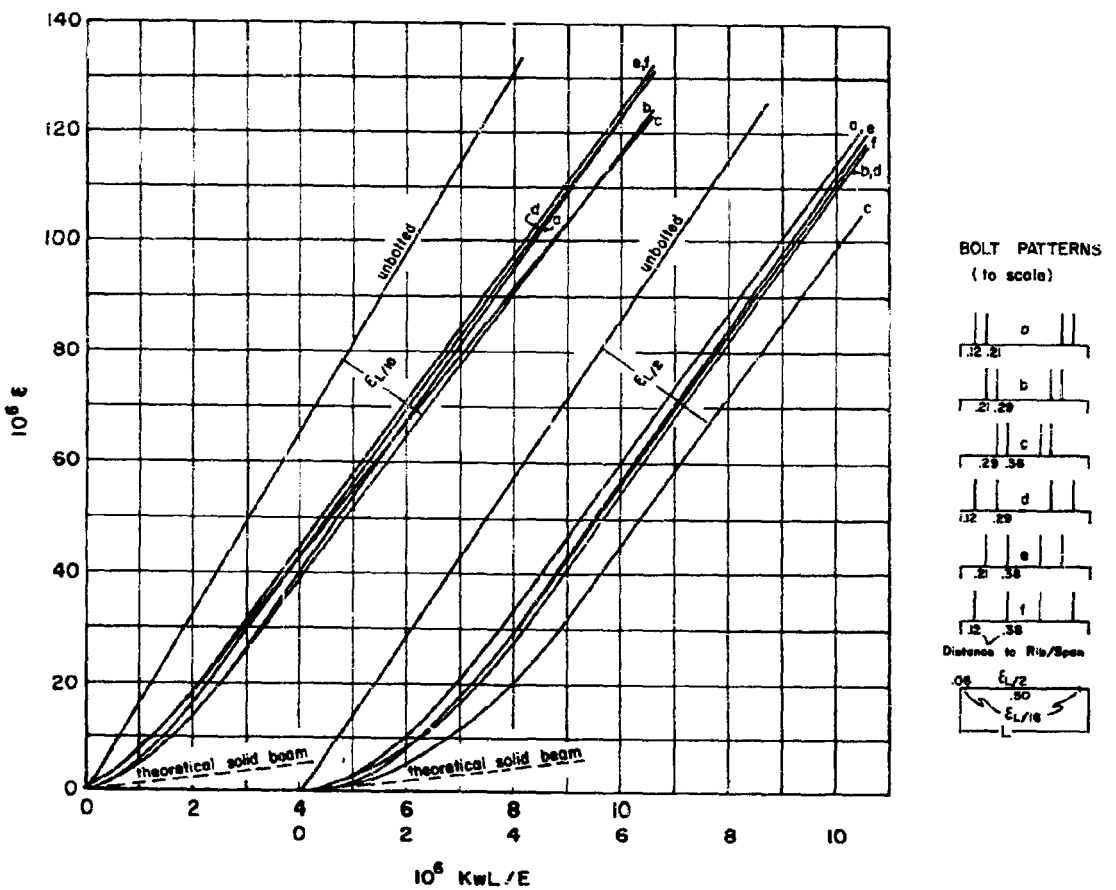


Figure 9.34. Load-strain graphs for lowest member of immediate roof; model A (Indiana limestone) for various bolting patterns. Slope of graph for theoretical solid beam = slope of graph for unbolted roof ÷ number of bolted beds.

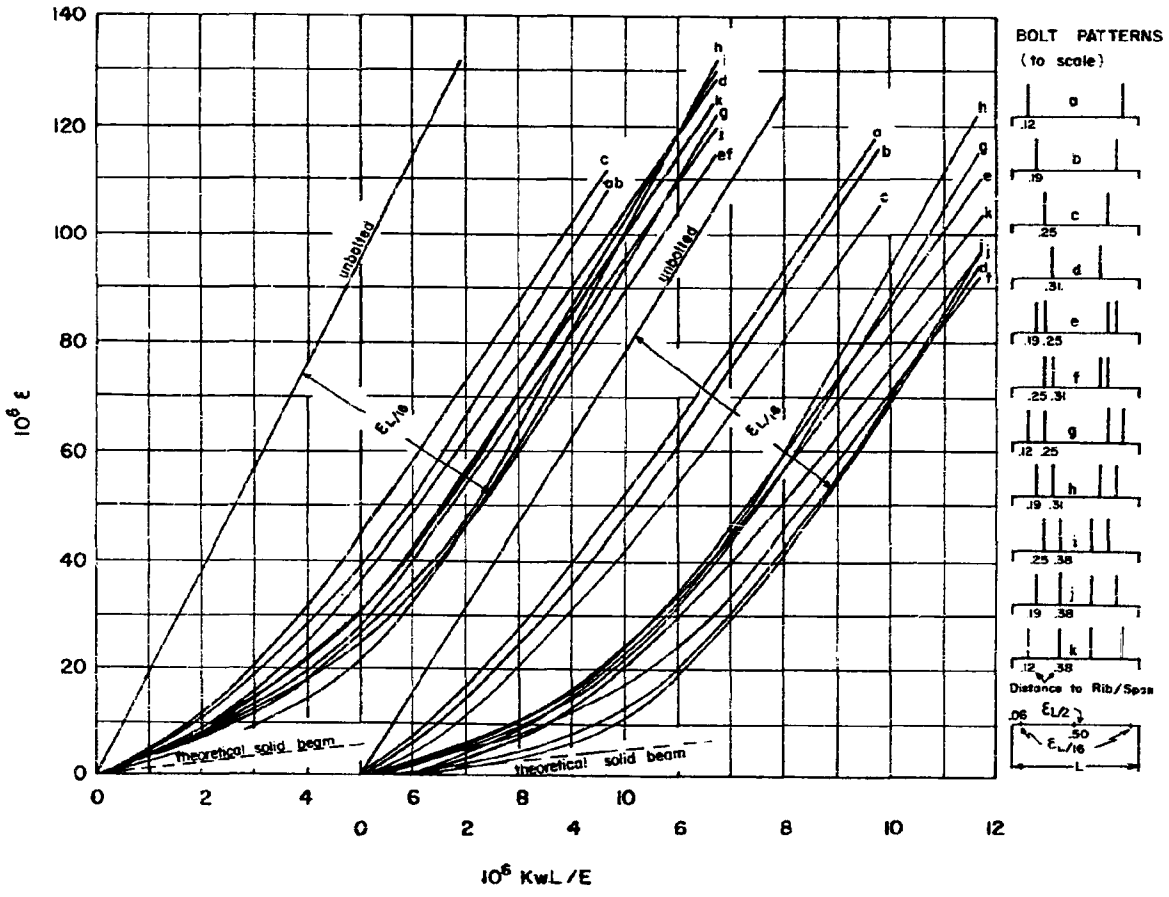


Figure 9.35. Load-strain graphs for lowest member of immediate roof; model B (Indiana limestone) for various bolting patterns. Slope of graph for unbolted roof ÷ number of bolted beds.

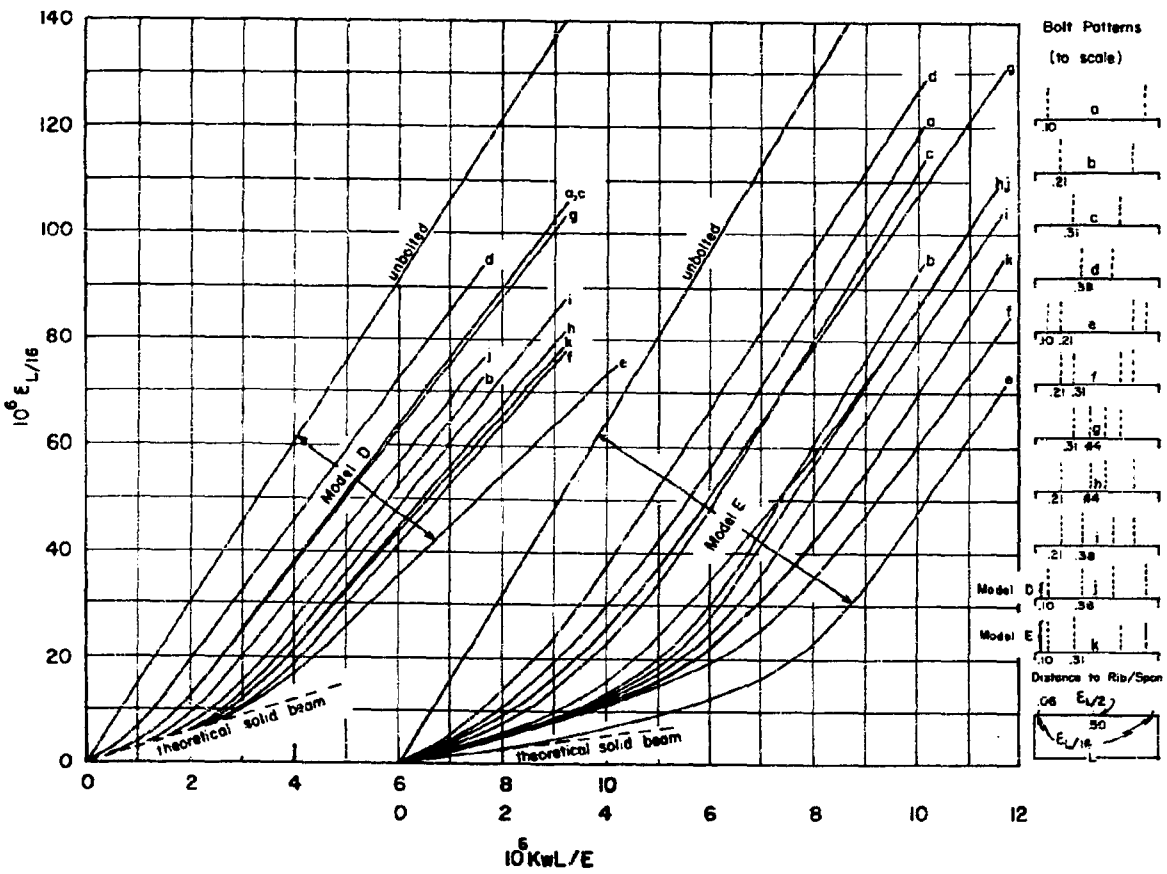


Figure 9.36. Load-strain graphs for lowest member of immediate roof; model D (Indiana limestone), model E (Hydrostone). Each curve is the average of two tests, various bolting patterns. Slope of graph for theoretical solid beam = slope of graph for unbolted roof ÷ number of bolted beds.

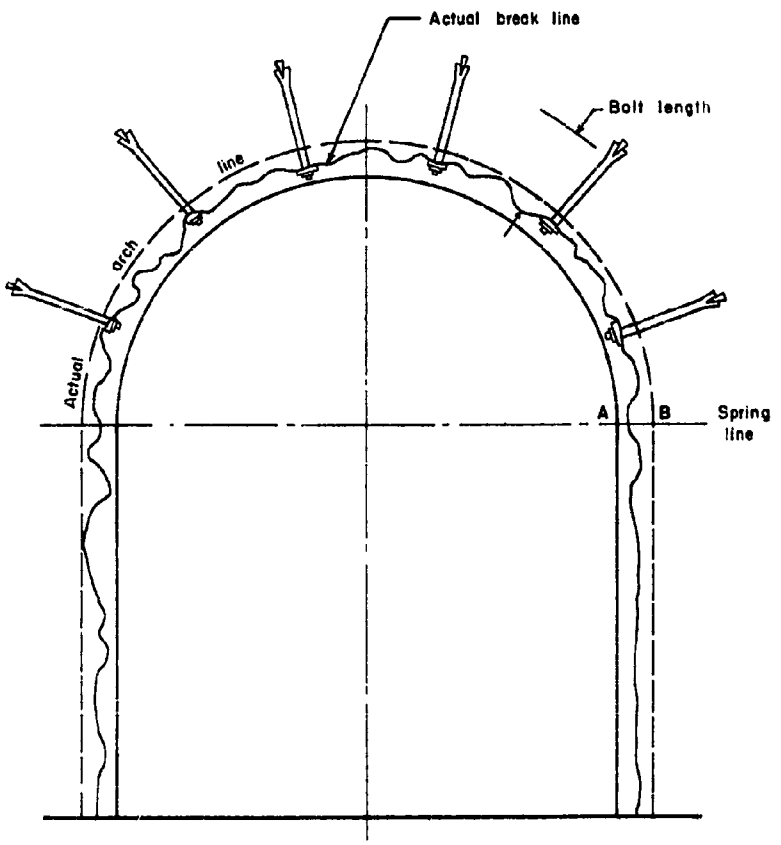

Actual break line
Bolt length
line
arch
Actual
A
B
Spring
line

Figure 9.37.

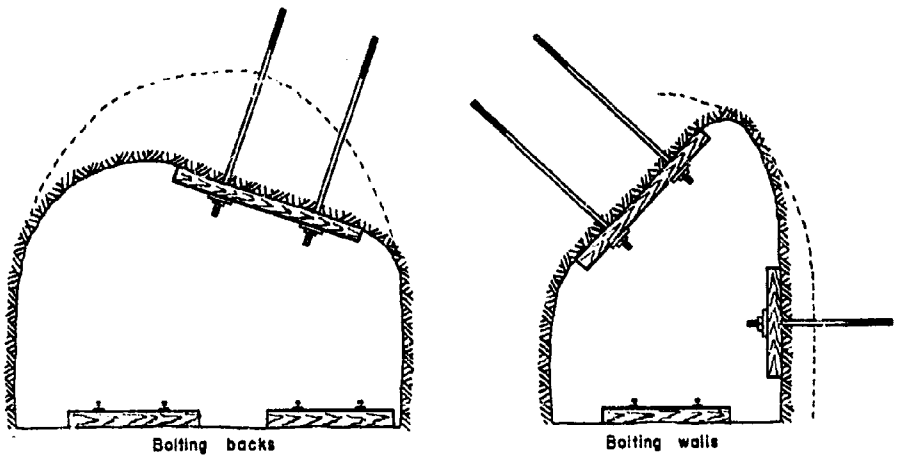


Figure 9.38.

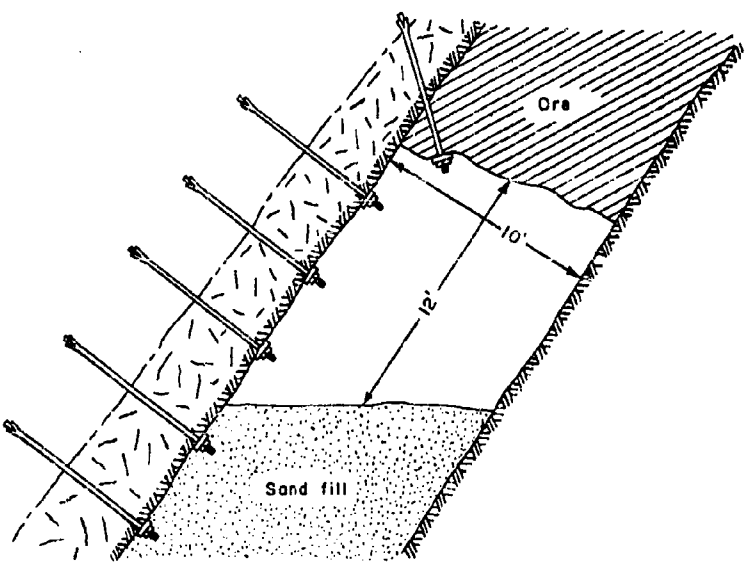


Figure 9.39.

In general, rock bolts are placed in underground openings on the basis of structural features and physical properties of rock. This is well illustrated by the process of beam building. Other specific cases (Figures 9.40 to 9.42) illustrate how bolts are employed to keep fragments from coming out of the hanging wall, or joints may be pinned together.

Torque investigations on roof bolts showed that a torque-tension relationship for 1 inch bolts was approximately 40 lb. of load for each ft. lb. of torque exerted (Figure 9.43).

Various types of artificial supports may be employed to support underground openings under static conditions. Some have been found effective in reducing secondary spalling from rock bursts. Timber sets, concrete, steel arches, and rock bolts have all proven useful in stabilizing underground openings. Their primary uses for protective construction will be very similar. They may be employed to reduce effects of spalling or used to offer some strength to the rock structure about the opening.

At present, however, it appears that the in situ rock about the opening will need to offer a very large portion of the resistance to collapse threatened by large transient loads generated by nuclear weapons.

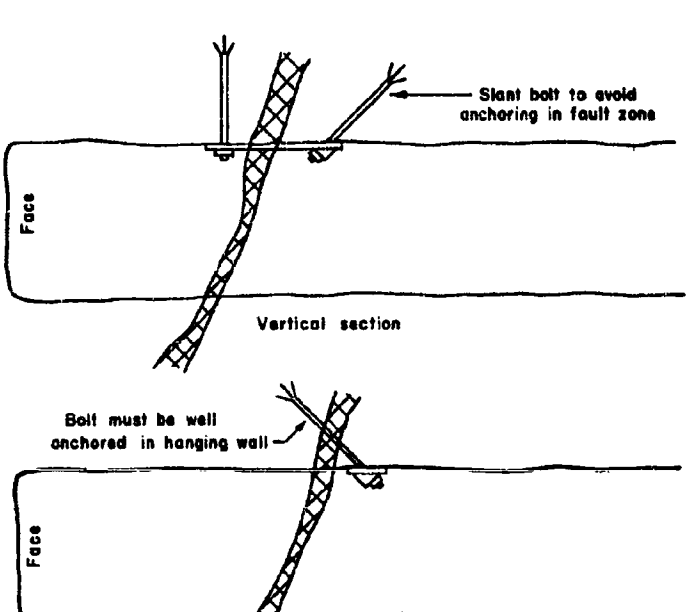


Figure 9.40.

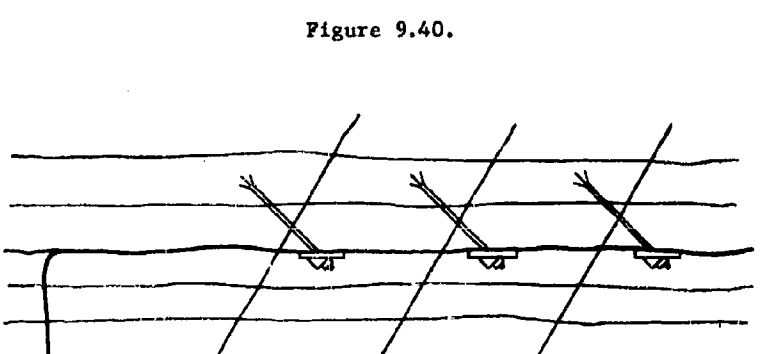


Figure 9.41.

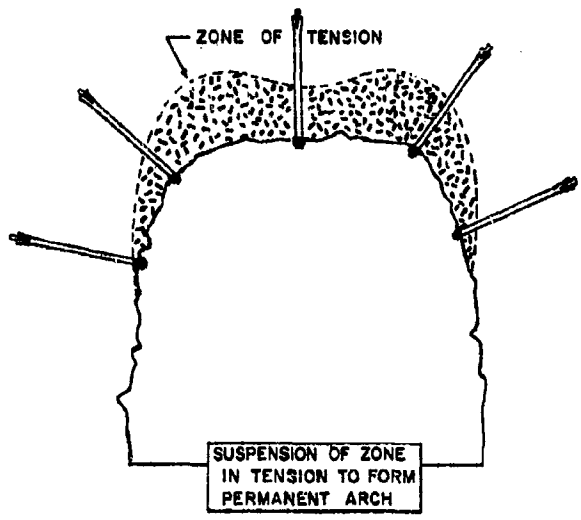


Figure 9.42. Diagram of zone of tension in arched opening.

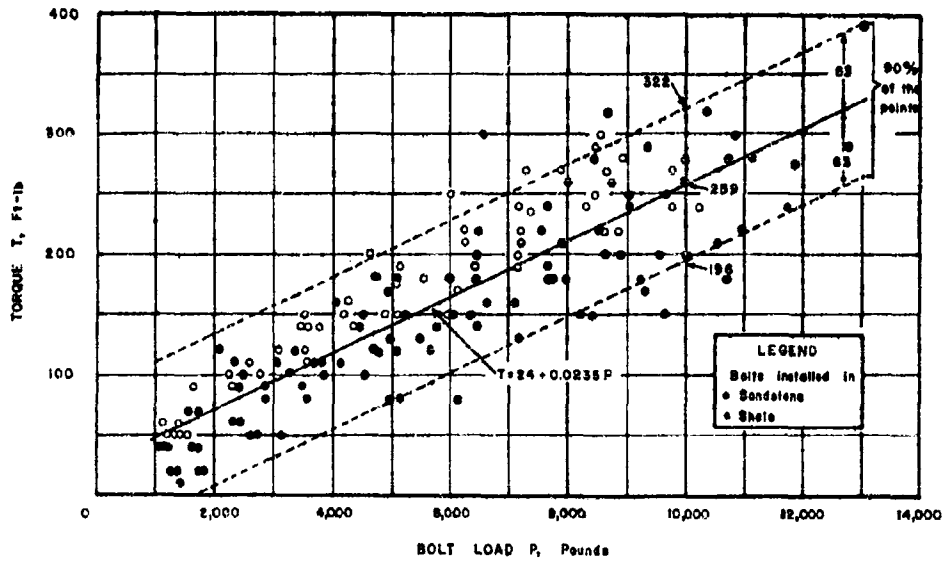


Figure 9.43.

NOTATIONS

$A, c_1, \ldots c_6$ = constants in the roof-bolting design formula

b = spacing between bolt sets along the opening, inches

D = decrease in roof bending strain due to bolting, expressed as a fraction of the theoretical value for unbolted roof

d = bolt-hole diameter, inches

d' = bolt diameter, inches

δ = deflection of a beam at midspan, inches

E = modulus of elasticity of immediate roof rock, p.s.i.

E' = modulus of elasticity of bolt material, p.s.i.

$\epsilon_x, \epsilon_y, \epsilon_z$ = unit strains, inches/inch, in the x, y, z directions

$\Delta\epsilon_{L/16}$ = decrease in outer-fiber bending strain $\epsilon_{L/16}$, inches/inch, due to bolting

$\epsilon_0, \epsilon_{L/16}, \epsilon_{L/2}$ = outer-fiber bending strains ϵ_x, at x = (0, L), x = (L/16, 15L/16), x = L/2, respectively

F = coefficient of friction on bedding planes

f_1, f_2, f_3 = undetermined functions

f = an undetermined function

G = a constant

g = acceleration of gravity = 32.2 ft./sec.^{2}

h = Bolt length = thickness of bolted roof, inches

I = moment of inertia of a beam cross section (= $bt^3/12$ for a rectangle)

K = centrifugal loading ratio (for prototypes, K = 1)

L = roof span, inches

M = moment applied to a beam at the supports, lb.-in.

μ = Poisson's ratio of roof rock

μ' = Poisson's ratio of bolt material

N = number of bolts per set, across the opening

n = revolutions per second

P = bolt tension, pounds

π = 3.1416

q = uniformly distributed beam load, lb./in. (= wbt for a gravity-loaded beam)

r = radius of rotation, inches

RF = reinforcement factor produced by bolting (=SF'/SF)

SF = safety factor for unbolted roof

SF' = safety factor for bolted roof

σ_x, σ_y, σ_z = unit stress, p.s.i., in the x, y, z directions

σ_0, $\sigma_{L/16}$, $\sigma_{L/2}$ = outer-fiber bending stresses σ_x, at x = (0, L), x = (L/16, 15L/16), x = L/2, respectively

t = thickness, inches, of bolted roof beds

T_{xy}, T_{yx} = unit shearing stresses, p.s.i., in the y, x directions on planes perpendicular to the x, y axes

w = unit weight of immediate roof rock, lb./cu. in.

w' = unit weight of bolt material, lb./cu. in.

x, y, z = rectangular coordinates

CHAPTER IX

REFERENCES

1. Lewis, R.S., Elements of Mining, Wiley.

2. Proctor, R.V., et al., Rock Tunneling with Steel Supports, Commercial Shearing & Stamping, 1946.

3. Cuncliffe, H., et al., Roadway Supports, with Special Reference to Yielding Arches, Trans. Inst. of Min. Engrs., Vol. 117, pp. 805-818, 1957-58.

4. Commercial shearing & Stamping Co., Commercial Yieldable Arches, Brochure, 1961.

5. Schmuck, H.K., Theory and Practice of Rock Bolting, Colorado School of Mines Quarterly, Vol. 52, No. 3, 1957.

6. Panek, L.A., Theory of Model Testing as Applied to Roof Bolting, U.S. Bureau of Mines, R.I. 5154.

7. Panek, L.A., Designs of Roof Bolting Systems to Reinforce Bedded Mine Roof, U.S. Bureau of Mines, R.I. 5155.

8. Panek, L.A., Principles of Reinforcing Bedded Mine Roof with Bolts, U.S. Bureau of Mines, R.I. 5156.

9. Panek, L.A., Centrifugal Testing Apparatus for Mine Structure Stress Analysis, U.S. Bureau of Mines, R.I. 4883.

10. Clark, G.B., and Caudle, R.D., Stresses Around Mine Openings in Some Simple Geologic Structures, Univ. of Illinois Exp. Sta. Bull. 430, 1955.

11. Thomas, E., Rock Stabilization Through Bolting, Second Protective Construction Symposium, Rand Corporation, 1959.

CHAPTER X

GEOLOGICAL EXPLORATION METHODS

Exploration Geophysics

The most obvious use of exploration geophysics in connection with deep underground protective installations is in predicting gross geologic structure at depth. This must be coupled with a knowledge of the general geologic structure of the local area, which may or may not be affirmed and checked in detail by drilling and excavation. The methods of geophysical exploration are (1) seismic, (2) gravity, (3) magnetic, (4) electrical and (5) radioactivity. Of these, the seismic methods have proven the most fruitful, particularly in predicting favorable geologic structures (See Table 10.1) for oil deposits. The remaining methods could readily have useful applications in particular cases of interest in this study. Magnetic and gravitational methods are often employed in combination to locate basement rocks of basic (high percentage of iron) composition. Radioactive methods would be limited to location of geologic formations containing radioactive minerals. Electrical methods also have limited but useful applications where differences in resistivity of constituent parts of the geologic structure are significant.

Seismic Prospecting

Seismic methods are the most widely used and give results which are easiest to translate into geological terms. They are basically more complicated because they require the transfer of measurable quantities of energy, usually from small amounts of high explosive, into the earth. In gravity and magnetic methods it is only required to measure existing influence fields, which is also true of the spontaneous polarization method. Both seismic methods, i.e., refraction and reflection, yield information on differences in elastic properties of rocks and these differences are correlated with geologic structure as a means of lithologic mapping. The elastic constants utilized, either directly or indirectly, are Young's modulus E, Poisson's ratio ν, rigidity or shear modulus G, and the bulk modulus k.

Several types of elastic waves may be generated in rock masses, the two most important being longitudinal and transverse. The speed of longitudinal (compressional) is given by

$$V_L = \sqrt{\frac{k + 4/3\ G}{\rho}} \qquad (10.1)$$

which may also be expressed in terms of the other elastic constants. The velocity of transverse waves is

$$V_T = \sqrt{\frac{G}{\rho}} \qquad (10.2)$$

TABLE 10.1[1]

Comparison of Major Geophysical Prospecting Methods

	Seismic refraction	Seismic reflection	Gravity	Magnetic	Electrical	Radioactivity
Principal applications	Reconnaissance exploration for geologic structure and oil Engineering Geology Regional geologic studies	Detailed exploration for geologic structure and for oil	Reconnaissance exploration Regional geologic studies	Exploration for minerals Reconnaissance exploration for oil Regional geologic studies	Exploration for minerals Engineering geology	Exploration for radioactive minerals
Principal instruments in current use	Geophones Recording system	Geophones Recording system	Gravimeter	Magnetic balance Fluxgate magnetometer Nuclear resonance magnetometer	Electrodes Potentiometers Detecting coils	Geiger counter Scintillation counter
Quantity actually measured	Time for explosion wave to return to surface after refraction by subsurface formations	Time for explosion wave to return to surface after reflection by subsurface formations	Variations in earth's gravitation field attributable to geologic structures	Variation in magnetic elements attributable to geologic structures	Natural potentials Current transmitted between electrodes, resulting potential drop Induced electric fields	Natural radioactivity of earth materials
Quantity computed from measurements	Depths to refracting horizons, horizontal speeds of seismic waves	Depths to reflecting horizons, dips	Density contrasts of rocks, depths to zones of anomalous density	Susceptibility contrasts of rocks, approximate depths to zones of anomalous magnetization	Resistivities of beds, approximate depths of interfaces between beds of contrasting resistivity	Uranium content of rocks
Geologic or economic features sought by method	Anticlines, faults, salt domes	Structural oil traps of all kinds, reefs	Salt domes, antiklinal axes, buried ridges	Basement topography, deposits of magnetic ores, dikes, and similar igneous features	Ore deposits having anomalous electrical properties, depth to bedrock, depth to ground water surface	Uranium deposits
Corrections applied to data	Weathering, elevation, "onset-to-trough"	Weathering, elevation, filter shift	Latitude, free-air, Bouguer, terrain	Diurnal variation, normal		
Size of crew (number of men)	15 or more	11-20	5	3 (ground)	2 or 3	1-4
Can measurements be made from aircraft?	No	No	No	Yes	Yes	Yes
Is method used offshore?	Yes	Yes	Yes	Yes	Yes	No
Cost per crew-month	$30,000-80,000 est.	$25,000-40,000	$6,000-9,000	$4,000 ground $6/mile airborne		

While transverse waves are of interest, only longitudinal waves are used in seismic prospecting. Two other types of waves are Raleigh (surface) and Love waves, the latter being observed only when there is a low-speed layer overlying a medium in which elastic waves have a higher speed. Transverse waves are of lower velocity than longitudinal.

Seismic Refraction[1]

Seismic refraction methods have long been employed by seismologists in the study of earthquake waves and the structure of the earth. By means of this method subsurface layering is detailed on a small scale using travel times of waves generated by near-surface explosions. While there currently is less activity in refraction than in reflection prospecting, the former has several advantages over reflection methods. The refraction method has been found to be particularly applicable for reconnaissance in areas where structures have high relief and where there is at least one high-speed marker bed overlain by lower velocity formations. Also, where subsurface geology is unknown, reflection surveys, which indicate only the geometry of the subsurface formations, can give little information about the composition of the geologic column. Refraction surveys yield data on seismic velocities of layers as well as their geometry and often make it possible to identify and map key formations. From an operational point of view refraction surveys must be spread out over a larger area and are thus more difficult to perform. For example, the separation between shot and detectors for refraction shooting in petroleum exploration ranges from about 4 to 12 miles.

Recent work by Richards[2] has proposed some new approaches to treatment of data in broadside or arc shooting over buried geologic structures such as anticlines or faults. Where subsurface topography is badly disturbed approximate methods are indicated.

Theory of Refraction Method

A brief outline of the basic principles of refraction shooting is requisite to an understanding of its application to the present problem, particularly with reference to the mechanism of transmission of refracted waves.

For a simplified case where the subsurface consists of two media, each with uniform elastic properties, the case may be analyzed for a horizontal interface at a depth z. The velocity of the longitudinal wave in the lower medium, V_1 is larger than that in the upper layer. (Figure 10.1). Waves generated at point S travel out in a hemispherical front, and will induce higher velocity waves in the lower layer. If the detecting instrument D is placed at a large distance x from the explosion the wave traveling along the path $ABCD_n$ will reach the detector before the wave traveling the path AD_n. (Figure 10.2). The wave will be refracted according to Snell's law.

$$\frac{\sin i}{\sin R} = \frac{V_o}{V_1} \qquad (10.3)$$

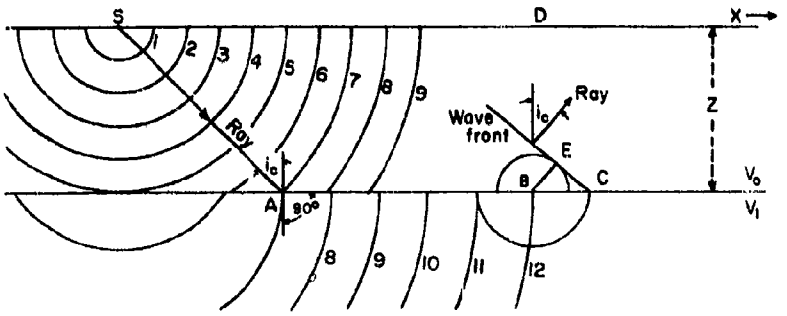


Figure 10.1. Mechanism for transmission of refracted waves in two-layered earth.

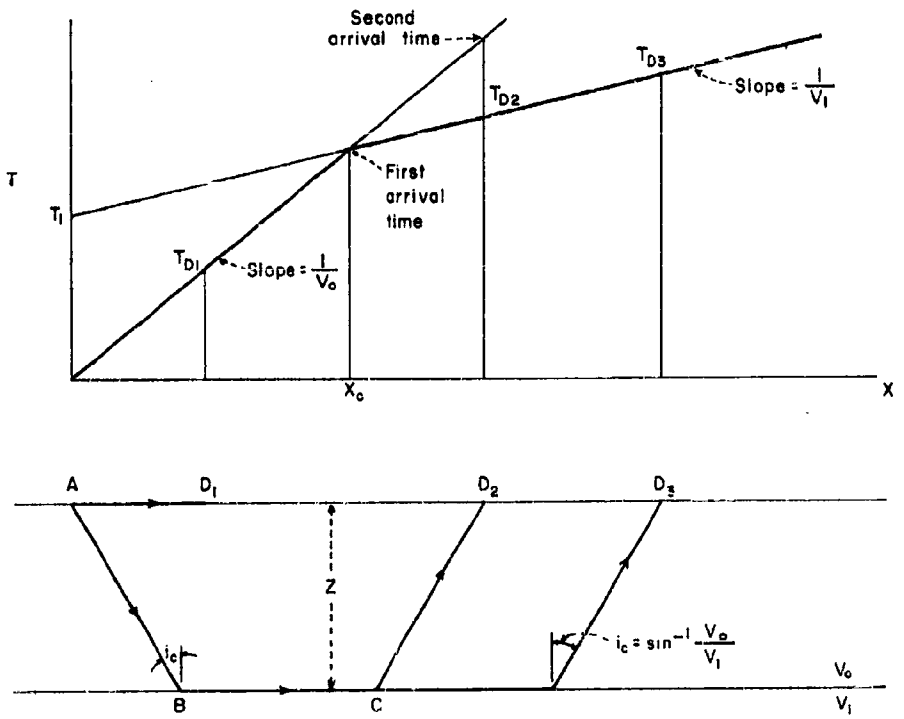


Figure 10.2. Ray paths of least time and time-distance curve for two layers separated by horizontal interface.

and the refracted wave reaching D_n will return to the surface at the critical angle i_c defined for the angle of refraction R equal to zero,

$$i_c = \sin^{-1} \frac{V_o}{V_1} \qquad (10.4)$$

A convenient method of representing refraction data is to plot the first arrival time T vs. the shot-detector distance $\underline{x}$. For the ideal case of a subsurface consisting of discrete homogeneous layers a time distance curve is simple to interpret since it consists of linear segments. Thus, for two-layer, three-layer and multiple layer cases where the speed for each layer is successively greater, the refraction method can be used to determine velocities and depths, in terms of the intercept time, the critical distance and the critical angle. All of these data may be deduced from the refraction observations. (Figures 10.3 to 10.5).

If a low-speed layer occurs in the geologic column, it cannot be detected by the indicated methods, because no wave will be refracted from the interface between it and the layer above. The presence of such a layer will lead to an error in the computation of depths to all deeper interfaces because its thickness will not be accounted for in the calculations.

For some configurations of layering and faulting it is possible to detect the faulting and measure the throw. If, for example, a high-speed bed of velocity V_1 underlies a low-speed overburden of velocity V_o if faulted vertically as shown in Figure 10.6, a refraction profile perpendicular to the strike of the fault often makes it possible to determine the above parameters. A method for the case where the shot is on the up-throw block and the detector is on the down-throw block was given by Barton[3]. The time distance curve and ideal geometric configuration of the geologic structure show that the curve consists of two parallel but displaced linear segments having an inverse slope equal to the speed in the faulted formation. The segments of the curve correspond to the arrival times of waves refracted respectively from the up-throw and down-throw blocks. The throw Z_T is determined from the difference between the intercept times of the two linear segments. The curve for the case where the shot is below the fault is derived in a similar manner.

Dipping beds may be detected and their depths evaluated by employing the time-distance plot indicated in Figure 10.7. For the mathematics of the above configurations the reader is referred to textbooks on exploration geophysics[1].

Seismic Reflection Method

This method, the most extensively used of all geophysical prospecting techniques (primarily for petroleum search), gives the most detailed and direct section of subsurface geologic structure of any geophysical method. Depths to subsurface interfaces may be mapped with accuracy, determined by the travel time of reflected waves. One advantage is that it permits mapping of many horizons with one shot and the precision for

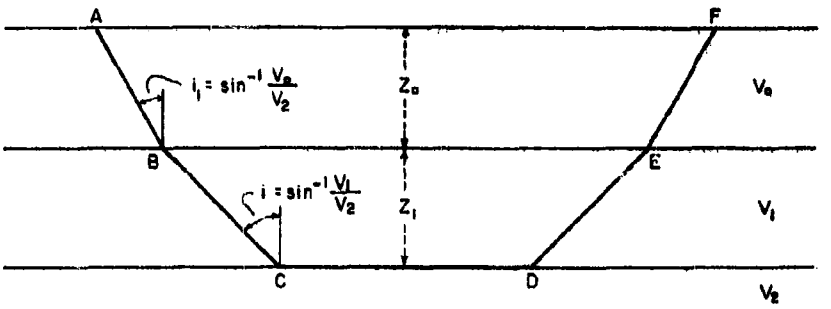


Figure 10.3. Ray paths of least time for three layers separated by horizontal interfaces.

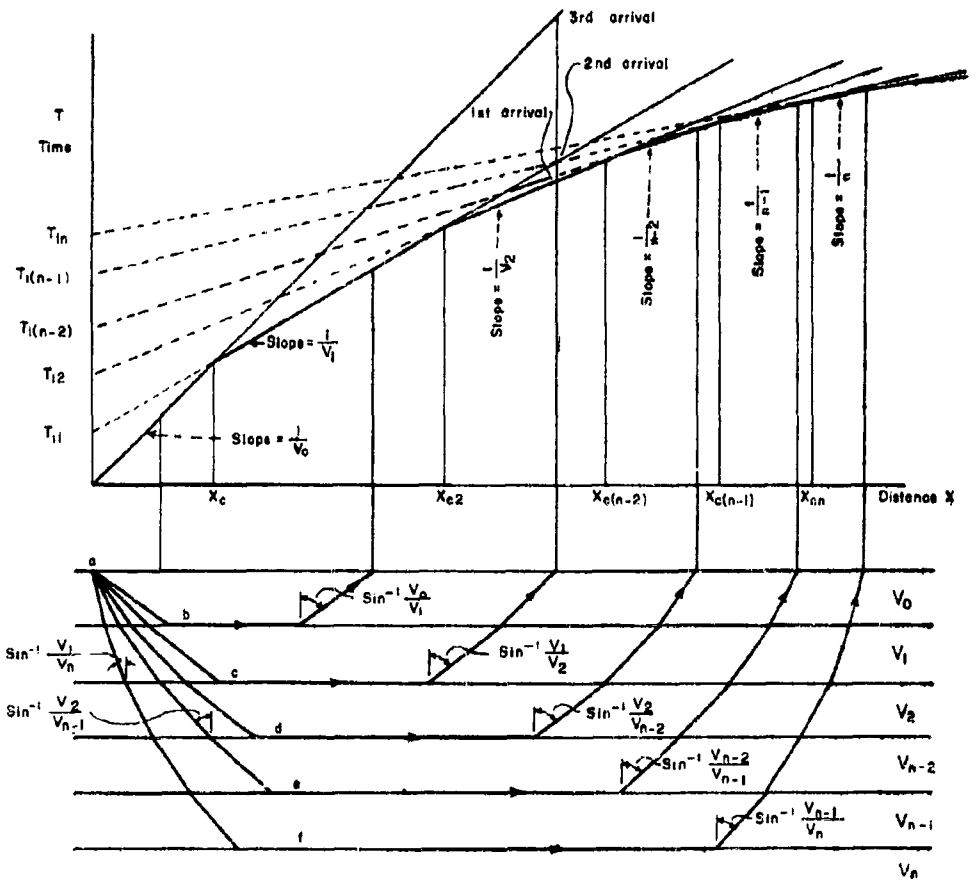


Figure 10.4. Ray paths, time-distance curve, and critical distances for multilayer case.

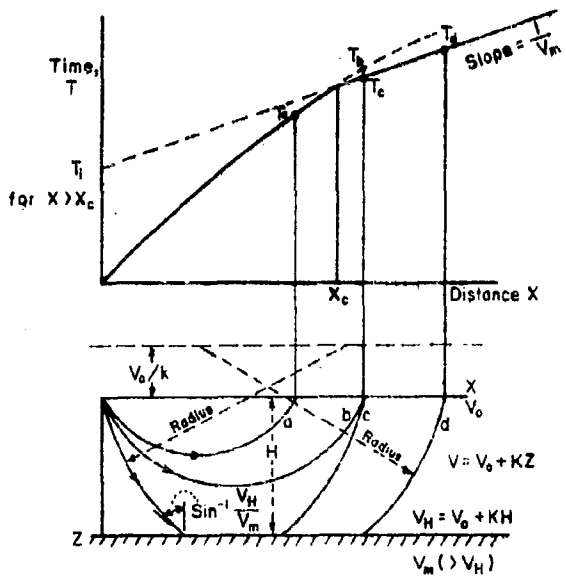


Figure 10.5. Time-distance curve and ray paths for high-speed marker below overburden with linear speed-septh relation.

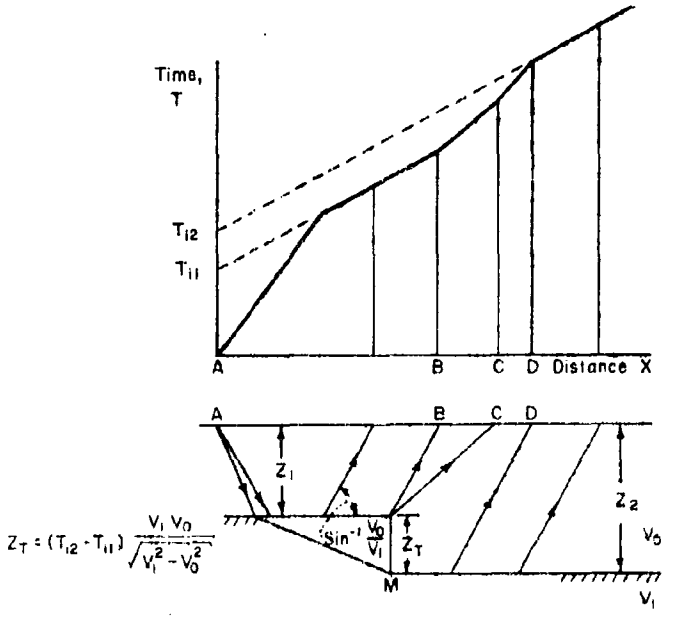


Figure 10.6. Wave paths and time-distance curve for refraction across fault (shot is on upthrown side).

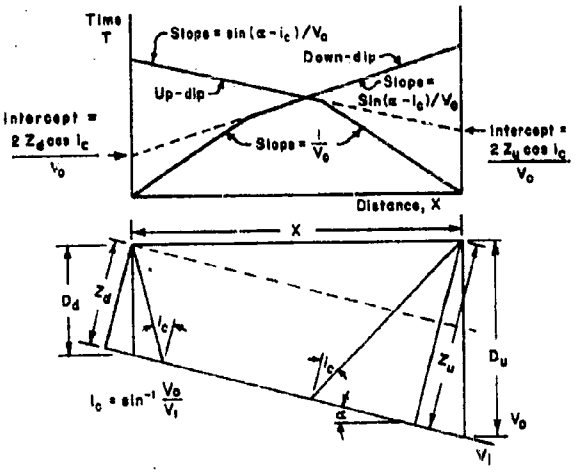


Figure 10.7. Refraction along an interface dipping at an angle α. Respective shots are at updip and downdip ends of profile.

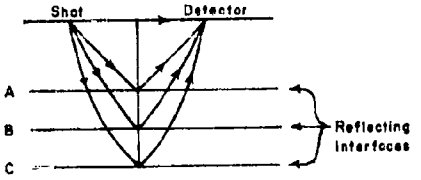


Figure 10.8. Waves reflected from a number of interfaces in area where speed increases continually with depth, except for discontinuities at interfaces themselves.

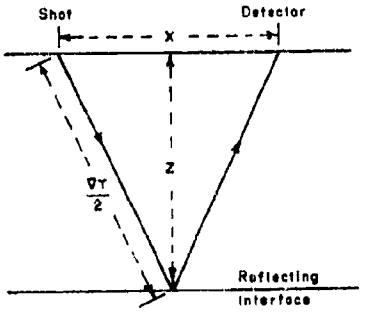


Figure 10.9. Wave reflected from single interface. Speed constant at V down to reflecting surface.

deeper horizons is the same as for shallow ones. Utilization of the reflection method is often preceded by magnetic, gravity or refraction reconnaissance surveys. The method is not usually applicable at very shallow depths.

Where there is a difference in acoustic impedance (density times velocity) on the two sides of an interface, the energy of an incident elastic wave will be partly reflected, the angle of incidence always being equal to the angle of reflection. For small seismic charges of HE set off just below the surface, each interface will reflect some of the wave energy back to the surface. A geophone placed at the surface will respond to the arrival of each reflected wave and the total travel time can be used to calculate the depth to the reflecting horizon when the speed along the wave path is known. If there is a continuous change of wave velocity with depth, the trajectories of the various reflected waves detected at a single geophone will be curves as shown in Figure 10.8. On the other hand, if the wave velocity has a constant value V, the wave will travel along straight lines and the depth to the interface of a horizontal interface and be easily calculated. (See Figures 10.9 and 10.10). The calculation of depths to inclined reflecting surfaces is somewhat more complicated. Reflections are required from two or more points on the dipping surface, from which the angle of dip can be determined from the difference in time between the two reflections. (Figure 10.11).

Where identified or unidentified geological markers persist over a large area it is possible to correlate reflections from them and contour them in a manner similar to that used in contouring from well data. Such correlation shooting gives the maximum accuracy and maximum detail, but is of high cost.

Where no velocity data are available from well shooting, an approximate velocity function may be determined from seismic measurements on the surface. Detectors are laid out over a wide range in an area of good reflection horizons and responses recorded in the usual way. The stepout times at various depths and distances can then be employed to calculate velocity from elementary formulas.

The proper interpretation of both refraction and reflection data involves their expression in geologic parameters. To be carried out competently it requires the assembling of all pertinent geological and geophysical information into an integrated representation of the structure than either source of information is likely to give alone. The coordination of geological information with reflection data should be a two way process. By close consultation with geologists and use of geological data the geophysicist can generally decrease the number of unknowns in the problems and can thus arrive at a more logically correct answer. Also the geologist benefits from the usage of the geophysical data in relating them to known geologic controls and completing the picture to the full extent that the art of seismic prospecting allows.

It must be recognized that there are certain limitations to the reflection method in yielding geological information. The resolving power of the method is limited in that discrete reflections cannot be expected from interfaces less than a wavelength apart, although a char-

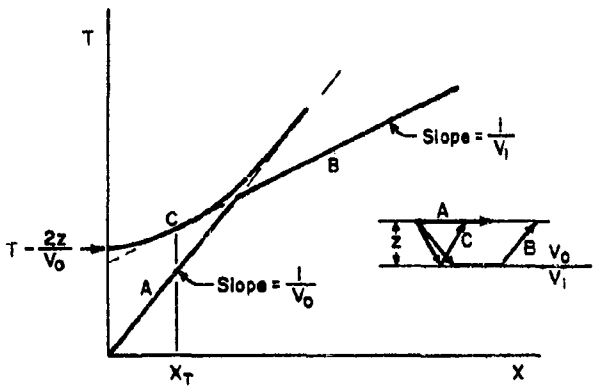


Figure 10.10. Time-distance curves for reflected and refracted waves observed with single velocity discontinuity.

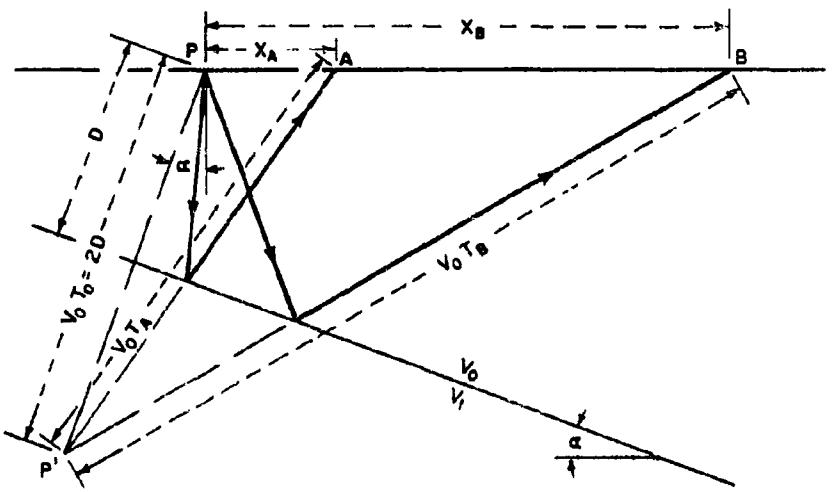


Figure 10.11. Reflections from a dipping interface. Shot is at P, geophones at A and B.

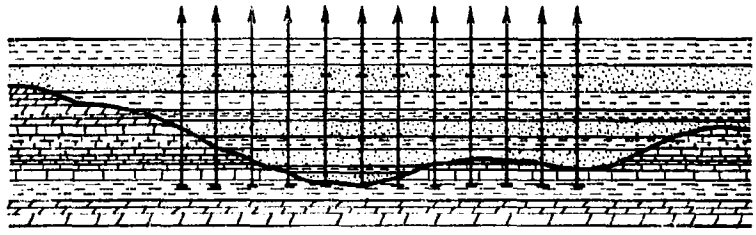


Figure 10.12. Reflection of seismic waves at an erosional surface. Vertical bars represent vertical distances covered by a seismic wave at reflecting positions for each channel of a 12-trace record. Erosional relief is generally not this great in nature.

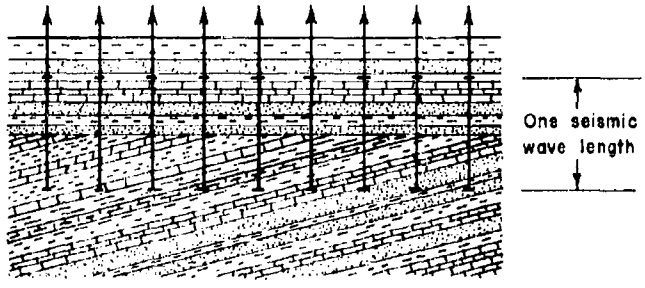


Figure 10.13. Reflection of seismic waves from zone of pinchout against unconformity. Poor resolution of reflections expected because of lateral variation of interference patterns.

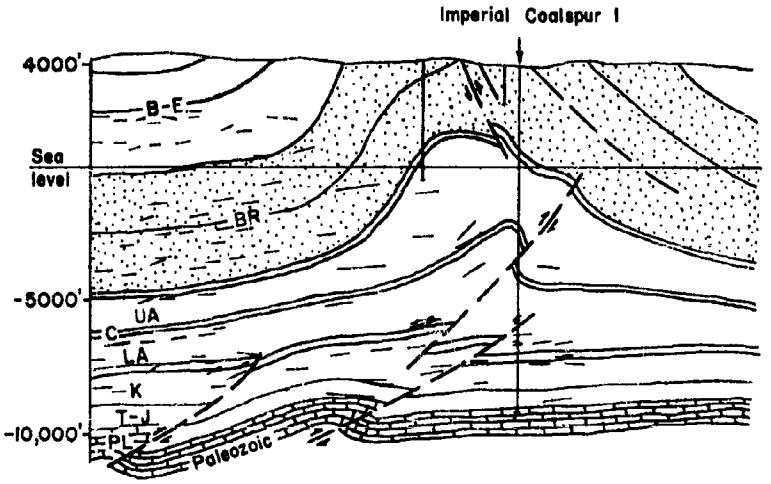


Figure 10.14. Construction of geologic section in foothills area of Alberta by combining surface geology, well information, and seismic reflection data.

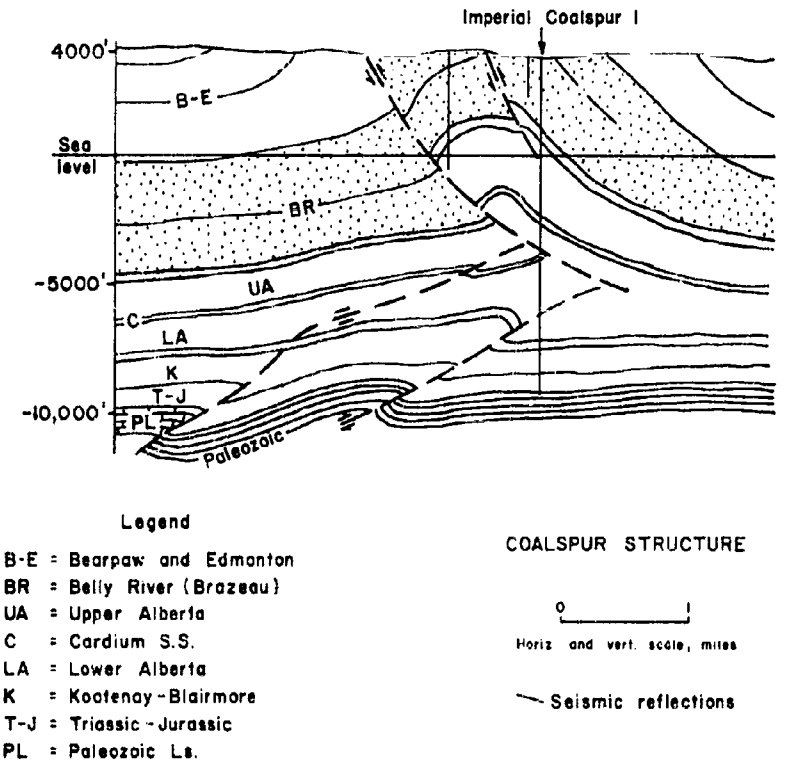


Figure 10.15. An alternative interpretation of the geological and seismic data used to obtain cross section of Figure 10.14.

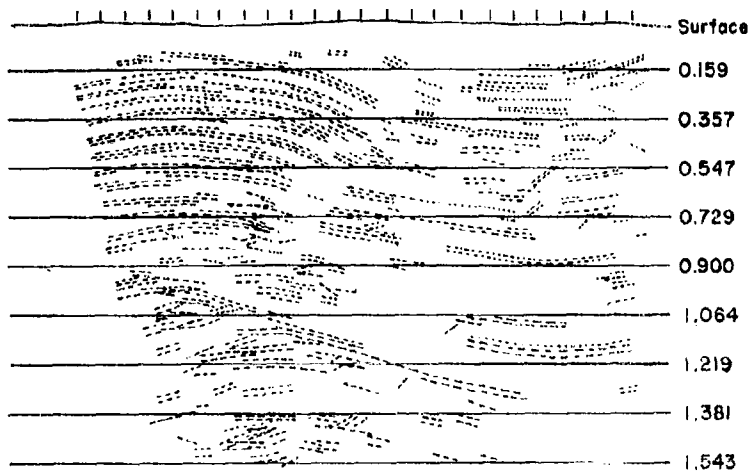


Figure 10.16. Reflection dip section from highly faulted and folded area before addition of geological information. Labels on horizontal lines represent times in sec.

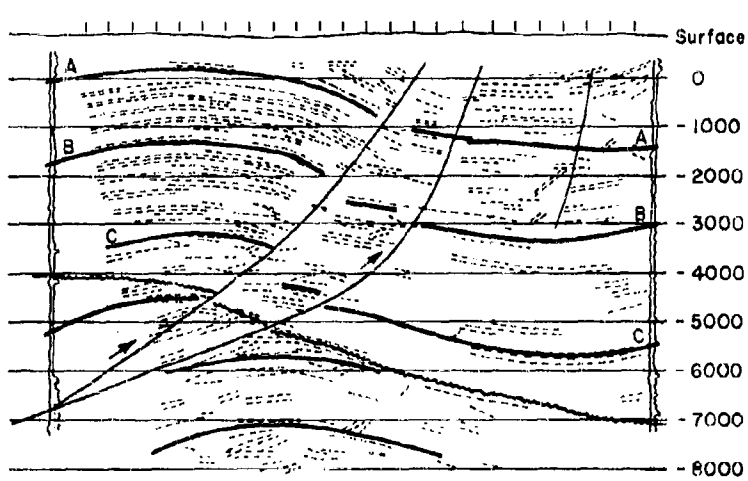


Figure 10.17. Section of 10.16 after information from two wells at opposite ends is used for geological interpretation. Labels on horizontal lines represent depths.

acteristic interference pattern made up of reflections closer together may be identifiable on the seismic record. Also, there are numerous lithological changes which may cause velocity changes as great as those which occur at interfaces between geological formations. Certain erosional surfaces and unconformities will not yield results which are interpretable because of shallow depth or other reasons. (See Figures 10.12 and 10.13).

Examples of geologic interpretation of prospected areas are given in Figures 10.14 to 10.17. The first two show alternate interpretations, while the latter two indicate reflection dip section before and after geological interpretation.

Summary - Seismic Methods. The successful application of seismic shooting to geologic problems in determining geologic structure in connection with prospecting for oil and other minerals indicates that they could be applied with equal success to exploration of subsurface structure in areas of interest for underground protective construction. They are subject to numerous limitations, but provide valuable aids in correlating geologic data and furnishing a reasonably accurate picture of subsurface geology before drilling, and are extremely useful in accurate plotting of geology between drill holes.

A further possible use of seismic surveys might be found in predicting a first approximation energy partition and distribution of blast wave energy in the rock from a surface or near surface explosion. That is, in the elastic range at some distance from a nuclear explosion crater much of the energy is reflected and refracted in accordance with known laws depending upon the particular geometrical configuration of formations and the relative acoustic impedances of each.

Gravity Method

The gravimetric method of prospecting is used to detect and measure lateral variations in the earth's gravitational attraction that are associated with differences in density in near-surface structures. Many geologic structures of interest in various phases of geological engineering give rise to variations in the normal density distribution within the earth's crust and are the source of diagnostic anomalies in the gravitational field. These differences are in many cases less than one ten-millionth of the earth's attraction and extremely sensitive instruments are required to measure them. Gravitational attraction is defined by Newton's law and the constant γ employed in the following equation is taken as 6.670×10^{-8}.

$$F = \gamma \frac{m_1 m_2}{r^2} \qquad (10.5)$$

Gravitational acceleration is about 980 cm/sec^2 or 980 gals. The practical unit of measurement employed in gravity exploration is a milligal or one thousandth of a gallon.

The vertical component of gravity is the quantity usually measured by a gravity meter and hence, it is usual to plot a profile of the var-

iation of this component in an area of interest. The theoretical variation for buried bodies of spherical, cylindrical and other shapes has been determined and field profiles are correlated with these theoretical profiles in attempts to determine the shape of the buried source of the anomaly.

One of the principle uses of the gravity meter has been in connection with the exploration for salt domes. Shallow domes of salt are usually covered by a cap of dense rock, while the salt is less dense than the surrounding rock. (See Figure 10.18).

In areas where the geologic section consists of formations with appreciable density contrast, folding of the rock will be reflected on a gravity map. For formations which have a greater than average density and are brought near the surface gravity methods are applicable.

It has been found that a number of widely different mass distributions below the ground surface can give the same type of gravity map on the surface. Any available independent geologic control such as that obtained from drilling logs or seismic data reduces the ambiguity of the interpretation. It is also possible to use information obtained from surface geology to guide the interpretations of gravity readings. Quantitative interpretations are most fruitful where there is already in existence a substantial control of the geology of the area. For example, if it is known from seismic data that a structure associated with a gravity high approximates a horizontal cylinder, and drilling information indicates uniform densities, the formula for a buried cylinder can be applied to approximate its size and depth. For cases where no simple geometrical form appears to be present, a number of structures may be assumed which are compatible with the independent geological control. The structure which gives the best calculated fit to observed results is considered to be the most likely to be present.

Magnetic Method

While magnetic prospecting is used for searching for both ore and oil, in the latter application it is ordinarily employed to determine the thickness of a sedimentary geologic section or to map structural features on the basement surface that might influence the structure of the overlying sediments. It has been found that sedimentary rocks exert such a small magnetic effect compared to the igneous rock below them that virtually all variations in magnetic intensity measurable at the surface are associated with the topography or lithologic changes in the basement rock. Both the magnetic and the gravity method of prospecting are similar in that they seek anomalies caused by changes in the physical properties of the subsurface rocks. Also both are used mainly for reconnaissance, and require fundamentally similar interpretation techniques.

In the last decade or so the number of magnetic surveys made by airborne magnetometers has steadily increased. The primary reasons are the speed economy, and convenience of airborne techniques.

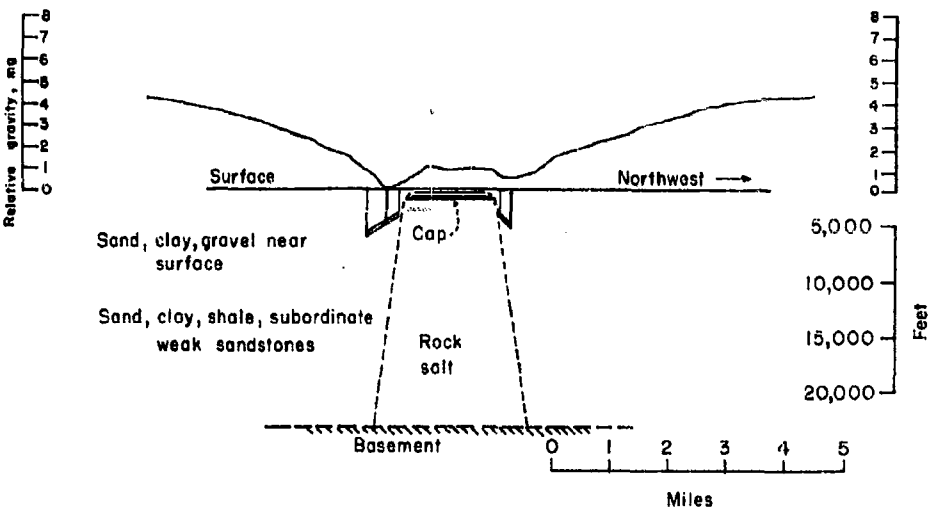


Figure 10.18. Northeast-southwest profile of anomalous relative gravity across Damon Mound salt dome, Texas.

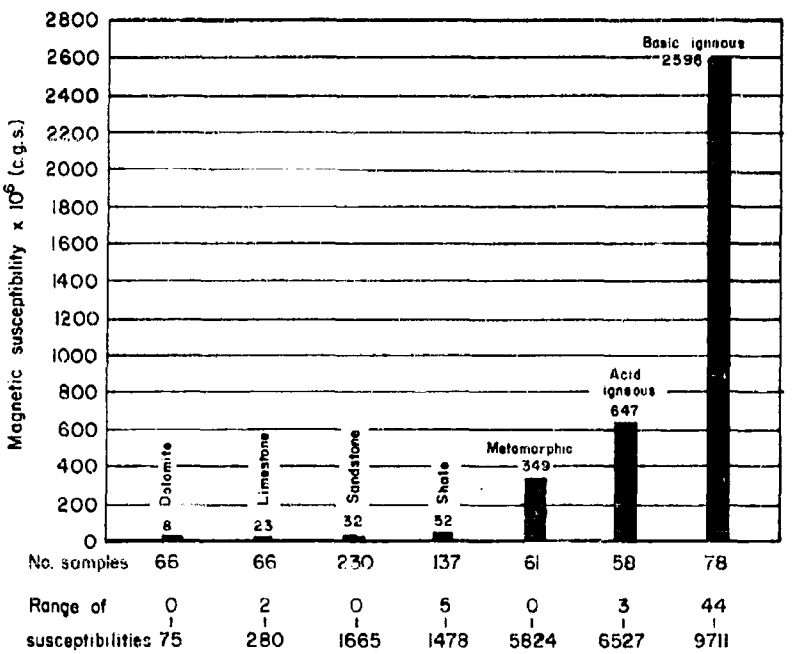


Figure 10.19. Average magnetic susceptibilities of surface samples and cores as measured in laboratory.

The magnetic method is employed to measure and evaluate magnetic anomalies in the earth's magnetic field which are caused by rocks or minerals of greater magnetic susceptibility than that of surrounding rocks. The unit of measurement is the gamma, which is defined as 10^{-5} oersted. Magnetic susceptibilities of a number of common rocks and minerals are listed in Figure 10.19.

The effects of buried magnetized bodies on the earth's magnetic field at the surface can be calculated from potential theory by methods similar to those used for determining the gravitational effects from geometrically similar bodies. The computations for magnetic fields, however, are considerably more difficult, since the dipoles distributed through the body cause both attraction and repulsion. The direction of polarization introduces another complication. Many of the formulas for forms such as spheres can be derived from the corresponding gravitational formulas by use of a relationship between magnetic and gravitational potentials. Figures 10.20 to 10.25 illustrate the theoretical types of vertical fields which might be expected from certain geometric forms.

Dobrin[1] lists three types of magnetic surveys over land whose subsurface features have been later detailed by drilling. These are: (1) magnetic ores sought directly: (2) non-magnetic materials associated with structures detectable by magnetic means; (3) oil-bearing structures in sediments associated with basement topographic features.

Perhaps the most spectacular of magnetic anomalies is that found over the Kursk iron deposit in Russia (Figure 10.27). The horizontal component of intensity varies from 20,000 to 70,000 gammas with a mile, and the vertical intensity reaches a maximum of three times its value at the North Pole. Also the declination varies by almost 180°. The anomaly was located in 1874, and the source was located by diamond drilling in 1923.

Magnetic surveys have been used to locate non-magnetic minerals by outlining structures favorable to their occurrence or by indicating magnetic materials with which other valuable minerals are commonly associated. A very large portion of the geophysical surveys on the Canadian shield in recent years consisted of magnetometer surveys for gold and base metals over drift covered areas. The non-magnetic metals are frequently found on the margins of batholiths and other intrusives which can be detailed under the drift by means of the magnetometer. In the Sudbury district of Canada, nickel and copper sulphide ore occurs at norite contacts. A magnetic anomaly indicated the host structure, and the presence of ore was subsequently determined by drilling. (Figure 10.28.)[4]

Figure 10.29 shows the structure and magnetic profile of the Cumberland oil field in Ohio where the pre-cambrian basement was faulted upward almost to the surface, whereas a definite magnetic low was associated with a salt dome and cap rock in the Hockley field in Texas. (Figure 10.30).

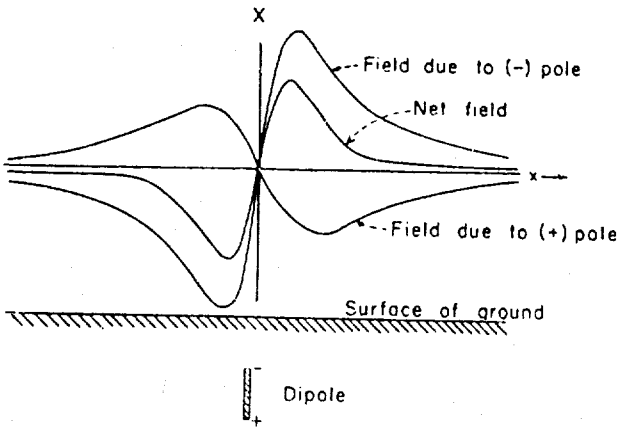


Figure 10.24. Horizontal field intensity X above vertical dipole.

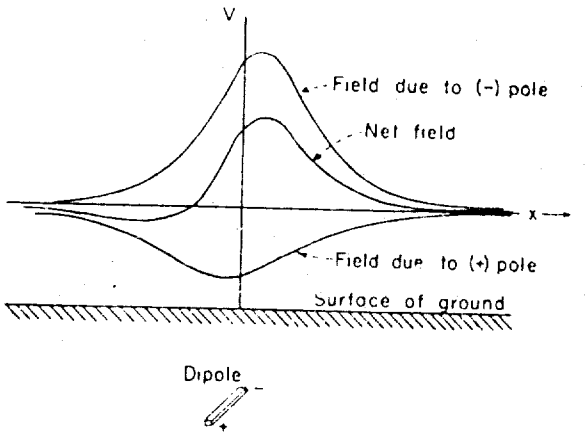


Figure 10.25. Vertical magnetic field of inclined dipole.

Preceding Page Blank

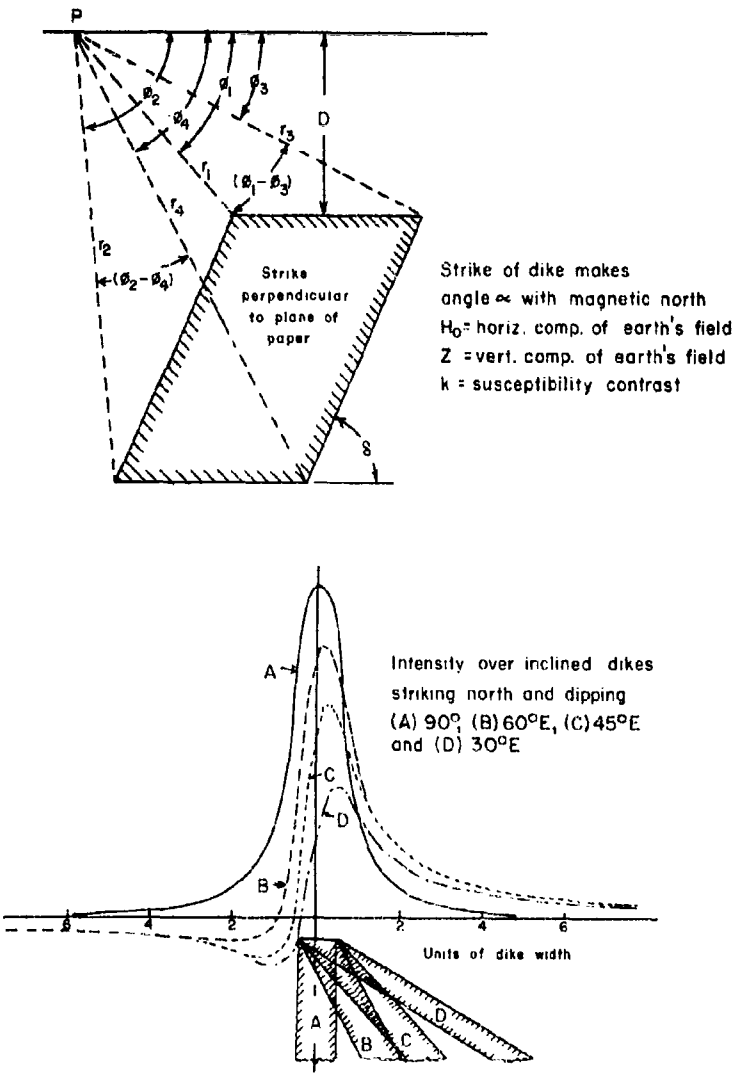


Figure 10.26. Formulas and typical profiles for vertical and inclined dikes.

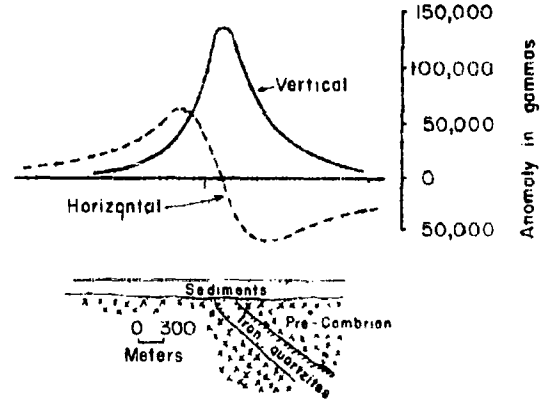


Figure 10.27. Magnetic anomalies across Kursk iron deposit.

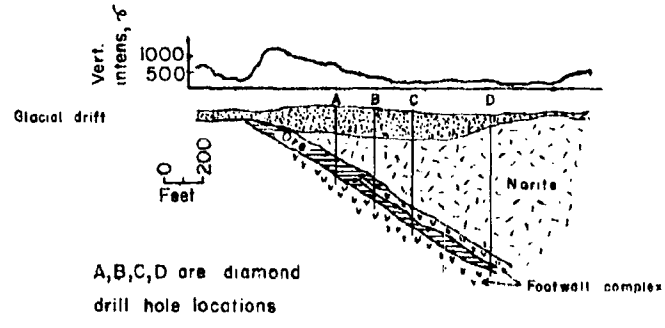


Figure 10.28. Magnetic field over drift-covered sulfide-ore body at Sudbury, Ontario.

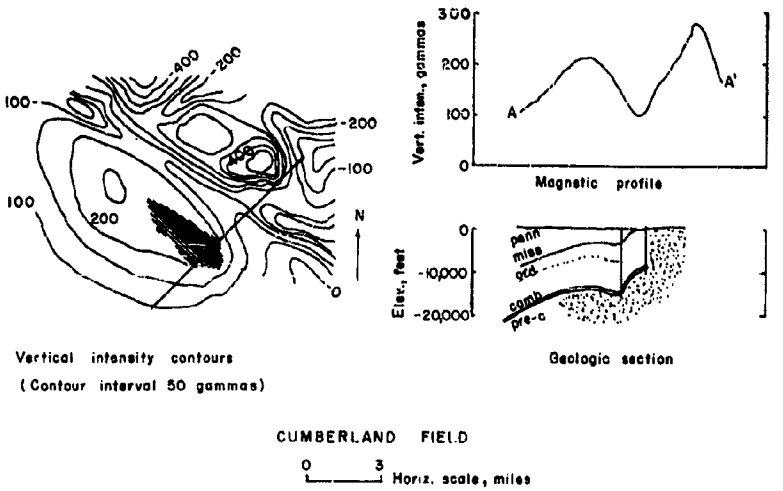


Figure 10.29. Magnetic intensities observed over Cumberland Field, Okla. Geologic section also shown.

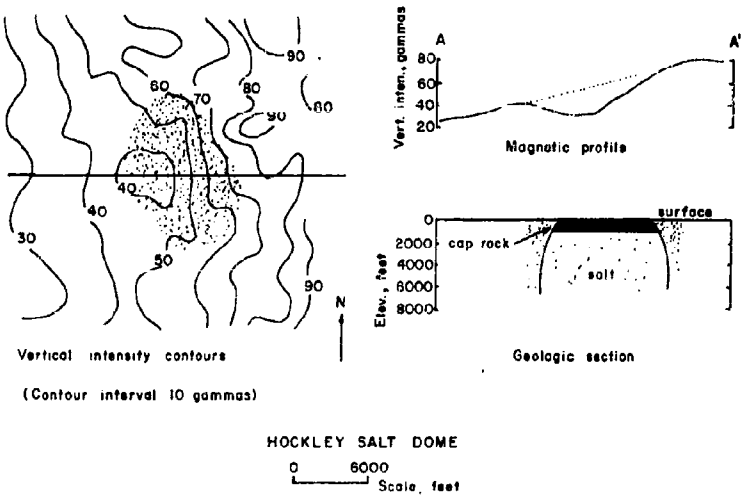


Figure 10.30. Negative magnetic anomaly over Hockley salt dome, Texas.

Electrical Prospecting Methods

These methods include the self-potential method, equi-potential line method, resistivity methods, methods utilizing telluric currents and induced potential methods. Electrical methods are characterized by shallow penetration, and limited resolution and interpretation. Their application has been essentially limited to the location of shallow mineral deposits and engineering surveys of immediate subsurface structure. Their effectiveness is limited by their emphasized response to near surface anomalies.

Exploration Drilling

In general there are three categories of drills employed in exploration drilling, churn drilling, rotary drilling, and percussion drilling. Of these, only rotary drilling is used extensively for probing for knowledge of geologic structure and the occurrence of mineral deposits. Large diameter bits with roller cones are employed in drilling for oil and are noted only for evaluation of gross geologic structure, i.e., bedding planes, individual members of the geologic column, structural traps, etc. Two types of drills yield cores as well as drill cuttings in coring rock, diamond drilling and calyx drilling. Diamond drills have been employed most extensively where detailed geology must be ascertained. That is, where cores are obtained solid samples of rock will yield quantitative as well as qualitative data on the competence of the rock which may be tested in the laboratory for its physical properties.

In exploration projects other than for petroleum, whether drilling is designed to ascertain the size and grade of an orebody or to secure geological engineering information, the choice of a method of drilling usually is between churn drilling and diamond drilling. Aside from the fact that it may yield a core, a diamond drill may be directed in any attitude with respect to the horizontal, while a churn drill may drill only vertically downward. Calyx drills can compete in rocks which are uniform and not too hard.

As might be expected most exploratory diamond drilling has been utilized in the past in searching for mineral deposits. The targets in mineral search programs and engineering geology projects are analogous in most respects. The immediate objective of a drilling program is to provide further data for geologic maps and sections.

Geologic Mapping

The translation of data obtained from drilling, together with exposed surface geology onto maps and sections provides a picture of the engineering structure available for building of underground protective installations. To serve as a basis for the value of drilling exploration and geophysical exploration results, it is well to understand which geologic data are important in the problem of design of underground openings. First, a usable map is a record of geological facts,

not theories, and there must always be a sharp distinction drawn between observation and inference. The failure to distinguish between geological facts and inference has been evidenced in otherwise excellent maps published by government surveys. The degree of uncertainty and inference should always be indicated.

The principles of mapping geologic detail for engineering structure design are similar to those employed in ore and oil search, although the emphasis on the category of geological features that are important is different in each case. As indicated in Chapters II to IV, the factors which effect structural strength and transmission of wave energy are concerned with both gross and detailed structure.

Many of the pertinent data on subsurface rock structure are obtained from the geologists log of a drill hole. This usually includes the following[5]:

Percentage of core recovered in each run
Grain size, expressed quantitatively
Recognizable minerals
Type and degree of alteration
Angle between structural planes and the axis of the core:
- Cleavage and schistosity
- Bedding
- Joints
- Veinlets or stringers

Location of sections in which core is crushed or broken or where only clay or mud is recovered (This may indicate a fault).

Solid cores which are recovered may be employed for preliminary laboratory tests for physical properties. In many cases the regional, local surface and subsurface geology, (the latter obtained by drilling) has furnished adequate information for planning extensive underground excavation projects.

The Snowy Mountain[6] project in Australia illustrates the effective utilization of diamond drilling to evaluate pertinent factors prior to actual excavation. It also illustrates some of the uncertainties involved.

All types of investigation were employed from broad regional surveys to detailed surveys of individual features. Usual methods of aerial and ground surveying were employed and a first order survey net established for overall control. Surface geology surveys, both regional and local, were carried out by usual geological methods. Subsurface methods included diamond drilling, seismic exploration and driving of investigation shafts and tunnels. A number of sites in the area was investigated progressively by surface mapping, air-photo interpretation and diamond drilling. The final site was chosen only after a careful assessment of the results of these investigations which showed the area to be free from major faulting.

The final site was explored initially by geological mapping of the surface and by diamond drilling. A total of five sloping holes was

drilled from the surface, varying in depth from 705 feet to 2005 feet, four of them extending below the level of the power station site. The site for the station was adopted tentatively based on the drilling results, and was explored further by an 8 x 8 foot tunnel 1100 feet long. Six more diamond drill holes were drilled from chambers near the end of this tunnel with a total of 1377 feet in the machine hall area and the surge race chambers. The joint pattern predicted from the surface exposures and the exploratory tunnel proved to be quite similar to that found in the site area, with the exception to two narrow, persistent faults. On the other hand a certain amount of shearing which was noted at boundaries between granite and gneiss did not occur in the actual excavation.

Diamond drilling has also been used successfully in evaluating the effects of underground nuclear detonations (See Chapter V).

Aerial Photography

In its relationship to geology aerial photography is employed to interpret various land forms for mapping of surface geology, and more importantly, in relation to the present study to identify rock types and rock structures where they are adequately expressed in earth surface features. The reader is referred to works on this subject for the details of theory and its application.

Rock Types

As pointed out earlier in this report, rocks may be classified as igneous, sedimentary or metamorphic. It is noted that each of these genetic classes covers a broad variety of rock types having generally typical, but specifically different modes of occurrence, gneiss, types of source, physico-chemical environment during solidification, alteration, or deposition and physico-chemical-mineralogical nature after formation. Lueder[7] proposes that rock classifications, based upon petrology and petrography support the suggestion that aerial-photographic techniques can be used to aid petrologic-petrographic surveys. It is also pointed out that there has been only a little work done (1959) on the true photographic patterns of specific rock types. Because of variations in the dominant mineral it is proposed that igneous rocks may have different responses to weathering that will be reflected in differences in land form, detailed surficial texture, drainage pattern, fracture and weather patterns, etc. Colors of rock may also offer a means of identification, and granitoid, felsitic, stratified, soluble limestones, shales and other types of rock have been found in many cases to exhibit characteristic textures and patterns in aerial photographs. Metamorphic rocks, in general, resemble the characteristics of rocks from which they were formed. Only a few rocks such as some slates, serpentines and quartzites exhibit any typical air-photo criteria.

Structural Geology

Many of the features of geologic structure which intersect the surface may be detected on an aerial photograph.

Faults[7]. Fault interpretation is based on one or more of the following criteria.

1. A persistent linear (linear feature of landscape) usually clearly defined.
2. Linear scarp, usually erosional, but may be actual fault scarp.
3. Persistent linear feature, near and parallel to a proven fault.
4. Offsetting of pattern of linears, with or without a change in trend.
5. Major regional change in lithology.
6. Offsetting of bedding linears, outcrop ridges, formations.

This is considered the most reliable criterion and it may be recognized only after careful detailed lithologic study.

Joints. Distinguishing between jointing and faulting is often difficult, Only where linears intersect clearly visible stratification on contacts is reliable determination possible. Joints also play an important role in that they tend to "fingerprint" a formation so that it can be traced or recognized more readily.

Bedding. The basic factor in the recognition of sedimentary bedding is that the successive beds usually differ in their physical and chemical properties. Topography in laminated structures rarely fails to show the strong influence of bedding after they have been acted upon by tectonic forces, erosion, etc. If the beds dip steeply, persistent close-space linears are evident. Prominent ridges, bands of color tone and contrasting weather patterns are conspicuous. Where beds are flat-lying they tend to follow contour patterns and certain beds become "cliff makers". Bedding should also conform with the regional structure. Where outcrops are scarce, bedding can often be interpreted from indirect evidence such as breaks in topography or changes in vegetation.

Schistosity and Gneissosity. While schists are highly foliated, unlike most sedimentary strata they display more homogeneity of composition and physical properties. Resulting foliation linears have less continuity, and ridges tend to be small and closely spaced.

Gneisses display abrupt lithologic changes as do schists, but to a lesser extent. Variations in weathering are less marked over wide thicknesses, however.

Summary

In general, aerial photographic methods are employed widely for reconnaissance in geological exploration and constitute valuable means of obtaining concepts of local and regional geologic structure. They

are employed extensively for accurate topographic mapping, and when coupled with geophysical techniques, surface geological surveys and subsurface probing, provide by far the most efficient, effective means of determining geologic structure.

CHAPTER X

REFERENCES

1. Dobrin, M.B., Introduction to Geophysical Prospecting, McGraw-Hill, 1960.

2. Richards, T.C., Broadside Refraction Shooting Geophysics, vol. 24, pp. 725-748, October 1959.

3. Barton, D.C., The Seismic Method of Mapping Geologic Structure, Trans. AIME, vol. 81, pp. 572-624, 1929.

4. Gailbraith, F.M., The Magnetometer a Geological Instrument at Sudbury, Trans. AIME, 1945.

5. McKinistry, H.E., Mining Geology, Prentice-Hall, 1948.

6. Lang, T.A., Underground Experience in the Snowy Mountains - Australia, Second Protective Construction Symposium, Project Rand, March 1959.

7. Lueder, Donald R., Aerial Photographic Interpretation, McGraw-Hill, 1959.

CHAPTER XI

CONCLUSIONS AND RECOMMENDATIONS

In general, it may be stated that the development of quantitative design criteria for resisting static loads in underground openings has seen only a few initial significant steps made toward an effective procedure; there is much less assurance concerning the utilization of existing data and methods in design to resist dynamic loads.

1. Rock Properties

A great number of tests of physical and mechanical properties of rocks has been reported, having been determined under a variety of laboratory and field conditions. Their primary value is to serve as a basis for further research.

The ultimate (ideal) objective of research into rock properties is to establish a procedure whereby the effective properties of rock at a proposed deep underground installation site may be determined by simple, inexpensive but reliable tests. The properties of interest are those which determine the stability of the overall rock mass subject to blast loading, and under static conditions as well. That is, one vital portion of the exploration program is a diamond drilling project which will provide solid cores of rock for testing. Most "standardized" laboratory tests, however, cannot be employed without question to evaluate rock parameters which can be utilized for design purposes.

Recommendations.

The most pressing needs are for research with the following objectives:

a. Determination of which rock properties are important in underground design, i.e., the effective design properties.

b. Evaluate further possible correlations of those which are most significant.

c. Investigate means of determining accurately the value of rock parameters which can be employed for design purposes, preferably by laboratory methods. This includes both design of openings and evaluation of any properties of the whole rock mass which may affect the stability of the protective installation.

d. One need may be for an in situ test to determine the utility of a site without need for elaborate preparation and particularly without requiring any extended period of time at the site.

2. Structural Engineering Geology.

There are several good books on engineering geology available, but none of them deal extensively with the subject of geology, rock properties and the factors related to deep underground protective construction.

Recommendations.

a. Investigate in more detail those principles of engineering geology pertinent to the problem and render a more definitive treatment of this subject.

3. Geology and Mine Stability.

The chief sources of information concerning the relationship of geology to the stability of underground openings subject to static and some types of dynamic loading are found in the case histories of operating mines, tunnels and underground power stations. The most important factors affecting the rock stability in underground opening structures are: (1) size of openings relative to structure, (2) faulting, fractures and joints, (3) weakening or strengthening mineralization, (4) type and basic strength of country rock, (5) destructive alteration and (6) depth. Most of the geologic studies found in the literature were made for exploration purposes and not to evaluate rock stability for purposes of mine operation. Hence, many pertinent details of geological engineering interest were not recorded and are not available for correlation and analysis.

Recommendations.

a. A detailed examination of the geology of operating mines with respect to its relation to opening stability would offer considerable valuable information beyond that currently available. Very few complete geological studies to date have been made with respect to mine stability problems.

b. Conduct a detailed investigation of rock bursts in their relation to the present problem.

c. A detailed examination and correlation of all of the military and civilian underground installations of the type most nearly resembling future needs should be made.

4. Geology and Stability of Underground Protective Construction.

The character of the geologic structure which constitutes the environment of an underground protective installation is more critical than that for a mine or tunnel because of the possibility of unpredictably high transient loads.

There appears to be considerable difference of opinion as to what the nature of the deep cover over an installation should be, competent or broken. That which would provide a significant amount of attenuation would ordinarily be preferred, but the installation itself should almost certainly be in competent rock. Steel, concrete or timber support will not resist heavy loads beyond low or medium level slabbing. Reflection and refraction properties are also important.

The direction of openings with respect to faults plays an important part in producing areas of high stress concentration in the rock near the opening. Thus, high static stresses plus a superposed dynamic stress field could readily result in a rock burst condition.

Recommendations.

a. Conduct an extensive investigation into the effects of geologic structure upon wave transmission and attenuation.

b. Conduct an intensive investigation into the effects of local geologic structure upon opening stability.

c. Investigate the effects of rock alteration, secondary mineralization, ground water and related problems.

5. Wave Mechanics and Instrumentation.

The type of wave of primary interest deep underground is the P wave or the dilatation wave. Damaging stress waves are generated by a detonation at the surface or from a subsurface position initially as a shock. Although most underground openings will be located at distances where the wave assumes an "elastic" behavior, pressures, strains and accelerations in zones from the position of the explosive downward within the damage distance are also of interest. Instrumentation to measure phenomena in some of the more distant zones is available, but for high pressure areas there appear to be few, if any, reliable devices available which will measure the important behavior parameters.

Recommendations.

a. Make an intensive investigation into the feasibility of developing pressure gages which will measure values successfully in the high pressure ranges.

b. Investigate the attenuation of high magnitude stress waves in various types of rocks and various types of rock media, i.e., broken, altered, etc.

c. Investigate the response of rock materials to high magnitude stress waves.

6. Rock Failure.

There has been a number of theories proposed to explain the failure of solid materials under stress. Of these, Griffith's and Mohr's theories seem to be the most generally applied. Some researchers have applied the theory of maximum strain to rock failure by slabbing.

On a large scale the failure of rock seems to be due to all three types of stress, i.e., compression, shear, and tension. Slabbing accounts satisfactorily for many of the observed failure phenomena in the formation of craters by HE and the Neptune crater. Geologic structure had some influence, due to difference in properties of strata, upon the limits of the fracture zone for the Rainier event, but all of the mechanisms involved are not clearly defined. Few data are available on configurations comparable to those which might be expected from an explosion over a deep protective installation.

Recommendations.

a. Intensify investigations already in progress on the relation of rock failure to rate of strain.

b. Investigate the basic mechanisms involved in rock failure in crushing, slabbing, fracturing, etc., to evaluate the relative effects of crystalline structure and bonding between crystals and grains; also on a larger scale to determine the influence of geologic structure upon mechanisms of failure.

7. Static Stresses and Design of Openings.

The analyses of static stresses around underground openings and the design of openings are based primarily upon elastic theory, and, hence are limited to simple symmetrical openings in near-ideal rock. Some analyses have been made for bedded rock, and a very few for structures intersected by fractures, joints or faults. Experience has shown that the location of openings with respect to faults can be critical.

Static stresses in the earth's crust are caused primarily by body forces, i.e., the weight of the overlying rock. Additional stresses may be superposed by tectonic forces in the rock. Resulting from these factors three types of stress fields are postulated and the preferred shape of opening for each is indicated. The principles of beam design for openings in stratified rock are given for the first layer of rock which acts as the immediate roof.

Recommendations.

a. Extend investigations of stress distributions for homogeneous structure to openings in broken, fractured rock, where the structure is more complex than in solid rock or simple stratified rock.

b. Examine in more detail the types of static stress fields which actually exist in the earth's crust due to depth, tectonic forces, and properties of the rock including geologic structure.

8. Dynamic Stresses and Design of Openings.

Analysis of pertinent types of stress waves currently has been concentrated upon the effects of a step type wave of limited horizontal extent applied to the surface of an ideal half space. The measurement of such a stress wave photoelastically, indicates that the stress at the surface of a cylindrical opening is multiplied by about 3.3 times the free stress field.

Cursory comparative analyses of effects of static stresses indicate that an elliptical or circular cross section is the best design for most geologic structures. Size should be kept as small as possible, because the total number of rock defects increases with size, and consequently the probability of limited failure or collapse of the opening.

Recommendations.

a. Extend both theoretical and experimental investigations of propagation of waves in a half-space and their impingement upon cavities of various analytical and non-analytical shapes.

b. Investigate the parameters involved in the superposition of dynamic and static stress fields.

c. Investigate the effects of gross and local geologic structure on dynamic stress fields.

d. Investigate the effects of local geological structure around openings upon stress concentration.

e. Investigate the effects of rock alteration and weathering on resistance to failure by dynamic loading.

9. Similitude and Scaling.

A plot of the effects of confined HE and nuclear explosives shows that within reasonable limits true cratering effects can be predicted by the cube root law. On a pound base (rather than kiloton) the most effective breakage, which includes the greatest volume broken plus the highest probability of breaking completely, is for scaled depths of 1.25 to 3.0, depending upon the type of rock. Such depths should result in Zone 1 damage. Resistance to cratering appears to be governed primarily by two factors: (1) ability of the rock to absorb impact energy, and (2) the strength of the rock.

At present it appears that the safest criterion to employ in calculating survival depth is to assume that the explosive is virtually unconfined.

Recommendations.

a. Conduct a series of small, medium and large scale tests with HE to define more clearly the parameters involved in dynamic stress concentration around deep openings.

b. Conduct a series of tests with nuclear devices to check the results of previous tests, those from HE, and to evaluate pertinent factors so that they are less speculative and more reliable for design purposes.

c. Investigate the principles of destressing and transfer of critical stresses on model and full scale.

d. Conduct a series of model "cratering" tests in several types of rock breaking to limited free surfaces and tunnels.

10. Support of Underground Openings.

Timber support has the particular advantage in that it is able to yield considerably before it fails, and it can absorb nominal impact loads. Rigid concrete or steel support is satisfactory for static support, but is not adapted to resisting high magnitude loads of long or short duration. Certain types of yieldable steel supports have been found capable of holding tunnels open while yielding with increasing resistance under gradually increasing (squeezing) loads. Little theory or experimental data is available concerning their behavior under either static or dynamic load. They appear to offer considerable promise to increase possibilities for survival in areas of Zone 4 damage.

Rock bolts will almost certainly be required in a protective installation. Their function in stabilizing rock structures under static load is well recognized from experience and experimentation. Their function in stabilizing rock structures under dynamic load is less well defined.

Recommendations.

a. Investigate various types of design of flexible support for openings subject to dynamic stresses. These might include systems such as damped elastic, frictionally resistant or hydraulic.

b. Investigate the characteristic behavior of rock bolts under dynamic loading.

11. Geophysics, Drilling and Aerial Photography.

Applicable methods of geophysical exploration are outlined in sufficient detail to show how they may be employed in the evaluation of a possible site for an underground installation. Seismic methods appear to be the most usable for this purpose, although they may often be supplemented with magnetic, gravitational or other geophysical techniques. Diamond drilling is a necessary procedure to project surface geology to depth and to add to and confirm geophysical findings. Aerial photo-

graphy is particularly useful for rapid mapping of new areas, both for topography and surface expressions of geologic structure.

Recommendations.

a. Write a detailed manual on the utilization of exploration geophysics in relation to underground protective construction.

APPENDIX I-A

PHYSICAL AND MECHANICAL PROPERTIES TESTS

Below are tabulated some of the standardized materials tests adapted for determining the physical properties of rock. Most of the properties listed in Appendix I-B were obtained by the following methods.

Young's Modulus.

Two standard methods are employed to determine value of Young's modulus: (1) static method and (2) dynamic method.

Static Method.[1,2] Cylindrical specimens of rock are prepared with the ends lapped to provide flat surfaces perpendicular to the main axis. These are cut to a length of approximately 2.5 times their diameter. Electric resistance strain gauges are cemented on the opposite sides of the specimen parallel to the longitudinal axis.

The same test procedure is followed as in that employed to determine compressive strength. The load is applied at the rate of 100 lb./sq. in./sec. to approximately 50 percent of the compressive strength, with five or six readings of load and strain being taken at evenly spaced load increments. One minute halts are made for each reading. A similar set of readings is made as the load is released. Six complete cycles of loading and unloading are then taken to the 50 percent load value, but normally data for these additional cycles are not recorded. During the next cycle, which is the seventh, readings are taken as on the initial portion of the first cycle and then the loading is continued until failure takes place.

A graph of the average stress and strain values is plotted. The secant value at the initial load is an approximation of the tangent value at zero load and therefore may be compared with the value obtained by the dynamic method.

Dynamic Method. Young's Modulus may also be calculated by determining the frequency of induced longitudinal vibrations in a specimen and substituting these values and the numerical density of rock in an appropriate formula. (Dynamic tests of elastic properties may be made all on one specimen and in one apparatus.) Longitudinal vibrations in a specimen (drill core) of rock which is suspended by a clamp at its center are measured in their fundamental frequency. (Figure I-A.1).

The longitudinal velocity is given by:

$$(1) \quad v_l = 2 f_l L \qquad \text{(I-A.1)}$$

where

v_l = longitudinal velocity of sound

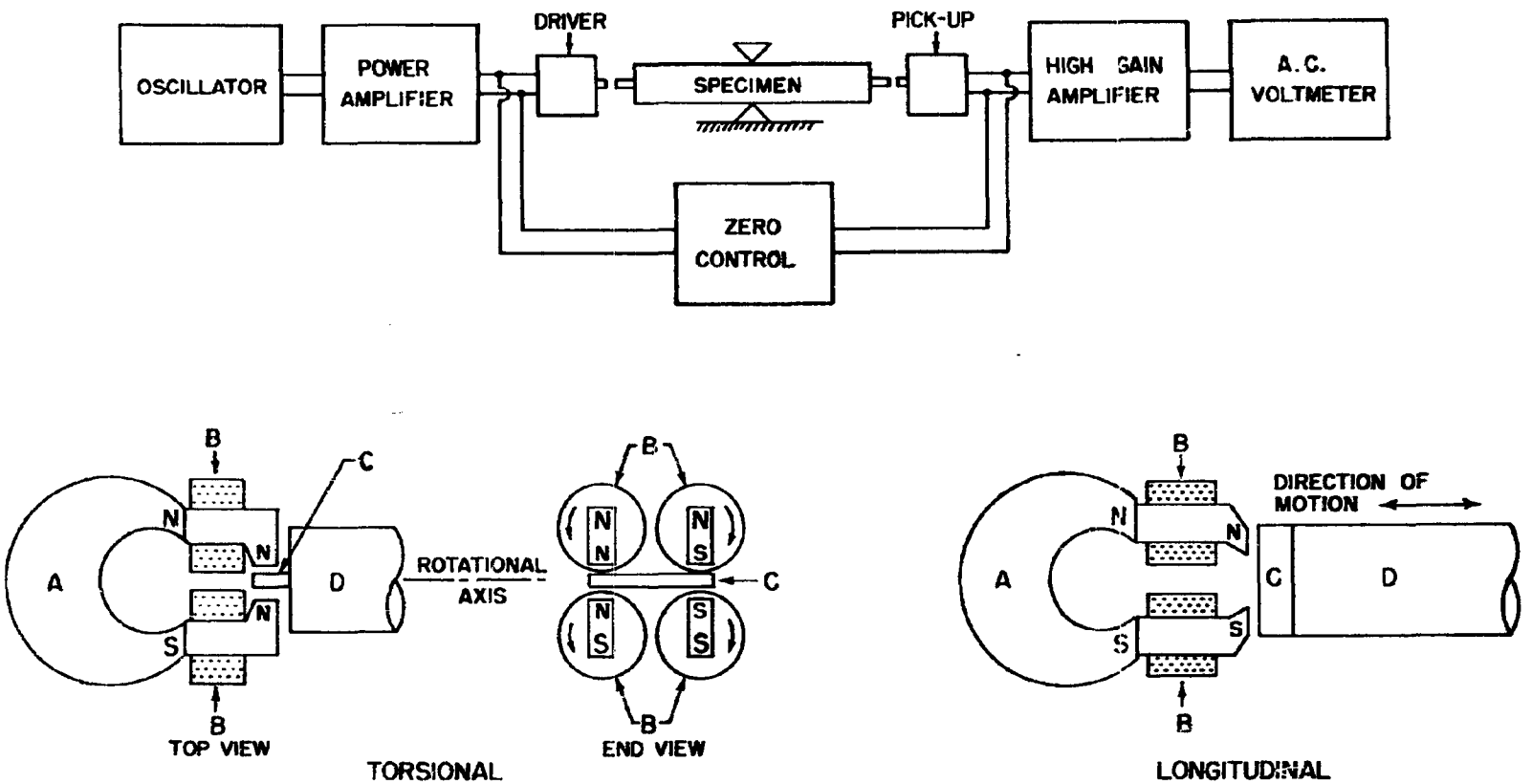


Figure I-A.1. Block diagram of electronic equipment utilized in dynamic modulus determination by the resonant frequency method. Insets show the specimen end configurations for torsional and longitudinal excitation.

f_1 = fundamental longitudinal frequency

L = length of specimen in feet

From the velocity determined by (1)

$$(2) \quad E = v_1^2 \rho \qquad \text{(I-A.2)}$$

where

E = Young's Modulus of Elasticity

ρ = density of the rock

Modulus of Rigidity

If a small block of elastic material is acted upon by two non-colinear forces (couple) a shearing stress is produced and the body is deformed. The modulus of rigidity is defined as the shearing stress divided by the deformation.

The modulus of rigidity may be determined with ease by a dynamic method. A cylindrical specimen is clamped as in the test to determine Young's modulus, and the fundamental frequency of torsional vibration is measured. The torsional velocity of sound in the specimen is then calculated from appropriate equations.

Tensile Strength

Rock specimens are tested for tensile strength in a standard testing machine with special tension grips which allow rock cores to be easily adjusted to insure alignment of the load with the axis of the test piece. The rate of loading is 100 pounds per minute. For rocks of non-uniform nature this test yields erratic results, and tensile strengths determined from rupture tests are preferred. (Figure I-A.2a).

Another method of determining the tensile strength of rock which has been accepted as a standard test is the so-called "indirect" or Brazilian test. This method was introduced in France for the determination of concrete tensile strength. A compressive load is applied perpendicular to the diametrically opposite generatrices of a rock cylinder as shown in Figure I-A.2b. Care must be taken that the compressive loading is uniform over the length of the cylinder. Assuming elastic behavior, the diametral plane connecting the generatrices under load is subjected to a uniform tensile stress over more than 80% of its area, given by

$$\sigma = \frac{2P}{\pi D \cdot l} \qquad \text{(I-A.3)}$$

Failure occurs when the tensile strength is exceeded and the specimen splits into two equal halves. Corrections can be calculated to account for the fact that the compressive loading is actually applied over a finite area rather than a single line. However, since these corrections are generally less than five percent they are seldom employed.

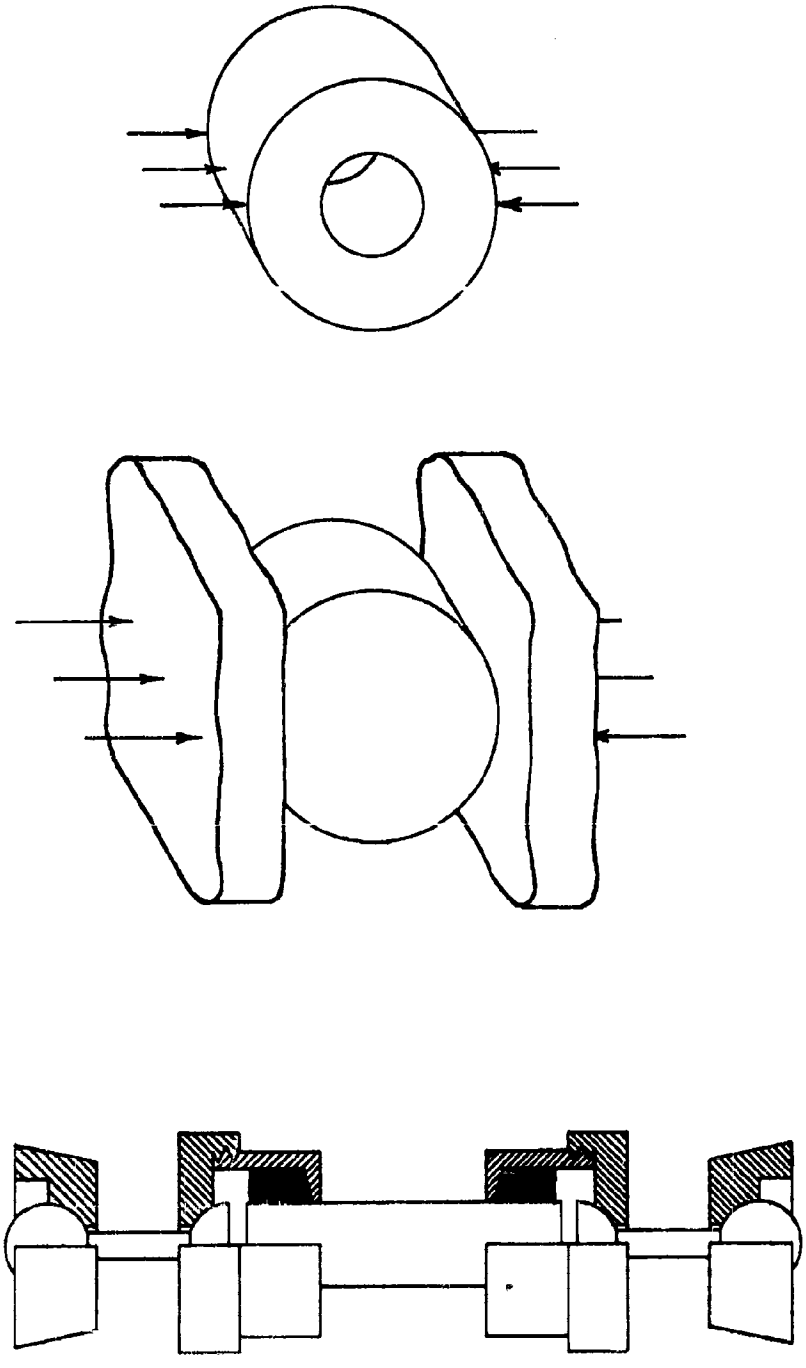


Figure I-A.2. Tensile test configurations. (a) direct tensile test, (b) indirect or Brazilian test, (c) ring test.

Although a compressive stress exists at right angles to the tensile stress calculated, its influence on failure is relatively insignificant due to the relative weakness of rock in tension.

In concrete testing, a tensile test is sometimes performed with the configuration depicted in Figure I-A.2c. It can be seen that this test differs from the indirect test above in that the specimen possesses a central hole. This hole provides a tensile stress concentration, and as a result the failure of the specimen generally originates at the central hole. Since calculation of the failing stress in this case is even more sensitive to the elastic nature of the material, and due to the difficulty of forming rock specimens of this type, this method has not received general acceptance in rock property testing.

Modulus of Rupture

The modulus of rupture is defined as the tensile stress in the extreme fibre of a beam computed by the familiar flexure formula $\sigma = \frac{Mc}{I}$. The testing procedure involves the preparation of 6-inch specimens which are placed on knife edges 5 inches apart. The load is then applied at the center, the load being increased until the specimen fails. The lower section of the test beam is in tension and a normal failure results in the rock breaking at the lower fibre. (Figure I-A.3).

Compressive Strength

Tests of compressive strength of rocks are made according to ASTM standards. Specimens are cut with their length equal to their diameter to avoid column effects, the ends are carefully lapped to insure that they are smooth and parallel and then they are tested in a standard testing machine. (Figure I-A.4).

Scleroscope Hardness

A Shore Scleroscope indicates the Scleroscope hardness of a substance by the height (or an arbitrary scale of 0 to 120 divisions) of rebound of a diamond pointed (pin-point - 0.03 in^2) hammer which is dropped vertically on the test surface. The impact of the point may produce some crushing of a microscopic nature, but this may be neglected for practical purposes. Data may be reproduced on a very non-homogeneous rock by an observer making at least fifty readings over a small surface. By comparison with values for rocks in Appendix I-B, a soft steel block exhibits a hardness measurement of 26.

Abrasive Hardness

This test employs a rotating abrasive wheel or plate against which two $2\frac{1}{2}$ inch diameter specimens are held at constant pressure. Silicon carbide powder is fed continuously onto the rotating circular plate and

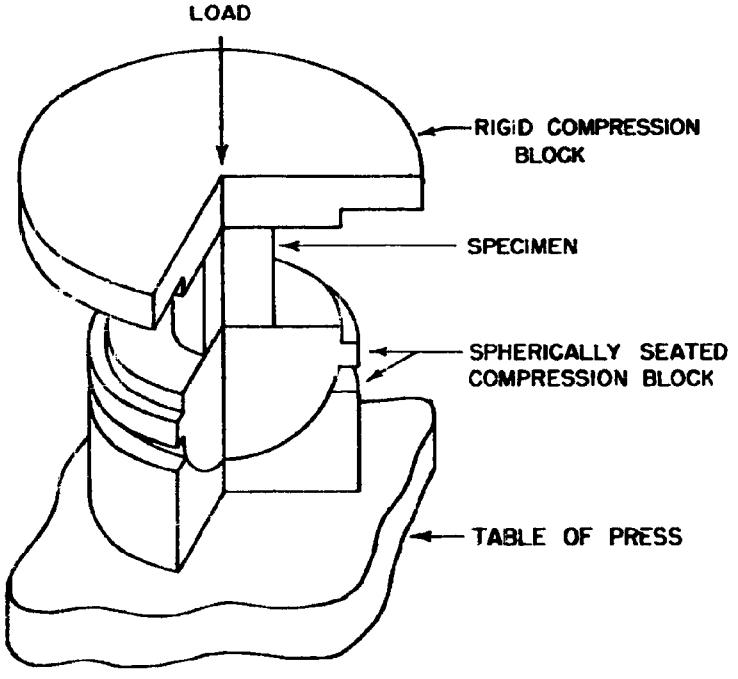


Figure I-A.4. Compressive test configuration.

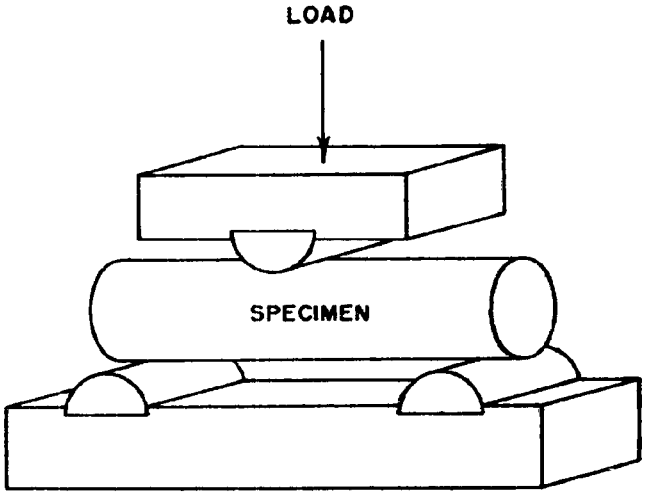


Figure I-A.3. Modulus of rupture test configuration.

the specimens are abraded for a given number of revolutions of the plate. The weight of material lost is determined and the abrasive hardness calculated from $H_d = \frac{10^{-3}}{M_d}$ where H_d is the abrasive hardness and M_d is the weight of material abraded in lb/sq. in. per revolution.

Impact Toughness

This method, known as the Page impact test, involves determination of the impact toughness of a rock by dropping a weight from successively greater heights upon a plunger in contact with a rock specimen, until such a height is reached that the specimen is fractured.

Apparent Porosity

This characteristic is defined as the ratio of the volume of open pore space in the specimen to the exterior volumes. It is obtained by measuring the difference in weight of a rock which is dessicator dried and when water saturated. The porosity of a rock so determined is also an indication of its granular structure.

Apparent Specific Gravity

This property is determined by the standard method of dividing the weight of a rock by the weight of an equal volume of water. The term "apparent specific gravity" is used because water cannot penetrate the closed pore spaces inside of the rock, and, hence, the specific gravity measured by water displacement methods includes the effect of internal pore spaces as well as that of the constituent minerals.

Strength of Rock Samples of Irregular Shape.

The use of rock samples of irregular shape could greatly reduce the time and labor involved in physical testing. Investigations in the United States have been performed primarily on diamond drill cores, although considerable work has been done with cubical specimens. In most instances it has been felt that smooth parallel surfaces are necessary for contact with loading heads. When results have been inconsistent error has often been attributed to improper preparation of the test specimens. Protodyakonov[3] has presented the following summary of methods of determining rock strengths based on irregularly shaped rock samples. These methods will undoubtedly find considerable use in the United States.

The results of tests performed on irregular specimens are more widely dispersed than those from regular specimens and therefore a greater number of samples is required to obtain the same degree of accuracy for the average strength. Even considering this additional

number of tests required the total labor involved for strength evaluation of a rock is considerably reduced.

Tensile Strength

Three separate methods for determining the tensile strength of irregularly shaped pieces of rock have been proposed.

Direct Tensile Test. A sample of irregular shape is embedded in cement between two metal dies, leaving a narrow transverse slit between the dies (Figure I-A.5a). The dies are pulled in a universal testing machine until the specimen fails. Carbon and white paper are pressed to the sample to obtain the rupture surface outline. The area of the rupture surface is then measured with a planimeter. The average resistance to lateral extension is

$$\sigma_t = \frac{P_t}{A} \qquad \text{(I-A.4)}$$

when P_t is the tensile load and A is the rupture surface area. This method has some disadvantages: the possible existence of a bending moment owing to non-centered loads on the sample, with resulting lowering of apparent strengths, and it is limited to rocks whose strength is less than that of cement. It also involves a time delay due to the period required for setting of the cement.

Indirect Tensile Test. Pieces of rock are chosen whose volumes do not differ by more than a factor of two, and whose sharp edges have been removed. These specimens are placed between platens of a compressive testing machine and crushed (Figure I-A.5b). The sample normally ruptures along a plane connecting the points of loading. The failure is assumed to be due to uniform tension applied across this surface. The area of the surface of rupture is approximately equal to V the volume of the sample raised to the 2/3 power with the result

$$\sigma_t = \frac{P_c}{V^{\frac{2}{3}}} \qquad \text{(I-A.5)}$$

where P_c is the compressive load at failure.

Failure of a Ring. A piece of rock of an irregular shape is prepared by drilling a central hole through it. A perforated tube within a rubber casing is inserted in the sample (Figure I-A.5c). Oil is injected into the tube, which produces a uniform pressure inside the sample. After the sample has been broken, its inner radius r and outer radius R are measured. The tensile failure stress is computed assuming that a crack first appears on the inner radius of the sample, gradually develops until it reaches the center of thickness of the sample, at which time instantaneous failure takes place. The formula so derived is obtained from Lame's formula for thick-walled cylinders taking into account the appearance of the first crack, giving

$$\sigma = \frac{2.69R}{Z} P_{max} \qquad \text{(I-A.6)}$$

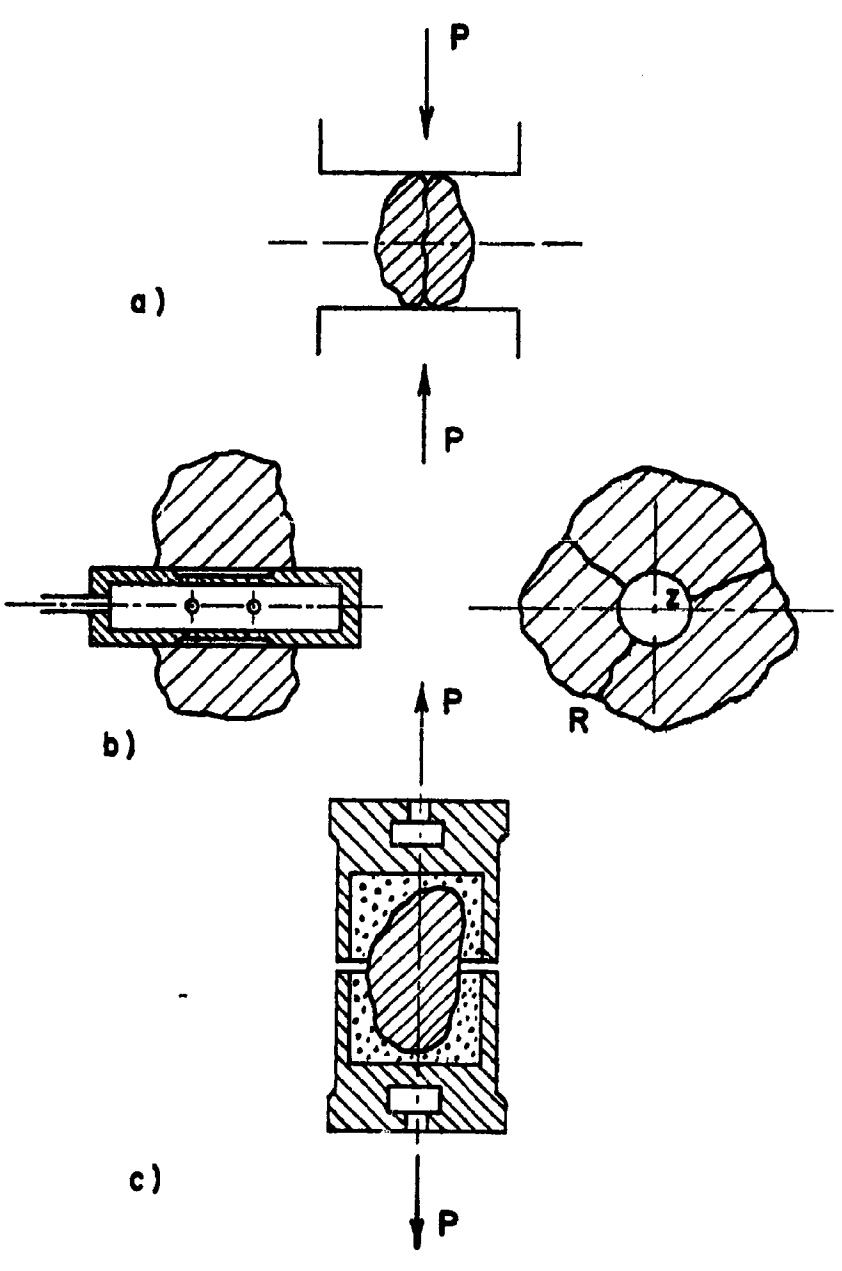


Figure I-A.5. Configuration of tensile tests performed by Russian investigators on irregularly shaped specimens. (a) Indirect tensile test, (b) Ring test, (c) Direct tensile test.

Combined Compression and Shear.

Tests to determine the strength of irregular rock specimens under combined shear and compressional stresses utilize specimens mounted between two dies in a concrete matrix (Figure I-A.6). The narrow slit between the two dies, which makes an angle α with the applied compressive load, controls the failure plane. The stresses at failure, where F is the area of the failure surface, become:

$$\sigma = \frac{P \cos \alpha}{F} \qquad \text{(I-A.7)}$$

$$\tau = \frac{P \sin \alpha}{F} \qquad \text{(I-A.8)}$$

Combined stress tests such as these permit inexpensive definition of Mohr's envelope for a particular rock type.

In all of the methods of testing irregularly shaped specimens selection is according to weight rather than dimensions. The only sample preparation is a smoothing of the sample by removing sharp edges with a hammer.

In Situ Determinations

Seismic[4]. In preparing the test sites, a series of shallow holes 1½ in. in diameter was drilled 8 inches deep in line vertically from a free surface; the outer holes on one or both ends were used as shot holes.

Gages were positioned in holes from 50 to 450 feet from the shot holes with mounts consisting of various shaped steel members welded to 6-inch-long studs grouted in the holes. The gages were oriented to measure particle motion perpendicular to a line from the shot hole to the gage position. Particle velocity gages and accelerometers with low cross-axial sensitivities were used and signals from them were amplified and recorded on a magnetic tape recorder.

In each test series, high explosive charges were detonated, trial shots being used to determine proper attenuator settings for preamplification. Other shots were fired for several purposes: (1) to determine optimum charge size for proper resolution of shear wave arrivals, (2) to vary travel paths and (3) to establish reproducibility of wave arrival times and wave forms. Preliminary charge sizes varied from 0.06 lb. to 0.4 lb.

Regular electric blasting caps were used, a chronograph contactor being inserted with the cap into the explosive charge to give an electrical pulse at detonation or zero time. Arrival times of longitudinal and shear waves were measured on the records from this zero time.

Tests were conducted by the Bureau of Mines in two rock types. The first test was in an underground opening at a depth of about 800 feet in a massive salt dome. A total of 9 shot holes and 6 gage holes was drilled

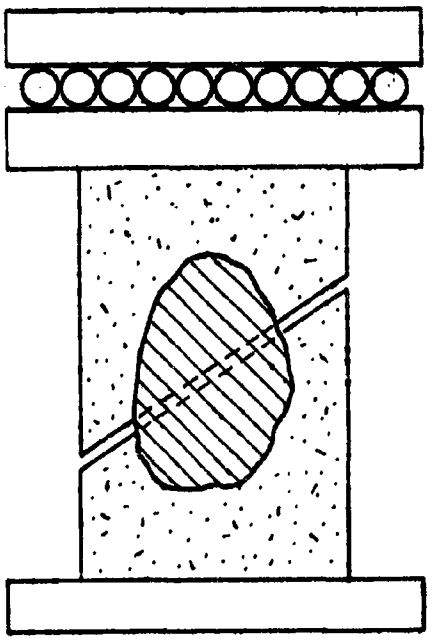


Figure I-A.6. Combined compression and shear test configuration as applied to irregularly shaped specimens by Soviet engineers.

in the floor of a drift. Gage mounts were simple L-shaped members welded to studs with gages fastened to the upright part of the ell and oriented to measure transverse motion. Optimum charge sizes for definition of shear wave arrivals in salt were found to be from 0.1 pound to 0.05 pound over travel paths in salt from 100 to 450 feet.

In more extensive tests conducted in a granite-gneiss outcrop, the same gage types and recording system were used. Shot holes were used on both ends of the array to minimize local velocity variations. Gages may be oriented to measure radial, vertical, and tangential components of particle velocity and acceleration. Elastic constants of field tested materials may be determined in the laboratory using standardized test procedures. (See Chapter I for mathematical formulae used to convert velocity measurements).

Load Bearing Tests[5]. Load bearing tests are being utilized to an increasing extent as a source of information for the design of heavily loaded surface structures such as dams and highways. Where load-bearing capacity is low and where deflections under load must not vary appreciably over the foundation, it has been considered essential that the physical characteristics of the foundation rock be investigated as a part of the design procedure.

Load bearing tests have supplanted seismic tests where the foundation rock is in a highly shattered condition. Consolidated and plastic flow, which might be expected under longterm, high intensity static loads, may not be detected by dynamic tests, particularly where the path of the shock wave is through saturated material. Dynamic tests conducted in the laboratory by the Bureau of Reclamation substantiate this conclusion. These dynamic tests indicated that water-filled joints between blocks of concrete had little effect on the average shock velocity. When the joints were air-filled, the travel times were somewhat greater, but erratic. The dynamic modulus of dry, shattered, concrete as computed from wave velocities was increased 50 percent by saturation.

Bearing load tests may be divided into two types, horizontal and vertical tests. Both types require excavation of a test pit into the region which is to be investigated. This test pit must be excavated with a minimum of blasting, with particular attention to the bearing surfaces to avoid disturbance of the foundation rock.

A hydraulic jack applies loads to bearing plates seated against opposite walls of the pit in the case of the horizontal tests. The thrust is applied 6 to 8 feet from the pit floor to minimize the effect of that boundary. Sufficiently large bearing plates eliminate local failure. Mortar is placed between the bearing plates and the rocks to secure uniform contact. Deflection of the load-bearing plates is measured by means of dial gages mounted two to a plate to get the average deflection. Deflections of the rock outside the bearing plates is also measured with dial gages.

A hydraulic jack, working against a dead weight, applies loads to a single bearing plate seated against the bottom of the pit in the case of the vertical tests. Where the rock is severely fractured, upward

movement of the area adjacent to the bearing plate is restricted by use of a reinforced concrete mat at the bottom of the test pit; the load being applied through a central hole in the mat. Dial gages are used in the same manner as in the horizontal tests. Tests are conducted for periods extending from a few hours to several weeks duration.

The load bearing tests have been based on the theoretical work of Boussinesq on the effect of a concentrated load on the plane boundary of a semi-infinite elastic body. This work has been extended to determine the modulus of elasticity of a semi-infinite solid from deflections caused by loading the rigid die giving

$$E_{die} = 0.5P(1-\nu^2)/aw \qquad \text{(I-A.9)}$$

where P is the total load, ν is Poisson's ratio, $\underline{a}$ is the radius of the area loaded and $\underline{w}$ is the deflection.

The moduli are normally computed as a secant to the load deformation curve. Since both consolidation and plastic flow take place under sustained load, as well as elastic action, the result is termed a "deflection modulus."

The performance of bearing tests in tunnels, test pits, and other restricted locations requires a knowledge of the corrections which must be applied to nullify the effects of restricting boundaries. Theoretically it has been determined that a correction of approximately 6.5 percent would be adequate to remove the effect of restraint due to the side walls of the pit in a horizontal load bearing test. Since this factor is small compared to the variability of test results, no correction of field data is normally made.

The load bearing tests performed to date have indicated that weathered surface rock materials may have load-deflection characteristics varying by several hundred percent at different locations separated by only a few hundred feet. Repeated loadings at the same location increase the stiffness of the rock mass. Although a direct comparison of horizontal and vertical tests is impossible due to differences in load magnitudes, loading duration, and variations in rock character, the average values of deflection moduli from the same location have been in reasonable agreement. Thus either test method may be utilized where the rock is reasonably similar in vertical and horizontal properties. Generally, the deflection of the rock mass is proportionally less at higher loads.

Additional Mechanical Property Tests Performed in the U.S.S.R.

Protodyakonov[3] has reported several methods of testing regularly shaped rock specimens which are mentioned here because they are quite different from tests performed for the same purpose in the United States.

Laboratory Tests. Figure I-A.7 illustrates four methods of obtaining the tensile strength of regular rock specimens utilized in the Soviet Union. In Figure I-A.7a, a sample in the shape of a disc is supported

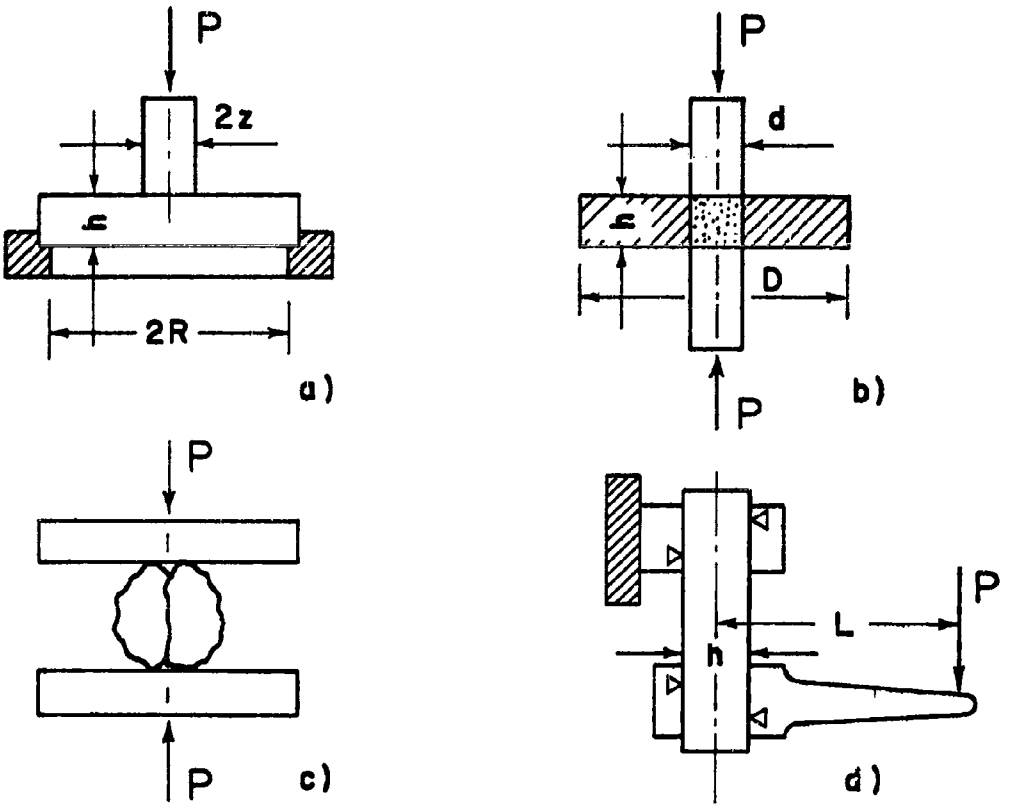


Figure I-A.7. Configurations of Russian standard tensile tests. (a) Bending of a disc, (b) extension of a ring, (c) indirect or Brazilian test, and (d) modulus of rupture.

along the perimeter and loaded at its center. The maximum tensile stress, σ, developed at a failing load, P, is given by the equation

$$\sigma = \frac{3P}{8\pi mh^2}\left[\, 4(m+1)\,\ln\frac{R}{Z} + \frac{4mR^2-(m-1)Z^2}{R^2} \,\right] \qquad \text{(I-A.10)}$$

where Z is the radius of the load applying die, h is the specimen thickness, R is the effective specimen radius, and $m = \frac{1}{\nu}$, the inverse of Poisson's ratio.

The tensile strength of rock has also been determined stretching a doughnut shaped sample by means of a uniform pressure applied to the interior wall. The pressure is developed between two coaxial punches (See Figure I-A.7b) acting against a rosin-paraffin putty. The tensile stress is taken as

$$\sigma_e = \sigma_p \frac{Z}{R-Z} \qquad \text{(I-A.11)}$$

where σ_p is the pressure applied to the butt of the punch.

The Russians are also using the so-called Brazilian or "indirect" tensile test with a compression load applied to rock cylinders placed on their sides as has been discussed previously. (See Figure I-A.7c). It is interesting to note that the equation relating the tensile stress developed to the applied compressive load, as used by the Russians is quite different from that utilized in the United States, being

$$\sigma = \frac{P}{D\,L}\quad\left(1 + \frac{10^{-4}P}{D\,L}\right)\ \mathrm{Kg/cm^2} \qquad \text{(I-A.12)}$$

Modulus of rupture tests have been performed using the configuration of Figure I-A.7d to apply a bending moment.

The search for data on shearing strength of rock has led to the adoption of several tests which combine both shear and compressive strength. In one test (See Figure I-A.8a) a prismatic sample is placed between two inclined dies and loaded to failure. Different combinations of shearing and compression stresses are made possible by changing the die angle. The resulting stresses are

$$\sigma = \frac{P\cos\alpha}{Lb} \qquad \text{(I-A.13)}$$

$$\sigma = \frac{P\sin\alpha}{Lb} \qquad \text{(I-A.14)}$$

where L and b are specimen cross-section dimensions.

Another shear-compression test performed combines double shear by means of a special press with an independently applied axial compressive load, as illustrated in Figure I-A.8b.

Several types of confined or triaxial strength tests have been reported by Protodyakonov. The simplest of these tests is illustrated

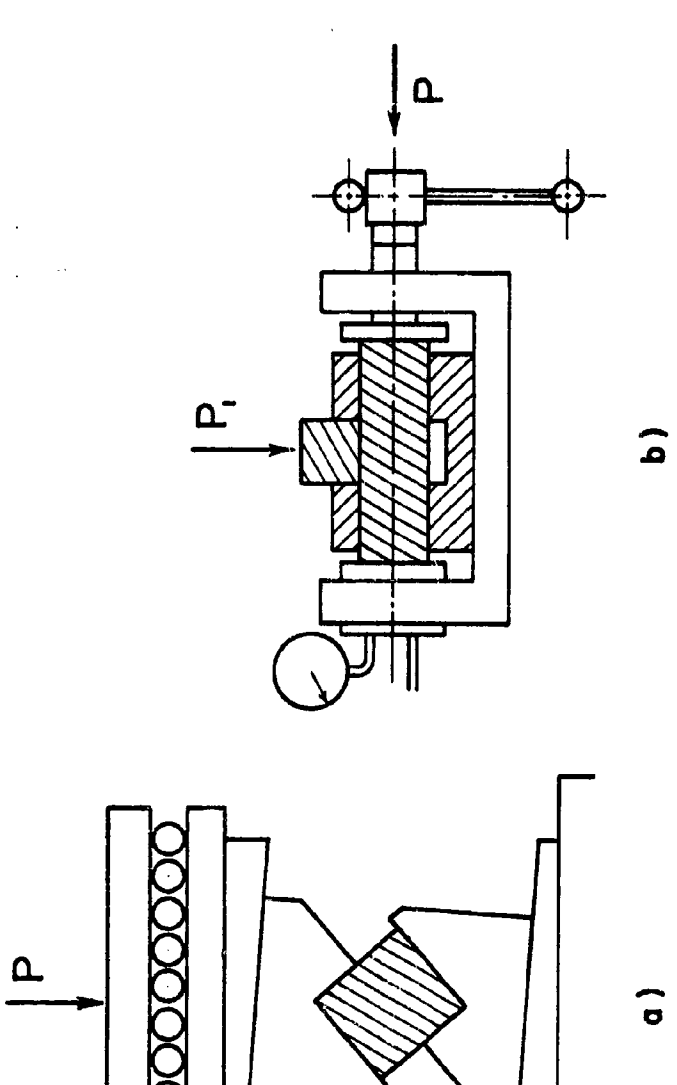


Figure I-A.8. Two methods utilized by Russian investigators to produce simultaneous shear and compression stresses.

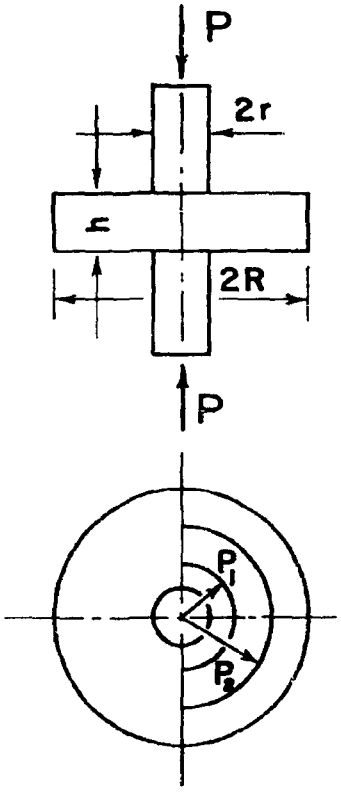


Figure I-A.9. Flat disc loaded by coaxial dies. Disc outer radius determines degree of confinement of central material.

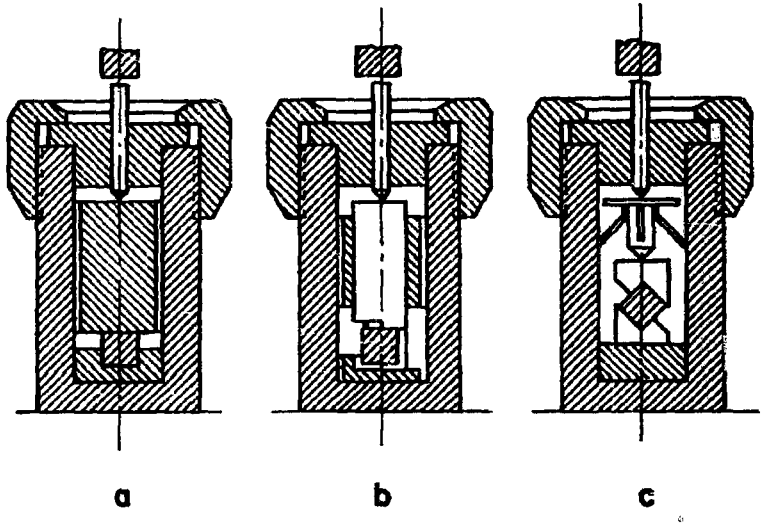


Figure I-A.10. Test configurations of hydrostatically loaded test specimens. (a) Superimposed compressive stress, (b) superimposed shear stress, and (c) superimposed combined shear and compression stress.

in Figure I-A.9. A flat disk is crushed by coaxial punches placed at its center. The outer part of the disk restrains the central portion. By increasing the outer radius of the disk the degree of confinement in the central portion is increased. The lateral pressure in the central part of the disk is

$$\sigma_z = \nu \frac{R^2 - Z^2}{2R^2} \sigma_p \qquad \text{(I-A.15)}$$

Cubic samples have been placed in pressure vessels and subjected to hydrostatic pressures simultaneously with compressive loadings, shearing loads, or combined compression shear loads as shown in Figure I-A.10. Oil or nitrogen has been used as the pressure transmitting fluid with pressures to 2000 atm. Samples have been soldered in foil sockets to prevent liquid penetration.

The deformation of samples in a compression chamber has been measured at pressures up to 5000 atmospheres. Samples are placed in the chamber whose deformation with pressure has been previously determined (Figure I-A.11). A transverse steel plate, rigidly connected between the sample and the casing measures the relative deformation by means of resistance strain gages, and specimen deformation is then calculated.

Another confined test performed consists of a rock sample which is subjected to a central bending force simultaneously with hydrostatic pressure of up to 5000 atm., as shown in Figure I-A.12. Deformation of the rock beam is measured by means of a calibrated cantilever steel plate with mounted resistance strain gages.

The Soviets have also performed a unique dynamic modulus of elasticity test during which cylindrical rock samples were subjected to 5000 atm. of hydrostatic pressure (See Figure I-A.13). A pulse method of testing was employed to obtain the dynamic modulus of elasticity using a piezoelectric pickup and receiver at each end of the sample made of ammonium dihydrophosphate. Frequencies of about 100 kc/sec. were employed. Velocity of pulse travel was used to compute the modulus of elasticity of the rock.

Static In Situ Tests. Tensile strength of rock in place has been determined by inserting rods similar to roof bolts in drill holes in the rock face and pulling the rods out of the face by means of a hydraulic jack. A cone-shaped cavity is left in the rock (See Figure I-A.14). The tensile stress developed is given by

$$\sigma = \frac{1.2P}{RL} \qquad \text{(I-A.16)}$$

where R is the crater radius and L is the crater depth.

Figures I-A.15a and I-A.15b illustrate two methods of hydraulically loading pillars left in place within an underground opening. Figure I-A.15a shows a means of producing compressive stresses within the pillar while shearing and compression are produced on the inclined plane shown in Figure I-A.15b.

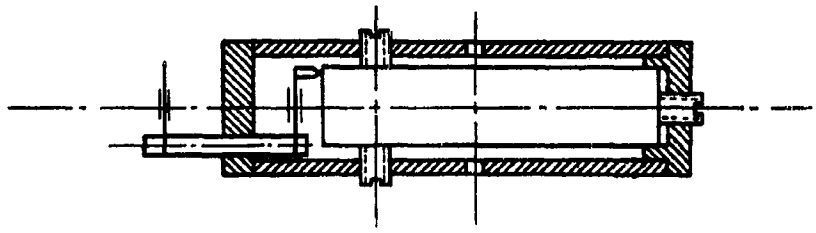


Figure I-A.11. Measurement of rock specimen deformation due to hydrostatic pressures.

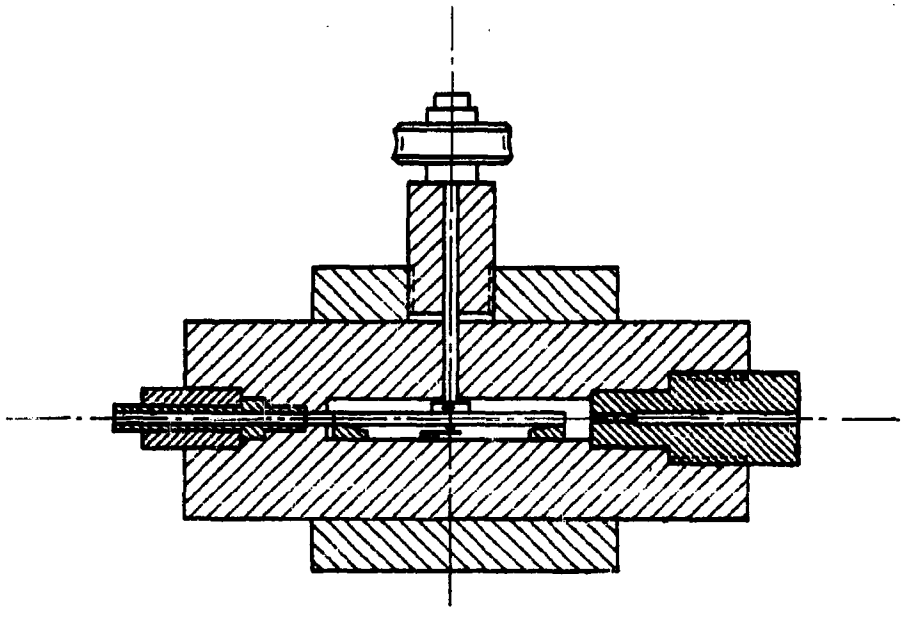


Figure I-A.12. Measurement of rock beam deflection under simultaneous central loading and hydrostatic pressure.

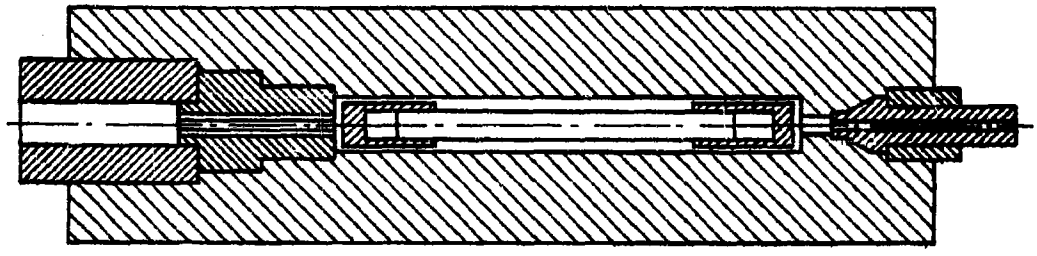


Figure I-A.13. Configuration for dynamic modulus of elasticity test as performed by Soviet scientists using a pulse velocity technique on specimens subjected to hydrostatic pressures.

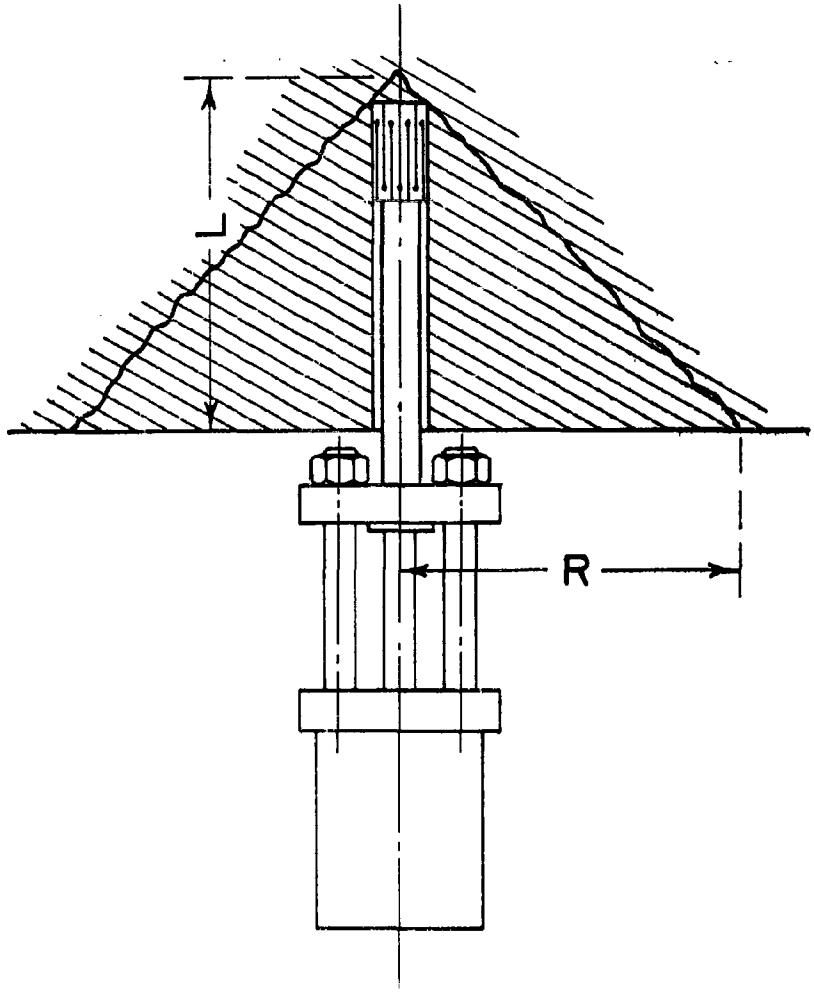
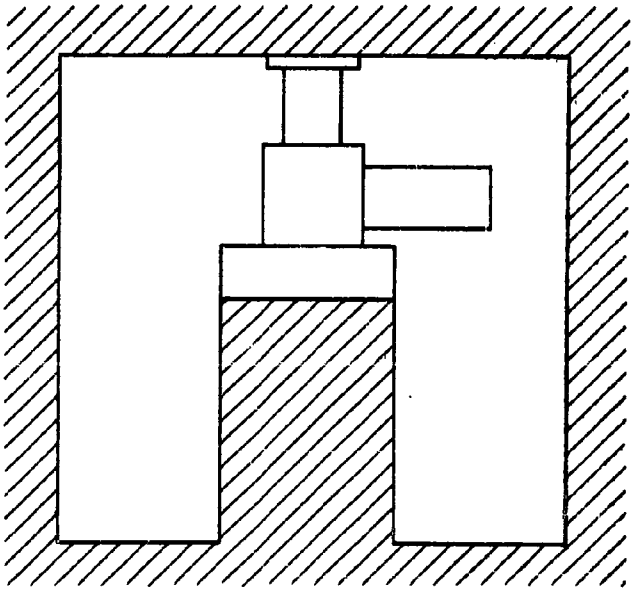


Figure I-A.14. In situ test configuration as used by Soviet investigators to determine tensile strength.



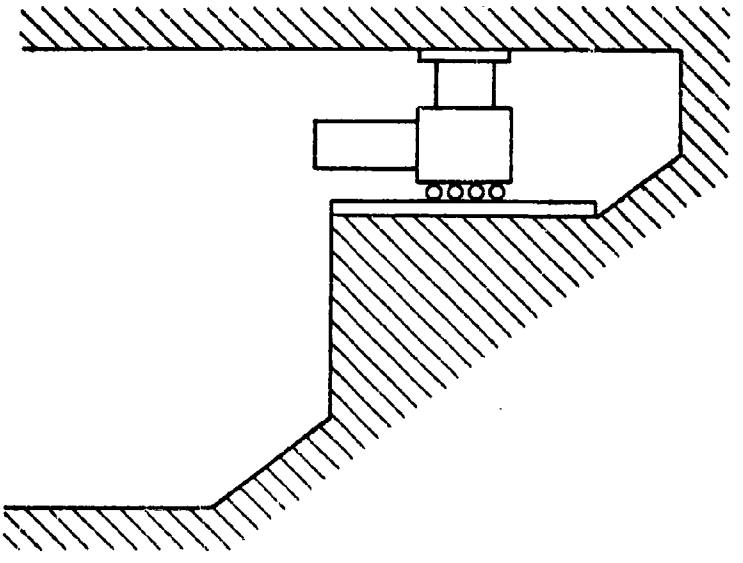


Figure I-A.15. Configuration of in situ tests for the determination of pillar compressive strengths and combined compression and shear strengths.

APPENDIX I-A

REFERENCES

1. Windes, S.L., Physical Properties of Mine Rock, Part II, Bureau of Mines Report of Inv. 4727, 1950.

2. Obert, L., Windes, S.L., and Duvall, W.I., Standardized Tests for Determining the Physical Properties of Mine Rock, Bureau of Mines Report of Inv. 3891, 1946.

3. Protodyakonov, M.M., Methods of Studying the Strength of Rocks Used in the U.S.S.R., Int. Symposium on Mining Research., Mo. School of Mines, Feb. 1961.

4. Nicholls, H.R., In Situ Determination of the Dynamic Elastic Constants of Rock, International Symposium on Mining Research, Mo. School of Mines, Feb. 1961.

5. Bureau of Reclamation, Foundation Bearing Tests at Davis Dam, Davis Dam Project, SP-18.

APPENDIX I-B

ANNOTATED TABLES OF PHYSICAL PROPERTIES OF ROCK

General

Appendix I-B has been included to provide the reader with a brief resume of a portion of the existing rock physical properties data for comparative purposes. The following tables represent neither the entire field of rock types nor even the entire span of physical properties for a single rock. Rather, the attempt has been made to summarize the results of physical property tests which have been performed which should have greatest significance in underground construction.

Data are presented in Table I-B.1 summarizing the result of triaxial compression tests. Table I-B.2 tabulates data from numerous mechanical and physical property tests. Tables I-B.3, I-B.4, and I-B.5 present data concerning heat capacity, heats of transformation and thermal conductivity of rocks, respectively.

Table I-B.1 - Triaxial Compression Test Data

Triaxial compression test data for a number of rocks are available within this table. These data are all from the work of the Bureau of Reclamation. The greater portion of these data were accumulated in one table by R. G. Wuerker[1], with current additions by the authors.

The results are presented as simple analytical expressions which enable comparisons of the strengths of various rocks. Lateral pressures applied in these tests are on the order of one-fifth to one-fourth the uniaxial crushing strength of the rocks.

Triaxial compression test data are presented in the form of two empirically determined expressions (1) shearing stress as a function of normal stress and (2) compressive strength as a function of confining pressure. A complete discussion of the test procedures and method of evaluation is given in the publications of the U.S. Bureau of Reclamation[2,3].

Equation of Mohr's Envelope

Since the development of Mohr's envelope and its defining equations have been described adequately elsewhere in this report, only those features peculiar to the data at hand will be discussed at this point.

The envelope, which is actually a curve tangent to each of the independently determined Mohr's circles, gives a mathematical relationship between the shearing stress and normal stress at a point within the rock at failure. In these tabulated results, Mohr's envelope is analyzed as a linear function under the assumption that a straight line adequately fits the data[2]. The method of least squares[4] was applied to

determine the equation of the straight line tangent to Mohr's circles. The envelope is characterized by two parameters (1) its intercept with the Y axis which has been denoted unit cohesive strength, c, and (2) its slope which is defined as the coefficient of friction, tan ø. Thus the equation of the envelope relating shear to normal stress is given by

$$\tau = C + \sigma \tan \phi \qquad \text{(I-B.1)}$$

The triaxial data presented would be of questionable value if confidence limits did not accompany it due to the extreme variability of the mechanical properties of most rocks. The minimum deviation of the confidence limits from the envelope, in terms of shearing strength, occurs at the average values of τ and σ and is designated as 2d. The minimum values of 2d are given in Table I-B.1 following the envelope equations.

Principle Stress Relationship - The principle stress relationship is presented in Table I-B.1 as a straight line, as it has elsewhere for concrete[5,6]. Curvilinear principal stress relationships have been used by other authors in the case of concrete specimens[7,4].

The principal stress relationship is utilized to aid in visualization of the increase of compressive strength with confinement.

References - The first column of the table gives the source from which the data was originally obtained. The identification symbols of the original publications have been used where possible.

Numbers with a prefix P- (for example: P5464) indicate that this is a sample tested by the U.S. Bureau of Reclamation, Denver, Colorado.

The prefix LR followed by a number refers to the bibliography at the end of the tables.

Table I-B.2 - Physical and Mechanical Properties of Rock

Data pertaining to nineteen rock properties are presented in Table I-B.2 for some 327 rock tests, from rocks commonly encountered in mining, milling and petroleum exploration. The tabulated data was derived almost entirely from the publications of the U.S. Bureau of Mines and the U.S. Bureau of Reclamation[8,2,9,10,11-14,15,16-28]. Credit for the basic compilation of rock physical property data is due R. G. Wuerker[1] and his monumental tables of rock physical properties. More recent data has been added by the authors together with modifications to Wuerker's original tables.

The majority of these rock properties were obtained under so-called "standard conditions". Unfortunately the standard conditions established by the Bureau of Mines and the Bureau of Reclamation are not always in complete agreement, as was explained in Appendix I-A. All of the data presented were obtained from laboratory measurements. A brief explanation of the data included in Table I-B.2 follows.

Source. Column 1 gives the reference from which data were obtained. The identification symbols of the original publications were used where possible. Decimal number identifications with numerals to the right of the decimal point which are less than 500.0 are the sample identification of the U.S. Bureau of Mines. They are the key to a reference system which includes area location, drill hole location, and position of the specimen along the drill hole.

Whole numerals greater than 500 refer to test numbers assigned by Allis-Chalmers Manufacturing Company to samples.

Test data with a prefix P- refer to samples tested by the U.S. Bureau of Reclamation, Denver, Colorado.

The prefix LR- followed by a number refers to a source report included in the bibliography accompanying these tables in which the particular test data is tabulated.

Type of Rock. Rock types are listed alphabetically using the nomenclature of the original reports. Some of the rocks which are recognized under more than one name are cross-referenced.

Static Elastic Constants. The secant modulus of elasticity in compression is presented here. The stress range over which the secant was drawn is indicated in column (4), the average secant modulus in column (5) and the range between highest and lowest values in the set of tests in column (6).

Poisson's ratio was determined directly as the ratio of lateral to longitudinal strain and is tabulated in column (7).

Dynamic Elastic Constants. The average modulus of elasticity as recorded in column (8) was obtained by measurement of either the resonant flexural or longitudinal vibration frequencies. It is beyond the scope of this appendix to differentiate between these methods. Chapter I contains a thorough discussion of the relative merits of different test methods, while Appendix I-A describes individual test techniques. The references at the end of this appendix should be consulted where knowledge of the specific details of a particular test is required.

Column (9) contains the tabulated values of the range of variation of test results for a rock sample.

The dynamic shearing modulus (dynamic modulus of rigidity) presented in column (10) was calculated from measured frequencies of resonant torsional vibration of rock cores.

Poisson's ratio as determined dynamically is not measured directly, rather it is calculated by means of the relationship

$$\nu = \frac{E}{2G} - 1 \qquad \text{(I-B.2)}$$

where ν is Poisson's ratio
E is the modulus of elasticity

G is the modulus or rigidity

It is apparent that errors in the dynamic elastic moduli result in disproportionately larger errors in Poisson's ratio.

Specific damping capacities of the various rock specimens are tabulated in column (12). Specific damping capacity, the ratio of energy dissipated per cycle of vibration to total energy input, is generally calculated from the width of the resonance curve at 0.707 of maximum amplitude. It may also be determined by means of the logarithmic decrement of free vibration of the sample.

The longitudinal velocity of sound waves, column (13), within the rock bars was calculated from the specimen dimensions and resonant frequency. In those instances where the longitudinal velocity is not given, it may be approximated by

$$v_l = \sqrt{\frac{E}{\rho}} \qquad \text{(I-B.3)}$$

where v_l = longitudinal bar velocity of sound
E = dynamic elastic modulus
ρ = density of the specimen

Selected Mechanical and Physical Properties. Grain sizes are listed in column (14). In most cases grain sizes were listed in the original report. In those areas where such data was not available, Wuerker[1] utilized the following conversion -

Very fine grained < 1 mm (shale)
Fine grained 1 mm (sandstone)
Medium grained 5 mm (diorite)
Coarse grained 10 mm (red granite)
Very coarse grained > 10 mm (salt)

Compressive strengths of rock samples are listed in column (15). The difference between maximum and minimum values for a particular set of samples is given in column (16).

Tensile strengths are tabulated in column (17). The sparcity of tensile test data may be attributed to the difficulty of obtaining valid results. Recent improvements in testing techniques have not as yet been reflected in any significant accumulation of comparative test data.

Modulus of rupture data are presented in column (18). These data are primarily the results of tests in which bending in rock beams is produced by a concentrated load at midspan.

The data on impact toughness listed in column (19) were obtained from a modification of ASTM standard D3-18 in terms of the height of drop required for a weight to break a unit volume of rock. Data from modulus of resilience determinations have been recorded in column (20) for comparative purposes. The modulus of resilience has been defined as the amount of energy stored by a unit volume of material in being stressed to the proportional limit. The area under the stress-strain curve of the rock sample is equal to the modulus of resilience.

The various concepts of hardness are grouped together in columns (21) Moh's hardness, (22) scleroscope hardness, and (23) abrasive hardness. Moh's hardness is presented based on an arbitrary scale where diamond is given the maximum hardness of 10, and talc the minimum hardness of 1. Moh's hardness data followed by the code letter s has been derived from scleroscope hardness data by means of the relationship

$$H_m = (SH + 26)/19 \qquad \text{(I-B.4)}$$

where H_m = Moh's hardness
SH = Shore scleroscope hardness

This relationship may be applied within the limits of Moh's hardness of 2-7. Scleroscope hardness measures the height of rebound of a diamond tip impinger in arbitrary units on a scale of 140 divisions, where pure high-carbon steel registers 100. Abrasive hardness is expressed in terms of the so-called hardness coefficients.

Column (24) summarizes work index data obtained for rock specimens. Work index is indicative of the energy required in comminution, and may be defined as the work input in kw-hr per shoot ton to reduce the rock from the theoretically infinite feed size to 80 percent passing 100 microns, the equivalent of 67 percent passing 200 mesh. The symbol IC following a piece of test data refers to an impact crushing test, RM-20 to a rod-mill grindability test at 20 mesh, BM-200 to a ball mill grindability test at 200 mesh.

Specific gravity of rock specimens and range of test data are presented in columns (25) and (26), respectively. Rock porosity and range of test data are tabulated in columns (27) and (28), respectively.

Table I-B.3 - Heat Capacities of Minerals and Rocks.

Table I-B.3a is a compilation of the heat capacities of minerals as tabulated by Goranson[29]. The minerals were classified alphabetically according to the elements appearing first in their chemical formulae, for example albite ($NaAlSi_3O_8$) is placed under sodium. Heat capacity is given in terms of absolute joules per gram.

In columns 3 to 8 inclusive are listed the instantaneous heat capacities for the respective temperatures (°C) given at the tops of the columns. The instantaneous heat capacity of the material at T°K can be expressed as

$$c_p = a + bT - cT^{-2} \qquad \text{(I-B.5)}$$

where c_p = heat capacity, j./gm.
T = temperature, T°K

The material parameters a, b, and c are listed in columns 9, 10, and 11, respectively. The equation has been assumed to have the proper characteristics for an interpolation formula above 0°C. The deviations of the formula from the data and the temperature range over which the formula was applied are given in column 12. Data references appear in the last column.

Table I-B.3b presents a tabulation by Goranson[29] of the heat capacities of some common rocks. He has stated that although some experimental data exist for mean heat capacities of rocks, these data are of uncertain value. Table I-B.3b consists of heat capacity data for rocks which were computed from the heat capacities of the constituent minerals. The material is presented in the same order as that in Table I-B.3a (Heat Capacity of Minerals).

Table I-B.4 - Heats of Transformation and Fusion of Minerals

The heats of transformation presented in Table I-B.4 are after Goranson[29]. In the first column the compounds are listed alphabetically according to the first elements of their chemical formulae. The second column contains the mineral designation. Columns 3, 4, and 5 contain phase change, temperature at which transformation occurs and heat absorbed per unit weight during the transformation, respectively. Column 6 contains the method used in determining the heats of transformation. Data were obtained from heat content data, differential heats of solution data, freezing point lowering and thermal analysis. It should be noted that the method of heat of transformation determination directly affects the accuracy of the data.

Table I-B.5 - Thermal Conductivities of Rocks.

The thermal conductivities of rocks presented in Table I-B.5 were tabulated by Birch[30]. The large number of values included for a particular rock was obtained from different investigators, and their lack of agreement may be primarily attributed to the variation in mineral content. The values serve as an indication of the possible range of conductivity rather than as definite figures for indiscriminate use. Conductivities of even relatively well-defined material show considerable variation as is exemplified by silica gel, which measurements by competent investigators have varied as much as 30 to 50 percent. The first column in the table lists the rock type and location. Column 2 gives the temperature at which conductivity measurements were made, and columns 4 and 5 the conductivity in cal sec^{-1} cm^{-1} deg^{-1} and watts $cm.^{-1}$ deg^{-1}, respectively. The last column refers to references following the table. In those cases where a temperature is not listed, the tests were usually performed at room temperature.

TABLE I-B.1

TRIAXIAL COMPRESSION TEST DATA

SOURCE	TYPE OF ROCK	EQUATION OF MOHRS ENVELOPE	PRINCIPAL STRESS RELATIONSHIP
LR76	Amphibolite, fine-to-medium-grained (Calif.)	$Y = 5,420 + 1.84X$	$S_1 = 42,500 + 15.4S_3$
P4802	Andesite, hypersthene, I (Palisades dam)	$Y = 4,060 + 1.0X$ $2D = \pm 270$, $Y = 10,520$	$S_1 = 20,070 + 6.1S_3$
P5348	Andesite, hypersthene, II (Palisades dam)	$Y = 3,970 + 1.0X$ $2D = \pm 210$, $Y = 10,040$	$S_1 = 18,900 + 5.7S_3$
P4861	Basalt, low strength (Medford, Oregon)	$Y = 4,500 + 1.2X$ $2D = \pm 450$, $Y = 13,130$	$S_1 = 24,570 + 7.4S_3$
--	Basalt, high strength	$Y = 6,340 + 1.1X$ $2D = \pm 630$; $Y = 16,440$	$S_1 = 32,440 + 6.6S_3$
LR79	Basalt, glassy, high strength (Idaho)	$Y = 1,570 + 1.38X$	$S_1 = 9,680 + 9.49S_3$
LR79	Basalt, glassy, medium strength (Idaho)	$Y = 610 + 1.54X$	$S_1 = 4,160 + 11.45S_3$
LR80	Basalt, vesicular, high strength (India)	$Y = 890 + 2.68X$ $(-320 < X < 640)$ $Y = 1,900 + 1.11X$ $(640 < X < 2800)$	$S_1 = 9,940 + 6.81S_3$
LR80	Basalt, vesicular, low strength (India)	$Y = 270 + 2.11X$ $(-120 < X < 280)$ $Y = 590 + 0.98X$ $(280 < X < 1380)$	$S_1 = 2,790 + 5.62S_3$
LR80	Breccia, tuff, high strength (India)	$Y = 360 + 1.46X$ $(-210 < X < 370)$ $Y = 570 + 0.89X$ $(370 < X < 760)$	$S_1 = 2,560 + 5.00S_3$
LR80	Breccia, tuff, low strength (India)	$Y = 160 + 1.74X$ $(-80 < X < 170)$ $Y = 350 + 0.61X$ $(170 < X < 600)$	$S_1 = 1,250 + 3.18S_3$

TABLE I-B.1 (Cont.)

TRIAXIAL COMPRESSION TEST DATA

SOURCE	TYPE OF ROCK	EQUATION OF MOHRS ENVELOPE	PRINCIPAL STRESS RELATIONSHIP
LR82	Claystone, silty (Texas)	Y = 36 + 1.02X	$S_1 = 176 + 6.04S_3$
LR82	Claystone, silty & calcareous (Texas)	Y = 52 + 0.84X	$S_1 = 220 + 4.59S_3$
LR81	Conglomerate, (India)	Y = 2,550 + 1.41X 2D = 1,080 @ 6,540	$S_1 = 15,960 + 9.8S_3$
P4823B	Diorite, quartz (Idaho)	Y = 2,010 + 1.4X 2D = ± 200, Y = 6,550	$S_1 = 12,180 + 9.2S_3$
P5123	Diorite, low strength	Y = 1,590 + 1.3X 2D = ± 270, Y = 4,840	$S_1 = 9,520 + 9.0S_3$
P5116	Diorite, high strength	Y = 2,540 + 1.4X 2D = ± 520, Y = 7,210	$S_1 = 16,090 + 10.0S_3$
P4885	Granite, (Grand Coulee, Wash.)	Y = 3,250 + 1.6X 2D = ± 420, Y = 11,600	$S_1 = 22,310 + 11.8S_3$
P5216	Granite, coarse-grained (Colo.)	Y = 2,000 + 1.5X 2D = ± 630, Y = 7,650	$S_1 = 13,350 + 11.1S_3$
P4883	Granite, slightly altered (Grand Coulee, Wash.)	Y = 1,420 + 1.6X 2D = ± 190, Y = 5,360	$S = 9,820 + 11.9S_3$
P5174	Granite, pegmatite, gp. A (Thompson, Colo.)	Y = 1,040 + 1.6X 2D = ± 310; Y = 5,540	$S_1 = 7,160 + 11.8S_3$
--	Granite, pegmatite, gp. B	Y = 1,110 + 1.3X 2D = ± 510; Y = 5,580	$S_1 = 6,640 + 8.9S_3$
LR83	Granite, (Wyo.), 1954	Y = 3,520 + 1.53X	$S_1 = 23,630 + 11.26S_3$
LR83	Granite, (Wyo.), 1959	Y = 4,380 + 1.50X	$S_1 = 28,880 + 10.92S_3$
LR83	Granite, altered (Wyo.)	Y = 2,020 + 1.48X	$S_1 = 12,920 + 10.15S_3$
LR84	Granite, coarse-grained, biotite (Ariz.)	Y = 3,730 + 1.40X	$S_1 = 23,370 + 9.79S_3$

TABLE I-B.1 (Cont.)

TRIAXIAL COMPRESSION TEST DATA

SOURCE	TYPE OF ROCK	EQUATION OF MOHRS ENVELOPE	PRINCIPAL STRESS RELATIONSHIP
P5620A	Graywacke, sub-, coarse-grained, high strength (Calif.)	Y = 1,700 + 1.1X 2D = ± 90, Y = 4,840	$S_1 = 8,720 + 6.5S_3$
P5624	Graywacke, sub-, coarse-grained, low strength (Calif.)	Y = 910 + 1.2X 2D = ± 300, Y = 3,670	$S_1 = 4,940 + 7.4S_3$
P5620C	Graywacke, sub-, fine-grained (Calif.)	Y = 1,640 + 1.0X 2D = ± 130, Y = 4,380	$S_1 = 7,660 + 5.5S_3$
P5620B	Graywacke, sub-, medium-grained (Calif.)	Y = 1,580 + 1.0X 2D = ± 80, Y = 4,420	$S_1 = 7,660 + 5.9S_3$
LR86	Hornfels, lime-silicate (Thailand)	Y = 3,640 + 1.14X	$S_1 = 19,360 + 7.09S_3$
P5463	Limestone, fine-grained (Marble Can., Ariz.)	Y = 2,150 + 1.6X 2D = ± 370, Y = 7,630	$S_1 = 15,320 + 12.6S_3$
P5468	Limestone, med.-grained (Marble Can., Ariz.)	Y = 5,300 + 0.7X 2D = ± 1,210, Y = 10,620	$S_1 = 20,470 + 3.7S_3$
P5465	Limestone, porous (Marble Can., Ariz.)	Y = 2,430 + 1.1X 2D = ± 1,280, Y = 8,080	$S_1 = 12,610 + 6.8S_3$
P5466	Limestone, chalcedonic (Marble Can., Ariz.)	Y = 2,610 + 1.5X 2D = ±510, Y = 6,440	$S_1 = 18,240 + 10.5S_3$
P5005	Limestone, reef breccia (Eniwetok)	Y = 180 + 0.6X 2D = ± 80, Y = 430	$S_1 = 610 + 2.9S_3$
P5469	Limestone, stylolitic (Marble Can., Ariz.)	Y = 1,920 + 1.7X 2D = ± 520, Y = 7,270	$S_1 = 13,860 + 13.0S_3$
P4880	Monzonite porphyry, low strength (Wash.)	Y = 2,390 + 1.7X 2D = ± 710, Y = 8,970	$S_1 = 17,460 + 13.4S_3$
P4880A	Monzonite porphyry, high strength (Wash.)	Y = 2,860 + 2.1X 2D = ± 420; Y = 11,300	$S_1 = 24,070 + 17.7S_3$
--	Monzonite porphyry, (Wash.)	Y = 3,170 + 1.5X 2D = ± 1,500; Y = 13,730	$S_1 = 20,420 + 10.3S_3$

TABLE I-B.1 (Cont.)

TRIAXIAL COMPRESSION TEST DATA

SOURCE	TYPE OF ROCK	EQUATION OF MOHRS ENVELOPE	PRINCIPAL STRESS RELATIONSHIP
P5618	Phyllite, graphitic (Sly Park Dam, Calif.)	$Y = 310 + 1.1X$ $2D = \pm 70$, $Y = 1,070$	$S_1 = 1,570 + 6.6S_3$
P5616	Phyllite, quartzose, slightly weathered	$Y = 250 + 1.2X$ $2D = \pm 60$; $Y = 860$	$S_1 = 1,370 + 7.5S_3$
P5615	Phyllite, sericite, moderately weathered	$Y = 280 + 1.1X$ $2D = \pm 60$; $Y = 840$	$S_1 = 1,470 + 6.9S_3$
P5270	Sandstone, low strength (Wyo.)	$Y = 1,690 + 1.1X$ $2D = \pm 220$, $Y = 6,420$	$S_1 = 8,780 + 6.8S_3$
P5254	Sandstone, high strength (Wyo.)	$Y = 2,450 + 1.1X$ $2D = \pm 390$, $Y = 7880$	$S_1 = 13,010 + 7.0S_3$
LR84	Sandstone, ferruginous, medium-grained (Ariz.)	$Y = 2,240 + 1.49X$	$S_1 = 14,730 + 10.77S_3$
LR84	Sandstone, quartzose, (Ariz.)	$Y = 2,230 + 1.71X$	$S_1 = 16,480 + 13.61S_3$
LR88	Sandstone, medium-grained, red (Ariz.)	$Y = 1,260 + 1.13X$	$S_1 = 6,650 + 7.0S_3$
P5089	Schist, biotite with pegmatite, low strength (Colo.)	$Y = 2,090 + 0.5X$ $2D = \pm 340$, $Y = 3,680$	$S_1 = 7,240 + 3.0S_3$
P5064	Schist, high strength	$Y = 1,260 + 1.9X$ $2D = \pm 260$; $Y = 3,900$	$S_1 = 9,990 + 15.7S_3$
P5082	Schist, biotite-chlorite, low strength (Colo.)	$Y = 370 + 1.7X$ $2D = \pm 280$; $Y = 2,570$	$S_1 = 2,770 + 13.7S_3$
P5083	Schist, high strength	$Y = 780 + 2.3X$ $2D = \pm 590$; $Y = 4,100$	$S_1 = 7,430 + 22.5S_3$
P5050	Schist, biotite-sillimanite, low strength (Colo.)	$Y = 480 + 1.3X$ $2D = \pm 200$, $Y = 1,700$	$S_1 = 2,840 + 8.6S_3$
P5095	Schist, high strength	$Y = 360 + 2.9X$ $2D = \pm 100$; $Y = 1,950$	$S_1 = 4,260 + 34.6S_3$

TABLE I-B.1 (Cont.)

TRIAXIAL COMPRESSION TEST DATA

SOURCE	TYPE OF ROCK	EQUATION OF MOHRS ENVELOPE	PRINCIPAL STRESS RELATIONSHIP
P5055	Schist, quartz injection, low strength (Colo.)	Y = 200 + 1.1X 2D = ± 160; Y = 1,190	$S_1 = 1{,}020 + 6.6S_3$
P5063	Schist, high strength	Y = 1,140 + 1.2X 2D = ± 510; Y = 4,440	$S_1 = 6{,}210 + 1.4S_3$
P5619	Schist, sericite, quartzose (Calif.)	Y = 350 + 1.4X 2D = ± 2.0; Y = 1,190	$S_1 = 2{,}210 + 9.9S_3$
LR83	Schist, (Fremont Canyon, Wyo.)	Y = 2,280 + 0.79X	$S_1 = 9{,}410 + 4.24S_3$
P5510	Shale, calcareous (Marble Canyon Dam, Ariz.)	Y = 1,160 + 2.1X 2D = ± 290; Y = 4,720	$S_1 = 10{,}230 + 9.7S_3$
P5500	Shale, quartzose (Marble Canyon Dam, Ariz.)	Y = 3,390 + 1.1X 2D = ± 480; Y = 9,760	$S_1 = 16{,}280 + 5.8S_3$
P5622	Siltstone, (Monticello Dam, Calif.)	Y = 720 + 1.2X 2D = ± 300; Y = 3,110	$S_1 = 3{,}970 + 7.7S_3$
LR82	Siltstone, (Texas)	Y = 75 + 1.36X	$S_1 = 460 + 9.34S_3$
LR81	Subgraywacke, calcareous (India), Group I	Y = 2,140 + 1.35X 2D = ± 330; Y = 5,540	$S_1 = 12{,}950 + 9.2S_3$
LR81	Subgraywacke, calcareous (India), Group II	Y = 1,540 + 1.49X 2D = ± 640; Y = 5,160	$S_1 = 10{,}140 + 10.8S_3$
P4860	Tuff, lithic (Ore.)	Y = 100 + 0.9X 2D = ± 10; Y = 220	$S_1 = 430 + 4.9S_3$

TABLE I-B.2

PHYSICAL AND MECHANICAL PROPERTIES OF ROCK

(1)	(2)	(3)	(4)	(5)	(6)	(7)	(8)	(9)	(10)	(11)	(12)	(13)
			STATIC ELASTIC CONSTANTS				DYNAMIC ELASTIC CONSTANTS					
			MODULUS OF ELASTICITY				MODULUS OF ELASTICITY					
NO.	SOURCE	TYPE OF ROCK	STRESS RANGE (10^3PSI)	(10^6PSI)	RANGE (10^6 PSI)	POISSON'S RATIO	(10^6PSI)	RANGE	SHEAR MODULUS (10^6PSI)	POISSON'S RATIO	SPECIFIC DAMPING CAPAC. $\cdot 10^{-6}$	LONGITUD. VELOCITY (FPS $\cdot 10^3$)
1	17.1a	Amphibolite, siliceous (India)										
2	17.1b	" , siliceous banded (India)										
3	17.2a	" , fine-grained (India)					15.1		6.64	0.14	2	19.0
4	17.2b	" , coarse-grained (India)										
5	17.3a	" , siliceous, coarse-grained (India)										
6	17.3b	" , siliceous, fine-grained (India)										
7	17.3c	" , siliceous, veined (India)										
8	17.4	" , biotite-rich (India)										
9	20.1	" , siliceous (India)										
10	20.1a	" , siliceous, parallel to foliation (India)					13.3		4.77	0.395	3	18.1
11	2159	" , (Fresno)										
12	P4802	Andesite, hypersthene, I (Palisades dam)	0-6.0	5.6	1.0	0.16						
13	P5348	" , hypersthene, II (Palisades dam)										
14	--	" , augite										
15	2560	" , (Stoughton, Mass.)										
16	2559	" , (Denver, Colo.)										
17	LR77	" , biotite, slight vesicular, mod. weathered (Oregon)		4.66		0.22						
18	"	" , pyroxene/chlorite & calcite, altered, vesicular (Oregon)		1.42		0.14						
19	"	" , agglomerate/chlorite & calcite, altered, (Oregon)		0.79		0.08						
20	"	" , biotite pyroxene/chlorite, mod. altered (Oregon)										
21	LR78	Argillite, metamorphosed (Alaska)	0-1.0	9.7	2.7	0.16	9.7	2.0	4.64	0.07		
22	5.5	Basalt and altered diabase, (New York)					13.9		5.51	0.28	1	18.7
23	6.1	Basalt, (Mich.)					8.03		3.80	0.150	4	15.2
24	10.2d	" , altered (Mich.)										
25	10.1	" , heavily altered, zeolitic (Mich.)					8.51		0.68	-0.04		5.80
26	P4861	" , low strength (Medford, Oregon)	0-6.0	8.7	5.2	0.22						
27	--	" , high strength										
28	10.2	" , amygdular, altered, epidatized (Mich.)					5.9		2.68	0.09	20	12.7
29	10.3	" , heavily altered, calcitized (Mich.)		8.7		0.15						
30	2455	" , (Durham, N. C.)										
31	2777	" , volcanic (Hawaii)										
32	LR79	" , glassy, high strength (Idaho)	0-1.5	5.14	4.71	0.11	4.68	5.80	2.15	0.11		
33	LR79	" , glassy, medium strength (Idaho)	0-1.5	5.14	4.71	0.11						
34	LR79	" , glassy, altered (Idaho)	0-1.5	.18	.12	0.01						
35	LR80	" , vesicular, high strength (India)	0-1.0	5.10	5.10	0.15	6.59	0.64	2.61	0.25		
36	LR80	" , vesicular, low strength (India)	0-1.0	5.10	5.10	0.15	1.62	0.27	1.51	0.29		
37	LR80	Breccia, tuff, high strength (India)	0-0.4	1.29	1.69	0.08	2.86	0.12	1.24	0.16		
38	LR80	" , tuff, low strength (India)	0-0.4	1.29	1.69	0.08	0.91	0.26	0.41	0.11		
39	LR81	Claystone, (calcareous siltstone) (India)	0-1.0	5.68		0.26	6.16		2.35	0.31		
40	LR82	" , silty (Texas)	0-0.05	0.033		0.22						
41	LR82	" , silty & calcareous (Texas)	0-0.01	0.033		0.22						
42	1.6	Conglomerate, (Ontario)					11.1		4.7	0.20	1	17.7
43	LR81	" , (India)	0-1.0	6.94		0.15	8.25		3.46	0.19		
44	--	Dacite										
45	--	Dam Breccia, (Hoover Dam)	0-5.0	6.28		0.222						
46	5.5	Diabase, altered & basalt (New York)					13.9		5.51	0.231	1	18.7
47	10.3a	" , coarse-grained (Mich.)					10.4		4.05	0.282	4	16.1
48	10.4a	" , fine-grained (Mich.)					11.1		4.35	0.275	4	16.7
49	10.5a	" , epidote-rich (Mich.)										
50	24.1	" , gabbro, olivine (Ariz.)										
51	11.1	" , amygdular, altered		10.0			10.2		4.10	0.25	5	16.5
52	--	"										
53	--	Diorite, (Minn.)										
54	2123	" , (Raleigh, N. C.)										
55	2625	" , (Mill City, Oregon)										
56	P4828	" , quartz (Idaho)	0-5.0	4.2	2.0	0.15	4.50	4.76	1.85	0.19		
57	5.4a	" , gneissic-gabbro (New York)					8.07		3.01	-0.005	4	15.9
58	12.1a	" , weath. augite & porphyry (Utah)					12.2		4.89	0.23	2	18.2
59	12.1b	" , weath. & alt. augite & porphyry (Utah)					11.6		4.61	0.26	2	17.8
60	12.2a	" , biotite, porphyry, alt. (Utah)					9.69		4.11	0.27	2	16.3
61	P5121	" , low strength	0-2.5	10.3	1.6	0.11						
62	P5116	" , high strength										
63	2.1	Dolomite, (Tenn.)					12.1		5.1	0.205	2	17.9
64	2386	" , (Sterling, Mass.)										
65	2715	" , (Glens Falls, N. Y.)										
66	--	" , (Harris Dam, Tenn.)		7.2	0.1	0.17						
67	[illegible]	Epidote, (Mich.)										
68	13.2	" , (Va.)					14.2		5.9		2	17.3
69	10.5a	" , epidote-rich (Mich.)										

TABLE I-B.2 (cont.)

PHYSICAL AND MECHANICAL PROPERTIES OF ROCK

(1)	(14)	(15)	(16)	(17)	(18)	(19)	(20)	(21)	(22)	(23)	(24)	(25)	(26)	(27)	(28)
NO.	GRAIN SIZE (mm.)	COMPRESSIVE STRENGTH AVERAGE (10^3psi)	COMPRESSIVE STRENGTH RANGE	TENSILE STRENGTH (10^3psi)	MODULUS OF RUPTURE (10^3psi)	IMPACT TOUGHNESS IN. LB./IN.^{3}	MODULUS OF RESILIENCE IN. LB./IN.^{3}	MOH'S HARDNESS	SCLEROSCOPE HARDNESS	ABRASIVE HARDNESS	WORK INDEX	SPECIFIC GRAVITY AVERAGE	SPECIFIC GRAVITY RANGE	POROSITY % AVERAGE	POROSITY % RANGE
1	0.5-1.5	74.9			6.0	18		6.37a	95	38		3.12			
2	0.5-1.5	62.4				18			94						
3	0.1-0.6	61.4			7.4	16	124.5		92	40					
4	0.1-2.0	61.7				16		5.79a	84						
5	0.25-2.0	59.0				10		5.89a	86						
6	0.1-0.6	51.5			4.2	15		6.26a	93	22		3.01			
7	0.1-0.6	30.4			5.3	6.0		4.74a		23		3.01			
8	0.25-2.0	32.8				8.9			64						
9	0.2-2.0	51.9				12.0		5.63a	81	22					
10	0.2-2.0	48.5					80.4					3.02			
11											16.11C	3.22			
13	0.3-1.6	19.15	3.51				27.0	6.17				2.57	0.04	4.8	3.2
14	0.3-1.6	18.71	3.36					6.17				2.57	0.02	3.6	1.5
15								6.25							
16											13.51C	3.07			
17											25.21C	1.75			
18		6.38										2.66		3.9	
19		4.39										2.11		17.6	
20		2.72										2.15		16.3	
21		19.32										2.78		20.8	
22		16.85	5.88									2.73	0.03	0.19	0.12
23	0.01-0.6	44.6			8.0	24	78.1	6.21a	92	37		2.94		0.2	
24	0.03-5.6	33.4			3.8	13	62.8	5.00a	69	15		2.85		0.9	
25	0.1-12.0	11.8						4.16a	53						
26	0.1-16.0	2.47			0.28	1.9	3.42			25		2.04		18	
27	1.0	24.45	9.87					6.09				2.72	0.11	4.3	2.79
28		31.85	16.78				57.3	6.09				2.74	0.09	1.63	2.76
29	0.1-20.0	17.3			2.1	3.5	25.4	3.95a	49	9.2		2.70		5	
30	0.1-16.0	49.6			4.1	8.8	141.0	5.84a	85	25.0		2.80		0.4	
31											11.41C	2.77			
32											20.11C	3.01			
33		8.37	5.72									2.62	0.16	3.64	1.83
34		5.46	2.27									7.56	0.17	6.06	5.76
35		3.30	1.11									2.06	--	24.81	--
35		9.85	8.73												
37		2.39	1.34												
38		1.55	1.16												
39		1.20	.54												
40		11.2													
41															
42															
43	10	24.					25.7	2.67							
44		17.43													
45								6.35							
46		17.1	11.3									2.48		15.0	
47	0.1-0.6	46.8			8.0	24	78.1	6.21a	92	37		2.94		0.3	
48	0.5-5.0	33.			4.5	5.6	52.4	5.37a	76	17		2.89		1.2	
49	0.5-1.0	44.2			5.3	5.3	87.5	5.58a	80	19		2.94		1.0	
50	1.0	34.9				5.6		4.74a	64	17					
51	1.0-2.0	30.7				2.4		4.86a	40						
52		22.6			4.3	3.7	25.0	4.68a	63	9.0					
53								6.04							
54				2.55											
55											28.51C	2.81			
56								6.31			14.01C	2.7			
57	0.3-6.0	12.67	1.4				22.4					1.0	2.5	2.7	0.1
58	0.3-1.0	27.			2.0	11.0	45.5	6.11a	90	11		3.03		1.0	
59		48.3				11.0	95.9	5.68a	82	30		2.74		0.25	
60		40.4				9.7	70.6	5.74a	83	23		2.72		0.56	
61		33.				6.9	56.2	5.42a	77	16		2.69		0.90	
62	0.2-10.0	9.31						6.26				2.66	0.27	0.49	1.07
63		19.14					11.6					2.87	0.09	0.22	0.10
64		46.7			3.8	5.9	88.6	5.26a	74	14		2.84		0.70	
65	3.5-4.0										8.01C	2.75			
66											18.61C	2.72			
67		28.15	19.9												
68	0.4-5.0	21.3			2.2	8.1		3.79a	46	9		2.93		5.3	
69	0.01-1.8	63.1			5.0	16.0	151.5	5.84a	85	40		3.26		1.5	
70															

TABLE I-B.2 (cont.)

PHYSICAL AND MECHANICAL PROPERTIES OF ROCK

(1)	(2)	(3)	(4)	(5)	(6)	(7)	(8)	(9)	(10)	(11)	(12)	(13)
			STATIC ELASTIC CONSTANTS				DYNAMIC ELASTIC CONSTANTS					
			MODULUS OF ELASTICITY				MODULUS OF ELASTICITY					
NO.	SOURCE	TYPE OF ROCK	STRESS RANGE (10^3PSI)	(10^6PSI)	RANGE (10^6 PSI)	POISSON'S RATIO	(10^6PSI)	RANGE	SHEAR MODULUS (10^6PSI)	POISSON'S RATIO	SPECIFIC DAMPING CAPAC. ψ	LONGITUD. VELOCITY (10^3FT/SEC)
71	934	Feldspar, (Erwin, Tenn.)										
72	1553	" , (Keene, N. H.)										
73	--	Fluorspar										
74	5.4	Gabro, altered (New York)					12.3		4.87		1	17.4
75	24.1	" , olivine, diabase (Ariz.)	(SEE DIABASE)									
76	24.1a	" , altered, diabase (Ariz.)	(SEE DIABASE)									
77	24.2	" , veined (Ariz.)										
78	4.4a	" , gneissic, diorite (N. Y.)	(SEE DIORITE)									
79	2626	" , (Lookout Pt. Dam, Oregon)										
80	P5116	Gneiss, diorite	(SEE DIORITE)									
81	27.1	" , augite, hornblende (N. J.)					15.0		5.90	0.27	2	18.2
82	27.2	" , biotite, hornblende (N. J.)					9.74		3.93	0.24	2	15.7
[illegible]							[illegible]		[illegible]		[illegible]	[illegible]
84	21.2	" , biotite, granitic (New York)										
85	21.3	" , hornblende, syenitic (New York)					6.51		3.26		3	13.2
86	21.4a	" , pyroxene, syenitic (New York)					9.35		4.19		3	15.5
87	21.4b	" , pyroxene-biotite, syenitic (New York)					8.28		3.70		3	14.9
88	4.1a	" , granitic & syenitic (New York)					3.48		2.07		4	9.33
89	4.2	" , quartz-magnetite (New York)					5.36		2.97		3	11.2
90	18.1	" , granitic, quartz-magnetite (New York)					9.67		4.17		4	15.3
91	18.1a	" , granitic, pegmatitic (New York)					6.47		3.07		4	13.5
92	P4885	Granite, (Grand Coulee, Wash.)	0-5.0	5.2	1.8	0.15						
93	P5216	" , coarse-grained (Colo.)	0-1.4	3.9	3.3	0.12						
94	P4883	" , slightly altered (Grand Coulee, Wash.)	0-2.5	1.6	1.4	0.20						
95	47.1	" , gneiss (Lithonia, Ga.)					5.65		1.71	-0.19	3	8.9
96	P5174	" , pegmatite, gp. A (Thompson, Colo.)	0-1.4	3.0	1.4	0.11						
97	--	" , pegmatite, gp. B										
98	1.3	" , (Vt.)					4.41		2.43		4	11.1
99	1.3a	" , parallel to bedding (Vt.)					3.97		2.20		5	
100	5.1	" , & quartz syenite (New York)					4.92		2.37		2	11.7
101	11.1	" , (Md.)					7.92		3.69		2	14.8
102	15.1	" , (Nev.)					7.44		3.26		2	14.5
103	22.1	" , (N. C.)					2.28		1.48		6	8.0
104	22.1a	" , parallel to foliation (N. C.)					4.39		1.80		3	11.2
105	1412	" , red (Spencer, S. D.)										
106	1630	" , (Pocelet, S. C.)										
107	LR83	" , (Wyo.)	0-4.0	10.6	2.1	0.17	10.44		4.40	0.19		
108	LR83	" , altered (Wyo.)										
109	LR84	" , coarse-grained, biotite (Ariz.)	0-8.0	9.03	3.03	0.14						
110	--	" , (Ark.)										
111	--	" , (Calif.)										
112	--	" , low strength (Brandford, Conn.)		8.33		0.25						
113	--	" , high strength (Conn.)										
114	--	" , (Delaware)										
115	--	" , low strength (Maine)										
116	--	" , high strength (Maine)										
117	--	" , low strength (Milford, Mass.)		5.13								
118	--	" , high strength (Mass.)										
119	--	" , low strength (Mo.)										
120	--	" , high strength (Mo.)										
121	--	" , low strength (N. H.)										
122	--	" , high strength (Troy, N. H.)		4.54		0.20						
123	--	" , low strength (Pa.)										
124	--	" , high strength (Pa.)										
125	--	" , low strength (R. I.)										
126	--	" , high strength (R. I.)										
127	--	" , low strength (Vt.)										
128	--	" , high strength (Vt.)										
129	--	" , (Va.)										
130	--	" , low strength (Wis.)										
131	--	" , high strength (Wis.)										
132	LR78	Graywacke, quartzose, fine-grained (Alaska)	0-1.0	9.8	1.1	0.15	10.8		4.6	0.20		
133	P5620A	" , sub-, coarse-grained, high strength (Calif.)	0-2.0	1.8	0.6	0.07	3.8	1.0	1.8	0.06		
134	P5624	" , sub-, coarse-grained, low strength (Calif.)	0-2.0	1.5	0.0	0.12	3.8	--	1.8	0.08		
135	P5620C	" , sub-, fine-grained (Calif.)	0-2.0	1.8	0.1	0.10	3.7	0.1	1.5	0.23		
136	P5620B	" , sub-, medium-grained (Calif.)	0-2.0	1.9	0.1	0.09	3.8	0.8	1.6	0.19		
137	51.2	Greenstone, amygdaloidal (Pen Mar, Pa.)					7.10		4.45	-0.21	5	13.1
138	1.7	" , (Va.)					13.25		6.10		2	19.2
139	7.9	" , schistose (Mich.)					11.5		4.62		1	17.1
140	7.10	" , & phyllite, low strength (Mich.)					10.8		4.71		2	16.4

TABLE I-B.2 (cont.)

PHYSICAL AND MECHANICAL PROPERTIES OF ROCK

(1)	(14)	(15)	(16)	(17)	(18)	(19)	(20)	(21)	(22)	(23)	(24)	(25)	(26)	(27)	(28)
NO.	GRAIN SIZE (mm.)	COMPRESSIVE STRENGTH AVERAGE (10^3PSI)	COMPRESSIVE STRENGTH RANGE	TENSILE STRENGTH (10^3PSI)	MODULUS OF RUPTURE (10^3PSI)	IMPACT TOUGHNESS IN./IN.^{2}	MODULUS OF RESILIENCE IN. Lb./IN.^{3}	MOH'S HARDNESS	SCLEROSCOPE HARDNESS	ABRASIVE HARDNESS	WORK INDEX	SPECIFIC GRAVITY AVERAGE	SPECIFIC GRAVITY RANGE	POROSITY % AVERAGE	POROSITY % RANGE
71								6.0			RM20-8,4-	2.6			
72											RM200-11.6	2.58			
73								4.0							
74	0.20-1.0	40.2			5.4	20	65.9	5.68s	82	22		2.93		0.3	
75															
76															
77	- 1.0	18.3				2.1		5.68s	63						
78															
79	1.0-5.0							6.14			16.81C	2.81			
80															
81	0.5-3.0	31.7				5.2	32.6	5.26s	74	16		3.34			
82	0.5-3.0	23.3				3.9	27.8	5.80	74	17		2.91			
83	0.5-18.0	32.4			2.5	3.9	65.8	5.86s	85	19		2.71		0.8	
85	1.0-8.0	33.3			1.9	4.3	85.2	5.68s	82	15		2.74		0.6	
86	0.5-9.0	29.7			2.5	3.7	47.3	5.12s	75	11		2.8		0.5	
87	0.5-9.0	22.8			3.1	2.7	31.4	5.92	71	12		2.76		0.6	
88	0.75-3.0	27.1			1.2	7.8	105.0	6.47s	97	12		2.97		0.8	
89	1.0-4.0	32.6			1.7	8.4	86.1	6.47s	97	11		3.18		0.7	
90	0.1-2.0	22.7			2.1	3.7	25.6	5.32s	75	10		3.04			
91	10.0	28.4				1.6	62.7	5.63s	81	27		2.65			
92	5.0	21.58	12.				48.7					2.63	0.07	1.59	1.38
93	2.0-12.0	10.46	7.63				14.1					2.63	0.03	1.0	0.6
94	5.0	9.4	4.89				34.0					2.61	0.04	2.36	1.91
95	0.1-2.1	28.0		0.41	2.0		69.2	5.63s	85			2.66			
96	5.0-10.0	6.19	0.26									2.62	0.09	1.0	1.4
97		8.44	0.1				12.7					2.62			
98	0.1-2.0	33.2		1.03	2.9	4.9	125.0	6.37s	95	19		2.66		0.7	
99	0.1-2.0	32.8			3.7	5.0	136.0	6.37s				2.66		0.9	
100	0.4-1.5	42.6			2.9	14.0	18.5	6.37s	95	24		2.69		0.8	
101	2.0-4.0	36.4			3.0	6.9	63.9	6.51s	98	26		2.65		0.8	
102	1.0-2.5	39.5			3.9	12.0	105.0	6.63s	100	12		2.63		0.9	
103	0.8-1.3	30.4			1.6	5.2	203.0	6.4-6.5	90	17		2.6		0.7	
104	0.8-1.3											2.6		0.7	
105											11.91C	2.6			
106											8.61C	2.56			
107		23.32	4.0	1.25								2.61	0.02	0.95	0.13
108		20.95	9.6	0.81								2.61	0.06	1.71	1.91
109												2.66	0.06	0.4	0.1
110		21.5	10.1												
111		21.1	2.0												
112		15.71										2.59			
113		31.66	4.6												
114		24.91	0.25												
115		14.09	2.17												
116		30.96	7.21												
117		18.99										2.58			
118		30.89													
119		18.23													
120		24.75	1.1												
121		17.95													
122		26.17										2.61			
123		6.10	1.1												
124		20.60	10.2												
125		21.97													
126		39.75													
127		17.18	5.9												
128		34.15	2.4												
129		27.07	3.1												
130		18.02	10.0												
131		45.89	3.7												
132		32.13	8.0									2.77	0.02	0.26	0.12
133	0.5-1.0	7.9	1.6	0.70			18.5					2.60	0.16	10.1	7.3
134	0.2-0.6	5.5	--				6.92					2.49	0.11	9.7	7.5
135	0.1-0.2	7.01	0.44				15.9					2.41	0.01	12.0	1.1
136	0.1-0.3	7.03	2.66				13.9					2.44	0.06	11.5	5.9
137	- 0.5	29.1		0.38	2.6	4.7	59.6	5.74s	64			2.94		0.5	
138	0.3-0.5	39.0			6.2	6.5	49.8	5.63s	81	20		3.02		0.7	
139	0.4-1.5	17.7			3.2	7.6	11.6	5.57s	58	7		2.93		0.6	
140	0.4-1.5	19.6			3.9	7.1	12.7	5.03s	53	6		2.81		0.4	

TABLE I-B.2 (cont.)

PHYSICAL AND MECHANICAL PROPERTIES OF ROCK

(1)	(2)	(3)	(4)	(5)	(6)	(7)	(8)	(9)	(10)	(11)	(12)	(13)
			STATIC ELASTIC CONSTANTS				DYNAMIC ELASTIC CONSTANTS					
			MODULUS OF ELASTICITY				MODULUS OF ELASTICITY					
NO.	SOURCE	TYPE OF ROCK	STRESS RANGE (10^6PSI)	(10^6PSI)	RANGE (10^6 PSI)	POISSON'S RATIO	(10^6PSI)	RANGE	SHEAR MODULUS (10^6PSI)	POISSON'S RATIO	SPECIFIC DAMPING CAPAC. $\cdot 10^{-6}$	LONGITUD. VELOCITY (10^3FT/SEC)
141	7.11	Greenstone, & phyllite, high strength (Mich.)					12.2		5.52		1	16.6
142	8.2a	" , (Minn.)										
143	8.2b	" , veined (Minn.)										
144	2177	Gypsum, hard (Nova Scotia)										
145	LR85	" , (Shoals, Indiana)		0.70		0.20						
146	12.2	Hematite Ore, parallel to bedding, low strength (Ala.)					10.1		3.90		7	14.1
147	14.6	" " , parallel to bedding, high strength (Ala.)										
148	8.3	" " , (Soudan, Minn.)					29.0		11.3		1	20.6
149	1515	" " , (Soudan, Minn.)										
150	7.3	" " , (Ishpeming, Mich.)					20.6		7.96		1	19.0
151	35.1	" " , (Ishpeming, Mich.)		15.1		0.20						
153	1377	" " , (Spaulding Mine, Ala.)										
154	2060	" " , (Rio Doce, Brazil)										
155	LR86	Hornfels, lime-silicate (Thailand)	0-5.0	8.9	10.0	0.20	6.1					
156	15.2	Hornstone (Nev.)					13.9		5.93		1	18.0
157	7.4	Jaspelite, (Ishpeming, Mich.)					15.0		7.0		1	18.2
158	8.4	" , (Soudan Mine, Minn.)					10.9		5.68		2	16.7
159	--	"										
160	P5463	Limestone, fine-grained (Marble Can., Ariz.)	0-3.5	9.9	1.6	0.25	10.3	3.3	4.0	0.28		
161	P5468	" , med.-grained (Marble Can., Ariz.)	0-2.5	5.2	1.4	0.23	7.6		2.9	0.31		
162	P5465	" , porous (Marbel Can., Ariz.)	0-1.4	3.0	3.0	0.22	4.1	3.6	1.7	0.20		
163	P5466	" , chalcedonic (Marble Can., Ariz.)	0-5.0	8.8	3.6	0.22	6.8	7.3	2.7	0.25		
164	P5000	" , reef breccia (Eniwetok)	0-2.0	5.4	2.7	0.16						
165	P5005	" , reef breccia (Eniwetok)	0-0.4	1.2	0.2	0.13						
166	P5001	" , reef head (Eniwetok)	0-1.5	3.5	1.8	0.23						
167	P5469	" , stylolitic (Marble Can., Ariz.)	0-3.5	6.5	2.1	0.19	8.2	4.2	3.2	0.27		
168	9.1	" , (Ohio)					7.97		3.04		4	15.4
169	28.6a	" , (Utah)					6.74		3.77	-0.12	8	13.7
170	28.6d	" , (Utah)					3.15		2.49	-0.37	10	9.4
171	31.2	" , (Utah)					9.43		3.93	0.20	2	15.9
172	34.1	" , (West Virginia)					9.56		3.96	0.21	3	16.4
173	34.2	" , (West Virginia)										
174	32.4	" , contact (Utah)										
175	12.5	" , coarse (Ala.)					7.64		1.91		4	14.2
176	1.2	" , fossiliferous (Ind.)					4.84		2.06		3	12.4
177	1.2a	" , fossiliferous, parallel to bedding (Ind.)					5.96		2.30		1	
178	23.2	" , (Tenn.)										
179	25.1	" , kerogenaceous, magnesian (marlstone) (Colo.)					1.8		1.0		22	7.8
180	25.2a	" , same parallel to bedding					3.1		0.98		18	10.2
181	14.4	" , limonitic (Ala.)					9.58		4.09		3	15.6
182	15.3	" , and marble (Nev.)					11.4		4.56		1	17.4
183	31.4	" , mineralized with shale (Utah)					9.53		4.07	0.17	2	15.6
184	--	"										
185	LR86	" , (Thailand)	0-5.0	6.7	0.5	0.23	9.1					
186	4.1	Magnetite ore, (New York)					4.56		2.70		4	8.24
187	5.1b	" " , (New York)					3.71		2.86		10	8.3
188	7.1	" " , siliceous (Mich.)					12.5		5.26		1	15.9
189	1.1	Marble, (Md.)					7.15		3.78		4	11.7
190	1.1a	" , parallel to bedding (Md.)					9.15		4.12		5	
191	15.1	" , & limestone (Nev.)	(SEE LIMESTONE)									
192	15.5	" , white (Nev.)					11.9		5.02		4	16.6
193	19.6	" , (New York)					7.84		3.35		1	14.5
194	19.7	Marble-pyroxene, mixed rock (New York)					10.0		4.89		2	19.1
195	25.1	Marlstone, calcareous shale (Colo.)										
196	25.2	" , kerogenaceous, magnesian, limestone (Colo.)	(SEE LIMESTONE)									
197	29.1	" , calcareous & dolomitic (Colo.)					3.61		1.41	0.11	15	10.5
198	29.2	" , kerogenaceous (Colo.)		0.6			2.7		1.11	0.18	11	9.4
199	29.3	" , calcareous and dolomitic (Colo.)					3.93		1.68	0.21	11	11.2
200	29.4	" , kerogenaceous (Colo)					1.89		0.84	0.02	16	7.6
201	29.5	" , calcareous & dolomitic (Colo.)					7.05		2.81	0.25	4	14.9
202	29.6	" , calcareous & dolomitic (Colo.)		4.0			5.0		1.94	0.28	7	12.8
203	29.7	" , kerogenaceous (Colo.)					4.47		1.47	0.58	11	17.1
204	29.8	" , kerogenaceous (Colo.)					3.83		1.00	0.96	12	11.2
205	29.9	" , kerogenaceous (Colo.)					2.87		1.00	0.45	11	9.90
206	41.4	" , (Colo.)					4.49			0.49		
26	LR87	Meta-andesite, (Shasta Dam)		11.6		0.27						
208	8.1a	Meta-rhyolite, (Minn.)					11.4		4.58		3	16.9
209	8.1b	" " , chloritic (Minn.)										
210	P4880	Monzonite porphyry, low strength (Wash.)	0-6.0	6.2	0.3	0.18	8.2	1.8	0.4	0.21		

TABLE I-B.2 (cont.)

PHYSICAL AND MECHANICAL PROPERTIES OF ROCK

(1)	(14)	(15)	(16)	(17)	(18)	(19)	(20)	(21)	(22)	(23)	(24)	(25)	(26)	(27)	(28)
NO.	GRAIN SIZE (mm.)	COMPRESSIVE STRENGTH AVERAGE (10^3psi)	COMPRESSIVE STRENGTH RANGE	TENSILE STRENGTH (10^3psi)	MODULUS OF RUPTURE (10^3psi)	IMPACT TOUGHNESS ft.-lb./in.^{2}	MODULUS OF ELASTICITY (10^6 lb./in.^{2})	NOE's HARDNESS	SCLEROSCOPE HARDNESS	ABRASTER HARDNESS	WORK INDEX	SPECIFIC GRAVITY AVERAGE	SPECIFIC GRAVITY RANGE	POROSITY % AVERAGE	POROSITY % RANGE
141	0.4-1.5	43.5			3.3	14.0	84.5	5.11a	71	14		3.30		0.5	
142	0.05-0.2	18.4				7.0		3.32a	37	6					
143	0.05-0.2	17.7				11.0		3.95a	49						
144											43IC	2.96			
145		3.2		0.35	1.20										
146	0.2-3.0	17.2			3.4	1.3	14.5	4.05a	51	5		3.78		3.0	
147	0.02-2.4	23.1				3.3		4.16a	53	53		3.67		2.3	
148	0.02-0.2	88.1			6.1	35.0	134.0	4.26a	74	24		5.07		1.3	
149											13.5IC	4.85			
150	0.1-0.3	47.8			3.2	18	35.4	4.68a	63	11		4.22		1.0	
151												4.68		1.1	
152															
153											4.5IC	3.3			
154											20IC	5.05			
155	0.26-2.0	14.7	10.3	0.67								2.82	0.32	0.73	1.17
156	0.01-0.1	77.3			3.8	7.1	215			52		3.19			
157	0.01-0.3	49.6			3.6	26	82	5.84a	85	20		3.39		0.6	
158	0.02-0.2	99.0				17	458	6.42a	96	48		2.90		0.3	
159								6.95							
160	0.003-0.2	11.66	3.41				69.4					2.71	0.07	3.4	4.7
161	0.02-0.2	18.48					34.1					2.66	0.05	4.7	1.4
162	0.03-2.0	19.32	22.3				69.5					2.44	0.05	13.9	10.0
163	0.02-80	15.58	8.7				14.5					2.60	0.17	5.4	6.9
164	> 5.0	4.96	4.08				2.28					2.30		13.	
165	> 5.0	0.86	0.19				0.336					1.82		32.71	
166		3.08	1.78				1.58					1.79		36.00	
167	0.01-0.85	11.53	12.69				11.7					2.73	0.06	3.9	5.6
168	0.1-0.5	28.5			2.9	8.6		4.42a	10			2.69		0.7	
169	0.05-0.45											2.67		1.3	
170												2.64		2.1	
171		28.0			2.2	2.5	41.7	4.11a	52	9.3		2.78		0.26	
172	0.001-0.1	23.0			1.9	2.5	27.7	4.38a	61	9.6		2.68		6.0	
173	0.001-0.5	29.5			2.5	2.0		4.42a	58	8.5					
174		23.6				3.1		4.11a	52	10.0					
175		24.0				6.6	37.8	4.84a	66	7.		2.83		0.9	
176	0.05-0.8	10.9		0.522	1.6	1.9	12.3	2.79a	27	3.		2.31		11.0	
177	0.05-0.8	9.7			1.9	2.1	7.96								
178	0.001-0.6	37.6			2.7	3.2		4.68a	63	11.					
179	0.005-0.15	16.6			0.4	3.7	7.68	4.32a	56	10.		2.25			
180	0.005-0.15				5.2			4.51a				2.18			
181	0.02-2.4	24.9			3.8	3.3	32.4	4.21a	61	8.		2.92		0.6	
182	0.1-1.0	22.1			2.6	3.9	21.8	4.74a	54	9.		2.79		0.4	
183		34.8			2.4	7.4	64.0		64	15.		2.92		0.62	
184								3.7							
185		4.22		0.47								2.60	0.00	0.43	0.13
186	3.0-10.0	20.5			1.5	5.1	46.1	5.5-6.5	72	3.		4.23		1.4	
187	< 1.5	17.6				4.4	41.8	4.53a	60	4.		3.55		0.6	
188	0.01-0.3	33.7			5.1	12.	45.6	4.16a	53	9.		3.64		0.8	
189	0.5-1.0	30.8		0.863	2.8	2.7	66.4	4.32a	56	8.		2.37		0.6	
190	0.5-1.0	31.2			3.3	2.4	53.								
191															
192	< 1.0				2.4		50.	3.7				3.2		2.3	
193	1.5-8.5	18.4			1.7	3.0	21.7	3.95a	49	7.		2.72		1.8	
194	1.0-10.0	18.8				3.0	11.8	3.79a	46	7.		3.02		0.4	
195	0.005-0.15	22.7				5.4		4.79a	65	5.					
196															
197	0.005-0.15	21.9			1.8	4.3	66.5	4.32a	56	6.7		2.31		4.9	
198	0.005-0.15	13.0			1.1	6.9	31.3	3.84a	47	8.7		2.24		0.51	
199	0.005-0.15	21.6			2.0	5.8	39.4	4.63a	62	10.		2.31		1.3	
200	0.005-0.15	12.5			0.87	6.2	41.3	3.84a	47	9.5		2.07		2.2	
201	0.005-0.15	28.2			4.8	2.8	56.5	4.47a	59	12.		2.45		5.2	
202	0.005-0.15	23.2			4.1	3.2	54.0	4.37a	57	6.9		2.26		12.0	
203	0.005-0.15	9.6			2.0	2.2	10.3	3.79a	46	12.0		2.19		1.7	
204	0.005-0.15	13.4			4.6	1.3	23.4	3.68a	44	11.		2.25		2.1	
205	0.005-0.15	10.4			3.6	4.8	18.8	3.84a	47	13.		2.08		0.24	
206	< 0.12			0.48	1.9							2.79			
207		12.05	30.00												
208	0.1-2.0	18.9			3.0	13.0	15.7	3.84a	47	7.		2.84		0.2	
209	0.1-2.0	34.1				12.0		4.95a	68	15.		2.69		0.4	
210	3.0-12.0	18.09	11.14									2.57	0.05	2.32	2.44

TABLE I-B.2 (cont.)

PHYSICAL AND MECHANICAL PROPERTIES OF ROCK

(1)	(2)	(3)	(4)	(5)	(6)	(7)	(8)	(9)	(10)	(11)	(12)	(13)
			STATIC ELASTIC CONSTANTS				DYNAMIC ELASTIC CONSTANTS					
			MODULUS OF ELASTICITY				MODULUS OF ELASTICITY					
NO.	SOURCE	TYPE OF ROCK	STRESS RANGE (10^3PSI)	(10^6PSI)	RANGE (10^6 PSI)	POISSON'S RATIO	(10^6PSI)	RANGE	SHEAR MODULUS (10^6PSI)	POISSON'S RATIO	SPECIFIC DAMPING CAPAC. $\cdot 10^{-2}$	LONGITUD. VELOCITY (10^3 ft/SEC)
211	P4880A	Monzonite porphyry, high strength (Wash.)	0-6.0	6.4	1.7	0.17						
212	--	" " , (Wash.)					8.94		3.30		4	16.0
213	19.1	Pegmatite, (New York)										
214	--	Peridodite										
215	P5618	Phyllite, graphitic (Sly Park Dam, Calif.)	0-0.5	1.4	1.0		3.9	--	1.0	--		
216	P5616	" , quartzose, slightly weathered	0-0.5	1.3	0.1	0.06	2.7	--	0.7	--		
217	P5615	" , sericite, moderately weathered	0-0.5	2.5	0.8							
218	7.8	" , green (Mich.)					11.1		4.75		2	15.9
219	7.10	" , & greenstone (Mich.)					10.8		4.71		2	16.4
220	7.11	" , & greenstone (Mich.)					12.2		5.52		1	16.6
221	24.4	Porphyry, altered (Ariz.)										
222	--	" , & diorite	(SEE DIORITE)									
223	--	" , [illegible] (Ontario)					10.3		4.4		2	16.8
224	[illegible]	[illegible]										
225	19.4a	" , fresh (New York)					18.0		7.29		3	19.8
226	19.4b	" , moderately altered (New York)					16.4		5.89		3	19.1
227	19.4c	" , heavily altered (New York)					3.19		1.10			9.7
228	19.4d	" , heavily altered (New York)					3.12		0.95		9	8.0
229	19.5	" , garnet (New York)					17.8		6.48		5	19.3
230	19.7	" , marble, mixed rock (New York)	(SEE MARBLE)									
231	52.3b	Quartzite, magnetite-bearing taconite (Minn.)					12.3		5.6	0.10	1	18.2
232	7.6	" , & slate (Mich.)										
233	7.7	" , & slate (Mich.)										
234	--	" , feldspathic										
235	16.1	Salt, rock-, (halite) (La.)										
236	LR12	" , rock-, (Retsof, New York)		0.17								
237	939	" , rock-, (Retsof, New York)										
238	LR12	" , potash, halite, sylvite mix. (N. M.)										
239	726A	" , rock-, (Alsace, France)										
240	P5270	Sandstone, low strength (Wyo.)	0-4.0	3.2	3.9	0.17						
241	P5254	" , high strength (Wyo.)										
242	1.4	" , (Ohio)					0.87		0.46		13	5.6
243	1.4a	" , parallel to bedding (Ohio)					0.97		0.46		12	
244	1.4b	" , parallel to bedding (Ohio)					1.28		0.64		12	
245	1.5	" , coarse-grained (Ohio)					1.03		0.58		7	5.9
246	1.5a	" , coarse-grained, parallel to bedding (Ohio)					1.54		0.70		6	
247	26.1a	" , (West Virginia)					3.12		1.99	-0.22	6	9.50
248	26.2a	" , (West Virginia)					5.56		2.19	-0.30	6	12.9
249	26.2b	" , (West Virginia)					3.10		1.99	-0.22	7	9.5
250	28.1	" , (Utah)		1.4			1.9		1.02	-0.01	10	8.0
251	28.2	" , (Utah)		1.2			2.1		1.02	+0.04	8	8.4
252	28.3	" , (Utah)		1.1			1.46		0.70	0.04	9	7.2
253	28.4	" , (Utah)					3.00		1.70	-0.11	10	9.7
254	28.5	" , (Utah)					2.77		1.48	-0.07	9	9.4
255	12.1	" , ferruginous (Ala.)					4.45		2.67		10	10.2
256	12.4	" , fossiliferous, red (Ala.)					6.46		3.26		1	12.2
257	14.2	" , ferruginous (Ala.)					7.02		3.51		7	13.3
258	14.3	" , siltstone & shale (Ala.)					5.79		3.29		10	12.5
259	LR19	" , ferruginous, weathered (Ill.)		0.725								
260	LR84	" , ferruginous, medium-grained (Ariz.)	0-4.0	4.16	0.19	0.06						
261	LR84	" , quartzose, medium-grained (Ariz.)	0-4.0	5.50	2.57	0.10						
262	LR84	" , quartzose, coarse-grained (Ariz.)	0-4.0	5.50	2.57	0.10						
263	LR88	" , medium-grained, red (Ariz.)	0-1.0	0.6		0.13	0.93	0.50				
264	P5089	Schist, biotite with pegmatite, low strength (Colo.)	0-2.5	6.0	1.2	0.08	8.6	1.6	3.7	0.16		
265	P5064	" , high strength					8.6	1.6	3.7	0.16		
266	P5082	" , biotite-chlorite, low strength (Colo.)										
267	P5083	" , high strength										
268	P5088	" , very high strength	0-2.0	9.9		0.20						
269	P5090	" , biotite-sillimanite, low strength (Colo.)	0-0.5	2.8	4.5							
270	P5091	" , high strength										
271	--	" , biotite sillimanite	0-1.0	3.3	1.7	0.06						
272	P5055	" , quartz injection, low strength (Colo.)										
273	P5063	" , high strength										
274	P5019	" , sericite, quartzose (Colo.)	0-0.5	1.3	0.3	0.12	2.6	1.1	0.9	0.44		
275	24.1	" , sericite (Ariz.)					8.7		3.8		5	15.5
276	LR83	" , (Fremont Canyon, Wyo.)	0-1.0	10.0	0.1	0.18	11.71		4.40	0.33		
277	P5510	Shale, calcareous (Marble Canyon Dam, Ariz.)	0-1.2	1.8	1.8	-0.04	3.6	3.1	2.3			
278	P5500	" , quartzose (Marble Canyon Dam, Ariz.)	0-1.2	2.0	3.7	0.07	3.2	3.8	1.7			
279	LR12	" , (Murdock, Ill.)		1.09		0.101						
280	31.1	" , (Utah)					8.44		3.86	0.09	5	14.9

TABLE I-B.2 (cont.)

PHYSICAL AND MECHANICAL PROPERTIES OF ROCK

(1)	(14)	(15)	(16)	(17)	(18)	(19)	(20)	(21)	(22)	(23)	(24)	(25)	(26)	(27)	(28)
NO.	GRAIN SIZE (mm.)	COMPRESSIVE STRENGTH AVERAGE (10^3PSI)	COMPRESSIVE STRENGTH RANGE	TENSILE STRENGTH (10^3PSI)	MODULUS OF RUPTURE (10^3PSI)	IMPACT TOUGHNESS IN./IN.^{2}	MODULUS OF RESILIENCE IN. LB./IN.^{3}	MOH'S HARDNESS	SCLEROSCOPE HARDNESS	ABRASIVE HARDNESS	WORK INDEX	SPECIFIC GRAVITY AVERAGE	SPECIFIC GRAVITY RANGE	POROSITY % AVERAGE	POROSITY % RANGE
211	3.0-12.0	25.02	9.41				52.0					2.58	0.04	2.40	2.03
212	3.0-12.0	24.73	22.31				49.1								
213	0.3-3.0	31.0			3.2	5.1	53.7	5.95a	87	26		2.59		1.1	
214								6.28							
215	0.08-0.23	0.97					0.336					2.35	0.17	15.3	5.7
216	0.01-3.0	1.36	0.86				0.775					2.18	0.22	22.4	8.5
217	1.0	1.42	0.52				0.388					2.34	0.05	17.4	8.9
218	0.01-0.7	18.3			3.3	7.7	15.1	3.47a	40	8		3.24		1.1	
219	0.01-0.7	16.6			3.9	7.3	12.7	3.00a	31	6		3.10		0.4	
220	0.01-0.7	45.5			3.3	14.0	84.5	5.11a	71	14		3.30		0.5	
221	0.05-2.5	32.2				6.2		4.84a	66						
222															
223	0.1-1.2	69.					122.9					2.70			
225	1.5-13	26.4			3.3	3.3	19.3	4.53a	60	14		3.48		0.6	
226	1.5-13	17.7			2.7	2.1	9.6	3.68a	44	10		3.31		0.5	
227	1.5-13	8.5			2.0	2.3	11.3	2.86a	26	6		2.53		3.3	
228	1.5-13	3.6				1.9	3.1	1.89a	10	2		2.43		14.0	
229	0.3-10.0	12.3			2.2	2.1	6.2	3.16a	34	4		3.40		1.0	
230															
231	0.3	91.2			3.4	4.6	338.5	5.75a	83	19		2.75		0.3	
232	0.01-0.7	30.6a			1.2	19.0		4.26a	55	9					
233		44.2			4.5	12.0		6.63	81	29					
234	0.01-0.7							6.10							
235	25-40	5.0										2.50			
236	10-20	1.08													
237											RH100-7.1	2.40			
238	10-30	4.18		0.402											
239											RH65-10.3	2.20			
240	0.11-0.8	8.81	7.47				28.0					2.28	0.78	16.43	6.20
241		12.2	5.21									2.17	0.27	11.21	6.87
242	0.2-0.3	10.4		0.12	0.5	1.8	61.6	3.00a	31	2		2.06		16.	
243	0.2-0.3	8.0			0.8	3.1	32.9								
244	0.2-0.3	7.7			0.8	3.1	21.2								
245	0.2-0.5	6.1		0.167	0.4	1.5	18.0	2.47a	20	1		2.17		16.	
246	0.2-0.5	5.2			0.7	1.4	8.6								
247	0.01	16.2			1.4	1.4	42.4	4.16a	53	5.5		2.6		4.3	
248	0.01	19.4			3.4	2.6	33.9	4.68a	63	8.1		2.5		3.1	
249	0.01	21.9			1.6	5.5	77.5			7.3		2.5		4.8	
250	0.05-0.45	15.5			0.42		61.4					2.20		10.0	
251	0.05-0.45	11.5			0.62		31.4					2.17		12.0	
252	0.05-0.45	14.2			0.58		69.2					2.14		13.0	
253	0.05-0.45	32.4			1.4		175.					2.15		5.0	
254	0.05-0.45	27.7			1.1		139.					2.13		7.0	
255	0.1-0.1	24.2			1.8	4.2	65.6	4.42a	58	5		3.14		3.1	
256	0.1-0.3	22.6			1.8	3.4	38.7	4.00a	50	7		3.26		2.9	
257	0.1-0.8	34.1			1.6	6.6	82.6	4.79a	65	9		2.93		1.4	
258	0.35-1.4	26.8			2.2	5.6	62.2	4.13	63	13		2.76		1.7	
259	0.4	2.27		0.216											
260	0.21-0.46	11.00	0.06									2.39	0.27	7.1	3.9
261	0.2-0.3	14.32	8.66	0.78								2.49	0.20	5.6	6.9
262	0.5-1.0	14.11	8.66	0.78								2.18	0.19	9.8	6.6
263												2.06	0.09	22.	
264		7.75										2.68	0.02	1.44	0.93
265		12.01					12.3	5.5				2.71	0.13	0.59	0.44
266	0.3-1.2	5.29										2.71	0.16	0.86	1.26
267		11.79										2.69	0.09	0.81	1.13
268		12.0					15.1					2.75		0.52	
269	0.1-1.0	1.16										2.72	0.10	1.13	1.20
270		4.93					5.81					2.71	0.11	0.85	0.76
271	2.0-5.0														
272		1.75						5.20				2.70	0.04	4.13	4.21
273		4.53	2.80				4.02					2.71	0.05	1.42	1.14
274	0.05-0.46	2.18					1.99					2.67	0.22	11.4	5.6
275	6.0	23.5				2.5	53.7	5.68a	82			2.7			
276		8.87	5.17	2.52								2.67		1.8	
277	2.00	5.22	0.75				6.42					2.59		6.6	
278	0.06	17.77	10.19				7.16								
279	0.01	4.47		1.598											
280	0.1	41.9			2.5	9.0	58.	4.42a	58	7.0		2.81		0.9	

TABLE I-B.2 (cont.)

PHYSICAL AND MECHANICAL PROPERTIES OF ROCK

(1)	(2)	(3)	(4)	(5)	(6)	(7)	(8)	(9)	(10)	(11)	(12)	(13)
			STATIC ELASTIC CONSTANTS				DYNAMIC ELASTIC CONSTANTS					
			MODULUS OF ELASTICITY				MODULUS OF ELASTICITY					
NO.	SOURCE	TYPE OF ROCK	STRESS RANGE (10^3PSI)	(10^6PSI)	RANGE (10^6 PSI)	POISSON'S RATIO	(10^6PSI)	RANGE	SHEAR MODULUS (10^6PSI)	POISSON'S RATIO	SPECIFIC DENSITY GM/CM³	LONGITUD. VELOCITY (10^3FT/SEC)
281	31.1a	Shale, silicified (Utah)					9.87		4.42	0.12	3	16.2
282	26.3a	" , silicified (W. Va.)										
283	26.4a	" , silicified (W. Va.)					6.73		1.82	0.92	9	13.6
284	26.4b	" , silicified (W. Va.)										
285	25.1	" , calcareous marlstone (Colo.)										
286	31.4	" , mineralized, limestone (Utah)					9.53		4.07	0.17	7	15.6
287	5.2	Shonkinite, syenite, gneissic dark (New York)					8.01		3.50		1	14.4
288	5.3a	" , syenite, gneissic dark (New York)					5.14		2.86		3	10.6
289	19.3	" , & syenite (New York)					9.93		4.13		3	16.4
290	12.6	Siltstone, & shale (Ala.)					7.72		3.67		5	14.4
291	14.1	" , & shale (Ala.)					9.33		4.15		5	15.8
292	14.3	" , sandstone & shale (Ala.)					5.79		3.29		10	12.5
293	P5622	" , (Monticello Dam, Calif.)	0-2.0	1.9	1.4	0.12	5.9	1.5	1.8	0.061		
295	LR82	" , (Texas)	0-0.1	0.10	0.05	0.27						
296	18.2	Skarn, garnet-pyroxene (New York)					12.5		5.05		4	16.8
297	21.5	" , calcareous-pyroxene (New York)										
298	1.6	Slate, (Pa.)										
299	1.6a	" , parallel to bedding (Pa.)					13.66		3.99		2	19.2
300	1.6b	" , parallel to bedding (Pa.)					12.11		3.71		4	
301	7.5	" , parallel to bedding (Mich.)					11.0		4.86		1	16.8
302	7.6	" , & quartzite	(SEE QUARTZITE)									
303	--	"										
304	LR81	Subgraywacke, calcareous (India)	0-1.0	2.82	0.65	0.07	4.92	2.03	1.96	0.25		
305	LR81	" , slightly calcareous (India)	0-1.0	1.64		0.05	3.26		1.66	+0.02		
306	LR81	" , calcareous (India)	0-1.0	5.18		0.17	6.12		2.59	0.18		
307	3.2	Syenite, basic (Ontario)					10.7		4.1		2	16.8
308	3.3	" , porphyry (Ontario)					10.3		4.4		2	15.8
309	3.5	" , basic (Ontario)					10.2		4.1		1	16.3
310	4.1a	" , gneiss, granitic (New York)					3.48		2.07		4	9.33
311	4.1b	" , gneiss granitic (New York)					6.12		3.00		2	12.9
312	4.1c	" , gneiss, granitic (New York)					7.68		3.60		1	14.5
313	5.1	" , granite & quartz (New York)					4.92		2.17		2	11.7
314	5.2	" , gneissic dark to shonkinite (New York)					8.01		3.50		1	14.4
315	19.2	" , granite & quartz (New York)					9.70		4.08		3	16.6
316	19.3	" , & shonkinite (New York)					9.93		4.13		3	16.4
317	31.3	Tactite, epidote- (Utah)					8.90		4.02	0.11	4	15.1
318	--	Trachyte										
319	6.2	Trap, amygdaloidal (Mich.)					9.37		3.94		4	15.7
320	3.1	Tuff, (Ontario)					12.6		4.7		1	18.3
321	LR77	" , ardosite, highly altered (Ore.)		1.22		0.09						
322	P4860	" , lithic (Ore.)	0-0.3	0.20	0.15	0.11						
323	LR26	Concrete, 28 days saturated					5.2					
324	LR27	" , (90 days), Cement: sandigravel ratio 1:2.29:3.38, w/c ratio 0.50 by weight										
325	LR28	Cement Mortar										
326	LR29	Concrete, 7 days moist, 21 days dry, Cement: sandigravel = 1:2,3:3,4, w/c ratio 0.5 by weight									5.4	
327	LR30	"										14.2

TABLE I-B.2 (cont.)

PHYSICAL AND MECHANICAL PROPERTIES OF ROCK

(1)	(14)	(15)	(16)	(17)	(18)	(19)	(20)	(21)	(22)	(23)	(24)	(25)	(26)	(27)	(28)
NO.	GRAIN SIZE (mm.)	COMPRESSIVE STRENGTH		TENSILE STRENGTH (10^3PSI)	MODULUS OF RUPTURE (10^3PSI)	IMPACT TOUGHNESS IN.-LB./IN.^{2}	MODULUS OF RESILIENCE IN. LB./IN.^{3}	MOH'S HARDNESS	SCLEROSCOPE HARDNESS	ABRASIVE HARDNESS	WORK INDEX	SPECIFIC GRAVITY		POROSITY %	
		AVERAGE (10^3PSI)	RANGE									AVERAGE	RANGE	AVERAGE	RANGE
281	0.01-2.0	33.5			2.1	7.4	56.18	5.11a	71	14.0		2.80		0.57	
282		15.0			0.15	2.9		3.16a				2.6		6.1	
283		11.6			4.2	0.9	10			4.3		2.4			
284		18.5			0.83	3.2				2.5					
285		22.7				5.4		4.79a	65	5.0					
286		34.8			2.4	7.4	64	4.74a	64	15.0		2.92		0.62	
287	> 1.0	37.3			2.7	14.0	86.8	6.11a	90	21		2.81		0.7	
288	1.0-5.0	26.9			1.6	7.2	70.6	5.47a	78	12		3.35		1.1	
289	0.1-4.0	34.5			3.2	6.3	59.9	5.68a	82	22		2.70		0.6	
290	> 0.1	37.2			2.7	8.7	89.4	3.5-4.0	71	11.0		2.76		0.8	
291	> 0.1	45.8			5.0	8.5	113	5.21a	73	18.0		2.77		1.0	
292		25.8			2.2	5.6	62.2	4.68a	63	13.0		2.76		1.7	
294		11.2													
295		0.69	0.10												
296	0.5-4.0	18.8				2.4	14.2	4.58a	61	6		3.28			
297	0.5-4.0	28.4			2.9	4.1		5.53a	79	15					
298	> 0.03	30.4				3.7		4.32a	56	3		2.74		1.0	
299	> 0.03	22.5					18.6								
300	> 0.03	30.5					38.4								
301	0.05-0.2	26.2			3.7	10	31.2	3.79a	46	7		2.93		0.6	
302															
303								6.30							
304		13.18													
305		9.28													
306		12.93													
307		44.					90.7					2.82			
308	0.1-1.2	63.					192.0					2.70			
309	0.1-1.5	37.					67.1								
310	0.75-3.0	27.1			1.2	7.8	106.0	6.47a	97	12		2.97		0.8	
311	0.75-3.0	31.2			2.3	8.9	79.6	6.58a	99	17		2.75		0.7	
312	0.75-3.0	34.3			2.8	12.0	76.8	6.58a	99	22		2.72		0.9	
313	0.4-1.5	42.6			2.9	14.0	18.5	6.37a	95	24		2.65		0.8	
314	> 1.0	37.3			2.7	14.0	86.8	6.11a	90	21		2.81		0.7	
315	0.5-4.5	39.9			3.0	7.2	82.2	6.09a	88	25		2.62		0.4	
316	0.5-4.0	34.5			3.2	6.3	59.9	5.68a	82	22		2.70		0.6	
317	0.05-6.0	38.6			2.7	4.8	87.2	4.79a	65	12		2.87		1.5	
318								6.33							
319	0.05-3.0	26.6			2.5	9.2	37.7		63	11		2.81		1.5	
320	0.12-0.25	40.0					63.5					2.78			
321		3.1										2.35		10.3	
322	< 6.0	0.53	0.19				0.780					1.45	0.17	42.48	12.17
323		1.0		0.35	0.5		0.865								
324															
325															
326		5.46		1.0											
327															

TABLE I-B.3a*

HEAT CAPACITY OF MINERALS

Compound	Mineral	C_p (joules per gram) for temperatures in °C.						C_p = a + b - cT^{-2} Constants in j./gm. (T°K.)			Error %; temp. range °C.	Reference
		-200°	0°	200°	400°	800°	1200°	a	10^3b	10^{-5}c		
2Ab-3An	labradorite		(.82 at 60°)									
3Ab-2An	andesine		.70	.97	1.07	1.18		.991	.20	.255	±1;0-900	18
	glass		.70	.99	1.09	1.21		1.016	.206	.278	1;0-900	18
4Ab-1An*	oligoclase		(.85 at 60°)									78*
Ag	native silver	.146	.233	.244	.256	.279		.217	.058	0	1;0-961	71
Ag	liquid						.32	.318	0	0	3;961-1300	71
AgCl	cerargyrite	.251	.354	.408	.462			.280	.271	0	2;0-453	72
	liquid							.410	0	0	5;453-533	72
Ag_3AsS_3	proustite		(.34 at 50°)									L.B.
Ag_2S	acanthite		.32					.317	0	0	5;0-175	73
	argentite			.37				.368	0	0	5;175-325	73
Ag_3SbS_3	pyrargyrite		(.32 at 50°)									L.B.
Al_2O_3	corundum	0.069	0.72	1.00	1.10	1.19	1.26	1.067	0.140	0.289	4;0-1700	1
	liquid							1.53			2230	
Al_2SiO_5	andalusite	.152	.77	1.03	1.11	1.165	1.20	1.136	0.050	0.281	3;0-1300	2
	cyanite	.077	.70	1.00	1.10	1.20	1.27	1.080	0.136	0.313	2;0-1400	3
	sillimanite	.133	.743	1.00	1.08	1.16	1.22	1.054	0.123	0.257	3;0-1200	4

TABLE I-B.3a from Reference 32, Appendix I-B.

TABLE I-B.3a (Continued)

Compound	Mineral	C_p (joules per gram) for temperatures in °C.						Constants in $C_p = a + bT - cT^{-2}$ j./gm. T°K.)			Error %; temp. range °C	Reference
		-200°	0°	200°	400°	800°	1200°	a	10^3b	10^{-5}c		
$Al_6Si_2O_{13}$	mullite		.77	.97	1.03	1.09	1.13	1.03	0.075	0.210	3;0-1100	5
$Al_8Si_3O_{18}$	kaolinite		.93	1.02				0.806	0.463	0.0	4;0-300	6
*$Al_2Si_2O_7 \cdot 2H_2O$	kaolin		.99	1.17	1.35			0.641	0.904	0.0	3;0-500	7
$Al_2Si_2O_7$	metakaolin		$.71_5$	1.00	1.10	1.20	1.27	1.062	0.151	0.289	2;0-1300	7
$2(AlF)O \cdot SiO_2$	topaz		(.83 at 50°)									8
Au	native gold		.127	.133	.140	.152	.	.119	.0306	).	2;0-1063	35
	liquid						.15				5;1063-1300	35
$BaCo_3$	α-witherite	.197	.44	.50	.55	.66		.366	.278	)	5;0-810	10
	β-witherite					.64		.64	0	)	10;810-980	10
$BaSO_4$	barite	.197	.45	.50	.55	.65		.383	.253	)	5;0-1050	10, 11
$BeAl_2O_4$	chrysoberyl		(.84 at 50°)									12
$Be_3Al_2Si_6O_{18}$	beryl		(.84 at 50°)									13
C	diamond		.435	1.06	1.37	1.86		.754	1.067	.4544	4;0-1040	25
	β-graphite		.635	1.18	1.45_5	1.88		.932	.913	$.407_7$	3;0-1040	26
$Ca_2Al_2H_2(SiO_4)_3$	prehnite		(.84 at 50°)									Joly
$Ca_2Al_2SiO_7$	gehlenite		.75	.97	1.03	1.09	1.12	1.042	.06	.2284	2;0-1300	19
$CaAl_2Si_2O_8$	anorthite		.70	.95	1.05	1.17	1.27	.950	.226	.2313	1;0-1400	18
	glass		.68	.96	1.06			1.014	.158	.282	1;0-700	18
$CaCO_3$	aragonite	.26	.78	1.00	1.13			.823	.497	.1286	3;0-750	16
	calcite	.28	$.79_3$	1.00	1.13			.823	.497	.1286		

TABLE I-B.3a (Continued)

Compound	Mineral	C_p (joules per gram) for temperatures in °C.						C_p = a + bT - cT^{-2} j./gm. (°K.) Constants in			Error %; temp. range °C.	Reference
		-200°	0°	200°	400°	800°	1200°	a	10^3b	10^{-5}c		
CaF_2	fluorite	.22	.85	.89	.93	1.01	1.10	.798	.204	0	5;0-1200	17
$CaMg(CO)_3$	dolomite		(.93 at 60°)									15
$CaMgSi_2O_6$	diopside		.69	.98	1.06	1.15	1.20	1.053	.111	.290	1;0-1300	20
	glass		.71	.98	1.07			.999	.188	.253	1;0-700	20
$CaSiO_3$	(α) pseudo-wollastonite	.174	.73	.92	.99	1.07	1.14	.926	$.150_2$	$.177_4$	2;0-1400	21
	(β) wollastonite	.172	.67	.92	1.00	1.06	1.10	1.007	.074	.269	2;0-1300	21
	glass		.69	.92	1.03			$.834_5$	.348	$.175_5$	2;0-700	21
$CaSO_4$	anhydrite		.52	.58	.60	.64		.569	.675	$.048_2$	5;0-1100	23
$CaSO_4 \cdot 2H_2O$	gypsum	.322	1.03									22
$CaWO_4$	scheelite		(.40 at 50°)									24
CdS	greenockite		.445	.50	.55	.653		.374	.2605	0	est.;0-1000	14
Cu	native copper	.161	.384	.40	.42	.46		.358	.096	0	2;0-1084	27
	liquid							.493	0	0	3;1084-1300	27
Cu_2O	cuprite		.47	.505	.54	.614		.419	.181	0	5;0-950	28
CuO	tenorite		.52	.63	.68			.572	.188	.079	2;0-537	29
$2CuO \cdot CO_2 \cdot H_2O$	malachite		(.74 at 57°)									
$CuFeS_2$	chalcopyrite		(.54 at 50°)									30
$CuPbSbS_3$	bournonite		(.31 at 50°)									
Cu_2Se	α berzelianite		.42					.42	0	0	5;0-100	31
	β berzelianite			.41				.41	0	0	5;100-200	31

TABLE I-B.3a (Continued)

Compound	Mineral	C_p (joules per gram) for temperatures in °C.						Constants : C_p = a + bT - cT^{-2} j./gm. (T°K.)			Error %; temp. range °C.	Reference
		-200°	0°	200°	400°	800°	1200°	a	10^3b	10^{-5}c		
Cu_2S	α chalcocite	.255	.470					.247	.82	0	3;0-103	32
	β chalcocite			.55	.55	.55		.55	0	0	10;103-900	32
CuS	covellite	.228	.49	.52	.54	.59		.464	.115	0	?;0-1000	33
$CuSiO_3H_2O$	dioptase		(.77 at 34°)									34
Fe	α iron		.44	.52	.60			.33	.40	0	3;0-755	36
	β iron					(.73)		.46	.25	0	3;755-903	36
	γ iron						.63	0.63	0	0	5;903-1401	36
	δ iron							.75	0	0	5;1401-1530	36
	liquid							.61	0	0	5;1530-1600	36
FeAsS	arsenopyrite		(.43 at 55°)									37
$FeCO_3$	siderite	.234	.68$_3$									38
Fe_2O_3	hematite		.61	.79	.90	1.08		.640	.420	111	3;0-800	39
Fe_3O_4	α magnetite		.60	.83	.93			.744	.340	.177	3;0-576	40
	β magnetite					1.03		.640	.362	0	5;576-800	40
$2Fe_2O_3 \cdot H_2O$	limonite		(.94 at 60°)									
Fe_2SiO_4	fayalite		.55	.79	.91	1.095		.69	.392	.181	3;0-900	41
$Fe_2Si_2O_6$	hypersthene		(.80 at 50°)									42
FeS	α troilite	.238	.606					1.00	1.85	0	7;0-138	43
	β troilite			.635	.66	.71		.574	.130	0	3;138-1195	43
FeS_2	pyrite	.075	.500	.594	.69			.373	.466	0	7;0-500	44

TABLE I-B.3a (Continued)

Compound	Mineral	C_p (joules per gram) for temperatures in °C.						Constants in $C_p = a + bT - cT^{-2}$ j./gm. (T°K.)			Error %; temp. range °C.	Reference
		-200°	0°	200°	400°	800°	1200°	a	10^3b	10^{-5}c		
Fe_7S_8	pyrrhotite		.594	.77				.406	2.81	.431$_3$	3;0-350	45
H_2O	ice	.653	2.06									
Hg	native mercury		.138	.138				.138	0	0	1;0-347	61
HgS	α-cinnabar		.214	.227	.240			.196	.066	0	2;0-580	14
$KAlSi_2O_6$	leucite		(.74$_5$ at 60°)									67
	glass		(.73$_2$ at 60°)									67
$KAlSi_3O_8$	adularia		.732	.842	1.00							18
	microcline		.680	.950	1.04	1.143		.988	.166	.263	1;0-1100	18
	orthoclase		.61	.94$_4$	1.05	1.145		1.043	.124	.351	1;0-1100	18
	glass		.70	.97	1.07	1.19		.976	.216$_5$	.247	2;0-1100	18
KCl	sylvite	.418	.682	.715	.749			.682	.168	0	2;0-770	65
KNO_3	α-niter	.326						.266	.219	0	10;0-128	66
	β-niter		1.19					1.19	0	0	5;128-338	66
	liquid			1.22				1.22	0	0	10;338-410	66
$LiAlSi_2O_5$	petalite		(.85 at 58°)									48
$LiAlSi_2O_6$	spodumene		(.90 at 60°)									49
	glass		(.91 at 60°)									49
$Mg_3Al_2Si_3O_{12}$	garnet		(.74 at 58°)									55

TABLE I-B.3a (Continued)

Compound	Mineral	C_p (joules per gram) for temperatures in °C.						C_p = a + bT · cT^{-2} Constants in j./gm. (T K.)			Error %; temp. range °C.	Reference
		-200°	0°	200°	400°	800°	1200°	a	10^3b	10^{-5}c		
$Mg_7B_{15}Cl_2O_{25}$	α-boracite		.796	1.18				.275	1.909	0	5;0-265	54
	β-boracite				1.41			.502	1.346	0	5;265-400	54
$MgCl_2$	chloromagnesite		.805	.84	.87			.760	.166	0	?;0-718	9
$MgCO_3$	magnesite	.161	.864									50
MgF_2	sellaite		.906	1.08	1.206	1.43		.857	.542	.0736	3;0-1000	51
$Mg(OH)_2$	brucite		(1.30 at 35°)									52
MgO	periclase	.066	.870	1.09	1.16	1.24	1.30	1.127	.124	.217	2;0-1800	53
$MgSiO_3$	pyroxene		.752	1.03	1.15			.973	.336	.233	1;0-500	56
	amphibole		.740	1.03	1.13	1.24		1.067	.183	.281	1;0-1100	56
	glass		.756	1.02	1.14			.971	.322	.226	1;0-700	56
$MgSO_4 \cdot H_2O$	kieserite		(1.00 at 9°)									57
$MgSO_4 \cdot 7H_2O$	epsomite		(1.51 at 32°)									52
$Mg_2Fe_2SiO_4$	olivine		(0.79 at 36°)									52
$Mg_3H_2Si_4O_{12}$	talc		(0.87 at 59°)									15
$MnCO_3$	rhodochrosite	.203	.70	1.08	1.46			.283$_5$	1.532	.33 X 10^{-11} T^4	4;0-500	58
MnO_2	pyrolusite		.975	1.00	1.01			.924	.227	.143X 10^{-11} T^4	?;0-500	59
$Mn_2O_3 \cdot H_2O$	manganite		(0.74 at 36°)									52
MnS	alabandite	.322*	.569*									60
MoS_2	molybdenite		.537	.554	.570			.515	.082	0	5;0-456	9

TABLE I-B.3a (Continued)

Compound	Mineral	C_p (joules per gram) for temperatures in °C.						Constants in $C_p = a + bT - cT^{-2}$ j./gm. (°K.)			Error %; temp. range °C.	Reference
		-200°	0°	200°	400°	800°	1200°	a	10^3t	10^{-5}c		
$NaAlSi_3O_8$	albite		.709	.986	1.085	1.196		1.018	.18[illegible]	.268	1;0-1100	18
	glass		.724	1.00	1.114	1.26		.978	.28[illegible]	.247	1;0-900	18
NaCl	halite	.466	.855	.915	.975	1.095		.773	.30[illegible]	0	2;0-800	77
	liquid					1.14		1.14	0	0	3;800-950	77
NaF	villiaumite		1.034	1.10	1.29			.473	1.19[illegible]	-.184	2;0-700	75
$Na_2B_4O_7 \cdot 10H_2O$	borax		(.161 at 35°)									74
Na_3AlF_6	cryolite		.909	1.18	1.39	1.78		.770	.9[illegible]	.0895	2;0-1000	76
NiS	millerite		.506	.565				.426	.29[illegible]	0	3;0-324	62
$PbCO_3$	cerussite	.177	.318									46
PbS	galena	.142	.207	.221	.235			.188	.0[illegible]	0	5;0-600	47
$PbSO_4$	anglesite		(.364 at 60°)									
Pd	palladium		.232	.246	.260	.289	.318	.212	.0[illegible]2	0	2;0-1549	63
Pt	platinum		.134	.139	.144	.154	.164	.127	.0[illegible]49	0	1;0-1600	64
S_8	rhombic sulfur							.482	.8[illegible]5	0	3;0-95.6	80
	monoclinic sulfur							.572	.5[illegible]6	0	3;95.6-119	80
	liquid							.656	.6[illegible]6	0	?;119-160	80
	viscous							1.22	0	0	?;160-270	80
Sb_2S_3	stibnite		.342	.375	.407			0.298	0.1[illegible]3	0.0	est;0-548	9
SiO_2	α-quartz	.173	.698	.969	1.129			.7574	.6[illegible]7	.168	1;0-575	68
	β-quartz					1.174	1.327	.763	.3[illegible]3	0	4;575-1600	68
	α-cristobalite	.186	.69	1.01				.254	1.6	0	4;0-250	69
	β-cristobalite				1.074	1.171	1.21	1.191	.0[illegible]2	.0625	2;250-1700	69
	glass	.184	.70	.95	1.06	1.21	1.34	.892	.3[illegible]5	.021	5;0-1700	70

TABLE I-B.3a (Continued)

Compound	Mineral	C_p (joules per gram) for temperatures in °C.						Constants in $C_p = a + bT - cT^{-2}$ j./gm. (T°K.)			Error %; temp. range °C.	Reference
		-200°	0°	200°	400°	800°	1200°	a	$10^{3}b$	$10^{-5}c$		
SnO_2	cassiterite		.34	.43	.48	.55		.387	.157	.07	4;0-1100	81
$SrCO_3$	strontianite	.211	.536									79
TiO_2	rutile, brookite		.70	.80	.88			.619	.395	.022	3;0-450	82
WO_3	tungstite		.33	.355	.382	.44	$.49_4$	.289	.14	0	5;0-1300	83
$ZnCO_3$	smithsonite	.238	.632									84
ZnO	zincite		.48	.58	.615	.66	.69	.586	.175	.094	2;0-1300	85
ZnS	α-wurtzite β-sphalerite	.430	.45	.53	.56	.587		.550	.141	.084	6;0-900	86
$ZrSiO_4$	zircon		(.61 at 60°)									87

REFERENCES FOR TABLE I-B.3a

Gen.: Landolt-Bornstein Tabellen, 1, 1242, 1923; 2, 1160, 1931; 3,2230, 1936; Kelley, Bulls. 371, 393, Bureau of Mines; Chem. Abstracts.

Heat Capacities of Minerals

1. Tilden, J. Chem. Soc. 559, 1905; Miehr, Immke and Kratzers, Tonind. Z., 50, 1671, 1791, 1926; Cohn, J. Am. Ceram. Soc., 7, 475, 1924; 10, 347, 1927; Roth and Bertram, Z. Electrochem., 35, 297, 1929; Kolossowsky and Skoulski, Bull. soc. chim. France, 47, 136, 1930; Newman and Brown, Ind. Eng. Chem., 22, 995, 1930; Wilkes, J. Am. Ceram. Soc., 15, 72, 1932; Esser, Averdieck and Grass, Arch. Eisenhuttenw., 6, 289, 1933; v. Gronow and Schwiete, Z. anorg. Chem., [illegible] Terebesi, Helv. Chim. Acta, 16, 922, 1933; Chipman, Trans. Am. Soc. Metals, 22, 414, 1934; Terebesi, Helv. Chim. Acta, (A) 804, 1934; Simon and Swain, Z. phys. Chem., 28, 189, 1935.
2. Neumann, Z. anorg. Chem., 145, 194, 1925.
3. Neumann, Z. anorg. Chem., 145, 194, 1925; Kolossowsky and Skoulski, Bull. soc. chim. France, 47, 136, 1930.
4. Cohn, J. Am. Ceram. Soc., 7, 475, 1924; Neumann, Z. anorg. Chem., 145, 194, 1925.
5. Kolossowsky, J. Gen. Chem. (U.S.S.R.), 1, 253, 1931; Bergeron, J. Soc. Glass Tech., 20, 680, 1936.
6. Kolossowsky and Skoulski (see 3).
7. Schwiete and v. Gronow, Zement, 24, 197, 1935.
8. Joly, Proc. Roy. Soc., 41, 250, 1887; Lindner, Diss. Erlangen, 1903.
9. Regnault, Pogg. Ann., 53, 60, 1841.
10. Regnault, Pogg. Ann., 53, 60, 1841; Joly, Proc. Roy. Soc., 41, 250, 1886; Laschschenko, J. Russ. Phys.-Chem. Soc., 43, 1604, 1910; Anderson, J. Am. Chem. Soc., 56, 340, 1934.
11. Latimer, Hicks Jr., and Schutz, J. Am. Schem. Soc., 56, 88, 1934.
12. Nilson and Pettersson, Ber. deut. chem. Ges., 13, 1459, 1880.
13. Oeberg, Ofs. Stockh., 42, 43, 1885; Joly, Proc. Roy. Soc., 41, 250, 1887.
14. Russell, Physik. Z., 13, 59, 1912.
15. Ulrich, Wollny Forsch. Geb. Agrikultur Phys., 17, 1, 1894.
16. Regnault, Pogg. Ann., 53, 60, 1841; Kopp, Phil. Trans. Roy. Soc., 155, 71, 1865; Thoulet and Lagarde, Compt. rend., 94, 1512, 1882; Joly, Proc. Roy. Soc., 41, 250, 1886; Pierce and Wilson, Nature, 61, 367, 1900; Nernst, Koref and Lindemann, Sitzber. Berlin Akad., 12, 247, 1910; Laschschenko, J. Russ. Phys.- Chem. Soc., 43, 793, 1911; Magnus, Physik. Z., 14, 5, 1913; Nernst and Schwers, Sitz., Berlin Akad., 355, 1914; Dannholm, Soc. Sci. Fennica, Commentationes Phys.-Math., 1, 1922; Anderson, J. Am. Chem. Soc., 56, 340, 1934; Simon and Swain, Z. phys. Chem., 28, 189, 1935.
17. Regnault, Ann. chim. phys., 1, 129, 1841; Neumann, Ann. phys., 126, 123, 1865; Kopp, Phil. Trans. Roy. Soc., 155, 1871; Joly, Proc. Roy. Soc., 41, 250, 1886; Eucken and Schwers, Phys. Gesell. Berlin, 15, 578, 1913; Kelley, Bull. 350, Bureau of Mines, 1932.
18. White, Am. J. Sci., 28, 334, 1909; 47, 17, 1919.
19. v. Gronow and Schwiete, Z. anorg. Chem., 216, 185, 1933.

20. White, Am. J. Sci., 47, 17, 1919; Wagner, Z. anorg. Chem., 208, 19, 1932; Cristescu and Simon, Z. phys. Chem., 25, 273, 1934.
21. White, Am. J. Sci., 47, 17, 1919; Roth and Bertram, Z. Electrochem., 35, 297, 1929; Huttig and Rosenkranz, Z. Electrochem., 35, 308, 1929; Parks and Kelley, J. Phys. Chem., 30, 1175, 1926; Wagner, Z. anorg. Chem., 208, 19, 1932; Cristescu and Simon, Z. physik. Chem., 25, 273, 1934.
22. Kopp, Phil. Trans. Roy. Soc., 155, 71, 1865; Latimer, Hicks Jr. and Schutz, J. Am. Chem. Soc., 56, 88, 1934.
23. Regnault, Pogg. Ann., 53, 60, 243, 1841; Kopp, Phil. Trans. Roy. Soc., 155, 71, 1865; Laschschenko and Kompanskii, J. Russ. Phys.-Chem. Soc., 60, 579, 1928.
24. Kopp, Phil. Trans. Roy. Soc., 155, 71, 1865.
25. Regnault, Bettendorf and Wullner, Dewar (black diamond) (see Ref. 18); Armstrong, Proc. Roy. Inst., 19, 393, 1908; Nernst and Lindemann, [illegible] Ewald, Ann. phys., 44. 1213, 1914.
26. Regnault, Pogg. Ann., 53, 243, 1841; Kopp, Phil. Trans. Roy. Soc., 155, 71, 1865; Bettendorf and Wullner, Pogg. Ann., 133, 293, 1868; Dewar, Phil. Mag., 44, 461, 1872; Magnus, Ann. Physik., 70, 303, 1923; Schlapfer and Debrunner, Helv. Chim. Acta, 7, 31, 1924.
27. Lorenz, Pogg. Ann., 13, 422, 1881; Bede, Fortschr. Phys., 11, 379, 1885; Naccari, Atti Torino, 23, 107, 1887-8; Gaede, Physik. Z., 4, 105, 1902; Glaser, Metallurgie, 1, 103, 121, 1904; Magnus, Ann. Physik, 31, 597, 1910; Nernst and Lindemann, Sitzber. Berlin Akad, 4, 94, 1911; Griffiths and Griffiths, Proc. Roy. Soc., A89, 561, 1914; Keesom and Onnes, Proc. Acad. Sci. Amsterdam, 18, 484, 1915; Schubel, Z. anorg. Chem., 184, 193, 1929; Harper, U.S. Bur. Stand. Bull., 11, 259, 1915; Wust, Meuthen and Durrer, Forsch. Arb. Ver. deut. Ing., 204, 1918; Doerinckel and Werner, Z. anorg. Chem., 115, 1, 1921; Umino, Sci. Repts. Tohoku Univ., 15, 597, 1926; Klinkhardt, Ann. Physik, 84, 167, 1927; Ruer and Kremero, Z. anorg. Chem,, 184, 193, 1929; Eucken and Werth, Z. anorg. allgem. Chem., 188, 152, 1930; Seekamp, Z. anorg. allgem. Chem., 195, 345, 1931; Bronson, Chisholm and Doherty, Can. J. Res., 8, 282, 1933; Maier and Anderson, J. Chem. Phys., 2, 513, 1934.
28. Magnus, Ann. Physik, 31, 597, 1910; Randall, Nielsen and West, Ind. Eng. Chem., 23, 388, 1931; Wohler, Jochum and Schmitt, Z. phys. Chem., 167, 169, 1933. Heat capacity depends on previous history through the temp. range of 450°to 750°C.
29. Regnault, Pogg. Ann., 98, 396, 1856; Kopp, Phil. Trans. Roy. Soc., 155, 71, 1865; Magnus, Habilitationsschrift, Eberhard-Karls Univ., Tubingen, 1910; Russell, Physik. Z., 13, 59, 1912.
30. Kopp, Phil. Trans. Roy. Soc., 155, 71, 1865; Oeberg, Ofs. Stockh., 42, 43, 1885.
31. Bellati and Lussana, Atti ist. Veneto, 7, 1051, 1888.
32. Regnault, Pogg. Ann., 53, 60, 1841; Kopp, Phil. Trans. Roy Soc., 155, 71, 1865; Beliati and Lussana, Atti ist. Veneto, 7, 1051, 1888; Bornemann and Hengstenberg, Metall u. Erz, 17, 313, 339; Randall, Nielsen and West, Ind. Eng. Chem., 23, 388, 1931; Anderson, J. Am. Chem. Soc., 54, 107, 1932; White, J. Am. Chem. Soc., 55, 1047, 1933. White got an abnormally high heat capacity around 300° indicating a maximum; and a minimum around 700°. A mean over the temp. range 300 - 900° is 0.55 ± 0.05.

33. Russell, Physik. Z., 13, 59, 1912; Bornemann and Hengstenberg, Metall u. Erz, 17, 313, 1920; Anderson, J. Am. Chem. Soc., 54, 107, 1932.
34. Kopp, Phil. Trans. Roy. Soc., 155, 71, 1865.
35. Wust, Meuthem and Durrer, Forschr. Arb. Ver. deut. Ing., No. 204, 1918; Schlapfer and Debrunner, Helv. Chim. Acta, 7, 31, 1924; Umino, Sci. Repts. Tohoku Univ., 15, 597, 1926.
36. Bystrom, Fortschr. Physik, 16, 369, 1860; Weinhold, Pogg. Ann., 149 186, 215, 1873; Lorenz, Pogg. Ann., 13, 422, 1881; Bede, Fortschr. Physik, 11, 379, 1885; Pionchon, Compt. rend., 102, 1454, 1886; Naccari, Atti Torino, 23, 107, 1887; Harker, Phil. Mag., 10, 430, 1905; Stucker, Sitzber. kgl. Akad. Wiss. Wien, 114, 657, 1905; Oberhoffer, Metallurgie, 4, 486, 1907; Weiss and Beck, Arch. sci. phys. nat., 42, 378, 1916 Von Pirani, Ber. deut. phys. Ges., 102, 1037, 1912; Griffiths and Griffiths, Proc. Roy. Soc., A88, 549, 1913; Levin and Schottky, Ferrum, 10, 193, 1913; Laschschenko, J. Russ. Phys.-Chem. Soc., 46, 311, 1914; Schubel, Z. anorg. Chem., 87, 81, 1914; Weiss, Piccard and Carrard, Arch. sci. phys. nat., 42, 378, 1916; Wust, Meuthen and Durrer, Forsch. Arb. Ver. deut. Ing., No. 204, 1918; Kawakami, Sci. Repts. Tohoku Univ., 15, 251, 1926; Klinkhardt, Z. Electrochem., 32, 534, 1926; Oberhoffer and Grosse, Stahl u. Eisen, 47, 576, 1927; Umino, Sci. Repts. Tohoku Univ., 16, 775, 1927; 18, 91, 1929; Zalesinski and Zulinski, Bull. int. acad. polonaise, pt. A, 479, 1928.
37. Sella, Nachr. kgl. Ges. Wiss, Gottingen, 311, 1891.
38. Roth and Bertram, Z. Electrochem., 35, 297, 1929; Anderson, J. Am. Chem. Soc., 56, 849, 1934.
39. Brown and Furnas, Trans. Am. Inst. Chem. Eng., 18, 309, 1926; Russell, Physik, Z., 13, 59, 1912; Roth and Bertram, Z. Electrochem., 35, 297, 1929; Kolossowski and Skoulski, Bull. soc. chim. France, 47, 136, 1930; Chipman and Murphy, Ind. Eng. Chem., 25, 319, 1933.
40. Weiss, Piccard and Carrard, Arch. sci. phys. nat., 43, 113, 1917; Brown and Furnas, Trans. Am. Inst. Chem. Eng., 18, 309, 1926; Roth and Bertram, Z. Electrochem., 35, 297, 1929; Kolossowski and Skoulski, Bull. soc. chim. France, 47, 136, 1930; Esser, Averdieck and Grass, Arch. Eisenhuttenw., 6, 289, 1932/3; Chipman and Murphy, Ind. Eng. Chem., 24, 319, 1933.
41. Roth and Bertram, Z. Electrochem., 35, 297, 1929; Esser, Averdieck and Grass, Arch. Eisenhuttenw., 6, 289, 1933.
42. Ulrich (see 15).
43. Regnault, Pogg. Ann., 53, 60, 1841; Bornemann and Hengstenberg, Metall u. Erz, 17, 313, 319, 1920; Anderson, J. Am. Chem. Soc., 53, 476, 1931.
44. Joly, Proc. Roy. Soc., 41, 250, 1886; Eucken and Schwers, Ber. deut. phys. Ges., 15, 578, 1913; Hengstenberg, Diss. Breslau, 1920; Maier, Rept. Invest. Bur. Mines, 1934.
45. Lindner, Diss. Erlangen, 1903; Hengstenberg, Diss. Breslau, 1920.
46. Anderson, J. Am. Chem. Soc., 56, 849, 1934.
47. Regnault, Pogg. Ann., 53, 60, 1841; Kopp, Proc. Roy. Soc., 155, 71, 1865; Joly, Proc. Roy. Soc., 41, 250, 1886; Rolla, Nuovo cimento, 9, 197, 1915; Eastman and Rodebush, J. Am. Chem. Soc., 40, 496, 1918; Anderson, J. Am. Chem. Soc., 54, 107, 1932.
48. International Critical Tables.
49. Schulz, Zentr. Mineral. Geol., 632, 1911.
50. Mitchell, J. Chem. Soc., 123, 1055, 1923; Anderson, J. Am. Chem. Soc., 56, 849, 1934.

51. Landolt-Bornstein Tabellen.
52. Kopp, Phil. Trans. Roy. Soc., 155, 71, 1865.
53. Russell, Physik. Z., 13, 59, 1912; Gunther, Ann. phys., 51, 828, 1916; Magnus, Ann. Physik, 70, 303, 1923; Wilkes, J. Am. Ceram. Soc., 15, 72, 1932.
54. Mallard, Bull. soc. min. France. 6, 122, 1883; Kroeker, Nachr. kgl. Ges. Wiss. Gottingen, 122, 1892.
55. Oeberg, Ofs. Stockh., 42, 43, 1885.
56. White, Am. J. Sci., 28, 334, 1909; 47, 1, 1919; Wagner, Z. anorg. Chem., 208, 19, 1932; Cristescu and Simon, Z. phys. Chem., 25, 273, 1934.
57. Rolla and Accame, Atti accad. Lincei, 22 II, 109, 1913.
58. Anderson, J. Am. Chem. Soc., 56, 849, 1934; Maier, from Kelley.
59. Kopp, Phil. Trans. Roy. Soc., 155, 71, 1865; Russell, Physik. Z., 13, 59, 1912; Maier, from Kelley.
60. Anderson, J. Am. Chem. Soc., 56, 476, 1934. He finds a hump at -133°C. (C_p=.64j./g.) above which temp. C_p drops rapidly to a cusp at about -126°C. (C_p=.55j./g.) above which temo. C_p again drops rapidly to a value and a slope $\partial C_p/\partial t$ very different from that on the low. temp. side of the hump.
61. Milthaler, Wied. Ann., 36, 897, 1889; Naccari, J. phys., 8, 612, 1889; Gaede, Physik. Z., 4, 105, 1902; Cohen, Kruisheer and Moesveld, Z. phys. Chem., 96, 437, 1920; Marttinen and Tiihonen, Soc. Sci. Fennica, 1, 11, 1922; Hirobe, J. Univ. Rokyo, 1, 155, 1926; Dixon and Rodebush, J. Am. Chem. Soc., 49, 1162, 1927.
62. Tilden, Phil. Trans. Roy. Soc., 203A, 139, 1904.
63. Jaeger and Dieselhorst, Wiss. Abhandl. physik.-tech. Reichsanstalt, 3,269, 1900; Jaeger and Rosenbohm, Proc. Acad. Sci. Amsterdam, 33, 457, 1930.
64. Bystrom, Fortschr, Physik, 16, 369, 1860; Tilden, Phil. Trans. Roy. Soc., 203A, 139, 1904; White, Am. J. Sci., 28, 334, 1909; Phys. Rev., 12, 436, 1918; Wust, Meuthen, and Durrer, Forsch. Arb. Ver. deut. Ing., No. 204, 1918; Jaeger and Rosenbohm, Proc. Acad. Sci. Amsterdam, 33, 457, 1930.
65. Plato, Z. phys. Chem., 55, 721, 1906; Magnus, Physik. Z., 14, 5, 1913; Southard and Nelson, J. Am. Chem. Soc., 55, 4865, 1933; Marley, Proc. Phys. Soc., 45, 591, 1933; Keesom and Clark, Physica, 2, 702, 1935.
66. Regnault, Pogg. Ann., 53, 60, 1841; Person, Pogg. Ann., 70, 300, 1847; Kopp, Phil. Trans. Roy. Soc., 155, 71, 1865; Neumann, Pogg. Ann., 126, 123, 1865; Goodwin and Kalmus, Phys. Rev., 28, 1, 1909; Ewald, Ann. Physik 44, 1213, 1914.
67. Bogajawlensky, Schr. Naturf. Ges. Dorpat, 1, 1904.
68. Pionchon, Compt. rend., 102, 1454, 1886; Laschschenko, J. Russ. Phys.-Chem. Soc. 42, 1604, 1910; Magnus, Physik. Z., 14, 5, 1913; White, Am. J. Sci., 28, 334, 1909; 47, 1, 1910; Nernst, Ann. phys., 36, 395, 1911; Bornemann and Hengstenberg, Metall u. Erz, 17, 313, 339, 1920; Wietzel, Z. anorg. Chem., 116, 71, 1921; Perrier and Roux, Mem. soc. vaud. sci. nat., 3, 110, 1923; Schlapfer and Debrunner, Helv. Chim. Acta, 7, 31, 1924; Cohn, J. Am. Ceram. Soc., 7, 475, 1924; Ber. deut. keram. Ges., 9, 289, 1928; Miehr, Immke and Kratzers, Tonind. Z., 50, 1671, 1926; Roth and Bertram, Z. Electrochem., 35, 297, 1929; Kolossowsky and Skoulski, Bull. soc. chim. France., 47, 136, 1930; Esser, Averdieck and Grass, Arch. Eisenhuttenw., 6, 289, 1932; Schwiete and v. Gronow, Zement, 24, 198, 1935.

69. Wietzel, Z. anorg. Chem., 116, 71, 1921; White, Am. J. Sci., 28, 334, 1909; 47, 1, 1919; Simon, Ann. phys., 68, 241, 1922; Cohn, J. Am. Ceram. Soc., 7, 475, 1924.
70. Stierlin, Viertel. naturforsch. Ges. Zurich, 52, 382, 1908; Laschschenko, J. Russ. Phys.-Chem. Soc., 42, 1604, 1910; Nernst. Ann. phys., 36, 395, 1911; Magnus, Physik. Z., 14,5, 1913; Wust. Meuthen and Durrer, Forsch. Arb. Ver. deut. Ing., 204, 1919; White, Am. J. Sci., 28, 334, 1909; 47, 1, 1919; Iitaka, Sci. Repts. Tohoku Univ., 8, 99, 1919; Bornemann and Hengstenberg, Metall u. Erz, 17, 313, 1920; Wietzel, Z. anorg. Chem. 116, 71, 1921; Cohn, J. Am. Ceram. Soc., 7, 359, 475, 548, 1924; Miehr, Immke and Kratzers, Tonind. Z., 50, 1671, 1926; Roth and Bertram, Z. Electrochem., 35, 297, 1929; Fischer, Z. anorg. Chem., 200, 332, 1931.
71. Bystrom, Fortschr. Physik, 16, 369, 1860; Naccari, Atti Torino, 23, 107, 1888; Tilden, Proc. Roy. Soc., 71, 220, 1903; Magnus, Ann. Physik, 31, 597, 1910; Nernst. Ann. phys., 36, 395, 1911; Griffiths and Griffiths, Proc. Roy. Soc., A88, 549, 1913; Schubel. Z. anorg. Chem., 87, 81, 1914; Weiss, Piccard and Carrard, Arch. sci. phys. nat., 42, 378, 1916; 43, 199, 1917; Wust, Meuthen and Durrer, Forsch. Arb. Ver. deut. Ing., 204, 1918; Eastman, Williams and Young, J. Am. Chem. Soc., 46, 1178, 1924; Umino, Sci. Repts. Tohoku Univ., 15, 597, 1926; Magnus and Young, J. Am. Chem. Soc. 46, 1178, 1924; Umino, Sci. Repts. Tohoku Univ., 15, 597, 1926; Magnus and Hodler, Ann. Physik, 80, 808, 1926; Jaeger, Rosenbohm and Veenstra, Proc. Acad. Sci. Amsterdam, 36, 291, 1933.
72. Ehrhardt, Wied. Ann., 24, 215, 1885; Goodwin and Kalmus, Phys. Rev., 28, 1, 1909; Magnus, Habilitationsschrift, Eberhard-Karls Univ., Tubingen, 1910; Eastman and Milner, J. Chem. Phys., 1, 444, 1933.
73. Regnault, Pogg. Ann., 53, 60, 1841; Bellati and Lussana, Atti ist. Veneto, 7, 1051, 1888; Sella, Nachr. kgl. Ges. Wiss. Gottingen, 311, 1891; Tilden, Phil. Trans. Roy. Soc., 203A, 139, 1904; Rolla, Proc. Acad. Sci. Amsterdam, 34, 808, 1931.
74. Kopp, Phil. Trans. Roy. Soc., 155, 71, 1865.
75. Krestownikow and Karetnikow, Leichtmetalle, 4, 29, 1934.
76. Roth and Bertram, Z. Electrochem., 35, 297, 1929; Krestownikow and Karetnikow, Leichtmetalle, 4, 29, 1934.
77. Plato, Z. phys. Chem., 55, 721, 1906; Magnus, Physik. Z., 14, 5, 1913; Roth and Bertram, Z. Electrochem., 35, 297, 1929; McGraw Jr., Landolt-Bornstien Tabellen.
78. Joly, Proc. Roy. Soc., 41, 250, 1886; Ulrich, Wollny Forsch. Geb. Akrikultur Phys., 17, 1, 1894. *Solid solutions of Ab = $NaAlSi_3O_8$, An = $CaAl_2Si_2O_8$ so that 4 Ab·1 An = $4NaAlSi_3O_8 \cdot 1CaAl_2Si_2O_8$.
79. Anderson, J. Am. Chem. Soc., 56, 340, 1934.
80. Person, Pogg. Ann., 70, 300, 1847; Dussy, Compt. rend., 123, 305, 1896; Wigand, Ann. Physik, 22, 64, 1907; Richards and Jackson, Z. phys. Chem., 70, 414, 1910; Nernst, Koref and Lindemann, Sitzber. Berlin Akad., 247, 1910; Nernst, Ann. phys., 36, 395, 1911; Lewis and Randall, J. Am. Chem. Soc., 33, 476, 1911; Dewar, Proc. Roy. Soc. 89, 158, 1913; Iitaka, Sci. Repts. Tohoku Univ., 8, 99, 1919; Monval, Bull. soc. chim., 39, 1349, 1926.
81. Huttig, Margierkiewicz and Fichmann, Z. phys. Chem., 141A, 8, 1929.
82. Regnault, Ann. chim. phys., 1, 129, 1841; Kopp, Phil. Trans. Roy. Soc., 155, 71, 1865; Nilson and Pettersson, Z. phys. Chem., 1, 27, 1887.

83. Regnault, Pogg. Ann., 53, 60, 1841; Russell, Physik. Z., 13, 59, 1912.
84. Anderson, J. Am. Chem. Soc., 56, 849, 1934.
85. Regnault, Pogg. Ann., 53, 60, 1841; Magnus, Physik. Z., 14, 5, 1913; White and Day, in J. Am. Chem. Soc., 48, 364, 1926.
86. Bornemann and Hengstenberg, Metall u. Erz, 17, 313, 339, 1920.
87. Kopp, Phil. Trans. Roy. Soc., 155, 71, 1865; Regnault, Pogg. Ann., 53, 60, 1841.

TABLE I-B.3b

HEAT CAPACITY OF ROCKS

(See also Table I-B.5)

Rock	C_p (joules per gram) for temperatures (°C.)					Constants in $C_p = a + bT - cT^{-2}$ j./gm. (T°K.)			Error %; temp. range °C.	Reference
	0°	200°	400°	800°	1200°	a	10^3b	10^{-5}c		
IGNEOUS										
Granite 65% Orthoclase 25% Quartz 9% Albite 1% Magnetite	.65	.95	1.07	1.13		.965 .966	.254 .199	.26 .22	Calc.; 0-575 Calc.; 575-1000	1
Japanese (Mean of 6)	.80 (.77 at 50°)	.95	1.09	1.39		.60	.74	0	±20; 0-800	2 3
Granodiorite 20% Quartz 60% Andesite 9% Amphibole 10% Pyroxene 1% Magnetite	.70	.97	1.08_5	1.17_5		.940	.289	.25	Calc; 0-900	1
Diorite, Japanese (Mean of 8)	(.81 at 65°)									3
Diorite 50% Andesine 40% Amphibole	.71	.99	1.09	1.18		1.024	.187	.23	Calc; 0-900	1

TABLE I-B.3b (Continued)

Rock	C_p (joules per gram) for temperatures (°C.)					Constants in $C_p = a + bT - cT^{-2}$ j./gm. (T°K.)			Error %; temp. range °C.	Reference
	0°	200°	400°	800°	1200°	a	10^3b	10^{-5}c		
9% Orthoclase 1% Magnetite										
Basalt Syracuse Aetna Kilauea	.85	1.04	1.14_5	1.32	1.49	.902	.402	.122	±5; 0-1200	2,4
Diabase	.70	.87	.98	1.19	1.36	.665	.50	.075	±5; 0-1200	5
Gabbro 45% Labradorite 45% Pyroxene, Olivine 5% Amphibole 5% Magnetite	.72	.99	1.10	1.18		.975 .969	.267 .268	.242 .234	Calc; 0-585 Calc; 585-900	1
METAMORPHIC										
Gneiss	.74	1.01				.38	1.33	0	±10; 0-200	6
Granite gneiss See Granite										1
Japanese	(.79 at 65°)									3
Slate	.71	1.00	1.10	1.20	1.27	1.06	.151	.29	Est; 0-1200	1

TABLE I-B.35 (Continued)

Rock	C_p (joules per gram) for temperatures (°C.)					Constants in $C_p = a + bT - cT^{-2}$ j./gm. (T°K.)			Error %; temp. range °C.	Reference
	0°	200°	400°	800°	1200°	a	10^3b	10^{-5}c		
Quartzite	.70	.97	1.13	1.17	1.33	.757 .763	.607 .383	.168 0	Calc.; 0-575 Calc.; 575-1600	1
Japanese (Mean of 9)	(.77 at 65°)									3
Marble (Mean of 6)	.79	1.00	1.13			.823	.497	.129	Calc.; 0-750	1 7
(.847 at 50°)										
SEDIMENTARY										
Sandstone	(.93 at 59°)									8
Micaceous	(.73 at 50°)									8
Japanese (mean of 4)	(.81 at 65°)									3
English (mean of 8)	(.81 at 50°)									7
(See Quartzite)										
Clay, Amorphous	.75	.94	1.13	1.51		.489	.953	0	±5;0-1000	9
(Shale)	(.77 at 65°)									3
Clay China Clay	.80	.94	1.08	1.78	1.78	.607	.707	0	±5;0-500	9
Kaolin						1.78	0	0	±7;600-1200	

TABLE I-B.3b (Continued)

Rock	C_p (joules per gram) for temperatures (°C.)					Constants in $C_p = a + bT - cT^{-2}$ C_p j./gm. (T°K.)			Error %; temp. range °C.	Reference
	0°	200°	400°	800°	1200°	a	10^3b	10^{-5}c		
Limestone	(1.00 at 58°)									7
English (mean of 3)	(.68 at 50°)									
Japanese (mean of 10).	(.83 at 65°)									3
See calc. marble										1

REFERENCES FOR TABLE I-B.3b

1. Calc. = calculated from mineral content; est. = computed by analogy. (R.W.G.)
2. Bartoli, Bull. mens. dell' acc. Gionenia, 3, 61, 1891; Poole, Phil. Mag. 27, 58, 1914.
3. Tadokoro, Sci. Reports, Tohoku Imp. Univ. 10, 339, 1921,
4. Roberts and Ricker, Phil. Mag. 32, 1891.
5. Barus, Phil. Mag. 32, 353, 1891.
6. Weber, Diss. Zurich. 1878.
7. Baldwin, Wiseman and Griffith, Proc. Inst. Civil Eng. 179, 290, 1909.
8. Hecht, Diss. Konigsberg, 1903.
9. Cohn, J. Am. Ceram. Soc. 7, 475, 1924.

TABLE I-B.4

HEATS OF TRANSFORMATION AND OF FUSION

Compound	Mineral	Phase Change	Temp., °C.	Δh joules per gram	Method*	Ref. Remarks
Ag_2S	acanthite	argentite	175	17.6± .2	H.C.	H.Cap.
	argentite	liquid	842	57	F.P.L.	38
Al_2O_3	corundum	γ α	20	0.41	H.C.	1
		solid liquid	2045	1070	F.P.L.	2
Au	gold	solid liquid	1063	65±4	H.C.	18
$BaCO_3$	witherite	α β	810	97.5±	H.C.	H.Cap.
$BaSO_4$	barite	solid liquid	1350	174	F.P.L.	4
$CaAl_2Si_2O_8$	anorthite	solid liquid	1550	440	F.P.L.	6
				440±65	H.C.	7
$CaCO_3$	calcite	aragonite		-21		
CaF_2	fluorite	solid liquid	1392	220	F.P.L.	5
$(CaMg)_4Si_3O_{10}$	Åkermanite	solid liquid	1458	380±65	H.C.	7
$CaMg(SiO_3)_2$	diopside	solid liquid	1391.5	(445±65	H.C.	8
				430	F.P.L.	9
$CaSiO_3$	pseudowollastonite	wollastonite	17	-45.5	H.C.	10
	pseudowollastonite	liquid	1512	483	F.P.L.	11
Ca_2SiO_4	larnite	β γ	20	26.8	H.C.	12
$CaSO_4$	anhydrite	solid liquid	1297	201	F.P.L.	13
Cu	copper	solid liquid	1084	200	H.C.	H.Cap.
CuO	tenorite	solid liquid	1447±	148	F.P.L.	14
Cu_2O	cuprite	solid liquid	1230	391±	F.P.L.	15

TABLE I-B.4 (Continued)

Compound	Mineral	Phase Change	Temp., °C.	Δh joules per gram	Method*	Ref. Remarks
Cu_2Se	berzelianite	α β	110	23±1	H.C.	16
Cu_2S	chalcocite	α β	103	35.2	H.C.	16
Fe	iron (Curie point)	α β	755	Uncertai	H.C.	20
		β γ	903	16.3	H.C.	20
		γ δ	1401	78.6	H.C.	20
		solid liquid	1530	279	F.P.L.	21
Fe_3O_4	magnetite	Curie point	576	Small	H.C.	H.Cap.
Fe_2O_3	hematite	amorph. α	33	341		22
Fe_2SiO_4	fayalite	solid liquid	1205	295	F.P.L.	23
FeS	troilite	α β	138	50	H.C.	H.Cap.
		solid liquid	1195	240±2	H.C. + F.P.L.	24
H_2O	ice I	solid liquid	0	332	H.C.	19
KCl	sylvite	solid liquid	770	360	H.C.	33
KNO_3	niter	α β	128	58.5	H.C.	H.Cap.
		solid liquid	338	117.5	H.C.	H.Cap.
$KAlSi_2O_6$	leucite	solid liquid	1686±5	130	F.P.L. + D.H.S.	34
$KAlSi_3O_8$	microcline glass		20	348	D.H.S.	35
	(adularia) orthoclase glass		20	418	D.H.S.	35

TABLE I-B.4 (Continued)

Compound	Mineral	Phase Change	Temp., °C.	Δ joules per gram	Method*	Ref. Remarks
$K_2Si_4O_9$		α β	592	9 6±1	H.C.	36
		solid liquid	765	147 30	H.C.	36
Li_2SiO_3		solid liquid	1177	336	H.C.	27
Li_4SiO_4		solid liquid	1249	260	H.C.	27
$MgCl_2$	chloromagnesite	solid liquid	712	356	F.P.L.	28
MgF_2	sellaite	solid liquid	1221	396	F.P.L.	29
$6MgO \cdot MgCl_2 \cdot 8B_2O_3$	boracite	α β	265	12 4	H.C.	H.Cap.
$MgSiO_3$	enstatite	solid liquid	1524	616	F.P.L.	30
Mg_2SiO_4	forsterite	solid liquid	1890	455	F.P.L.	31
$MnSiO_3$		solid liquid	1274	270	F.P.L. + D.H.S.	32
NaCl	halite	solid liquid	800	530	H.C.	39
Na_3AlF_6	cryolite	solid liquid	1000±	330	H.C.	40
$NaNO_3$		solid liquid	310	185	H.C.	H.Cap.
$NaAlSi_3O_8$	albite	solid liquid	1105	203	F.P.L.	41
$NaAlSiO_4$	carnegieite	(β-nephelite) liquid	1526	340	F.P.L.	42
Na_2SiO_3		solid liquid	1087	343	F.P.L.	43
$Na_2Si_2O_5$		solid liquid	884	193	F.P.L.	43
PbS	galena	solid liquid	1114	73	F.P.L.	25
$PbSO_4$	anglesite	solid liquid	1090±	131	F.P.L.	26
S	sulfur	rhombic monoclinic	95.6	11 ±1	H.C.	44a
		monoclinic liquid	119	38 .5	H.C.	44b
		liquid viscous	160	1 .5	H.C.	44c
Sb_2S_3	stibnite	solid liquid	546	12	F.P.L.	3

TABLE I-B.4 (Continued)

Compound	Mineral	Phase Change	Temp., °C.	Δh joules per gram	Method*	Ref. Remarks
SiO_2		α quartz β quartz	575	14.6	H.C.	37a
		α cristobalite β cristobalite	250	13.2	H.C.	37b
		β cristobalite α quartz	77	-117	D.H.S.	37c
		quartz liquid	1470	244	D.H.S.	37d
		cristobalite liquid	1713	142	T.A.	37e
TiO_2	rutile	solid liquid	1825	597±	F.P.L.	2
Zn_2SiO_4	willemite	solid liquid	1509	170	H.C.	35
ZnS	sphalerite	solid liquid	(1645)±	391±	F.P.L.	45

*H.C. - from heat content data
D.H.S. - from differential heats of solution data
F.P.L. - from freezing point lowering

H. Cap. - Data here obtained from literature on interval heat capacities; reference found under heat capacities.
T.A. - Thermal analysis

REFERENCES FOR TABLE I-B.4

1. Roth and Troitzsch, Z. ang. Chem., 40, 198, 1936.
2. Computed (K.K.) from Al_2O_3 - TiO_2 (Bunting, Bur. Standards J. Research, 11, 719, 1933).
3. Computed (K.K.) from Sb_2S_3 - SnS (Parravano and De Cesario, Gazz. chim. ital., 42, 1, 1912).
4. Computed (K.K.) from $BaSO_4$ - Na_2SO_4 (Calcagni, Atti accad. Lincei, 21, 483, 1912) and $BaSO_4$ - K_2SO_4 (Calcagni, op. cit.; Grahmann, Z. anorg. Chem., 81, 257, 1913).
5. Computed (K.K.) from CaF_2 - AlF_3 (Fedotieff and Iljinsky, Z. anorg. Chem., 80, 113, 1913) and CaF_2 - $Ca_3(PO_4)_2$ (Nacken, Zentr. Mineral. Geol., 530, 1912).
6. Mean computed (R.W.G.) from albite-anorthite across diagram (Bowen, Am. J. Sci., 38, 207, 1914, computes same value). Initial [illegible] slope yields 407 j./g. The system, diopside-anorthite, yields 370 j./g.; leucite-anorthite 392 j./g.; and carnegieite-anorthite 373 j./g.
7. Vogt, Silikatschmelz, 1904.
8. White, Am. J. Sci., 28, 486, 1909 (Vogt, Silikatschmelz, 1904, gives 427 ± 65 j./g. as the heat of fusion).
9. Computation (R.W.G.) from diopside-anorthite (Bowen, Z. anorg. Chem., 94, 23, 1916) yields 450 j./g.; from diopside-leucite (Bowen and Schairer, Am. J. Sci., 18, 301, 1929) 407 j./g. Mean value taken as 430 j./g. Slopes in systems, diopside-forsterite, and diopside-silica, not accurate enough for computations.
10. Wagner, Z. anorg. Chem., 208, 19, 1932. The transformation temp. of wollastonite ⇌ pseudowollastonite is 1190 ± 10°C. for which this value 45.5 j./g. is an approximation.
11. Computed from $CaSiO_3$ - $MgSiO_3$ (Allen and White, Am. J. Sci., 27, 1, 1909).
12. Johannson and Thorvaldson, J. Am. Chem. Soc., 56, 2327, 1934.
13. Computed (K.K.) from $CaSO_4$ - K_2SO_4 (Muller, Neues Jahrb. Mineral. Geol., Beilage Bd., 30, 1, 1910; Grahmann, Z. anorg. Chem., 81, 257, 1913).
14. Computed (K.K.) from CuO - Cu_2O (Roberts and Smyth, J. Am. Chem. Soc., 43, 1061, 1921).
15. Computed (K.K.) from Cu_2O - CuCl (Truthe. Z. anorg. Chem., 76, 161, 1912).
16. Bellati and Lussana (see under Heat capacity).
17. Computed (K.K.) from Cu_2S - CuCl (Truthe, Z. anorg. Chem., 76, 161, 1912), Cu_2S - Ni_2S_3 and Cu_2S - Ni_2S (Friedrich, Metall u. Erz, 11, 160, 1914).
18. For H.C. see under Heat capacity. The heat of fusion calculated from freezing point lowerings averages 63 j./g.
19. Barnes and Maass, Can. J. Research, 3, 205, 1930.
20. Umino, Sci. Repts. Tohoku Univ., 18, 104, 1929; Tammann and Bandel, Arch. Eisenhuttenw., 7, 371, 1934; Steinwehr and Schulze, Z. Metallkde, 27, 129, 1935. Awbery and Griffiths. Proc. Roy. Soc. A174, 1, 1940. The Curie point transformation is spread over a temperature interval with the peak at 755°. The data are not good enough to indicate definitely whether or not the heat capacity slope becomes infinite at this temperature. One integration yields the value 20 j./g. for the heat of transformation.

REFERENCES FOR TABLE I-B.4 (Continued)

21. Mean value computed (K.K.) from Fe - Au (Isaac and Tammann, Z. anorg. Chem., 55, 63, 1907), Fe - P (Konstantinow, Z. anorg. Chem. 66, 209, 1910) and Fe - Sb (Kurnakow and Konstantinow, Z. anorg. Chem., 58, 1, 1908).
22. Fricke and Klenk, Z. Electrochem., 41, 617, 1935.
23. Computed (R.W.G.) from forsterite-fayalite (Bowen and Schairer, Am. J. Sci., 29, 151, 1935). Vogt (Silikatschmelz, 1904) gives 356 ± ? j./g. for fayalite slag.
24. From scattered heat content measurements Δh is 222 j./g. Mean value computed (K.K.) from FeS - Cu_2S (Bornemann and Schreyer, Metallurgie, 6, 612, 1909), FeS - As_2S (Schoop, Metallurgie, 8, 737, 1905), FeS - Fe (Friedrich, Metallurgie, 7, 257, 1910), and FeS - PbS (Friedrich, Metallurgie, 4, 671, 1907) is 257 j./g. Mean taken as 240 j./g.
25. Computed, Maier, Rept. Invest. Bur. Mines, 1934.
26. Mean value computed (K.K.) from $PbSO_4$ - Li_2SO_4 (Calcagni and Marotta, Atti accad. Lincei, 21: II, 93, 1912), $PbSO_4$ - $PbMoO_4$ (Jaeger and Germs, Z. anorg. Chem., 119, 145, 1921).
27. Schwarz and Sturm, Ber. deut. chem. Ges., 47, 1730, 1914.
28. Mean computed (K.K.) from $MgCl_2$ - AgCl, - $CaCl_2$, -$CdCl_2$, -CuCl, -KCl, - $PbCl_2$, - $SnCl_2$, - $ZnCl_2$ (Menge, Z. anorg. Chem., 72, 162, 1911) and $MgCl_2$ - $BaCl_2$, - $SrCl_2$ (Sandonnini, Atti accad. Lincei, 21:II, 634, 1912).
29. Computed (K.K.) from MgF_2 - $Mg_3(PO_4)_2$ (Winter, Diss. Leipzig, 1913).
30. Computed from $MgSiO_3$ - $CaSiO_3$ (Allen and White, Am. J. Sci., 27, 1, 1909). Vogt (Silikatschmelz, 1904) gives 524 j./g.
31. Computed (R.W.G.) from forsterite-fayalite (Bowen and Schairer, Am. J. Sci., 29, 151, 1935). Vogt (Silikatschmelz, 1904) gives 544 ± ? j./g.
32. From differential heats of solution Mulert (Diss. Gottingen 1912) got 271 j./g. Mean value computed (K.K.) from $MnSiO_3$ - $MgSiO_3$ (Lebedew, Z. anorg. Chem., 70, 301, 1911) and $MnSiO_3$ - $MnTiO_3$ (Smolensky, Z. anorg. Chem., 73, 293, 1911) is 262 j./g.
33. Plato, Z. phys. Chem., 55, 721, 1906.
34. Value computed (R.W.G.) from diopside-leucite (Bowen and Schairer, Am. J. Sci., 18, 301, 1929) is 130 j./g. Mulert (Diss. Gottingen, 1912) gives 109 j./g. as the diffl. heat of soln. of glass and crystals at room temp.
35. Mulert, Diss. Gottingen, 1912.
36. Goranson and Kracek, J. Phys. Chem., 36, 913, 1932.
37. (a) and (b) From heat content data - see under Heat Capacities. (c) Troitzsch, Diss. Braunschweig, 1936. (d) Roth and Chall (Z. Electrochem., 34, 185, 1928) got 239 j./g. at 1470°C. Roth and Troitzsch (Arch. Eisenhuttenw., 6, 82, 1932/33) got 244 ± 7 j./g. from differential heats of solution. Mulert (Diss. Gottingen, 1912) got 154 j./g. as the differential heat of solution of amorphous SiO_2 and quartz at room tem. (3) This value is computed from (d and c). It is in substantial agreement with the value 159 j./g. computed from SiO_2 - TiO_2 (Bunting, Bur. Standards J. Research, 11, 719, 1933) and the mean of 131 j./g. obtained by Kracek (J. Am. Chem. Soc., 52, 1441, 1930) from the systems studied by him.

REFERENCES FOR TABLE I-B.4 (Continued)

38. Mean value computed (K.K.) from Ag_2S - AgCl (Sandonnini, Atti accad. Lincei, 21: I, 479, 1912), Ag_2S - FeS (Schoen, Metallurgie, 8, 737, 1905), and Ag_2S - ZnS (Friedrich, Metallurgie, 5, 114, 1908).
39. Roth and Bertram, Z. Electrochem., 35, 305, 1929. (Plato, Z. phys. Chem., 55, 721, 1906, gives a value of 517 j./g.)
40. Roth and Bertram (Z. Electrochem., 35, 305, 1929) data yield 331.4 j/g. Some other data yield a value slightly lower.
41. Computed from albite-anorthite (Bowen, Am. J. Sci., 35, 577, 1913).
42. Computed (R.W.G.) from carnegieite-anorthite (Bowen, Am. J. Sci., 33, 551, 1912) and carnegieite-kaliophilite (Bowen, Am. J. Sci., 43, 121, 1917).
43. Computed from Na_2SiO_3 - $Na_2Si_2O_5$ - $NaAlSiO_4$ (Tilley, Mineralog. petrog. Mitt., 43, 406, 1933).
44. See references under Heat Capacities. (a) Neumann, Z. phys. Chem., 171 A, 416, 1934. (b) Monval.
45. Computed (K.K.) from ZnS - Ag_2S (Friedrich, Metallurgie. 5, 114, 1908).

TABLE I-B.5

THERMAL CONDUCTIVITY OF ROCKS
(1 Atmosphere)

Rock	Tempera-ture °C.	Conductivity K Cal. Sec. cm. deg.	Watts Cm. deg.	Refer-ence
Granite	100	5.69×10^{-3}	23.8×10^{-3}	25
	500	3.80	15.9	
	30	7.2-5.0	30-21	10
(h^2 = .027 to .015)		(9.6-7.7)	(40-32)	27
Japan (h^2 = .014 to .006)	60	(6.0-2.9)	(25-12)	29
Aberdeenshire	30	8.1	34	20
Barre, Vermont	0	6.66	27.9	3
	50	6.25	26.2	
	100	5.90	24.7	
	200	5.50	23.0	
Westerly, R.I.	0	5.80	24.3	
	50	5.60	23.4	3
	100	5.42	22.7	
	200	5.12	21.4	
Dubbeldevlei Bore, S.A. (mean of 4 specimens)	25	6.8	28.4	42

TABLE I-B.5 (Continued)

Rock	Temperature °C.	Conductivity K Cal. Sec. cm. deg.	Watts Cm. deg.	Reference
Rockport, Mass.	0	8.4	35.1	3
(These values are probably too	50	7.8	32.6	
high; see reference)	100	7.2	30.1	
	200	6.5	27.0	
	300	5.9	24.5	
Granite gneiss		6.7-4.3	28-18	15
		5.1	22	10
Osogna Tessin (h^2 = .0156)		(8.2)	(34)	27
Pelham, Mass.	0	7.42	31	3
Parallel to foliation	100	6.58	27.5	
Perpendicular to foliation	0	5.17	21.6	
	100	4.82	20.1	
Granite schist		6.5	27.2	15
Quartz monzonite, California	0	7.56×10^{-3}	31.6×10^{-3}	3
	50	6.98	29.2	
	100	6.55	27.4	
	200	5.91	24.7	
Quartz-feldspar porphyry, Jacoba Bore, S.A. (mean of 5 specimens)	25	8.0	33	42
Tonalite, California	0	6.42	26.9	3
	100	5.90	24.7	
	200	5.52	23.1	

TABLE I-B.5 (Continued)

Rock	Temperature °C.	Conductivity K Cal. Sec. cm. deg.	Watts Cm. deg.	Reference
Syenite, Ontario	50	5.25	22.0	3
	100	5.08	21.3	
	200	4.99	20.9	
Syenite (h^2 = .0089)	20	(4.43)	(18.5)	27
Diorite, Japan (h^2 = .0123)	60?	(5.52)	(23.1)	29
Andesite, Japan	60?	(3.06)	(13)	29
(h^2 = .0124)	20	(7.1)	(30)	27
Trachyte	20	(6.0-4.1)	(25-17)	27
Trachyte (h^2 = .0096-.0103)	17-20	(5.5-6.0)	(23-25)	1
Leucitite, Mt. Vesuvius		4.9-4.0	21-17	15
Albitite, Pennsylvania	0	4.85	20.3	3
	100	4.80	20.1	
	200	4.70	19.7	
	300	4.55	19.0	
Anorthosite, Transvaal (bytownite)	0	4.43	18.5	3
	100	4.54	19.0	
	200	4.69	19.6	
Quebec (labradorite)	0	4.13	17.3	3
	100	4.20	17.6	
	200	4.34	18.2	
	300	4.50	18.8	

TABLE I-B.5 (Continued)

Rock	Temperature °C.	Conductivity K Cal. Sec. cm. deg.	Watts Cm. deg.	Reference
Montana (bytownite)	0	4.02	16.8	3
	100	4.10	17.2	
	200	4.27	17.9	
Diabase, Maryland	0	5.62×10^{-3}	23.5×10^{-3}	3
	100	5.35	22.4	
	200	5.37	22.5	
Diabase, Vinal Haven, Maine	0	5.23	21.9	3
	100	5.10	21.3	
	200	5.03	21.1	
	300	4.99	20.9	
Diabase, Westfield, Mass.	0	5.04	21.1	3
	100	5.01	21.0	
	200	5.01	21.0	
	300	5.03	21.1	
	400	5.06	21.2	
Diabasic basalt	30	4.04	16.9	4
	75	4.14	17.3	
"Trap," Calumet and Hecla	50	3.3	14	22
"Trap," Calumet and Hecla ($h^2 = .0075$)				11
"Trap"		5.8-3.5	24-15	10

TABLE I-B.5 (Continued)

Rock	Temperature °C.	Conductivity K Cal. Sec. cm. deg.	Watts Cm. deg.	Reference
Amygdaloidal lava (Ventersdorp lava, Jacoba Bore, S.A.)	25			
(mean of 4 specimens from depths between 312 and 1197 feet)		8.0	33.5	42
(mean of 5 specimens from depths between 3560 and 6732 feet)		6.9	28.9	42
Silicified dike rocks, Gerhardminnebron Bore	25	10.6-7.8	44-33	42
Basalt		5.3-4.3	22-18	25
(h^2 = .0083)		(5.3)	(22)	9
Japan (h^2 = .0068)	60?	(3.44)	(14)	29
Mittelrhein (h^2 = .0115)	20	(6.8)	(28)	27
Whin Sill		3.4	14.2	10
Gabbro, Japan (h^2 = .0132 - .0079)	60?	(7.2-4.3)	(30-18)	29
Sligachan	30	6.1	25.5	20
Skye	30	5.9	24.7	20
French Creek, Pa.	0	5.55	23.2	3
	100	5.25	22.0	
	200	5.13	21.5	
Mellen, Wisconsin	0	4.75×10^{-3}	19.9×10^{-3}	3
	100	4.75	19.9	
	200	4.76	19.9	
	300	4.78	20.0	
	400	4.81	20.1	

TABLE I-B.5 (Continued)

Rock	Temperature °C.	Conductivity K Cal. Sec. cm. deg.	Watts Cm. deg.	Reference
Bronzitite, Transvaal	0	11.1	46.3	3
	50	9.2	38.5	
	100	8.5	35.6	
	200	7.8	32.8	
	300	7.3	30.6	
Hypersthenite, Montana (bronzitite)	0	11.0	46	3
	100	9.3	39	
	200	8.7	36	
Dunite, Balsam Gap, N.C. (mean of 3 specimens)	0	12.4	52	3
	50	10.5	44	
	100	9.4	39	
	200	8.1	34	
Limestone, Japan (h^2 = .012-.005)		6 to 2	25 to 9	29
Solenhofen	30	5.24	21.9	4
	75	4.52	18.9	
Solenhofen	0	7.2	30.1	3
	100	5.5	23.1	
	200	4.8	20	
Pennsylvania (carbonaceous) Parallel to bed	0	8.2	34.5	3
	100	7.0	29.5	
	200	6.5	27.4	

TABLE I-B.5 (Continued)

Rock	Temperature °C.	Conductivity K Cal. Sec. cm. deg.	Watts Cm. deg.	Reference
Perpendicular to bed	0	6.1	25.5	3
	100	5.4	22.6	
	20	5.7	24	25
	350	3.2	13	
	0	5.4	23	5
	100	4.9	20	
"compact"		$8.1\text{-}4.8 \times 10^{-3}$	$34\text{-}20 \times 10^{-3}$	10
"porous"		5.3-2.6	22-11	10
Rankham, "impure, shelly"	17	6.28	26.3	41
"very hard, impure, shelly"	17	7.95	33.3	41
Limestone, ("Rama"), dolomitic, Longford Mills, Ontario	130	3.9	16	44
	181	3.8	16	
	268	3.7	15	
	377	3.2	13	
Limestone, dolomitic, Queenston, Ontario	123	3.4	14	44
	177	3.4	14	
	254	3.3	14	
	332	3.2	13	
Chalk		2.2	9.2	10

TABLE I-B.5 (Continued)

Rock	Temperature °C.	Conductivity K Cal. Sec. cm. deg.	Watts Cm. deg.	Reference
Marble (17 varieties)	30	7.7-5.0	32-21	23
Japan (h^2 = .0107)	60?	(5.5)	(23)	29
Carrara (h^2 = .0147)		(8.2)	(34)	27
h^2 = .0085, .0099, .0103)		(5.5-4.8)	(23-20)	9
Proctor, Vermont, Parallel to bed.	0	7.36	30.8	3
	100	6.0	24.9	
	200	5.2	21.7	
Perpendicular	0	7.2	30.1	
	100	5.7	23.9	
	200	5.1	21.1	
	0	7.2	29.9	6
	0	8.9-8.4	37-35	7
	30	7.1	29.8	17
		8.6-4.8	36-20	10
Marble (black), St. Albert, Ontario	124	3.7	16	44
	210	3.6	15	
	334	3.3	14	
Marble (white), Phillipsburg, Quebec.	125	3.4×10^{-3}	14×10^{-3}	44
	170	3.4	14	
	238	3.6	15	
	342	3.3	14	

TABLE I-B.5 (Continued)

Rock	Temperature °C.	Conductivity K Cal. Sec. cm. deg.	Conductivity K Watts Cm. deg.	Reference
Marble (brown), St. Marc des Carriers, Quebec	118	4.0	17	44
	196	3.6	15	
	245	3.3	14	
	360	2.7	11	
Dolomite	0	11.9	49.8	3
	100	9.3	38.9	
	200	8.0	33.3	
Japan (h^2 = .0085)	60?	(4.3)	(18)	29
Gerhardminnebron Bore (mean of 7 samples)	25	10.9	45.6	42
Quartzite, Japan (h^2 = .031 - .012)		(13-7)	(54-27)	29
Witwatersrand, from Gerhardminnebron Bore				
"feldspathic" (4 samples) 25°		10.7	43.8	42
"nonfeldspathic" (7 samples)		14.2	59.4	
"chloritoid-bearing" (6 samples)		15.6	65.4	
(mean of 17 samples)		13.6	56.9	
Quartzitic sandstone				
Parallel to bed	0	13.6	56.9	3
	100	10.6	44.4	
	200	9.0	31.7	
Perpendicular	0	13.1	54.8	
	100	10.3	43.1	
	200	8.7	36.2	

TABLE I-B.5 (Continued)

Rock	Temperature °C.	Conductivity K Cal. Sec. cm. deg.	Watts Cm. deg.	Reference
Quartzite	0	14.9	62.5	5
	100	12.5	52.3	
	20	9.3	39	19
Quartz schist	30	9.7	40.6	20
"Recrystallized sandstone"	30	11	46	20
"Hard sandstones"		10.8-6.2	45-26	10
Sandstone, Boreland Bore	17	10×10^{-3}	41.8×10^{-3}	41
"Soft sandstones"		4	17	10
Sandstone (h^2 = .0133, .0046)		(5, 2.4)	(21, 10)	9
"Greensand"		1.9	8	10
Amygdaloid, Calumet and Hecla	50	3.5	14.6	22
Conglomerate, Calumet and Hecla	50	5	21	22
Micaceous flagstone				
along cleavage		7	29	10
across cleavage		4.8	20	
Phyllite		7	29	15
Serpentine		7-6	29-25	9
(h^2 = .0131)		(7.2)	(30)	29
Soapstone		8.1	34	30
Slate, Wales				
Parallel to schistosity		6.7	28	10
Perpendicular to schistosity		3.9	17	

TABLE I-B.5 (Continued)

Rock	Temperature °C.	Conductivity K Cal. Sec. cm. deg.	Conductivity K Watts Cm. deg.	Reference
Slate,				
Pennsylvania, perpendicular to bedding	0	4.6	19.4	3
	100	4.2	17.7	
	200	4.1	17.1	
	0	5.2	21.6	5
	100	4.7	19.8	
	60	5.4	22.6	18
Slate, Madoc, Ontario	120	3.7	16	44
	188	3.9	16	
	304	3.5	15	
Shale		4.1-2.4	17-10	10
"very fine-grained"	17	1.4	5.9	41
"with sand"	17	2.8	11.7	41
Gerhardminnebron Bore				
from 6457 feet	25	6.6	27.6	42
from 4190 feet	25	4.4	18.4	
Blaes (shale), Boreland Bore	17	1.4×10^{-3}	5.9×10^{-3}	41
Fakes, Boreland Bore	17	3.25	13.5	41
Silty clay	17	3.7	15.4	41
"Gault" ($h^2 = .0037$)		2.7	11.3	46

Best Available Copy

TABLE I-B.6

EFFECT OF WETTING AND OF SIMPLE COMPRESSION ON THE THERMAL CONDUCTIVITY OF CERTAIN ROCKS

(Ref. 45)

K_o = conductivity of dry, uncompressed rock at 45°C., in 10^{-3} $\frac{\text{cal.}}{\text{cm. sec. deg.}}$

ΔK_w = increase of conductivity after soaking in water.

ΔK_p = increase of conductivity of dry rock on compressing to 10,000 $\frac{\text{lbs.}}{\text{in.}^2}$

ΔK_{wp} = increase of conductivity of wet rock on compressing to 10,000 $\frac{\text{lbs.}}{\text{in.}^2}$

K_m = maximum observed conductivity for compressed, wetted rock.

Rock	Bulk density	Porosity %	K_o	$\frac{\Delta K_w}{K_o}$ %	$\frac{\Delta K_p}{K_o}$ %	$\frac{\Delta K_{wp}}{K_o}$ %	K_m
Marble, Danby, Vt.	2.67	[illegible]	5.80	11	13	2	6.62
Limestone:							
Solenhofen	2.60	3.4	5.03	23	13		6.19
Bedford, Ind.	2.31	13.2	4.40	14	7	1	5.06
Bermuda	1.55	43	2.11		22		2.57
Sandstone:							
Doubling Gap, Pa.	2.64	0.5	9.20	13	18	4	10.9
Owl Canyon, Colo.	2.17	22	4.43	36	30	6	6.3
Shale, Sunderland, Mass.	2.67		3.87		10		4.25
Slate, Pennsylvania	2.76		4.32		4		4.50
Anorthosite	2.72		4.13		1		4.17
Gabbro, Wis.	2.87		4.51		2		[illegible]
[illegible]	2.83		1.67		4		

Preceding Page Blank

APPENDIX I-B

REFERENCES

1. Wuerker, Rudolph G., Annotated Tables of Strength and Elastic Properties of Rocks, University of Illinois, Pet. Branch, AIME, December 1956.

2. U.S. Bureau of Reclamation, Physical Properties of Some Typical Foundation Rocks, Concrete Laboratory Report SP-39, 1953.

3. U.S. Bureau of Reclamation, A Revised Method of Interpretation of Triaxial Compression Tests for the Determination of Shearing Strength, Structural Research Lab. Rep. SP-9, December 1946.

4. Balmer, G., A General Analytic Solution for Mohr's Envelope, Proceedings ASTM, vol. 52, 1952, p. 1260.

5. U.S. Bureau of Reclamation, Determination of Boundary Porosity by Triaxial Compression Tests of Concrete, Structural Research Laboratory Report SP-15, 1947.

6. Richart, F.E., Brandtzaeg, A., and Brown, R.L., A Study of the Failure of Concrete under Combined Compressive Stresses, Bull. 185, Engineering Experiment Station, University of Illinois, Urbana, Ill., 19[illegible].

7. U.S. Bureau of Reclamation, Triaxial Stress, Computation of Mohr's Envelope as a Curve, Structural Research Laboratory Report SP-23, 1949.

8. Obert, L., Windes, S.L., and Duvall, W.I., Standardized Tests for Determining the Physical Properties of Mine Rock, U.S. Bureau Mines, RI 3891, 1946.

9. Windes, S.L., Physical Properties of Mine Rock, Part I, U.S. Bureau Mines, RI 4459, 1949.

10. Windes, S.L., Physical Properties of Mine Rock, Part II, U.S. Bureau Mines, RI 4727, 1950.

11. U.S. Bureau of Reclamation, Tensile and Triaxial Compression Tests of Rock Cores from the Passageway to Penstock Tunnels N-4 at Boulder Dam, Laboratory Report No. Sp. 6, 1945.

12. U.S. Bureau of Reclamation, Laboratory Tests of Rock Cores from Monticello Dam Site, Solano Project, Concrete Laboratory Report No. C-746, 1954.

U.S. Bureau of Reclamation, Strength and Elastic Properties of Navajo Sandstone Core from Glen Canyon Dam Site---, Structural Laboratory Report No. SP-30, Part I, 1 Oct. 1951.

APPENDIX I-B

REFERENCES

14. U.S. Bureau of Reclamation, Strength and Elastic Properties of Black Canyon Dam Concrete and Rock, Boise Project, Idaho, Concrete Laboratory Report No. SP-36, 24 November 1952.

15. Blair, F.E., Physical Properties of Mine Rock, Part III, U.S. Bureau of Mines, RI 5130, 1955.

16. U.S. Bureau of Reclamation, Laboratory Tests on Orville Dam Foundation Rock Core--Feather River Project--State of California, Laboratory Report No. C-876, 1958.

17. U.S. Bureau of Reclamation, Tests on Foundation Rock Cores from Debenger Dam Site, Medford Project, Oregon, Laboratory Report No. C-186, 1942.

18. U.S. Bureau of Reclamation, Laboratory Tests of Foundation Rock Cores from Devil Canyon Dam Site--Devil Canyon Project, Alaska, Laboratory Report No. C-933, 1960.

19. U.S. Bureau of Reclamation, Strength and Elastic Properties of Black Canyon Dam Concrete and Rock, Boise Project, Idaho, Laboratory Report No. SP-36, 1952.

20. U.S. Bureau of Reclamation, Laboratory Tests of Rock Cores from the Foundation of Koyna Dam, India, Laboratory Report No. C-859, 1958.

21. U.S. Bureau of Reclamation, Laboratory Tests of Rock Cores from the Foundation of Dam BR-9, India, and Analysis of Load-Bearing Tests, Laboratory Report No. C-731, 1954.

22. U.S. Bureau of Reclamation, Tests of Foundation Cores for the Spillway at Sanford Dam--Canadian River Project, Texas, Laboratory Report No. C-718, 1953.

23. U.S. Bureau of Reclamation, Laboratory Tests of Rock Cores from Fremont Canyon Tunnel Area--Glendo Unit--Missouri River Basin Project, Wyoming, Laboratory Report No. C-945, 1960.

24. U.S. Bureau of Reclamation, Laboratory Tests of Rock Cores from Bridge Canyon Dam Site,--Bridge Canyon Project, Arizona, Laboratory Report No. C-786, 1955.

25. Chan, Samuel Shu Mou, Physical Property Tests of Rock, Centrifugal Tests and the Design of Mine Openings, Unpublished master's thesis, School of Mines and Metallurgy, University of Missouri, 1960.

26. U.S. Bureau of Reclamation, Laboratory Tests of Foundation Rock Cores from Bhumiphol Dam (formerly Yanhee), Yanhee Project, Thailand, Laboratory Report No. C-771A, 1959.

APPENDIX I-B

REFERENCES

27. U.S. Bureau of Reclamation, Tests of Rock Cores from Shasta Dam Foundation, Laboratory Report No. C-94, 1940.

28. U.S. Bureau of Reclamation, Strength and Elastic Properties of Navajo Sandstone Core from Glen Canyon Dam Site, Mile 15--Colorado River Storage Project, Arizona, Laboratory Report No. SP-30, Part I, 1951.

29. Goranson, Roy W., Handbook of Physical Constants, Section 16: Heat Capacity; Heat of Fusion, G.S.A. Special Papers Number 36, January 31, 1942.

30. Birch, Francis, Handbook of Physical Constants, Section 17: Thermal Conductivity and Diffusivity, G.S.A. Special Papers Number 36, January 31, 1942.

31. Wuerker, R.G., The Status of Testing Strength of Rocks, Trans. AIME, TP 3556A, Mining Engineering, Nov. 1953, 1108/13.

32. Geological Society of America, Handbook of Physical Constants, Special Paper 36, 1942.

33. Handin, J.W., An Application of High Pressure in Geophysics, Experimental Rock Deformation, Trans. ASME, April 1953, p. 315.

34. Griggs, D.T., Deformation of Rocks under High Confining Pressure, Jour. of Geology, vol. 44, p. 541-577.

35. Griggs, D.T., Miller, W.B., Deformation of Yule Marble, Part I, Compression and Extension Experiments on Dry Yule Marble at 10,000 atm Confining Pressure, Room Temperature, Bull. Geolog. Soc. Am. vol. 62, 1951, p. 853-862.

36. Handin, J.W., and Griggs, D.T., Deformation of Yule Marble, Part II, Predicted Fabric Changes, Bull. Geolog. Soc. Am., vol. 62, 1951, p. 863-885.

37. Turner, F.J., and Ch'ih, C.S., Deformation of Yule Marble, Part III, Observed Fabric Changes due to Deformation at 10,000 atm. Confining, Pressure, Room Temperature, Dry, Bull. Geolog. Soc. Am., vol. 62, 1951, p. 887-905.

38. Phillips, D.W., Tectonics of Mining, Part II, Colliery Engineering, vol. 281, August 1948.

39. Mielenz, R.C., Petrography and Engineering Properties of Igneous Rocks, U.S. Bureau of Reclamation.

40. Stoecke, K., Die Pruefung der Natuerlichen Bausteine (Testing of Building Stones) in Handbuch der Werkstoff pruefung (E. Siebel, Editor), vol. 3.

APPENDIX I-B

REFERENCES

41. Wuerker, R.G., Measuring the Tensile Strength of Rocks, Trans. AIME TN 253-A, Mining Engineering, vol. 157, February, 1955.

42. How to Determine Crusher and Grinding Mill Sizes Accurately, Allis-Chalmers Manufacturing Co., Milwaukee, Wis. A-C Bull. 07 R 7995A.

43. Gilbert, B.W., Shore Scleroscope Hardness Tests Made on Moh's Scale Minerals from Talc to Quartz, Inclusive, Dept. of Mining and Metallurgical Engineering, University of Illinois, Urbana, Ill. 1954.

44. Gyss, E.E. and Davis, E., Hardness and Toughness of Rocks, Mining and Metallurgy, vol. 8, 1927, p. 261.

45. Tertsch, H., Die Festigheitserscheinungen der Kristalle, (Strength Properties of Crystals) Springer Verlag, Vienna, vol. 182, 1949.

46. Griffith, J.H., Physical Properties of Typical American Rocks, Iowa Engineering Experiment Station, Bull. 161, 1937.

47. Scott, F.L., Hard Rock Rotary Drilling, The Oil Weekly, 7 October 1946.

48. Kesler, Clyde, E., Personal communication.

49. Smith, F.C. and Brown, R.Q., The Shearing Strength of Cement Mortar, University of Washington, Engineering Exp. Station, Bull. 106, 1941.

50. Hall, H.N., Compressibility of Reservoir Rock, Trans. AIME, vol. 198, 1953, p. 309.

51. Jones, R., Testing of Concrete by Ultrasonic-Pulse Technique, Highway Research Board, Proc. 32nd Annual Meeting, 1953, p. 258.

52. Scott, P.P., and Bearden, W.G., and Howard, G.C., Rock Rupture as Affected by Fluid Properties, Trans. AIME, vol. 198, III, 1953.

53. Fatt, I., and Davis, D.H., Reduction in Permeability with Overburden Pressure, Jour. Pet. Tech., vol. 147, December 1952, p. 16.

54. Fatt, I., The Effect of Overburden Pressure on Relative Permeability, Journ. Pet. Tech., vol. 194, October 1953, p. 15.

55. Bays, G.S., and Taylor F., With Increasing Depths -- Comes What?, Oil Weekly, 9 May 1938.

56. Payne, L.L., and Chippendale, W., Hard Rock Drilling, The Drilling Contractor, June 1953, p. 58.

APPENDIX I-B

REFERENCES

57. Tentative Method of Test for Fundamental Transverse and Torsional Frequencies of Concrete Specimens, ASTM Standard C 215-52 T.

58. Kesler, C.E., and Chang, T.S., Review of Sonic Methods for the Determination of Mechanical Properties of Solid Materials, University of Illinois, Department of Theoretical and Applied Mechanics, Report 54.

59. Kesler, C.E., and Higuchi, Y., Determination of Compressive Strength of Concrete by Using Its Sonic Properties, Proc. ASTM, vol. 53, 1953, p. 1044.

60. Kesler, C.E., and Chang, T.S., Utilization of Data Obtained in Sonic Tests of Plain Concrete, University of Illinois, Department of Theoretical and Applied Mechanics, Report 77.

61. Obert, L., and Duvall, W.I., Discussion of Dynamic Methods of Testing Concrete, with Suggestions for Standardization, Proc. ASTM, vol. 41, 1941, p. 1053.

62. Born, W.T., The Attenuation Constant of Earth Materials, Geophysics, vol. 6, 1941, p. 132.

63. Wuerker, R.G., Testing of Roof Bolting Systems Installed in Concrete Beams, Trans. AIME, TP 3554-A, Mining Engineering, June 1953, p. 606.

64. Shepherd, R., Physical Properties and Drillability of Mine Rock, Colliery Engineering, (Dec. 1950), p. 468; (Jan. 1951), p. 28; (Feb. 1951), p. 61; (March 1951), p. 121.

65. Head, Jr., Albert L., A Drillability Classification of Geological Formations, World Oil, Drilling Section, October 1951, p. 125.

66. Hartman, H.L., and Pfleider, E.P., Chapter: Formation of Cuttings in Exhaust Dust Control in Dry Percussion Drilling, Trans. AIME, TP 4005-A.

67. Shepherd, B.F., Drilling--The Problem--What-Why-How?, Mining Congress Jour., November 1954.

68. Goodrich, R.K., Rock Classification Tests, Unpublished Manuscript, Joy Manufacturing Co., Claremont, N. H.

69. Koch, W., Die Pruefung der Bohrbarkeit von Gesteinen, (Testing the Drillability of Rock) in: Mitteilungen der Forschungsstelle fuer Bohr-und Schiesstechnik, vol. 1, 11, Bergakademie Clausthal.

APPENDIX I-B

REFERENCES

70. Dunlap, G.E., and Fellows, J.A., Ferrous Castings for Abrasion Resistance, American Brake Shoe Co., 230 Park Ave., New York.

71. Bond, F.C., Crushing and Grinding Calculations, Allis-Chalmers Manufacturing Co., Milwaukee, Wis.

72. Pfleider, E.P., and Blake, R.L., Research on the Cutting Action of the Diamond Drill Bit, Trans. AIME, February 1953, p. 187.

73. Fraenkel, K.H., Editor, Manual on Rock Blasting, AB Atlas Diesel, Stockholm.

74. Toughness of Rock, ASTM Designation D3-18, ASTM Standards, Part II, 1942, p. 427.

75. Goldbeck, A.T., and Jackson, F.H., Physical Tests of Rock for Road Building, Office of Public Roads, Bull. 44, 1912.

76. Woolf, D.O., The Results of Physical Tests of Road-Building Rock, U.S. Dept. of Agriculture, Misc. Publ. 76, 1930.

77. Bresler, B., and Pister, K.S., Failure of Plain Concrete under Combined Stresses, Separate Publ. 674, ASCE, Proceedings, April, 1955.

78. Lacabanne, W.D., and Pfleider, E.P., Rotary Percussion Blast-hole Machine May Revolutionize Drilling, Mining Engineering, vol. 7, Sept. 1955, p. 850.

79. Kochanowsky, P.J., Blasting Research Leads to New Theories and Reductions in Blasting Costs, Trans. AIME, TP 4045-A, Mining Engineering Sept. 1955, p. 861.

80. Brodrhauer, R.G., Strength Characteristics of Rock Samples under Hydrostatic Pressure, Master Thesis, The Rice Institute, Houston, Texas, April 1955.

81. Murray, A.S., and Cunningham, R.A., Effect of Mud Column Pressure on Drilling Rates, Trans. AIME, TP 4166, Jour. Pet. Tech., Nov. 1955, p. 196

82. Pennington, J.V., Rock Failure in Percussion, The Pet. Engineer, May 1954, vol. 26, 5 B-76.

83. Stumm, J.J., What is this Sonic Drill?, The Pet. Engineer, October 1954, vol. 26, 10, 5-52.

84. McCutchen, W.R., The Behavior of Rocks and Rock Masses in Relation to Military Geology, Colorado School of Mines Quarterly, January 1949, vol. 44, p. 1.

APPENDIX I-B

REFERENCES

85. Robertson, E.C., Experimental Study of the Strength of Rocks, Bull. Geol. Soc. Am., October 1955, vol. 66, p. 1275-1314.

86. Harrison, E., Kieschnik, W.F., Jr., and McGuire, W.J., The Mechanics of Fracture Induction and Extension, Trans. AIME, vol. 201, TP 3916.

87. Willmore, T.A., Degenkolb, R.S., Herron, R.H., and Allen, A.W., Application of Sonic Moduli of Elasticity and Rigidity to Testing of Heavy Refractories, Jour. Am. Ceramic Soc., vol. 37, October 1954, p. 10, 445-457.

88. Felts, L.L., Clark, G. B., and Yancik, J. J., A Laboratory Method for Determining the Thermodynamic Efficiency of High Explosives, Trans. AIME, TP 4213-A, Mining Engineering, March 1956, p. 318.

89. Chang, T.S., and Kesler, C.E., Correlation of Sonic Properties of Concrete with Creep and Relaxation, University of Illinois, Department of Theoretical and Applied Mechanics, Report 94.

90. Kesler, C.E., and Siess, C.P., Static and Fatigue Strength of Concrete, ASTM Preprint 96-a.

91. Hubbert, M., and Willis, D.G., Mechanics of Hydraulic Fracturing, Trans. AIME, Preprint 686-G.

APPENDIX III-A

CASE HISTORIES OF UNDERGROUND STRUCTURE STABILITY

The following are given as examples of typical case histories of underground rock structure stability which are tabulated in Chapter III.

Open Stopes with Pillars

Southeast Missouri District.[1]

The disseminated ores of southeast Missouri are found at various horizons in the Bonne Terre dolomitic limestone, which is of Cambrian age. (See Figure III-A.1). The lower part of this formation consists of a transition zone of alternating, thin-bedded, and sometimes cross-bedded layers of limestone, shale and sandstone inter-bedded with thin layers of "chloritic" material.

Ore occurs at various horizons throughout the 365 feet thickness of the formation, but most of it is confined to the lower hundred feet. Shale layers, usually thin, are often impregnated with galena while the limestone beds above and below are only lightly mineralized. As a rule the richest ore is in rock which is soft and somewhat decomposed.

The ore body itself is composed of rich layers of galena separated by bands of lean ore. That of the middle horizon is harder and breaks into larger blocks than that in the upper and lower horizons due to the presence of marked bedding and jointing. There is considerable variation in the strength of individual beds of the formation, but in general they are strong and will support themselves over wide spans. Some of the spans are 100 feet between pillars or between pillars and marginal walls. In areas of weakness it is necessary to limit spans to 17 or 18 feet. Upon exposure to air, shaly layers tend to slack, and together with vertical channels, slips and joints constitute sources of weakness in both the ore and roofs of the stopes. The presence of "water channels" requires great care in mining operations, both because they weaken roofs and because sometimes they are active water courses.

Jonathan Limestone Mine.[2,3]

The Bureau of Mines conducted an investigation of the behavior of roof strata under natural conditions of mining and with the roof strata artificially loaded with compressed air above the immediate roof layer in the Jonathan mine. In each case the roof was considered to be composed of individual layers vertical sections of which could be treated as simple or multiple layered beams. Stress distribution in this type of structure is given in Chapter VIII. Only the geological structure which permitted a successful study of the applicability of beam theory to horizontal mine roofs is given here.

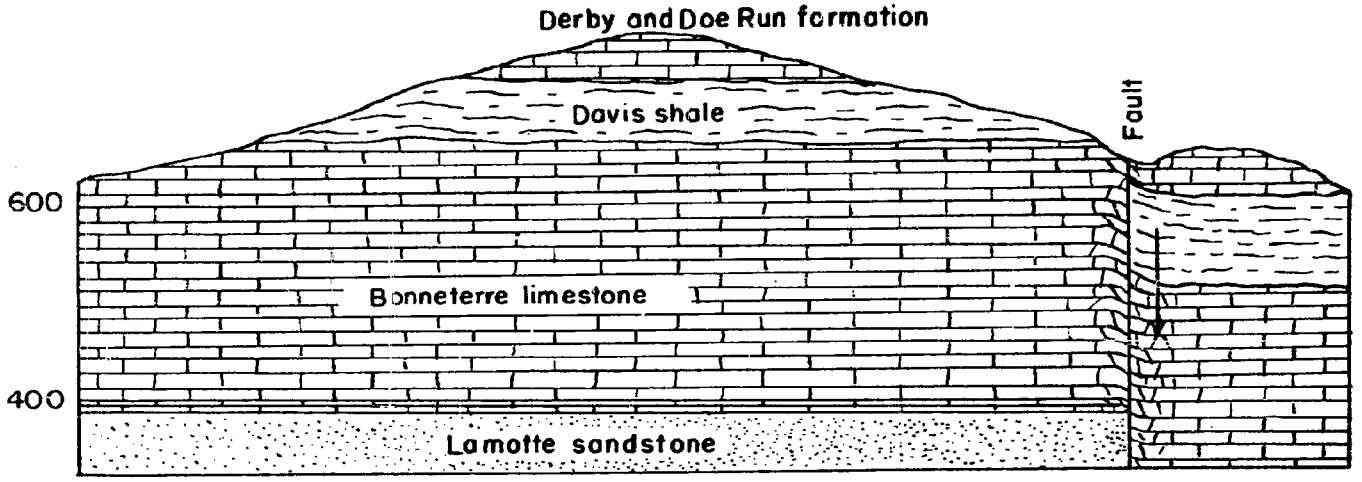


Figure III-A.1. Generalized section of geologic structure in lead mines in Southeast Missouri, St. Joseph Lead Company.

The first part of the investigation included: (1) a study of geology and stratigraphy of the formations; (2) evaluation of physical properties of the roof rock; (3) strata exploration for a suitable roof horizon; (4) computation of possible roof spans; and (5) initial investigations to check the applicability of calculations.

The Jonathan mine is in the flat lying Maxville limestone, which is about 41 feet thick and is overlain with sandstone and shales. The lower half is described as clayey limestone, while the upper half is stratified in somewhat continuous layers 2 to 18 inches thick which increase in calcium content toward the top. Overlying sediments are 50 to 300 feet thick of black shale, gray shale, and thin coal lenses which lie on an erosion surface. "Washes" and "cutters" in the old erosion surface have been exposed in open pit mines. The shale washes (filled with shale) form a V-shaped troughs which vary in depth from a few inches to 4 feet. Cutters, about 1 inch thick feather out from the bottom of the washes and are filled with shale and/or calcite. Vertical NE-SW joints cut the limestone at about 10 foot intervals and are filled with calcite. Uncemented or closely cemented joints are uncommon, while no faults, fissures, local rolls or voids have been encountered.

The mine roof was diamond drilled to obtain more specific information concerning thickness of beds, physical properties of rock and structure of the roof. The limestone was found to be quite uniform and cored in lengths from 2 to 18 inches, broken along thin (hairline) seams of shale. The sediments over the limestone were drilled from 20 to 25 feet, which was found to consist of layers of varying thickness of black shale and gray shale with lenses of coal up to 6 inches in thickness.

The pertinent physical properties are given in Table III-A.1. These were quite consistent for the limestone but considerably more variable for the shale.

Table III-A.1
Physical properties of limestone and shale (holes 1, 2, and 3)

	Average value	Standard deviation, percent	Number of Observations
Limestone:			
Apparent specific gravity.....	2.69	0.7	16
Modulus of rupture.....p.s.i.	2,600	30	17
Modulus of elasticity..... do.	10.4×10^6	4	11
Lower black shale:			
Apparent specific gravity.....	2.[illegible]	0.7	17
Modulus of rupture..... p.s.i.	2[illegible]	48	26
Modulus of elasticity..... do.	1.4×10^6	--	1

Cost studies indicated a preferred roof span of 30 feet, while the fact that the higher grade limestone was near the top of the bed dictated a minimum thickness of limestone roof. Roof spans of 18 to 20 feet had been employed, with 28 inches to 12 feet of limestone as roof. Roof partings were formed at thin, shale-filled partings, most of which showed some bonding or cohesive strength. Closely controlled drilling and blasting were required to prevent overbreak into the roof. Occasional shale washes were encountered at the shale horizon 3 feet below the contact and these required guniting and bolting.

Studies beyond physical property tests were made of the shale by opening up two areas of shale roof at the limestone-shale contact. The roof in Area 1 was black shale, while that in Area 2 consisted of 14 inches of black shale, 12 to 18 inches of coal and then more shale. The exposed areas were approximately 20 by 60 feet, both being bolted on 4 foot centers. A shale wash was exposed in Area 1 and several cracks in Area 2. Both areas showed air slacking with small pieces falling in 3 weeks. One year later a block of shale and coal in Area 2 failed, forming an arch. Shale which had as little as 2 inches of limestone cover showed no signs of failure.

It was therefore concluded that (1) a roof could be formed at any shale stringer, (2) joints in limestone did not materially affect roof behavior, (3) bolting and guniting would be required on shale washes, and (4) shale would not form a satisfactory roof.

The purposes of the roof span studies were (1) to observe the behavior of shale stringer, joints, etc., at spans greater than 20 feet, (2) evaluate physical properties of roof in place, (3) study time deterioration of roof, and (4) determine whether shale would load the limestone. Room widths and beam (roof strata) depths were calculated from appropriate beam formulae, bridging of stringers was considered good and the experimental room was located at least three pillar widths from adjoining openings.

The experimental room was opened from a pilot drift and a 6 foot raise was driven to check the roof stratigraphy. All defects (mostly vertical) were found to be parallel to the shorter dimension of the room (see Figure III-A.2). The roof was core drilled at 5 points to 20 feet and at 4 points in the raise horizontally to a depth of 10 feet. The logs of the roof holes are shown in Figure III-A.3. The roof strata along the center line of the room were uniform; limestone was 28 to 30 inches thick; the black shale, coal, and gray shale were of variable thickness, the black shale coring well. A number of lateral stringers parallel to the bedding were noted, the bond across the stringers varying in strength. The physical properties of limestone and shale parallel to the bedding are given in Table III-A.2. The modulus of rupture values of horizontal cores was about 1.7 times that of vertical cores.

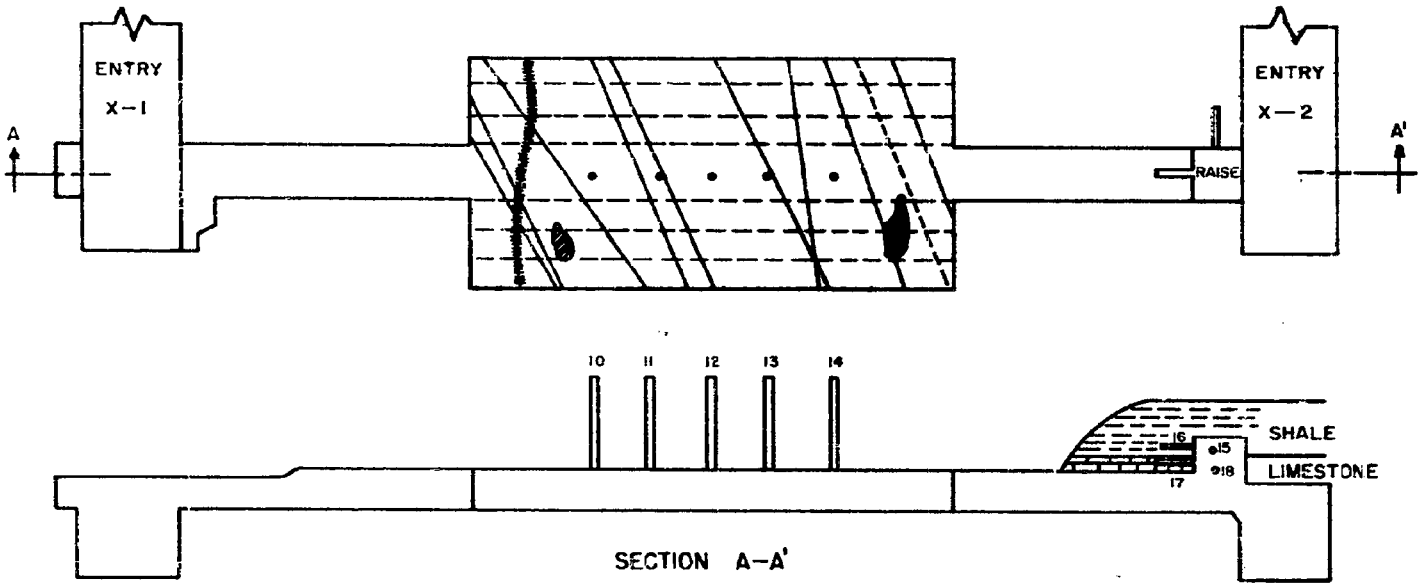


Figure III-A.2. Plan and section of experimental room, Jonathan Mine.

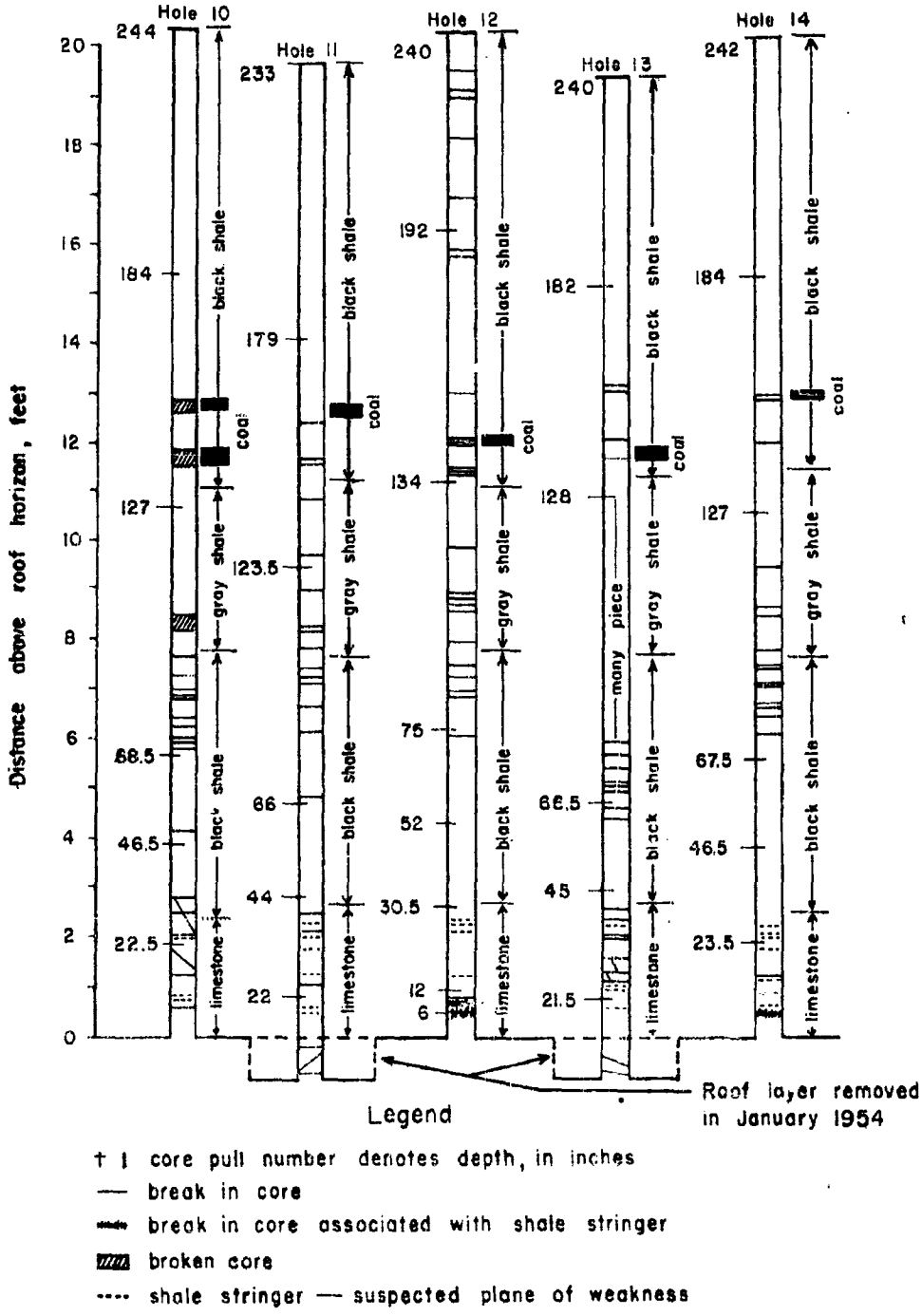


Figure III-A.3. Logs of drill holes into roof, Jonathan Mine.

Table III-A.2
Physical properties of limestone and shale parallel to bedding (holes 15, 16, 17, and 18)

	Average value	Standard deviation, percent	Number of Observations
Shale:			
Specific gravity.....	2.67	2.5	32
Modulus of rupture.....p.s.i.	1,260	22	6
Tensile strength.....do.	342	28	4
Limestone:			
Specific gravity.....	2.80	1.5	36
Modulus of rupture.....p.s.i.	4,668	8.1	8
Tensile strength.....do.	1,088	23	4
Modulus of elasticity.....do.	10.0×10^6	8	6

Both roof sag measurements and microseismic noises were recorded. Threaded rods were anchored in the roof strata (See Chapter XI). The room was widened from 10 to 40 feet in 10 foot increments, sagged with each increase in width and finally separated at 6 inches and 2 feet 4 inches in the limestone and at 8 and 12 feet in the shale. It was concluded that the limestone beds were gravity loaded and that the shale was self-supporting. The separated 6 inch layer was not easily removed.

In a subsequent phase of the investigation compressed air was injected in the separation between the limestone and the shale. Failure stress agreed with that calculated by appropriate beam equations and that measured by modulus of rupture tests.

Oil Shale, Rifle, Colorado

Introduction. As part of a program of development of the oil reserves in the oil shales of Colorado, the Bureau of Mines has conducted extensive tests of the behavior of the strata in roofs and pillars of a mine excavated in some of the richer of the oil shales.[4] A study of geology and structure of the deposit indicated open stoping (room and pillar), the design problem being the calculation of optimum safe roof span, pillar size and consequent extraction ratio. These were determined from the geologic structure of the deposit, physical properties of the oil shale, and the magnitude and distribution of stresses in the rock resulting from excavation. Both theoretical calculations and model stress studies were employed. Model tests were checked with full scale tests to measure roof sag, separations in roof strata and rock failure. Roof dimensions were increased from 50 x 100 feet to 80 x 200 feet with a period of 14 months for measurement of sag.

Roof sag was greater than that predicted by theory with some anomolous behavior. No significant separations were observed in the 8 foot thick roof layer. Failures were predicted by the microseismic method; and numeroud planes of weakness appeared at different elevations in the roof. While the safe extraction ratio was computed to be 82 percent, 75 percent was used with 60 foot roof spans and 60 foot square pillars.

Geology. The oil bearing "shales" are about 500 feet thick. The Mahogony bed is one of possible economic importance. (See Figure III-A.4). The shales contain "kerogen", but no free oil or carbon. A room mined 59 feet in diameter had stood for 25 years with no failures. Exploratory drilling (1945-46) in three holes showed that the oil-shale formations are persistent, of uniform thickness and dip approximately 4° to the north. A 6 inch iron stained layer of tuff was used as a stratigraphic reference (Mahogony marker). No faults, fissures or significant jointing were disclosed by the drilling. The rock is relatively tough, strong, fine bedded, and the bedding is influenced more by the organic content of the rock than by changes in physical properties, partings or planes of weakness.

Cores obtained from drilling were employed to find a suitable roof rock; a small raise was made for the same purpose; and an adit was examined for pillar structure. Partings or weak beds, such as volcanic ash, were carefully noted. Blasting in early room development disclosed a parting near the top of the Mahogony ledge, which was selected as the roof horizon. The cores indicated a solid 8 foot layer above this plane, and then a shale layer 44 to 54 feet thick, capped by thick layers to the surface forming a total overburden of 300 to 700 feet. A series of nearly parallel fractures was noted in possible pillar rock, the distance between them being 5 to 40 feet, their dip being 75° to 90°. Some were discontinuous while others penetrated into higher elevations with seeping water.

There was considerable fragmentation to a distance of 100 feet in from the surface, probably caused by weathering. Consequently all haulage adits were driven 200 feet beyond the outcrop and beyond the weathered zone.

Physical Properties of Oil Shale. Physical properties of the oil shale were investigated by the Bureau of Mines and Columbia University. The results of tests from the laboratories are in general agreement and are given in Tables III-A.3, III-A.4, III-A.5, III-A.6, III-A.7, and III-A.8. Variations are attributed to differences in methods of testing, and the fact that samples were from different locations.

Oil shale is moderately strong, the modulus of rupture averaging 4000 psi and the compressive strength 16000 psi. The modulus of rupture was higher for the roof than for pillars, also being higher in samples cut parallel to the bedding. The higher the "oil" content of the shale, the weaker it is. Moisture and time deterioration tests indicated no significant changes in properties by wetting and drying or by heating.

Safe roof span estimates were made considering the 8 foot roof bed as a gravity loaded beam or plate. Calculations were based on the elastic theory and model tests in a centrifuge.

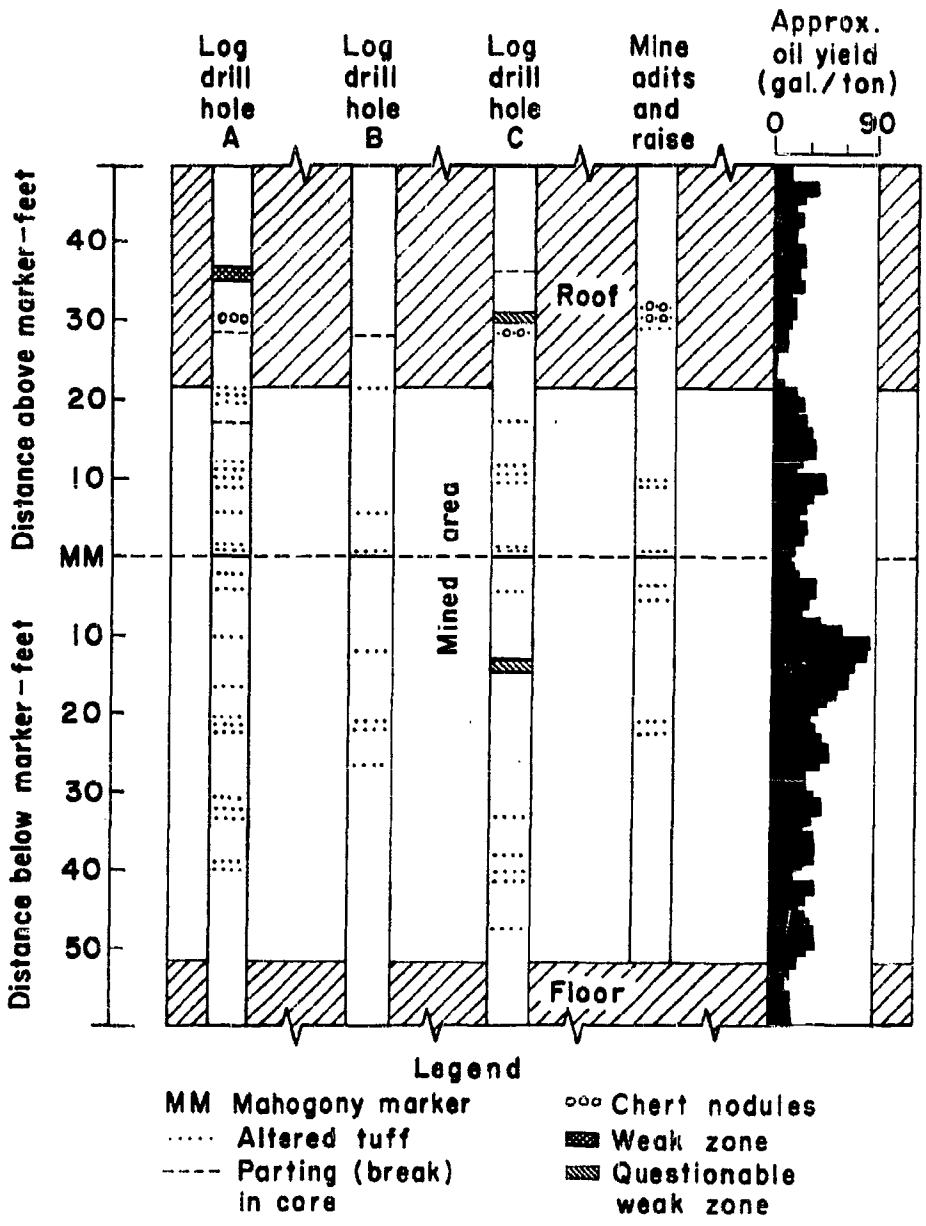


Figure III-A.4. Log of cores and mine opening, Oil Shale Mine[4].

Table III-A.3
Physical properties of oil-shale samples from roof cored parallel to bedding, College Park, Md.

	Average Value	Standard deviation, percent	Number of Observations
Apparent specific gravity.....	2.18	2.0	4
Modulus of rupture.....lb./sq.in.[1]	3,000	18	6
Elastic constants:			
a) Young's Modulus..lb./sq.in..	3.1×10^6	15	4
b) Modulus of rigidity.. ...do.	0.98×10^6	16	4
c) Specific damping capacity...	0.18[2]	10	4
d) Apparent Poisson's ratio....	0.58	12	4
e) Velocity of sound...ft./sec.	10,200	6.5	4

1 Load applied perpendicular to strata.
2 Estimate.

Table III-A.4
Physical properties of oil-shale samples from roof cored perpendicular to bedding, College Park, Md.

	Average Value	Standard deviation, percent	Number of Observations
Apparent specific gravity.....	2.25	--	2
Compressive strength....lb./sq.in.[1]	16,600	19	18
Modulus of rupture.....lb./sq.in.[1]	360	51	6
Elastic constants:			
a) Young's modulus..lb./sq.in.	1.8×10^6	--	2
b) Modulus of rigidity.....do.	1.0×10^6	--	2
c) Specific damping capacity..	0.22	--	2
d) Apparent Poisson's ratio...	0.10	--	2
e) Velocity of sound..ft./sec.	7,750	--	2
Hardness:			
a) Schleroscope.schleroscope units	56	8	85
b) Abrasive.rev.sq.in.lo-3/lb.....	9.8	14	12
Impact toughness.....	3.7	34	17

1 Load applied parallel to bedding.

Table III-A.5
Compressive strength of oil-shale samples from roof and pillar specimens cut perpendicular to bedding, Columbia University

Distance from Mahogany marker, feet	Bed designation[1]	Number of specimens tested	Compressive strength, p.s.i.	Standard deviation, percent
3166 above.....	Roof	2	15,380	--
21.5-26.8 above...	do.	2	14,890	--
20 above.....	do.	3	12,430	1.0
18.5 above.....	A	1	17,100	--
10 above.....	B	2	15,000	--
4.2 above.....	C	1	17,100	--
2.5 below.....	D	1	19,000	--
4.5 below.....	D	2	12,650	--
7 below.....	D	2	11,730	--
10 below.....	D	1	10,700	--
12.5 below.....	E	1	12,520	--
14 below.....	E	3	8,280	5.0
14.6 below.....	E	5	7,350	2.6
15.5 below.....	F	3	11,910	.4
17 below.....	F	1	9,190	--
17.5 below.....	F	1	12,080	--
18.5 below.....	F	8	8,160	3.4
20 below.....	G	1	14,480	--
20.5 below.....	G	1	14,470	--
23 below.....	G	2	10,250	--
23 below.....	G	2	8,600	--
26.6 below.....	G	2	14,090	--
27 below.....	G	3	12,960	7.2
31 below.....	H	3	8,560	5.7
33 below.....	H	1	13,600	--
37 below.....	H	1	15,390	--
39.5 below.....	H	2	17,280	--
46.5 below.....	I	2	12,700	--

[1] In accordance with their oil content and caking tendency, the minable oil-shale beds were grouped into 10-lettered beds.

Table III-A.6
Shear strengths of oil-shale samples from roof, Columbia University

Direction of shearing force to the bedding planes	Shear strength lb./sq.in.	Number of samples tested	Standard deviation, percent
Perpendicular.....	3,490	5	4.9
Do.....	4,640	5	3.1
Parallel.....	1,770	5	10.5
Perpendicular.....	3,560	5	5.1
Do.....	3,145	5	6.0
Parallel.....	890	5	8.3
Perpendicular.....	3,205	5	5.2
Parallel.....	920	5	9.1

Table III-A.7
Modulus of rupture of oil-shale samples from roof beams cut perpendicular to bedding, Columbia University

Depth of beam, inches	Span, inches	Ratio of span to depth	Modulus of rupture, lb./sq.in.
.2256	3.0	13.32	6,590
.1775	3.5	19.72	4,320
.2440	6.0	24.6	4,730
.1722	6.0	34.84	4,240
.1499	6.0	40	4,070
.1198	6.0	50.1	3,370
.1141	6.0	52.6	3,350

Table III-A.8
Modulus of elasticity of oil-shale samples from roof and pillar, Columbia University

Bed Designation	Stress limits for constant E, lb./sq.in.	Modulus of elasticity (E), lb./sq.in.
Roof.....	0-3000	1.13×10^6
Do.....	0-3000	3.56×10^6
Do.....	0-3000	3.54×10^6
Do.....	0-8500	1.09×10^6
G.....	0-5000	2.66×10^6
G.....	0-2000	$.513 \times 10^6$
E.....	0-2400	$.588 \times 10^6$

Limestone Mine.[5]

A limestone mine in western Missouri is of interest because of the roof stability requirements in supporting roads and pipelines which lie over the mine.

The geologic column of rocks in the area is given in Figure III-A.5. Limestone is mined from the Bethany Falls bed which is overlain with 150-180 feet of interbedded limestones and shales. Some of the beds of limestone are fairly competent and would be reasonably strong if supported by other limestone. However, the high percentage of shale results in a weak structure which has caved three times in a period of ten years. There is no significant faulting in the mine and a single joint system predominates, with little evidence of solution activity or alteration.

In haulage ways in the mine only the lower 15 feet of the Bethany Falls limestone is mined, leaving a roof which is fairly stable. Where the formation is mined to a height of 30 feet, however, the limestone roof is less competent and the top 12 feet of the pillars are formed of shale, shaly lime, and thin beds of limestone which are subject to spalling on exposure to atmosphere. This results in the formation of pillars of the shape shown in Figure III-A.6, which produces a high percentage reduction of effective support area of the pillars.

A combination of jointing, pillar spalling, shale and limestone roof has contributed to roof failure at the juncture of rooms where larger than average roof spans are created. Safe roof spans are in the range of about 30 to 40 feet. Actual roof spans in the neighborhood of 75 feet result from mining and spalling.

Sublevel Stoping

Horne Mine.[6,7,8,9]

The Horne Mine is found in an "island" of rhyolite flows, tuffs, and agglomerates, surrounded on three sides by andesites, and cut off on the north side by the Horne Creek Fault. The ore bodies are believed to have been formed as replacement deposits in shear and breccia zones in these rocks. The existence of the highly complex and disturbed structure was one of the basic controls of ore deposition. The greater part of the ore was deposited in or near the intersection of two systems of shearing.

Remarkable features of the deposit are (1) the massive character of the sulphide ore with its lack of gangue minerals, (2) the relatively small amounts of included rock, (3) the sharply defined contacts with the wall rocks, and (4) in general the presence of a score of massive sulphide lenses and their accompanying siliceous bodies all within an area less than 1,800 feet square.

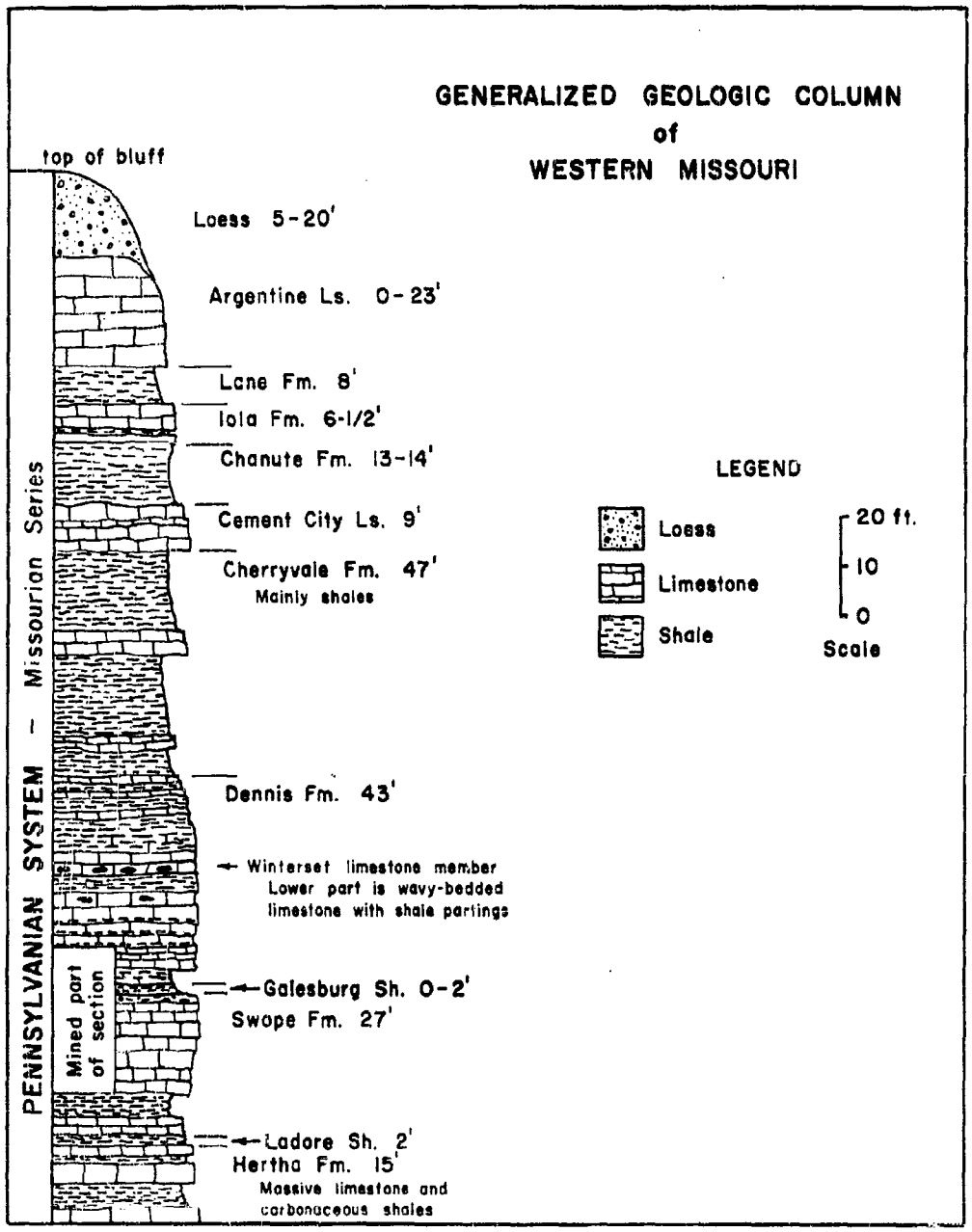


Figure III-A.5. Generalized geologic column of western Missouri.

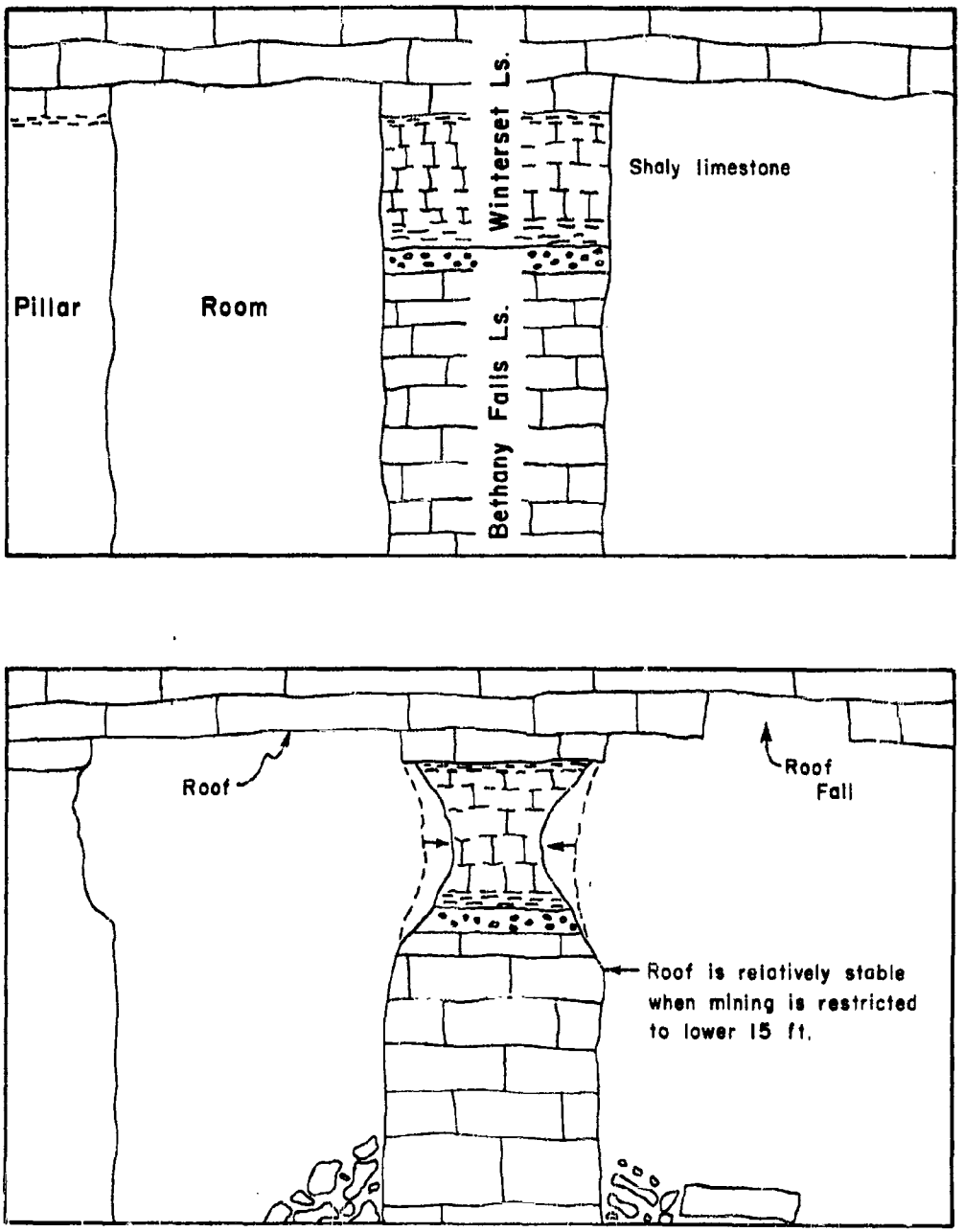


Figure III-A.6. Typical deterioration of shaley portion of pillars in limestone mine in western Missouri, Missouri Portland Cement Co.

Geologically there are four types of ore: (1) massive sulphide, (2) siliceous flux, (3) chloritic gold ore, and (4) a small deposit of disseminated sphalerite and pyrite in rhyolite.

The strength of the massive sulphide ore is considered phenomenal. It is mined by benching in sublevel stopes to avoid dangerous heating and oxidation which would interfere with flotation. The siliceous fluxing ore bodies are removed either by benching or by shrinkage stoping. The ore bodies are compact in character and stand up with comparatively long roof spans. Practically no timber is necessary except in shafts, one or two sets in stations, chutes and cribbed manways. The ores are classed as medium to hard for drilling. The occurrence of slips in siliceous rhyolite is more frequent than in the massive sulphide ore and it must be carefully watched during mining.

In general, the Horne mine has exceptionally strong ground and can use mining methods that could not be considered in weaker structures. As the mine progresses in depth, more attention must be paid to bad ground due to the increase in lithostatic pressure, the dimensions of the lower level stations and drifts being held to a minimum. Gunite is used where the rock has a tendency to slough, together with rock bolts, reinforcing and gunite in shafts and stations.

Rock alteration has minor effects upon mining and is of three types: silification, sericitization, and chloritization.

Silicification--the Horne rhyolites consist mainly of quartz, and the amount of quartz increases as the main mineralized area is approached.

Sericitization--the formation of sericite is widespread. It occurs (1) as a stress mineral consequent to the folding, (2) in highly faulted and shear zones (sericite schists), (3) as veinlets of leter origin, with pyrite and chlorite, formed during the mineralization period, and (4) as massive sericite consequent to the replacement of sheared and mashed rhyolite by sulphides. The fourth type is confined to margins of the sulphide bodies.

Chloritization--this has an influence on the occurrence of gold values and is believed to have been formed with the sericite during the mineralization period.

Figures III-A.7 to III-A.10 show the relative position of the upper and lower H ore bodies, together with the very complicated geological structure which exists in the vicinity of the deposits and the method of mining. In spite of the complex structure, the presence of faults and occurrence of some weakening alteration, the general structure is competent and permits a method of mining which requires no support in the stopes

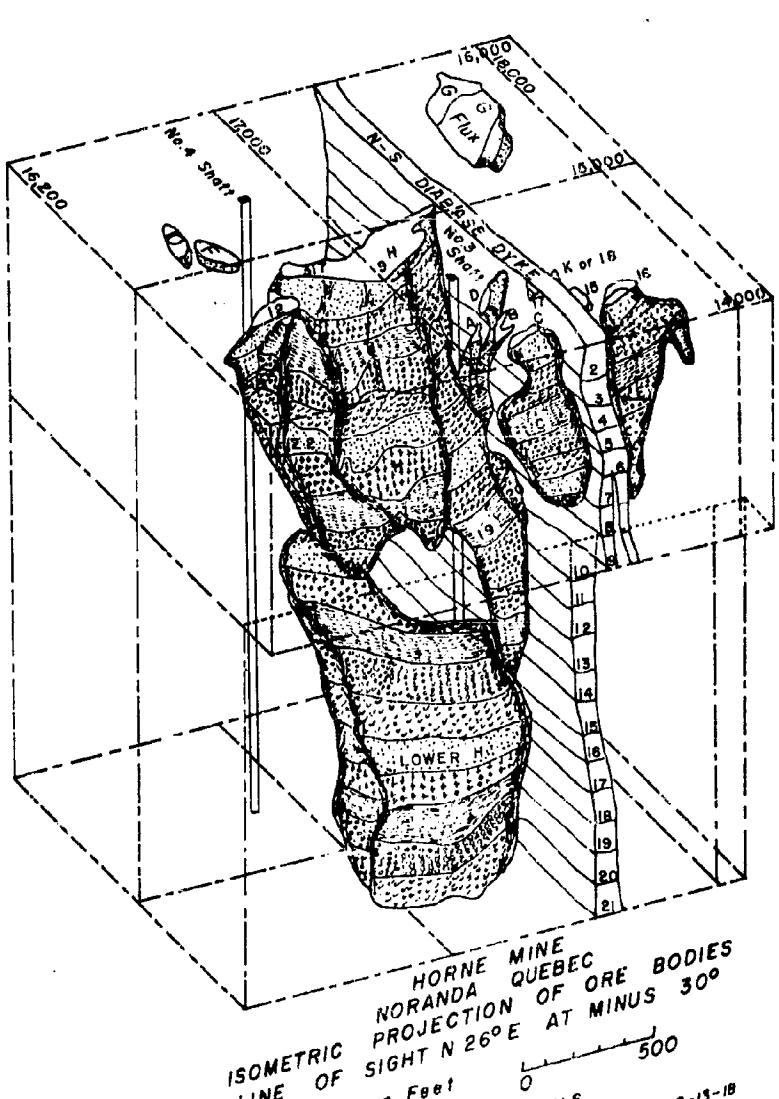


Figure III-A.7. An isometric drawing of the geology of the Horne ore bodies[5].

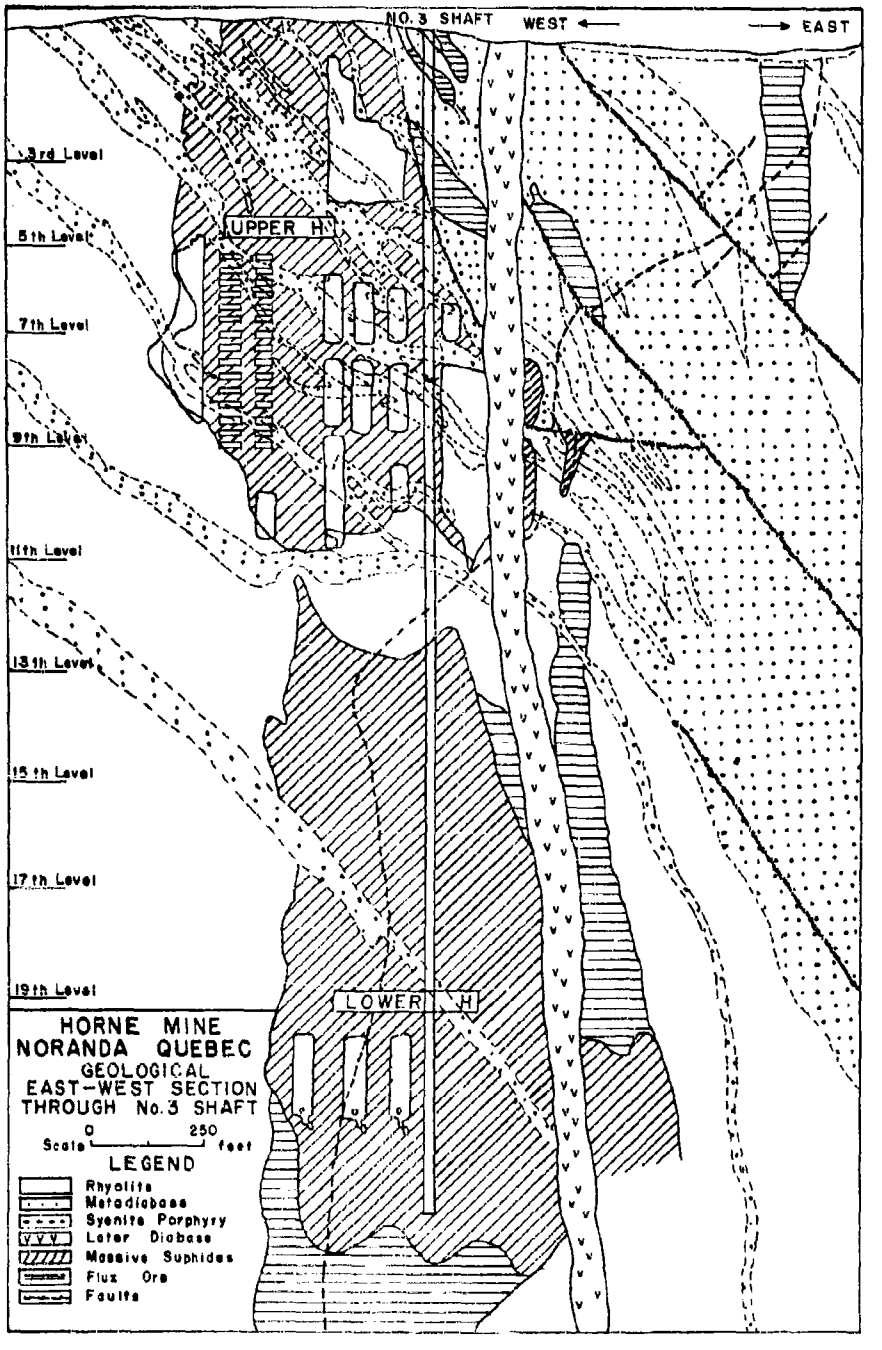


Figure III-A.8. Vertical Section through the Horne mine showing the ore bodies and the enclosing rocks[5].

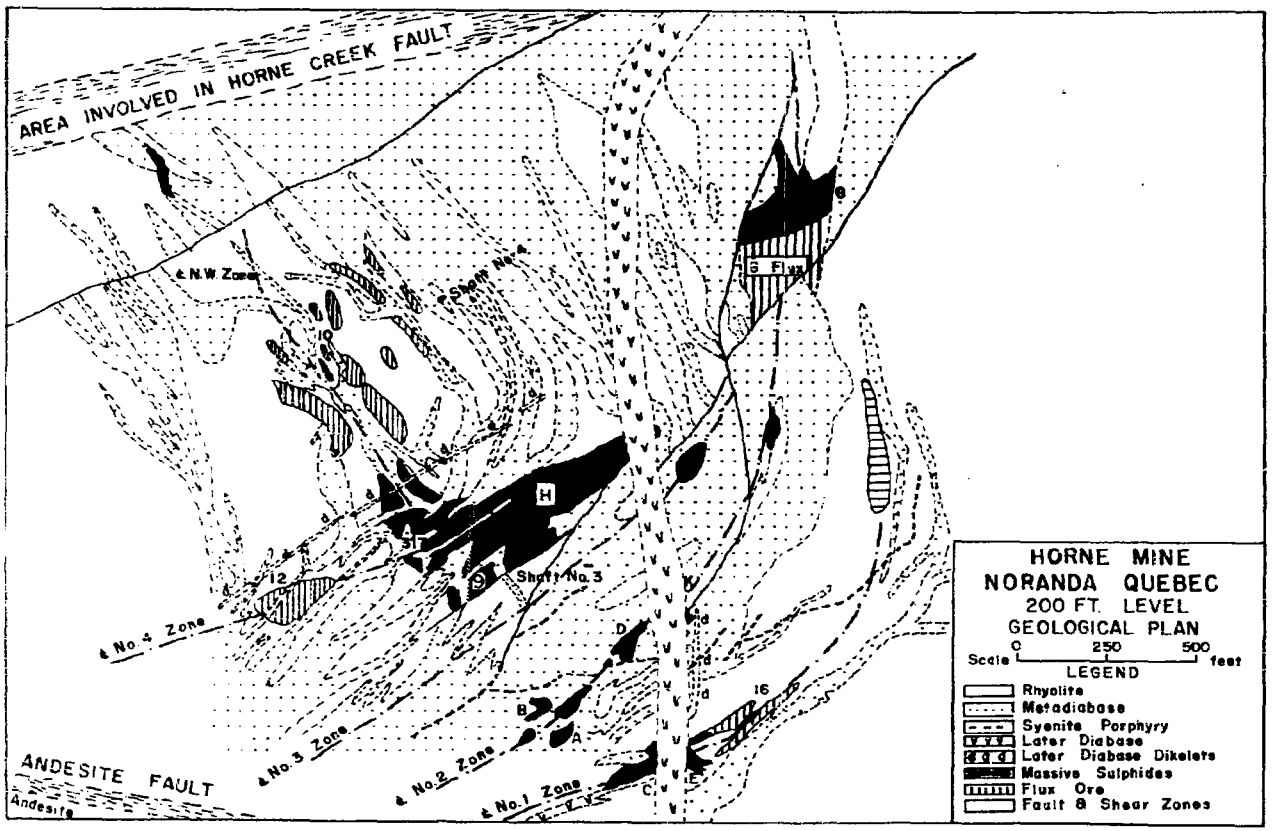


Figure III-A.9. Plan view of the geology on the 200 level of the Horne mine. Structure is complex with faults and dikes, but silicified rock and strong massive sulphide ore permit use of sublevel stoping[5].

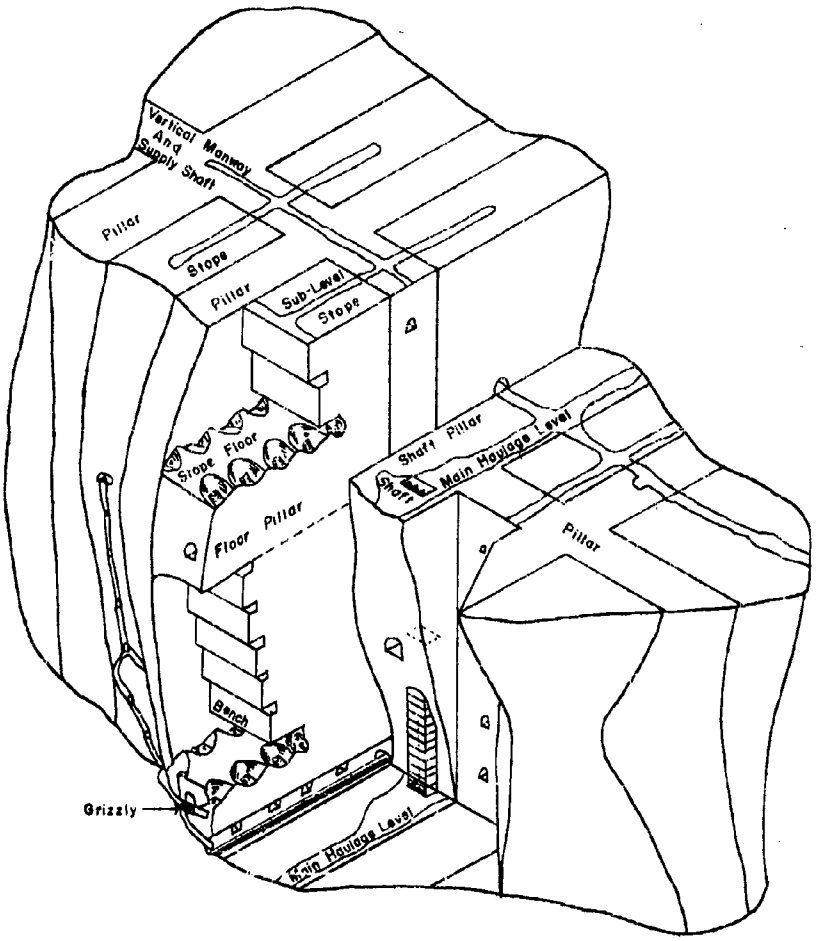


Figure III-A.10. Block diagram of the massive lower H ore body showing the method of sublevel stoping applied to mine the ore, Horne Mine. Method requires no stope support[5].

Burra Burra Mine. [10,11]

The rocks of the Ducktown district all belong to the Great Smoky Mountain formation of Lower Cambrian age. They consist almost entirely of metamorphosed sediments, the geologic column being constituted mainly of graywacke with arkose, graywacke conglomerate, conglomerate, mica schist, slate, staurolite schist, and garnet schist in the order named. The ore deposits are found upon the limbs of a large anticlinorium, which is the main geologic structure of the district. They are believed to be replacements of a limestone bed which has been thickened in places by thrust folds and by strike faults in the bodies themselves.

The general strike of the Burra ore body is N. 62° E., and dips 75° to the S.E. at the surface, flattens to 50° at the sixteenth level with local dips as low as 35°. The ore body itself is over 2,300 feet long on the fourteenth level of the Burra Burra mine, where the minable thickness varies from a few feet to a maximum of 180 feet.

The immediate wall rocks are highly metamorphosed schists and graywackes, whose bedding planes parallel the ore in dip and strike. In general, but not everywhere, the schistosity parallels the bedding. The tendency of the rock is to break along bedding planes rather than parallel to the less prominent schistosity. In most parts of the mine the walls stand well. Spans of 100 feet are usually self-supporting except where the ground is fractured by folding.

There are but few prominent slips and joints in the ore, but where they do appear they are generally horizontal. There are also minor vertical joints, the whole forming a system of more or less rectilinear planes, much stronger horizontally than vertically. The distance between these joints and slips is measured in terms of feet rather than inches. The ore tends to adhere to the wall rock rather than to break away from it, and is not as self-supporting over long spans as is the country rock. Haulage levels stand without support both in ore and wall rock.

In the zone of primary ore, the principal ore minerals are massive sulphides: pyrrhotite, pyrite, and chalcopyrite, with smaller percentages of zinc in the form of sphalerite. The gangue minerals are chiefly lime silicates, quartz, and calcite, with which the sulphide minerals have intergrown. The ore tends to break into large angular blocks and slabs which wedge in chutes and hang up in flat stopes.

The original sedimentary rocks in the district were closely folded, faulted, and metamorphosed. The faults show strong tendencies to parallelism with a well defined cleavage or schistosity. The ore-bearing rocks are found near the main axis of the synclinorium. Many of the beds are cut by closely spaced faults which represent warped planes along which they were fractured during folding. The irregularity in width of the ore bodies is believed to be due in a large measure to faulting, although the original limestone beds which they replaced were not of uniform thickness. This faulting took place before the limestone was replaced by the ore and silicates, or perhaps when it was a relatively weak member of the series. The stresses which were imposed on the formations were

relieved to a certain extent by fracturing of the weak beds. Thus, the ore bodies are cut by faults in many places, although faults are not universally present along or in the walls. These faults are of minor importance in mining operations.

Microscopic studies of the ore show that many of the gangue minerals in the sections have been bent and fractured, but the fractures have been later healed by the sulphides. This probably accounts in a large measure for the strength of the ore.

Shrinkage Stoping

Creighton Mine.[12,13]

The Creighton mine (Figure III-A.11) ore bodies occur along a shear zone where the norite hanging wall forms a bulge into the granite footwall. They are large lenticular deposits, largely of massive chalcopyrite and pyrrhotite with nickel. The average dip of the main ore body is 45° and has a maximum width of 300 feet. At some places below the sixteenth level greenstone forms the hanging wall of the deposit.

There are many brecciated areas that occur in the Sudbury district, in which the Creighton mine is one of the most important. The fragments of rock composing the breccia may be cemented by some of the more finely crushed rock and in places where the cementing material is composed of sulphides, those breccias constitute the commercial ore bodies. The position, size and continuity of the breccia zones was controlled largely by the ability of the various rocks to resist crushing. Thus, the tougher greenstone rocks are possibly less broken, and the fault movements expended themselves in the more brittle granite, gneiss, quartzite or graywacke. At some places in the mine hazardous ground, irregularities of the deposit, rock inclusions in the ore and need for rock disposal have been the cause for the adoption of cut-and-fill and square-set stoping.

The complex structural controls of ore deposition have resulted in frequent, and sometimes complicated mining problems. The intersections of shear zones cause prominent irregularities which in some cases rake across several stopes between adjacent levels. The ore bodies have many tag ends that require special attention, and the range in grade of ore (disseminated) necessitates frequent inspection to determine proper mining limits. Constant geological supervision is necessary in order that mining programs may be modified in accordance with new geological information as it becomes available.

Disseminated sulphide ores are confined to noritic rock and the sulphide component ranges from zero to almost 100 percent. Higher grade ore bodies are mined by selective methods (square-set, etc.). Outlying lower grade ore is mined by non-selective methods. Remote parts of the deposit are too low grade to be mined by any method.

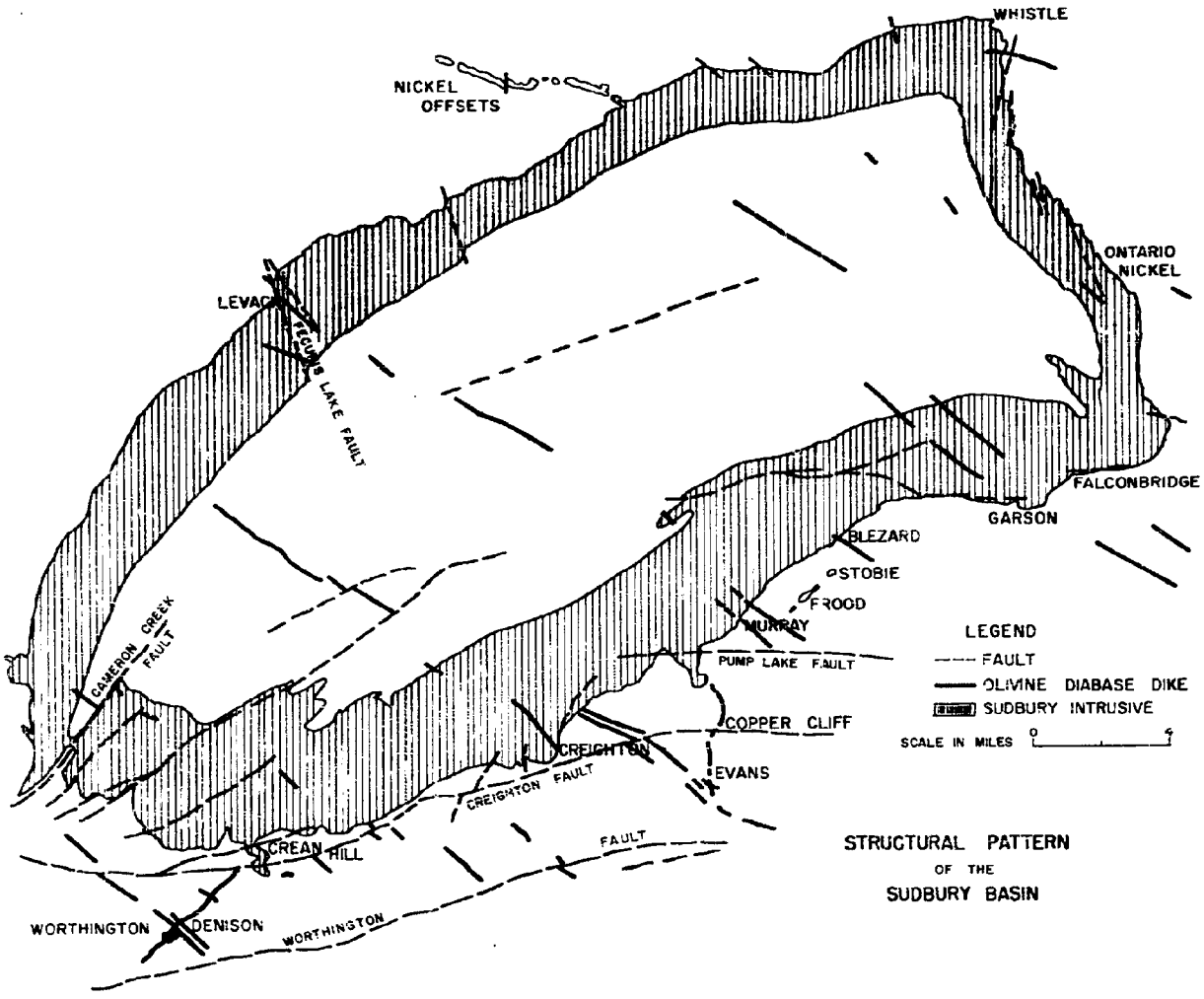


Figure III-A.11. Geologic structure pattern of the Sudbury Basin and the location of the important mining centers.

The massive sulphides occur as the matrix of a breccia that contains inclusions consisting of large and small fragments of all kinds of footwall rocks. Massive ore also occurs as veins in disseminated ore and in massive footwall rocks. The typical massive sulphide ore body lies along a shear zone and passes obliquely from one side to the other of the lower contact of the norite, the upper portion lying in or against disseminated norite and the lower portion within the footwall rock.

The principal country rocks, aside from the norite, are granite and gabbro. The norite is structurally strong and all workings located in it are easily maintained. The gabbro acts much as the norite, but rockbursts are fairly common in the granite, occurring soon after the ground is opened up. Since the granite and the gabbro are components of the footwall complex and cannot be projected safely, it has become common practice to obtain advance information by diamond drilling before new crosscuts are laid out.

Hollinger Mine.[14]

This description is singularly complete with reference to the geology of the Hollinger mine as it affects the mining operations. It is rich in details of the factors which illustrate the total dependence of effective mining operations upon knowledge of geology. (See Figures III-A.12 and III-A.13).

The rocks of the Porcupine district are classified in the following geologic column:

Pleistocene

Glacial and recent: Boulder clay, stratified clay, sand gravel, peat.

Pre-Cambrian

Keweenawan: Olivine diabase
Intrusive contact

Matachewan: Quartz diabase
Intrusive contact

Algoman: Granite, granite porphyry, quartz porphyry
Intrusive contact

Haileyburian (?): Serpentine
Intrusive contact

Timiskaming: A series of sediments consisting of conglomerate, graywacke, slate and quartzite, in places much impregnated with carbonate.
Unconformity

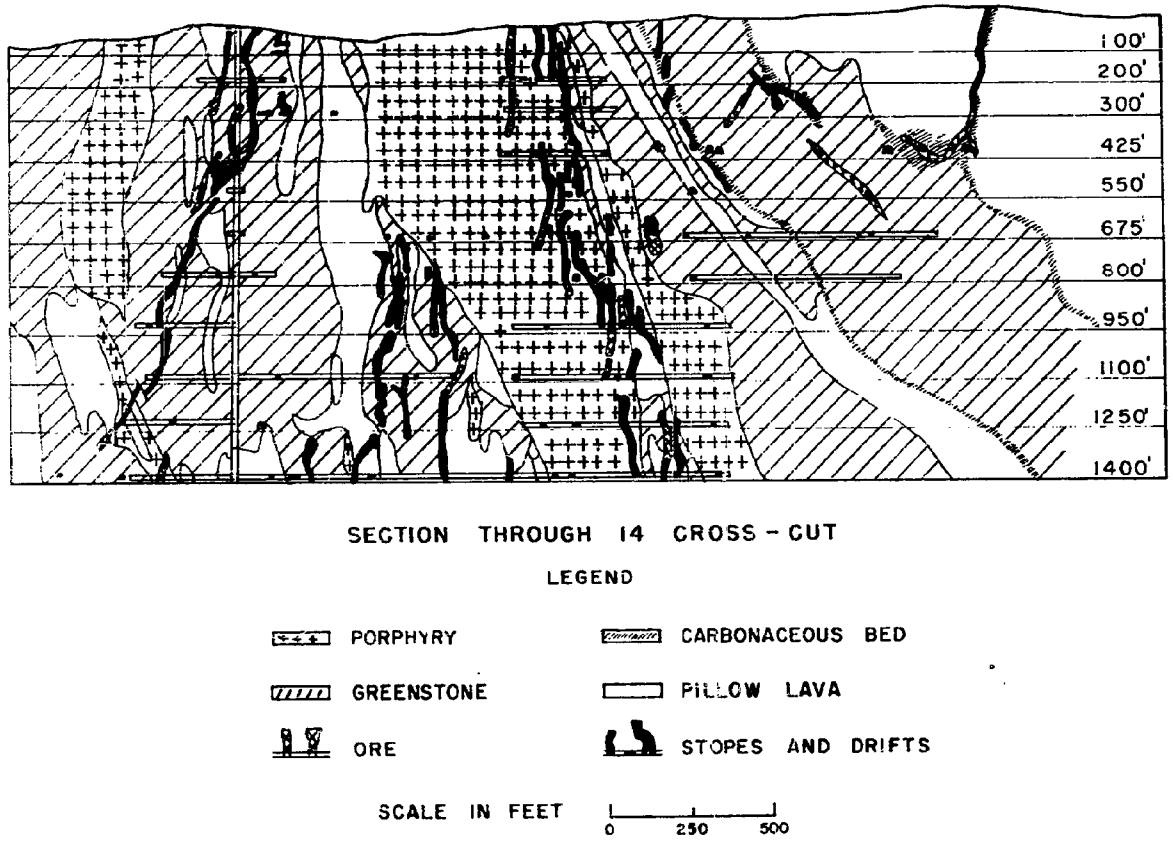


Figure III-A.12. Typical cross section of the Hollinger mine showing the distribution of rocks and ore.

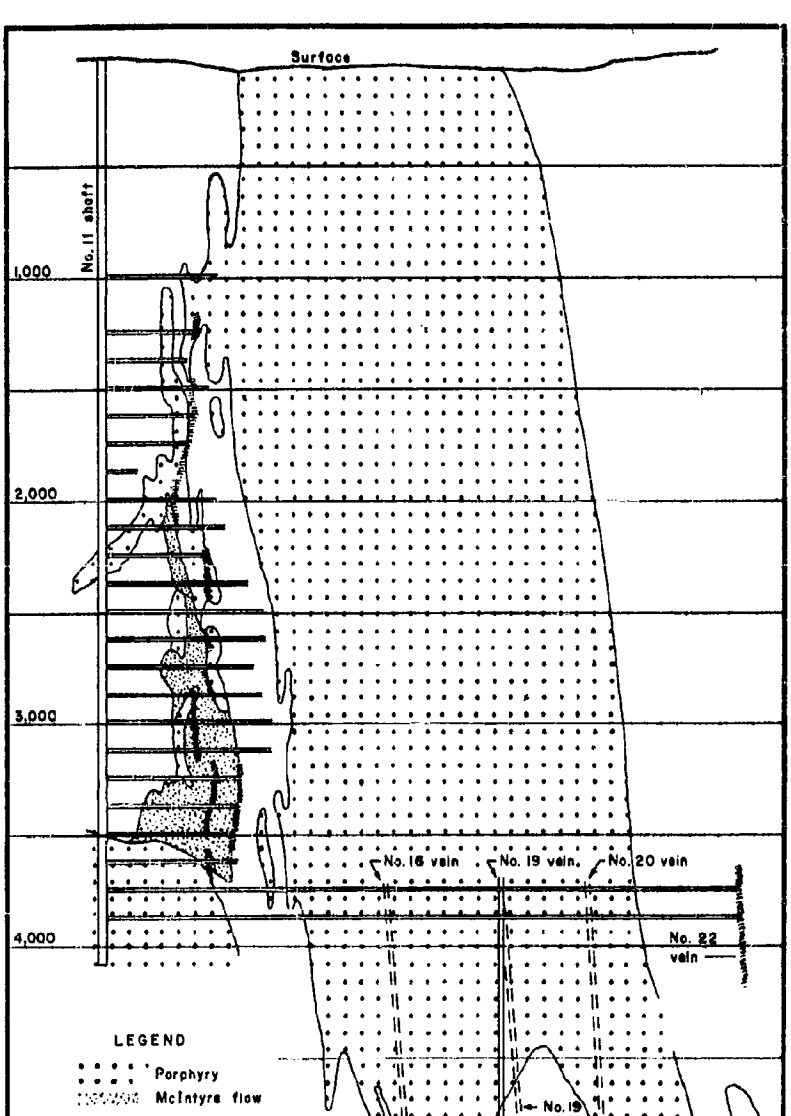


Figure III-A.13. Vertical geological section of the McIntyre mine depicting the relationship between the igneous country rocks, the ore and mine openings.

Keewatin: A complex of basic to acid lava flows; andesite, dacite, rhyolite, volcanic gragmental, tuffs, and agglomerate, now altered to green and grey schists, carbonate schist, carbonate-talc-chlorite schist, iron formation and slates.

Figure III-A.12 shows a typical distribution of the rocks in a vertical plane across the strike of the main geological structures. In the central portion of the property repeated dynamic action and igneous intrusions have so changed the flows by distortion, shearing, schisting, and alteration of original minerals that it is usually not possible to differentiate between them. The principal intrusive rock is the quartz porphyry. Where it is highly schistose the feldspars have undergone alteration and the rock has become essentially a sericite schist.

Minimum Series of Geological Events in the Porcupine District

1. Building up of essentially conformable Keewatin lava flows on an unknown basement.
2. Local folding along E-W axis.
3. Intrusion of Alaskite porphyry with marginal brecciation.
4. Erosion of Keewatin-porphyry surface.
5. Deposition of Timiskaming sediments.
6. Cross-folding along N-W axis.
7. Intense folding along E-W axis.
8. Development of shearing and schistosite, accompanying and/or following E-W folding.
9. Buckling of schistosity, perhaps during erosion and uplift.
10. Intrusion of quartz monzonite, and/or albitite dikes.
11. Fracturing of rocks in a highly complicated manner.
12. Complex period of vein deposition and attendant mineralization.
13. Intrusion of diabase dikes.
14. Post vein faulting.
15. Feeble mineralization along late faults.
16. Uplift and erosion.
17. Glaciation.
18. Modern erosion, sedimentation and weathering.

The observed results of events 2 to 11 inclusive upon the varied group of rocks was shearing, schisting, fracturing and rock alteration over wide areas. Local areas show variations in type and intensity of these results. The existence of these conditions made the area exceptionally favorable to the entrance of mineralizing solutions and ore deposition in the host rock. The intensity of fracturing varies from place to place and is probably influenced locally by the texture, structure, and weakness of the rock types as well as by the stresses induced during the major geological events. The schistosity in the Hollinger mine dips steeply to the south and, like the larger fractures, pitches east.

The structure, including the fracturing, played an important part in the vein formation. The intricate system of closely spaced veins lies within a zone of shearing and fracturing, which itself occurs where a coincidence of three sets of folds and the porphyry masses produced the maximum of structural complexity at the point of greatest diversity in rock type. Over 100 of these veins have been productive.

Post-mineral faulting of the quartz veins has displaced them slightly in some areas. Mineralization (sulphides and quartz-ankerite) sometimes is found in the wall rock. Shearing adjacent to and parallel to the vein is common where definite quartz veins cut the schistosity. The veins vary from a few inches to several feet in thickness. Features of the Hollinger ore deposits which affect the choice of stoping methods are as follows:

1. Intricate vein systems extending for long distances both along their strike and vertically. These are composed of parallel, frequently connected ore bodies which may branch upward, downward, or laterally.

2. The requirement that a maximum recovery of ore be obtained with minimum dilution with barren rock, maximum safety, and prevention of subsidence.

3. Wall rock conditions are partly favorable because the schisting usually makes a small angle with the strike of the veins. This tends to "key" slabs into the stope walls. Conditions are unfavorable where cross fractures and slips or flat-lying planes of weakness decrease the strength of the walls and the ore, thus affecting the support required.

4. Wide variations in the width of veins horizontally and vertically frequently occur within short distances. There are places where widths of 100 feet are opened up in mining.

5. Variations in vein filling occur from a preponderance of quartz, through mixtures of quartz, to other minerals and included wall rock in different proportions. These, taken in conjunction with the fracture patterns, give rise to different strengths of vein fillings and determine the artificial support required to hold the stope backs.

The stoping method which best meets the requirements imposed by these geological conditions is horizontal cut-and-fill stoping. However, shrinkage stoping is employed where veins are narrower than 6 feet and the walls are strong. Cut-and-fill stopes are usually started as shrinkage stopes.

Cut-and-Fill Stoping

McIntyre Porcupine Mines.[15,16,17]

Most of the deposits at McIntyre are mined by horizontal cut-and-fill, although square-sets are used locally to mine pillars and in stopes where the ground is blocky.

The McIntyre mine is located on the north limb of the Porcupine syncline which lies within the area of Keewatin lavas and later intrusives. An area of Temiskaming sediments, which occupy the central trough of the Porcupine syncline, lie to the southeast of the McIntyre property. (See Figures III-A.14 to III-A.16). The Keewatin lavas have been classified in considerable detail, and are known as basalt and greenstones. The greenstones are the coarse-grained flows or parts of flows, and the basalts are the finer-grained variations. There were three periods of intrusive activity with entirely different types of rocks formed during each. These are constituted of diabase dikes, albitite dikes and quartz-porphyry masses. The diabase dikes cut the lava flows, porphyries and veins, strike N-S ore NE-SW and have steep or vertical dips. They sometimes interfere with operating conditions underground. The albitite dikes cut the lava flows, porphyries, but are cut by the veins. These dikes are coarse-grained and consist essentially of acid plagioclase and rounded fragments of granitic character. Several stocks of quartz-porphyry are intruded into the tilted and folded lavas. They are all of the same type, differences in hand specimens being due to different degrees of alteration and schistosity.

The rocks in the area near the ore have been subjected to compressive forces at several times in their history. The complex folding, the fractures now occupied by the veins, the pre-mineral and post-mineral faulting, and a broad belt of schist are evidences of these tectonic forces. The schist strikes N 65° E and most of the productive veins of the Pearl Lake area occur in it.

It is believed to be reasonable that the lavas were folded and a regional pattern of stress control was in existence before the porphyry intrusion. The later stresses were the original stresses complicated by the action of cooling porphyry masses, which had a marked effect on the fracturing of the schisted and unschisted areas. There are several planes of fracturing cutting and the schisting at a small and the ore is found in these fractures.

The ore is of two types: (1) quartz veins with included schist fragments, and (2) irregular replacement bodies. An ore body may include both types, and inasmuch as they occur in fractures which are common to all the rock types of the area, it follows that the wall rocks may be any

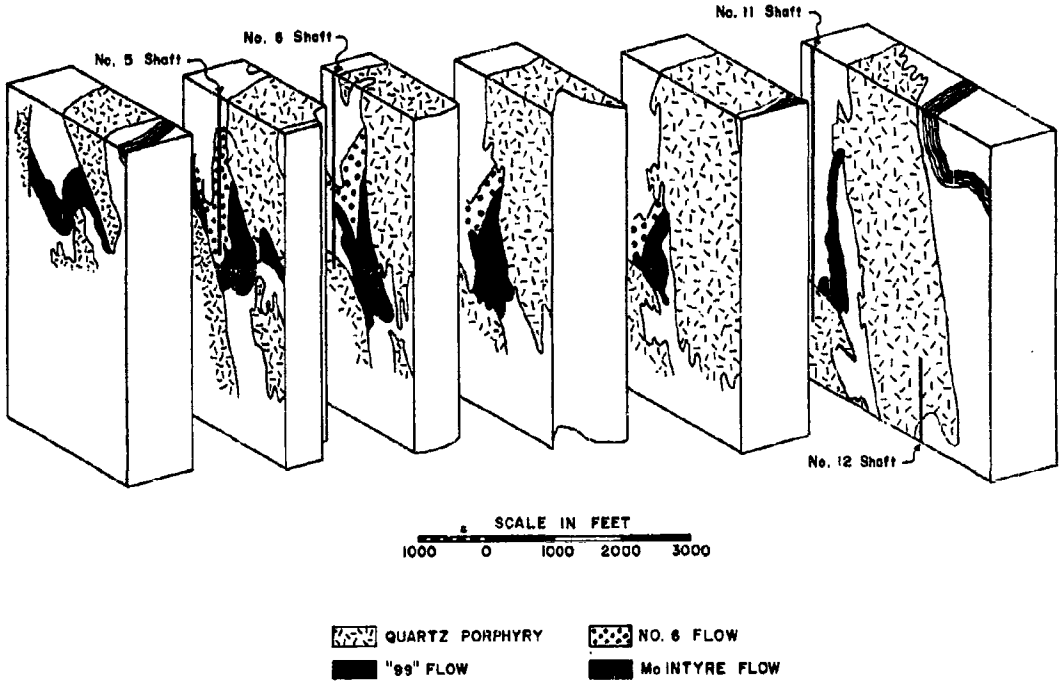


Figure III-A.14. Offset block diagram of the geology of the McIntyre-Porcupine mine. Ore occurs in the McIntyre flow.

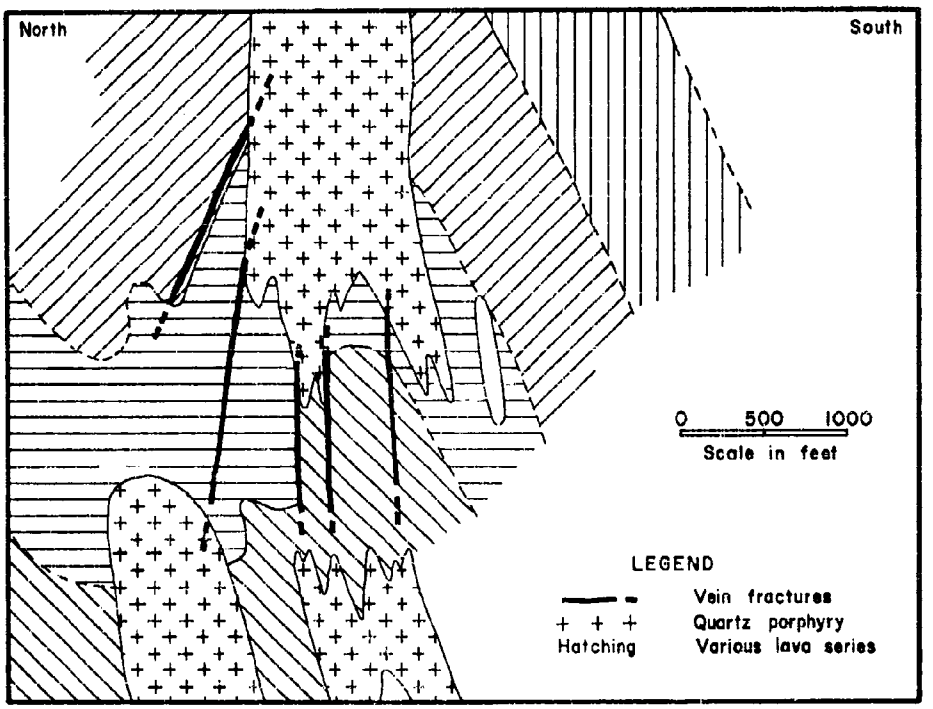


Figure III-A.15. Plan view of geology of McIntyre mine.

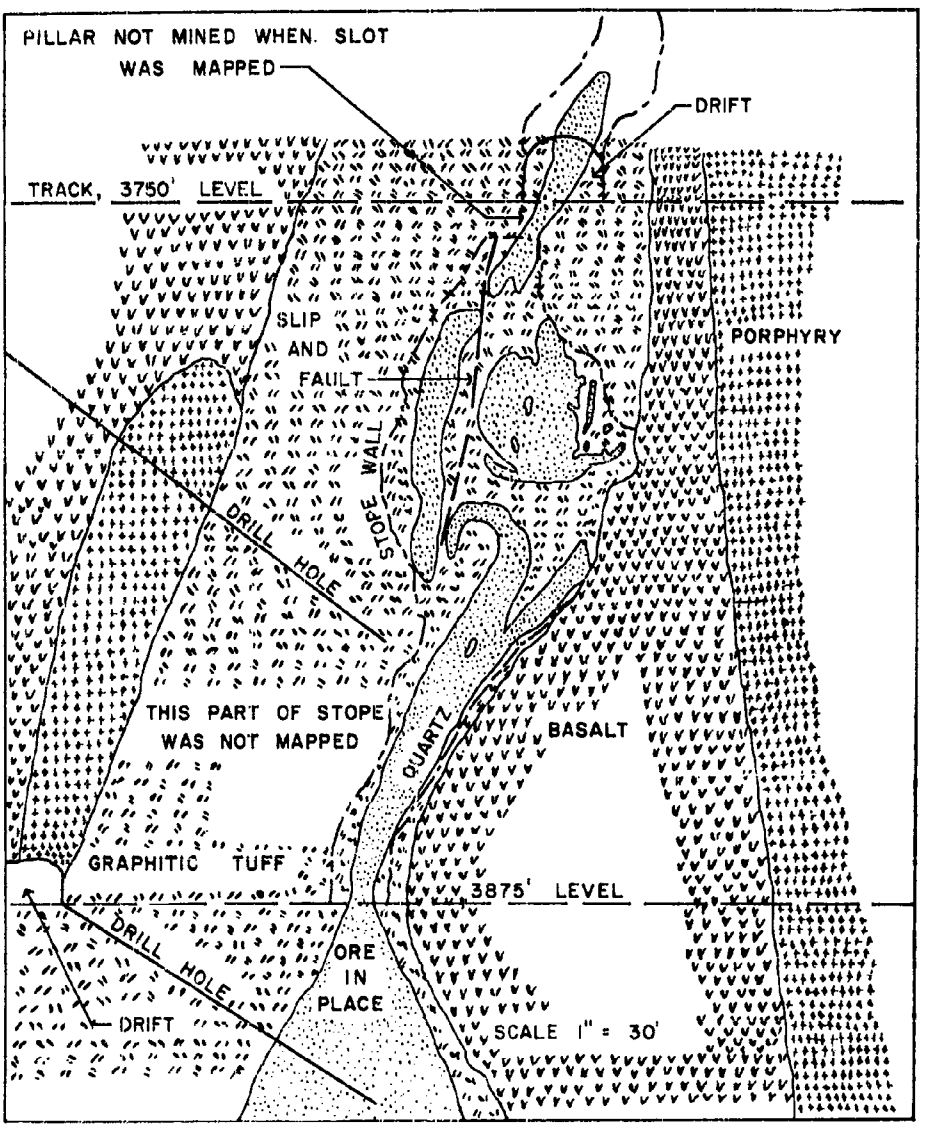


Figure III-A.16. Stope section showing the type of stope geology encountered in the McIntyre mine. Note the complex structure, faults and the graphitic tuff.

of the types or their derivatives. The following may be said in general concerning the principal alteration processes of the various rock types: The basalts may show any type of alteration to any degree, while the greenstone and dacites also show any type of alteration, but to a much less marked degree than the basalts. Porphyrys are not chloritized like other rocks. The wall rocks made up of the lava schists or their derivatives usually stand well unless broken up by faults. The wall rocks of contact ore bodies in porphyry are usually carbonated and sericitized. They tend to be slabby and are difficult to hold. Disseminated sulphide ore bodies usually occur with irregular walls due to the fact that mineralization often extends away from the main fissure into the walls along joint planes and fractures.

Ore bodies dip from 60° to vertical. Lengths vary from 1,200 feet to smaller footages, widths up to 100 feet, with the average width being 10 feet. The ore deposits possess the same physical characteristics at all horizons. There is also a zone characterized by the unusual development of an amorphous carbon rock, which may contain as high as 7 percent of carbon in local areas where minor cross faulting occurs. This zone strikes about N 60° E and dips to the S. It is important in mining operations because it intersects three of the principal vein systems. Where this occurs there is often a considerable displacement and consequent dilution of the original vein material with wall rock of a more or less carbonaceous nature. At these intersections the vein walls are difficult to support and such areas are usually mined by square-sets or square-sets and fill. Employment of these methods of stoping prevents excessive dilution, allows a certain amount of sorting, and makes for safer mining conditions. (Figure III-A.16).

The major part of the ore developed to 1933 was in lava schist of a friable character in or relatively close to a prophyry contact. The type of ore body and the type of wall rock may vary considerably within short distances. This factor has an important influence on the method of mining to be used in a given area. The basalt and porphyry contact areas are usually highly carbonated and sericitized. In the areas characterized by this type of alteration the wall rocks tend to slab off and dilution of the ore becomes a serious problem. Hence, close wall support is necessary during the mining process.

In the irregular replacement veins, the mineralization has tended to follow joint planes and fractures into the walls. For clean mining and for complete extraction, close wall support is necessary. In local areas faulting has weakened the structure so that the back must be supported as well as the walls. During 1933, 60 percent of the mining was by cut-and-fill methods. It was then predicted that this percentage would increase as depth of mining increased.

Anaconda Copper Mining Company.[18,19]

In the Butte mines, closely filled flat-back square-set stopes are employed where square-set rill stopes or horizontal cut-and-fill stopes, or ordinary filled-rill methods are not applicable. Geological details of structure of the mines in this district are also exceptionally complete, and for this reason are described here in detail.

Essentially all of the Butte ores occur in two sets of faults or fractures in a country rock of quartz-monzonite which constitutes a portion of a large mass that intruded Paleozoic and Cretaceous beds and Cretaceous andesite flows. One set of faults, the Anaconda system, has a prevailing east-west strike and a southerly dip. The other set of faults, the Blue vein system, strikes toward the north-east and dips steeply toward the south. The Continental fault (post-ore) bounds the east end of the district. It strikes north, dips 67° west and has a vertical displacement of about 1,500 feet. In addition there is present a series of post-mineral faults in the district which have affected the ore-bearing faults locally. (Figures III-A.17 and III-A.18). These are typical sections which show the manner in which the district has been faulted and disturbed, creating the "horsetail" structure described by Sales.[18] Three zones of mineralization are recognized: (1) central zone of copper arsenic minerals with intense alteration, (2) intermediate zone containing sphalerite-galena, and (3) north or peripheral zone containing zinc and manganese.

Due to the complexity of the vein and fault structures and the small scale of Figure III-A.17, only larger features and more general structure can be shown. The Anaconda fissures, which are continuously mineralized, and vein filling other than crushed granite are shown in black.

The fault systems are:

1. Anaconda ore east-west systems, comprising the oldest known fractures--highly mineralized, most important commercially.

2. Blue system (thrust faults)--earliest post-Anaconda fault fissure, typical fault fissure with ore occurring in shoots.

3. Mountain View breccia faults--cut Anaconda and Blue vein systems.

4. Steward system--sparingly mineralized.

5. Rarus fault--unmineralized, post-Blue, displacement 120-350 feet.

6. Middle faults--unmineralized.

7. Continental fault--regarded as seventh period of fissuring; unmineralized, lies outside of copper producing area.

Rock Alteration. Most of the important rock alteration in the area is associated with the Anaconda vein system in the vicinity of Anaconda hill. Alteration has taken place not only within and along veins and faults, but the whole rock mass including granite, aplite and quartz-porphyry has been subjected to metasomatic processes, producing a rock of marked difference in physical and chemical character from the fresh rock. The dark granite has been altered to a whitish, less firm rock, showing considerable amounts of fine pyrite. The quartz-porphyry has been altered to a yellowish-white rock with glassy phenocrysts of quartz. When these altered rocks are subjected to the action of meteoric

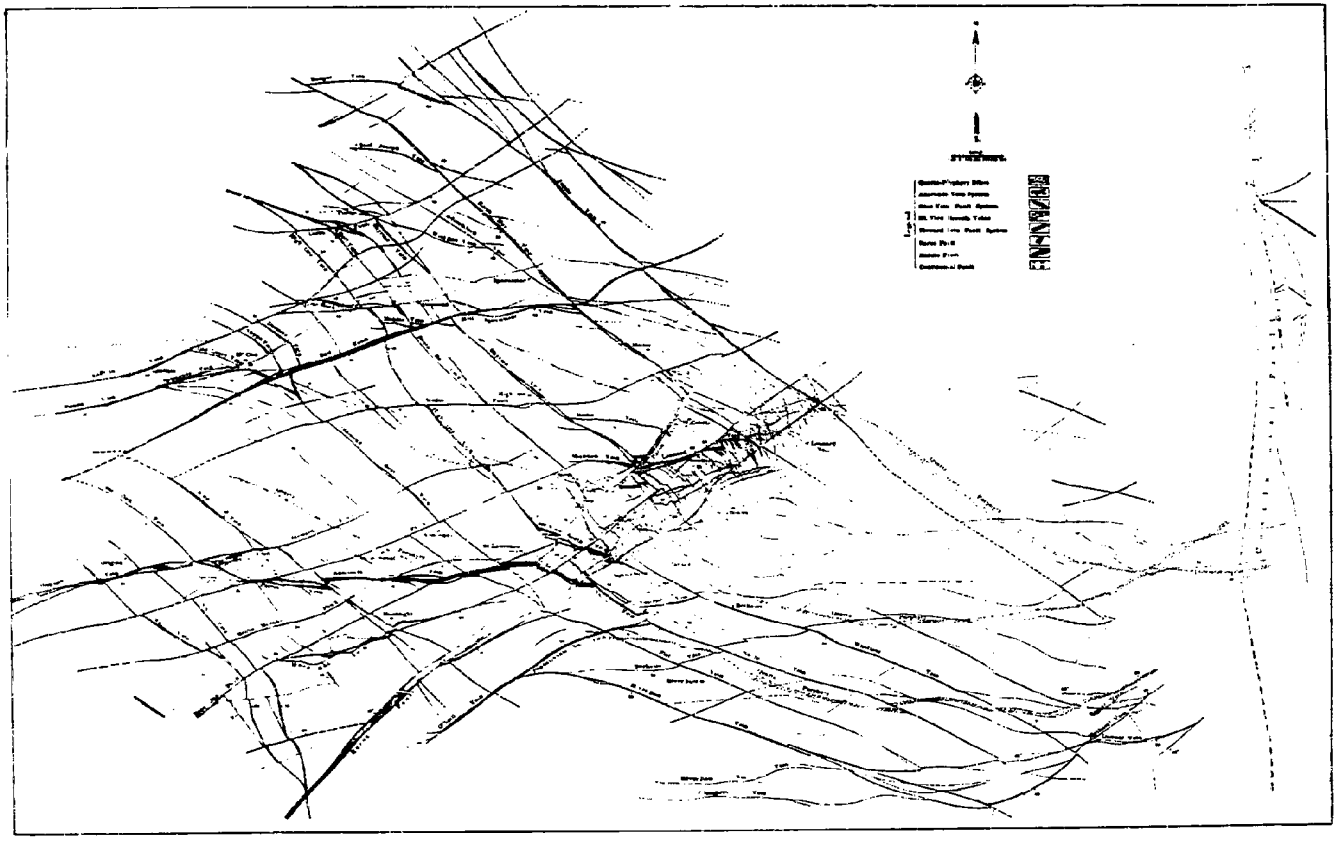


Figure III-A.17. Horizontal section of the Butte District, 4,600 ft. above sea level (1,500 ft. below surface), showing structural relations of the fissure systems[17].

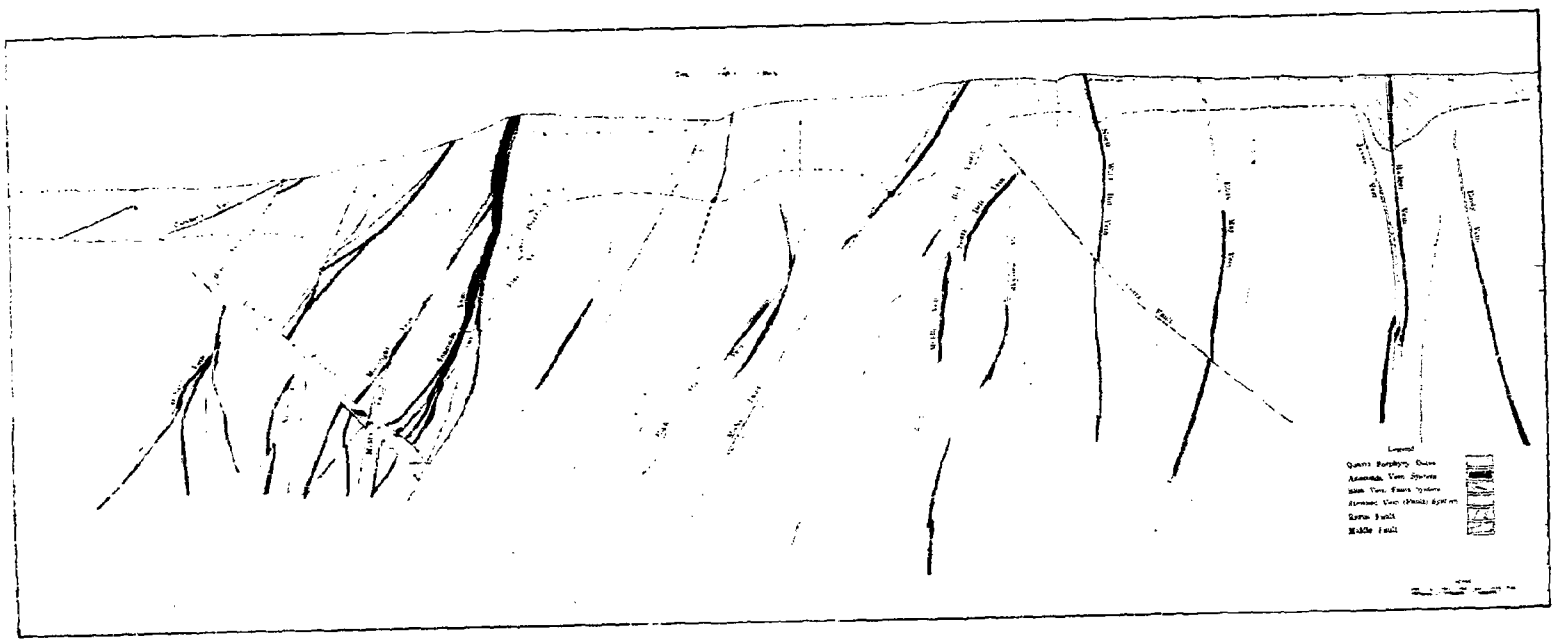


Figure III-A.18. North-south vertical section through the copper district near the Anaconda Shaft, showing the structural relations of the veins and fissures[17].

waters, they become weaker, more porous and show a little more uniformity in structure. In some cases in new workings in the upper levels, the rock breaks into great slabs, the fracture planes extending across the rock without reference to joint planes.

The alteration is attributed to three causes: (1) vein formation, where the alteration was caused by solutions which formed the ores: (2) hydro-metamorphism or the effect of descending meteoric waters; and (3) oxidation processes.

Alteration is not necessarily most intense in regions of greatest crushing and brecciation of rock. This is attributed to the fact that the earliest ascending water and gases were more active due to their higher temperature and more concentrated chemical composition. Impervious crushed granite and fault clay were not present in earliest fractures and fissures, thus the gases and solutions were permitted access to the wall rock at all points. The regions of oldest fractures were subjected to vein forming processes over greater periods of time than areas near later fault veins. Chemical agents were aided considerably by dynamic action in the granite and other rocks. Breaking and crushing of the rock on a large scale not only provided channels for gases and solutions but exposed greater areas of the rock to their attack.

Alteration accompanying vein forming processes took place on and near principal channel fractures. By means of the main channels, associated fissures and joint planes in fissured areas, the solutions penetrated practically all of the granite in the fissured area. Formation of chlorite and pyrite by metasomatic processes characterized this stage of change in the rock character. The thermal solutions attacked first the iron silicates, augite, hornblende, and biotite, forming chlorite, epidote, secondary silica and pyrite, followed later by reaction with plagioclase and orthoclase feldspar to form sericite and additional secondary silica. Continuation of these processes resulted in the disappearance of the chlorite and epidote and the formation of a "pyritized" granite, consisting principally of quartz, sericite, and disseminated pyrite. Inasmuch as metasomatism proceeds outward from the main solution channels, the alteration is more intense near these fractures.

Cold meteoric waters percolating through unaltered granite have resulted in little or no chemical change. The oxidation of pyrite, formation of iron sulphates and free sulphuric acid, which is carried by these waters, makes the action of the cold solutions much more effective at depths to 300 feet. Here the sericite is converted to kaolin which, in turn, makes the granite weaker and more porous.

Water flow through the rocks decreases in the upper levels as more openings are made at greater depth in the near vicinity. The slow rate of flow of water from greater distances indicates that the circulation of ground water in the Butte granite is extremely sluggish, if not practically stagnant, as well as being meteoric in origin.

Ore-Anaconda Vein. Of the seven distinct fissure systems named above, only the Anaconda system, the Blue system and the Steward system are ore producing.

The Anaconda veins are relatively continuous in width and character. Where the ore has replaced relatively firm rock, it is unusually hard and massive, exhibiting some imperfect banding due to replacement of sheared granite or deposition along closely spaced fractures.

Splitting of veins on both the strike and dip gives rise to two or more separate "footwall and hanging wall streaks" varying in width from one to 100 feet. The inter-vein granite is highly altered and netted with veinlets of mineralogical composition similar to the larger veins. Composition may vary mineralogically over wide ranges of percentage over small distances both along the strike and the dip, the principal minerals being chalcocite, bornite, enargite, and pyrite. The relative proportions of these minerals also vary from one extreme to the other. The component veins may or may not be well defined, an ore band usually being wider and more persistent than the rest; the smaller veins remaining roughly parallel, separated by vein granite. Stoping widths vary from 5 feet to 100 feet, averaging about 20 feet.

Faults in Anaconda Veins. Where the Blue veins system intersects the Anaconda system the vein material is shattered and broken, exhibiting step faulting, strike faulting, and general disturbance of the hanging wall rock and footwall rock. The effect of faults intersecting at right angles is more marked than that of faults intersecting at obtuse angles. In strike faults the movement may take place along either the hanging wall or the footwall, or both, the degree of breakage of vein material being determined by the amount of movement. Later solutions may remineralize these new fractures again into a solid mineral complex, a common feature of the Butte veins.

Blue Vein System. The Blue veins are displaced fissures of variable dip but relatively uniform strike. There is considerable branching and rejoining of the mineralized fissures to include horses of granite. The fault zone, which varies in width from 5 feet to 25 feet, often exhibits two well-defined movement planes characterized by seams of fault clay from 0.25 to 2 inches in thickness. These seams are usually accompanied by crushed granite of variable thickness, sometimes occupying the whole width of the fault zone. It represents a distinct zone of finely ground granite between the clay seams described, the whole being bounded by solid granite hanging wall and footwall.

Ore minerals are chalcocite, enargite and bornite, occurring in irregular shoots, either along the main fissure or along branches in the fault zone. Along the strike the ore shoots are separated by barren stretches of crushed granite between the characteristic clay seams. The ore is less massive than that of the Anaconda system. Ore formed by replacement of crushed granite retains its brecciated structure and may be distinguished thereby from ore formed by replacement of solid granite. Valuable minerals also often occur in crushed altered granite as stringers and veinlets of copper minerals with quartz and pyrite in limited amounts, or as disseminated chalcocite in crushed granite.

With respect to the physical character of the ore, that found in the Anaconda system is usually harder, wider, and more massive and seldom exhibits breccia structure. The metasomatic action has been more intense and complete than in fault veins where vein formation processes were disturbed by fault movements. Geological evidence all leads to the conclusion that the ores were derived primarily from igneous sources.

Geological Factors and Operation. In many sections of the Butte district the alteration is most pronounced along the joint planes where the wall rock of the vein has been altered and decomposed for considerable distances from the vein itself. Alteration, in addition to the adjusting movement of the rock, has so diminished the structural strength of the country rock that stope walls, and even walls of drifts and crosscuts, lack self-supporting cohesiveness and tend to crumble in blocky masses. This characteristic is greatly magnified by even small quantities of percolating water. The continuity of structural rock support is practically destroyed along the planes of numerous and complex post-mineral faults that are characterized in most placed by impalpable gouge seams. Frequently these faults follow the walls of the vein, in many cases leaving them at acute angles to enter either the vein or the country rock, often returning again to the wall of the vein. These unfavorable geological structural conditions cause sloughing and squeezing of the walls and backs of openings, require close timbering and filling of stopes before prolonged exposure to air and demand frequent repair and replacement of timber. In order to permit support, drifts, and crosscuts must be of small dimensions, which prevent the use of cars, locomotives or mechanical loaders of large size. Except in unusual cases when veins are small, these geologic conditions prevent the adoption of stull timbering, open stoping, shrinkage stoping or caving methods. They also restrict the size of shaft compartments and loading pockets that may be used without danger of prohibitive expense of jacketsetting and other maintenance. For the same geological reasons and because of the limited life of timber, it is impractical to explore or develop ore reserves extensively, so that plans for mining ventilation, etc., cannot be made without reliable knowledge of the size and shape of the ore bodies.

The Butte vein systems are very complex, exhibiting considerable variation in strike and dip, and displacements of the veins and ore bodies are of magnitudes up to 300 feet. Post-mineral faults described above cut the veins at many different angles, and often divide the ore bodies into separated blocks of ore of relatively small dimensions. This greatly complicates the work of development and the location of chutes and manways, stoping operations, timbering, etc. Vein dips are seldom flatter than 40°, which permits the ore to run down the footwall by gravity unless it is wet. Walls of the vein are predominantly distinct, though occasional irregular mineralization extends into the wallrock. Except where the vein is broken by faulting, the width of the oreshoot is usually small compared to the length and depth. Many of the ore bodies are from 15 to 100 feet in width, so that single timbers are not long enough to make suitable caps or stulls for timbering in a large part of stoping operations. This has resulted in the general adoption of square-set stoping, except for the narrow veins that have walls suitable for rill stoping. Ore is likely to be considerably wider and of higher grade at the intersection of veins, either on the strike

or dip. In some of the larger vein systems, the ore frequently occurs in shoots occupying only a portion of the width of the vein, the remainder being too low grade to be commercial. Frequently, roughly parallel shoots occur in the vein, one of which may be on the footwall and the other against the hanging wall, with sufficient valuable mineralization between the two to make continuous ore. In other instances, the two walls may be connected by ore shoots traversing either the strike or dip or both. The ore in many veins may occur in lenticular form, the vein in the barren portions frequently pinching out to such small dimensions that it is not of importance. The largest oreshoot of the district is in the original vein system of the Anaconda Mining Company. It varies in width from 10 to 100 feet, averaging approximately 25 feet, and has a continuous stoped length of 7,700 feet, and a developed depth of about 3,600 feet.

The complication of geological conditions and the resultant uncertainty of shape and location of branching or faulted portions of ore shoots make it impractical if not impossible to follow any orderly plan of development or mining without deviation, and frequent intermediate levels and other openings are necessary.

In the lower levels of the Butte mines, the rock and water temperature are 100°F., with a geothermal gradient of 10°F. to 100 feet of depth. The methods and costs of mining are effected by the copper-acid water. Most pump lines must be constructed of lead or be wood-lined. All underground metal equipment must be protected from corrosion. The high temperature requires extensive and careful ventilation engineering to direct considerable volumes of fresh air to each working face.

Because of the complexity of geological structure, unusually comprehensive surveys and geological mapping must be made. And on account of the large amount of valueless sulphide material in the copper ores, it is difficult to determine visually the relative value of the ores, requiring in turn complete and systematic sampling and assaying.

Conclusions

1. Processes of alteration accompanying the formation of the Butte veins seriously affect the strength of ore and country rock. Alteration by thermal solutions depositing the ores vitally affected the strength of the wall rocks, while additional chemical changes superimposed by meteoric waters upon thermally altered granite cause further weakening in the upper portions of the rock mass.

2. Solid veins composed of quartz, pyrite, and copper minerals tend to strengthen the ore complex. It is the alteration and fault movements which cause the Butte veins to require timber.

3. The addition of silica and solid veins and stringers tend to strengthen what might have been normally a weak altered country rock.

4. In general, faulting, jointing, and alteration tend to weaken the mine structure, while the mineralization tends to strengthen it.

Square-Set Mining

Bunker Hill and Sullivan Mine[20,21,22]

The stratigraphy of the district has been listed as follows:

Wallace formation--calcareous shales, calcareous quartzitic sandstone and a thin bed of limestone.

Other formations total 19,800 feet of quartzites and shales.

The Wardner district is believed to be one of the most extensively faulted regions in the world, 97 faults having been identified and named in the district. Most of the deposits of the Coeur d'Alene occur as metasomatic fissure veins, tabular in shape and formed largely by replacement along fissures and shear zones. The veins strike in a N-W direction and are nearly vertical. The fissures appear to have been made by faulting, yet the displacement of the faults is not measurable. None of the ore zones represent a structurally important fault. Veins vary in thickness, in some places having been formed by fissure filling and other places by extension into the wall by replacement.

The Bunker Hill fissure shows evidence of considerable movement, the plane of maximum movement being marked by a clay gouge one to two inches in thickness. Immediately under the gouge is a band of crushed quartzite which measures a few inches in thickness up to a foot or more. The crushed quartzite grades into shattered rock and then into an irregularly fissured quartzite. The hanging wall quartzite is considerably fissured and shattered, in some places for about 300 feet. Most of the ore occurs as large irregular bodies in the hanging wall, the whole 300 feet of the fissured zone being regarded as a lode deposit on a grand scale. The typical ore deposit is described as an obscurely bounded mass of shattered quartzite which has been largely altered to siderite and encloses numerous irregular bunches of galena of all sizes up to masses of nearly pure lead sulphide several feet in cross section. These bodies of galena are irregularly distributed, have ragged boundaries, and grade outwardly into siderite, traversed by innumerable stringers of galena, which then coalesce here and there to form bunches of considerable size. The stringers are very small, few of them being over a fraction of an inch in width and many not much thicker than a sheet of paper. They are characterized by an intimate and close reticulation. They are so closely crowded near the best ore that a slight increase in thickness would result in the formation of a mass of pure galena, and it is evident that they represent an intermediate stage in the complete replacement of quartzite by galena. The fragments of the shattered quartzite have been attacked by the ore-bearing solutions not only on their outer surfaces, but along multitudes of originally microscopic cracks within each fragment. The result has been that such fragments have been in many areas replaced completely by galena. Scarcely any of the ore shows the concentric and shelly structure observed where the ore-bearing solutions have been limited, by lack of permeability of the rock affected, to a peripheral attack on the fragments. Not all bodies are of this type. Much of the ore occurs as large solid stringers in clearly filled open fissures. The relation of the ore-bearing fissures to structurally important faults is not known.

The mining methods employed at the Bunker Hill and Sullivan mine have been found to be suited to irregular occurrence of ore, and permit clean mining and high extraction. The ore bodies at this mine occur in a severely faulted zone of Algonkian quartzites and have been much disturbed by later faults. Although the metamorphism of the region is attributed to the underlying intrusives, no connection between these intrusives and the deposition of ore has been shown.

The deposits occur in two types of veins: the Bunker Hill vein and the Jersey vein. The Bunker Hill type consists of wide irregular masses of galena with siderite and quartz gangue. There is ordinarily one well-defined wall, but never two. The dip is between 40° and 50°. About 80 percent of the ore has been produced from this type of vein. Veins of the Jersey type vary in width from a few inches up to 40 feet and have dips of 45° to 50°. They carry some siderite, but the ore is siliceous as compared to the Bunker Hill type vein. The Jersey veins traverse hard quartzite. The method of mining used is square-set and fill. Mining practice is to remove all material showing galena. A definite hanging wall is seldom found, and the overlying rock is invariably heavy.

The following is stated by Easton:[23] The process of cutting out the sill floor, and stoping the ore so exposed, calls for means and methods which are definitely related to the shape of the ore body and its mineralization. These conditions must be met and allowed for as they are encountered. The structure of the enclosing country rock is pretty much disregarded, because square sets do not permanently support the rocks which enclose the void created by stoping. They are used primarily for protecting the workmen from falls of rock and to afford passageways for manways and ore chutes when the stope is filled. Good mining practice, especially in heavy ground, is to keep this filling right up to the face. No timber can withstand the enormous crushing effect which is generated by large underground rock openings. Where the stope is small enough, simpler and cheaper methods of timbering can be used, but all of them must be filled with waste rock to avoid the risk of caving which might result in injuries or fatalities to the workmen and losses of ore except in the case of rare instances where the country rock is uniformly hard and strong.

In this mine it does not make any difference whether the enclosing rocks are affected by faults, intrusion, metamorphism, alteration by thermal solution, alteration by meteoric water or other geologic condition, the opening created by mining is temporarily sustained by timbering. Square-sets are used where the ore body is large, and where shrinkage and caving methods are not practical. The geological details, no matter what they are, do not make it possible to depart from the rigid necessity of replacing the ore by waste filling.

McIntyre Mine.[24] (See also cut-and-fill stoping)

Figures III-A.15 and III-A.16 are, respectively, a plan view and a cross-section through a stope on the No. 25 vein between the 3875 and 3750 levels showing the geology and the timber.

There are very few stopes at McIntyre which have followed the square-set method from level to level. Most of them are mined by the flat back cut-and-fill method. Square-sets are commonly used for removing floor pillars of variable height depending on the condition of the ground.

In some stopes, however, where widths are considerably above the average (10 feet) and where the ground is blocky, these conditions have forced a change to the square-set method after a very few lifts (floors) have been completed. Figure III-A.16 is a good example of this condition. The ore is a quartz vein with inclusions of graphitic slaty tuff or argillite. The vein lies in or along one side of the tuff which may be strongly sheared and considerably contorted. The faults, chiefly post-ore, are marked by an apparent concentration of graphite, which is perhaps merely a reorientation of the flakes. The tuff bed is about 30 to 45 feet wide in addition to the vein. It lies between carbonated basalt flows and is cut by porphyry dikes. There has been enough movement along the vein walls and larger inclusions to produce graphitic slips which cause the rock to break in slabs.

After considerable trouble was experienced in this stope by falls of ground in the flat back cut-and-fill method, it was decided to mine the remainder in vertical slices using square sets for support. A similar method is in use in several other stopes in this same vein system.

Frood Mine[25,26]

The formations in the Sudbury basin consist of a complex group of igneous, sedimentary, and metamorphic rocks. The structure includes dikes and sills, intrusions of granites of various ages, norite, greenstone, pegnatites, and many others. Quartz-diabase dikes are later in age than the granite. One period of formation of such dikes was followed by a period of faulting. The faults strike northeast and are of the overthrust type. The Frood breccia, "crush conglomerate," which is found at or near every major contact in the area as well as in places of minor disturbance such as folds and small faults were also formed during a related period.

Most of the valuable mineralization is found in areas of quartz-diorite and quartz-diorite breccias and commercial deposits are located in these formations at the intersection of breccia zones.

The Frood-Stobie ore body lies in a dike-like noritic rock body known as the Frood offset. This offset was the localizing agent for the mineralizing solutions, and is nearly all mineralized. A good portion of it is ore and the geometry of the deposit is essentially the geometry of the offset. Although a large tonnage of ore does occur in adjacent rocks, it parallels the structure of the offset and the amount is small compared with the tonnage in the offset.

The dike-like ore body strikes northeasterly, dips 75° to the northwest, and has an overall length of 9,500 feet. The principal ore body being mined is a lobe of the deposit which extends below the 1200 level.

At the 1600 level it is 3,500 feet long and averages 85 feet in width. The width becomes greater at higher horizons because the hanging wall dips more steeply than the footwall. The outline of the ore is habitually smooth except where it is broken by a minor fault, which displaces the ore about 50 feet. Also, there are several rolls or spurs of ore which extend into the hanging wall rocks, approximately perpendicular to the dip of the ore body. These irregularities are due to the local structural control of the hanging wall rocks, and each has a characteristic rake which permits reliable projection of its position for reasonable distances.

The ore has been classed in four divisions: (1) disseminated ore, (2) breccia ore, (3) massive sulphides, and (4) siliceous ore. The bulk of the ore is constituted of disseminated pyrrhotite, pentlandite, and chalcopyrite in the noritic rock.

The breccia ore and massive sulphide occur as a thin discontinuous sheath around the disseminated ore and as an important solid body of high grade sulphides extending 500 feet down the dip from the disseminated ore. The latter, however, is associated with the surrounding rocks rather than the offset rock. The breccia ore consists of schist remnants and rounded rock fragments embedded in a matrix of fine-grained sulphides flecked with black silicate minerals.

The siliceous ore is found below the heavy sulphide types where the latter fingers out as stringers and weak disseminations in rock which consists mostly of schisted Frood breccia.

The disseminated ore, together with the surrounding breccia ore and the massive sulphide, constitute a compact mining unit. Mineralization terminates rather abruptly at the margins of the ore body, at places against clean partings. Gradational boundaries which require control sampling do not occur except in the siliceous ore. The disseminated ore is a structurally strong body which tends to break to an arched back in stoping. It is considered good mining ground. The massive sulphide ore tends to slab horizontally, and where ore projections extend into the hanging wall, particularly heavy ground conditions are sometimes encountered.

The country rocks surrounding the offset rock belong to the Frood series of interbanded quartzite, rhyolites, greenstones, and gabbroic sills, all of which are penetrated, particularly along their contacts, by the Frood breccia. The physical behavior of these rocks under mining conditions is of prime interest. The rhyolite is brittle, well jointed, and has a high bursting potential, which gives rise to the worst mining conditions in the mine. The breccia tends to slough because it is heterogeneous and somewhat schisted, although sloughing is not serious. The quartzite is found impure, commonly sericitic or micaceous, and provides reasonably good ground. The gabbro and greenstone are medium to fine-grained rocks which are firm except where they have been loosened along the joints. These members of the Frood series are relatively thin and since they lie at low angles to the ore body, attempts to locate openings in the safer rocks are hampered. Longer cross-cuts may traverse all types of rock, but it is sometimes possible to favor the best ground in laying out drifts and raises.

The square-set method of mining is employed to mine higher grade ore deposits where complete extraction is desirable, where the ore and walls require support during stoping operations, and where it is necessary to prevent caving and subsidence of overlying and surrounding ground. It is applicable to ore deposits of all sizes, shapes, dips and degrees of irregularity. This method is also used to mine rib pillars, crown pillars, and floor pillars in filled stope areas. Remnants of ore left in place, not recoverable by other methods, and broken ore left between chutes in filled shrinkage stopes, have been recovered by the use of square sets. Inclined cut-and-fill is used in narrow, irregular ore, where back support is not necessary but wall support is necessary. Horizontal cut-and-fill was first chosen as the method of mining, but as the stopes were opened up, great numbers of cleavage planes and numerous cross fractures in the ore made square-setting necessary.

Lake Shore Mine[27,28]

The productive veins of the Kirkland Lake district lie within a belt of pre-Cambrian sedimentary rocks composed of metamorphosed tuff, conglomerate, and greywacke, which occupies a synclinal trough in the old Keewatin basement. The syncline is about two miles across, and the strike of the beds is N 60° E. Intrusives occur in the form of dikes and bosses, and these make up a greater part of the ore zone. The most important of the intrusives is the porphyry, which is believed to be related to the mineralization.

The Lake Shore ore bodies are made up of secondary minerals which are deposited in the crushed and brecciated zones formed by an earlier system of faults. The important geological events leading up to and following the mineralization are as follows:

(1) Folding of sedimentary rocks and development of the syncline now found at Kirkland Lake.

(2) The intrusion of the granitic offshoots along the ore zone.

(3) The formation of a series of overthrust faults as a result of pressure applied from the southwest.

(4) The injection of deep-seated mineral solutions along some of the faulted zones. It is probable that a good part of the mineral deposition took place during the period of faulting.

(5) Tangential strain acting on the country to the east produced a series of post-ore faults, accompanied by the deposition of calcite, barite, quartz, and chlorite in narrow seams. This same type of mineralization is found in cross faults.

The Lake Shore vein system is part of the general fracture pattern which was produced by the faulting referred to in (3) above, which formed a parallel series of easterly-striking sheared zones jointed by weaker diagonal fractures.

At the Lake Shore mine there are two veins, the north and the south vein-faults which represent the main structures. Each fault zone is made up of several parallel fractures with characteristically diagonal breaks joining them. The resulting structure is that of vein zones broken up into roughly diamond-shaped blocks of all sizes. The same block pattern exists between the two veins.

North Vein Zone. This vein is the most productive, extends more than 2,800 feet horizontally, 4,500 feet vertically, strikes N 70° E and dips 75° to 82° to the south. The fracture zone is more than 100 feet wide in the west portion of the ore body, but is narrower to the east. Within the fracture zone there are heavy parallel shears or mud seams marking the planes of movement, and the rock between the breaks is highly crushed and brecciated. While the heaviest shear is on the footwall side of the ore, this is not always the case, and where the fracturing is widespread, there are two or more well defined east-west shears. It is along the heavy breaks where the most continuous and uniform ore bodies are found. However, in some places where the main channels have apparently been rendered impervious to the flow of solutions by the mud and gouge, they contain very little ore, and the subsidiary cracks and branching fissures may be mineralized.

Parallel ore bodies are found in the vein zone on the west side of the mine where parallel fractures have been mineralized. In some cases the veins are separated by horses of waste, while in others the crushed ground between contains sufficient amounts of valuable minerals to permit mining of the whole width.

The minable width of ore varies considerably from place to place along the vein, depending upon the extent of the fracturing because the latter was the primary control in ore deposition. Where branching ore shoots join due to difference in dip, this creates a difficult mining problem because stoping above wide sections of ore eventually reaches a point where it becomes necessary to divide the width into two parts. The intervening waste pillars are usually highly crushed and are consequently very difficult to support. Numerous cross slips occur in the wider ore bodies in certain parts of the deposit, but these appear to be part of the pre-ore fracture pattern. In general, the hanging wall of the ore body is not well defined, and its outline is less regular than the footwall side. Test holes are drilled into the hanging wall side to determine the ore limits.

South Vein Zone. The South vein is in a strong fractured zone which parallels the North vein and lies about 400 feet south. While the fracturing is similar in appearance to that in the North vein, the structure is not as strong and the ore shoots are less continuous and narrower. This was due in part to the fact that the crushing was less intense and the rock between fractures is firmer and not so badly broken up. The ore may be lower in grade, and parallel ore bodies are much less common. Post-mineral faulting has caused very few mining problems. Only one large fault and a few small ones are known to exist which have been subject to movement subsequent to mineralization. The ore in the North vein is practically one continuous body of ore, while that in the South vein occurs in several important shoots.

Nature of Ore and Wall Rocks. The porphyry and syenite are very highly altered in the vicinity of the North vein and the rocks are much lighter in color. The whole fault zone is intensely crushed and brecciated, including the ore body itself. Quartz has been introduced as fillings around broken fragments of rock, as irregular masses and stringers, and not as clear cut veins. The quartz itself contains many fractures around which additional quartz containing gold, tellurides, sulphides, and a minor amount of carbonates were deposited.

Coarse sulphides are lacking, except for local segregations of chalcopyrite, and lesser amounts of galena, in some of the post-ore calcite seams. Due to the intense fracturing, the ore in the North vein tends to become loose during mining operations. This is particularly true in the other sections, where parting frequently takes place along horizontal planes. The result is the formation of rather large blocks of loose ore or rock which must be supported by timber cribs in the stopes. Horses of waste in stope areas and thin pillars between parallel ore bodies fail easily and are difficult to hold. Inasmuch as these pillars always contain some values they may be included with the ore rather than to attempt to hold them in place if they are not too large.

In the South vein, although the rock has been less severly crushed than that in the North vein, there has been more intense silicification close to the main shears and considerably more fine sulphide mineralization has been introduced into the ore. The result is a firmer rock and ore which requires less support in mining. Parting along flat seams is also less frequent in this type of ore.

Jointing is an important feature of the wall rocks of both vein zones. As a result, the walls are weak along both ore bodies. The effect is more noticeable in the North vein, due to the more intense crushing. During mining, particularly if the wall rock is porphyry, smaller angular blocks are formed along the walls and, if they are unsupported by backfill or timber, the sloughing will extend for some distance into the walls of the ore body. When the walls are made up predominantly of basic syenite, larger lenticular slabs are formed. They are usually bounded by smooth planes coated with chlorite and other secondary minerals, the presence of which results in treacherous stope walls which require very careful attention. Sulphide mineralization is more plentiful in the South vein.

Effects of Pressure. One of the problems encountered in deep mining is the movement of rock around mine openings induced by the increasing rock pressure accompanying increasing depth. Evidence of increased pressure is usually indicated by a sag in the hanging wall which may be accompanied by bursting of the rock. Rock bursts are the sudden failure of rock under stress of pressure, with considerable expenditure of energy. They occur at comparatively great depths and depend upon local geological conditions.

Rock Bursts. The factors influencing the incidence and severity of rock bursts are summarized as follows: (1) depth of workings, (2) structural features of ore and enclosing rocks, (3) dip of the ore body, (4) concentration of mining operations, and (5) rate of mining.

(1) Depth of workings:

For similar geological structures, the incidence of rock bursts and possibly their violence increase with the depth of the mine workings. Movement of the rock around openings at shallow depths is usually limited to sloughing while the rock structure adjusts itself to the presence of the new openings. At greater depths, however, there is a tendency for the rock around the opening to move toward it in an attempt to establish equilibrium conditions. According to the doming theory, this action causes the formation of arches over the opening as successive layers of the rock reach their ultimate strength and fail. This process continues until the dome becomes large enough that it will maintain itself. The size of the dome depends upon the size of the excavation, the nature of the wall rocks, the method of support, and the depth of the workings. The most severe bursts occur where there is a merging of domes from contiguous stopes.

The primary cause of all movements of rock at depths in a mine is believed to be the rock pressure due to the weight of the overlying mass. This pressure might increase linearly with depth only if hydraulic conditions are assumed, but the rigidity of the rock and discontinuities of geologic structure almost preclude such an assumption.

(2) Structural features of ore and enclosing rocks:

The walls of mine openings are not homogeneous in structure, consequently the presence of joints, contacts, bedding planes, fractures, dikes, etc., tend to relieve the stresses which would otherwise be built up in the rock. Pieces of rock have been known to fly off of the face of contacts with explosive violence. The physical character of the rock is also important, because hard, brittle rocks are more susceptible to bursting than soft, weaker ones.

(3) Dip of the ore body:

Rock bursts are more likely to occur in steeply dipping deposits than in those which dip at low angles. If the downward pressure is resolved into normal and tangential components, it is suggested that in the case of flat lying deposits, most of the pressure is normal to the deposits or openings, and all of the cumulative effect of the pressure is not transmitted to the lower workings. In steeply dipping deposits, the pressure is mostly tangential and is carried downward in a cumulative manner.

(4) Concentration of mining operations:

Mining extensively in one area tends to increase the instability of the rock and the tendency toward rock-bursts, because of the greater amount of open space and the merging of domes.

(5) Rate of mining:

Mine development opens up only small areas and has little effect upon rock movement. When stoping is well under way, however, and a larger portion of the solid support of the walls furnished by the ore body has been removed, the effects of the pressure become serious.

The most common bursts in the Lake Shore mine are (1) strain bursts in exceptionally hard brittle rock, and (2) pillar bursts where the pillars are too small or too few to support the constantly increasing load.

The porphyry, and the syenite to a lesser extent, are strong and somewhat brittle rocks. They are resistant up to a point of failure, as compared to soft schistose rocks where the relief of stress is a more gradual process. To what extent the fracture system in the rock affects the occurrence of rock bursts is not known conclusively.

The type of rock burst experienced at the Lake Shore mine has been associated with the floor pillars developed as part of the cut-and-fill method of mining. As a result of a study of the causes of rock bursts, a square-set filled-rill method was evolved to mine the block of ore from the 2575 level to the 3200 level. This effectively eliminated the objectionable features of the cut-and-fill method which resulted in bursts of the floor pillars left during mining.

Top Slicing and Sublevel Caving

Gogebic Range.[29,30]

Both top slicing and sublevel caving are employed to mine iron ore deposits on the Gogebic Range. The ore bodies are found in several horizons in a series of steeply dipping (55° to 70°) cherty and slaty beds which rest on a quartzite footwall. The formations are very regular both along their strike and dip. The deposits usually occur as iron concentrations in V-shaped pitching troughs which are formed by the intersection of igneous dikes with the footwall quartzite and with impervious slaty members of the geologic column. (Figures III-A.19 and III-A.20).

The size and shape of the ore bodies vary, with dimensions from a few to several hundred feet in width and depth, and from several hundred to several thousand feet in length. The ore is composed of soft, red, partly dehydrated hematite with lesser amounts of hard or specular hematite.

From the accompanying geologic section (Figure III-A.19), it is noted that the hanging wall consists of a partly leached cherty iron formation and slates which, as capping, vary considerably in tenacity and hardness. As a rule they break into blocks or slabs which form an interlocking gob as they cave, and arch over so that they require only light temporary support while the slices are being driven and caved back.

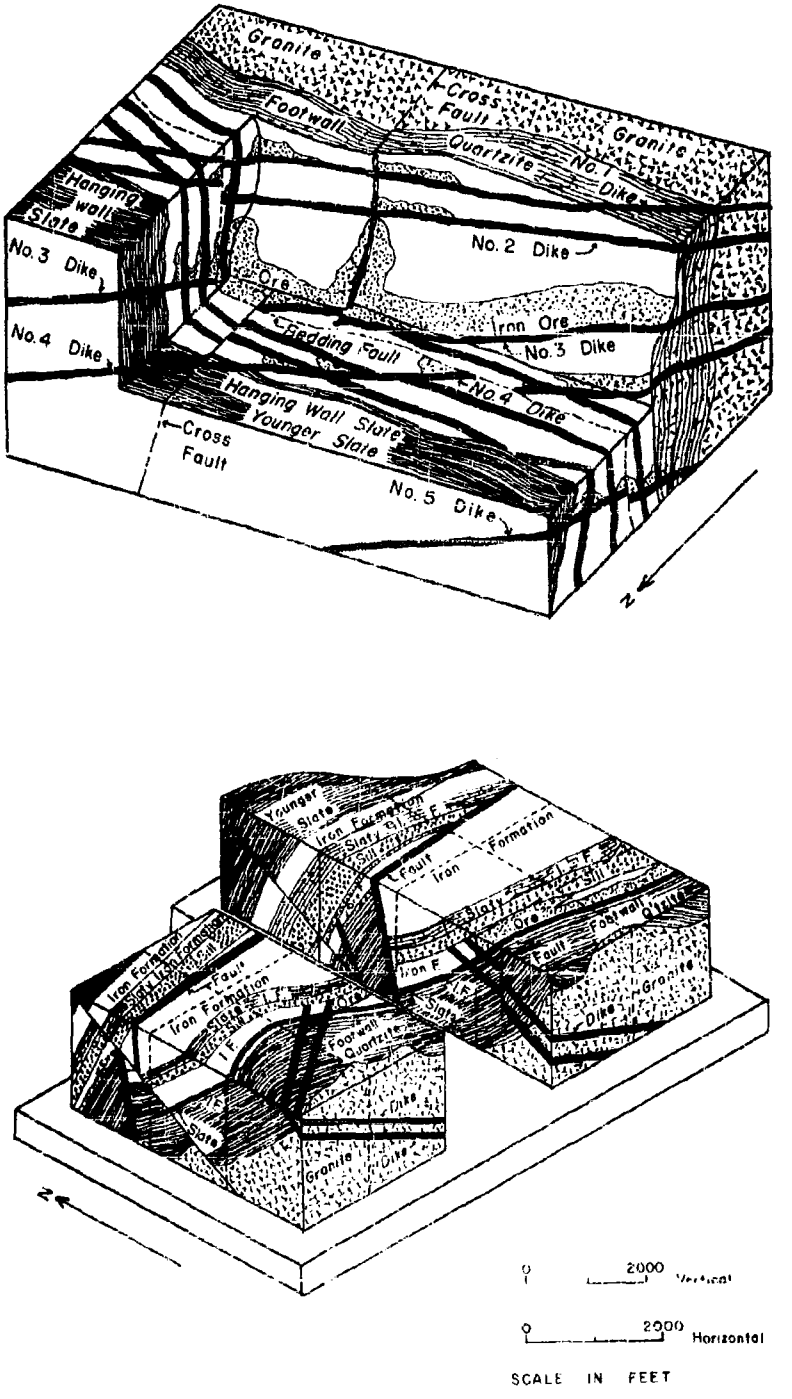


Figure III A.19. Block diagrams of the ore formations in the Gogebic Range.

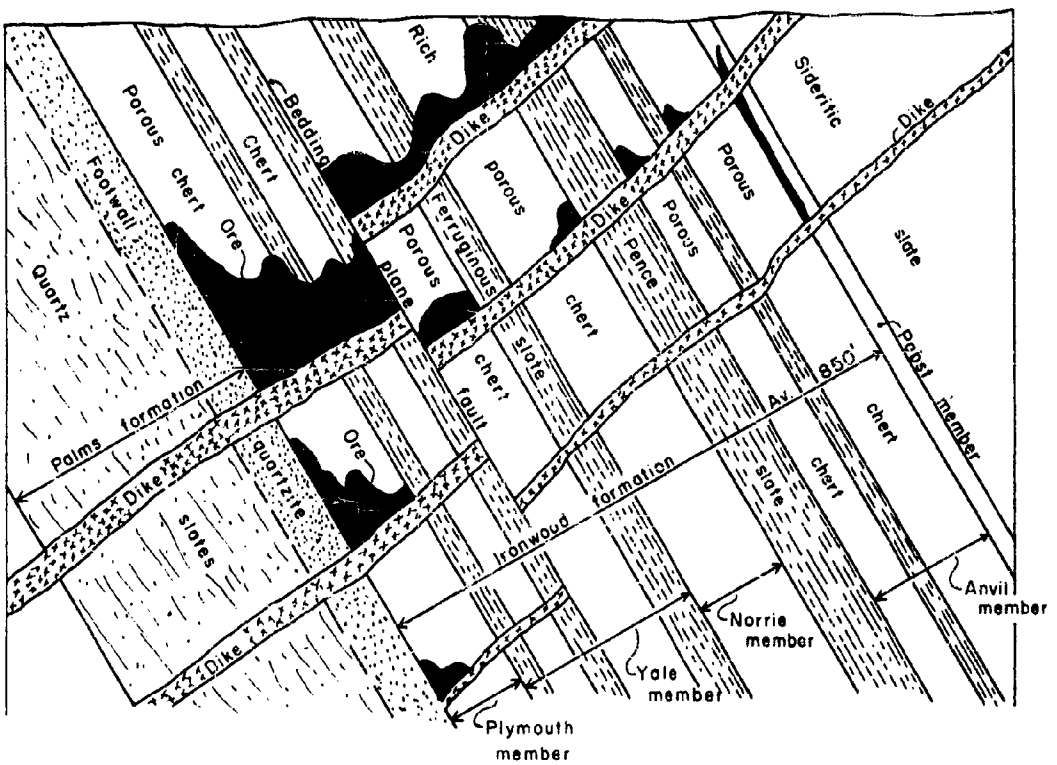


Figure III-A.20. Generalized geological section of the Gogebic Range.

Most of the ore bodies are V-shaped in transverse section, which makes them especially suitable to mine by sublevel caving. This follows from the fact that the shape delays the caving of the gob due to the ore bodies being narrower on each successively lower sublevel, which in turn assists in producing an arch effect in the gob.

The boundary between the ore and the wall rock is often well defined, but is sometimes very irregular. The hanging wall rocks in some places contain considerable amounts of iron minerals. However, where this is the case any small dilution of the ore by hanging wall rock does not seriously affect the grade of the ore being mined. As a rule, the outlines of the ore bodies are very irregular, due to the cross-fault zones and erratic occurrence of ore above the impervious bottoms of the troughs.

Some of the mines in this area are deeper than 3,000 feet, which causes heavy pressures around the ming openings. Consequently, all drifts in ore require timber support. In some places, drifts in the immediate footwall require even more timbering, although this is not usually the case. Also, in some localities the beds are broken and displaced by faults of variable strikes.

In the Eureka mine, the beds are displaced by numerous faults, displacements varying from 100 feet to 600 feet. The faults dip and strike in all directions. In some cases, they have aided in formation of the ore bodies and other cases have served to prevent deposition in otherwise favorable localities.

Most of the ore is a soft red hematite which requires timber support in all mine openings. The top of the footwall is constituted of a band of soft red slate which has the characteristics of shale where it is adjacent to ore bodies. It slabs off easily and is a constant cause of dilution of the ore. The hanging wall or capping is usually found to be a cherty iron formation, and the contact between this formation and the ore is very irregular. The hanging rock is usually structurally strong enough to stand without support. However, when blocks of this rock are weakened by mining operations, they slab off after ore has been removed.

Two types of ore bodies are found in the Eureka mine. (Figure III-A.21). The most typical one consists of masses of ore which are triangular in cross section lying at the intersection of diorite dikes with the footwall. The other type consists of narrow blankets of ore 5 to 20 feet in width which lie on the footwall. The capping is strong and hard, but has been weakened longitudinally by seams of ore and transversely by cross-jointing planes 8 to 20 inches apart.

Block Caving

Climax Molybdenum Mine

The geological conditions at the Climax mine are summarized by Bucky as follows:[31]

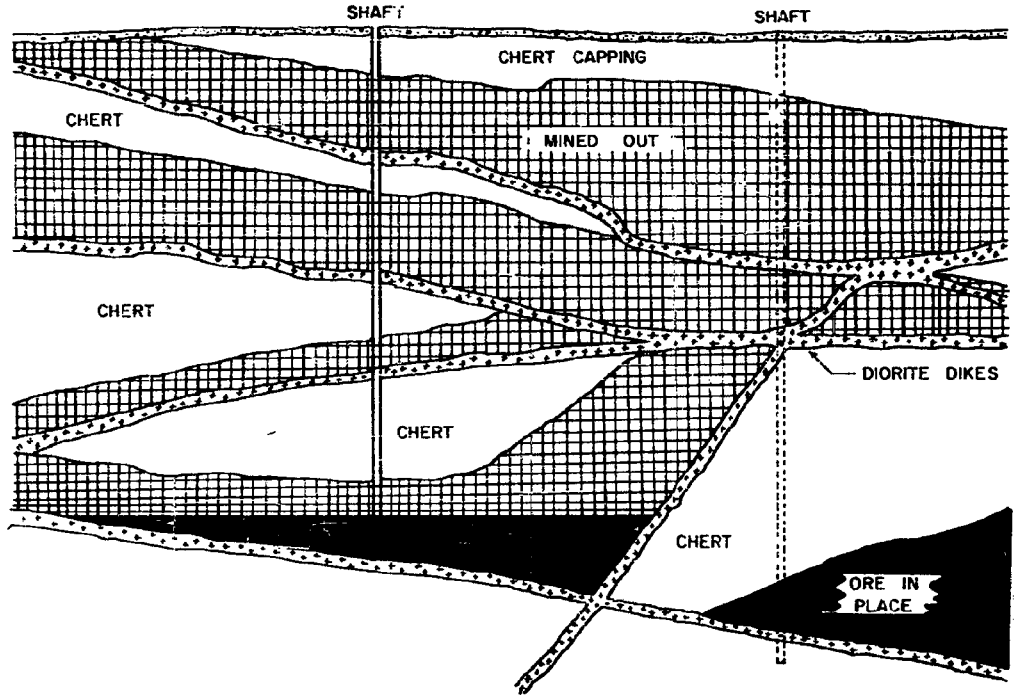


Figure III-A.21. Longitudinal section of the iron deposits showing the succession of formations overlying the ore, Eureka Mine.

Shape. The top portion of the deposit is dome-shaped, the next lower portion being an elliptical ring with the center area barren and siliceous. The ore body beneath this is also elliptical in shape with the center ore-bearing.

Dimensions. At the Phillipson level the ore body is an elliptical ring with an axis of 3,000 feet in the northeasterly direction and an axis of 2,800 feet in a southeasterly direction. The mineralized section is 400 feet wide. Its depth is unknown.

Dip. The dip is steep and variable, from 90° to doming over the top.

Capping. The thickness varies from 0 to considerably over 300 feet.

Estimated Tonnage. Over 100,000,000 tons.

Ore Mineralization. Molybdenite is found finely disseminated in quartz veinlets in fractures.

Ore Characteristics. Valuable minerals occur in a silicified schist and granite, and in early porphyry.

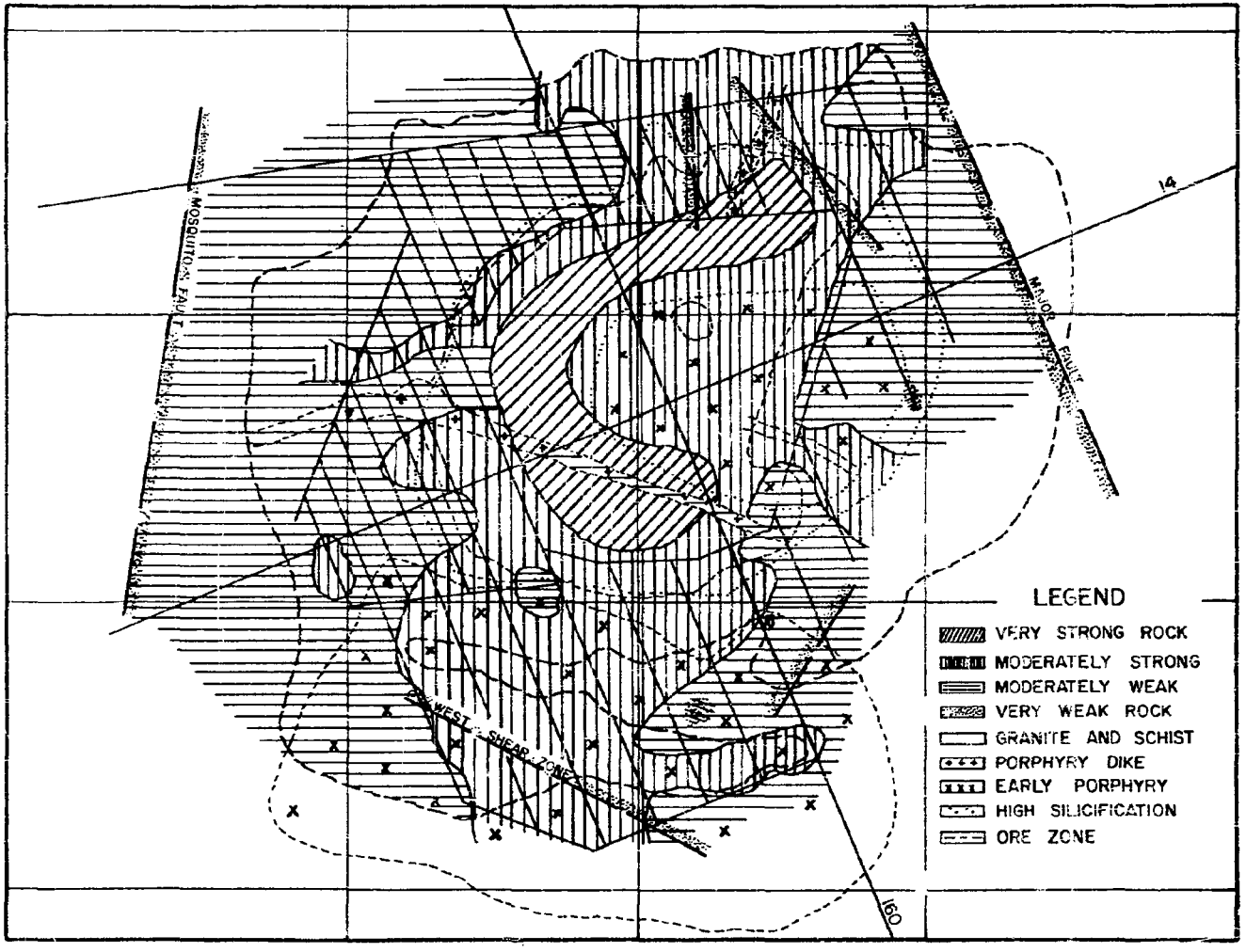
Mineral Content of Ore. Varies, estimated fraction of 1 percent.

Physical Characteristics of Ore Body. The granite is hard but is cut by numerous small sericitic fractures. The ore body in general is intensely fractured. The degree of silicification varies from intense at the footwall to slightly altered at the hanging wall.

Physical Characteristics of Capping. Composed of the same type of rock as the ore body, but has been subject to considerable surface alteration and less silicified. It is softer and weaker than the ore body.

Descriptions from a recent study of King[32] are repeated here in considerable detail because his work illustrates the qualitative geologic principles of rock mechanics and block caving. A horizontal section of the mine on the Phillipson level (Figure III-A.22) shows that the outer ore zone is an annular ring varying in width from 300 to 800 feet, surrounding barren silicified rock. Vertical sections (Figures III-A.23 and III-A.24) reveal the ore zone to be dome shaped with its apex truncated by glaciation. An outer ore zone overlies the barren core described above, and is itself overlain on the flanks of the dome with unmineralized rock. The central ore zone of similar shape lies under the core of barren rock.

The molybdenite is distributed uniformly through a zone of moderately silicified granite, schist, and quartz monzonite porphyry, around the highly silicified core. It occurs in veinlets associated with fine granular quartz and pyrite, these minerals replacing altered and fractured granite, schist, and porphyry, and as coatings on numerous fractures in these rocks.



F.gure III-A.22. Plan view of the Phillipscn level and the rock distribution according to type and class, Climax Molybdenum Co.

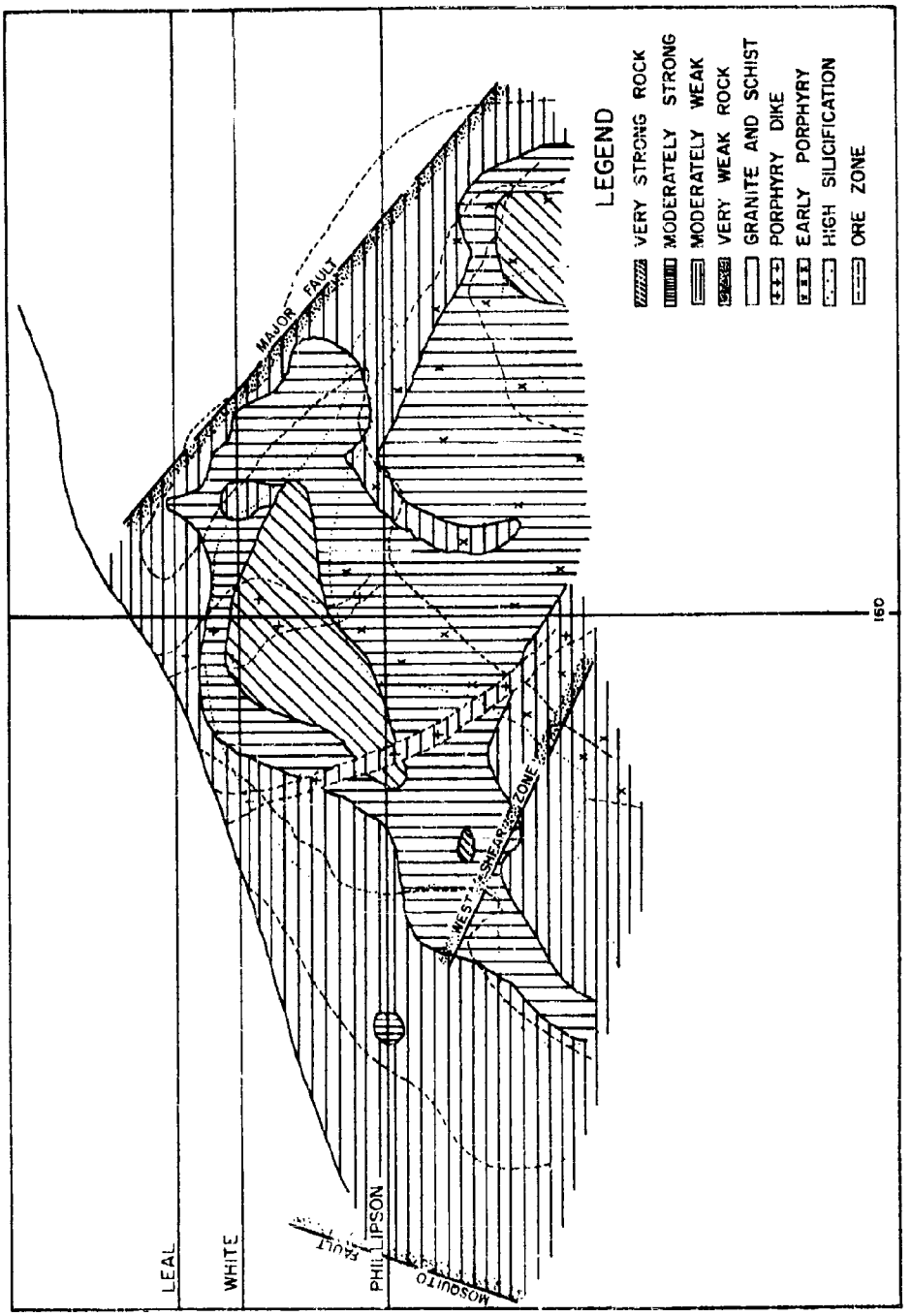


Figure III-A.23. Vertical section at right angles to that in Figure III-A.22, Climax Mine.

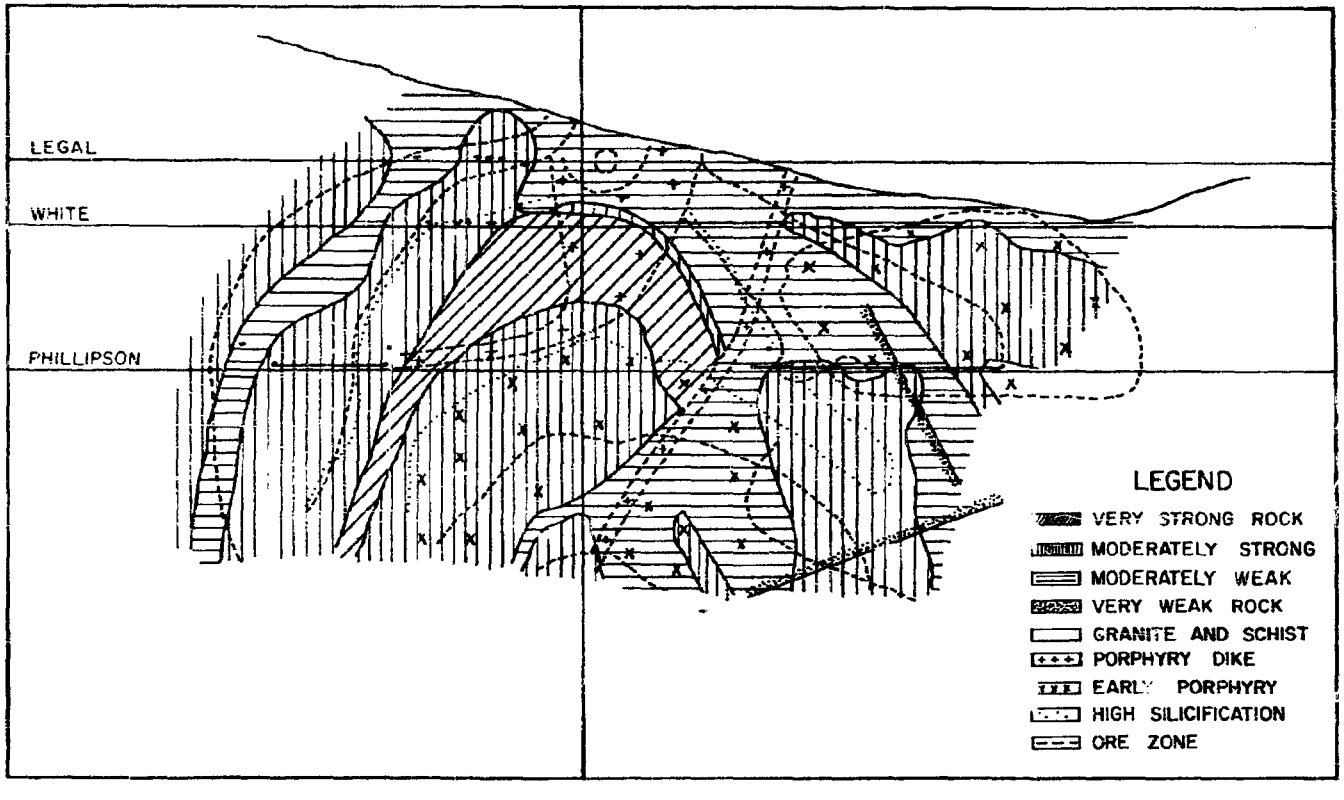


Figure III-A.24. Vertical section through the Climax ore body, Climax Mine.

While the Climax ore body is intensely fractured, many fractures are mineralized and no longer represent planes of weakness. Much of the fracturing is post-mineral, however. These fractures are generally filled with sericite and gouge, or they remain as unmineralized joints separating otherwise massive rock into blocks of various size.

Important differences in the behavior of ore and various types of rock were recognized and a study was made to determine the relation of the cave-ability of the rocks to their physical characteristics. This study brought out the importance of geological structures, including mineralization, silicification, sericitization, and decomposition.

For classification purposes the rock was divided into four types: (1) very strong, (2) moderately strong, (3) moderately weak, and (4) very weak. Each can be readily distinguished from the others and their distribution is shown in the accompanying sections.

The rocks in class (1) are very strong, hard, and competent. They are constituted of that material which is unmineralized and relatively unfractured around the ore body, and of rock which has been highly mineralized, such as that occurring inside the footwall of the ore zone. Here the original rock is almost completely replaced by quartz and fracturing and jointing are present in minimum amounts. Rock of this description represents that at one extreme end of the range of physical characteristics.

The rocks with properties of those in class (4) are very weak, soft, and incompetent, and are best represented by the broken and crushed rock found along fractures and faults. Characteristic features include intense fracturing and crushing sericitization, banded quartz with vugs, coarse fluorite and pyrite. This type of rock constitutes not more than one percent of the area of any section.

Most of the rock falls in classes (2) and (3). Moderate silicification, generally fresh rock, wide spacing of fractures (6 inches to more than 2 feet) are characteristic features of moderately strong rock. Post-mineral faults are not prominent in this class, nor is there much sericite or soft material filling the new fractures that are present.

Moderately weak rock is distinguished from class (2) by a more closely spaced (1 inch to 2 feet) fracture pattern, by the presence of more iron oxide and sericite along the fractures, and by partly decomposed rock.

The caving properties of these rocks are as follows:

1. The first class is considered uncaveable because it is capable of maintaining support and can arch over openings of several hundred feet. Also, if sufficiently large stopes could be developed to cause failure in this type, the caved rock would break into blocks too large for efficient handling. This type of rock occurs in the silicified core, but affects mining adversely in only one area.

2. Moderately strong rock is caved successfully, but stopes should be more than 200 feet by 200 feet to initiate caving if the stope is isolated from other caved rock. The caved blocks of rock are generally large and will conform somewhat to the spacing of fractures and joints. There is little tendency to pipe or funnel because arches form and become stable over several draw points. This causes high hangups and prevents excessive draw from the individual points. When the draw is extended laterally, the rock eventually caves over a larger area. This type of rock is stable for most underground openings and constitutes about 40 percent of the total. Little or no timber is required at intersecting drifts or raise and shaft stations.

3. Moderately weak rock caves readily and the rock breaks to a size (up to 10 feet) that is easy to handle through draw points and in slusher drifts. Two slusher stopes are sufficient to start caving (200 feet by 100 feet). Large drifts in this type of rock require timbering. It makes up about one-half the total volume of the mineralized area.

4. Very weak rock is not stable for large openings, and drifting or raising through this type of ground requires complete, close timbering. Unsupported openings as large as 25 feet fail and cave. The problem is not in getting the rock to cave, but in maintaining slusher drifts and stations, and fingers long enough to draw large tonnages.

It is believed that the general fracturing of the mineralized area makes block caving possible. A good portion of the rock between fractures is hard and strong, and the whole mass would be very competent if it were not separated into blocks by fracturing. The majority of breaks occur along existing planes of weakness. The weak structures are those that have fractures filled with sericite, or thin pyrite and molybdenite veins.

Following are some important principles regarding the distribution of rock classes relative to the surface, silicification, rock types, and mineralization. The rock within one hundred feet of the surface has been weakened as a result of the processes of chemical change and decomposition characteristics of the surface rocks. This is shown in the accompanying vertical sections. Most fractures exhibit iron oxide or iron-stained sericite filling, and in many places actual oxidation has penetrated the rock. Diamond drill cores from this rock are soft, vuggy, and break into gravel when they are split.

Other moderately weak rock occurs west of the ore body adjacent to the Mosquito fault. Here the rock is predominantly schist with little silicification and exhibits a moderately close spaced fracture pattern. Difficulty in diamond drilling is above average and core recovery is lower than average.

The extremely strong rock can be correlated roughly with high silicification, but it does not occupy the entire zone of silicification. Here is found a minimum of post-mineral fracturing, and definite pyrite and molybdenite veinlets are not present. However, widely separated fracture zones and joints coated with molybdenite do occur, and these

probably cause the relatively stable rock to break up after it has been undermined by caving on the lower levels. The central silicified barren core is an arch-shaped mass of very strong rock, with but few fractures which would permit caving if it were ore.

Moderately strong rocks and moderately weak rocks occur irregularly in all formations. These include granite, schist, and quartz monzonite porphyry, which have been equally fractured. Porphyry dikes cutting across the ore body are prominent weak structures. Two major faults are important because of their location, primarily because they must be avoided when large openings are planned.

Conclusions

1. Silicification is closely related to strength where there has been no post-mineral faulting.

2. General fracturing makes caving possible. This is aided considerably by alteration and thinly mineralized fissures of pyrite and molybdenite. The weak structures are fractures filled with sericite, or the thinly mineralized veins.

3. Schist, porphyry, and granite are equally fractured, mineralized, and altered. All strengths of rock may occur in any of them.

4. The caving characteristics of the Climax ore body are thus related in a quantitative manner to the geologic structure and physical properties of the ore and rock.

Vanderwilt[33] notes that alteration increases gradationally from the hanging wall side of the ore zone to the footwall side. The footwall is a massive fine-grained quartz replacement of the host rock (granite, schist, and quartz prophyry). The alteration consists of quartz and orthoclase replacement as well as general decomposition of the feldspars which makes it difficult to distinguish rock types in some areas in the ore zone.

The rock throughout the whole ore zone is cut by closely spaced fractures which show no predominant pattern or orientation except in local areas. The spacing of fractures in the ore varies on the average from less than an inch to about 6 inches. In the fine-grained quartz in the footwall the spacing is about 6 inches to 24 inches. This quartzose rock is stronger than the rock in the ore zone.

The rock between fractures is moderately hard and strong, the best visible evidence of strength being the number and type of fractures present. As described above, King used these as a basis for mapping the caveability of the rock.

The various kinds of fractures and lines of weakness may be classified in four groups: (1) The first is the oldest and includes small (0.05 to 0.1 inch) quartz-molybdenite veins, some of which have been well cemented with quartz. (2) The second group to develop consists of many quartz-topaz-pyrite seams carrying minor quantities of chalcopyrite,

sphalerite, galena, and wolframite. (3) The third group contains numerous tight joints and open fractures filled with sericite, which cut both molybdenite and pyrite veins. (4) The last group includes many partly cemented fractures which were reopened by post-mineral movement. As the rock caves during mining operations, the post-mineral fractures and sericite-filled fractures are the most favorable planes of weakness along which separation takes place. Separation along pyrite seams is common, while the quartz-molybdenite veins are the least important lines of weakness.

Inspiration Mine.[31]

The Inspiration ore body is a mass of irregular outline with a bottom which is reasonably regular. Its average length is 8,000 feet, average width is 800 feet, and average thickness is 200 feet. The dip of the deposit varies from 0° to 30° and the capping varies from 0 to 500 feet in thickness. The ore minerals are chalcocite, malachite, asurite, and chrysocolla, which are distributed along cracks, fractures, and in crevices. Chalcocite and cuprite are found disseminated in (Pinal) schist and (Schultz) granite.

The ore body has been completely fractured and is very weak. Due to the fractures it caves readily. The ore body is bounded on the east by a fault on the other side of which lies the Miami deposit. On the west the deposit becomes too thin for possible mining.

The capping is also very weak, but breaks too fine, does not pack and flows readily.

Case History of Underground Power Station

Power Station, Snowy Mountains, Australia.

One of the most successful applications of a combined knowledge of rock mechanics and its relationship to structural geology is found in the construction of a power station in Snowy Mountains, Australia.[34,35] The station is eleven hundred feet underground in a granite mass which exhibits sheeting, faulting, and jointing. The dimensions of the machine hall are 306 feet in length by 77 feet in maximum width with a height of 104 feet maximum. Physical properties of rocks were determined together with residual rock stresses. These were utilized in relationship to rock structure in an effort to orient the openings in order to avoid weakening the underground structure. Photoelastic studies were also made to ascertain important stress concentrations.

Geology. The regional geology of the area is shown in Figure III-A.25. Rugged mountains in the area are composed predominantly of granitic rocks and slightly metamorphosed sedimentary rocks whose age varied from Ordovician to Devonian. In plateau areas the granite is intensely altered but in low stream valleys is found to be fairly fresh. The Tumut River near the power station has cut a steep V-shaped valley about 2000 feet deep in the table land, while to the east the basalt from a plateau fills a floor of an ancient valley. Both of these structures may have affected the residual underground stresses. As shown in Figure III-A.26 the T1 and T2 power stations have been located in a complex mass of granitic paragneiss and granulite which has been intruded by sheets of granite. The metamorphic rocks are known as the Boomerang Creek granitic gneiss and the igneous granite as Happy Valley granite. Marginal zones of the granite are heavily faulted and sheared. The immediate area in the vicinity of the power station is intersected by a series of overthrust faults with zones of crushed rock, clay, and close jointing near or in fault zones. Because of the instability of surface soil and weathered surface rock the penstocks were placed underground. The geology of the T1 power site is shown in Figures III-A.26 and III-A.27.

Geological Structure of the Site. As indicated above, the rock in the area of the power station site is of two types, gneiss and granite. The granite is found in sheet-like masses 100 to 300 feet thick intruding into the gneiss. The contact between these two types of rock is gradational, varying in thickness from a few feet to as much as 20 feet. These rock masses are intersected by a series of overthrust faults which trend northeast and generally dip 30° to 40° southeast. A large fault is found in the locality of the headrace surge-tank which is about 1000 feet in elevation above the main machine hall. The fault zone ranges in thickness between 50 and 90 feet and consists mainly of closely jointed granite which contains several seams composed of crushed rock and clay one to five feet thick.

A second fault zone is found in the tailrace tunnel 4,000 feet downstream of the station. Tectonic action has resulted in a very closely jointed and softened gneiss which contains many thin crushed zones and clay seams up to one foot in width. The power station is

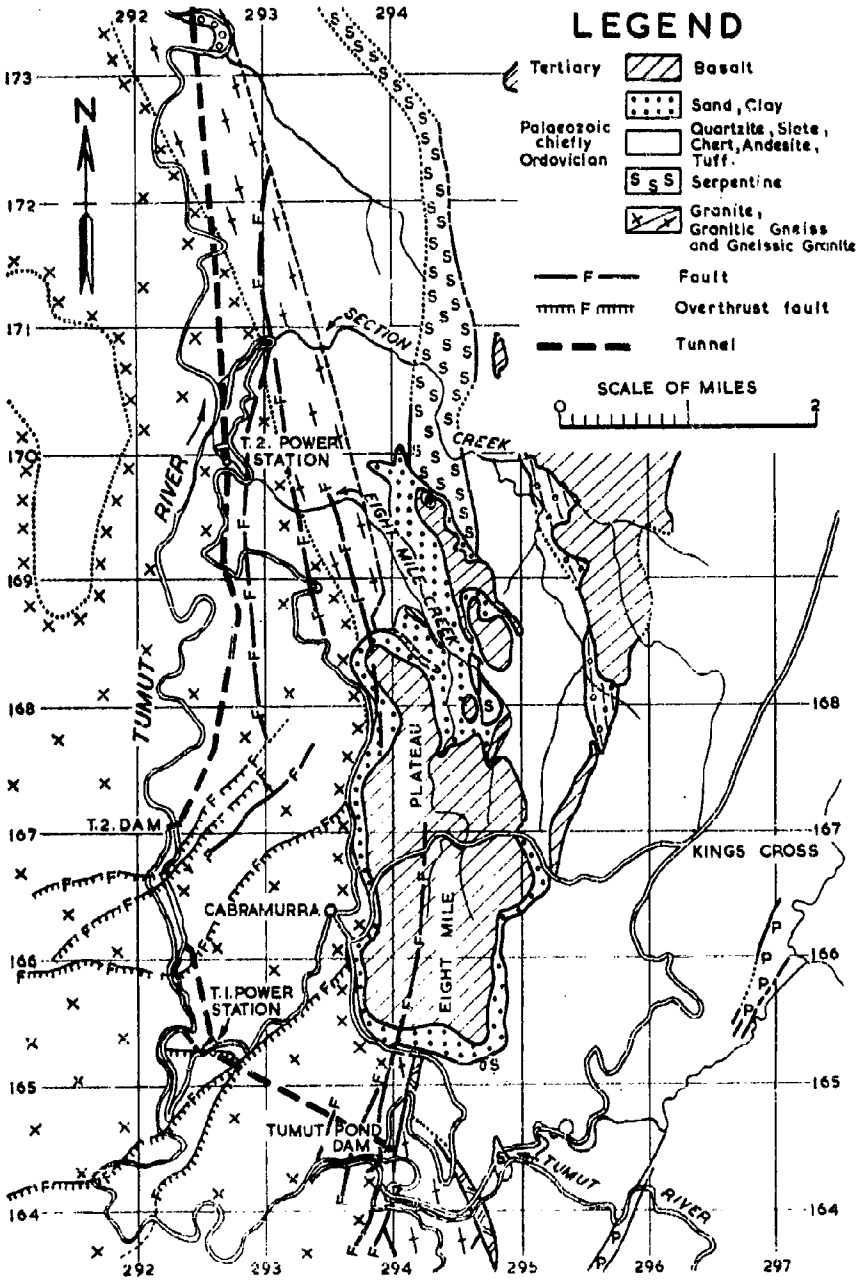


Figure III-A.25. Regional Geology, Snowy Mountain Power Station.

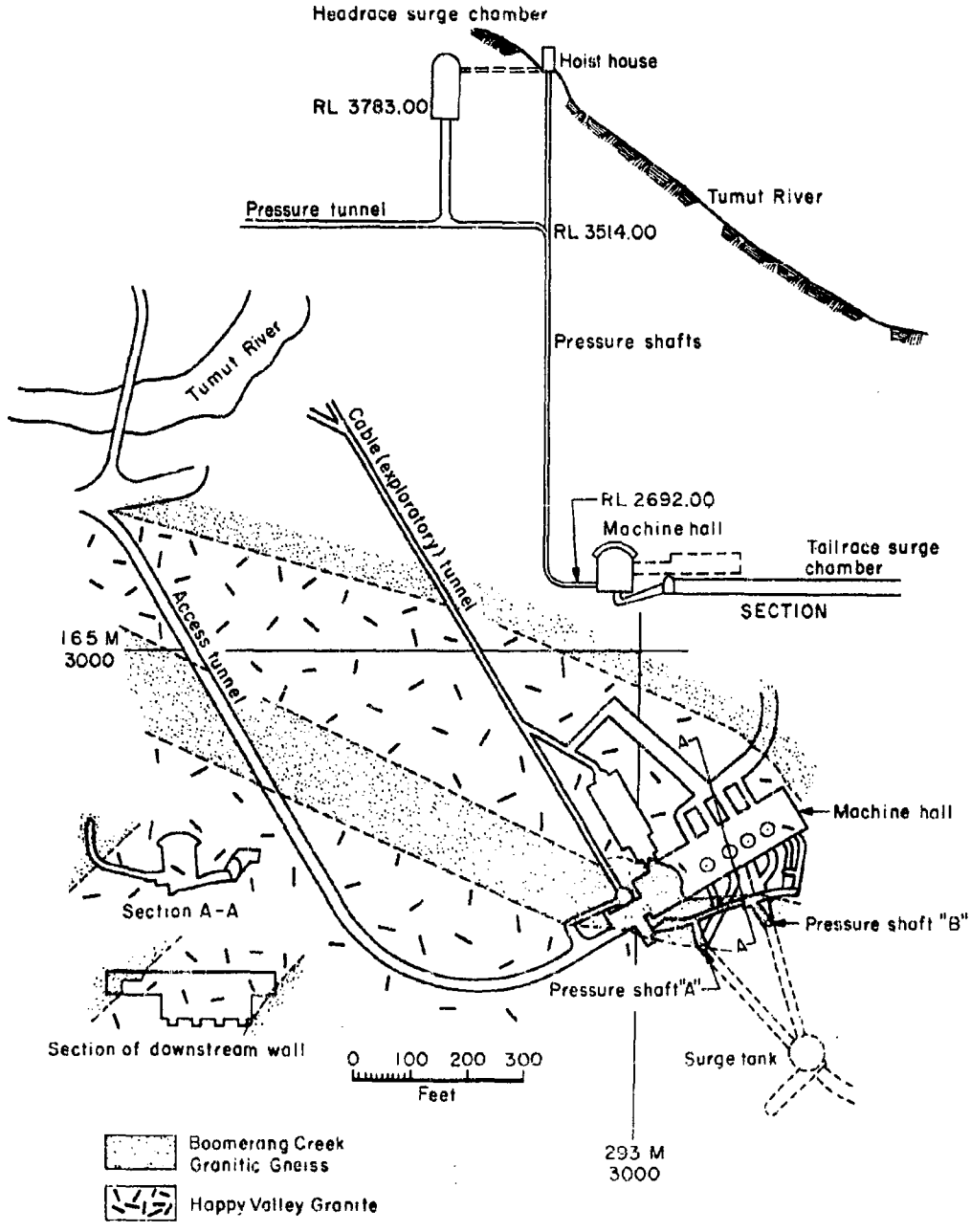


Figure III-A.26. Plan showing rock types T.1. power stations - general layout, Snowy Mountain Power Station.

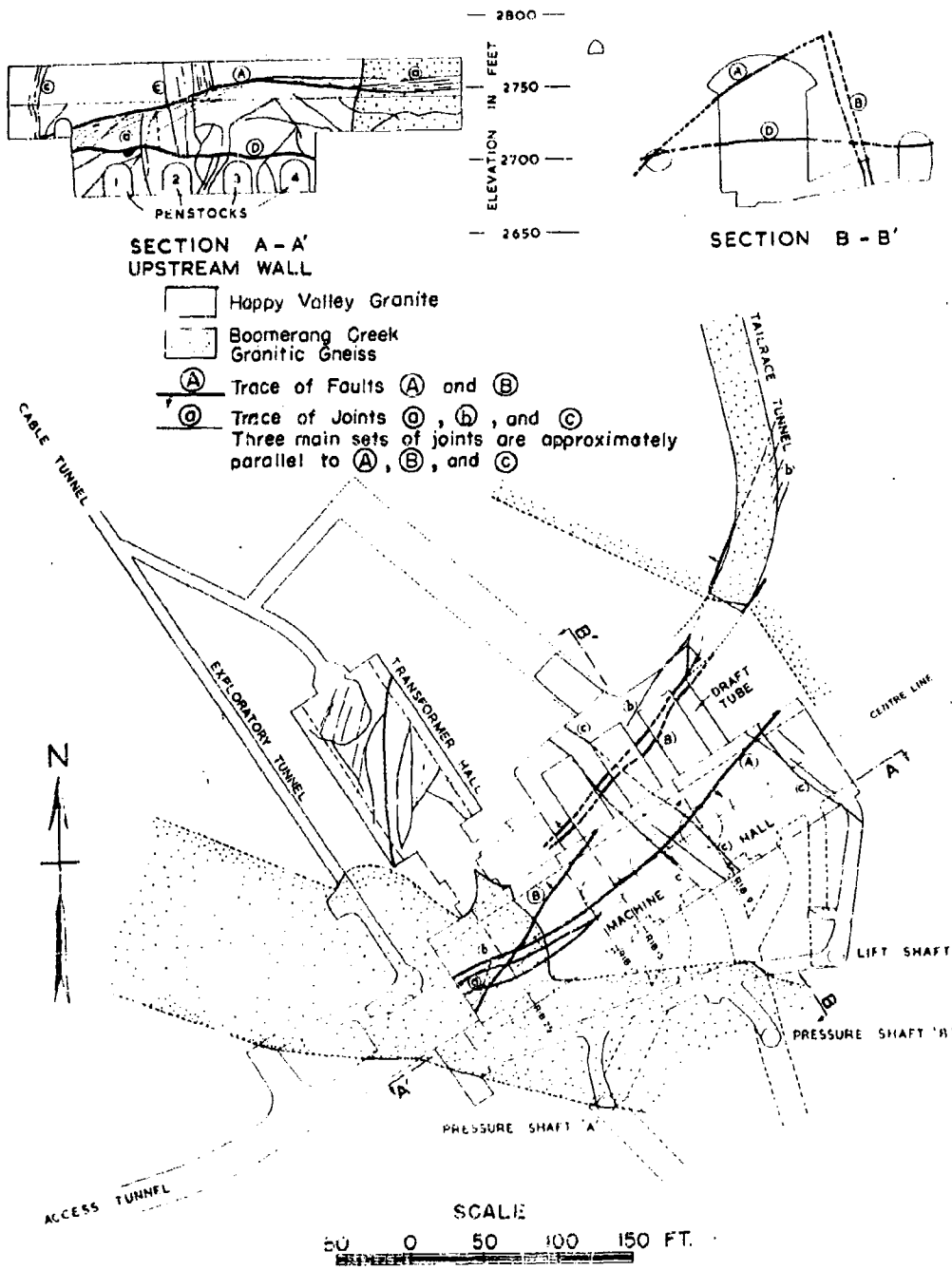


Figure III-A.27. Geology of site - Snowy Mountain Power Station.

thus in a mass of rock which lies between these two faults. The site itself is free from major faults but the rock mass evidences much previous strain in the form of slickensides along joints and by the presence of minor faults which are related to the ones of major size. Two small faults which show little displacement intersect the machine hall. Both have resulted in fracturing and jointing in the granite and gneiss. An additional fracture zone occurs in the lower part of one of the power station walls but is found only in the granite.

Both types of rock are jointed, the pattern being similar in each. Spacing of the joints in the gneiss however, is closer than that in the granite and the character of the joint surfaces is also different. The joint pattern has indicated that the joints may be grouped into three principal sets (Figure III-A.27). Most of the ground water inflows into the excavations were found to come in through the joints of set c, whereas the other two sets were practically dry.

While many of the joints appear to be slickensided the majority were rough enough to have a high coefficient of friction. The effect of this is to offer considerable resistance to slipping or rotational shear. Much of the jointed rock immediately around the excavation was comparatively loose. Slight movements in the crushed blocks here relieved the stress and transferred it to the layers behind. Thus, it is postulated that a destressed zone of rock exists immediately about the openings. Two forms of supports were used to hold this loose rock in place, that of conventional steel supports and rock bolts. The manner of placing the bolts in supports was based upon the results of a program of investigation designed to evaluate the best techniques for bolt installation.

The first considerations concerning geologic structure were the placement of roof bolts to offer support to the immediate surface of the excavations, such support to be of both temporary and permanent nature.[35] The bolts were ten to fifteen feet long and were spaced on centers of about four or five feet. Spacing was varied somewhat to conform with the directions of fracturing and jointing. In areas where excessive loosening of rock fragments occurred, particularly in the vicinity of faults, steel mesh was employed between rock bolts. Rock failure by rupturing or spalling was noted only in the case of isolated pillars. Strain measurements were made both in reinforced concrete arch ribs and horizontal aluminum points at the ends of concrete ribs and angular rotation points on reinforced concrete abutment beams. Certain asymmetries in roof strain were observed and were believed to be at least in part due to the topography of the valley near the installation site. The presence of faults nearby may also have an effect. (See also Chapter I and VI).

APPENDIX III-A

REFERENCES

1. Jackson, C.F., Methods of Mining Disseminated Lead Ore at a Mine in Southeast Missouri District, USBM & IC 6170.

2. Merrill, Robert H. and Mongan, Thomas A., Method of Determining the Strength of a Mine Roof, Bur. of Mines Rpt. of In. 5406.

3. Merrill, Robert H., Roof Span Studies in Limestone, Bur. of Mines Rpt. of Inv. 5348.

4. Merrill, Robert H., Design of Underground Mine Openings - Oil Shale Mine, Rifle, Colorado, Bur. of Mines Rpt. of Inv. 5089, 1954.

5. Clark, George B., Private Report.

6. Price, Peter, The Geology and Ore Deposits of the Horne Mine, Noranda, Quebec, Tr. CIMM 37:108, 1934

7. Bu[illegible]er, W.M., Geology of [illegible]e Horne Mine, Can. Mg. Jl. 55:149-154, April 1934

8. Henderson, E., Mining at Noranda, Can. Mg. Jl. 55:155-160, April 1934.

9. Hall, O., Mining at Noranda Tr. CIMM 40:141-164, 1937.

10. McNaughton, G.H., Mining Copper at Ducktown Tennessee, E & M J, vol. 128, July 1929.

11. Emmons, W.H., and Laney, F. [illegible], Geology and Ore Deposits of the Ducktown Mining District, Tennessee, USGS, pp. 139.

12. Parker, R.D., Mining a Cre[illegible]on, E & M J 131:437, 10 Nov. 1930.

13. The Operations and Plants of the International Nickel Company of Canada, Ltd., Can. Mg. Jl. 67:[illegible]24, May 1946.

14. Ringaleben, W. G., The Hollinger Mine--Geology, Can. Mg. Jl. 56:364, September 1935.

15. Shavlem, H.G., Mining Methods and Costs at the McIntyre Porcupine Mines, Ltd., Schumacher, Ontario, USBM IC 6745.

16. Company Staff, The Story of McIntyre-McIntyre Geology, E & M J 134:454, November 1933.

17. Langford, C.B., Geology of the McIntyre Mines, AIME Tech. Paper 903, 1938.

REFERENCES (cont.)

18. Sales, R. H., Ore Deposits of Butte, Montana, Tr. AIME 46:3-127, 1931.

19. Daly, W. B., et al., Mining Methods in the Butte District, Tr. AIME 72:234, 1925.

20. Hershey, O. H., Genesis of Lead Silver Ores in Wardner District, Idaho, Min. and Sci. Press, 104:750, 1 June 1912.

21. Ransome, R. L. and Calkins, F. C., The Geology and Ore Deposits of the Coeur d'Alene District, Idaho, USGS, pp 62.

22. Brown, U. E., Mining Methods of the Bunker Hill and Sullivan Mining and Concentrating Co., Kellog, Idaho, USBM IC 6407.

23. Personal communication from Stanley A. Easton, President, Bunker Hill and Sullivan Mining Company, Kellog, Idaho.

24. Personal communication from George D. Furse, Geologist, McIntyre Porcupine Mines, Ltd., Schumacher, Ontario.

25. The Operations and Plants of the International Nickel Company of Canada, Ltd., Can. Mg. Jl. 67:328, May 1946.

26. Company Staff, The Operation and Plants of the International Nickel Co., Ltd., Can. Min. Jl. 58, November 1937.

27. Robson, W. T., Lake Shore Geology, Tr. CIMM 39:99, 1936.

28. Weldon, L. S., Mining Methods and Practices at Lake Shore, Tr. CIMM 39:142, 1936.

29. Jackson, C. F., Mining by the Top Slicing Method, with some notes on Sublevel Caving, USBM IC 6410.

30. Schaus, O. M., Methods and Cost of Mining Hematite at the Eureka-Asteriod Mine on the Gogebic Range, Gogebic Co., Mich., USBM IC 6348.

31. Bucky, P. G., Mining by Block Caving, Hercules Powder Co., 1945.

32. King, R. U., A Study of Geologic Structure at Climax in Relation to Mining and Block Caving, Tr. AIME 163, 1946.

33. Vanderwilt, J. W., Ground Movement Adjacent to a Caving Block in the Climax Molybdenum Mine, AIME Tech. Paper 2000, 1946.

34. Moye, D. G., Rock Mechanics in the Investigation and Construction of T1 Underground Power Station, Snowy Mountains, Australia, CSA Eng. Geology Case Histories No. 3, May 1959.

35. Lang, Thomas A., Underground Experience in the Snowy Mountains-Australia, Protective Construction Symposium, Rand 1959.

APPENDIX IX-A

DETAIL PROCEDURE FOR COMPUTATION OF STRESSES [1]

Introduction

In this appendix a method of computing stresses in ribs is explained step by step. To illustrate this explanation the stresses in a 2-piece continuous rib for a tunnel with a semi-circular roof, Example No. 1, is computed.

Example No. 2 is included to show the effect of side pressure on straight-legged ribs and the beneficial effect of converting the tunnel cross-section to a full circle when side pressures are encountered.

Example No. 1 24 Ft. x 27 Ft. Tunnel

Construction of Load Diagram

See Fig. IX-A.1, a tunnel 24 ft. wide, semi-circular arch, 13 ft. vertical side walls. Crown is assumed to be hinged and the ends of the arch are fixed.

1. Draw the outside "design" line of the concrete for half the tunnel.
2. Draw in the rib, with its outside flange on the outside design concrete line. Assume 1" rib depth for each 3 feet of tunnel width. Draw neutral axis of rib: 8" rib.
3. Draw in the "overbreak" line parallel to outside flange of rib: 8" offset from rib.
4. Assume the maximum blocking point spacing and indicate the blocking points on the outside flange of the rib. One blocking point should be at the junction between arch and straight leg (at or near the spring line); another located not more than 6 in. from the crown joint. Label the blocking points 1, 2, 3, etc., starting at the spring line.

As the rib must be designed for maximum conditions, the second and third blocking points from the crown joint should be at the maximum spacing from the first blocking point. This induces maximum thrust in the arch. A maximum blocking space should separate the spring line blocking point from the one next above to induce maximum bending moment in the straight leg: 50 in. maximum blocking point spacing.

5. Project blocking points radially to the overbreak line and neutral axis.

---

[1] Proctor, R.V., et. al., Rock Tunneling with Steel Supports, Commercial Shearing and Stamping, 1946.

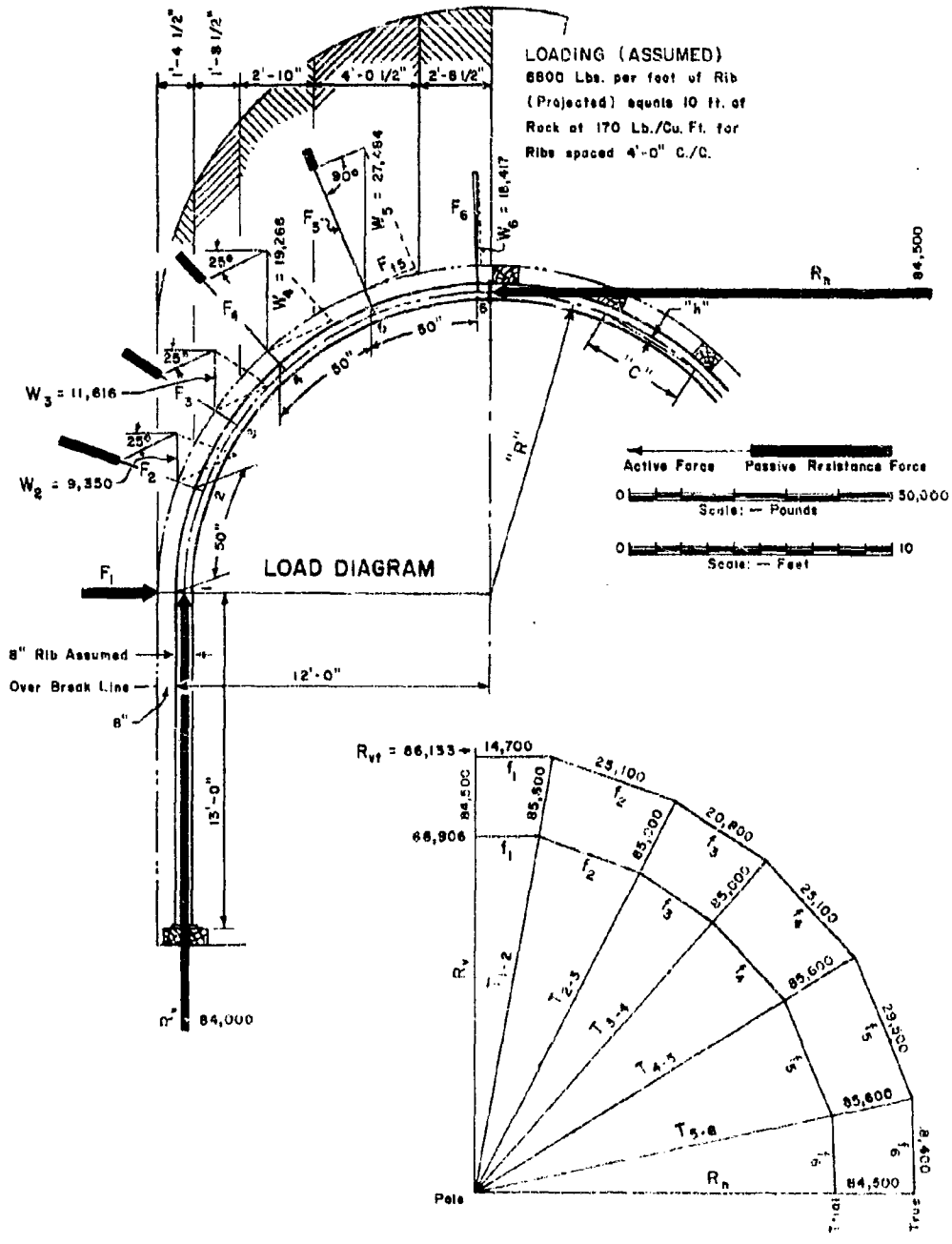


Figure IX-A.1. A tunnel 24 ft. wide, semi-circular arch, 13 ft. vertical side walls.

6. Assume the upper boundary of the body of rock which is to be carried by the rib. Draw vertical lines upward from the mid-points between the overbreak blocking points. The panels thus obtained represent the volume of rock acting at each blocking point: 10 ft. of rock.

7. Assume a rib spacing, and weight per cubic foot of rock. Compute the vertical load at each point and, to some suitable scale of pounds per inch, show each load acting vertically on the overbreak blocking point, as W_5 in Fig. IX-A.1.

Data: 10 ft. of rock; 4 ft. rib spacing; weight of, 170 lbs. per cu. ft. = 6800 lb. per ft. of rib, projected on a horizontal line.

8. As shown in Fig. 9.25 resolve each vertical force W at the overbreak blocking point into a radial load force F and a tangential component F_t if the tangent is inclined less than 25^o to the horizontal, otherwise at 25^o component as in Fig. 9.24h.

9. Show an upward vertical reaction R_v at the spring line (point 1).

10. Draw in the chords connecting the neutral axis blocking points. These chords represent the direction of the thrust in each panel.

Construction of Force Polygon

11. From a common point (pole) draw a vertical ray R_v and rays parallel to each thrust line (chord) and label them T_{1-2}, T_{2-3}, etc. End up with a horizontal ray R_h.

12. Compute the sum R_{vt} of all the vertical loads W which act on one-half of the tunnel roof. According to Fig. IX-A.1 the roof carries only one of the two components of each of the weights W. Therefore the total vertical pressure R_v on one-half of the roof is smaller than R_{vt}. However, its real value is not yet known. Hence, it is necessary to construct a trial polygon starting at an arbitrarily selected point on the ray R_v. For the sake of convenience, it is advisable to assume this point at a distance 0.80 R_{vt} from the pole. Starting at this point draw a line f_1 (parallel to force F_1 on the load diagram) to intersect ray 1-2. From this intersection draw a line f_2 parallel to force F_2 to intersect ray 2-3, and repeat until the horizontal ray R_h is reached, thus completing the trial force polygon.

R_{vt} is 86133 lbs. 80% of R_{vt} is 68906 lbs.

13. Now compare f_2 on the polygon with force F_2 on the load diagram, f_3 with force F_3 and so on. Usually at one or more points the radial component F on the load diagram will exceed the corresponding trial polygon force f.

14. Transfer all forces F which exceed the corresponding trial polygon forces f to the polygon, extending the rays as necessary, and complete a new polygon for the force f farthest removed from the pole. This is the true force polygon. It will be noted that all the other true polygon forces f are now greater than the corresponding forces F on the load diagram. The excess represents the force of passive resistance mobilized by the rock against the active tendency of the rib to advance toward the rock. Maximum excess is at point 6. In Fig. IX-A.1 the passive resistance furnished by the rock has been plotted as the thick part of the arrow.

Determination of Thrusts

15. The length of the rays of the true force polygon represent thrust. Since the design must be based on the most unfavorable stress conditions, determine which is the longest ray. Thrust is uniform and maximum in all panels of maximum block spacing because of constant curvature of rib. Thrust scales 85600 lbs.

Note: The excess of R_{vt} over R_v in Fig. IX-A.1 represents that part of the rockload on the roof which is transferred by friction forces onto the rock located next to the tunnel. It is always very small compared to the total load which the friction forces could carry. Thus, for instance, in Fig. IX-A.1 the excess amounts to about 0.02 R_h whereas the friction forces could carry at least R_h x tan 25^o = 0.45 R_h. This is due to the fact that the vertical component of the passive forces (thick part of the arrows F_2 to F_5) relieves the load which would otherwise be carried by the friction forces.

Bending Moment

16. As stated in Chapter IX it is not worth while to determine the intensity of the various moments as the rib, being of constant section, must be proportioned for the maximum. This maximum occurs at the blocking point next to the crown joint blocking point. The bending moment M_{max} cannot exceed .86 M_t and for design purposes may be taken as .86 M_t. Maximum moment is at point 5.

Maximum Total Stress

17. The sum of the compressive stress due to the thrust and the maximum compressive stress due to bending is the maximum total stress.

Computations for Stresses in Arch Rib

18. The following symbols are used in the formulas below:

C = Chord length between neutral axis blocking points, in inches, (measured on the load diagram or computed): 48.4 in., computed.

R = Radius of neutral axis of rib, in inches, from load diagram: 140.0 in.

h = Rise of arc between blocking points, in inches, computed.

M_t = Bending moment in inch-pounds if rib sections could be pin connected at blocking points, computed.

M_{max} = Maximum bending moment, in inch-pounds, in rib continuous for at least 4 blocking points, computed.

T = Thrust, in pounds, scaled from true force polygon: 85600 lbs.

S = Section Modulus of beam under consideration, from structural hand book: S = 18.0 $in.^3$ 8 x 5¼ in. WF-beam, 21 lbs. per foot.

A = Sectional Area of beam under consideration, less holes, in sq. inches, from structural hand book, reduced by computation: A = 6.18 sq. in. less .22 sq. in. for 7/8 in. tie rod hole = 5.96 sq. in.

f_c = Stress in arch portion of rib, in pounds per sq. in., computed.

The following formulas are used in stress computations:

$$h = R - \sqrt{R^2 - \left(\frac{C}{2}\right)^2}$$

$$h = 140 - \sqrt{140^2 - \left(\frac{48.4}{2}\right)^2} = 2.1 \text{ in.}$$

$$M_t = hT \quad \text{(equation 1)}$$

$$M_t = 2.1 \times 85600 = 179{,}760 \text{ in.-lbs.}$$

$$M_{max} = .86\ M_t \quad \text{(equation 4)}$$

$$M_{max} = .86 \times 179760 = 154594 \text{ in.-lbs.}$$

$$f_r = \frac{T}{A} + \frac{M_{max}}{S}$$

$$f_r = \frac{85600}{5.96} + \frac{154594}{18} = 22950 \text{ lbs. per sq. in.}$$

f_{all} = Allowable fibre stress = 24000 p.s.i., for temporary construction. (May be set at any desired figure). Since the stress f_r of 22950 p.s.i. is less than the allowable stress f_{all} of 24000 p.s.i., this rib is considered satisfactory.

Leg Checked as a Column

19. Having thus selected the beam to be used for the arch, it may be interesting to investigate whether this beam is capable of acting as a column to carry the forces down to subgrade. In Chapter IX it is shown that the leg is normally amply strong, but a check is made here for the benefit of those interested.

First, the permitted stress in the leg is computed by means of one of the customary column formulas. This computation takes care of lack of true homogeneity in the metal, variation in the shape and thickness of the section, and eccentricity of application of the forces. All of these departures from perfect conditions cause the axial force to set up a bending moment in the leg. This moment is maximum at the middle of the leg and requires reduction of the allowable stress.

Second, the stress in the leg is computed and compared to the reduced allowable stress.

20. The following symbols are in addition to those in Paragraph 18.

f_{red} - Maximum permitted fibre stress at mid-point, in lbs. per sq. in., computed.

f_{all} = Allowable fibre stress = 24,000 p.s.i., for temporary structures, assumed.

M_1 = Bending moment at spring line in inch-lbs., computed.
M_c^1 = Bending moment at point of maximum deflection of leg in upper half of middle third, in inch-lbs., computed.
d_1 = Deflection of the leg caused by bending moment M_1, in inches, computed.
d_2 = Total deflection of leg in the upper half of the middle third, caused by the sum of the moments, in inches, computed.
E = Modulus of Elasticity of the structural steel used in the rib, which is 29,400,000 lbs. per sq. in.
I = Moment of Inertia of the beam under consideration, from structural handbook: $I = 73.8$ in.^{4}
R_V = Thrust acting on the leg, in pounds, scaled from true force polygon: $R_V = 84500$ lbs.
l = Length of leg below spring line blocking point, in inches, from load diagram: $l = 156$ in.
f_1 = Stress in leg at spring line, in lbs. per sq. in., computed.
f_c = Stress in the leg at point of maximum deflection, in lbs. per sq. in., computed.
r = Radius of gyration for the major axis of the section, from structural handbook: $r = 3.45$ in.

Stresses in Leg

21. Reduction of allowable stress. Two commonly used formulas for reduction of allowable stress in columns are given below.

$$f_{red} = \frac{f_{all}}{1 + \frac{l^2}{f_{all} r^2}}$$

$$f_{red} = \frac{24000}{1 + \frac{156^2}{24000 \times 3.45^2}} = 22,115 \text{ p.s.i.}$$

This is the American Institute of Steel Construction formula for Strut Loading.

$$f_{red} = \frac{f_{all}}{18000} \times \left[17000 - .485 \left(\frac{l}{r}\right)^2\right]$$

$$f_{red} = \frac{24000}{18000} \times \left[17000 - .485 \left(\frac{156}{3.45}\right)^2\right] = 21,345 \text{ p.s.i.}$$

This is the well-known straight line formula adjusted to an allowable fibre stress other than 18000 p.s.i. This straight line formula will ordinarily give somewhat lower values than the A.I.S.C. formula in the range of l/r commonly encountered in rib design.

22. Computation of stresses in leg. The following formulas are used.

$$M_1 = .67M_t = .67h_T$$

$$M_1 = .67 \times 2.1 \times 85600 = 120{,}440 \text{ in.-lbs.}$$

$$f_1 = \frac{T}{A} + \frac{M_1}{S}$$

$$f_1 = \frac{85600}{5.96} + \frac{120440}{18.0} = 21050 \text{ p.s.i.}$$

$$d_1 = .0642 \frac{M_1 l^2}{EI}$$

$$d_1 = .0642 \times \frac{120440 \times 24{,}336}{29400000 \times 73.8} = .087 \text{ in.}$$

$$M_c = \frac{(.578M_1)^2}{.578M_1 - d_1R_v}$$

$$M_c = \frac{(.578 \times 120440)^2}{.578 \times 120440 - .087 \times 84500} = 77800 \text{ in.-lbs.}$$

$$f_c = \frac{R_v}{A} + \frac{M_c}{S}$$

$$f_c = \frac{84500}{5.96} + \frac{77800}{18.0} = 18500 \text{ p.s.i.}$$

To be satisfactory, the stress in the leg must satisfy both conditions below.

f_1 must be less than f_{all}: 21050 is less than 24000.

f_c must be less than f_{red}: 18500 is less than 21345 (or 22115)

Thus the beam selected for the arch rib is also quite satisfactory for the leg.

Example No. 2 - Tunnel Support Subject to Side Pressure

This example (Figure IX.A-2) sets forth the computations made to illustrate the advantages of a full circle rib over a straight legged rib when side pressures are encountered. Where side pressure is present it is necessary to lag tight and pack solid, as would be the case in squeezing rock. Hence the blocking point spacing is reduced to zero and because of this, there are no bending stresses in the curved portion of the rib.

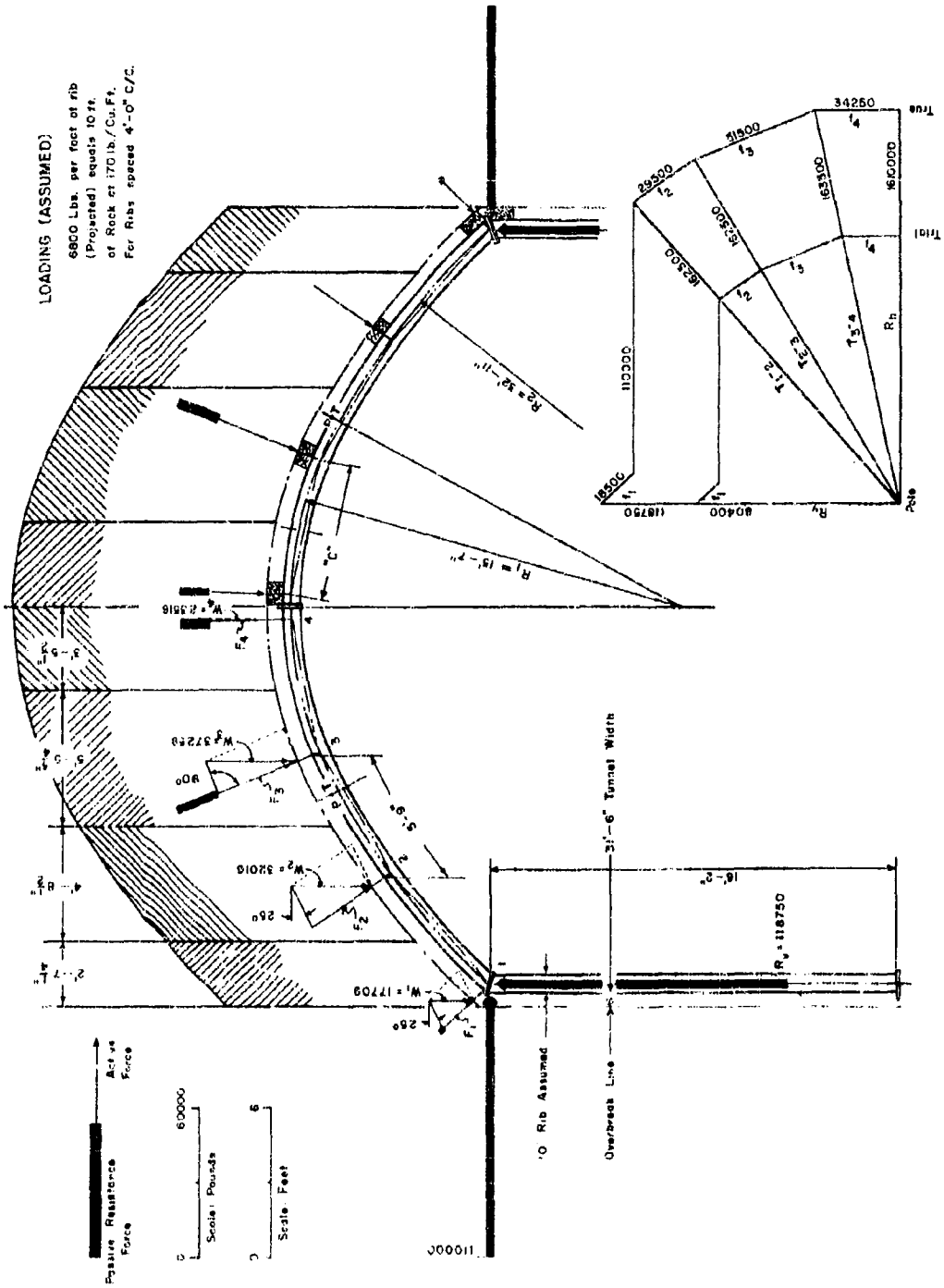


Figure IX-A.2. Sets forth the computations made to illustrate the advantages of a full circle rib over a straight legged rib when side pressures are encountered.

In the following paragraphs, the maximum stress in the rib is computed for each type under vertical and under combined loading. This is done for 10 ft. of rock, weighing 170 lbs. per cu. ft. with ribs spaced at 4 ft. The respective carrying capacities in ft. of rock are then obtained by increasing the load till the fiber stress reaches the permitted stress.

Case 1 - Vertical Load Only on Straight Legged Rib

An inspection of the force polygon shown in Example 1, where a 50-in. blocking point spacing was used, reveals that the thrust T is less than the total vertical reaction R_{vt}. As the blocking point spacing is reduced the thrust T increases until at zero spacing $T = R_{vt}$.

R_{vt} = the vertical load on half the tunnel.

$T = R_{vt} = \frac{24}{2} \times 4 \times 10 \times 170 = 81600$ lbs.

A = 8.870 sq. in., for 8 x 8 in. WF-beam, 31 lbs. (after deducting for tie rod hole).

$f = \frac{T}{A} = \frac{81600}{8.87} = 9200$ p.s.i.

Inasmuch as there is no bending moment in the arch rib, f_r is also the stress in the straight leg, or $f_r = f_c$. However, the leg is considered to be a slender column and whereas the allowable figure stress f_{all} in the arch may be taken as 24000 p.s.i. the fibre stress f_{red} permitted for the leg is smaller on account of the danger of buckling.

r = 3.47 in., for 8 x 8 in. WF-beam, el lbs.

l = 114.8 in., the length of the straight leg.

$$f_{red} = \frac{24000}{18000} \left| 17000 - .485 \left(\frac{l}{r} \right)^2 \right| = 21900 \text{ p.s.i.}$$

As f_c cannot exceed f_{red}, the leg limits the capacity of the rib set. The capacity H_p in feet of rock then is

$$H_p = \frac{f_{red}}{f_c} \times 10 \text{ feet of rock or } \frac{21900}{9200} \times 10 = 23.8 \text{ ft.}$$

Case 2 - Side Unit Pressure Equal to 1/3 the Unit Vertical Pressure Acting on the Straight Legged Rib.

The thrust T in the arch remains the same as in Case 1 as the vertical load on the arch rib causes the rib to press outward against the rock with a greater force than the assumed inward horizontal pressure. (Note: This statement is true for the ratios of leg length to arch rise and horizontal pressure to vertical pressure in this example. A longer leg and/or greater ratio of horizontal to vertical pressure may vitiate this statement.)

There is no bending moment transmitted into the leg from the arch as in Example 1. Bending and deflection in the leg does result, however, from the horizontal pressure. Hence the leg is subjected to combined stress, i.e., compression due to the thrust T transmitted into it from the arch rib, and bending stress from two causes, one being from the active external horizontal ground pressure, and the other from the thrust acting about the deflection resulting from the first.

Since the thrust T and consequently the stress in the arch is known, as explained in Case 1, the following computations deal only with the stresses in the leg, which limit the capacity of the rib set. For the sake of simplicity the straight leg is considered to be vertical.

The following additional symbols and formulas are used in the computations.

M_h = Bending moment caused by lateral pressure, in in.-lbs. M_h is maximum at .125 x l below mid-point of leg.
M_c = Bending moment from all causes combined at point of maximum deflection, in in.-lbs. The maximum deflection is slightly below mid-point of leg.
d_1 = Maximum deflection of leg caused by moment M_h in inches. This occurs at .078 x l below mid-point of leg.
d_2 = Total maximum deflection, from all causes combined, in inches. Maximum slightly below mid-point of leg.
E = Modulus of Elasticity, 29,400,000 p.s.i.
I = Moment of Inertia, 109.7 $in.^4$, for 8 x 8-in. WF-beam, 31 lbs.
$R_v = R_{vt} = T$ = Thrust acting on leg, 81600 lbs.
f_c = Stress in leg at point of maximum deflection, in p.s.i.
W = Total horizontal pressure of rock on straight leg, in pounds.
H_p = Height of rock causing vertical load, 10 ft.
w = Weight per cu. ft. of rock, 170 lbs.
l = Length of straight leg in inches, = 114.8 in.
s = Rib spacing, 4 ft.

$$W = \frac{sH_p wl}{3 \times 12} = \frac{4 \times 10 \times 170 \times 114.8}{3 \times 12} = 21700 \text{ lbs.}$$

$M_h = \frac{Wl}{14.2}$ for a beam fixed at one end and with simple support at the other $= \frac{21700 \times 114.8}{14.2} = 175{,}440$ in.-lbs. This occurs at .125 x l or 14.3 in. below mid-point of leg.

$d_1 = \frac{Wl^3}{185EI} = \frac{21700 \times 1512954}{185 \times 29400000 \times 109.7} = .055$ in. This occurs at .078 x l or 9 in. below mid-point of leg.

The above moment and deflection are increased by the thrust T acting around d_1 as a lever arm. These are both maximum near the mid-point of the leg so that when added to M_h the resulting total moment M_c is maximum just below the mid-point. It is not important to find out just where.

$$M_c = \frac{M_h^2}{M_h - d_1 R_{vt}} = \frac{175440^2}{175440 - .055 \times 81600} = 180{,}050 \text{ in. lbs.}$$

$$f_c = \frac{R_{vt}}{A} + \frac{M_c}{s} = \frac{81600}{8.87} + \frac{180050}{27.4} = 9200 + 6571 = 15770 \text{ p.s.i.}$$

This stress was caused by 10 ft. of rock. The capacity of the rib set then is

$$H_p = 10 \times \frac{f_{red}}{f_c} = \frac{10 \times 21900}{15770} = 13.9 \text{ ft.}$$

Thus it may be seen that when side pressure is acting the straight leg reduced considerably the load which may be carried by a horseshoe shaped rib.

This limitation may be removed by converting to a circular extrados. Design for the circular shape is described below.

Case 3 - Full Circle Rib

A circular rib, using the same rib profile as the horseshoe shape is drawn over the horseshoe layout, allowing for minimum concrete thickness at the bottom corners and the crown. The size required for the 24 ft. by 24 ft. tunnel under consideration is 26 ft. O.D.

Since the ribs are fully lagged and dry packed there is no bending moment in the rib. Passive resistance of the surrounding ground causes the thrust line to pass through the centroid of the rib section at all points as previously described. Therefore, the stress is entirely compressive, and is equal to one-half the vertical load. (Horizontal thrust in the ring due to vertical load is greater than the active horizontal load from the ground.)

The number of feet of rock which the rib will carry is determined from the compression strength of the rib.

$$T = R_{vt} = Af_{all} = 8.87 \times 24000 = 212{,}880 \text{ lbs.}$$

$$H_p = \frac{2T}{(O.D.)\ sw} = \frac{2 \times 212880}{26 \times 1 \times 170} = 24.1 \text{ feet of rock}$$

APPENDIX IX-B

TABLE IX-B.1 CONTINUOUS RIBS

CAPACITY IN POUNDS PER FOOT OF TUNNEL WIDTH MAXIMUM FIBER STRESS—24000 LBS. PER SQ. IN.

BEAM			B = Width of Tunnel to Outside Design Concrete Line S = Maximum Blocking Point Spacing												
Depth & Flange Width	Type	Weight Per Foot	S	14'-0" 40"	16'-0" 42"	18'-0" 44"	20'-0" 46"	22'-0" 48"	24'-0" 50"	26'-0" 52"	28'-0" 54"	30'-0" 56"	32'-0" 58"	34'-0" 60"	36'-0" 62"
				2750	2470										
				3750	3370										
				4780	4310	3910	3570								
				4030	3620	3280	2990								
				5760	5180	4690	4270								
				6920	6220	5630	5130								
				7860	7060	6390	5820								
				5590	5030	4540	4130	3790							
				7100	6380	5770	5260	4830	4450						
				5519	5940	4460	4060	3730							
				7540	6760	6110	5570	5100	4470						
				7410	6670	6030	5490	5033	4650						
				8590	7780	7040	6410	5870	5420	5030					
					12010	10660	9890	9060	8370	7760	7220	6740			
				9550	8560	7740	7050	6460	5960	5530	5140				
				13850	10370	9370	8710	8040	7360	6830	6350	5930			
						5990	5450	4990	4610						
						7640	6950	6370	5860	5450					
						8640	8290	7600	7010	6500	6040	5640	5280	4960	4670
						6320	5750	5270	4860						
						7310	6680	6120	5650	5240					
						9210	8390	7680	7090	6570	6100	5700			
						10600	9650	8400	8150	7560	7020	6560	6150	5770	5440
						12920	10850	9930	9160	8500	7900	7380	6910	6480	
						13820	12590	11530	10640	9860	9160	8560	8020	7530	7100
						15640	14250	13110	12040	11160	10370	9690	9070	8530	[illegible]
						17870	16270	14890	13750	12740	11840	11050	10360	[illegible]	9160
							18150	17990	16600	15390	14290	[illegible]	[illegible]	11760	11090
								21700	20030	18560	[illegible]	[illegible]	15110	14210	13400
								25100	23190	[illegible]	19970	18650	17470	16420	15480
								9610	[illegible]	8210	7630	7130	6680	6280	5920
								[illegible]	11540	10740	9940	9290	8700	8170	7710
								8220	7580	7020	6520	6090	5710	5370	5060
								10320	9500	8820	8180	7640	7160	6740	
								13130	12080	11210	10430	9740	9130	8580	8090
								16460	15170	14070	13060	12210	11440	10760	
									18290	16970	15770	14730	13820	12990	12250
									20200	18750	17410	16270	15260	14340	13530
									24950	22900	21280	19870	18630	17520	16520
										26760	24840	23230	21780	20480	
										30930	28710	26850	25165	23650	
												14170	13280	12490	11790
												16570	15520	14680	14040
												20780	19500	18230	17290

APPENDIX IX-B

TABLE IX-B.2 MAIN PLATE RIBS

D = WEIGHT IN POUNDS PER FOOT OF TUNNEL WIDTH MAXIMUM FIBER STRESS = 12000 LBS. PER SQ. IN.

Line	S = Spacing of Tunnel to Outside Design Concrete Line								S = Maximum Blocking Point Spacing.							
	8	12'-0"	14'-0"	16'-0"	18'-0"	20'-0"	22'-0"	24'-0"	16'-0"	28'-0"	30'-0"	32'-0"	34'-0"			
		30"	32"	34"	36"	38"	30"	32"	34"	36"	38"	40"	42"			
				3910	3570											
				4285	3990											
				4695	4270											
				5035	5130											
				5290	5820											
				5450	6740	5740										
				5770	6560	6830										
				6090	7060	8730										
				6210	7570	9100										
				6470	7980	9730										
				6610	8190	10060										
				6870	8590	10690										
				7130	8990	11320										